

Adipose derived stem cells for cell therapy of amyotrophic lateral sclerosis

Yuri Ciervo MSc



Thesis submitted for the degree of Doctor of Philosophy,

The University of Sheffield

and

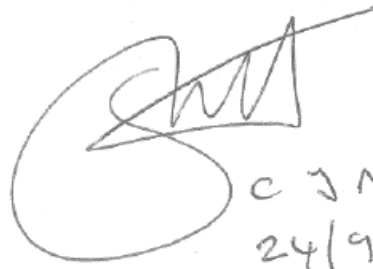
Tongji University

September 2019

Statement from Professor Christopher McDermott, Head of Department of Neuroscience

The following PhD thesis 'Adipose derived stem cells for cell therapy of amyotrophic lateral sclerosis' submitted to the University of Sheffield by Y. Ciervo contains published material from the review article 'Advances, challenges and future directions for stem cell therapy in amyotrophic lateral sclerosis'. This was published in Molecular Neurodegeneration (DOI: 10.1186/s13024-017-0227-3), under a Creative Commons Attribution Licence (CC BY).

Permission has been given by the co-authors Professor P. J. Shaw, Dr R. Mead, Dr K. Ning and Professor J. Xu for the reuse of the material in this thesis. Y. Ciervo wrote the manuscript and prepared the figures, Professor P. J. Shaw, Dr R. Mead, Dr K. Ning and Professor J. Xu edited the manuscript. Given the contribution that Y. Ciervo made towards the original manuscript, I am happy that reuse of the material in this thesis is appropriate.



C J McDermott
24/9/19

Acknowledgements

Firstly, I would like to express my sincere gratitude to my supervisors Professor Dame Pamela Shaw, Dr Richard Mead, Dr Ke Ning and Professor Jun Xu for giving me the opportunity of a PhD and for the continuous support and guidance during my studies. It really was a fantastic experience.

A huge thank you to Richard for all the encouragement, support and constant precious feedback during my PhD. I could have never imagined to have such a kind and supportive supervisor – working together and exchanging ideas has been a real pleasure. I am extremely grateful to Professor Shaw for always believing in me and for the precious guidance throughout my PhD – thank you for all the time you have invested in me. I am also grateful to Dr Ning for his support and encouragement and to Professor Xu for the guidance and support during my wonderful and rich experience in China.

A big thank to the past and present members of the Mead Group, in particular to Dr Matt Stopford, Dr Jodie Stephenson, Dr Heledd Brown-Wright and Amy Keerie, thank you for all the help and fun we had. I am also grateful to the members of the Xu Team at Tongji, with a special mention to Milong, Jin and Lesley – thank you for making my experience in China easier and so enjoyable. I am particularly grateful to Dr Laura Ferraiuolo, Ian Coldicott, and Dr Adrian Higginbottom for sharing their valuable knowledge, teaching me and helping during my studies. I would like to extend my thanks to Santiago Coelho, Dr Evangelia Karyka, the Ferraiuolo Group, the Flow Cytometry Team and BSU staff at the University of Sheffield for the assistance and technical help. Many thanks also to all the colleagues in the office and the SITraN community as a whole. SITraN is truly a great place to work! Thank you to The University of Sheffield, Tongji University and the National Institute for Health Research (NIHR) Sheffield Biomedical Research Centre (BRC) for funding my PhD.

Further, thank you to my sister and parents for the support and words of encouragement. A very special gratitude goes to my wife Rachel, for her patience and for always providing me with moral and emotional support. Undertaking this PhD has been a truly life-changing experience and it would not have been possible to do without you, thank you! Last but not least, thank you to my son Nathan, who has always provided a ray of sunshine, even in the hardest times.

Abstract

Amyotrophic Lateral Sclerosis (ALS) is a devastating neurodegenerative condition characterised by progressive motor neuron loss leading to paralysis and ultimately death. Because of the complexity and high heterogeneity of the disease, single drugs have failed as effective therapeutic options and new therapies are urgently needed.

Cell-based therapy is a promising therapeutic strategy in ALS. Given their immunomodulation properties and the capacity to secrete neuroprotective factors, adipose derived stem cells (ADSCs) represent an excellent candidate for clinical application. It is hypothesised that intrathecal injection of ADSCs may be beneficial in ALS, because of the capacity of these cells to modulate the toxic microenvironment that leads to motor neuronal degeneration.

The therapeutic potential of mouse derived ADSCs is first investigated by injecting GFP⁺-ADSCs into the cerebrospinal fluid of transgenic SOD1^{G93A} ALS mice. ADSCs persisted for 4 weeks and were unable to migrate into the spinal cord parenchyma. Despite these limitations, ADSCs improved motor function and delayed disease onset in SOD1^{G93A} mice compared to vehicle-injected animals. Pathological analysis in the spinal cord showed that ADSCs attenuated motor neuron (MN) death and reduced glial activation.

The neuroprotective potential of ADSCs was then evaluated *in vitro*, in astrocyte/MN co-cultures where astrocytes show toxicity. Through the secretion of soluble factors, ADSCs protected MNs from both astrocytes derived from symptomatic SOD1^{G93A} mice, and from human iAstrocytes obtained by reprogramming fibroblasts from patients with either sporadic or familial ALS. Further, ADSCs displayed the capacity to reduce the inflammatory phenotype of SOD1^{G93A} astrocytes by inhibiting the release of pro-inflammatory mediators and inducing the secretion of neuroprotective factors.

In conclusion, our data in two translational models of disease show that through paracrine mechanisms ADSCs support MN survival and modulate the toxic microenvironment that contributes to neurodegeneration, indicating these cells as potential candidates for the development of a cell-based therapy in ALS.

Contents

Acknowledgements	i
Abstract	ii
Contents	iii
List of Figures	ix
List of Tables	xii
Abbreviation	xiv
1 Introduction	1
1.1 Amyotrophic Lateral Sclerosis	1
1.2 Diagnosis, clinical features and prognosis of ALS	1
1.3 Aetiology and pathology of ALS	2
1.3.1 SOD1	2
1.3.2 TARDBP and FUS	4
1.3.3 C9orf72	6
1.4 ALS is non-cell autonomous disease	7
1.4.1 Astrocytes	9
1.4.2 Role of astrocytes in ALS	9
1.4.3 Pathological mechanisms of ALS astrocytes	11
1.4.4 Inflammation-mediated neurotoxicity of ALS astrocytes	13
1.4.5 Microglia	15
1.4.6 Role of microglia in ALS	16
1.4.7 Oligodendrocytes in ALS	18
1.5 Treatment options for ALS	19
1.6 Stem cell therapy in ALS	20
1.6.1 Human Embryonic Stem Cells (hESCs)	20
1.6.2 Foetal Neuronal Stem Cells (NSCs)	21
1.6.3 Induced Pluripotent Stem Cells (iPSCs)	22
1.6.4 Mesenchymal Stem Cells (MSCs)	23
1.6.5 Proof-of-concept for MSC therapy in the SOD1 ^{G93A} model of ALS	24
1.6.6 MSCs in ALS: Clinical trials	33
1.7 Adipose tissue: a fat tissue source for mesenchymal stem cells	37
1.7.1 In vitro neuronal differentiation capacity of ADSCs	38
1.7.2 Proof-of-concept for ADSC therapy in the SOD1G93A model of ALS	41

1.7.3 ADSCs in ALS: clinical trials	42
1.8 MSCs for ALS therapy: summary of proposed mechanisms of action	43
1.9 Summary and Hypothesis.....	48
1.10 Aims and Objectives	49
2 Materials and Methods.....	50
2.1 Ethics statement	50
2.2 Mouse Adipose Derived Stem Cells	50
2.2.1 Isolation of mouse Adipose Derived Stem Cells (ADSCs).....	50
2.2.2 Culture and expansion of mADSCs	52
2.2.3 mADSC characterisation by flow cytometry	54
2.2.4 In vitro tri-lineage differentiation of mADSCs	56
2.2.5 Production of EGFP-expressing lentivirus particles	60
2.2.6 Lentivirus titration by Flow Cytometry	62
2.2.7 Transduction of mADSCs and long-term cell storage	64
2.3 In vivo therapeutic study	65
2.3.1 Transgenic C57BL/6J-Tg (SOD1G93A)1Gur/J mice	65
2.3.2 Intrathecal transplantation of mADSCs in SOD1G93A mice: study design.....	67
2.3.3 Intrathecal injection of GFP-mADSCs: surgical procedure	68
2.3.4 Tissue collection for the detection of injected GFP-ADSCs in the whole CNS.....	71
2.3.5 Weighing and the accelerating rotarod test.....	72
2.3.6 Catwalk gait analysis.....	72
2.3.7 Neuroscoring	73
2.3.8 Tissue collection for histology	73
2.3.9 Immunohistochemical staining on spinal cord.....	74
2.3.10 Immunohistochemical staining image analysis	75
2.3.11 Nissl staining and Motor Neuron counts	75
2.3.12 Tissue collection for RNA extraction	76
2.3.13 Gene expression in mouse spinal cord: RT-qPCR	76
2.4 Astrocytes, Motor Neurons and ADSCs co-culture experiments	79
2.4.1 Isolation of cortical mouse astrocytes	79
2.4.2 Characterisation of cortical astrocytes by flow cytometry	80
2.4.3 Generation of human iAstrocytes	81
2.4.4 HB9-GFP mouse Motor Neurons (HB9-GFP-MNs)	82

2.4.5 HB9-GFP-MNs, mouse astrocytes and ADSCs triple separated co-culture	83
2.4.6 HB9-GFP-MNs, human iAstrocytes and ADSCs triple separated co-culture	84
2.4.7 Separated co-culture between mAstrocytes and ADSCs.....	85
2.4.8 Separated co-culture between iAstrocytes and ADSCs.....	85
2.4.9 Multiplex Bead-Based Immunoassay	85
2.4.10 Enzyme-linked Immuosorbent Assay (ELISA)	86
2.4.11 Gene expression after co-culture experiments by qPCR	88
2.5 Human Adipose Derived Stem Cells	89
2.5.1 Isolation of human Adipose Derived Stem Cells	89
2.5.2 hADSC characterisation by flow cytometry	90
2.5.3 In vitro differentiation of hADSCs	92
2.5.4 Recombinant human C-C chemokine Receptor 2B (hCCR2B) lentiviral vector design and production	94
2.5.5 Production of infectious viral particles with 3rd or 2nd generation packaging plasmids.....	101
2.5.6 hADSCs transduction optimization.....	102
2.5.7 Analysis of hCCR2B expression by Flow Cytometry	103
2.5.8 Analysis of hCCR2B expression by Western blot	104
2.5.9 Analysis of hCCR2B expression by IF	105
2.6 Statistical analysis	106
3 Characterisation of Mouse Adipose Derived Stem Cells (mADSCs)	107
3.1 Introduction	107
3.2 Aims	109
3.3 Isolation and expansion of mADSCs	110
3.3.1 Foetal Bovine Serum (FBS) test results	112
3.4 The immunophenotype of mADSCs: flow cytometry results.....	115
3.5 Tri-lineage differentiation of mADSCs: results.....	117
3.5.1 Adipogenic differentiation	117
3.5.2 Osteogenic differentiation	121
3.5.3 Chondrogenic differentiation	125
3.6 EGFP-expressing lentivirus production: titration results	127
3.7 Transduction of mADSCs: MOI test results	129
3.8 Lentivirus transduction of mADSCs and long-term storage	131

3.9	Characterization of GFP-mADSC	133
3.9.1	Immunophenotype of GFP-mADSCs: flow cytometry results	133
3.9.2	Tri-lineage differentiation of GFP-mADSCs	135
3.10	Discussion	138
3.10.1	Isolation and expansion of mADSCs.....	138
3.10.2	Immunophenotype of mADSCs.....	139
3.10.3	Tri-lineage differentiation of mADSCs.....	140
3.10.4	Generation of GFP-mADSCs, long-term storage and characterisation	142
3.10.5	Conclusions.....	144
4	Intrathecal transplantation of mADSCs in SOD1 ^{G93A} mice	145
4.1	Introduction	145
4.2	Aims	146
4.3	Estimation of cell viability before in vivo transplantation.....	147
4.4	Optimization of cell dosage for transplantation.....	147
4.5	Engraftment, distribution and survival of GFP-mADSCs in SOD1G93A mice	151
4.6	mADSCs increase body weight in SOD1G93A mice.....	158
4.7	mADSCs delay motor performance decline in SOD1G93A mice	159
4.8	mADSCs improve gait parameters in SOD1G93A mice.....	161
4.9	mADSCs delay disease onset in SOD1G93A mice	165
4.10	ADSCs increase MN survival in SOD1G93A mice: Nissl staining results .	166
4.11	ADSCs reduce astrogliosis in SOD1G93A mice: glial fibrillary acid protein (GFAP) staining results.....	168
4.12	ADSCs reduce microgliosis in SOD1G93A mice: IBA-1 staining results...	171
4.13	Gene expression analysis in spinal cord tissue: qPCR results.....	174
4.14	Discussion	176
4.14.1	Optimization of the cell number to inject in SOD1 ^{G93A} mice	176
4.14.2	Engraftment and distribution of GFP-ADSCs in SOD1 ^{G93A} mice	177
4.14.3	Effect of ADSC injection on body weight	179
4.14.4	Effect of ADSC injection on the rotarod task.....	179
4.14.5	Effect of ADSC injection on gait parameters	180
4.14.6	Effect of ADSCs on disease onset	181
4.14.7	Effect of mADSCs on MN loss	182

4.14.8	Effect of ADSCs on astrogliosis	183
4.14.9	Effects of ADSCs on microgliosis.....	183
4.14.10	Effect of ADSCs on cytokines and growth factor gene expression	184
4.15	Conclusions	186
5	The therapeutic potential of ADSCs on in vitro models of ALS.....	187
5.1	Introduction	187
5.2	Aims	190
5.3	Purity of mouse astrocyte cultures.....	191
5.4	ADSCs protect MNs from SOD1 ^{G93A} -linked mouse astrocyte toxicity.....	192
5.5	Expression of growth factors in ADSCs is modulated by SOD1 ^{G93A} mouse astrocytes	195
5.6	ADSCs modulate the expression of growth factors in SOD1 ^{G93A} astrocytes	200
5.7	ADSCs modulate the expression of cytokines/chemokines in SOD1G93A astrocytes	204
5.8	mADSCs protect MNs from human ALS iAstrocyte toxicity	208
5.9	iAstrocytes/ADSCs separated co-culture: gene expression analysis for inflammatory cytokines and growth factors.....	214
5.10	Discussion	220
5.10.1	ADSCs protect MNs from SOD1 ^{G93A} mAstrocyte toxicity	220
5.10.2	Expression and secretion of growth factors in ADSCs is modulated by SOD1 ^{G93A} astrocytes	221
5.10.3	ADSCs modulate the expression and secretion of neurotrophic factors in mAstrocytes.....	223
5.10.4	ADSCs reduce the inflammatory signature of SOD1 ^{G93A} astrocytes	227
5.10.5	ADSCs protect MNs from human ALS iAstrocyte toxicity	229
5.10.6	Gene expression of cytokines and growth factors in iAstrocytes: differences with murine SOD1 ^{G93A} astrocytes	231
5.11	Conclusions	234
6	CCR2 overexpression in human Adipose Derived Stem Cells (hADSCs)	235
6.1	Introduction	235
6.2	Aims	237
6.3	hADSCs isolation and expansion	238
6.4	hADSC characterisation by flow cytometry.....	240

6.5 Tri-lineage differentiation of hADSCs	243
6.5.1 Adipogenic differentiation	243
6.5.2 Osteogenic differentiation	246
6.5.3 Chondrogenic differentiation	248
6.6 Construction of hCCR2B-IRES-ZsGreen1 lentivirus vector.....	251
6.7 CCR2 overexpression in hADSCs	256
6.7.1 Lentivirus transduction optimization	256
6.7.2 Quantification of CCR2 overexpression in hADSC by Western blotting	261
6.7.3 CCR2 overexpression in hADSCs: imunocytochemistry.....	262
6.7.4 Phenotypic and functional characterization of CCR2-hADSCs.....	263
6.8 Discussion	265
6.8.1 Isolation, expansion and characterisation of human ADSCs	265
6.8.2 Rationale behind CCR2B overexpression on hADSCs.....	266
6.8.3 CCR2B overexpression on hADSCs by lentivirus gene delivery	266
6.8.4 Lentivirus transduction optimization	267
6.8.5 CCR2B overexpression in hADSCs in feasible and does not alter the MSC characteristics	268
6.9 Conclusions	269
7 Discussion.....	270
7.1 ADSCs for cell therapy of amyotrophic lateral sclerosis	270
7.2 Choosing mouse derived ADSCs for in vivo therapeutic investigation	271
7.3 Intrathecal injection of ADSCs into SOD1 ^{G93A} ALS mice	272
7.4 Triple separated co-culture: a method to screen for ADSC therapeutic potential and to investigate the molecular mechanisms of protection	277
7.5 From the bench to the clinic: trial design for cell therapy in ALS	278
7.6 Concluding remarks and future directions	280
8 References.....	284
Appendices.....	320
Project Outputs and Achievements	322

List of Figures

Figure 1.1.	Molecular mechanisms in the pathophysiology of ALS.....	8
Figure 1.2.	Potential mechanisms of mesenchymal stem cell efficacy in neurodegeneration.	47
Figure 2.1	Isolation process to obtain ADSCs from C57BL/6 adult mice.....	52
Figure 2.2.	pLV-SIN-eGFP lentivirus vector map.....	61
Figure 2.3.	eGFP-expressing lentivirus titration.....	63
Figure 2.4	Disease course in C57BL/6J-Tg (SOD1 ^{G93A})1Gur/J mice.....	66
Figure 2.5.	<i>In vivo</i> study design.....	68
Figure 2.6.	Exposure of the atlanto-occipital membrane for cell transplantation.....	69
Figure 2.7.	Mouse head position during cisterna magna injection.....	70
Figure 2.8.	Representative image of the catwalk analysis software 7.1 dashboard.....	73
Figure 2.9.	Triple Separated co-culture system.....	84
Figure 2.10.	Multiplexed Bead-Based Immunoassay.....	87
Figure 2.11.	ELISA principle.....	88
Figure 2.12.	Isolation process to obtain ADSCs from human lipoaspirate.....	90
Figure 2.13.	hCCR2B cDNA shuttle vector map.....	95
Figure 2.14.	pLVX-IRESZsGreen1 lentivirus vector.....	96
Figure 3.1.	Appearance of p0 mADSCs.....	111
Figure 3.2.	Appearance of early passages mADSCs.	112
Figure 3.3.	Growth kinetics of mADSCs.....	113
Figure 3.4.	Morphology of mADSCs at early and late passages.....	115
Figure 3.5.	Surface marker expression of mADSCs.....	117
Figure 3.6.	Adipogenic induction of p3 mADSCs.....	119
Figure 3.7.	Adipogenic differentiation of p3 mADSCs: Oil Red O staining 1.....	120
Figure 3.8.	Adipogenic differentiation of p3 mADSCs: Oil Red O staining 2.....	121
Figure 3.9.	Adipogenic differentiation of p14 mADSCs: Oil Red O staining.....	122
Figure 3.10.	Osteogenic induction of p3 mADSCs.....	123
Figure 3.11.	Osteogenic differentiation of p3 mADSCs: Alizarin Red S staining.....	124
Figure 3.12.	Osteogenic differentiation of p12 mADSCs: Alizarin Red S staining.....	125

Figure 3.13.	Chondrogenic differentiation of p3 mADSCs in 3D pellet cultures.....	126
Figure 3.14.	Chondrogenic differentiation in 3D pellets cultures: Alcian Blue staining.....	127
Figure 3.15.	EGFP-lentivirus titration by flow cytometry.....	129
Figure 3.16.	Optimization of EGFP-lentivirus transduction of mADSCs.....	131
Figure 3.17.	Lentivirus transduction of passage 1 mADSCs.....	133
Figure 3.18.	Immunophenotype of GFP-mADSCs.....	135
Figure 3.19.	Adipogenesis of GFP-mADSCs.....	136
Figure 3.20.	Osteogenesis of GFP-mADSCs.....	137
Figure 3.21.	Chondrogenesis of GFP-mADSCs.....	138
Figure 4.1.	GFP-ADSCs engraftment in SOD1 ^{G93A} mice 48 hours after intrathecal injection of 1x10 ⁶ cells.....	150
Figure 4.2.	Optimization of cell dose for transplantation in SOD1 ^{G93A} mice.....	151
Figure 4.3.	Distribution of GFP-mADSCs 1 week post-injection 1.....	153
Figure 4.4.	Distribution of GFP-mADSCs 1 week post-injection 2.....	154
Figure 4.5.	Distribution of GFP-mADSCs 2 weeks post-injection.....	155
Figure 4.6.	Distribution of GFP-mADSCs 3 weeks post-injection.....	156
Figure 4.7.	Distribution of GFP-mADSCs 4 weeks post-injection.....	157
Figure 4.8.	Histology on control PBS-Injected mice.....	158
Figure 4.9.	Effect of ADSC-transplantation on body weight.....	159
Figure 4.10.	Effect of ADSC-transplantation on Rotarod performance.....	161
Figure 4.11.	Effect of ADSC-transplantation on onset of motor function decline.....	162
Figure 4.12.	Effect of ADSC-transplantation on gait parameters: stride length, stand time and duty cycle.....	164
Figure 4.13.	Effect of ADSC-transplantation on gait parameters: walking duration, percent of time spent on diagonal paws and percentage of time spent on three paws.....	165
Figure 4.14.	Effect of ADSC-transplantation on disease onset.....	166
Figure 4.15.	Effect of ADSC-transplantation on MN survival in SOD1 ^{G93A} mice.....	168
Figure 4.16.	Effect of ADSC-transplantation on astrocyte activation in SOD1 ^{G93A} mice.....	170

Figure 4.17.	Effect of ADSC-transplantation on microgliosis in SOD1 ^{G93A} mice..	172
Figure 4.18.	Effect of ADSC-transplantation on microglial morphology in SOD1 ^{G93A} mice.....	173
Figure 4.19.	Gene expression of inflammatory cytokines/chemokines in spinal cord of SOD1 ^{G93A} mice.....	175
Figure 4.20.	Gene expression of growth factors in spinal cord of SOD1 ^{G93A} mice.....	176
Figure 5.1.	Characteristics of mouse astrocytes.....	192
Figure 5.2.	Validation of the separated co-culture method.....	193
Figure 5.3.	Effect of ADSC exposure on MN survival after co-culture with NTg and SOD1 ^{G93A} astrocyte.....	195
Figure 5.4.	Growth factor gene expression in ADSCs.....	197
Figure 5.5.	Secretion levels of VEGF and IGF-1 in ADSCs.....	200
Figure 5.6.	Growth factor expression in SOD1 ^{G93A} and NTg astrocytes.....	202
Figure 5.7.	Growth factor secretion from SOD1 ^{G93A} and NTg astrocytes.....	204
Figure 5.8.	Cytokine/chemokine expression in SOD1 ^{G93A} and NTg astrocytes.....	206
Figure 5.9.	Cytokine/chemokine secretion from SOD1 ^{G93A} and NTg astrocytes.....	208
Figure 5.10.	iAstrocyte characterization by ICC.....	209
Figure 5.11.	Effect of ADSCs on MN survival after co-culture with control or ALS derived human iAstrocytes.....	211
Figure 5.12.	Effect of ADSCs on MN mono-cultures.....	212
Figure 5.13.	Effect on MN survival of SOD1 ^{G93A} iAstrocytes exposed and then withdrawn from ADSCs.....	214
Figure 5.14.	Gene expression of pro-inflammatory cytokines in iAstrocytes at basal levels.....	216
Figure 5.15.	Gene expression of pro-inflammatory cytokines in iAstrocytes after co-culture with ADSCs.....	217
Figure 5.16.	Gene expression of growth factors in iAstrocytes at basal levels....	219
Figure 5.17.	Gene expression of growth factors in iAstrocyte after co-culture with ADSCs.....	220
Figure 6.1.	Morphology of cultured hADSCs.....	240
Figure 6.2.	Immunophenotype of hADSCs.....	242

Figure 6.3.	Flow Cytometry multicolour analysis of hADSCs.....	243
Figure 6.4.	Adipogenesis of hADSCs: phase-contrast microscopic images.....	245
Figure 6.5.	Adipogenesis of hADSCs: Oil Red O staining.....	246
Figure 6.6.	Osteogenesis of hADSCs: phase-contrast microscopic images.....	247
Figure 6.7.	Osteogenesis of hADSCs: Alizarin Red O staining.....	249
Figure 6.8.	3-dimensional chondrogenesis of hADSCs: Alcian Blue staining...	249
Figure 6.9.	2-dimensional chondrogenesis of hADSC.....	250
Figure 6.10.	2-dimensional chondrogenesis of hADSC: Alcian Blue staining.....	251
Figure 6.11.	Enzymatic diagnostic digestion of hCCR2B shuttle vector clones...	252
Figure 6.12.	Gel electrophoresis of hCCR2B cDNA PCR amplification product..	253
Figure 6.13.	Enzymatic diagnostic digestion of pLVx-hCCR2B-IRES vector clones.....	255
Figure 6.14.	pLVx-hCCR2B-IRES vector sequencing.....	256
Figure 6.15.	hADSCs lentivirus transduction optimization: volume test.....	257
Figure 6.16.	hADSCs lentivirus transduction optimization: polybrene test.....	258
Figure 6.17.	Transduction of hADSCs with pLV-CCR2B 3 rd generation lentivirus.....	259
Figure 6.18.	Transduction of hADSCs with pLV-CCR2B 2 nd generation lentivirus.....	260
Figure 6.19.	Transduction of hADSCs with pLV-SCR 2 nd generation lentivirus...	261
Figure 6.20.	CCR2 overexpression in hADSCs: western blot analysis.....	262
Figure 6.21.	CCR2 overexpression in hADSCs: immunocytochemistry.....	263
Figure 6.22.	Immunophenotype of CCR2-hADSCs.....	264
Figure 6.23.	Tri-lineage differentiation of CCR2-hADSCs.....	265
Figure 7.1.	Delivery strategies for the transplantation of MSCs in ALS0.....	276

List of Tables

Table 1.1.	Summary of MSC transplantation studies in ALS rodent models.....	30
Table 2.1.	Foetal Bovine Sera tested to support the growth of mADSCs.....	53
Table 2.2.	Fluorescent-conjugated antibodies used for Flow Cytometry.....	55
Table 2.3.	List of antibodies used in IHC.....	74
Table 2.4.	List of optimized mouse specific primers for qPCR.....	78
Table 2.5.	Skin Fibroblast donor's information.....	81
Table 2.6.	List of human primers optimized for qPCR.....	88
Table 2.7.	Fluorescent-conjugated human antibodies used in flow cytometry.....	91
Table 2.8.	hCCR2B cloning primers detail.....	98
Table 2.9.	hADSCs transduction optimization.....	102

Abbreviation

ADM	Adipogenic differentiation medium
ADSCs	Adipose derived stem cells
AIM	Adipogenic induction medium
ALS	Amyotrophic lateral sclerosis
ANG	Angiotensin
APC	Allophycyanin
BAC	Bacterial artificial chromosome
BBB	Blood-brain-barrier
BDNF	Brain derived neurotrophic factor
bFGF	Basic fibroblast growth factor
BM-MSCs	Bone marrow-derived MSCs
BrdU	Bromodeoxyuridine
BSA	Bovine serum albumin
C1 _q	Complement component 1q subcomponent
C9ORF72	Chromosome 9 open reading frame 72
CCR2	C-C chemokine receptor type 2
CD	Cluster of differentiation
Chat	Choline acetyltransferase
CMV	Cytomegalovirus
CNS	Central nervous system
CSF	Cerebrospinal fluid
CTNF	Cliliary neurotrophic factor
CXCR4	C-X-C chemokine receptor type 4
DAPI	4'6-diamino-2-phenylindole
DMEM	Dulbecco's modified eagle medium
DMSO	Dimetyl sulfoxide
DNA	Deoxyribonucleic acid
EEAT2	Excitatory amino acid transporter 2
EBs	Embryoid bodies

EBSS	Earle's balanced salt solution
EDTA	Ethylenediaminetetraacetic acid
EGF	Epidermal growth factor
EGFP	Enhanced green fluorescent protein
ELISA	Enzyme-linked immunosorbent assay
FACS	Fluorescent-activated cell sorting
fALS	Familial ALS
FBS	Foetal bovine serum
FC	Flow cytometry
FDA	U.S Food and Drug Administration
FITC	Fluorescein isothiocyanate
FTD	Fronto-temporal dementia
FTLD	Frontotemporal lobar degeneration
FUS	Fused in sarcoma protein
GABA	Gamma-aminobutyric acid
GAPDH	Glyceraldehyde 3-phosphate dehydrogenase
GDNF	Glial-derived neurotrophic factor
GFAP	Glial fibrillary acid protein
GLT-1	Glutamate reuptake transporter
GMP	Good manufacturing practice
HBSS	Hank's Balanced Salt Solution
hESCs	Human embryonic stem cells
HGF	Hepatocyte growth factor
hNSCs	Human neural stem cells
Iba1	Ionized calcium binding adaptor molecule 1
IBMX	3-Isobutyl-1-methylxanthine
ICC	Immunocytochemistry
ICV	Intracerebroventricular
IFATS	International Federation for Adipose Therapeutics and Science
IFN- γ	Interferon gamma
IGF-1	insulin-like growth factor 1

IHC	Immunohistochemistry
IL-1 β	Interleukin 1 beta
IL-4	Interleukin 4
IL-6	Interleukin 6
IM	Intramuscular
iNPCs	Induced neural progenitor cells
iPSCs	Induced pluripotent stem cell
IRES	Internal ribosome entry site
ISCT	International Society for Cellular Therapy
ISL-1	Insulin gene enhancer protein
ITS	Insulin-transferrin-selenium
IV	Intravenous
KLF4	Kruppel-like factor 4
LB	Luria-Bertani broth
LPS	Lipopolysaccharide
M1	Classically activated microglia
M2	Alternatively activated microglia
MAO-B	Monoamine oxidase B
MAP2	Microtubule-associated protein 2
MCP-1	Monocyte chemoattractant protein 1
MCS	Multiple cloning site
MHCI	Major histocompatibility complex class I
MHCII	Major histocompatibility complex class II
MND	Motor neuron disease
MNLCs	Motor neuron-like cells
MNPs	Motor neuron progenitors
MNs	Motor neurons
MOI	Multiplicity of infection
mPGK	Mouse phosphoglycerate kinase
MRI	Magnetic resonance imaging
mRNA	messenger RNA

MS	Multiple sclerosis
MSCs	Mesenchymal stem cells
MTC1	Lactate transporter
NF-kB	nuclear factor kappa-light-chain-enhancer of activated B
NGF	Nerve growth factor
Ngn1	Neurogenin1
NMJ	Neuromuscular junction
NPs	Nanoparticles
NRF2	Nuclear factor erythroid 2-related factor 2
NSE	Neuron-specific enolase
NT-3	Neurotrophin-3
NTg	Non transgenic
O/N	Overnight
OCT	Optimal cutting temperature compound
OCT4	Octamer-binding transcription factor 4
ORF	Open Reading Frame
PBMCs	Peripheral blood mononuclear cells
PBS	Phosphate-buffered saline
PCR	Polymerase chain reaction
PD	Parkinson's disease
PDL	Population doubling level
PDR	Population doubling rate
PE	Phycoerythrin
PE-Cy7	Phycoerythrin-cyanine7
PET	Positron emission tomography
PFA	Paraformaldehyde
PLS	Primary lateral sclerosis
PMA	Progressive muscle atrophy
PNN	Perineural net
RA	Retinoic acid
RBC	Red blood cell

RNA	Ribonucleic acid
ROS	Superoxide reactive oxygen species
RT	Room temperature
sALS	Sporadic ALS
SC	Spinal cord
SCI	Spinal cord injury
SD	Standard deviation
SDS	Sodium dodecyl sulphate
Shh	Sonic hedgehog factor
SOD1	Superoxide dismutase 1
Sox2	Sex determining region Y-box 2
SPF	Specified pathogen free
SVF	Stromal vascular fraction
TAE	Tris-acetate-EDTA
TARDBP	TAR DNA-binding protein 43
Tg	Transgenic
TGF- β	Transforming growth factor beta
TNF- α	Tumor necrosis factor alpha
Trk-A	Tropomyosin receptor kinase A
TUNEL	Terminal deoxynucleotidyl transferase dUTP nick end labeling
VEGF	Vascular endothelial growth factor
VLA4	Integrin very late antigen 4
WAT	White adipose tissue
WB	Western blot
WT	Wild type

1 Introduction

1.1 Amyotrophic Lateral Sclerosis

Amyotrophic Lateral Sclerosis (ALS), also known as Lou Gehrig's disease, is a rapidly progressive neurodegenerative condition characterized by selective degeneration of both upper motor neurons (MNs) in the motor cortex, and lower motor neurons in brainstem and ventral horn of the spinal cord (Walling, 1999). ALS is the most common form (97%) of motor neuron disease (MND). The other forms of MND are progressive bulbar palsy (PBP), progressive muscular atrophy (PMA) and primary lateral sclerosis (PLS) (Walling, 1999).

1.2 Diagnosis, clinical features and prognosis of ALS

The estimated ALS incidence across the world is 2/100,000 with a prevalence of up to 7.4/100000 (Andersen and Al-Chalabi, 2011). The disease typically manifests during the fifth-sixth decade of life leading to progressive muscle atrophy, weakness and paralysis. Usually, patients die within 2 to 5 years after diagnosis due to respiratory failure (Andersen and Al-Chalabi, 2011). About two-third of patients present with limb onset disease characterized by spasticity and weakness in one particular upper or lower limb that will later appear in the contralateral limb. In about 30% of patients the disease manifests with bulbar onset characterized by dysarthria and/or dysphagia symptoms, while the remaining 5% of patients present with respiratory difficulties (Hardiman et al., 2017a). Frontotemporal lobar degeneration (FTLD) is present in almost 15% of ALS patients, and likewise, a proportion of FTLD cases show motor neuron impairment (Robberecht and Philips, 2013). These genetic and pathological overlaps showed a strong association between ALS and frontotemporal dementia, however, the molecular basis for this association has not yet been elucidated (Robberecht and Philips, 2013).

Because of the lack of specific biomarkers, the diagnosis of ALS is based on the El-Escorial criteria which require in depth clinical investigation in order to exclude the presence of other diseases with similar symptoms and the evidence for disease progression (Turner et al., 2013). A definitive ALS diagnosis takes on average 12 months from the time the patient start feeling the first symptoms (Mitchell et al., 2010). The revised ALS functional rating scale (ALSFRS-R) is currently used to evaluate disease progression, and together with survival, represents the typical measure for clinical trial endpoint (Cedarbaum et al., 1999, Rutkove, 2015). There is urgent need for the identification of a definitive biological marker which would not only speed up

the diagnostic process, but more importantly provide a tool to monitor disease progression and evaluate the effect of therapeutic products in clinical trials (Verber et al., 2019).

1.3 Aetiology and pathology of ALS

ALS is mainly sporadic in origin (sALS) but a family history of the disorder can be found in ~10% of cases (Hardiman et al., 2017b). Hereditary forms of the disease are considered as familial (fALS), predominantly autosomal dominant transmitted and rarely X-linked or recessive (Andersen and Al-Chalabi, 2011).

More than 20 mutated genes have been found to cause fALS so far including SOD1 (Rosen et al., 1993), TARDBP (Kabashi et al., 2008, Rutherford et al., 2008), FUS (Kwiatkowski et al., 2009, Vance et al., 2009), OPTN (Maruyama et al., 2010), VCP (Johnson et al., 2010, Shaw, 2010), UBQLN2 (Deng et al., 2011), C9orf72 (Renton et al., 2011, DeJesus-Hernandez et al., 2011), TBK1 (Cirulli et al., 2015, Freischmidt et al., 2015) and very recently GLT8D1 (Cooper-Knock et al., 2019). sALS and fALS are clinically indistinguishable, and since mutations in fALS genes are also present in some sporadic or isolated cases of ALS, the disease can be interpreted as complex and multi-factorial (Poppe et al., 2014). Nevertheless, clinical variability such as rate of progression, onset type (limb or bulbar) and survival within patients and even relatives who carry the same gene mutation highlight the importance of external factors which may play a role in the susceptibility, age of onset and rate of progression of the disease (Poppe et al., 2014).

Given the complexity and high degree of heterogeneity of ALS, the precise mechanisms behind disease onset, development and progression are incompletely understood. However, the discovery of causative inherited genes and de novo gene mutations, together with the generation of in vitro and animal models, has uncovered important pathophysiological mechanisms. In the next sections, the most relevant causative genes will be described in detail.

1.3.1 SOD1

Superoxide dismutase 1 (SOD1) was the first gene in which mutations have been identified in fALS patients (Rosen et al., 1993), and over 180 SOD1 pathogenic mutations have been associated with ALS so far, accounting for 20% of fALS cases and for 2-7% of sporadic ALS (Abel et al., 2012). SOD1 is a ubiquitously expressed enzyme involved in the detoxification of superoxide reactive oxygen species (ROS) (Carri et al., 2015). Given the importance of SOD1 as a ROS scavenger and the

evidence of increased oxidative stress in ALS pathology, a loss of enzyme activity may play a role in the disease (Barber and Shaw, 2010). However, even though the precise mechanism is still uncertain, the generation of several SOD1-mutated ALS models certainly demonstrated a SOD1 toxic gain-of-function in ALS aetiology and pathology (Cleveland et al., 1996). In addition, mutations that preserve the dismutase activity of the enzyme still cause motor neuron degeneration (Borchelt et al., 1994), and overexpression of wild type SOD1 worsened disease progression in mutant transgenic ALS mice (Jaarsma et al., 2008). The use of SOD1 mutants and the generation of transgenic animal models expressing different SOD1 mutations, revealed important cellular mechanisms by which alterations of this gene might cause motor neuron death (Gurney et al., 1994). At the present, most of the proposed pathological mechanisms involved in SOD1 mutations rely upon its capacity to misfold and escape from the cell's protein degradation system. In fact the misfolded protein forms aggregates which in turn may affect several physiologic cellular functions including: 1) Perturbation of the proteasome and autophagy systems (Kitamura et al., 2014); 2) Activation of the ER-stress response leading to secondary microglial activation (Saxena et al., 2009); 3) Mitochondrial impairment (Shi et al., 2010); 4) Axonal transport dysfunction (Zhang et al., 1997) and astrocyte activation (Yamanaka and Komine, 2018). Interference by oligomeric complexes and/or protein aggregates to cellular protein homeostasis mechanisms is considered a hallmark in ALS and in other neurodegenerative diseases. Other evidence in support of imbalance in proteostasis as a pathogenic mechanism for ALS comes from the detection of mutations in genes encoding for components of the proteasome machinery (Deng et al., 2011, Maruyama et al., 2010, Johnson et al., 2010, Shaw, 2010). However, the specific molecular mechanisms of the process and whether impairment of proteostasis may be an initiating event in ALS or a consequence is not completely understood and needs further investigation (Paez-Colasante et al., 2015). In addition, a pathogenic role for wild-type SOD1 in non SOD1-ALS has been proposed. For example, reducing the levels of wild-type SOD1 in astrocytes derived from patients with sporadic disease, improved MN survival in co-culture experiments (Haidet-Phillips et al., 2011). Moreover, misfolded SOD1^{WT} intracytoplasmic inclusions have been detected in MNs and glial cells of patients with sporadic or familial disease lacking SOD1 mutations (e.g. in the presence of C9orf72, TDP-43, FUS and VAPB mutations) (Forsberg et al., 2019, Forsberg et al., 2010, Pokrishevsky et al., 2012).

1.3.1.1 The SOD1^{G93A} mouse model of ALS

Although the specific molecular mechanisms behind ALS onset, development and progression are not fully understood, the generation of the SOD1^{G93A} transgenic mouse model uncovered important pathological mechanisms in ALS (Gurney et al., 1994, Cleveland et al., 1996). The most commonly used SOD1 transgenic mice express a large amount of a human mutant form of SOD1, characterized by a pathogenic substitution of glycine with alanine at amino acid position 93. The SOD1^{G93A} mice demonstrate many of the features seen in the human ALS pathology and represent the most widely used and best characterised *in vivo* model for the study of ALS. Indeed, axon retraction, selective spinal motor neuron death, loss of innervation of motor end-plates, muscular atrophy and progressive motor deficit with terminal paralysis of hind limbs are observed in this murine model (Gurney et al., 1994, Cleveland et al., 1996). Several therapeutic interventions that showed positive effects in SOD1^{G93A} mice have failed to translate into the clinic, and therefore the use of this model for therapy development has been questioned (Scott et al., 2008). However, computer modelling and statistical analysis of data collected from more than 5,000 SOD1^{G93A} mice, coupled with re-testing of several drugs, revealed that one key reason for poor translation into humans of therapies that demonstrated efficacy in this model was due to inadequately designed pre-clinical methods (Scott et al., 2008). To overcome this issue, guidelines for experimental design, power analysis methods and standardised procedures for pre-clinical animal research in ALS have been released (Ludolph et al., 2010).

Other murine models expressing different human SOD1 mutations (G37R, G85R, A4V and D90A) have also been generated (Wong et al., 1995, Bruijn et al., 1997, Deng et al., 2006, Jonsson et al., 2006). Although these models recapitulate some of the features seen in human disease, their use has been limited due to later onset of disease (7 to 12 months) and different rate of disease progression (rapidly progressive or slowly progressive) compared to the SOD1^{G93A} model.

1.3.2 TARDBP and FUS

After fifteen years from the identification of SOD1 mutations, linkage analysis studies enabled the discovery of another two fALS related genes: TARDBP (Sreedharan et al., 2018) and FUS (Vance et al., 2009). TARDBP (TDP-43) is a DNA- RNA-binding protein which functions in the nucleus by regulating transcription and splicing processes (Scotter et al., 2015). About 4% of fALS and 1% of sALS are linked to mutations in TDP-43. Pathological TDP-43 ubiquitinated inclusions in the cytoplasm

of neurons are detected in almost 97% of ALS cases and in most of FTLD post-mortem tissues, but not in the ALS patients with SOD1 and FUS mutations (Scotter et al., 2015).

The mechanisms by which mutated TDP-43 exerts its pathological effects may comprise both loss- and gain-of-function and its amount within the cell seems to require tight regulation. Indeed, while on the one hand the protein mislocalization in the cytoplasm and subsequent irreversible accumulation in stress granules may explain its toxic effect by establishing a pro-aggregation environment (Johnson et al., 2009), on the other hand, the TDP-43 reduction within the nucleus may adversely affect the RNA processing apparatus (Polymenidou et al., 2011, Arnold et al., 2013). As a result, erroneously controlled RNA degradation, production of aberrant proteins, and altered gene expression occur, so disturbing the physiology of motor neurons (Highley et al., 2014, Arnold et al., 2013, Lagier-Tourenne et al., 2012).

The subsequent finding of FUS mutations in fALS and sALS patients highlighted once again the importance of anomalous RNA processing in the pathogenesis of ALS (Vance et al., 2009). Like TDP-43, the fused in sarcoma protein (FUS) is a ribonucleoprotein designed to shuttle in and out of the nucleus to accomplish its role in mRNA biogenesis and regulation (Schwartz et al., 2015). Basophilic FUS-positive cytoplasmic inclusions are present in fALS patients with FUS-linked mutations, sALS patients without SOD1 or TDP-43 inclusions and in 10% of TDP-43-negative FTLD cases (Kobayashi et al., 2013). Both TDP-43 and FUS regulate and target more than 10,000 genes and more than 2,000 different RNAs including pre-mRNAs, mRNAs and micro-RNAs (Lagier-Tourenne et al., 2012). Therefore, it is not surprising that defects in these proteins may have a massive impact on dysregulation of gene expression, especially in neurons where metabolism is extremely active. Moreover, given their prion-like properties, Fus and TDP-43 are predisposed to aggregate and form stress granules, sequestering other proteins and RNAs which in turn may have toxic effects in the cell (Pradat et al., 2015). Their prion-like characteristics may also suggest a radial propagation of the aggregates to contiguous cells, which may be consistent with the observed anatomical spread of ALS (Pradat et al., 2015).

The molecular pathology of TDP-43 and FUS in ALS is still under investigation, and despite significant similarities in structure and function, they may contribute to the disease through separate mechanisms (Lagier-Tourenne et al., 2012). Several approaches have been tested in order to generate a TDP-43 ALS-like rodent model but apart from elucidating important roles of TDP-43 in neural development and

embryogenesis, degeneration of motor neural circuits with consistent upper and lower motor neuron death has not been achieved yet (Scotter et al., 2015). Of interest, a study conducted in transgenic mice carrying two different human TDP-43 mutations with expression levels analogous to endogenous wild-type TDP, showed an ALS motor phenotype, but without cytoplasmic TDP-43 inclusions or depletion of nuclear TDP-43 (Arnold et al., 2013). After ten months of age the neurodegeneration processes in these mice appear to slow down and stabilize without additional disease progression (Arnold et al., 2013). This may limit the use of this model for the study of early pathological mechanisms or therapeutic intervention during the early stage of ALS.

1.3.3 C9orf72

The discovery of mutations in chromosome 9 open reading frame 72 (C9orf72) in fALS, sALS and FTLD provided firm evidence of the strong relationship between ALS and fronto-temporal dementia (DeJesus-Hernandez et al., 2011, Renton et al., 2011). In particular, mutations in C9orf72 account for about 40% of fALS, 25% of FTLD and are identified in almost 7% of sporadic ALS, making C9orf72 the most common mutated gene in ALS (Majounie et al., 2012). Therefore, discovering the role of C9orf72 mutations in ALS may be fundamental in order to uncover pathological mechanisms in ALS. Although the physiological role of C9orf72 is not fully understood, recent evidence suggests its involvement in the regulation of endosomal trafficking and initiation of autophagy in neuronal cells (Farg et al., 2014, Aoki et al., 2017, Webster et al., 2018).

Patients with C9orf72 mutations incorporate an anomalous expansion of the GGGGCC repeat (G4C2) situated in a noncoding region of the gene (intron 1), and albeit still incomplete, various hypothesis have been formulated to explain its role in ALS pathology (Cooper-Knock et al., 2015). The presence of intranuclear RNA foci containing RNA-binding protein in C9orf72-ALS post-mortem tissue suggests a gain-of-function RNA toxicity pathology (DeJesus-Hernandez et al., 2011). Moreover, it has been demonstrated that the toxicity of the G4C2 repeats is strongly correlated with the length of the repeat in C9orf72 mutant cell lines (Lee et al., 2013). Specifically, the higher the number of repeats the higher the toxicity measured by the viability of a neural cell line (Lee et al., 2013). However, loss of function is not to be excluded as ALS patients showed reduced C9orf72 mRNA levels and the exact physiological role of the protein within the cell still remains to be elucidated (DeJesus-Hernandez et al., 2011, Renton et al., 2011).

Another proposed mechanism of neuronal toxicity in the C9orf72 spectrum comes from the detection of dipeptide repeat (DPR) inclusions generated by repeated-associated non-ATG (RAN) protein translation (Mori et al., 2013). As in the majority of ALS cases, in C9orf72-related ALS TDP-43 proteinopathy is present (Cooper-Knock et al., 2015). The specific mechanisms by which C9orf72 mutations give rise to ALS is still unexplained, but given that mutations in this gene contribute to a high percentage of ALS cases, analysis of C9orf72-ALS pathological mechanisms gained considerable interest among researchers since its discovery and mouse models have been generated (Liu et al., 2016, Peters et al., 2015, O'Rourke et al., 2015, Jiang et al., 2016). The C9orf72 BAC transgenic mouse model generated by Liu et al. displays pathological and clinical features similar to human disease. However, the model is characterised by incomplete penetrance, sex-dependent effects and high phenotypic variability in between animals (Liu et al., 2016).

1.4 ALS is non-cell autonomous disease

Several pathological mechanisms selectively affecting the MN population have been proposed including cytoplasmic protein mis-localisation and aggregation (Lagier-Tourenne et al., 2012), aberrant protein homeostasis (Kitamura et al., 2014), RNA toxicity (DeJesus-Hernandez et al., 2011), dysregulation of RNA processing (Highley et al., 2014), excitotoxicity mediated by excessive glutamate receptor activation (Alexander et al., 2000), mitochondrial dysfunction (Shi et al., 2010), endoplasmic reticulum stress response (Saxena et al., 2009), abnormal rearrangement of the cytoskeleton, impaired axonal transport (Zhang et al., 1997) and oxidative stress (Barber and Shaw, 2010).

In addition to the above-mentioned pathological mechanisms, the contribution of microglial cells, oligodendrocytes and astrocytes seems to be critical in ALS, influencing significantly the speed of disease progression after onset (Robberecht and Philips, 2013). The first evidence indicating the involvement of neighbouring non-neuronal cells in ALS came from studies demonstrating that restricted expression of human SOD1 mutations in neurons was not able to reproduce a motor neuron degeneration phenotype in mice (Pramatarova et al., 2001, Lino et al., 2002). Subsequent studies using allografted chimeric mutant SOD1 mice or conditional expression of wild-type SOD1 in specific non-neuronal sub-populations in SOD1^{G93A} mice, provided strong evidence of a central role in disease progression for glial cells (Clement et al., 2003, Papadeas et al., 2011, Yamanaka et al., 2008a). It is now widely accepted that ALS is a non-cell autonomous disease, where the motor neuron

degeneration processes seem to be strongly associated with and modulated by complex interaction among different cell types, together with the development of a sustained inflammatory milieu (Ferraiuolo, 2014). The major pathological mechanisms contributing to motor neuron injury in ALS are summarized in figure 1.1.

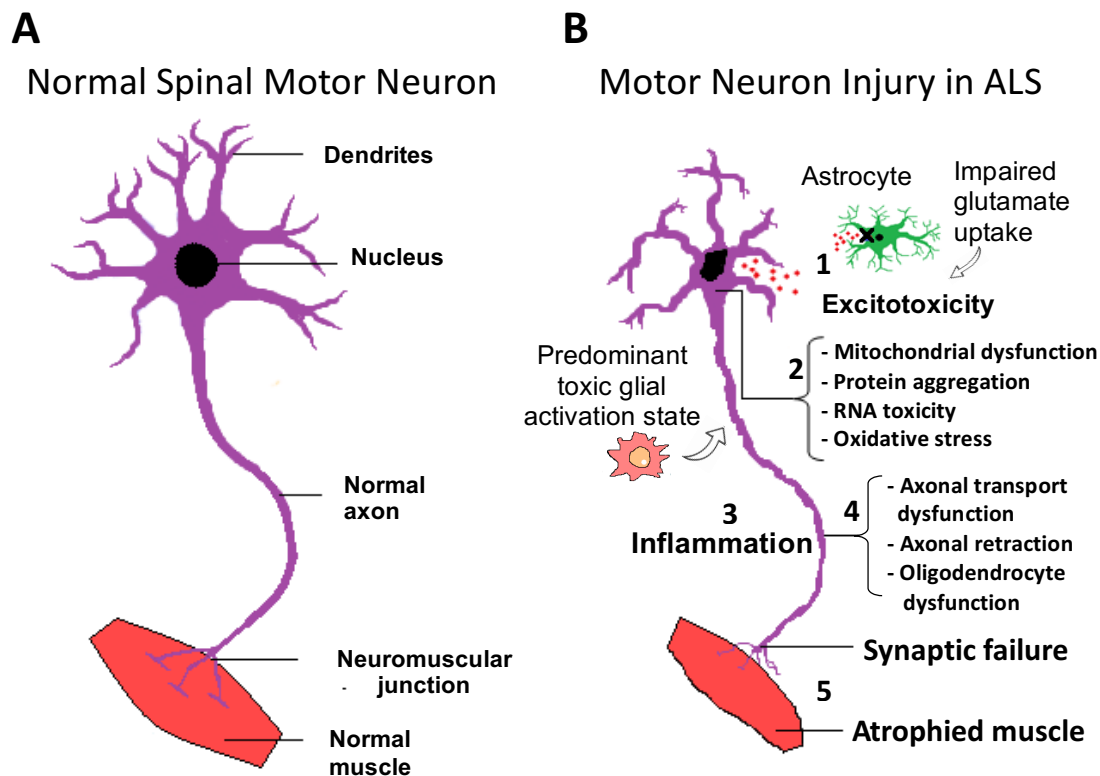


Figure 1.1. Molecular mechanisms in the pathophysiology of amyotrophic lateral sclerosis. A) Schematic representation of healthy spinal cord motor neuron. B) Schematic representation of ALS affected spinal cord motor neuron: 1) Astrocytes are not able to support neuronal functions and impaired glutamate clearance leads to neuronal excitotoxicity; 2) Defects in protein degradation pathways and disturbances in RNA processing result in protein aggregate formation, RNA toxicity and mitochondrial dysfunction; 3) The secretion of pro-inflammatory cytokines by activated microglia contributes to the development of an inflammatory milieu; 4) Failure of axonal architecture and transport functions, together with the alteration of the physiological role of oligodendrocytes results in 5) synaptic failure, denervation and finally, muscle atrophy. Adapted with permission from “Advances, challenges and future directions for stem cell therapy in amyotrophic lateral sclerosis”, *Molecular Neurodegeneration*, 2017 (Ciervo et al., 2017).

1.4.1 Astrocytes

Astrocytes represent the most abundant cell type in the central nervous system (CNS) and are important in neurodevelopment, neurophysiology and injury. Astrocytes constitute a complex and heterogeneous population of cells that differ depending on their anatomical location and functions. Some of their fundamental physiological activities consist in providing structural, metabolic and trophic support to neurons, regulation of ion homeostasis and synaptic activity, neurotransmitter buffering and maintenance of the blood-brain barrier (BBB). In addition, astrocytes are important during CNS injury and disease by actively participating in tissue repair processes and mediating neuroinflammation. Indeed, following injury astrocytes “activate” undergoing proliferation, and morphological and phenotypic changes, which could be protective or detrimental depending on the surrounding microenvironment and the duration and amplitude of the inflammatory response (Liddel and Barres, 2017).

1.4.2 Role of astrocytes in ALS

Astrogliosis, characterized by the up-regulation of the glial fibrillary acid protein (GFAP), enhanced expression of inflammatory markers and down-regulation of metabolic genes is observed both in humans and in transgenic murine models of ALS (Pehar et al., 2017). The generation of chimeric mice and application of Cre-loxP systems in mutant SOD1 rodent models shed some light on the role of astrocytes in ALS progression (Clement et al., 2003, Yamanaka et al., 2008a). Although astrocyte-specific expression of human mutant SOD1 did not lead to motor neuron degeneration in mice (Gong et al., 2000), selective knock-out of mutant SOD1 in astrocytes of SOD1^{G93A} and SOD1^{G85R} transgenic mice slowed down disease progression and increased life span (Yamanaka et al., 2008b, Wang et al., 2011a). Moreover, focal intraspinal transplantation of SOD1^{G93A} rat glial-restricted progenitors induced MN death and caused motor dysfunction in WT rats (Papadeas et al., 2011). Conversely, transplantation of WT astrocyte precursors into the spinal cord of SOD1^{G93A} rats, reduced MN loss, delayed motor performance decline and extended disease duration compared to controls (Lepore et al., 2008). More recently, xenotransplantation of human derived glial precursor cells in rodent models provided further insight into the role of astrocytes in human ALS. Chen et al. convincingly demonstrated that glial precursor cells, generated from induced pluripotent stem cells (iPSCs) obtained from a human ALS patient with a familial SOD1 mutation, can engraft, differentiate into astrocytes and induce motor function deficits when transplanted into WT mice (Chen et al., 2015b). Similarly, transplantation of iPSC-

derived astrocyte precursors generated from ALS patients with sporadic disease into immunodeficient (SCID) mice, led to MN damage, pre-synaptic defects at neuromuscular junctions (NMJs) and motor behavioural changes (Qian et al., 2017). In contrast, transplantation of glial-rich neural progenitors derived from iPSCs generated from a human healthy donor into SOD1^{G93A} mice, improved motor function and extended survival (Kondo et al., 2014).

A central role for astrocytes in ALS pathology has also been extensively corroborated by using *in vitro* models. Similarly to what has been found *in vivo*, expression of mutant SOD1 in spinal MNs *in vitro* did not cause cell death *per se*, but only mild abnormalities such as diminished axonal projections and reduced cell body diameter (Nagai et al., 2007). On the contrary, murine or human astrocytes carrying SOD1 transgenes, were able to induce MN death *in vitro*. (Nagai et al., 2007, Di Giorgio et al., 2007, Marchetto et al., 2008). Moreover, there is strong evidence demonstrating that mutated SOD1 astrocytes trigger MN death by releasing soluble toxic factors. Indeed, conditioned media from SOD1^{G93A} astrocytes induced MN death both *in vitro* and *in vivo* (Nagai et al., 2007, Fritz et al., 2013, Rojas et al., 2014, Ramirez-Jarquin et al., 2017). In addition, astrocyte toxicity appears to be selective for MNs, since murine SOD1^{G93A} astrocytes did not affect the survival of either human embryonic stem cells (ESC)-derived inter-neurons (Di Giorgio et al., 2008), primary spinal GABAergic neurons or dorsal root ganglion (DRG) neurons (Nagai et al., 2007). Recently, down-regulation of major histocompatibility complex class I (MHC I) in MNs following co-culture with ALS astrocytes has been indicated as a possible explanation for the MN restricted toxicity (Song et al., 2016). ALS astrocytes were not able to reduce MHC I expression in GABA neurons. Moreover, restoring the levels of MHC I in MNs after exposure to ALS astrocytes, protected against toxicity (Song et al., 2016).

Similar to astrocytes derived from ALS rodents, astrocytes derived from ALS patients with sporadic or familial disease with mutations in SOD1, C9orf72 or FUS, triggered the selective death of either mouse or human MNs *in vitro* (Haidet-Phillips et al., 2011, Kia et al., 2018, Re et al., 2014, Meyer et al., 2014). These findings emphasize the pivotal role of astrocytes in mediating neurotoxicity not only in fALS, but also in sporadic ALS. It is worth mentioning that the role of astrocytes in the pathogenesis of fALS with mutations in the TDP-43 gene is not completely elucidated. For example, expression of mutant TDP-43 exclusively into MNs is sufficient to produce an ALS-like phenotype in rats (Huang et al., 2012), and transplantation of mutant TDP-43 glial restricted precursors into wild type rats did not lead to MN degeneration (Haidet-

Phillips et al., 2013). In addition, several authors reported that mutant TDP-43 astrocytes are not toxic to MN in co-culture (Haidet-Phillips et al., 2013, Serio et al., 2013). In contrast, other studies did demonstrate a role for astrocytes in TDP-43 ALS. Tong et al. showed that the selective expression of a mutant form of TDP-43 in astrocytes is enough to provoke an ALS-like phenotype in rats (Tong et al., 2013), and Rojas et al. showed that conditioned medium collected from primary astrocytes derived from a transgenic TDP-43 mouse model was actually toxic to MNs *in vitro* (Rojas et al., 2014). Thus, although the molecular mechanisms are still unclear, astrocyte dysfunction in TDP-34 linked ALS has been shown.

1.4.3 Pathological mechanisms of ALS astrocytes

Although how mutant astrocytes contribute to disease progression in ALS is still unclear, dysfunction in several molecular mechanisms has been unravelled. One of the first identified and most studied pathological mechanisms by which astrocytes contribute to MN degeneration is related to their reduced capacity for the re-uptake of glutamate from the synaptic cleft, which results in glutamate-mediated excitotoxicity. Indeed in both humans and rodent models of ALS, astrocytes display reduced expression and function of the glutamate transporter (EAAT2/GLT-1) resulting in extracellular glutamate excess and in turn MN toxicity due to excessive influx of calcium following overstimulation of post-synaptic glutamate receptors (Howland et al., 2002, Pardo et al., 2006, Rothstein et al., 1995, Rothstein et al., 1992). For instance, strategies to increase astrocyte glutamate transporter expression in ALS models, resulted in excitotoxicity modulation and neuroprotection (Guo et al., 2003, Rothstein et al., 2005, Benkler et al., 2016). Other examples of loss of homeostatic functions in ALS-linked astrocytes are represented by reduced supply to MNs of lactate, which serves as a source for energy production (Ferraiuolo et al., 2011, Madji Hounoum et al., 2017), and dysregulation in neurotrophic factor release such as for example glial-derived neurotrophic factor (GDNF) (Brambilla et al., 2016).

In addition to loss of support/functions, astrocytes are known to contribute to ALS through the release of toxic factors which selectively kill MNs. This is supported by several pieces of evidence showing MN death following exposure to conditioned medium collected from either murine or human ALS astrocytes. For example, although on the one hand reduced metabolic or growth factors support is involved in MN loss, on the other hand excessive production of pro-nerve growth factor (pro-NGF) from neonatal SOD1^{G93A} mouse astrocytes caused MN apoptosis *in vitro* (Ferraiuolo et al., 2011). Alteration in transforming growth factor beta 1 (TGFβ-1)

signalling has also been associated with SOD1-linked astrocyte toxicity both *in vivo* and *in vitro* (Phatnani et al., 2013). In particular, enhanced secretion of TGF β -1 from astrocytes obtained from adult SOD1^{G93A} mice, induced axonopathy, cytoplasmic protein inclusions and autophagy defects in cultured MNs, culminating in cell death (Tripathi et al., 2017). Interestingly, increased immunoreactivity for pSmad2/3 inclusion in spinal MNs of sporadic and familial (SOD1) ALS patients was reported (Nakamura et al., 2008). The phosphorylation of Smad2/3 is the first signalling event occurring after the binding of TGF β -1 with its receptor on the cell surface.

Another mechanism of toxicity is linked to mitochondrial dysfunction in ALS astrocytes. Mitochondrial dysfunction in mutated SOD1 astrocytes leads to increased production of ROS, which can contribute to motor neuron injury (Cassina et al., 2008, Marchetto et al., 2008). In support of this, transgenic SOD1^{G93A} mice overexpressing the nuclear factor erythroid 2-related factor 2 (NRF2) under the control of the GFAP promoter, displayed later onset and prolonged life span, likely due to enhanced secretion from NRF2-astrocytes of the antioxidant glutathione (Vargas et al., 2008).

Astrocytes can also be toxic to MNs via unconventional secretory pathways as for example via exosomes (Prada et al., 2018). Exosomes are membrane vesicles originating from the inner cell membrane containing proteins, mRNAs and microRNAs which are released into the extracellular space. The content of exosomes can be transferred between cells and this represents an important way of cell-to-cell communication and signal transduction with resulting modulation of cellular functions in both physiology and disease (They et al., 2002). Interestingly, it has been shown that even though SOD1^{G93A} mouse astrocytes are characterised by down-regulation of proteins involved in secretory pathways, their exosome release is enhanced compared to control astrocytes (Basso et al., 2013). Moreover, exosomes released by SOD1^{G93A} astrocytes induced selective MN death *in vitro* (Basso et al., 2013). Recently, Varcianna *et al.* demonstrated dysregulation of miRNA cargo in exosomes secreted by induced iAstrocytes derived from fALS patients with the C9orf72 expansion mutation through genetic reprogramming of skin fibroblasts (Varcianna et al., 2019). In particular, exosomes purified from C9orf72 iAstrocytes, but not from healthy control iAstrocytes, were able to affect neurite outgrowth and induce MN death *in vitro* (Varcianna et al., 2019).

1.4.4 Inflammation-mediated neurotoxicity of ALS astrocytes

Neuroinflammation is a common feature in neurodegenerative conditions and it is well documented in both sALS, fALS and transgenic animal models of ALS (McCombe and Henderson, 2011). Although the role of inflammation in ALS is not well established, astrocytes participate in neuroinflammation by acting in synergy with microglia and infiltrating T lymphocytes (Liu and Wang, 2017). Several pieces of *in vitro* evidence showed that spinal cord astrocytes derived from post-mortem tissue of ALS patients or activated astrocytes derived from murine ALS models produce pro-inflammatory cytokines and inflammatory mediators such as prostaglandins and NOX-2 that can directly affect MN survival (Haidet-Phillips et al., 2011, Hensley et al., 2006, Aebischer et al., 2010, Di Giorgio et al., 2008). For example, elevated secretion of IFN- γ from astrocytes carrying a mutated form of SOD1 caused MN death *in vitro* (Aebischer et al., 2010). Interferon gamma (IFN- γ) is a cytokine critical for the regulation of innate and adaptive immunity, and elevated levels of the cytokine were detected in the spinal cord of sALS and SOD1^{G93A} mice (Wang et al., 2011b). Similarly, mouse spinal cord astrocytes expressing the human R521G FUS mutation were able to secrete high levels of tumor necrosis factor alpha (TNF- α), which in turn mediated motor neuron toxicity *in vitro* (Kia et al., 2018). TNF- α is a potent pro-inflammatory cytokine and although its role in ALS disease progression is still controversial, there are several mechanisms by which TNF- α may be deleterious in ALS. For example, through its receptor TNFRF1, TNF- α can exacerbate excitotoxicity by inducing release of glutamate from microglia and inhibiting its clearance from astrocytes (Tortarolo et al., 2017). Moreover, through the activation of the nuclear factor kappa-light-chain-enhancer of activated B cells (NF- κ B) pathway TNF can stimulate microglia proliferation, leukocyte infiltration and promote muscle wasting (Ouali Alami et al., 2018). Interleukin 1 beta (IL-1 β) is another potent pleiotropic cytokine and elevated levels have been detected in cerebrospinal fluid (CSF) of ALS patients (van der Meer and Simon, 2010). Interestingly, damage of the BBB may contribute to motor neuron degeneration in ALS and IL-1 β secretion from activated astrocytes has been associated with BBB breakdown mediated by endothelin-1 and TNF- α (Didier et al., 2003, Winkler et al., 2014). Moreover, blockage of IL-1 β with anakinra slowed disease progression and extended survival in SOD1^{G93A} mice (Meissner et al., 2010).

Interestingly, exposure of rat healthy astrocytes to CSF from sALS patients induced significant up-regulation of interleukin 6 (IL-6), suggesting a role for the cytokine in promoting a vicious chronic inflammatory cycle in ALS (Mishra et al., 2016). Recently,

it was suggested that increased humoral levels of IL-6 may trigger endothelial cell damage and subsequently affect the BBB integrity (Garbuzova-Davis et al., 2018). IL-6 is a bi-functional cytokine with both pro- and anti-inflammatory properties that can be secreted by astrocytes in the CNS (Sekizawa et al., 1998). The anti-inflammatory effects of IL-6 have been associated with exercise and muscle contraction, however, in ALS it is proposed to mediate a pro-inflammatory response (Ono et al., 2001, Ehrhart et al., 2015).

In neuroinflammatory conditions reactive astrocytes appear to be the principal source of the monocyte chemoattractant protein-1 (MCP-1) (Mayo et al., 2014). MCP-1 is considered the most potent chemoattractant molecule for recruiting immune cells to sites of inflammation and its sustained production during several neurodegenerative conditions is strongly associated with neuronal damage (David et al., 2017, Conductier et al., 2010). Immunohistochemistry of the spinal cords of ALS patients revealed that MCP-1 expression was mostly localized to astrocytes and to a lesser extent to microglia and neurons (Baron et al., 2005, Henkel et al., 2004). Elevated levels of MCP-1 in CSF, serum and post-mortem tissue of ALS patients, and spinal cord of SOD1^{G93A} mice have been reported (Wilms et al., 2003, Kawaguchi-Niida et al., 2013, Henkel et al., 2006, Tateishi et al., 2010, Gupta et al., 2011, Henkel et al., 2004). Also, MCP-1 concentrations showed a negative correlation with disease progression in ALS (Tateishi et al., 2010). Interestingly, MCP-1 secretion from reactive astrocytes promoted microglia activation towards pro-inflammatory polarization (He et al., 2016).

One of the principal regulators of the inflammatory response is the transcription factor NF-κB, which regulates the expression of several pro-inflammatory genes (Swarup et al., 2011). Although NF-κB is considered the master regulator of microglia activation in ALS (Frakes et al., 2014), strong up-regulation of its expression in astrocytes obtained from ALS patients has been reported (Haidet-Phillips et al., 2011, Swarup et al., 2011). However, selective downregulation of NF-κB in astrocytes did not protect MNs *in vitro* and did not delay disease onset in the transgenic SOD1^{G93A} mouse model (Frakes et al., 2014, Crosio et al., 2011). This body of evidence may suggest a secondary role for astrocytes in driving neuroinflammation in ALS. However, redundancy and the complex interplay between astrocytes and cell components of the innate immune response make the understanding of the inflammatory response in ALS really difficult. Very recently, Alami *et al.* deeply investigated the role of astrocyte-specific NF-κB activation in the SOD1^{G93A} mouse model by using a tetracycline-regulated conditional expression system under control of the GFAP

promoter. The authors elegantly showed that restricted NF- κ B activation in astrocytes evokes a differential stage-specific immunological response which is beneficial during the pre-symptomatic stage but detrimental and toxic during disease progression (Ouali Alami et al., 2018). The astrocyte NF- κ B-dependent activation during different stages of the disease was strictly associated with the regulation of microglia functions. In addition, Fumito et al, recently showed that secretion of elevated levels of transforming growth factor beta 1 (TGF- β 1) from reactive astrocytes in SOD1^{G93A} mice interferes with the neuroprotective functions of microglia and T-cells by reducing the levels of anti-inflammatory cytokines and neuroprotective factors such as interleukin 4 (IL-4) and insulin-like growth factor 1 (IGF-1) (Endo et al., 2015). Recently, Liddelow et al., showed that harmful reactive astrocytes (termed A1) which are able to rapidly kill MNs *in vitro*, and are present in many neurological conditions including ALS, are induced by pro-inflammatory activated microglia through the secretion of IL-1 α , TNF- α and complement component 1q subcomponent (C1_q) (Liddelow and Barres, 2017).

Taken together, these data highlight how important is the interplay between astrocytes and microglia in regulating the inflammatory response in ALS, which can be protective at least during the first phases of disease, but deleterious during disease progression. This delicate interplay may explain why therapeutic interventions aimed to correct single pro-inflammatory pathways has not been successful in the clinic (Petrov et al., 2017).

1.4.5 Microglia

Microglia are considered the resident immune cells of the CNS which in the healthy brain, although defined as in a “resting” state, represent a highly dynamic cell population which participates in several physiological functions such as neurogenesis and synaptic plasticity. Microglia constantly monitor their microenvironment by migrating and by using their ramified processes that retract and elongate (Perry and Teeling, 2013). Their main role in the brain and spinal cord is to survey the surrounding extracellular space and rapidly respond to abnormalities in case of injury, disease or infection. Upon activation, microglia undergo morphological changes such as retraction of processes and enlargement of the cell body, and start releasing effector molecules that can be neuroprotective or neurotoxic depending on the stimulus (Kierdorf and Prinz, 2013). Indeed, similar to peripheral macrophages, microglia exist within a spectrum of phenotypic/functional states extremes of which are generally and simplistically termed M1 for the “classical” pro-inflammatory

activation state, and M2 for the “alternative” anti-inflammatory state (Geloso et al., 2017). The M1 microglia activation response is usually a consequence of pro-inflammatory stimuli such as for example exposure to IFN- γ or lipopolysaccharide (LPS) which, activating the classical NF- κ B pathway, drives microglia to enhance the inflammatory response by releasing nitric oxide, pro-inflammatory cytokines, prostaglandins, chemokines and ROS and by reducing the production of protective growth factors (Geloso et al., 2017). Thus, the classical M1 activation state can be harmful and neurotoxic. On the contrary, the M2 “protective” activation induced by anti-inflammatory cytokines including IL-4 and IL-13, is characterized by the release of immunosuppressive cytokines such as for example IL-10 and neuroprotective growth factors such as IGF-1 and brain-derived neurotrophic factor (BDNF) (Liu and Wang, 2017). M2 microglia also promote tissue repair by phagocytizing cell debris and promoting the reconstruction of the extracellular matrix (Cherry et al., 2014).

1.4.6 Role of microglia in ALS

Microglial activation and proliferation is a common feature in ALS which is histologically documented in both sporadic and familial forms of the disease in post-mortem tissue and in transgenic SOD1^{G93A} rodents (Hall et al., 1998, Henkel et al., 2004, Borchelt, 2006). Moreover, the use of positron emission tomography (PET) imaging allowed the demonstration of microglial activation in living ALS patients, where a negative correlation between levels of microgliosis and clinical disease severity was documented (Alshikho et al., 2018, Zurcher et al., 2015). Similar to astrocytes, the role of microglia in ALS has been investigated in detail by using transgenic murine models of disease.

Transplanting bone marrow derived from SOD1^{G93A} mice into PU.1^{-/-} mice, which are not able to produce myeloid and lymphoid cells, it has been shown that expression of mutant SOD1 exclusively in microglia is not sufficient to cause motor neuron degeneration (Beers et al., 2006). However, when backcrossing PU.1^{-/-} mice with SOD1^{G93A} mice, transplantation of bone marrow from wild type mice reduced MN loss and extended survival, demonstrating that to acquire a toxic phenotype SOD1 mutant microglia may require signals from affected MNs and other cell type such as astrocytes (Beers et al., 2006). Conversely, exogenous mutant SOD1 induced MN death *in vitro* only in the presence of microglia, which in response to the extracellular mutant protein activated by increasing the secretion of pro-inflammatory cytokines and superoxide (Zhao et al., 2010). Although the elimination of proliferating microglia did not protect MNs in SOD1^{G93A} mice (Gowing et al., 2008), selective microglia

knockdown of SOD1^{G85R} or SOD1^{G73R} in transgenic mice slowed down disease progression and increased survival (Wang et al., 2009a), confirming a detrimental role for microglia carrying mutant SOD1 during disease progression.

The harmful properties of microglia isolated from SOD1^{G93A} transgenic mice or carrying mutations in TDP-43 have also been reported *in vitro* by several studies, in which, compared to wild type microglia, mutant microglia displayed enhanced secretion of pro-inflammatory mediators including TNF- α , IL-1 β , MCP-1 and NADPH oxidase 2 (NOX-2), which in turn promoted MN damage (Zhao et al., 2015, Weydt et al., 2004, Xiao et al., 2007, Beers et al., 2006, Sargsyan et al., 2009). Frakes *et al.*, showed that microglia isolated from adult SOD1^{G93A} mice are toxic to MNs *in vitro*, and inhibition of the NF- κ B pathway results in MN rescue (Frakes et al., 2014). In support of the hypothesis that the main mechanism driving MN toxicity in ALS microglia is through the activation of the NF- κ B pathway, the authors also showed that constitutive activation of the pathway in microglia not expressing mutant SOD1 is sufficient to cause MN death (Frakes et al., 2014).

In ALS transgenic mice, microgliosis is well documented and increases during disease progression (Clement et al., 2003). A study using selective Cre-mediated inactivation of mutant SOD1, showed that reduction of the mutated protein specifically in MNs results in a delay in disease onset and a slowdown in the early stages of disease progression in SOD1^{G37R} mice (Boillee et al., 2006). Conversely, knockdown of mutant SOD1 in microglia does not affect disease onset but consistently reduces the rate of progression during the later stages of disease. This indicates a pathological role for microglia during disease progression but not during the initiation of the neurodegenerative process (Boillee et al., 2006). However, as already discussed, microglial activation may be beneficial or detrimental and it is unclear whether mutant microglia in this study were actively damaging MNs or whether they were losing their neuroprotective properties (Borchelt, 2006). However, in a report where the selective downregulation of the NF- κ B pathway in microglia reduced MN loss and extended survival in SOD1^{G93A} mice, the beneficial effects observed appeared to be due to a reduction in M1 (toxic) microglia rather than an induction of M2 (neuroprotective) microglial phenotype (Frakes et al., 2014).

Although still unclear, it seems that during the early stages of disease the activation of microglia towards a M2 phenotype may represent a neuroprotective response to MN death, while the shift to a M1 toxic microglia activation during disease progression may exacerbate neuroinflammation resulting in neurotoxicity (Beers and Appel,

2019). For example, microglia isolated from SOD1^{G93A} mice at disease onset expressed increased mRNA levels of M2 markers such as CD163 and BDNF, but lower levels of the M1 marker Nox2, compared to microglia obtained from end-stage mice (Liao et al., 2012). Moreover, mixed astroglial/microglial co-culture experiments showed that the end-stage M1 microglia were toxic to MNs, while the M2 microglia isolated at disease onset were neuroprotective, increasing MN survival even when compared to wild type microglia (Liao et al., 2012). In line with this, targeted NF-κB activation in astrocytes only before disease onset, prolonged the pre-symptomatic phase and increased overall survival in SOD1^{G93A} mice by inducing microglial proliferation and thus enhancing their neuroprotective effects (Ouali Alami et al., 2018). In contrast, astrocytic activation of NF-κB after disease onset accelerated disease progression and shortened life span as a consequence of microglia activation (Ouali Alami et al., 2018). In this study, astrocytic activation of NF-κB exclusively modulated the proliferation of microglia, but not their phenotypic state. In addition, astrocytic overproduction of TGF-β1 in SOD1^{G93A} mice, resulted in inhibition of microglial activity as demonstrated by a decrease in antigen presentation functions and a reduction in IGF-1 release, which ultimately aggravated disease progression (Endo et al., 2015). In agreement with the aforementioned studies, it has been recently shown in SOD1^{G93A} mice that before disease onset, brain microglia are characterized by an anti-inflammatory phenotype documented by the expression of high levels of IL-10 in response to LPS stimuli (Gravel et al., 2016)

Although the shift of microglial functions during disease onset in transgenic ALS mice have been demonstrated by several groups, the separation of microglia into M1 or M2 phenotypes is too simplistic and it has been suggested not to accept this semantic generalization (Ransohoff, 2016). In contrast to what has been found with macrophages, microglial polarization *in vivo* has not been proven yet, thus the use of the M1/M2 paradigm in the study of a such complex cell population must be used with caution (Ransohoff, 2016).

1.4.7 Oligodendrocytes in ALS

Another non-neuronal cell population which is involved in ALS pathology is represented by oligodendrocytes. The main function of these cells in the CNS is to insulate axons by producing myelin. In addition, oligodendrocytes provide metabolic support to neurons through the secretion of lactate (Lee et al., 2012). Although the role of oligodendrocytes during disease progression in ALS has not been extensively investigated at a degree comparable to the study of astrocytes and microglia, there

is evidence demonstrating that these cells contribute to neurodegeneration. For example, Lee *et al.* showed that the lactate transporter MTC1, which is highly expressed by oligodendrocytes, is significantly reduced in both post-mortem tissue of ALS patients and in the spinal cord of symptomatic SOD1^{G93A} mice (Lee et al., 2012). In addition, the authors showed that downregulation of MTC1 leads to motor neuron death and axonopathy both *in vitro* and *in vivo* (Lee et al., 2012). More recently, it has been shown that oligodendrocytes degenerate before disease onset in SOD1^{G93A} rodents, and although oligodendrocytes precursors proliferate during disease progression, they do not mature into functional cells, thus being unable to properly support remyelination and trophic functions (Kang et al., 2013, Philips et al., 2013). Moreover, selective deletion of human mutated SOD1 in oligodendrocyte precursors, increased the expression of the MTC1 transporter in mature oligodendrocytes, delayed disease onset and increased the life-span in mutant SOD1 ALS mice (Kang et al., 2013). Finally, very recently it has been shown that oligodendrocytes derived from mutant SOD1^{G93A} mice, or obtained from ALS patients with either sporadic or familial disease are able to damage and kill MNs *in vitro*, through both release of soluble factors and cell-to-cell contact mechanisms (Ferraiuolo et al., 2016). Interesting, while SOD1^{G93A} oligodendrocyte MN toxicity mediated by paracrine mechanisms was dependent on reduced lactate provision, cell-to-cell contact mediated toxicity was independent of lactate production, suggesting multiple and separate mechanisms of toxicity (Ferraiuolo et al., 2016).

1.5 Treatment options for ALS

The complex heterogeneity of ALS, where several molecular mechanisms contribute to the pathology, enables various opportunities for therapeutic intervention. However, the complexity of the disease and clinical variability within patients inevitably makes the identification of a universal single drug or therapy capable of fighting ALS in its totality, very difficult. Various therapeutic strategies are being experimentally evaluated such as immunomodulation, approaches to improve mitochondrial function, induction of autophagy and anti-oxidant agents (Poppe et al., 2014). However, after over twenty years of encouraging results in preclinical studies, no efficacious treatment has been developed so far. The only two FDA approved drugs for ALS are riluzole, that prolongs life expectancy by only approximately 3-4 months (Poppe et al., 2014), and edaravone, which showed mild beneficial effects on the decline of the ALS-FRSR over a short time-scale in a small subset of patients (Hardiman and van den Berg, 2017).

1.6 Stem cell therapy in ALS

During the last decade, progress in stem cell biology paved the way for potential cellular based therapy for neurological disease. Albeit still at an early stage and with several issues to be solved, stem cell therapy holds great promise for the treatment of ALS. Stem cells are considered as a population of cells which are defined by functional characteristics. They are undifferentiated cells capable of self-renewal, able to form clones *in vitro* and capable of differentiation into mature cell types of various tissues. There are several reasons that make the use of stem cells in ALS therapy potentially attractive:

- 1) The complexity of ALS pathology may not allow the use of a single drug or target treatment;
- 2) The capability of stem cells to differentiate into neuron-like cells and potentially replace neuronal population lost in ALS;
- 3) The degeneration of existing motor neurons could be prevented by the release of neuroprotective trophic factors and by immunomodulatory properties of transplanted cells, thus modifying the toxic microenvironment in ALS.

There are different types of stem cells which differ according to the source, clonogenic capacity, differentiation potential and availability.

1.6.1 Human Embryonic Stem Cells (hESCs)

Human embryonic stem cells (hESCs) are derived from the inner cell mass of blastocyst and can indefinitely propagate *in vitro*, preserving the capacity to differentiate into any cell type of the three embryonic germ layers (endoderm, mesoderm and ectoderm) (Thomson et al., 1998). For the first time in 2005, Shin and colleagues obtained motor neuron-like cells expressing markers such as islet1 and choline acetyltransferase from hESCs using a conditioned media containing basic fibroblast growth factor (bFGF), retinoic acid (RA) and sonic hedgehog factor (Shh) (Shin et al., 2005). The survival, differentiation and beneficial neurotrophic support of motor neuron progenitors (MNP) derived from hESCs has been also demonstrated after lumbar intraspinal or intracranial transplantation into SOD1^{G93A} mice and other MND models (Rossi et al., 2010, Wyatt et al., 2011). Wyatt et al., transplanted hESC derived MNP directly into the spinal cord of immunosuppressed SOD1^{G93A} mice, spinal muscular atrophy (SMA) $\Delta 7$ SMN pups and rats with spinal cord injury (SCI), demonstrating the *in vivo* differentiation of the engrafted cells into a mixed population of mature and immature motor neuron cells (Wyatt et al., 2011). The axons of the

differentiated cells did not reach the periphery, and the authors did not prove the integration of the differentiated cells into the existing neural circuit. However, the transplanted cells were able to reduce motor neuron loss in proximity to the injection site by actively releasing neurotrophic factors such as neurotrophin-3 (NT-3) and nerve growth factor (NGF). In particular, in SOD1^{G93A} mice that received MNPs, 43 ± 5 endogenous neurons cranial to the injection site survived until the end of the study (110 days old), in comparison to the vehicle control group in which 27 ± 3 neurons were counted (Wyatt et al., 2011). Yet, the use of hESCs in the clinic is hindered because of ethical concerns, potential tumorigenicity *in vivo* and the potential for graft rejection (Toma et al., 2015).

1.6.2 Foetal Neuronal Stem Cells (NSCs)

Foetal neural progenitors (NSC) are multipotent stem cells derived from foetal spinal cord or brain, capable of *in vitro* self-renewal and able to differentiate into astrocytes, neurons and oligodendrocytes. Given their partial maturation state they have less propensity to form teratomas *in vivo* (Mothe and Tator, 2015). Several studies investigated the safety and therapeutic potential of spinal, intrathecal or intracranial transplantation of human neural stem cells (hNSC) in ALS rodent models (Xu et al., 2009, Xu et al., 2011, Yan et al., 2007). In particular, a well-characterized hNSC cell line (NSI-566RSC) derived from an 8-week human foetal spinal cord showed very promising results in transplanted SOD1^{G93R} rodent animals (Yan et al., 2006, Xu et al., 2006). In 2006, Yan et al. performed spinal cord injections of NSI-566RSC cells into the ventral horn of 8-week-old SOD1^{G93A} mice at the lumbar level L4-L5, under combined immunosuppression or CD4 antibodies (Yan et al., 2006). Four separate injections were carried out per mouse, with a total of 8 x 10⁴ cells. The authors showed that the graft survived for more than two months after transplantation, with most of the engrafted NSCs showing differentiation into TUJ1⁺ neurons, and evidence of synaptic contacts with host neurons (Yan et al., 2006). Moreover, in mice injected with live NSCs cells, disease onset was delayed by 15 days and life span extended by 12 days in comparison to the control group that received injections of dead cells. A statistically significant later onset and a slowing of disease progression, was also confirmed by analysis of motor performance (Yan et al., 2006).

The same group of authors, investigated the therapeutic potential of the NSC-566RSC cell line after injection of around 8 x 10⁵ cells into the lumbar spinal cord of SOD1^{G93A} rats at a pre-symptomatic disease stage (Xu et al., 2006). In this study, rats that received live NSCs showed an increase in survival of around 11 days and a delay

in disease onset of 7 days when compared to the control placebo group. The beneficial effect could be associated with the release of neurotrophins such as glial-derived neurotrophic factor (GDNF) and brain-derived neurotrophic factor (BDNF), which in turn delayed the death of α -motor neurons in the lumbar region (Xu et al., 2006). Despite these encouraging data, the restricted number of cells available for transplantation represents a potential limitation for obtaining therapeutic efficacy in humans.

1.6.3 Induced Pluripotent Stem Cells (iPSCs)

Induced pluripotent stem cells (iPSCs) are an adult source of pluripotent stem cells derived from somatic cells (e.g. dermal fibroblasts) by forced genetic induction of four factors that preserve pluripotency in ESCs: Kruppel-like factor 4 (KLF4), sex determining region Y-box 2 (SOX2), octamer-binding transcription factor 4 (OCT4) and c-MYC (Takahashi and Yamanaka, 2006, Takahashi et al., 2007). The differentiation of human iPSCs into electrically active motor neurons has been accomplished by several groups both *in vitro* and *in vivo* (Dimos et al., 2008, Karumbayaram et al., 2009). Interestingly, Popescu et al. demonstrated *in vivo* differentiation of human iPSC-derived neural progenitors (NPs) in presymptomatic SOD1^{G93A} rats following stem cell injection into the ventral horns of the lumbar spinal cord (Popescu et al., 2013). At 30 days post-transplantation human mitochondria positive cells displayed expression of the neuronal precursor marker doublecortin (DCX), indicating the presence of undifferentiated progenitors. Substantial differentiation into mature motor neurons could be observed only after 60 days, with the majority of engrafted cells expressing the neuronal marker microtubule-associated protein 2 (MAP2) (Popescu et al., 2013). This relatively long time is something to bear in mind, considering that transplantation was performed before disease onset and NPs could survive and differentiate within a less toxic environment in comparison to the symptomatic stage. If cells were transplanted during disease progression, as would occur in the clinic, NPs may not have a permissive environment and/or the necessary time to differentiate into mature motor neurons.

The therapeutic potential of iPSC-derived NPs has also been investigated in the SOD1^{G93A} mouse model of ALS (Nizzardo et al., 2014). iPSC-derived neural stem cells (NSCs), further selected for the expression of the integrin very late antigen 4 (VLA4⁺), were transplanted either by repeated (n=3) intrathecal or weekly intravenous injections. Intrathecal injection of cells extended survival by 10 days, while systemic delivery increased survival by 23 days, compared to control PBS injected mice

(Nizzardo et al., 2014). The molecular protective mechanism of iPSC-derived NSCs may be attributed to the capacity of these cells to secrete trophic factors such as glial derived neurotrophic factor (GDNF), BDNF, NT-3 and TGF- α , which in turn protects resident motor neurons and reduces astrogliosis (Nizzardo et al., 2014).

The opportunity for reprogramming somatic cells into neural stem cells could overcome the immune rejection problem by autologous transplantation, and bypass the ethical problems related to the use of embryonic and foetal cells. However, several issues need to be addressed, such as reprogramming efficiency, epigenetic memory and safety before translation of the use of iPSCs into clinical practice.

1.6.4 Mesenchymal Stem Cells (MSCs)

Adult mesenchymal stem cells (MSCs) are stromal multipotent stem cells that can be derived from umbilical cord, bone marrow, adipose tissue and peripheral blood and have the capacity to differentiate into different components of mesoderm origin (cartilage, bone, fat, muscle and stroma) (Pittenger et al., 1999). These cells can be expanded and maintained by several passages in plastic-adherent culture. MSCs show fibroblast-like morphology, they do not differentiate spontaneously and are characterized by the expression of specific surface markers (Pittenger et al., 1999). In addition to mesodermal commitment, several authors showed the potential of bone marrow-derived MSCs (BM-MSC) to differentiate into neuron-like cells, oligodendrocytes and astrocytes (Woodbury et al., 2000, Hermann et al., 2004, Rivera et al., 2006, Boucherie et al., 2009, Sanchez-Ramos et al., 2000, Wislet-Gendebien et al., 2005, Joe et al., 2014, Chan-II et al., 2013, Choi et al., 2014).

Several characteristics make the use of MSCs very attractive in ALS cell therapy. MSCs can be obtained and expanded from adults relatively easily, bypassing the ethical constraints related to the use of embryonic and human foetal derived stem cells. Also, they are less immunogenic and can be harvested from ALS patients allowing both allogenic and autologous transplantation (Pittenger et al., 1999). Moreover, these cells are capable of homing to areas of insult, possess immunomodulatory and anti-apoptotic properties, and are capable of secreting several cytokines, extracellular matrix proteins and growth factors relevant in neuroprotection and tissue repair (Lewis and Suzuki, 2014). Because of these properties, MSCs are receiving significant attention amongst researchers.

1.6.5 Proof-of-concept for MSC therapy in the SOD1^{G93A} model of ALS

Several studies were performed in ALS rodent models in order to investigate the potential of either human (hMSC) or murine (mMSC) bone marrow-derived MSCs (BM-MSCs) for cell therapy in ALS. Different approaches have been tested by varying the delivery method, the amount of injected cells, the time of intervention, and the differentiation state. Table 1.1 shows a summary of preclinical studies described in the literature with injection of BM-MSCs in ALS models.

1.6.5.1 Intravenous delivery

In 2007, Zhao and colleagues delivered 3 million hBM-MSCs into 60 day pre-irradiated SOD1^{G93A} mice by intravenous infusion (Zhao et al., 2007). The recipient mice showed a 14 day delay in disease onset, and prolonged survival of about 18 days in comparison to untreated mice. Moreover, the decrease in motor performance (rotarod test) was delayed by 3 weeks (Zhao et al., 2007). However, immunostaining experiments showed that only a few transplanted cells migrated and penetrated into the grey and white spinal cord matter, surviving for no more than 20 days (Zhao et al., 2007).

In another study, 1 million engineered hBM-MSCs overexpressing neurogenin1 (Ngn1) were injected in the tail vein of pre-symptomatic SOD1^{G93A} mice (Chan-Il et al., 2013). Ngn1 is a transcription factor able to induce neuronal differentiation in MSCs (Chan-Il et al., 2013). Two weeks after transplantation, injected cells were found within the brain, spinal cord and liver, and some cells had migrated into the spinal cord parenchyma (Chan-Il et al., 2013). The neural induction of hMSCs with neurogenin1 seemed to potentiate the migration capacity and survival of engrafted cells into the CNS of SOD1^{G93A} mice, resulting in enhanced and prolonged benefits (Chan-Il et al., 2013). The migration capacity might be explained by high expression of chemokine receptors such as C-C chemokine receptor type 2 (CCR2) and C-X-C chemokine receptor type 4 (CXCR4), which were significantly more expressed after neurogenin1 induction. (Chan-Il et al., 2013). Interestingly, when MSCs were injected at a pre-symptomatic stage, disease onset in the treated group was delayed by 5 days with an increase in life span of only 3 days. Conversely, when injected close to disease onset, Ng1-MSCs were able to increase survival by about 7 days, suggesting the importance of the time of intervention for stem cell therapy in ALS (Chan-Il et al., 2013).

Furthermore, the Uccelli group demonstrated that mouse BM-MSCs isolated from non-transgenic mice, were therapeutically effective when transplanted during the

symptomatic stage of the disease in the SOD1^{G93A} mice (Uccelli et al., 2012). In this study, mBM-MSCs expanded *ex-vivo* for 8-15 passages, were transfected with the luciferase gene reporter vector pL-Luc-HI for *in vivo* tracking and injected into the tail vein of SOD1^{G93A} mice. The mice that received the MSC transplantation showed an extended survival of 17 days, delayed decline in motor performance and decreased weight loss when compared to the control PBS-injected mice (Uccelli et al., 2012). In addition, the transplantation of MSCs alleviated the pathology of the disease in the ALS spinal cord, by reducing astrogliosis and microglial activation, and by restoring antioxidant components such as glutathione-S-transferase and metallothioneins to their baseline level of expression and activity. However, the engraftment efficiency of intravenous delivered cells within the CNS was very low, with luciferase-positive cells almost completely absent twenty days post- injection. This suggested that MSCs delivered by the intravenous route, can exert clinically positive effects during the disease course that do not correlate with the efficiency of long-term engraftment in the host (Uccelli et al., 2012).

1.6.5.2 Intrathecal delivery

Using a different approach, several authors have injected a variable number of BM- MSCs directly into the cisterna magna of pre-symptomatic SOD1^{G93A} mice (Habisch et al., 2007, Kim et al., 2010, Zhang et al., 2009, Forostyak et al., 2014). Direct injection into the CSF allows the obstacle of the BBB to be bypassed. Moreover, the injected cells may migrate along the spinal cord possibly reaching segments specifically affected by motor neuron degeneration. Indeed, it has been demonstrated that the injected BM- MSCs were able to delay disease onset, improve motor performance, ameliorate motor neuron death and prolong survival in transplanted SOD1^{G93A} mice (Zhang et al., 2009, Kim et al., 2010, Forostyak et al., 2014, Zhou et al., 2013). These beneficial effects were enhanced by multiple intrathecal injections or by using a considerable number of MSCs (1×10^6) (Kim et al., 2010, Zhang et al., 2009). However, injected cells rarely migrated into the parenchyma, suggesting a neuroprotective effect of MSCs from the CSF (Zhang et al., 2009, Zhou et al., 2013, Kim et al., 2010). In fact, it was shown that injection of MSCS into the CSF of SOD1^{G93A} mice consistently inhibited microglial activation and the release of inflammatory molecules, possibly by diffusion of soluble factors where direct contact between cells is not a requirement (Zhou et al., 2013).

In 2009, Boucherie and colleagues, investigated the therapeutic potential of rat wild-type (WT) bromodeoxyuridine-labelled BM- MSCs (BrdU- MSC) by intrathecal injection

in SOD1^{G93A} transgenic rats, at disease onset (Boucherie et al., 2009). Stem cell transplantation in SOD1^{G93A} rats resulted in a reduction in the rate of disease progression, as the first signs of paralysis were detected 2 weeks later in comparison to control mice. Moreover, treated rats showed reduced local inflammatory response and an increase in life span of 16 days (Boucherie et al., 2009). Interestingly, this is the only study to show a significant trans-differentiation of MSCs into astrocyte-like cells *in vivo*. Indeed, transplanted BrdU-MSCs were found to penetrate into the grey matter of the ventral horns, and stained positively for the astrocyte marker GFAP (Boucherie et al., 2009). Remarkably, around 40% of the BrdU-MSCs that successfully migrated in proximity to motor neurons, co-localized with the astrocyte marker, and about 30% of the GFAP-positive cells were actually positive for BrdU. This study demonstrated a considerable local chimerization of the astroglial population near the site of motor neuron injury in the lumbar spinal cord of SOD1^{G93A} rats (Boucherie et al., 2009). However, cell fusion events with resident astrocytes cannot be excluded. Surprisingly, the overall level of astrogliosis was not changed upon MSC treatment, and the loss of expression of the astrocyte glutamate reuptake transporter (GLT-1), typically observed in SOD1^{G93A} rats, was not rescued (Boucherie et al., 2009).

The perineural net (PNN) is a specialized matrix structure present at a high density around motor neurons and is fundamental in axon development as well as neuronal plasticity (Forostyak et al., 2014). Modification and deterioration of the PNN has been observed in the spinal cord of SOD1^{G93A} rats during neurodegeneration (Forostyak et al., 2014). Interestingly, intrathecal delivery of hBM-MSCs into early post-symptomatic SOD1^{G93A} rats, resulted in partial rescue of PNN structures suggesting a role of MSCs in reactivating CNS plasticity (Forostyak et al., 2014). In this study, stem cell injection increased survival by 14 days in comparison to the placebo group.

Boido et al. (2014) injected a total of 300,000 bisbenzimidate pre-labelled hMSCs into the cisterna lumbaris (L5-L6 level) of early symptomatic SOD1^{G93A} mice (Boido et al., 2014). Although the treated mice showed only a slight delay in motor neuron loss and slowing of motor performance decline, astrogliosis and microgliosis were consistently attenuated in recipient mice in comparison to the controls (Boido et al., 2014). Two weeks post-transplantation, transplanted cells were found mostly concentrated on lumbar, thoracic and cervical meninges, but considerable numbers of bisbenzimidate positive cells were found in proximity to motor neurons within the spinal cord (Boido et al., 2014). It is noteworthy that the use of bisbenzimidate as a marker for cell

transplantation has been questioned since the dye may transfer from labelled cells to host cells (Iwashita et al., 2000).

More recently, Sironi *et al.* tested the therapeutic effect of multiple intracerebroventricular injections of human umbilical cord derived MSCs (UC-MSCs) in SOD1^{G93A} mice (Sironi et al., 2017). For tracking purpose, cells were double labelled with polymethyl methacrylate nanoparticles (NPs) and Hoechst-33258 before being injected bilaterally into the lateral ventricles of SOD1^{G93A} mice. Mice received 4 separate injections of 250,000 hUC-MSCs once every two weeks from the age of 98 days when the mice started showing the first symptoms of disease. Although stem cell transplantation significantly protected MNs and reduced neuroinflammation in the lumbar spinal cord, NMJ denervation was not prevented and no differences in disease progression or survival were detected compared to control PBS-injected mice (Sironi et al., 2017). In this study, the engraftment and distribution of the transplanted cells during time was also reported, showing a cluster of double labelled hUC-MSCs confined to the lateral ventricles and associated with the choroid plexus. In contrast to a previous study from the same authors showing migration of hUC-MSCs into the spinal cord and brain parenchyma of SOD1^{G93A} mice after a single intracerebroventricular (ICV) injection (Violatto et al., 2015), in the Sironi *et al.* paper, the cells were not able to migrate caudally from the lateral ventricles even following multiple injections.

1.6.5.3 Intraparenchymal delivery

Other authors have attempted to inject human or mouse MSCs directly into the dorsal horn of spinal cord of SOD1^{G93A} mice (Vercelli et al., 2008, Knippenberg et al., 2012b). In the Vercelli group experiments, hMSCs were found to engraft, migrate to the ventral horn close to α -motor neurons and survive more than 10 weeks after surgery, although without signs of differentiation into neurons or astrocytes (Vercelli et al., 2008). Also, male but not female recipient mice showed a consistent (38%) increased motor neuron survival as well as reduced gliosis and attenuated astrocyte activation in comparison to control mice (Vercelli et al., 2008). Though the authors claimed an extended lifespan in male treated mice, not all of the experimental groups were followed until the disease end-point, and a Kaplan-Meier survival curve was not shown.

1.6.5.4 Intramuscular delivery

Since early pathologic mechanisms of disease involve destruction of neuromuscular junctions before motor neuron death, intramuscular injection of MSCs at early stages

of disease has also been proposed. hBM-MSCs, genetically engineered to express green fluorescent protein (GFP) and to constitutively secrete GDNF, were injected into the forelimb triceps brachii muscles of pre-symptomatic SOD1^{G93A} rats (Suzuki et al., 2008). The intramuscular transplantation of MSCs did not delay disease onset, however, survival was prolonged by 18 days. Furthermore, a reduction of endplate denervation in SOD1^{G93A} rats was observed, when compared to the control vehicle group (Suzuki et al., 2008). However, MSCs were not able to regenerate motor endplates, nor to reduce neuroinflammation (Suzuki et al., 2008). Moreover, to obtain significant survival and integration of MSCs in the host, the induction of focal muscle injuries was necessary.

1.6.5.5 Combined intrathecal and intramuscular delivery

Very recently, the Jendelova' group by transplanting hBM-MSCs onto SOD1^{G93A} rats, compared the effect of repeated intrathecal injections (IT), repeated intramuscular (IM) or a combination of the two delivery routes (IT +IM) (Rehorova et al., 2019). The first stem cell injection was performed after early signs of disease onset, while the second and third injections at two weeks intervals. At each treatment, a total of 5×10^5 cells were transplanted into the cisterna lumbaris and 6×10^5 cells (distributed in three separate locations) into the quadriceps femoris of both hind limbs. Compared to the vehicle, all the rats receiving MSCs showed improvement in rotarod performance and a delay in the decline of motor function and physical condition, although with no significant differences between the treated groups. Body weight and grip strength test were not affected by the treatment. Of interest, overall survival was increased in all the treated groups compared to the controls. However, the combined intrathecal and muscular treatment, or intrathecal injections alone were more effective compared to the muscular treatment alone. In particular, survival was increased by about 18 days in the IT and IT + IM groups and about 6 days in the IM group compared to the vehicle (Rehorova et al., 2019). The differences in life span between the IT and IM groups correlated with the survival of the transplanted cells. Indeed, while cells injected intrathecally survived for more than 2 weeks in the subarachnoid space, only a few cells survived in muscles 1 week after transplantation. Although no major differences were found between the IT and IT+IM groups in motor performance and life span, the combined IT+IM treatment resulted in the greatest pathological and molecular changes, as documented by reduced MN loss, partial preservation of NMJs, and reduction in levels of proteins involved in apoptosis and necroptosis (Rehorova et al., 2019).

The authors, in parallel to the MSC treatment also tested repeated intrathecal administration of conditioned media from the same batch of cells used for transplantation. Interestingly, the beneficial effects observed with the use of the conditioned media were limited compared to the cell therapy approach, with no improvement in survival (Rehorova et al., 2019).

Table 1.1. Summary of MSC transplantation studies in ALS rodent models

ALS model	Cells	Delivery Method	Cell numbers	Age	Outcomes	Cell graft	Reference
SOD1^{G93A} mice	hBM-MSC after 5 passages in culture	Intravenous	3x10 ⁶ in 0.3 ml of L-DMEM	Pre-symptomatic (8 w)	Increased lifespan of 18 days, delayed disease onset of 14 days and reduced motor neuron loss	14 days post-injection, very few cells into grey and white matter of lumbar spinal cord, but also in kidney, lung and spleen.	(Zhao et al., 2007)
SOD1^{G93A} mice	mBM-MSCs expressing Luciferase expanded for 8-15 passages	Intravenous	1x10 ⁶ in 0.2 ml of PBS	Symptom onset	Increased lifespan of 17 days, delayed decline in motor performance and weight loss.	Cells detected in spinal cord and hypothalamus after 24h and 48h. Very few cells after 20 days. No cells after 35 days	(Uccelli et al., 2012)
SOD1^{G93A} mice	hBM-MSC expressing Ngn1 after 5 passages in culture	Intravenous	1x10 ⁶ in 0.1 ml of PBS	Pre-symptomatic (8 w) or symptom onset (14-16 w)	Increased lifespan of 3 days, delayed disease onset of 5 days and reduced motor neuron loss	14 days post-injection, very few cells in brainstem and spinal cord, but also in kidney.	(Chan-II et al., 2013)
SOD1^{G93A} mice	hBM-MSC-derived neural-like cells from neurosphere propagated for 3 weeks	Cisterna Magna	1x10 ⁵ in 10 µl of PBS	Pre-symptomatic	No benefits	10 days post-injection, cells in the subarachnoid space near cisterna magna and within cerebellum.	(Habisch et al., 2007)
SOD1^{G93A} mice	ALS-hBM-MSC after 3 passages in culture	Cisterna Magna	1 x 10 ⁶ in 10 µl of ALS-CSF	Pre-symptomatic	Increased lifespan of 8 days, slowed decline in rotarod test and increased motor neuron survival	7 weeks post-injection, cells in ventricular system and subarachnoid space. Some cells into brain and spinal cord.	(Kim et al., 2010)

ALS model	Cells	Delivery Method	Cell numbers	Age	Outcomes	Cell graft	Reference
SOD1^{G93A} mice	hBM-MSC after 5 passages in culture	Intravenous	3x10 ⁶ in 0.3 ml of L-DMEM	Pre-symptomatic (8 w)	Increased lifespan of 18 days, delayed disease onset of 14 days and reduced motor neuron loss	14 days post-injection, very few cells into grey and white matter of lumbar spinal cord, but also in kidney, lung and spleen.	(Zhao et al., 2007)
SOD1^{G93A} mice	mBM-MSCs expressing Luciferase expanded for 8-15 passages	Intravenous	1x10 ⁶ in 0.2 ml of PBS	Symptom onset	Increased lifespan of 17 days, delayed decline in motor performance and weight loss.	Cells detected in spinal cord and hypothalamus after 24h and 48h. Very few cells after 20 days. No cells after 35 days	(Uccelli et al., 2012)
SOD1^{G93A} mice	hBM-MSC expressing Ngn1 after 5 passages in culture	Intravenous	1x10 ⁶ in 0.1 ml of PBS	Pre-symptomatic (8 w) or symptom onset (14-16 w)	Increased lifespan of 3 days, delayed disease onset of 5 days and reduced motor neuron loss	14 days post-injection, very few cells in brainstem and spinal cord, but also in kidney.	(Chan-II et al., 2013)
SOD1^{G93A} mice	hBM-MSC-derived neural-like cells from neurosphere propagated for 3 weeks	Cisterna Magna	1x10 ⁵ in 10 µl of PBS	Pre-symptomatic	No benefits	10 days post-injection, cells in the subarachnoid space near cisterna magna and within cerebellum.	(Habisch et al., 2007)
SOD1^{G93A} mice	ALS-hBM-MSC after 3 passages in culture	Cisterna Magna	1 x 10 ⁶ in 10 µl of ALS-CSF	Pre-symptomatic	Increased lifespan of 8 days, slowed decline in rotarod test and increased motor neuron survival	7 weeks post-injection, cells in ventricular system and subarachnoid space. Some cells into brain and spinal cord.	(Kim et al., 2010)

SOD1^{G93A} rats	GFP-hBM-MSC engineered to secrete GDNF	Intramuscular after focal injuries	1.3x10 ⁵ in PBS	Pre-symptomatic (80 days)	Prolonged survival, reduction in denervated motor endplates and reduced motor neuron loss	Between basal lamina and muscle fibres at the end of the study	(Suzuki et al., 2008)
SOD1^{G93A} rats	hBM-MSC	Repeated (3 times) combined intramuscular (IM) and intrathecal (IT)	5x10 ⁵ IT in 50 µl of PBS + 3X 2x10 ⁵ IM in 100 µl of PBS	Symptom onset	Delayed motor function decline, increased survival of 18 days. Partial preservation of NMJ, reduced apoptosis and necroptosis markers in spinal cords	Folds of arachnoidea in the cauda equina for no more than 2 weeks. Very few cells surviving in muscles 1 week post-injection	(Rehorovai et al., 2019)

hBM-MSC = human bone marrow-derived mesenchymal stem cells; DMEM = Dulbecco's modified eagle medium; Ngn1 = neurogenin-1; PBS = phosphate buffer saline; mBM-MSC = mouse bone marrow-derived mesenchymal stem cells; ALS-hBM-MSC = human bone marrow-derived mesenchymal stem cells derived from ALS patient; ALS-CSF = cerebrospinal fluid derived by ALS patient; GFP-hBM-MSC = green fluorescent protein labelled hBM-MSC; PNN = perineural net; BrdU = bromodeoxyuridine; NPs = nanoparticles; hUC-MSC = human umbilical cord-derived MSC; ICV = intracerebroventricular; GDNF = glial derived neural factor; IM = intramuscular; IT = intrathecal.

1.6.6 MSCs in ALS: Clinical trials

1.6.6.1 Mazzini trials: Intraparenchymal delivery of autologous BM-MSCs

Despite the absence of any preclinical data, in 2001 Mazzini *et al.* embarked upon the first clinical trial in order to evaluate the safety and feasibility of MSC injection into the spinal cord of sporadic ALS patients (Mazzini *et al.*, 2003). The study comprised the recruitment of 7 sALS patients with spinal onset and severe lower limb impairment without respiratory complications (Mazzini *et al.*, 2003). Autologous mesenchymal bone marrow-derived stem cells were expanded for 3-4 weeks under good manufacturing practice (GMP) conditions and cytogenetic analysis, viability and cytofluorimetric analysis for characterization of antigens were carried out before infusion (Mazzini *et al.*, 2003). However, no detailed data were provided. In this study, following three hours in serum-free medium, a variable number of cells ranging from 7 to 152 million were suspended in 1-2 ml of autologous CSF and transplanted directly into the parenchyma of spinal cord at thoracic level (T7-T9) (Mazzini *et al.*, 2003, Mazzini *et al.*, 2008). The patient follow-up was performed every 3 months for six years.

After surgery, no signs of increased neurological defects or toxicity were observed, indicating that implantation into the spinal cord of *ex vivo* expanded MSCs was safe and well tolerated by patients (Mazzini *et al.*, 2003, Mazzini *et al.*, 2008). To further validate the safety of the therapy, in 2010 a second Phase I clinical trial was conducted in another 10 patients following the same protocol as described above, with slight modifications (Mazzini *et al.*, 2010). Cells (11-122 million) were transplanted in the anterior horn at the thoracic level (T4-T6) with different numbers of injection sites (2 to 5) (Mazzini *et al.*, 2010). Two years post-surgery, no tumour formation, side effects or toxicity had been detected (Mazzini *et al.*, 2010).

A long-term (9 years) safety study, concluded in 2012, was carried out by the same authors on the basis of 19 ALS patients who underwent autologous MSCs implantation in two separate phase I studies from 2001 to 2003 (Mazzini *et al.*, 2012). Importantly, magnetic resonance imaging (MRI) analysis demonstrated no tumour formation or abnormal cell growth, indicating that *ex vivo* expansion of ALS patient-derived MSCs does not affect karyotype or cellular senescence, making their use safe in the clinic (Mazzini *et al.*, 2012). No data describing stem cell characterization were shown and evidence of engraftment in post-mortem CNS tissue has not yet been described.

1.6.6.2 Karussis trials: Intrathecal and intravenous delivery of autologous MSCs

In 2010, a phase 1/2 clinical trial was conducted in Israel in 15 patients with multiple sclerosis (MS) and 19 ALS patients (Karussis et al., 2010). In order to enhance the potential benefits of MSC transplantation, after 40-60 days in culture, a median of 60 million autologous MSCs were transplanted intrathecally in combination with a mean of 20 million MSCs delivered intravenously (Karussis et al., 2010). Also, in 9 patients MSCs were pre-labelled with ferumoxides in order to track their fate *in vivo* by MRI (Karussis et al., 2010). At the end of 25 months of follow-up, no severe adverse effects were registered in any of the patients, with signs of disease stabilization in some patients during the first 6 months after the intervention (Karussis et al., 2010). Furthermore, MRI screening 24h, 48h, 1 and 3 months after the infusion of cells, showed the presence of ferumoxides in nerve roots, meninges and the parenchyma of the spinal cord. However, these results are not conclusive of the presence of MSCs in the CNS, since the contrast agent can be ingested by phagocytes which have migrated to inflammatory lesions (Karussis et al., 2010). In addition, flow cytometry analysis and subsequent proliferative response assay of peripheral blood monocytes obtained from ALS patients 4h and 24 h after infusion of MSCs, showed a dramatic increase in CD4⁺ CD25⁺ regulatory T cells, coupled with a reduction in activated dendritic cells and lymphocyte proliferation, demonstrating the immediate immunomodulatory properties of MSCs following transplantation (Karussis et al., 2010).

1.6.6.3 Oh trials: Repeated intrathecal infusions of autologous BM-MSCs

Recently, a single open-label clinical trial was performed in order to evaluate the clinical feasibility and safety of two repeated infusions of autologous MSCs into the CSF by lumbar puncture in 8 ALS patients (Oh et al., 2015). At intervals of 26 days, 1×10^6 MSC cells per kg were injected diluted in autologous CSF (Oh et al., 2015). After 1 year, no deaths were recorded and the procedure was considered safe, without long-term adverse effects (Oh et al., 2015). In addition, CSF samples of two patients were collected before both the first and the second injection in order to evaluate cytokine levels. IL-10, TGF- β (I, II and III) and IL-6 levels were increased after MSC transplantation, while the level of the monocyte chemoattractant protein 1 (MCP-1) was decreased (Oh et al., 2015).

The same group performed repeated intrathecal MSC injections in another 37 patients between 2007 and 2010, with the aim of identifying MSC markers capable of

predicting the response in ALS patients (Kim et al., 2014a). First, they measured the level of various trophic factors in MSC cultures from each patient by enzyme-linked immunosorbent assay (ELISA). They then transplanted MSCs from different patients in the SOD1^{G93A} mouse model and analysed differences in onset, MN loss and immunoreactivity (Kim et al., 2014a). The authors concluded that the beneficial effects (symptom improvement and slowing of decline) observed in a proportion of patients, were positively correlated with the increased capacity of MSC cells to secrete vascular endothelial growth factor (VEGF), angiotensin (ANG) and TGF- β *in vitro* (Kim et al., 2014a). Moreover, the clinical efficacy observed in some patients was confirmed also in SOD1^{G93A} mice which exhibited prolonged survival and lower levels of neuroinflammation (Kim et al., 2014a).

These promising results led to a phase II parallel-group, randomized, and controlled trial in 64 ALS patients with sporadic disease, investigating the safety and efficacy of 2 repeated intrathecal injections of autologous MSCs (ClinicalTrials.gov Identifier: NCT01363401). Importantly, this is the first worldwide clinical trial reporting published results on the safety and efficacy of MSC transplantation in ALS patients that included a control group (Oh et al., 2018) However, the control group was not representative of a proper placebo group, since for ethical reasons sham procedures such as BM aspiration and lumbar puncture were not performed. In the study, patients were divided into the treatment group (MSCs and riluzole, n=31) or control group (riluzole alone, n=33). In the treatment group, patients received 2 intrathecal injection of 1×10^6 cells/Kg at a 26 days interval. The primary efficacy outcome considered changes in the ALSFRS-R scale from baseline (before first injection) to 4 and 6 months after transplantation, while secondary outcomes included the monthly rate of decline, changes in forced vital capacity and responder analysis (Oh et al., 2018). The incidence of adverse effects were not different between the two groups, with the MSCs treatment group reporting mild and transient headache, back pain and musculoskeletal pain (Oh et al., 2018). Interestingly, both the mean ALSFRS-R score and change in slope were significantly reduced in the MSC group compared to the controls at both 4- and 6-month follow-up time points. Responder analysis revealed that 69% of patients responded to the treatment at 4-month follow-up, while 63% responded at 6-month follow-up, with good responders representing 25% of the treated cohort (Oh et al., 2018). However, Kaplan-Meier analysis of survival, did not find any significant difference between MSC-treated and control groups.

Analysis of cytokines in CSF from patients treated with MSCs showed a reduction in pro-inflammatory cytokines (e.g. TNF- α , MCP-1) accompanied by a shift towards an

anti-inflammatory environment such as increased levels of IL-10 and TGF- β 1. Interestingly, post-hoc analysis of CSF cytokines and long-term effectiveness, showed that in good responders, levels of TGF- β 1 inversely correlated with low MCP-1 levels. This correlation pattern was not found in poor responders, suggesting the use of the inverse correlation between levels of TGF- β 1 and MCP-1 as a potential biomarker to predict treatment response (Oh et al., 2018).

1.6.6.4 Brainstorm Cell Therapeutics trials: autologous NurOwn[®] MSC-NTF cells

Brainstorm Cell Therapeutics, a privately owned biotech company founded in Israel, optimized and patented a method to differentiate human BM-MSCs into astrocyte-like cells capable of secreting enhanced levels of neurotrophic factors (MSC-NTF), but at the same time able to preserve the MSC immunomodulatory properties (Gothelf et al., 2014, Bahat-Stroomza et al., 2009, Sadan et al., 2008). These cells and their scalable manufacturing process are registered under the name of NurOwn[®] technology and showed promising results in animal models of Parkinson's disease, Huntington's disease and autism (Perets et al., 2017, Sadan et al., 2009, Sadan et al., 2012). Compared to MSC obtained from the same donor, following differentiation MSC-NTFs secrete significantly enhanced levels of GDNF, BDNF, VEGF and hepatocyte growth factor (HGF) (Gothelf et al., 2017).

Recently, the results from phase 1/2 and 2a clinical trials testing the safety profile and effects of MSC-NTFs in ALS patients were published. In the phase 1/2 trial, 12 ALS patients were randomized to receive one intrathecal injection (IT) of 1×10^6 cells/Kg (n=6), or to receive intramuscular injections (IM) in 24 separate sites into biceps and triceps (1×10^6 cells per site, n=6) (Petrou et al., 2016). In the phase 2a trial, 14 patients were injected with escalating doses (3 doses) of MSC-NTFs both IT and IM, with the maximum cell dosage being 2×10^6 cells/Kg IT and 48×10^6 cells IM (Petrou et al., 2016). In both studies, patients were followed at 3 and 6-months after transplantation. No serious adverse effects related to the treatment were encountered in either clinical trial stages, with most of the adverse effects observed being mild and transient (up to 72h following transplantation). Although a control group was not included in the studies, patients that received IT injection or IT+IM injections of MSC-NTFs, but not patients receiving only IM transplantation, showed a significant reduction in the rate of disease progression (changes in ALSFRS-R score and predicted FVC) during the 6-month follow-up, compared to the 3-month run-in period preceding the treatment (Petrou et al., 2016). Post-hoc analysis identified a total of

16 patients (89%) and 13 patients (87%) as good responders to the therapy at 3-month and 6-month follow-up respectively.

Based on the results from these two open-label trials, a phase 2 randomized, placebo controlled, double-blind trial (NCT02017912) testing 1 single IT dose of MSC-NTFs was performed on 48 ALS patients. The results of the study were presented at the 70th Annual Meeting of the American Academy of Neurology (Los Angeles, USA, 2018). The treatment met the primary safety outcomes and showed a reduction in the rate of ALS progression compared to the placebo group. Interestingly, the authors reported that the effect was statistically significant in a subgroup of patients with rapid disease progression, but not in slowly progressive disease (Kern et al., 2018). Analysis of CSF markers evidenced increased concentration of VEGF and decreased levels of MCP-1 which correlated with ALSFRS-R slope improvement in treated patients. A phase 3, placebo controlled (1:1) multicenter trial is now enrolling patients (n=200) to evaluate the efficacy of repeated (n=3) intrathecal injections of MSC-NTFs (NCT03280056).

1.7 Adipose tissue: a fat tissue source for mesenchymal stem cells

Mesenchymal stem cells represent an ideal source of adult stem cells for cell therapy given their immunosuppressive nature, low potential for immunogenicity and trans-differentiation capacity. However, the collection of MSC from bone marrow is an invasive procedure which can be painful and anaesthesia is often required (Zuk et al., 2001). Moreover, the proportion of stem cells within the total cell population in bone marrow aspirate is usually about 0.001-0.002% which leads to extended culture times and increased expense in order to obtain sufficient GMP cells for clinical application (Zuk et al., 2001).

Subcutaneous (buttocks and abdomen) and visceral (omentum) white adipose tissue (WAT) may represent an alternative source of stromal adult stem cells since they can be obtained by minimally invasive, simple procedures such as liposuction or lipectomy and they are relatively abundant, representing 1% of WAT cells after processing (Zuk et al., 2001, Meyer et al., 2015, Baglioni et al., 2009). Several names and abbreviations have been used to refer to adipose-derived mesenchymal stem cells. Here, the abbreviation ADSC will be used. In spite of some differences in the expression of a cluster of differentiation (CD) markers such as CD49d and CD106, ADSC cells are phenotypically similar to BM-MSC cells, showing fibroblast-like morphology, characteristic expression of mesenchymal stem cell markers (CD44⁺, CD105⁺, CD73⁺, CD90⁺, CD29⁺, CD45⁻, CD34⁻, CD14⁻ CD19⁻), lack of major

histocompatibility complex class II (MHC-II) and the capacity to differentiate into osteoblasts, chondrocytes and adipocytes in specific culture conditions (Zuk et al., 2001). Thus, hADSCs comply with all the minimum criteria for the characterization of hMSCs, established in 2005, by the International Society for Cellular Therapy (ISCT) (Dominici et al., 2006). Like MSCs obtained from bone marrow aspirates, hADSCs secrete several soluble factors such as BDNF, NGF, HGF, VEGF, IGF-1 and bFGF that may contribute to neurotropism, neuroprotection and tissue regeneration by paracrine mechanisms (Han et al., 2014). Moreover, hADSCs showed a greater proliferation capacity *in vitro* than hBM-MSCs both pre- and post-cryopreservation, showing signs of senescence after 30 passages in culture opposed to 20 passages for hBM-MSC (Han et al., 2014).

Even though the literature appears controversial, there is evidence supporting the potential of ADSCs to trans-differentiate into progenitors or mature cells of ectodermal origin, therefore opening the way to a future investigation of the feasibility of cell replacement in neurodegenerative disorders (Safford et al., 2002; Krampera et al., 2007; Ahmadi et al., 2012; Feng et al., 2014).

1.7.1 In vitro neuronal differentiation capacity of ADSCs

The capacity of ADSCs to differentiate *in vitro* into mature, stable and functional neurons is an open field of debate among researchers. Usually, the differentiation protocol consists of expanding ADSCs as adherent cells for several passages, followed by induction with media containing different cocktails of chemical agents, cytokines and growth factors (Safford et al., 2002, Zuk et al., 2002, Ashjian et al., 2003, Krampera et al., 2007, Jang et al., 2010).

A different method to obtain neuron-like cells from ADSCs is based on neurosphere formation capacity, generally achieved by culturing cells in epidermal growth factor (EGF) and bFGF conditioned serum-free media (Qian et al., 2010, Ahmadi et al., 2012). A neurosphere is a cluster of cells containing neural precursors able to proliferate and survive as floating and non-adherent structures. The neurosphere can be dissociated, seeded onto a poly-L-lysine feeder layer and differentiated by adding neuronal induction components (Qian et al., 2010, Ahmadi et al., 2012, Feng et al., 2014). Alternatively, ADSCs are cultured in the presence of ESCs or Schwann cells either in the presence or absence of induction factors (Krampera et al., 2007, Bahmani et al., 2014). In particular, when co-cultured with Schwann cells, ADSCs showed long-lasting (12 days) Schwann-like cell morphology and expression of myelin protein (Krampera et al., 2007). Pre-irradiation of Schwann cells excluded

eventual cellular fusion artefacts (Krampera et al., 2007). Since the addition of supernatant from Schwann cell cultures failed to differentiate ADSCs, the authors speculated that the addition of specific chemical components or growth factors to the ADSC cultures, may promote the initial steps toward differentiation *in vitro*, which can be completed in the appropriate microenvironment and by required cell-to-cell interaction with mature cells *in vivo*.

The trans-differentiation of ADSCs towards motor neuron-like cells has also been reported. In 2012, Abdanipour and Tirahini (Abdanipour and Tiraihi, 2012) induced rat ADSCs to trans-differentiate into motor neuron-like cells by a two-step protocol. ADSCs were committed to neural progenitors expressing nestin, neurofilament 68 and neuro D by pre-induction for 24h with selegiline. Selegiline is an inhibitor of monoamine oxidase B (MAO-B) which was used to trans-differentiate BM-MSCs into dopaminergic neural-like cells and proved to be a safer pre-inducer in comparison to the toxic β -mercaptoethanol and butylated hydroxyanisole compounds, widely used for ectodermal differentiation of MSC (Abdanipour and Tiraihi, 2012). The maturation of the pre-induced ADSCs into a motor-neuron phenotype was then achieved by incubation with Shh and RA, resulting in a differentiation efficiency of around 70%. The resultant motor neuron-like cells (MNLCS) were characterized by an initial and transient high expression of oligo-2 and islet-1 (markers for early motor neuron commitment during *in vitro* differentiation), followed by a decrease in these two markers accompanied by an increase in the expression of the motor neuron marker HLBX9 (Abdanipour and Tiraihi, 2012). Mature MNLCS, but not high HLBX9 expressing cells, were functionally tested for the capacity to release pre-synaptic vesicles by staining and destaining with the fluorescent probe FM1-43. Quantitative analysis of vesicle release after stimulation, showed a 4-fold increase in comparison to pre-induced ADSCs. MNLCS, also formed innervation-like contacts with myotubes in a co-culture *in vitro* system (Abdanipour and Tiraihi, 2012). Very recently, the same authors proposed a different method to obtain MNLCS from rat ADSCs (Darvishi et al., 2016). ADSCs were first converted into neurospheres by induction with NM medium consisting of DMEM, B27, EGF and bFGF for 7 days. Next, neural stem cells (NSC) were obtained by neurosphere dissociation into single cells, and incubation for 10 days with NM supplemented with 10% FBS. Maturation into motor neurons was achieved by incubation with Shh and RA for 5 days, followed by addition in culture media of BDNF, GDNF, ciliary neurotrophic factor (CNTF) and NT-3 for another 7 days (Darvishi et al., 2016). During the maturation process of ADSC-NSCs into motor neurons, an increase in the expression of insulin gene enhancer protein ISL-1 (islet-

1), homeobox HB9 and choline acetyltransferase (ChAT) was observed, with MN-like cells positive for the neural marker MAP2 at day 14 of maturation. These findings were documented by both immunocytochemistry and RT-PCR. The functional activity of mature MNLCs was investigated by quantification of the release of synaptic vesicles by FM1-43 loading and release experiments upon ion stimulation. The synaptic vesicle activity correlated with changes in intracellular calcium concentration and membrane depolarization, as demonstrated by further investigations utilizing calcium and voltage-sensitive dyes (Darvishi et al., 2016).

Is the trans-differentiation of ADSCs into neurons real?

The differentiation into neurons is commonly described as morphological changes such as body retraction, bi- or multi-polar shape and branching extension, and by the expression of neuronal markers revealed by immunohistochemistry (IHC), western blotting (WB) and quantitative RT-PCR analysis. However, several studies showed that the neural-like phenotype obtained by chemical induction was a very fast but transient event which may be a result of cytoskeletal rearrangement due to the toxicity of compounds added into the induction media (Neuhuber et al., 2004, Lu et al., 2004a). Furthermore, several neuronal markers considered to confirm neuron maturation such as nestin, neuron-specific enolase (NSE), tropomyosin receptor kinase A (trk-A) and vimentin are already present at low levels in undifferentiated ADSCs (Woodbury et al., 2002, Zuk et al., 2002, Ashjian et al., 2003, Feng et al., 2014, Jang et al., 2010). Thus, morphological changes and expression of neuronal markers on the cell surface should not be considered as a definitive proof of neuronal differentiation, and functional characterization (i.e. electrophysiology) is necessary. However, very few studies confirmed electrical activity of ADSC-derived neurons by patch-clamp experiments (Jang et al., 2010, Feng et al., 2014). In addition, the efficiency and reproducibility of differentiation protocols described in the literature is low, and neuronal induction of ADSCs gives rise to a heterogeneous population of undifferentiated cells, neuron-like cells and astroglial-like cells with different degrees of maturation (Jang et al., 2010, Krampera et al., 2007). Together with the fact that untreated ADSCs often show slight expression of neuronal progenitor markers, these results suggest the presence of specific cell subtypes with different neuronal differentiation potential (Fu et al., 2008). This is supported by the existence of variability in the secretome of hADSCs obtained from different donors and maintained in separated cultures (Kalinina et al., 2015)

1.7.2 Proof-of-concept for ADSC therapy in the SOD1^{G93A} model of ALS

For the first time in 2013, the therapeutic potential of ADSCs was investigated in the SOD1^{G93A} mouse model (Marconi et al., 2013). ADSCs were isolated from C57BL/6 GFP-expressing mice, and a total of two million cells were injected into the tail vein of B6SJL-SOD1^{G93A} mice after the first clinical signs of disease. The control group received injection of PBS only as vehicle. mADSCs delayed the motor performance decline and transiently attenuated motor neuron death, in comparison to the controls. However, no differences in astrogliosis levels, nor in survival were observed between the two groups (Marconi et al., 2013). Even if the authors claimed that GFP-positive cells were found to migrate into damaged CNS areas, such as the grey matter in the spinal cord, low magnification images of grafted cells were not shown and histology on PBS-treated control spinal cord sections was not performed. Finally, increased levels of trophic factors such as GDNF and bFGF were found in spinal cord homogenates of ADSC injected mice. Interesting, since mADSCs in this study were not capable of producing GDNF *in vitro*, it is likely that in addition to trophic factor production and secretion, ADSCs could have an indirect biological effect by stimulating the secretome of surrounding astrocytes, which are known to produce GDNF (Marconi et al., 2013).

Another group tested the therapeutic potential of human ADSCs isolated from three healthy donors aged 64, 69 and 84 (Kim et al., 2014b). Female transgenic SOD1^{G93A} mice before clinical evidence of disease received 1×10^6 of hADSCs by intravenous (IV) or 2×10^5 hADSCs by intracerebroventricular (ICV) injections. As a control, the sham group received PBS only. Rotarod test and paw grip endurance were monitored as behavioural tests and their reduction by 15% was considered as disease onset. The endpoint (survival) was defined by the lack of a righting reflex within 30 seconds after being placed on their side (Kim et al., 2014b). The authors found that disease onset in mice that received ICV injections was significantly delayed by 26 days, while in mice infused IV there was only an 11 day delay in disease onset. Remarkably, survival was prolonged by 24 days and 9 days respectively in ICV and IV mice when compared to the controls (Kim et al., 2014b). IHC evaluation of the spinal cord of ICV transplanted mice revealed that 6.8% of transplanted cells survived up to 4 weeks post-injection. However, only 0.7% migrated to the grey matter of the lumbar spinal cord and very few cells were positive for neuronal markers (MAP2 or I-NFM). In contrast, after IV infusion very few undifferentiated cells were found to engraft in the meninges of the spinal cord (Kim et al., 2014b). In addition, terminal deoxynucleotidyl transferase dUTP nick end labeling (TUNEL) assay performed on spinal cord from

ICV mice showed reduced levels of apoptosis in the anterior grey matter compared to IV and control recipients. Also, RT-PCR and ELISA assays on spinal cord homogenates showed a significantly higher concentration of neurotrophins in the ICV group in comparison to controls (Kim et al., 2014b). ELISA assay on the supernatant from hADSCs cultures showed high levels of neurotrophic factors that are relevant in neuroprotection such as IGF1 and VEGF (Kim et al., 2014b). The anti-apoptotic effect was further confirmed *in vitro* by culturing primary neural cells from normal mice with hADSC conditioned media. (Kim et al., 2014b).

To date, these are the only two published studies using ADSCs in an experimental model of ALS. However, the therapeutic potential of ADSCs has been tested in other neurodegenerative experimental models. In particular, the use of ADSCs showed encouraging results in animal models of chronic stroke, Parkinson's disease, Alzheimer's disease, traumatic brain injury and ageing (Kim et al., 2007, Park et al., 2013, Yan et al., 2014, Schwerk et al., 2015).

1.7.3 ADSCs in ALS: clinical trials

Few clinical trials have tested or are currently investigating the safety of ADSCs transplantation in ALS patients. In 2016, Staff et al. at the Mayo Clinic (Rochester, USA) published the results of a phase I dose-escalation safety trial in which autologous ADSCs were delivered intrathecally via lumbar puncture in 27 ALS patients (Staff et al., 2016). The intervention consisted of either a single dose or two monthly doses of ADSCs, ranging from 1×10^7 to 1×10^8 cells. The intrathecal transplantation was found to be safe in all participants with only moderate and tolerable side effects such as headache, and back and leg pain from week 1 to week 3 after treatment. However, in some patients receiving the double injection at the highest cell dose, moderate pain was reported to last for up to 2 months. CSF analysis before the treatment, 1 week and 4 weeks after injection, revealed an escalating increase in protein concentration and an increase in the number of monocytes from baseline to week 1, which began to normalize at week 4 (Staff et al., 2016). MRI of brain and spinal cord 3 weeks after transplantation revealed nodular abnormalities, reminiscent of arachnoiditis, in the lumbosacral nerve roots of patients receiving the highest cell dose. However, autopsies from 4 patients, including 3 in which MRI abnormalities were observed, did not show any sign of arachnoiditis or tumour formation (Staff et al., 2016). Based on the results from the phase I study, a phase II open label clinical trial to evaluate safety and efficacy of repeated intrathecal administration of autologous ADSCs is currently recruiting patients (ClinicalTrial.gov

identifier: NCT03268603). In this study, ADSCs will be injected every 3 months for a total of 4 injections starting with a dose of 1×10^8 cells. The study will be performed at the Mayo Clinic in Rochester (USA).

The Andalusian Initiative for Advanced Therapies recently completed the recruitment of 40 ALS patients for a phase I/II, multicentre, randomized, controlled with placebo clinical trial to evaluate the safety and efficiency of intravenous infusion of different concentration of autologous ADSCs (ClinicalTrials.gov identifier: NCT02290886). Patients will be randomized into 4 arms: a placebo group, a group receiving 1 million ADSC/Kg, a group receiving 2 million ADSCs/Kg and a group receiving 4 million ADSCs/kg. The study is expected to be completed in July 2021.

The Kuzma-Kozakiewicz group, is recruiting a total of 30 ALS patients to evaluate the safety and efficacy of 1 intraspinal injection followed by 2 intrathecal infusions of ADSCs to be delivered every 3 months (ClinicalTrials.gov Identifier: NCT03296501).

Finally, a clinical trial sponsored by The Royan Institute in Iran tested the safety of intravenous injections of ADSCs derived from healthy donors (2 million cells/kg) in 19 ALS patients with sporadic disease (ClinicalTrial.gov identifier: NCT02492516). The study was completed in 2016, however, no results have been published to date.

1.8 MSCs for ALS therapy: summary of proposed mechanisms of action

The *in vitro* differentiation of mesenchymal stem cells into neuron-like cells brought great enthusiasm into the idea of cellular replacement as a therapeutic strategy in ALS. However, there are many practical issues to be solved. The real trans-differentiation of MSCs into neurons has been questioned and further investigation in order to study molecular pathways and optimized protocols enhancing the efficiency, stability and degree of maturation are needed. Also, only a few studies have reported MSCs showing signs of *in vivo* maturation when transplanted into mice (Boucherie et al., 2009, Vercelli et al., 2008). More importantly, for therapeutic efficacy, the transplanted cells should engraft, migrate to affected areas of degeneration, survive, mature and integrate into the pre-existing neuronal circuits forming synapses, extending long axon projections to reach muscles and regenerating neuromuscular junctions. All this must occur within a hostile microenvironment where other motor neurons are dying and activated microglia and astrocytes are sustaining an inflammatory milieu (Feeney et al., 2001, Alexianu et al., 2001). Moreover, different pathological mechanisms described in ALS such as glutamate excitotoxicity (Alexander et al., 2000), oxidative stress (Barber and Shaw, 2010) and loss of

metabolic support (Ilieva et al., 2009) may affect the viability of transplanted cells and inhibit maturation. Finally, stem cell maturation and integration into the host neuronal circuits could take a relatively long time, which may not be compatible with the fast progression rate of the disease.

Besides the challenge of cell replacement in ALS, in recent years increased attention has been paid to the “bystander effect” mechanism through which MSCs could exert their therapeutic effect. Different mechanisms have been proposed to explain the role of MSCs in neuroprotection. Although the precise mechanisms are still unknown, the secretion of anti-inflammatory cytokines and growth factors by MSCs may influence the progression of ALS in multiple ways, including endogenous regenerative processes such as neuronal plasticity, angiogenesis and axonal re-myelination (Kingham et al., 2014, Forostyak et al., 2014). The delivery of growth factors such as BDNF, IGF-I, VEGF and GDNF into ALS experimental models has been very promising since these factors were shown to be neuroprotective, improved motor function and prolonged motor neuron survival (Henriques et al., 2010). However, translation into the clinic failed to provide any beneficial effect in ALS patients (Henriques et al., 2010). This is thought to be related to the small amount of growth factor that effectively reached the CNS either because of an inability to cross the blood brain barrier or because of the short half-life after intravenous injection (Henriques et al., 2010). Moreover, intrathecal injections of growth factors did not result in relevant benefits for ALS patient (Henriques et al., 2010).

The use of MSCs as “carriers” for the uninterrupted supply of growth factors has been proposed, having shown positive results in an ALS rodent model (Krakora et al., 2013, Knippenberg et al., 2012a). Indeed, MSCs transduced to overexpress specific growth factors (GDNF, VEGF) or neuroprotective agents (*e.g.* glucagon-like peptide 1) transplanted into SOD1^{G93A} rodent models, significantly preserved neuromuscular junctions, attenuated motor neuron death, improved motor function, delayed symptom onset and prolonged survival (Krakora et al., 2013, Knippenberg et al., 2012a). Through paracrine activity and cell-to-cell contacts, MSCs were able to induce astrocytes and glial cells to secrete enhanced levels of GDNF, VEGF and CNTF both *in vitro* and in the SOD1^{G93A} mice, resulting in anti-apoptotic effects and motor neuron protection (Marconi et al., 2013, Sun et al., 2013).

Another potential mechanism by which MSCs could participate in tissue repair, is in the secretion of exosomes (Han et al., 2016). The content of exosomes, after their secretion from stem cells, could be transferred to neighbouring cells and mediate a

plethora of biological pathways from free radical scavenging to the activation of self-regenerative programmes (Bonafede et al., 2015). The neuroprotective potential of MSC-derived exosomes seems to be mainly mediated by the presence of miRNAs cargos, that once transferred to neurons, have the potential to regulate several functions including inhibition of apoptotic pathways, reduction of glutamate release and enhanced neuroplasticity (Galieva et al., 2019). Moreover, exosomes derived from MSCs possess immunomodulatory properties, for example the capacity to stimulate regulatory T cell proliferation, suppress the release of TNF- α , INF- γ and IL-1 β , and promote the skewing of type 1 T helper cells (pro-inflammatory Th1) towards type 2 T helper cells (anti-inflammatory Th2) (Galieva et al., 2019). Interestingly, exosomes derived from murine adipose derived stem cells (ADSCs), were able to protect both naïve and SOD1^{G93A} transfected NSC34 motor neuron-like cells from oxidative stress in an *in vitro* culture system, with a significant reduction of apoptotic events and an increase in cell viability (Bonafede et al., 2016). In addition, exosomes derived from human ADSCs showed the ability to reduce SOD1 protein aggregation in neuronal cells obtained by *in vitro* differentiation of NSCs, which were previously isolated from adult SOD1^{G93A} mice (Lee et al., 2016b).

MSCs may act by modulating astrocyte dysfunction since they showed the ability to induce expression of glutamate re-uptake transporter 1 (GLT1) and inhibit caspase-3 cleavage in SOD1^{G93A} mutated astrocytes, thus limiting excitotoxicity (Gu et al., 2010). Several studies on experimental models of ALS demonstrated the capacity of MSCs to attenuate astrogliosis (Zhou et al., 2013, Vercelli et al., 2008, Boido et al., 2014). When transplanted into SOD1^{G93A} mice, MSCs may exert immunomodulatory effects indirectly by stimulating host cells to secrete anti-inflammatory interleukins (IL) such as IL-10, IL-3 and IL-13 (Boido et al., 2014). Intrathecal delivery of hMSCs into SOD1^{G93A} mice slowed disease progression, but increased lymphocyte infiltration into the spinal cord (Kwon et al., 2014). However, hMSCs cultured with peripheral blood mononuclear cells (PBMC) derived from ALS patients increased the proportion of regulatory T cells accompanied by enhanced production of anti-inflammatory cytokines such as IL-4, IL-10 and TGF β (Kwon et al., 2014). Thus, when injected into the CSF of ALS mice, MSCs could exert their beneficial immunomodulation by stimulating regulatory T cell proliferation, activation and migration to areas of CNS inflammation (Kwon et al., 2014). MSCs were shown to inhibit maturation and activation of dendritic cells *in vitro*, and prevent lymphocyte migration into the spinal cord of experimental autoimmune encephalomyelitis mice (Zappia et al., 2005, Ramasamy et al., 2007). MSCs were also able to suppress proliferation, maturation

and activation of pro-inflammatory Th1 and Th17 cells, with a concomitant switch toward active CD4⁺ CD25⁺ Foxp3 regulatory T cells *in vitro* (Luz-Crawford et al., 2013).

T regulatory cells are reduced in patients with aggressive ALS and reduced levels of these cells in early disease correlates with rapid progression of neurodegeneration (Henkel et al., 2013). Interestingly, peripheral blood monocytes obtained from ALS patients 4h and 24 h after an intravenous infusion of MSCs, showed a dramatic increase in CD4⁺ CD25⁺ regulatory T cells, coupled with a reduction in activated dendritic cells and lymphocyte proliferation (Karussis et al., 2010).

The establishment of a sustained pro-inflammatory milieu in ALS spinal cord has been demonstrated which is probably accompanied by a shift of microglial cells from an anti-inflammatory state (often referred to as M2 in the literature) to an active neurotoxic state (often referred to as M1 in the literature) (Brites and Vaz, 2014). Of interest, MSC-conditioned media significantly inhibited the production and secretion of pro-inflammatory cytokines in microglia activated by LPS (Ooi et al., 2015) (Noh et al., 2016). This, has been attributed to the capacity of MSCs to secrete TGF- β , which in turn inhibited the NF κ B pathway and restored a protective microglial phenotype (Noh et al., 2016). Thus, through paracrine effects, MSCs could modulate the functional properties of microglia by switching the detrimental activated microglial state to the beneficial activated microglial state after LPS induction (Noh et al., 2016). Therefore, the immunomodulatory properties of MSCs may play an important role in attenuating neuroinflammatory processes during the progression of ALS and further work is needed in order to explore this specific mechanism. An overview of the potential beneficial effects that MSCs could exert in modulating pathophysiology in neurodegenerative conditions is summarized in figure 1.2.

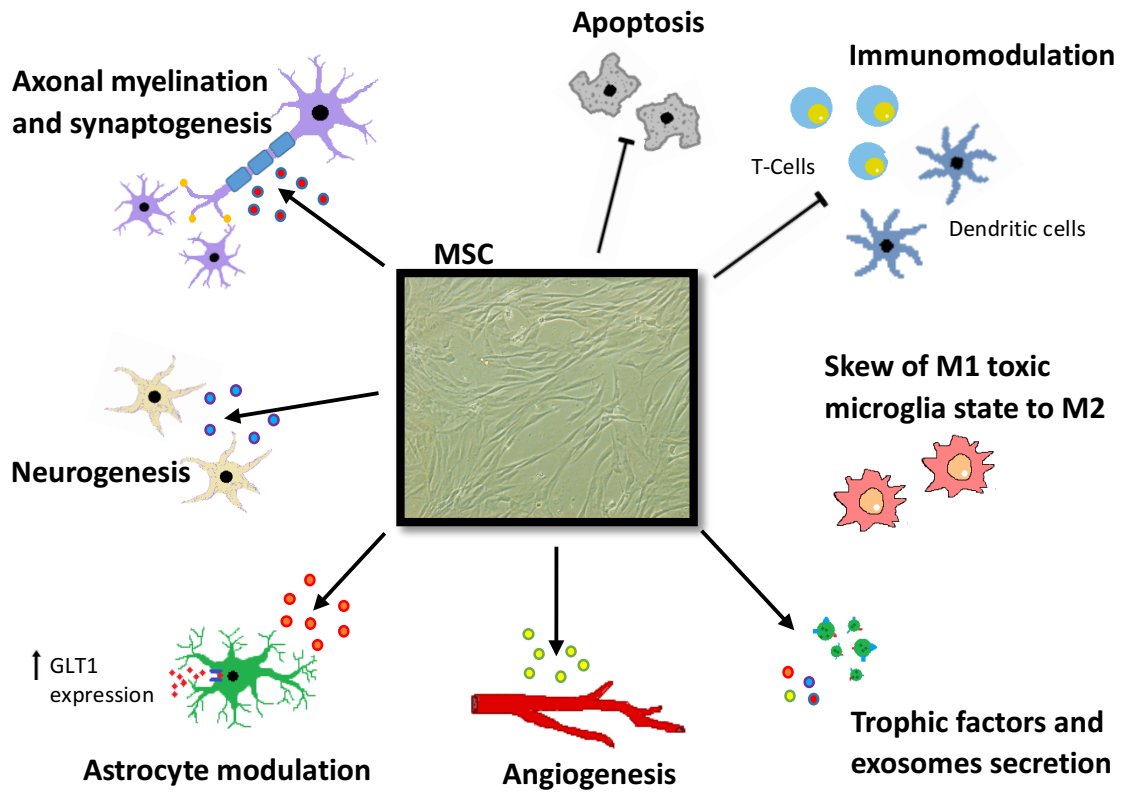


Figure 1.2. Potential mechanisms of mesenchymal stem cell efficacy in neurodegeneration. Transplanted MSCs may provide therapeutic responses through paracrine effects and cell-to-cell contacts with resident neural cells. The capacity of MSCs to secrete cytokines, growth factors and exosomes could potentially induce and support regeneration processes, including angiogenesis, synaptogenesis, axonal re-myelination and neurogenesis. Because of their immunomodulatory properties, MSCs could attenuate inflammatory responses in the central nervous system by inhibiting maturation and migration of dendritic cells, suppression of lymphocyte activation and proliferation, and by reducing gliosis. Moreover, MSCs possess anti-apoptotic properties, and may limit excitotoxicity by modulating astrocyte functions.

1.9 Summary and Hypothesis

ALS is an adult-onset, fast progressive fatal disease with unmet medical needs. Although the selective death of motor neurons is considered as the main pathological feature of ALS, it is widely established that non-neuronal neighbouring cells such as astrocytes, microglia and oligodendrocytes play an important role during the progression of the neurodegenerative process. Moreover, it is well established that a sustained pro-inflammatory milieu in ALS spinal cords is accompanied by the shift of glial cells from an anti-inflammatory state to an active neurotoxic state (Brites and Vaz, 2014). A myriad of molecular mechanisms are thought to be implicated in ALS pathology, however, due to the heterogeneous nature of the disease, single drugs or target treatments have failed to translate into clinical benefits for ALS patients.

The development of a cell-based therapy could provide a broad therapeutic approach, by targeting different pathways and by alleviating the toxic spinal cord milieu. Given their immunosuppressive nature, neuroprotective properties and trans-differentiation capacity, mesenchymal stem cells (MSCs) have raised great enthusiasm as a potential therapeutic strategy in ALS patients. Moreover, MSCs display low immunogenicity, thus potentially allowing both allogenic and autologous cell transplantation. Injection of bone marrow (BM) derived MSCs into the SOD1^{G93A} ALS mouse model has been shown to transiently preserve motor neurons, delay onset of motor symptoms, reduce neuroinflammation and extend survival (Lewis and Suzuki, 2014). It is likely that the observed positive effects are the results of the paracrine activity of MSCs, which through the secretion of a plethora of bioactive soluble factors are able to modulate the toxic micro-environment that leads to neuronal loss. However, bone marrow represents a difficult source in order to obtain clinically relevant numbers of cells for human transplantation. Adipose derived stem cells (ADSCs) may represent a better option for clinical translation, given their abundance, biological characteristics and higher proliferation capacity *in vitro*.

It is hypothesised that treatment with ADSCs can improve motor performance and delay disease onset in the SOD1^{G93A} animal model of ALS, by immunomodulation and neurotrophic support to neurons and surrounding non-neural cell components.

One of the major challenges in the development of cell-based therapies in ALS is to safely and efficiently deliver stem cells into the CNS. The injection of stem cells directly into the CSF surrounding the spinal cord by intrathecal injection may represent a safe and valid route of administration. Indeed, through a minimally

invasive intervention, the injected cells may be able to survive, migrate and home close to areas of degeneration.

Therefore, it is hypothesised that injection of ADSCs into the CSF of SOD1^{G93A} mice via the Cisterna Magna, may represent an efficient delivery route for cell homing to degenerative areas within the parenchyma of the spinal cord.

Amongst several mechanisms by which ADSCs may provide therapeutic benefit in ALS, the capacity of these cells to modulate glial functions has been proposed. In particular, MSC conditioned media showed the ability to reduce the inflammatory signature of microglia and to improve the glutamate uptake functions of ALS astrocytes.

It is hypothesised that by modulating astroglial functions, ADSCs may limit ALS-linked astrocyte toxicity towards motor neurons.

1.10 Aims and Objectives

Aim:

The overall aim of this project is to investigate the therapeutic potential of ADSCs as a cell therapy strategy for ALS. This, will be evaluated both *in vivo* by using the SOD1^{G93A} transgenic mouse model of ALS, and *in vitro* by using novel and well characterised models of ALS.

Objectives:

- To isolate, expand and characterise ADSCs derived from C57BL/6 Ntg mice.
- To investigate the fate of engrafted GFP-labelled mADSCs in SOD1^{G93A} mice after intrathecal injection.
- To investigate the effect of ADSC transplantation in pre-symptomatic SOD1^{G93A} mice by evaluating motor function, disease onset and pathology.
- To investigate whether ADSCs are able to protect MNs from ALS-linked astrocyte toxicity *in vitro*, and from this, ascertain the potential molecular mechanisms of protection.
- To stably overexpress the human C-C chemokine receptor 2B (hCCR2B) on the cell surface of human ADSCs, and ensure that they retain their ADSC character.

2 Materials and Methods

2.1 Ethics statement

All experiments involving mice were conducted in accordance with the animal (Scientific Procedures) Act 1986 under the UK Home Office project licence number 40/3640 approved by the Sheffield University Ethical Review Committee Project Applications and Amendments Sub-Committee and by the UK Animal Procedures Committee (London, UK).

2.2 Mouse Adipose Derived Stem Cells

2.2.1 Isolation of mouse Adipose Derived Stem Cells (ADSCs)

Mouse adipose derived mesenchymal stem cells (mADSCs) were obtained from 8- to 12-week-old non-transgenic C57BL/6J mice. The procedure for the isolation of mADSCs was adapted from previous studies (Marconi et al., 2013, Cao et al., 2015) (figure 2.1) as follows. Mice were sacrificed by cervical dislocation, and inguinal (subcutaneous) fat pads were aseptically removed and collected into a 50 ml Falcon tube containing sterile ice cold Hank's Balanced Salt Solution with Ca^{++} and Mg^{++} (HBSS, Gibco) and 50 U/ml penicillin-streptomycin (Pen/Strep, Lonza). From the inguinal adipose tissue lymph nodes were carefully excised and eliminated to avoid leukocyte contamination. After tissue collection, all procedures were performed under sterile conditions in a class 1 flow cabinet.

The adipose tissue was extensively washed at room temperature (RT) with HBSS, transferred into a 100 mm² culture dish and weighed. The fat was then minced into small pieces (1-3 mm³) by using sterile scissors and scalpel blades and re-suspended in an equal volume of 37°C pre-warmed HBSS containing 1 mg/ml collagenase type I (C0130, Sigma), 2% (w/v) Bovine Serum Albumin (BSA) and 50 U/ml penicillin-streptomycin (Lonza) for extracellular matrix digestion. The suspension was then transferred into a sterile 50 ml falcon tube and incubated at 37°C in a water bath for 60-90 minutes, with gentle manual shaking every 5-10 mins, until the tissue appeared smooth on visual inspection. At the end of the incubation period, the collagenase enzymatic activity was neutralized with an equal volume of HBSS containing 10% foetal bovine serum (FBS). The resulting homogenate, containing the cell suspension, was filtered through a 70 µm sterile mesh cell strainer (Fisher) to remove debris and undigested tissue. The solution was then centrifuged at 400g for 5 minutes at RT to obtain a high density dark red pellet, representing the so-called stromal

vascular fraction (SVF) containing ADSCs. Complete separation of the SVF from mature adipocytes was performed by shaking the tube vigorously by hand for 10 seconds, followed by another centrifugation step. Next, the top yellow layer containing mature adipocytes and oil, and the remaining supernatant containing pre-adipocytes, was carefully aspirated and discarded without disturbing the cell pellet. Following a washing step in HBSS, the dark red pellet was re-suspended in 10 ml of red blood cell (RBC) lysis buffer (160 mM NaH₄Cl, 14 mM NaHCO₃, 0.1 mM EDTA; pH 7.3) and incubated at RT in the dark for 7 minutes to lyse contaminating red blood cells. The buffer activity was neutralized with 10 ml of DMEM-10% FBS, the cell suspension filtered through a 70 µm cell strainer and centrifuged at 400g for 4 minutes at RT. The resultant white stromal cell pellet, tightly packed at the bottom of the tube, was re-suspended in complete ADSC culture media consisting of DMEM (with 4500 mg/L glucose, L-glutamine, and sodium bicarbonate) supplemented with 10% (v/v) heat-inactivated FBS and 50 U/ml Pen/Strep.

Cells were counted using a haemocytometer and seeded into 25 cm² (T25) or 75 cm² (T75) tissue culture NuncTM Cell Culture Treated EasyFlasksTM (Thermo Fisher Scientific) at a concentration of 30-40 X 10⁴ cells/cm² and incubated at 37°C with 20% O₂, 5% CO₂ and 95% humidity. Twenty four hours after plating, the non-attached cells and cellular debris were removed by washing twice with 5-10 ml of sterile phosphate buffer saline (PBS) and fresh complete media was added. Cells were then placed back into the incubator for expansion.

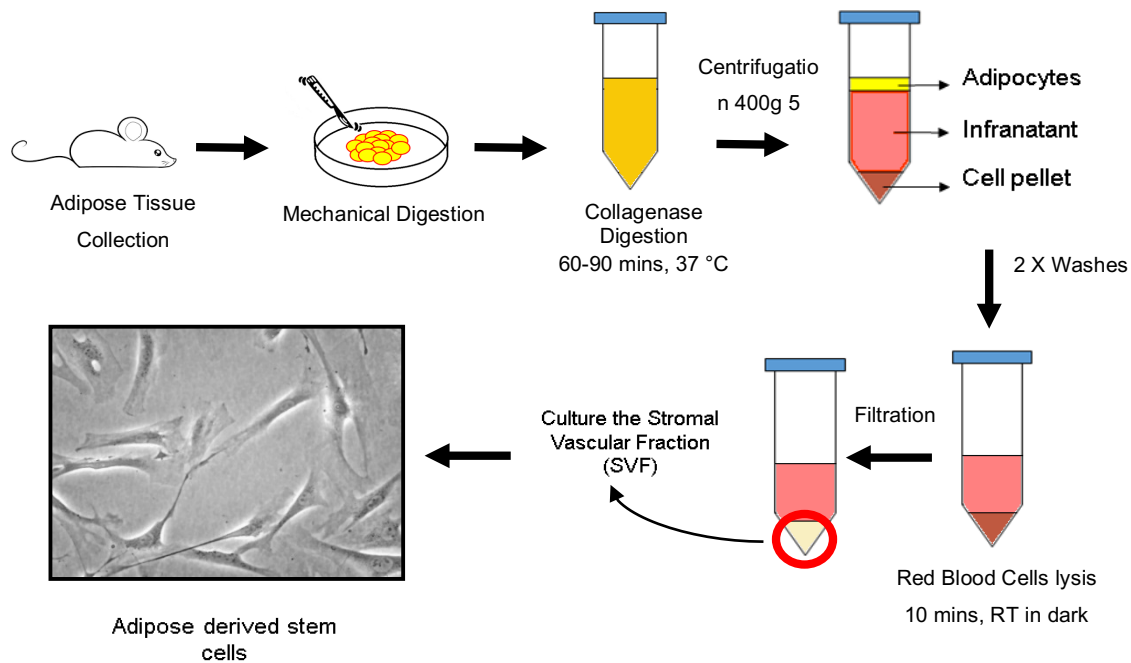


Figure 2.1. Isolation process to obtain ADSCs from C57BL/6 adult mice. Whole adipose tissue is mechanically and enzymatically digested and the SVF is obtained by filtration and centrifugation. Culture of the SVF on standard plastic tissue culture flasks results in the selection and expansion of the adipose stem cell population.

2.2.2 Culture and expansion of mADSCs

All cell culture procedures were performed under sterile conditions in a laminar airflow Class 2 biological safety cabinet. The cell culture working area, including bottles, tissue culture flasks, materials and gloves, were sprayed with 70% industrial methylated spirit and wiped clean. mADSCs were grown in proliferation media consisting of DMEM, containing 10% FBS and 50 U/ml Pen/Strep. The medium was changed every 3 days. When the cultures reached 80-90% confluence, the cells were passaged and placed in new culture flasks for expansion. Cells were washed twice with sterile PBS without $\text{Ca}^{++}/\text{Mg}^{++}$ and incubated with 1X trypsin-Versene (0.5 g/L trypsin 1:250 and 0.2 g/L EDTA, Lonza) for at least 3 minutes at 37°C. For efficient dissociation of the adherent cells from the culture surface, the flask was tapped firmly on each side several times. The trypsin activity was neutralized with an equal volume of complete media and cells centrifuged at 400g for 5 minutes at RT. The cell pellet was then re-suspended in complete media for cell counting, and cells plated in new T75 or T175 tissue culture Nunc™ flasks at a seeding density of 5.000 cells/cm².

2.2.2.1 Foetal Bovine Serum Test

Initially, mADSCs were cultured in complete proliferation media containing 10% (v/v) of standard (not of USA origin) FBS (F9665, Sigma). Since one of the main critical factors in culturing ADSCs resides in the choice of the appropriate serum, three different sources of FBS were tested. The different sera tested for the growth of ADSCs are summarized in table 2.1.

Table 2.1. Foetal Bovine Sera tested to support the growth of mADSCs

FBS	Origin	Supplier	Source, lot n°
FBS-SA	South America	Labtech.com	408110
Qualified-FBS	United States	Thermo Fisher- Gibco®	10082139
Mesenchymal Stem Cells-FBS	Mexico	Thermo Fisher- Gibco®	12763012

To define the optimal serum capable of supporting the *ex vivo* expansion of mADSCs, the cell growth kinetics were estimated by calculating the cumulative population doubling levels (PDLs) (Greenwood et al., 2004). PDL represents an estimation of the total number of times that a primary cell population has doubled after *in vitro* isolation, thus containing a more accurate measure of the age of the cell population compared to the “passage number”. Briefly, mADSCs cultured in the presence of the different FBS, were seeded in T-25 flasks at a concentration of 5000 cells/cm². When cultures reached 80-90% confluence, cells were harvested, counted and reseeded in new T25 culture flasks at the same initial density. This procedure was carried out for at least 10 passages or until cells were not able to reach 80% confluence within 2 weeks of repeated (every 3 days) refeeding.

For each passage in culture, the PDL was calculated by using the following formula:

$$PDL = [\log_{10} (N / N_0)] / \log_{10} (2)$$

where N is the number of harvested cells and N₀ is the number of cells seeded to start that subculture. To generate and compare the growth curves, the PDL from each passage were added and plotted on a graph as a function of the time in culture. Also, the population doubling rate (PDR), after 10 passages in culture, was measured as

the maximum number of cumulative PDL divided by the number of days necessary to reach that maximum cumulative PDL (Lee et al., 2016a).

To investigate whether the different types of sera tested for the expansion of mADSCs could affect the cellular phenotype, the cell morphology was monitored microscopically and recorded during each passage in culture. Phase contrast images of mADSCs during culture were visualized with a Leica inverted microscope and images captured with an Apex Minigrab Camera.

2.2.3 mADSC characterisation by flow cytometry

The cell surface phenotype of cultured mADSCs was analysed by flow cytometry (FC). mADSCs were expanded for four to five passages (p4-p5) and characterized for mesenchymal stem cell (CD44, CD90, CD29, CD106, CD105), endothelial (CD31) and haematopoietic (CD34, CD45, CD11b) surface marker expression.

Briefly, when cultures reached 80-90% confluency, cells were lifted with trypsin, centrifuged at 366g for 4 minutes, re-suspended in complete media and viability was determined using the Trypan Blue exclusion method. It is to be noted that cells were not analysed if viability was less than 90%. Cells were re-suspended in ice cold FC buffer, consisting of PBS containing 2% (v/v) of FBS, and aliquoted into micro centrifuge tubes (1.5 ml) at a concentration of 5×10^5 cells/tube. Following 10 minutes incubation on ice, cells were washed with FC buffer by centrifugation at 366g for 3 minutes at 4°C and re-suspended in 100µl of FC buffer. Next, the specific fluorescent-labelled antibody, conjugated with either phycoerythrin (PE), allophycyanin (APC), isothiocyanate (FITC) or phycoerythrin-cyanine7 (PE-Cy7), was added to the sample and the cell suspension was incubated for 30 minutes on ice in the dark.

As a negative control, unstained cells were incubated in the presence of FC buffer alone. For the identification of the specific interaction between antigens and antibodies, cells were stained with an equal concentration of matched fluorescent-labelled isotype control antibodies. The antibodies used for FC analysis were all purchased from Biolegend™ and are summarized in table 2.2. Following the incubation period, cells were pelleted, washed three times with 500µl of FC buffer by centrifugation, re-suspended with 400µl of FC buffer and transferred to 5ml FACS tubes (12 x 75 mm, BD Falcon).

Stained cells were acquired on a BD LSRII FACS instrument (Biosciences Company) and analysed with FlowJo 7.6.1 (FlowJo LLC, Oregon). For analysis, unstained cells were used to set the gates and isolate the single cell population. Forward scatter

(FSC) and side scatter (SSC) parameters were used to exclude debris, doublets and cell clumps. From each sample at least 10,000 single cell events were collected and analysed.

Table 2.2: Fluorescent-conjugated antibodies used for Flow Cytometry

Antibody	Host species	Clone		Concentration
PE anti-mouse CD90.2	Rat IgG2b	30-H123		0.15 µg per 5 x 10 ⁵ cells
PE anti-mouse CD34	Rat IgG2a	MEC14.7		0.13 µg per 5 x 10 ⁵ cells
APC anti-mouse CD31	Rat IgG2a	MEC13.3		0.15 µg per 5 x 10 ⁵ cells
APC anti-mouse CD44	Rat IgG2b	IM7		0.13 µg per 5 x 10 ⁵ cells
FITC anti- mouse/human CD11b	Rat IgG2b	M1/70		0.13 µg per 5 x 10 ⁵ cells
FITC anti-mouse CD45	Rat IgG2b	30-F11		0.15 µg per 5 x 10 ⁵ cells
PE/Cy7 anti- mouse CD106	Rat IgG2a	429 (MVCAM.A)		0.20 µg per 5 x 10 ⁵ cells
PE/Cy7 anti- mouse CD105	Rat IgG2a	MJ7/18		0.50 µg per 5 x 10 ⁵ cells
PE/Cy7 anti- mouse/rat CD29	Armenian Hamster IgG	HMβ1-1		0.50 µg per 5 x 10 ⁵ cells
PE Rat IgG1 Isotype	Rat IgG1	RTK2071		0.25 µg per 5 x 10 ⁵ cells
PE Rat IgG2b Isotype	Rat IgG2b	RTK4530		0.15 µg per 5 x 10 ⁵ cells
PE Rat IgG2a Isotype	Rat IgG2a	RTK2758		0.13 µg per 5 x 10 ⁵ cells
APC Rat IgG2a Isotype	Rat IgG2a	RTK2758		0.15 µg per 5 x 10 ⁵ cells

APC Rat IgG2b Isotype	Rat IgG2b	RTK4530		0.13 µg per 5 x 10 ⁵ cells
FITC Rat IgG2b Isotype	Rat IgG2b	RTK4530		0.15 µg per 5 x 10 ⁵ cells
PE/Cy7 Rat IgG2a Isotype	Rat IgG2a	RTK2758		0.20 µg per 5 x 10 ⁵ cells
PE/Cy7 Armenia Hamster IgG Isotype	Armenian Hamster IgG	HTK888		0.50 µg per 5 x 10 ⁵ cells

2.2.4 In vitro tri-lineage differentiation of mADSCs

To demonstrate the multi-lineage differentiation potential of mADSCs, expanded cells were induced to differentiate into adipocytes, osteocytes and chondrocytes by using conditioned media. mADSCs were induced to differentiate into adipocytes and osteocytes both at early passages (p3), and late passages (p14) in culture, when the cells reached a population doubling level of 15. For chondrogenesis, mADSCs were differentiated only at early passage (p3). Protocols for differentiation were adapted according to the literature (Baglioni et al., 2009, Zheng et al., 2006, Guasti et al., 2012).

2.2.4.1 Preparation and storage of reagents for differentiation media

- Dexamethasone (FW 392.5) (D4902, Sigma-Aldrich):
A 5 mM stock solution was prepared by dissolving 0.0196 g of dexamethasone in 5ml of absolute ethanol and stored at -80°C. Fresh working solution was made by diluting ethanol stock in complete DMEM media to yield 10 µM stock and filtered with sterile 0.2 µm Minisart® syringe filters (17597, Sartorius).
- Insulin, recombinant human (FW 5807.57) (I2643, Sigma-Aldrich):
A 500 µM stock was prepared by dissolving 25 mg of Insulin in 8.61 ml of Earle's Balanced Salt Solution (EBSS, 14155, Life Technologies™, Invitrogen) acidified with 43 µl of 0.005M HCl and sterile filtered with 0.2 µm HT Tuffryn membrane low-protein binding acrodisc syringe filter (PN4192, Pall Life Sciences). Aliquots (0.5 ml) were dispensed in sterile cryovials and stored at -80°C.
- Indomethacin (FW 357.8) (I8280, Sigma-Aldrich):

A 200 mM stock solution was prepared by dissolving 0.5367 g of Indomethacin in 7.5 ml of dimethyl sulfoxide (DMSO) (D2650, Sigma-Aldrich) and sterile filtered with a 0.2 µm Minisart® syringe filter. Aliquots (250 µl) were stored at -80°C in sterile cryovials.

- 3-Isobutyl-1-methylxanthine (IBMX) (FW 222.2) (I5879, Sigma-Aldrich):
A 250 mM stock solution was prepared by dissolving 100 mg of IBMX in 1.8ml of DMSO filtered with a sterile 0.2 µm Minisart® syringe filter. Aliquots (100 µl) were stored at -20°C.
- (+)-Sodium L-ascorbate (FW 198.11) (A4034, Sigma-Aldrich):
1 g of Ascorbic acid was diluted in 20 ml of distilled water (dH₂O) to yield 50 mg/ml stock solution, sterile filtered with a 0.2 µm HT Tuffryn acrodisc syringe filter, dispensed in 250 µl aliquots and stored at -20°C.
- β-Glycerol Phosphate (β-GP) (FW 216.04) (G9422, Sigma-Aldrich):
A 1M stock solution was prepared by dissolving 5.25 g of β-GP disodium salt hydrate in 11.6 ml of pre-heated water and sterile filtered with a 0.2 µm HT Tuffryn acrodisc syringe filter. 1.5 ml aliquots were stored at -20°C.
- Recombinant human transforming growth factor-β1 (TGF- β1) (AF-100-21C, PreproTech):
A 20 ng/µl stock was made by reconstituting 10 µg of lyophilized TGF-β1 in 0.5 ml of 0.1% BSA in dH₂O acidified with 3 µl of 1.2M HCl. The solution was sterile filtered and stored at -80°C.

2.2.4.2 Adipogenic differentiation

mADSCs were grown in complete standard medium. When cultures were 80% confluent, the cells were detached by trypsinization and reseeded at a density of 15,000-20,000 cells/cm² in 12-well culture plates or onto autoclaved 13 mm circular glass coverslip in 24-well plates. After 24 hour of incubation in control medium, or until cultures reached sub-confluence, the culture medium was replaced with the adipogenic induction medium (AIM). The AIM consisted of DMEM supplemented with 10% (v/v) FBS, 50 U/ml Pen/Strep, 1 µM dexamethasone, 1 µM insulin, 200 µM indomethacin and 0.5 mM IBMX. Cells were cultured in AIM for three days. At the fourth day of adipogenic induction, the AIM was switched to the adipogenic differentiation medium (ADM) consisting of DMEM plus 10% (v/v) FBS, 50 U/ml Pen/Strep, 1 µM dexamethasone, 1 µM insulin and 200 µM indomethacin. The medium was changed every three days with fresh ADM prepared each time before

feeding the cells. During the differentiation process, cell morphology was monitored daily by microscopic observation, and documented with the use of the Apex Minigrab Camera. Induction to adipogenic differentiation was carried out for a maximum duration of two weeks. mADSCs growing in parallel with standard complete medium (non-induction of differentiation) were used as a control to check for spontaneous differentiation.

2.2.4.3 Oil Red O staining

Adipogenesis was detected by Oil Red O (O-R-O) staining assay after one and two weeks of adipogenic induction as previously described (Peister et al., 2004). Oil Red O is a lipophilic dye that specifically stains neutral triglycerides and lipids and it is widely used to document intracellular accumulation of fat globules in adipocytes. Oil Red O stock solution (0.5% w/v) was prepared by dissolving 500 mg of Oil Red O powder (1052300025, Merck) in 100 ml of iso-propanol and stored at RT. Working solution was prepared by mixing three parts Oil red O stock with two parts of distilled water (dH₂O), followed by 10 minutes incubation, and filtration through Whatman filter paper. Cells were washed with PBS and fixed with 4% (w/v) paraformaldehyde (PFA) pH 7.4 at RT for 20 minutes. Next, the wells were washed twice with dH₂O for 5 minutes with agitation and stained with O-R-O working solution for 15 minutes at RT. After incubation, cells were washed three times with dH₂O for 5 minutes with agitation and rinsed once in 60% iso-propanol in order to remove any excess stain. Finally, coverslips were mounted face-down on glass slides with 10 µl of aqueous mounting solution (VectaMount™, Vector) and allowed to air dry for at least 5 hours. Images were then captured with an upright Nikon Eclipse Ni microscope. Cells differentiated in the 12-well plates were rinsed with dH₂O and observed under an inverted microscope (Leica) and photomicrographs were acquired with an Apex camera.

2.2.4.4 Osteogenic differentiation

For osteogenic differentiation, mADSCs were plated in 12-well plates or onto circular coverslip in 24-well plates, at a concentration of 30,000 cells/cm². Differentiation was induced when cells were confluent, by replacing the standard medium with DMEM supplemented with 10% (v/v) FBS, 50 U/ml Pen/Strep, 0.1 µM dexamethasone, 50 µg/ml ascorbic acid and 10 mM β-glycerol phosphate. Every three days, cells were fed with freshly made osteogenic differentiation media for a maximum period of four weeks. Parallel cultures of non-induced mADSCs were used as a control for spontaneous differentiation.

2.2.4.5 Alizarin Red S staining

To assess mADSC differentiation toward osteogenic lineage, cells were stained with 2% Alizarin Red S after two, three and four weeks of culture in the induction media. Alizarin Red S staining is the standard biochemical method used to detect extracellular mineralization during differentiation of osteoblasts in culture, which indicates successful *in vitro* bone formation (Wang et al., 2009b). The assay is based on the capacity of the organic red-dye 1,2-dihydroxyanthraquinone, to complex with calcium deposits. The Alizarin Red S staining solution was prepared by dissolving 2g of Alizarin Red S powder (MFCD00013049, Amresco®) in 100 ml of dH₂O, and the pH was adjusted to 4.2 with 0.1% (v/v) ammonium hydroxide (NH₄OH). The solution was filtered through Watman paper and stored at RT in the dark. Cells were gently washed once with PBS and fixed for 30 minutes at RT with a fixation solution consisting of 39.7% (v/v) dH₂O, 59.5% (v/v) acetone and 0.8% (v/v) citrate concentrated solution (sodium citrate tribasic dehydrate 1M). After fixation, cells were washed with PBS and stained with an adequate volume of 2% Alizarin Red S solution for 45 minutes at RT. After the incubation period, cells were washed at least 5 times with dH₂O to remove any trace of free dye and rinsed in PBS. Cells in the 12-well plates were observed under an inverted microscope, while coverslips were mounted on glass slides and visualized with the Nikon microscope.

2.2.4.6 Chondrogenic differentiation

The protocol for chondrogenic differentiation was adapted from Guasti et al., in which chondrogenic differentiation is performed on three dimensional cell pellets (Guasti et al., 2012). Passage 3 mADSCs were detached with trypsin and centrifuged at 300g at RT for 4 minutes. Cells were then counted and 0.5×10^6 cells were aliquoted in 15ml falcon tubes. After a further centrifugation step, the supernatant was removed and pellets re-suspended with 500 µl of chondrogenic differentiation media consisting of DMEM containing 1% (v/v) FBS, 50 U/ml Pen/Strep, 1% (v/v) Insulin-transferrin-selenium (ITS) (1843306, Gibco), 1% (v/v) sodium pyruvate, 50 µg/ml ascorbic acid, 0.1 µM dexamethasone and 10 ng/ml transforming growth factor β1. Cells were then centrifuged at 300g for 3 minutes at RT and tubes placed in an incubator without disturbing the pellet. Media was changed every day for the first 3 days with fresh made medium. From the fourth day onward, medium was changed every 3 days. For non-induced controls, pellets were cultured in the presence of control medium consisting of DMEM, 1% (v/v) FBS and 50 U/ml Pen/Strep.

2.2.4.7 Alcian Blue staining

Differentiation was assessed by Alcian blue 8G (A5268, Sigma) staining three weeks after induction. Alcian Blue is a polyvalent basic dye widely used to stain cartilage tissue because of its affinity for glycosaminoglycans. Cell pellets were washed twice in PBS and fixed in 4% (w/v) PFA at RT for 30 minutes. Pellets were then washed in PBS and cryo-protected in 30% (w/v) sucrose/PBS at 4°C O/N. The next day, pellets were embedded in Optimal cutting temperature compound (OCT) (KMA-0100-00A, CellPath) and rapidly frozen on dry ice soaked in methanol. Frozen pellets were cut with the cryostat at 20 µm thickness and sections were collected on glass slides. The chamber and objective temperature of the cryostat was set at -21 °C. Slides were left at RT for 20 minutes before being dried at 37°C for 30 minutes in order to improve tissue adhesion to the glass. For Alcian Blue staining, tissue sections were incubated for 5 minutes at room temperature with 0.1M HCl in order to bring the pH to 1. Slides were then stained with Alcian blue 1% (w/v) in 0.1M HCl for one hour at RT. After incubation, sections were rinsed in 0.1M HCl, extensively washed with ddH₂O and mounted with Vectashield Antifade mounting medium (H-1400, Vector Laboratories).

2.2.5 Production of EGFP-expressing lentivirus particles

The pLV-SIN-EGFP lentivirus vector was a kind gift from Dr Evangelia Karyka (SITraN, University of Sheffield). pLV-EGFP is a HIV-1 based expression vector in which the transcription of the enhanced green fluorescent protein (EGFP) is driven by the mouse phosphoglycerate kinase (mPGK) promoter. The vector contains all the viral processing elements for the production of self-inactivating (SIN) 3rd generation lentivirus particles. The vector map is illustrated in figure 2.2.

To produce viral particles, HEK 293T cells at early passage (10 to 15) were used. One day before transfection, HEK 293T cells were plated onto 20 petri dishes (10cm) at a seeding density of about 3×10^6 cells/plate and cultured in DMEM, 10% FBS and 1% Pen/Strep. The day after, cells were co-transfected by the calcium-phosphate method with the pLV-SIN-EGFP plasmid together with the 3rd generation packaging plasmids (pCMVΔ8.92, pRSV-Rev, pMDG). For each plate, 13 µg of pLV-SIN-EGFP, 13 µg of pCMVΔ8.92, 3 µg of pRSV-Rev and 3.75 µg of pMDG were combined in a small T25 culture flask and gently mixed to a final volume of 5 ml with sterile ddH₂O. Then, 5ml of 0.5M calcium chloride (CaCl₂) was added dropwise to the DNA solution. The DNA-CaCl₂ solution was successively added dropwise to 10 ml of pre-warmed 2X HBS (280mM NaCl, 100mM HEPES free-acids, 1.5mM Na₂HPO₄, 0.2% dextrose in ddH₂O, pH 7.05) while air bubbling gently with a pipette and incubated for 10

minutes for DNA precipitation. For each HEK 293T plate, 1ml of the DNA solution was added dropwise trying to cover the whole plate. Plates were swirled gently prior to incubation at 37°C, 5% CO₂ overnight. The next morning, the medium containing the precipitated DNA was replaced with 10ml fresh medium and cells incubated for a further 48h before collecting the virus-containing medium (orange/yellow at this stage). The virus-containing medium was then filtered through 0.45 µm filter to remove cells and debris. A high-titre viral preparation was finally achieved by ultracentrifugation at 68,580g for 90 min at 4°C. The virus was finally re-suspended over several hours on ice in 300 µl of 1% (w/v) BSA in PBS, aliquoted and stored at -80°C.

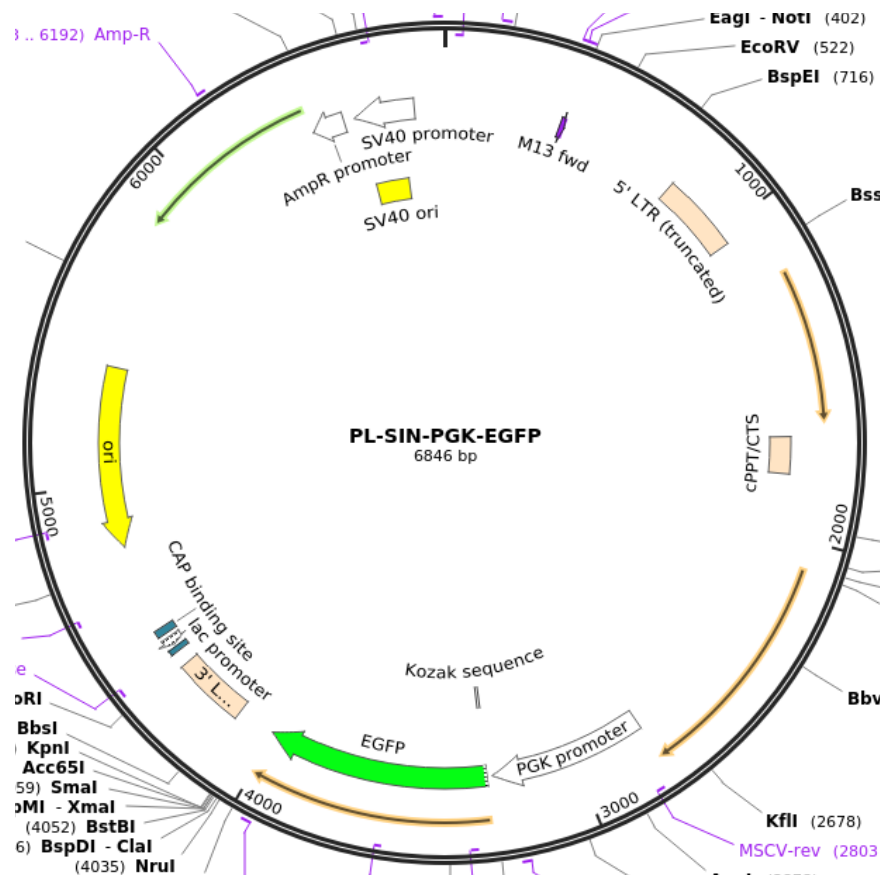


Figure 2.2. pLV-SIN-eGFP lentivirus vector map.

2.2.6 Lentivirus titration by Flow Cytometry

Lentivirus preparations were functionally titred in order to measure infectious viral particles. Virus titre (TU) was calculated by quantifying the number of GFP-positive HeLa cells after transduction with serial dilutions of the concentrated lentivirus. One day before transduction HeLa cells were plated in a 12-well plate at a seeding density of 75,000 cells per well and incubated at 37°C in complete medium (DMEM containing 10% (v/v) FBS and 50 U/ml Pen/Strep). On the day of transduction cells from two representative wells were collected and counted. The lentivirus was thawed on ice and diluted in fresh complete media to the final concentrations corresponding to 10^{-2} , 10^{-3} and 10^{-4} μ l of vector. HeLa cells were infected with 450 μ l of medium containing virus in duplicate for each serial dilution (figure 2.3). Complete medium without virus was used as a negative control. After 6 hours of incubation at 37°C, the medium containing virus was replaced with fresh complete medium and cells left in the incubator.

Three days post-transduction cells were collected by trypsinization, fixed with 4% (w/v) PFA in PBS for 15 minutes at RT, washed in PBS by centrifugation and finally re-suspended in 200 μ l of PBS. Samples were kept on ice until ready to be analysed. Cells were acquired on a BD LSRII FACS instrument (Biosciences Company) and analysis was carried out with FlowJo software (Version 7.6.1). For analysis, unstained cells were used to set the gates and isolate the single cell population. Forward scatter (FSC) and side scatter (SSC) parameters were used to exclude debris and doublets. From each sample at least 10,000 single cell events were collected and analysed. Viral titre was calculated as Transduction Units per mL (TU/ml) using the volume of virus used for infection by applying the formula:

$$\text{Vector titre} = \frac{(\% \text{ positive cells} \times \text{no. of cells during transduction} \times \text{dilution factor})}{\times 2} \text{ TU/ml}$$

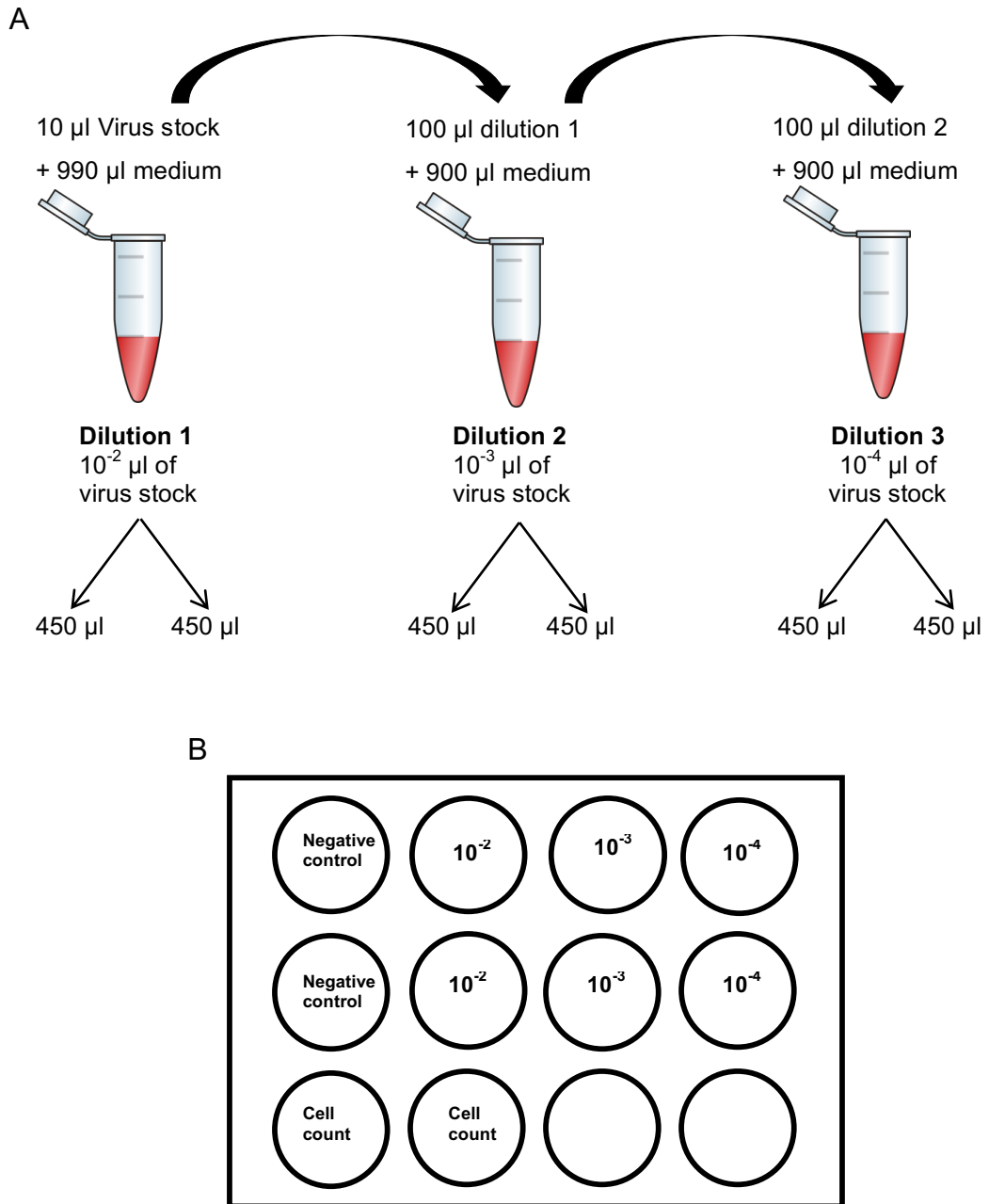


Figure 2.3. EGFP-expressing lentivirus titration. (A) Schematic diagram showing virus stock serial dilutions. (B) Example of 12-well tissue culture plate set up for titration of virus preparation by transduction of HeLa cells.

2.2.7 Transduction of mADSCs and long-term cell storage

mADSCs were transduced with the EGFP-encoding lentivirus for *in vivo* tracking purposes. To optimise the lentivirus transduction efficiency of mADSCS, cells were infected at different multiplicity of infection (MOI) (30, 50, 80, 100) with the EGFP-expressing lentivirus in the presence or absence of 4 µg/ml polybrene (107689, Sigma). Passage 3 mADSCs were seeded at low density (7,000 cells/cm²) in 12-well plates and incubated under standard culture conditions for 16 hours. Cells were then transduced for 7 hours with a final volume of 0.5 ml/well of medium containing virus before adding another 0.5 ml/well of fresh complete medium. After 24 hours, the lentivirus containing medium was replaced with fresh medium and cells left in an incubator for a further 72 hours. Transduction efficiency and cell morphology was monitored daily by fluorescent microscopy before quantification of GFP-positive cells by flow cytometry on PFA fixed cells. An MOI of 30 in the presence of 4 µg/ml polybrene was used in the following experiments as nearly 96% of the cells were positive for GFP and cell morphology was similar to the non-transduced mADSCs.

For long-term cell storage of GFP-mADSCS, cells were transduced at passage 1 and expanded in culture. Passage 3 GFP-mADSCs were grown to 80% confluency and collected for storage. Briefly, cells were lifted with trypsin, washed in PBS by centrifugation and resuspended in freezing medium (80% (v/v) FBS, 10% (v/v) DMEM and 10% (v/v) dimethylsulfoxide (DMSO)) at a concentration of 1 million cells per ml of cryopreservation medium. Cells were then aliquoted in cryovials, labelled and placed in isopropanol freezing container and frozen at -80°C. After 24 hours, cryovials were transferred into liquid nitrogen. To revive GFP-mADSCS, cells were rapidly thawed at 37°C, washed in complete medium by centrifugation and plated at a concentration of 1 x 10⁴ cells/cm². GFP-mADSCs were then grown for one or two more passages before being characterized by flow cytometry and tested for multidifferentiation capacity.

2.3 In vivo therapeutic study

2.3.1 Transgenic C57BL/6J-Tg (SOD1^{G93A})1Gur/J mice

Transgenic C57BL/6J-Tg (SOD1^{G93A})1Gur/J mice of the defined C57BL/6J inbred genetic background were used in this study (Mead et al., 2011). B6SJL-Tg (SOD1-G93A)1Gur/J mice, carrying a high copy number of the human SOD1 with the G93A substitution mutation, were originally obtained from the Jackson Laboratory (stock number 002726). These mice were successively backcrossed with C57BL/6J OIaHsd mice (Harlan, UK) for >20 generations to generate an inbred genetic background (Mead et al., 2011). Since there are not significant differences between males and females in this model, hemizygous transgenic males were bred with wild type females to maintain the SOD1^{G93A} transgene while hemizygous females were used for experiments (Mead et al., 2013). All experimental procedures were conducted in compliance with the Animals (Scientific Procedures) Act 1986 and under a UK Home Office Project Licence (40/3640) approved by the Sheffield University Ethical Review Committee Project Applications and Amendments Sub-Committee and by the UK Animal Procedures Committee (London, UK). The mouse colony was maintained in a specific pathogen free (SPF) environment before being moved for experiments to a conventional animal facility following the Home Office code of practice for the housing and care of animals used in scientific procedures (12h light/dark cycle and room temperature maintained at 21 °C). Each mouse cage was covered with a layer of fine sawdust (eco-pure flakes 6, Datesand, UK) and contained a plastic house and paper wool (Datesand, UK). Female mice from the same litter were housed together in pairs, triplets or quadruplets and rodent diet (Harlan, UK) and water were provided *ad libitum*.

Identification of mice was accomplished by ear clipping and ear tissue used for genotyping. Genomic DNA was extracted from ear tissue by incubation at 65°C for 20 minutes with 30 µl of QuickExtract™ DNA Extraction Soln 1.0 (QE09050, Lucigen), followed by incubation at 98°C for 2 minutes. Transgenic SOD1^{G93A} mice were identified by PCR amplification performed in a 10 µl volume of 5x FIREPol® Master Mix Ready to Load (04-12-00115, Solis Biodyne), 0.5 µl of DNA, 0.5 µM of each of the human SOD1 primer (forward 5'-CATCAGCCCTAATCCATCTGA-3', reverse 5'-CGCGACTAACAATCAAAGTGA-3') and 0.5 µM of each of the mouse interleukin-2 receptor control primer (forward 5'-CTAGGCCACAGAATTGAAAGATCT-3', reverse 5'-

GTAGGTGGAAATTCTAGCATCATC-3'). The PCR reaction mix was run on a thermo cycler machine (G-storm, UK) and the automated cycling was set as follows:

Step	Temperature	Time	
Initial Denaturation	94 °C	5 min	
Denaturation	94 °C	1 min	} 30 cycles
Annealing	60 °C	45 sec	
Elongation	72 °C	30 sec	
Final elongation	72 °C	10 min	
Storage	10 °C	Infinite	

The PCR products (9 µl) were then loaded into the wells of a 2% (w/v) agarose/1x TAE gel containing 1% (v/v) ethidium bromide. For identification of the approximate size of the DNA amplicons, 4 µl of 100bp DNA hyperladder (Bioline) was added to the first well of each gel row. Electrophoresis was performed for 40 min at 105 Volt (V) and bands visualized at ~320bp for mouse IL-2R and ~250bp for hSOD1 when present. Positive and negative controls were used.

The SOD1^{G93A} mice of the defined C57BL/6J inbred genetic background used in this study display a really consistent disease course which is schematized in figure 2.4 (Mead et al., 2011).

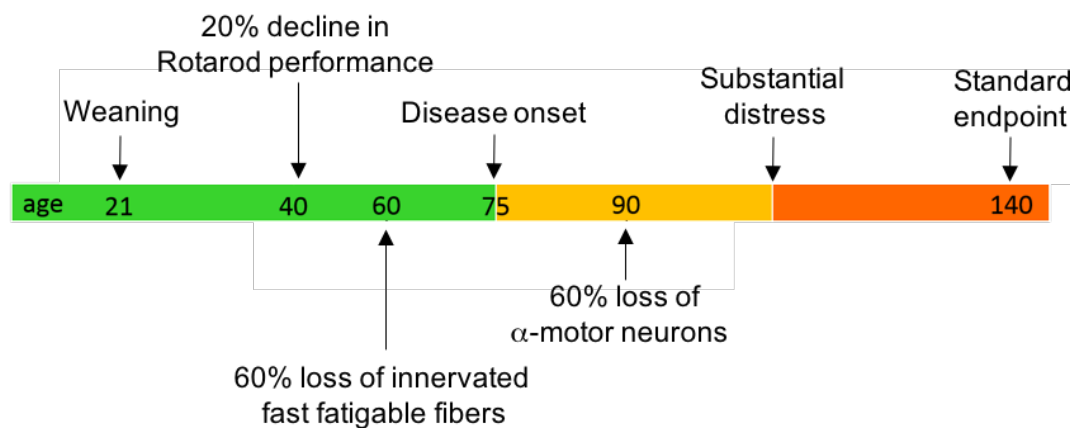


Figure 2.4. Disease course in C57BL/6J-Tg (SOD1^{G93A})1Gur/J mice. Schematic diagram illustrating the main behavioural and pathological features observed in our SOD1^{G93A} mice and the times at which they are detected.

In particular, compared to control NTg animals, the SOD1^{G93A} mice are characterised by an early decline in motor function at the age of 40 days which corresponds to the denervation of fast fatigable motor units (Mead et al., 2011). The decline can be objectively measured by testing the mice for rotarod performance. At the age of 60, SOD1^{G93A} mice start displaying a significant increase in glia activation in the ventral horns of the lumbar region of the spinal cord compared to NTg mice. Moreover, at the age of 90 days, these mice show a reduction of ~ 60% in the number of α -motor neurons in the lumbar enlargement of the spinal cord (Kirby et al., 2018). Clinical signs of the disease, defined as the presence of tremor and hind-limb splay defect, usually appear between 70 and 80 days of age. The standard end-point, corresponding to righting reflex > 10 seconds, is reached at 140 days of age (Mead et al., 2011).

2.3.2 Intrathecal transplantation of mADSCs in SOD1G93A mice: study design

First, the optimal cell dose of GFP-mADSCs to be transplanted in SOD1^{G93A} mice was defined by performing a pilot study. Different cell numbers (0.3 million, 0.5 million or 1 million) were transplanted into the CSF of 30 day-old SOD1^{G93A} mice (n=2) and brain/spinal cord collected 48 hours or 1 week post-injection to evaluate stem cell engraftment and distribution. Following optimization of the cell dose, SOD1^{G93A} transgenic mice were recruited for the therapeutic study. The litters were split in order to evenly distribute the parentage and mice between 30 and 32 days of age (pre-symptomatic stage) were randomly assigned to the treatment (5×10^5 GFP-ADSCs re-suspended in PBS, n=15) or to the control (PBS only, n=15) group. PBS was chosen as a vehicle based on previous transplantation studies, in which the control group is usually injected with the same solution used to resuspend the cells to be transplanted in the treatment group (Ciervo et al., 2017). Statistical power analysis using G*Power 3.1. was carried out to determine group size (Faul et al., 2017). Performing statistical power analysis to determine group size is a fundamental step in the design of pre-clinical studies. This assures that the sample size is sufficiently large to allow the detection of a statistically significant difference. Moreover, it allows to reduce the number of animals used in the experiment to a minimum, in compliance with the guideline on the principles of regulatory acceptance of 3Rs testing approaches. Power analysis was performed based on the detection of a 10-day shift in the time taken to reach a 20% decline in rotarod performance. A power of 80% was used with a two-tailed Student's T test ($\alpha=0.05$, $\beta=0.8$). The analysis suggested that 14 mice per group are required to detect a 10-day difference in time taken to reach the rotarod decline. The group size was finally increased by one (n=15) in order to account for eventual unexpected (unrelated health problems) loss. Body weight and

rotarod performance was monitored twice a week from 33 days of age until the study terminated. Neurological evaluation was performed three times a week from 60 days of age onward, and disease onset was defined as the evidence of simultaneous hind limb splay defect and tremors. Gait analysis was performed at day 70 and 84 (n=5/group). During the study, mice (n=3/time point) were sacrificed for histological evaluation of stem cell engraftment within the whole CNS. At the end of the study (day 90) mice were culled and tissue collected for pathology. Figure 2.5 is a schematic diagram illustrating the study design.

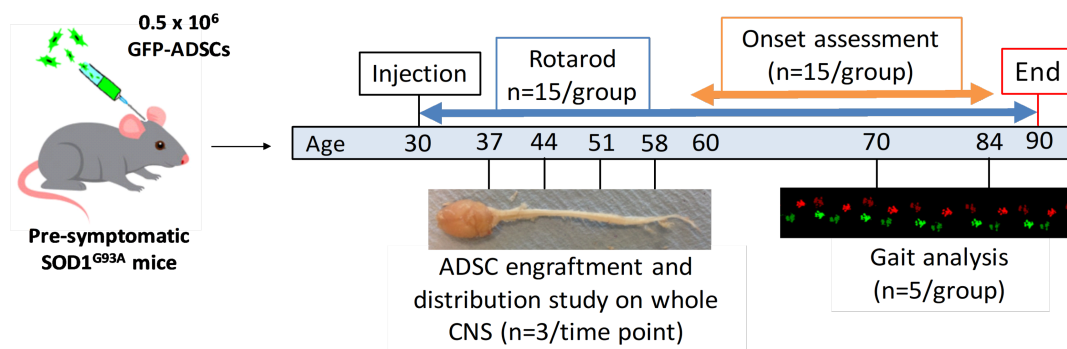


Figure 2.5. *In vivo* study design. Schematic diagram illustrating the pre-clinical study design to investigate the effect of intrathecal transplantation of GFP-mADSCs in pre-symptomatic SOD1^{G93A} mice.

2.3.3 Intrathecal injection of GFP-mADSCs: surgical procedure

Passage 3 GFP-mADSCs were thawed from the liquid nitrogen stock and cultured for 4-5 days before being used for transplantation. When cultures reached 80% confluence, cells were detached by trypsinization, washed in PBS, counted and vitality evaluated by Trypan Blue exclusion. Cells were then aliquoted, resuspended in 250 μ l of HypoThermosol® FRS solution (BioLife Solutions, USA) and stored at 4°C until ready to be transplanted. The HypoThermosol® FRS solution is a clinical grade optimized hypothermic solution that enables preservation of cells, tissues and organs at 2-8°C for an extended period of time (2-4 days) (Ginis et al., 2012).

Cells were injected directly into the CSF of mice via the cisterna magna. The surgical procedure was adapted from previous studies (Janowski et al., 2008, Iannitti et al., 2018). Before surgery, mice were placed in an induction chamber and anaesthetized with 5% isoflurane (5ml/min). Unconscious mice were then shaved, placed prone on a heat pad and the head was fixed to a stereotactic apparatus with the help of tooth and ear bars. The tooth bar was used to adjust and locate the top of the head at an

angle of approximately 30° with the table surface, and the posterior part of the head (at the level of the distal part of the occipital bone) at 45°. These coordinates allowed a good view of the cisterna magna after exposure of the atlanto-occipital membrane, while allowing the mouse to breathe normally. During the surgery deep anaesthesia was maintained with 1-2% isoflurane (2ml/min). To expose the atlanto-occipital membrane, the skin was incised from the nuchal line to the level of the second/third cervical vertebrae and the muscles separated by blunt dissection. To keep the muscles apart a pair of microretractors was used.

Representative images illustrating the mouse head after exposure of the atlanto-occipital membrane are shown in figure 2.6.

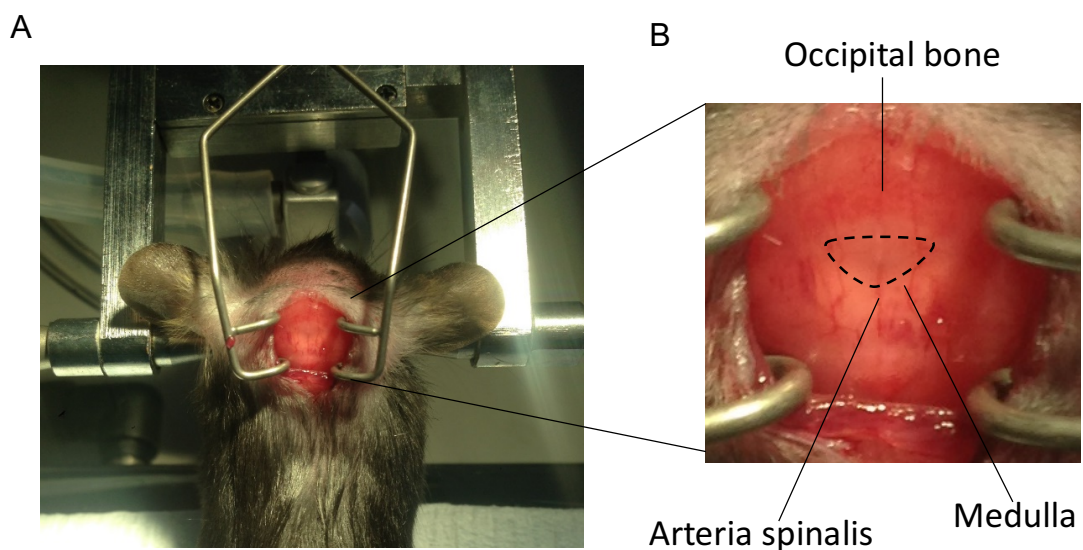


Figure 2.6. Exposure of the atlanto-occipital membrane for cell transplantation. (A) The head of the mouse is kept in position with the use of tooth and ear bars. After a midline incision of the skin and blunt separation of the dorsal muscles, the atlanto-occipital membrane is exposed. (B) The cisterna magna appears as dark reverse triangle located between the occipital bone and the top of the medulla oblongata (dashed box).

After exposure of the atlanto-occipital membrane, GFP-mADSCs were prepared for transplantation. Cells were spun at 366g for 4 minutes and re-suspended in sterile room temperature PBS at a concentration of 30,000 cells/ μ l, 50,000 cells/ μ l or 100,000 cells/ μ l depending on the experiment. For injection, cells were taken into a Hamilton syringe (702 RN 25 μ l, 7636-01). The syringe was then placed in a standard

infuse/withdraw programmable syringe pump (Harvard Apparatus 350) connected to the micromanipulator on the stereotaxic apparatus. The needle (Gauge 31, point style 4 at 45°) was carefully directed towards the midline of the atlanto-occipital membrane at an angle of 30° to the table surface. The dura mater was pierced and the needle withdrawn to allow outflow of CSF. The needle was then moved forward and stopped 1 millimeter inside the cisterna magna. The mouse head position during the injection is illustrated in figure 2.7.

A volume of 10 μ l of cell suspension (equivalent to a total number of either 3×10^5 , 5×10^5 or 1×10^6 cells) was injected at a rate of 1 μ l/min. At the end of the injection period, the needle was kept in place for further 10 minutes to avoid cell leakage and then slowly withdrawn. The dorsal muscles were sutured with absorbable 6-0 coated vicryl (W9500, Ethicon) and the skin with non-absorbable 5-0 Mersilk nylon monofilaments (W468, Ethicon). The mouse was then moved into an incubator set at 28°C until complete recovery. Mice were able to walk normally 15-25 minutes post-surgery. For the vehicle group, mice were injected with 10 μ l of sterile PBS alone.

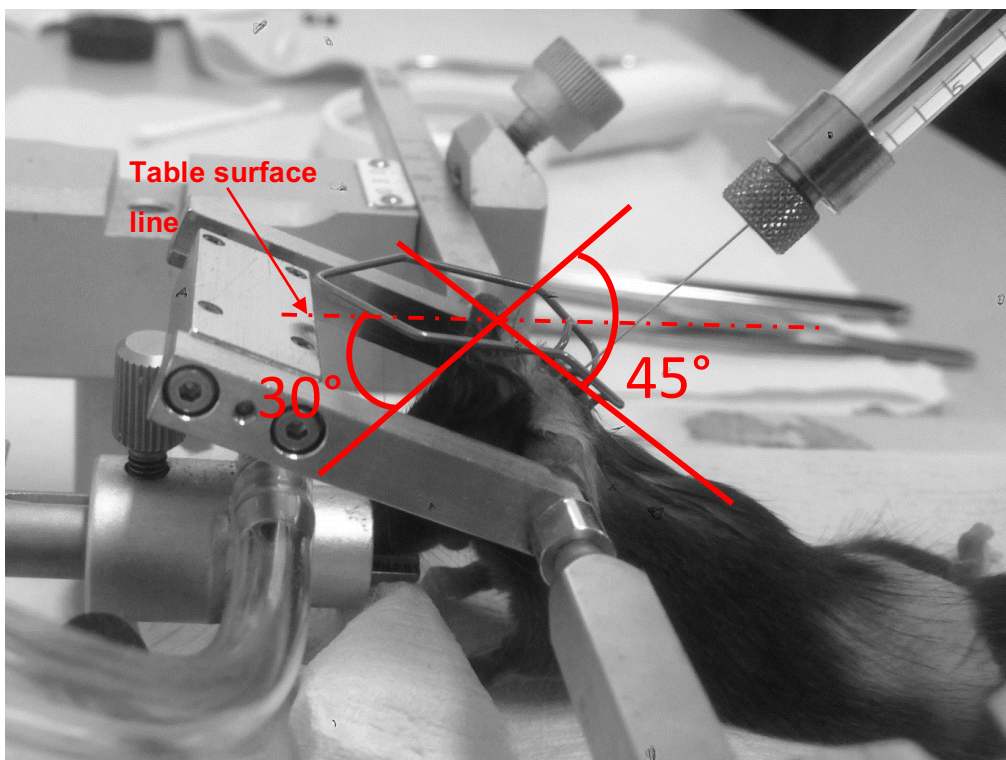


Figure 2.7. Mouse head position during cisterna magna injection. The dashed line represents the horizontal line corresponding to the table surface. The front top part of the mouse occiput forms an angle of approximately 30° with the horizontal line. The posterior part of the occiput is inclined at an angle of about 45° to the table surface.

2.3.4 Tissue collection for the detection of injected GFP-ADSCs in the whole CNS

Mice were sacrificed with an anaesthetic overdose of pentobarbitone (2.5ml/Kg) injected into the peritoneum. Before cessation of cardiac function but in the absence of the pedal reflex (a sign of deep anaesthesia), a thoracotomy was performed to expose the heart. The left ventricle was cannulated with a syringe containing ice cold PBS and a mild pressure applied to induce right atrial extension. The right atrium was then cut and the mouse perfused with 7.5 ml of cold PBS, followed by perfusion with 20 ml of 2% (w/v) paraformaldehyde (PFA) in PBS. Following perfusion, limbs, thorax and visceral soft tissue were dissected from the body and discarded, while the whole skull and vertebral column were post fixed in 2% (w/v) PFA at 4°C O/N. The following day, dissection of whole CNS with intact dura mater was performed under the microscope. The dissection protocol was adapted from the literature (Janowski et al., 2008). After extraction of the brain from the skull and the spinal cord from the spinal canal, tissue was cryoprotected by immersion in 20% (w/v) sucrose in PBS at 4°C O/N. The spinal cord was then sectioned into cervical, thoracic and lumbar segments, while the brain was dissected into forebrain, midbrain and hindbrain regions. Tissue was finally frozen in OCT medium (CellPath, UK) over methanol/dry ice and stored at -80°C.

Frozen tissue was acclimatised at -20°C for 30 minutes and successively sectioned with a cryostat. The chamber temperature was set at -21°C and the objective temperature at -20°C. Samples (forebrain, midbrain, hindbrain and cervical, thoracic and lumbar spinal cord segments) were individually sectioned at 20 µm thickness and mounted serially over 12 uncoated glass slides, covering the whole brain and spinal cord tissue (total of 72 slides per mouse). For brain samples, each slide contained 10 sections, while for spinal cords each slide contained 50 sections. Slides were finally dried at RT for 20 minutes and stored at -20°C until use.

For detection of GFP-mADSCs, 3 slides per sample covering 7.5 mm and 3.6 cm of brain and spinal cord tissue respectively, were processed and imaged. Briefly, slides were dried at 37°C for 30 minutes, washed in PBS with gentle agitation three times (10 minutes per wash) at RT and finally mounted in Vectashield aqueous hard set mountant containing 4',6-diamidino-2-phenylindole (DAPI) (Vector Laboratories, UK). Slides were left to air-dry in the dark at RT O/N. Sections were screened for the presence of GFP signal (Excitation 490 20x, Emission 525_36m) with the INCell Analyzer 2000 (GE Healthcare, UK) and images were captured.

2.3.5 Weighing and the accelerating rotarod test

Weight was measured twice per week in the afternoon immediately prior to the rotarod test. The rotarod test was carried out for a maximum period of 300 seconds, with the rotarod (Ugo Basile 7650) set to accelerate from 4 to 40 rpm in 270 seconds. On each testing day, mice were tested twice with a rest period of 3 minutes in between tests and latency to fall was recorded in seconds. The highest score was used for analysis.

The first rotarod testing day started at the age of 30-32 days old after the mice received training for three consecutive days. In order to determine rotarod decline, the best score among the first test and the three training tests was selected to define the peak of performance. Rotarod performance was carried out until the end of the study.

2.3.6 Catwalk gait analysis

Gait parameters were captured with the catwalk gait system (Noldud Instruments 7.1, Netherlands) in groups of 5 SOD1^{G93A} transgenic mice (ADSC injected and PBS injected mice) at 70 and 84 days of age. Mice were placed on the catwalk apparatus glass floor in the dark and allowed to walk without interference. Runs were recorded only when straight and continuous. Out of at least 6 runs recorded, the most similar 3 were selected and used for analysis. Gait data was analysed using dedicated Catwalk software. Each paw print was labeled manually followed by automatic detection of gait parameters. A demonstration of the catwalk software dashboard is shown in figure 2.8.

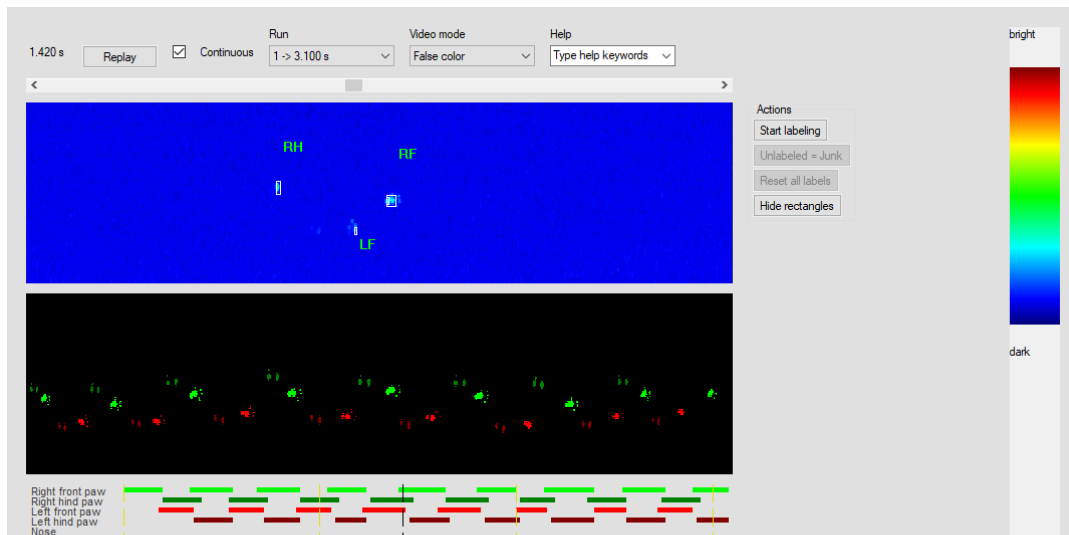


Figure 2.8. Representative image of the catwalk analysis software 7.1 dashboard. The labelling of each individual paw print is performed manually in the blue (top) panel. The black (bottom) panel shows the correct assignment of the limbs where left paws are in red and right paws are in green; forepaws are bright while hind paws are dull.

2.3.7 Neuroscoring

Neuroscoring was performed in the afternoon every 3 days from 60 days of age onward by using a neurological deficit scoring system previously described in the literature (Mead et al., 2011). This was performed by the same investigator who was blinded to the groups. Forelimb and hindlimb tremors were individually scored based on a scale of 0-3 (0-normal, 1-mild, 2-moderate, 3-strong) during mouse suspension by the tail. At the same time, hindlimb splay defects were evaluated individually for left and right hindlimbs on a scale 0-4 (0-normal, 1-mild, 2-moderate, 3-strong, 4-paralysed). The neurological deficit was delineated by an overall score (0-normal, 0.5-onset, 1-abnormal gait, 2-severe waddle, 3-dragging on one hindlimb, 4-paralysis of one limb) and onset of disease defined by coexisting hindlimb splay defect and hindlimb tremor for two consecutive neuroscore tests.

2.3.8 Tissue collection for histology

Mice (n=6 per group) were culled at the age of 90 days by trans-cardiac perfusion under terminal anaesthesia. The mouse was perfused with 10 ml of ice cold 4% (w/v) PFA following perfusion with 8 ml of ice cold PBS. The spinal column was then collected and post-fixed O/N in 4% (w/v) PFA/PBS at 4°C. The following day, the spinal cord was dissected from the column, washed in PBS and divided into cervical,

thoracic and lumbar segments. The lumbar enlargement (12mm) was cut in half and embedded in paraffin within a single block with the two median extremities oriented upward. Tissue was then sliced at 10 µm thickness using a microtome. Sections were mounted serially over a series of 5 slides with 5 sections being discarded in between each series, for a total of 60 slides covering 4.8 mm of spinal cord tissue. This ensured that there was a distance of at least 100µm between serial sections. Each slide contained 8 sections.

2.3.9 Immunohistochemical staining on spinal cord

Sections were rehydrated by using the following sequence: 2 x 5 minutes in xylene, 5 minutes in 100% ethanol, 5 minutes in 95% ethanol, 5 minutes in 70% ethanol and 5 minutes in water. Following deparaffinisation, heat-induced epitope retrieval was performed. Slides were completely submerged in Access Super RTU pH 8 (MP-606PG1, Menarini) and placed in an antigen access unit (Menarini) for 30 minutes at 125 °C with a pressure of 20 psi. At the end of the cycle, slides were allowed to cool at RT and washed in PBS for 10 minutes with gentle agitation. Sections were then blocked/permeabilised for 20 minutes at RT with 5% (w/v) BSA and 0.25% Triton™ X-100 (Sigma-Aldrich) in PBS. After blocking/permeabilisation, slides were incubated with the primary antibodies (see table 2.3) diluted in 1% BSA, 0.25% (v/v) Triton X-100/PBS at 4 °C O/N. Slides were then given 6 quick washes and 3 x 8 minutes washes in PBS with gentle agitation, blocked in 5% (w/v) BSA/PBS for 10 minutes at RT and incubated with the secondary antibodies (see table 2.3) at RT for 90 minutes. Following incubation, slides were washed with 2x quick washes in PBS, 4 x 8 minutes washes in PBS and 1 x 5 minutes wash in distilled water in agitation in the dark. Slides were dried to remove water excess, mounted with Vectashield hard set aqueous solution containing DAPI (Vector Laboratories, Peterborough) and left to dry at RT O/N in the dark.

Table 2.3. List of antibodies used in IHC

Antibody	Specific for	Raised in	Supplier	Catalog n	Dilution
Anti-GFAP	Astrocytes	Chicken	Abcam	Ab4674	1/500
Anti-IBA-1	Microglia	Rabbit	GeneTex	GTX100042	1/500
Alexa fluor anti-rabbit 555	Anti-rabbit primary	Donkey	Thermo Fisher	A27039	1/1000
Alexa fluor anti-chicken 488	Anti-chicken primary	Donkey	Thermo Fisher	A11039	1/1000

2.3.10 Immunohistochemical staining image analysis

All images were captured with the INCell Analyzer 2000 (GE Healthcare, UK). For each spinal cord section (8 sections/slide), GFAP and IBA-1 staining was captured at a magnification of 60x within each ventral horn. For analysis, the GE Developer Toolbox 1.9 (GE Healthcare, UK) was used. The staining was first segmented based on the grey intensity level and a threshold set. This was followed by a sieve filter retaining objects with an area over 4 μm^2 . For GFAP, the threshold was set at 220 gray levels. While for IBA-1, a threshold of 200 gray levels was chosen. Total staining area (μm^2) and main staining index [(unstained pixels – stained pixels)/2xSD] were recorded for GFAP. Total staining area (μm^2) was recorded for IBA-1. For analysis, ADSC-treated and PBS-treated transgenic SOD1^{G93A} mice (n=6 per group) were compared.

2.3.11 Nissl staining and Motor Neuron counts

Paraffin serial sections of lumbar spinal cord were processed for Nissl staining. The staining was performed on every 5th section (total of 12 slides per mouse) covering a total length of about 4.8 mm of the lumbar spinal cord, with at least 80 μm of space between each section. Nissl staining was performed according to the literature. Briefly, sections were dewaxed in xylene, rehydrated through graded alcohols and stained with pre-filtered 0.1% Cresyl fast violet for 20 minutes. Sections were then rinsed quickly in distilled water and differentiated in 0.25% ethanoic acid for 10 seconds. After washing in distilled water, sections were dehydrated by immersion baths in crescent graded alcohols with the following sequence: 5 minutes in 70% ethanol, 5 minutes in 95% ethanol, 2 x 5 minutes in 100% ethanol and 5 minutes in xylene to clear. Slides were dried, mounted in permanent mounting medium (H-5000, VectaMount®) and dried at 37°C O/N.

Nissl-positive α -motor neurons were identified and counted depending on their topography, morphology and size. Only multipolar cells located in the ventral horn of the lumbar spinal cord, characterised by the presence of a large nucleus with intensely labelled nucleoli and a diameter size of at least 25 μm were counted as α -MNs. Motor neuron counts was performed by the same investigator who was blinded to the treatment groups. A total of 96 sections (192 ventral horns) were screened for each mouse (n=6 per group).

2.3.12 Tissue collection for RNA extraction

Mice were sacrificed at 90 days of age by injection of an overdose of pentobarbitone (2.5ml/Kg). In the absence of pedal reflex mice were exsanguinated via cardiac puncture by using a 1 ml syringe (5 Gauge needle). The head was removed and the spine was cut at the level of the hips. The spinal cord was flushed from the rostral end of the column by pushing PBS into the spinal cavity using a 10 ml syringe fixed to a pipette tip. The spinal cord was then cut into two halves (upper and lower) and snap frozen in liquid nitrogen. Samples were stored at -80°C until use.

2.3.13 Gene expression in mouse spinal cord: RT-qPCR

2.3.13.1 RNA extraction from spinal cord tissue

The lower half of the spinal cord was processed for RNA extraction by using the RNeasy Lipid Tissue Mini Kit (74804, Qiagen). Frozen samples were immersed into 200 µl of QIAzol Lysis Reagent (79306, Qiagen) and homogenised with the help of a pellet pestle motor (Fisher Scientific). Following homogenisation, another 800 µl of QIAzol reagent was added and samples incubated at RT for 5 minutes. After adding 200 µl of chloroform, samples were shaken vigorously for 15 seconds and centrifuged at 12,000g for 15 minutes at 4°C. The supernatants were carefully collected, transferred to new Eppendorf tubes and mixed with one volume of 70% ethanol. Samples were then transferred into RNeasy spin columns and the kit manufacturer's instructions were followed. Finally, RNA was eluted with 50 µl of RNase-free water into a new tube and RNA concentration and purity estimated with the NanoDrop™ 2000/2000c Spectrophotometer (Thermo Fisher Scientific). Samples were stored at -80°C until use.

2.3.13.2 cDNA synthesis

To eliminate any genomic DNA contamination, DNase treatment was performed with Recombinant DNase I (471678001, Merck). To a total of 2 µg of RNA was added 1 µl of enzyme, 1µl of DNase reaction buffer (10x) and DEPC water to a final volume of 10 µl. The reaction mixture was placed in a PCR machine (G-storm) and incubated for 10 minutes at 37°C. The DNase was then inactivated by incubation for 10 minutes at 75°C in the presence of 1µl of 2.5 mM Ethylenediaminetetraacetic acid (EDTA). Following DNase treatment, cDNA was synthesised by reverse transcription. A 1 µl volume of 40 mM random hexamer primers (Sigma) and 1 µl of 10 mM of dNTP Mix (BIO-39053, Bioline) were added to the RNA solution, mixed, briefly centrifuged and

incubated at 75°C for 5 minutes. At the end of the incubation, samples were immediately transferred to ice (to avoid the generation of secondary structures in the RNA) and allowed to cool. For cDNA synthesis, the M-MLV Reverse Transcriptase (28025013, Thermo Fisher Scientific) was used. Briefly, 4 µl of First Strand Buffer (5x), 2 µl of 100mM DTT and 1 µl of M-MLV-RT were added to the RNA solution (13 µl) and sample placed in the PCR machine for 1 hour at 37°C, followed by 5 minutes at 95°C. Finally, 40 µl of DEPC water was added to the sample (20 µl) and stored at -20 °C.

2.3.13.3 qPCR

Primers were designed and validated using Primer-BLAST (NCBI) free software as follows:

- product size between 100 and 200 bp;
- primer melting temperature (T_m) between 58 and 61 °C with a Max T_m difference between forward and reverse primers of 8 °C;
- primer size between 15 and 25 nucleotides;
- GC content between 40 and 60%;
- whenever possible primers were designed to span across an exon-exon junction.

Once primer pairs were generated the OligoAnalyzer® Tool (Integrated DNA Technologies) software was used to identify unwanted hairpins and dimers. All primers were validated and optimized before running the final experiment. qPCR assay specificity verification was carried out by running a qPCR with serial dilutions of the primer mix (100, 10, 5, 2.5 and 1.25 µM) and by performing a melt curve analysis. An agarose gel electrophoresis was also run with the qPCR products in order to exclude secondary non-specific amplicons and to confirm that the single band was of the correct expected size. The construction of a standard curve was finally performed in order to determine the reaction efficiency and reproducibility of the qPCR assay. This was carried out by making serial dilutions (neat, 1/4, 1/16, 1/64 and 1/250) of the cDNA sample and plotting C_T against dilution. The qPCR assay was accepted only with an efficiency of at least 90% and R^2 of 0.95. All the primer pairs validated and used for experiments are listed in table 2.4.

Table 2.4. List of optimized mouse specific primers for qPCR

Gene	Forward sequence	Reverse sequence	Conc (µM)
GAPDH	CATCACTGCCACCCAGAAGACTG	ATGCCAGTGAGCTTCCCGTTTCAG	5
VEGF _a	CAGACGTGTAAATGTTCTGCAAA	TGGTGACATGGTTAATCGGTCTTT	5
GDNF	CTCTTGCTCCCGACCTTCTG	ACAGCCACGACATCCCATAA	5
BDNF	GGCTGACACTTTTGAGCACGTC	CTCCAAAGGCACTTGACTGCTG	2.5
IGF1	CCTCAGACAGGCATTGTGGA	CTTCTCCTTTGCAGCTTCGTT	1.25
TGF-β1	TGATACGCCTGAGTGGCTGTCT	CACAAGAGCAGTGAGCGCTGAA	5
HGF	GGGATTCGCAGTACCCTCA	ACTTGACACGTCACACTTGG	2.5
bFGF	CTTCCCACCAGGCCACTTC	GTTGGCACACACTCCCTTGA	5
IL-1β	TGGACCTTCCAGGATGAGGACA	GTTTCATCTCGGAGCCTGTAGTG	1.25
IL-6	TACCACTTCACAAGTCGGAGGC	CTGCAAGTGCATCATCGTTGTTTC	2.5
TNF-α	AGCACAGAAAGCATGATCCG	GCCATTTGGGAAGTCTCATCC	1.25
MCP-1	TTTCCACAACCACCTCAAGC	TTAAGGCATCACAGTCCGAGTC	2.5

Each qPCR reaction mixture was prepared as follows:

- 1 µl cDNA
- 1 µl diluted primer mix (forward plus reverse)
- 5 µl Brilliant SYBR® green qPCR master mix (600882, Agilent Technologies)
- 3 µl DEPC water

Each sample was pipetted in duplicate in non-skirted, thin-wall 0.2ml 96-Well Low-Profile plates (MLL9601, Bio-Rad). Glyceraldehyde 3-phosphate dehydrogenase (GAPDH) was used as house-keeping gene. For each primer pair an internal non-template control was pipetted. Plates were then covered with 0.2ml flat optical wide area 8-cap strips (TCS-0803, Bio-Rad) and centrifuged for 1 minute at 1,700 RPM. Plates were finally placed in the qPCR machine (CFX384 Touch™ Real-Time, Bio-Rad) and run on the following protocol:

- 95°C for 10 minutes
 - 95°C for 30 seconds
 - 60°C for 30 seconds
 - 72°C for 1 minute
 - 95°C for 1 minute
 - 60°C for 30 seconds
 - 60°C for 5 seconds
 - +0.5°C/cycle Ramp 0.5°C/s
 - Plate reader
- } X 45
- } X 70

2.3.13.4 qPCR analysis

The CFX Manager Software (Bio-Rad) was used to control real-time PCR parameters and to extract the Cycle threshold (Ct) values. qPCR data analysis was then performed using Microsoft Excel 2016 (Microsoft) and GraphPad Prism 6 (GraphPad). Relative expression concentrations were calculated by using the double delta Ct analysis method ($\Delta\Delta Ct$). For each duplicate the Ct value mean was calculated and data was used only when Ct values differed by ≤ 0.6 . GAPDH was used as housekeeping gene. The difference between the gene being tested and GAPDH (ΔCt) was calculated for both tested control (ΔCt_{TC}) and tested experimental (ΔCt_{TE}) samples. The ΔCt_{TC} is representative of the control PBS-injected mice (n=7) while the ΔCt_{TE} represent the ADSC-injected mice (n=7). The mean ΔCt_{TC} was calculated and subtracted from each ΔCt value (both ΔCt_{TC} and ΔCt_{TE}) to arrive at the double delta Ct values ($\Delta\Delta Ct$). Finally, the relative concentration, or expression fold change, was calculated using the formula: $2^{-\Delta\Delta Ct}$.

2.4 Astrocytes, Motor Neurons and ADSCs co-culture experiments

2.4.1 Isolation of cortical mouse astrocytes

Mouse cortical astrocytes were isolated from symptomatic (90 days) female transgenic SOD1^{G93A} and control sex and aged matched non-transgenic (NTg) mice. Isolation and culture of astrocytes was performed as previously described with minor modifications (Frakes et al., 2014). Mice (3 to 4) were sacrificed by cervical dislocation and brains were isolated and pooled together. Brains were washed thoroughly with PBS. Cerebellum and meninges were carefully dissected and tissue digested with papain (200U/ml) (1071440025, Sigma-Aldrich) diluted in enzymatic buffer (116mM NaCl, 5.4mM KCl, 26mM NaHCO₃, 1mM NaH₂PO₄, 1.5mM CaCl₂, 1mM MgSO₄, 25mM glucose, 1mM cysteine in ddH₂O).

For each brain preparation 60 μ l of papain in 6 ml of enzymatic buffer was used. Digestion was carried out for 60 minutes at 37°C in water bath with gentle agitation every 10-15 minutes. The enzymatic reaction was then quenched with an equal volume of 40% FBS (v/v) in HBSS (Ca²⁺/Mg²⁺) and the solution centrifuged at 200g for 4 minutes. The supernatant was discarded and the pellet resuspended in 2 ml of 0.5 mg/ml DNase I (DN25, Sigma-Aldrich) in HBSS and incubated at RT for 5 minutes. Following DNase treatment the tissue homogenate was gently disrupted with fire-polished Pasteur pipettes, filtered through a 70 μ m cell strainer and centrifuged at 200g for 4 minutes. The pellet was resuspended in 10 ml of 20%

isotonic Percoll (P1644, Sigma-Aldrich) (v/v in HBSS) and 10ml of HBSS were dispensed on top of the Percoll cell suspension taking care not to disrupt the formed density gradient. The solution was then centrifuged for 20 minutes at 200g with slow acceleration and no brake. The interphase layer containing cell debris and myelin was discarded and the cell pellet washed with 3 ml HBSS by centrifugation at 200g for 4 minutes.

The pellet was finally resuspended in complete medium consisting of DMEM, 10% (v/v) FBS (Life Science production), and 50 U/ml Pen/Strep. Cells were plated in standard culture flask previously pre-coated with 0.01% (v/v) poly-L-ornithine (A-004-C, Sigma-Aldrich). Cells were grown in incubator at 37°C with 20% O₂, 5% CO₂ and 95% humidity. Medium was replaced every 3 days for approximately 14 days. When cultures reached confluence, flasks were placed on an orbital shaker at 230rpm, 37°C for 3 hours to remove contaminant microglia. Astrocytes were then detached with mild trypsinization (1x trypsin diluted 1 in 3 in PBS) and expanded (Saura et al., 2003). For experiments, astrocytes were used at passage 3 to 4.

2.4.2 Characterisation of cortical astrocytes by flow cytometry

Mouse astrocyte purity was confirmed by flow cytometry (FC). Astrocytes were expanded for four passages (p4) and stained for CD44 (astrocyte marker) and CD11b (microglia marker). Briefly, cells were lifted with trypsin, centrifuged at 200g for 4 minutes, re-suspended in complete media and viability was determined by the Trypan Blue exclusion method. Cells were then resuspended in ice cold FC buffer (2% (v/v) FBS in PBS), and aliquoted into micro centrifuge tubes (1.5 ml) at a concentration of 1×10^6 cells/tube. Following 10 minutes incubation on ice, cells were washed with FC buffer by centrifugation at 200g for 3 minutes at 4°C and resuspended in 100µl of FC buffer containing APC-conjugated anti-mouse CD44 (0.26 µg) and FITC-conjugated anti-mouse CD11b (0.26 µg) antibodies (Biolegend™). As a negative control, unstained cells were incubated in the presence of FC buffer alone. For the identification of the specific interaction between antigens and antibodies, cells were stained with an equal concentration of matched fluorescent-labelled isotype control antibodies. Following the incubation period, cells were washed three times with 500 µl of FC buffer by centrifugation, re-suspended with 400 µl of FC buffer and analysed on a BD LSRII FACS instrument (Biosciences Company). Data analysis was carried out with FlowJo 7.6.1 (FlowJo LLC, Oregon). Unstained cells were used to set the gates and isolate the single cell population. Forward scatter (FSC) and side scatter

(SSC) parameters were used to exclude debris and doublets. From each sample at least 10,000 single cell events were collected and analysed.

2.4.3 Generation of human iAstrocytes

Human induced astrocytes (iAstrocytes) were generated by Dr Laura Ferraiuolo's laboratory through genetic reprogramming of skin fibroblasts. Skin biopsy collection from ALS patients and healthy donors (table 2.5) was approved by the Research Ethics Committees of Sheffield (study number STH16573, reference 12/YH/0330) or by the Institutional Review Board of the Ohio State University (ethics number IRB08-00402) after informed consent was obtained.

Table 2.5. Skin Fibroblast donor's information.

Cell line	Diagnosis	Mutation	Age at collection (years)	Onset to death (months)	Sex	Source
3050	Non-ALS	/	68	/	M	UoS
155	Non-ALS	/	40	/	M	UoS
78	fALS	C9orf72	66	31.7	M	UoS
183	fALS	C9orf72	50	27	M	UoS
100	fALS	SOD1 ^{A4V}	-	100	F	OSU
102	fALS	SOD1 ^{A4V}	-	200	F	OSU
12	sALS	/	29	90	M	OSU
17	sALS	/	47	72	M	OSU

fALS = familial ALS, sALS, = sporadic ALS, UoS = University of Sheffield, OSU = The Ohio State University

Fibroblasts from 2 non-ALS controls, 2 C9orf72, 2 SOD1^{A4V} and 2 sporadic patients were reprogrammed into neural progenitor cells (iNPC) as previously described (Meyer et al., 2014). Fibroblasts were grown into one of a six-well plate for 24 hours before being transduced with retroviral vectors expressing Oct-3/4, Sox 2, Klf 4 and c-Myc. Cells were allowed to recover for 1 day in basal fibroblast medium composed of DMEM (Gibco) and 10% (v/v) FBS (Life Science Production) and switched to NPC conversion medium consisting of DMEM/F12 (1:1) GlutaMax (Gibco), 1% (v/v) N2 (Gibco), 1% (v/v) B27 (Gibco), 20 ng/ml bFGF (Preprotech), 20 ng/ml EGF (Preprotech) and 5 ng/ml heparin (Sigma-Aldrich). Following morphology changes, sphere-like cells were switched to NPC proliferation medium consisting of DMEM/F12 (1:1)

GlutaMax, 1% (v/v) N2, 1% (v/v) B27 and 40ng/ml bFGF. iAstrocytes were obtained as previously described (Varcianna et al., 2019). iNPCs were seeded in 10 cm dishes coated with fibronectin and induced to differentiate for 7 days by culture in astrocyte proliferation medium composed of DMEM (Fisher Scientific) containing 10% (v/v) FBS (Life Science production) and 0.2% (v/v) N2 (Gibco).

2.4.4 HB9-GFP mouse Motor Neurons (HB9-GFP-MNs)

Murine HB9-GFP MNs used in this study were generated and kindly provided by Dr Laura Ferraiuolo's laboratory. HB9-GFP MNs were obtained from mouse embryonic stem cells (mESC) containing a GFP gene under the MN-specific promoter HB9. mESCs were cultured on primary mouse embryonic fibroblasts (Merck) in mESC media consisting of KnockOut DMEM (Gibco), 15% (v/v) embryonic stem-cell FBS (Gibco), 2mM L-glutamine (Gibco) and 0.00072% (v/v) 2-mercaptoethanol (Sigma-Aldrich). Differentiation into MNs was performed through embryoid bodies (EBs). mESCs were detached by trypsinization, resuspended in EB medium (DMEM/F12, 10% knockout serum replacement (Gibco), 1% N2, 1mM L-glutamine, 0.05% (w/v) glucose (Sigma-Aldrich) and 0.0016% (v/v) 2-mercaptoethanol and plated on non-adherent Petri dishes. EB media was replaced every day. To induce differentiation, from day 2 to day 7 post-plating, 2 μ M retinoic acid (Sigma-Aldrich) and 0.5 μ M smoothed agonist (Sigma-Aldrich) were added. At the end of the differentiation protocol (7 days), the HB9-GFP MN enriched fraction was obtained by EBs dissociation with papain.

EBs from 2-3 10cm dishes were collected and spun at 200g for 2 minutes. The EBs were washed by centrifugation with PBS and 2.75 ml of enzymatic buffer (116mM NaCl, 5.4mM KCl, 26mM NaHCO₃, 1mM NaH₂PO₄, 1.5mM CaCl₂, 1mM MgSO₄, 25mM glucose, 1mM cysteine in ddH₂O) containing 200 μ l of papain (20 U/ml) were added. The EBs were then mixed with a 1 ml pipette for 10 times and incubated in water bath at 37°C for 10 minutes with gentle shaking every 2 minutes. After incubation, the solution was carefully pipetted 5 times before being centrifuged at 300g for 5 minutes. The supernatant was discarded and the pellet resuspended in 3 ml of enzymatic buffer containing 300 μ l of FBS and 150 μ l of DNase I. The cell suspension was then slowly added on top of 5 ml of FBS in order to prepare a cushion solution. Following centrifugation at 100g for 6 minutes, cells were resuspended in MN complete medium consisting of KnockOut DMEM, F12 medium, 10% (v/v) KnockOut Serum Replacement, 1mM L-glutamine, 0.5% (w/v) glucose, 1% (v/v) N2,

0.0016% (v/v) 2-mercaptoethanol, 20 ng/ml BDNF (Prepotech), 40 ng/ml CNTF (Prepotech) and 20 ng/ml GDNF (Prepotech) and counted.

2.4.5 HB9-GFP-MNs, mouse astrocytes and ADSCs triple separated co-culture

For co-culture experiments, three separated astrocyte preparations per genotype (SOD1^{G93A} and NTg) were established (biological replicates). Passage 4 mAstrocytes from symptomatic (90 day-old) SOD1^{G93A} or NTg age matched control mice were seeded in triplicate (technical replicates) into separate wells of a 24-well plate, previously coated O/N with 1:1000 poly-L-ornithine (Sigma-Aldrich) and 1:200 laminin (Sigma-Aldrich), at a concentration of 50,000 cells/well. mAstrocytes were maintained for 24 hours in astrocyte basal medium (DMEM, 10% (v/v) FBS, 50 U/ml Pen/Strep). On the same day, 30,000 ADSCs were plated onto sterile glass coverslips (22 mm²) containing 2 mm² paraffin wax dots. The next day, the HB9-GFP-MN enriched fraction was obtained and 30,000 HB9-GFP-MNs/well plated onto the mAstrocyte monolayer in 1 ml of complete MN medium, thus establishing a mixed astrocyte/MN co-culture. Before seeding the MNs, the astrocyte medium was removed and astrocytes washed with PBS. After 5 hours, coverslips containing the ADSCs were washed in PBS, inverted and laid onto the astrocytes/HB9-GFP MNs mixed co-culture, establishing a “triple separated co-culture system”. Thus, ADSCs were physically separated from astrocytes and MNs but could share the same culture medium (Ferraiuolo et al., 2007). Every other day, 500 µl of medium was replaced with fresh complete MN medium until day 7 of co-culture. As a control, empty coverslips were added to the mixed astocyte/MN co-culture.

HB9-GFP MNs were imaged using the INCell 2000 analyser (GE Healthcare) 24 hours after the initiation of the co-culture to measure the number of cells corresponding to day 1. Plates were then imaged again at day 7. The number of viable MNs were counted using the ColumbusTM Data Storage and Analysis System (RRID:SCR 007149; Perkin Elmer). Only GFP positive motor neuronal cell bodies with at least one axon were counted as viable cells. Finally, the percentage of MN survival was calculated as the number of viable MN at day 7 as a percentage of the number of viable MN at day 1. A schematic diagram of the co-culture system is illustrated in figure 2.9.

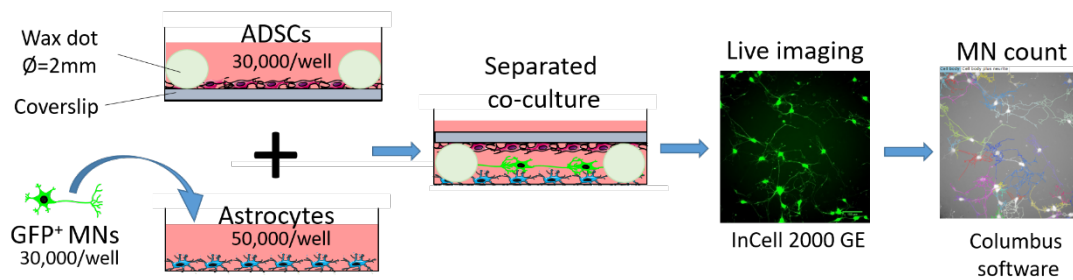


Figure 2.9. Triple Separated co-culture system. Schematic illustration of the astrocyte/HB9-GFP-MN/ADSC separated triple-co-culture system. MNs are seeded on top of a confluent layer of astrocytes and ADSCs onto glass coverslips containing tiny paraffin wax dots. The coverslips containing ADSCs are then inverted and added to the astrocyte/MN co-culture to obtain the triple separated co-culture system. ADSCs are physically separated from astrocytes and MNs but can communicate through the exchange of soluble factors. As a control, empty coverslips are added to the co-culture. Culture plates are imaged at day 1 and 7 of co-culture with the IN Cell 2000 analyser to identify alive HB9-GFP-MNs. MNs are finally quantified with the use of the Columbus software.

2.4.6 HB9-GFP-MNs, human iAstrocytes and ADSCs triple separated co-culture

Human iAstrocytes were grown in 10 cm dishes in complete iAstrocyte proliferation medium (DMEM, 10% (v/v) FBS, 0.2% (v/v) N2). At day 6 of differentiation, cells were lifted with accutase (A1110501, Gibco) and plated in quintuplicate onto one well of a 24-well plate previously coated with 1:400 fibronectin (FC010, Millipore). Cells were seeded at a concentration between 10,000 and 40,000 cells/well depending on the cell line. ADSCs were plated onto glass coverslips (22 mm²) containing paraffin wax dots at a concentration of 30,000 cells/well. After 24 hours (day 7 for iAstrocytes differentiation), 50,000 HB9-GFP-MNs were seeded on top of the iAstrocytes and medium switched to complete MN medium. After 5 hours, the coverslips containing ADSCs were inverted and added to the iAstrocytes/MNs mixed co-culture to obtain the triple-separated co-culture (as described in figure 2.7 above) . Empty glass coverslips were used as controls. The following day, plates were imaged with the INCell 2000 analyser (GE Healthcare) for quantification of viable MN at day 1. HB9-GFP-MNs were imaged again at day 3 and percentage of MN survival calculated as number of viable cells at day 3 as percentage of viable MNs at day 1.

2.4.7 Separated co-culture between mAstrocytes and ADSCs

mAstrocytes derived from SOD1^{G93A} and age matched NTg mice obtained from three separate preparations were plated onto 24-well plates coated with 1:1000 poly-L-ornithine (A-004-C, Sigma-Aldrich) at a concentration of 50,000 cells per well. mAstrocytes were allowed to recover for two days before adding 30,000 ADSCs/well previously seeded onto glass coverslips containing wax dots as above. Separated co-cultures were maintained for 48 hours in complete mAstrocyte medium (DMEM, 10% (v/v) FBS, 50 U/ml Pen/Strep). Empty coverslips were used as a negative control.

At the end of the co-culture period, for supernatant protein analysis, the coverslips containing ADSCs were removed, washed in PBS and cultured for further 24 hours in 500 µl of control medium. mAstrocyte cultures were also washed in PBS twice, and 300 µl of fresh culture medium added. After 24 hours, the supernatant from both astrocytes and ADSCs was collected, spun at 600g at 4°C for 10 minutes and snap frozen in liquid nitrogen. Samples were stored at -80°C until ready to use. Following supernatant collection, mAstrocytes were fixed with 4% (v/v) PFA in PBS for 10 minutes and stained with Hoechst 33342 Solution (62249, Thermo Fisher Scientific) diluted 1:5000. Plates were then imaged with the In Cell 2000 analyser (GE Healthcare) and cell nuclei counted with the ColumbusTM Data Storage and Analysis System (RRID:SCR_007149; Perkin ElmerWaltham). For gene expression analysis, following 48 hours of co-culture, mAstrocytes and ADSCs were separated, washed in PBS and processed for RNA extraction.

2.4.8 Separated co-culture between iAstrocytes and ADSCs

Control or patient derived iAstrocytes obtained from three separate differentiation batches were lifted at day 6 of the differentiation protocol and seeded onto 24-well plates pre-coated with 1:400 fibronectin at a concentration depended on the cell line. iAstrocytes were allowed to recover for 24 hours and coverslips containing 30,000 ADSCs/well were added for the separated co-culture. Separated co-cultures were maintained for 72 hours in complete iAstrocyte medium (DMEM, 10% (v/v) FBS, 0.2% (v/v) N2). Empty coverslips were used as a negative control. At the end of the co-culture cells were separated, washed in PBS and total RNA extracted.

2.4.9 Multiplex Bead-Based Immunoassay

The content of soluble cytokines in supernatants from mAstrocytes after separated co-culture with or without ADSCs was measured with the use of the BDTM Cytometric

Bead Array (CBA) Flex Set Multiplexed Bead-Based Immunoassay (BD Biosciences). The assay allows the building of a specific multiplex analysis by choosing up to 30 analytes to be measured simultaneously. Samples were analysed for IL-6, IL-1 β , TNF- α and MCP-1. Figure 3.10 shows a schematic representation of the assay principle.

The assay was carried out by the “Medical School Flow Cytometry Core Facility” following the manufacturer’s instructions and samples were acquired on an Attune dual-laser flow cytometer (Thermo Fisher). The raw data files were received as Microsoft Office Excel documents and analysed with the use GraphPad 7. First, a nonlinear regression standard curve (Curve Fit) was generated. This was then used to extrapolate the sample values. Protein concentration (pg/ml or pg/ml) for each well/sample was finally normalized to the number of cells counted at the end of the experiment in that specific well.

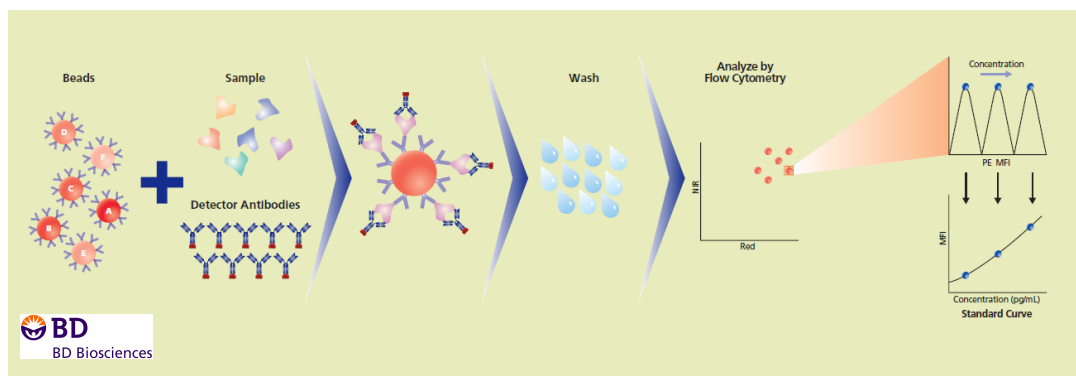


Figure 3.10. Multiplexed Bead-Based Immunoassay. Schematic diagram showing the Immunoassay principle. Each cytometric bead is coated with a cytokine-specific antibody and can be distinguished from one to another because of their different associated red fluorescence. The beads are first incubated with the sample and then with a detector antibody conjugated with the fluorochrome phycoerythrin (PE). Samples are finally collected through a flow cytometer which measures the mean Fluorescence Intensity (MFI). Protein quantification is calculated through the generation of a standard curve. Image obtained from BD Biosciences website.

2.4.10 Enzyme-linked Immunosorbent Assay (ELISA)

VEGF-A and IGF-1 protein concentration in supernatant collected from mAstrocytes and ADSCs after separated co-culture was quantified by sandwich enzyme-linked immunosorbent assay (ELISA) by using commercial ELISA kits (figure 2.11). For

VEGF-A measurement, the Mouse VEGF-A Platinum ELISA kit (BMS619/2, Thermo Fisher Scientific) was used following the manufacturer's instruction. IGF-I protein concentration was quantified with the Mouse IGF-1 ELISA Kit (EMIGF1, Thermo Fisher Scientific) following the manufacturer's instructions. Before starting the protocol, samples stored at -80° were thawed on ice and diluted with the assay diluent provided in the kit. The lyophilized standard (VEGF or IGF-1) was then reconstituted and serial dilutions were made. The standard and the samples were then pipetted in duplicate into the specific antibody pre-coated 96-well strip plate provided in the kit and the manual instructions followed. At the end of the protocol, absorbance was read at 450 nm with the PHERASStar microplate reader (BMG, Labtech) and absorbance values transferred to an Excel data sheet. Data were finally analysed with GraphPad 7. Briefly, the optical density value from the control (medium alone) was subtracted from the standard and samples reading values. Data were then plotted on GraphPad 7 and a nonlinear sigmoidal standard curve (Curve Fit) was drawn. Protein concentration in the samples was then extrapolated and normalized to the number of cells counted at the end of the co-culture.

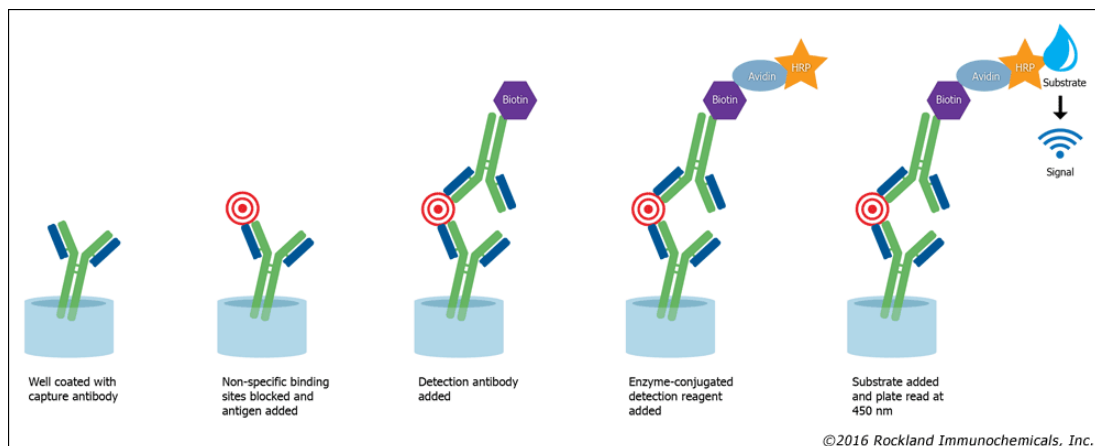


Figure 2.11. ELISA principle. Schematic diagram showing the ELISA principle. Each well of a 96-well plate is coated with the antibody specific for the protein of interest. The supernatant containing the antigen is added to the well and during incubation the antibody binds the peptide. Following washing steps a second biotinylated detection antibody specific to the antigen is then added. After a washing step a streptavidin-HRP is added and binds the biotin-conjugate antibody. A substrate solution reactive with HRP is added and a coloured product is formed in proportion to the amount of the protein of interest present in the sample. Finally, the reaction is stopped with an acid and absorbance read at 450 nm. Protein concentration is then calculated with the help of a standard curve. Image obtained from Rockland Immunochemicals, Inc website.

2.4.11 Gene expression after co-culture experiments by qPCR

At the end of the separated co-culture, ADSCs were separated from astrocytes (mouse model or human model derived), washed in PBS and total RNA extracted with the RNeasy Mini Kit (74104, Qiagen) following the manufacturer instructions. For each cell type/condition RNA was extracted by lysing 6 wells of a 24-well plates pooled together. cDNA was synthesised from 1 µg of mRNA by reverse transcription using the M-MLV Reverse Transcriptase (28025013, Thermo Fisher Scientific) as described in paragraph 2.3.13.2. For real-time qPCR, cDNA was amplified using the Brilliant SYBR® green qPCR master mix (600882, Agilent Technologies). For details on primer design and optimization and the qPCR protocol please see paragraph 2.3.13.3. Each sample was run in duplicate with the CFX384 Touch™ Real-Time thermocycler (CFX384 Touch™ Real-Time, Bio-Rad) and analysis performed with the CFX Manager Software (Bio-Rad). Data were analysed with the double delta Ct method ($\Delta\Delta C_t$) relative to GAPDH. In table 2.4 is the list of mouse primers used for amplification of cDNA from mouse astrocytes and mADSCs. The list of human primers used to amplify cDNA from human iAstrocytes is shown in table 2.6.

Table 2.6. List of human primers optimized for qPCR

Gene	Forward sequence	Reverse sequence	Conc (µM)
GAPDH	CAACTTTGGTATCGTGGAAGGAC	ACAGTCTTCTGGATGGCAGTG	5
VEGF-A	CAGGTCAGACGGACAGAAAGA	AGCAGGTGAGTAAGCGAA	2.5
GDNF	AGGATTGCGAACTCTTGCCC	CAGCCACGACATCCCATAACT	2.5
BDNF	CCCGTGAGGTTTGTGTGGA	CCACCTTGTCTCGGATGTT	5
IL-1β	CCTGTCTGCGTGTTGAAAG	GGGAACTGGGCACTCAA	5
IL-6	AGAGGCACTGGCAGAAAACA	TCACCAGGCAAGTCTCCTCA	5
TNF-α	GCTGCACTTTGGAGTGATCG	TCACTCGGGGTTTCGAGAAGA	5

2.5 Human Adipose Derived Stem Cells

2.5.1 Isolation of human Adipose Derived Stem Cells

Abdominal subcutaneous adipose tissue was obtained by liposuction from a consenting healthy donor of 34 years of age under ethical approval from the Ethics Committee of East Hospital Affiliated to Tongji University School of Medicine (approval number 038). The lipoaspiration procedure was carried out by the surgical team in the hospital clinic. To isolate human primary adipose derived stem cells (hADSCs) fresh lipoaspirate was processed as described in the literature with minor modifications (Zuk et al., 2002). In figure 2.12 is a schematic representation of the hADSCs isolation process.

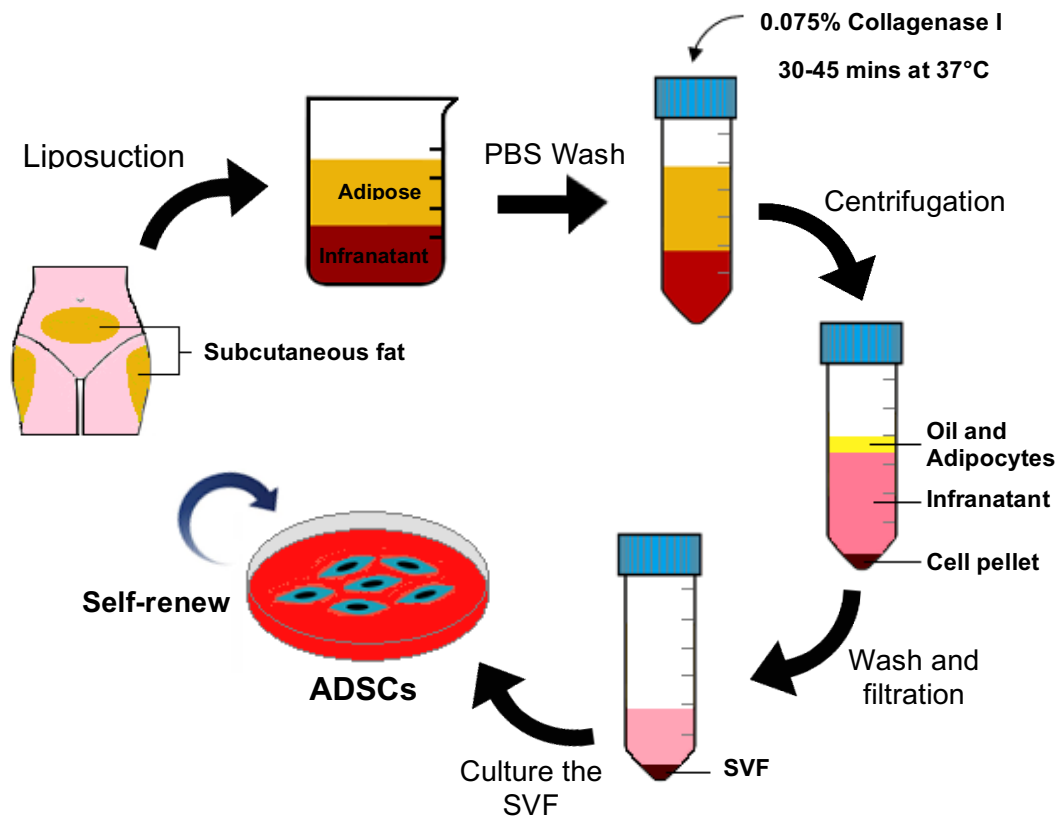


Figure 2.12. Isolation process to obtain ADSCs from human lipoaspirate. Fresh lipoaspirate is extensively washed in PBS to remove blood and contaminants. The adipose tissue is then enzymatically digested with collagenase I and the stromal vascular fraction (SVF) is obtained by filtration and centrifugation steps. Culture of the SVF on standard plastic tissue culture flasks results in the selection and expansion of the adipose stem cell population. Adapted with permission from “Advances, challenges and future directions for stem cell therapy in amyotrophic lateral sclerosis”, *Molecular Neurodegeneration*, 2017 (Ciervo et al., 2017).

Raw adipose tissue was extensively washed (3 to 4 times) with equal volumes of sterile PBS without calcium and magnesium containing 100 U/ml of Pen/Strep (Gibco) in order to remove contaminants from blood. The resulting floating yellow adipose tissue was collected and digested with an equal volume of 0.075% (w/v) Collagenase type I (17100-017, Gibco), containing 100 U/ml Pen/Strep in PBS for 60 minutes at 37 °C with manual shaking every 5 to 10 minutes. At the end of the incubation period, the collagenase activity was neutralized by adding an equal volume of PBS containing 10% (v/v) FBS (10099-141, Origin secure: Australia, Gibco) and the homogenate was filtered through a 70 µm nylon mesh filter to remove undigested tissue. The filtrate was then centrifuged at 400g for 5 minutes at RT to obtain the high-density stromal vascular fraction (SVF) pellet. The resultant top yellow layer and infranatant containing adipocytes, oil and pre-adipocytes was discarded and the SVF pellet was washed in DMEM/F-12 (11330032, Gibco) containing 10% (v/v) FBS and 100 U/ml Pen/Strep by centrifugation at 300g for 3 minutes. Finally, the pellet containing the ADSC fraction was re-suspended in complete proliferation medium consisting of DMEM/F-12, 10% (v/v) FBS, 10 ng/ml human basic fibroblast growth factor (bFGF) (10014-HNAE, Sinobiological) and 100 U/ml Pen/Strep. The cell solution was filtered through a sterile 70 µm nylon mesh, and cultured in a humidified incubator at 37 °C, 20% O₂, and 5% CO₂. After 48 hours, cultures were washed twice with pre-warmed PBS to remove debris and non-adherent cells and placed back in the incubator with fresh complete medium for cell expansion. Medium was changed every 2-3 days and to avoid spontaneous differentiation and/or inhibition of proliferation, cells were not allowed to reach confluence. When cultures reached 80-90 % confluence, cells were washed in PBS, detached with 0.25% trypsin-EDTA (25200056, Gibco) at 37°C for 2-3 minutes and passaged at a seeding density of 10,000 cells/cm² or at a ratio of 1:3 culture dishes.

2.5.2 hADSC characterisation by flow cytometry

hADSCs were phenotypically characterized by a multicolour flow cytometry analysis for expression of specific mesenchymal stem cell, hematopoietic and endothelial surface markers. All the fluorescent-conjugated antibodies used were from the Human MSC Analysis Kit (562245, BD Biosciences), which provides MSC positive markers (CD73, CD105, CD90, CD44) both as single and cocktail mixture, a cocktail mixture of negative markers (CD34, CD31, CD45, CD11b, CD19 and HLA-DR) to allow identification of potential contaminants, and a cocktail of corresponding fluorescent conjugated isotype control antibodies. All the antibodies are summarized in table 2.7.

Cells at 90% confluency were collected by trypsinization, centrifuged at 400g for 5 minutes and re-suspended in complete hADSCs medium for cell counting. Cells were then aliquoted into micro-centrifuge tubes at a concentration of 0.5×10^6 /tube and washed in 500 μ l of ice-cold flow cytometry buffer (FCB) consisting of PBS and 2% FBS. After centrifugation at 300g for 3 minutes, cells were re-suspended in FCB and incubated for 10 minutes on ice. Cells were then centrifuged again and re-suspended in 100 μ l of FCB containing the specific individual fluorescent conjugated antibody, antibodies cocktail or isotype controls at the manufacturer recommended concentration. For the unstained negative control, no antibody was added. After 30 minutes incubation on ice in the dark, cells were washed three times with 500 μ l of FCB by centrifugation at 300g for 3 minutes at 4°C, re-suspended in 400 μ l of FCB, and transferred to FACS tubes (Falcon) ready for analysis

Cells were acquired on a Caliber flow cytometer (BD, USA) and analysed with FlowJo 7.6.1 software. Unstained cells were used to set the gates and isolate the single cell population. Forward scatter (FSC) and side scatter (SSC) parameters were set with a logarithmic scale to exclude debris and dead cells. From each sample at least 10,000 single cell events were recorded. Fluorescence compensation was performed by the Flow Cytometry Facility technical team (Tongji University, Shanghai).

Table 2.7 Fluorescent-conjugated human antibodies used in flow cytometry

Antibody	Host species	Clone
PE – CD34	Mouse IgG1	30-H123
PE – CD45	Mouse IgG1	HI30
PE – CD11b	Mouse IgG1	ICRF44
PE – CD19	Mouse IgG1	HIB19
PE – HLA-DR	Mouse IgG1	G46-6
FITC – CD90	Mouse IgG1	5E-10
PerCP/Cy5.5 – CD105	Mouse IgG1	266
APC – CD73	Mouse IgG1	AD2
PE – CD44	Mouse IgG1	G44-26
PE mouse IgG1 Isotype	Mouse IgG1	X40

FITC mouse IgG1 Isotype	Mouse IgG1	X40
PerCP/Cy5.5 mouse IgG1 Isotype	Mouse IgG1	X40
APC mouse IgG1 Isotype	Mouse IgG1	X40

2.5.3 In vitro differentiation of hADSCs

To assess the multipotential differentiation capacity of cultured hADSCs, cells expanded for three generations (p3) were induced to differentiate *in vitro* into adipocytes, osteocytes and chondrocytes. hADSCs were differentiated by using specific conditioned media consisting of chemical cocktails and growth factors. All chemical reagents were purchased from Sigma-Aldrich unless otherwise specified.

2.5.3.1 Adipogenic differentiation

hADSCs were grown in complete medium consisting of DMEM/F-12, 10% FBS, 10 ng/ml human bFGF, and 100 U/ml Pen/Strep. When cultures were 80% confluent, cells were collected by trypsinization and plated in 12-well culture plates or in 24-well plates onto glass coverslips at a seeding density of 30,000 cells/cm². After 24-48 hours of incubation, expansion medium was replaced with adipogenic induction medium (AIM) consisting of DMEM/F12, 10% (v/v) FBS, 100u/ml Pen/Strep, 1 μM dexamethasone, 10 μM insulin, 200 μM indomethacin and 0.5 mM Isobutylmethylxantine (IBMX). To check for spontaneous differentiation, control cells were cultured with standard complete medium. Media was replaced every 2-3 days with fresh prepared differentiation media. After 6 days, the AIM was switched to the adipogenic maintenance medium (AMM) in which IBMX was removed from the differentiation cocktail and cells cultured for another 6 days. The differentiation process was monitored daily by microscopic observation for a total of 12 days. Adipogenic differentiation was confirmed by Oil Red O staining 6 and 12 days after starting the differentiation protocol as described in paragraph 2.2.4.3.

2.5.3.2 Osteogenic differentiation

Osteogenic differentiation of hADSCs was performed on 6-well standard culture plates. hADSCs were plated at a seeding density of 50,000 cells/cm². When cultures became confluent, basal proliferation medium was replaced with osteogenic differentiation media consisting of DMEM/F12, 10% (v/v) FBS, 100 U/ml Pen/Strep,

0.1 μM dexamethasone, 50 $\mu\text{g/ml}$ ascorbic acid and 10nM β -glycerol phosphate. Media was changed every 3 days with fresh made media for a maximum period of three weeks. In parallel, hADSCs were cultured in control basal media to monitor for spontaneous differentiation. Osteogenesis was assessed by Alizarin Red O staining after 1, 2 and 3 weeks of the initiation of the differentiation as described in paragraph 2.2.4.5.

2.5.3.3 Chondrogenic differentiation

For chondrogenic differentiation, two different methods were employed. The first protocol was performed on three dimensional cell pellets as described in detail in paragraph 2.2.4.6. Briefly, hADSCs were induced to grow as cell pellets in 15 ml tubes and cultured in chondrogenic differentiation medium consisting of DMEM/F12 containing 1% (v/v) FBS, 100 U/ml Pen/Strep, 1% (v/v) Insulin-transferrin—selenium (ITS), 1% (v/v) sodium pyruvate, 50 $\mu\text{g/ml}$ ascorbic acid, 0.1 μM dexamethasone and 10 ng/ml transforming growth factor β 1 (TGF β 1) (10804-HNAC, Sinobiological). Fresh prepared chondrogenic medium was added every 2-3 days. Control non-induced cell pellets were cultured in DMEM/F12, 1% (v/v) FBS and 100 U/ml Pen/Strep. Differentiation was assessed by Alcian blue 8G (A5268, Sigma) staining at week 3 of differentiation (see paragraph 2.2.4.7).

Chondrogenic differentiation was also performed by a two dimensional cell culture system on standard 12-well culture plates. hADSCs were expanded for three passages and plated at a cellular density of 30,000 cells/cm² in control basal medium. After 24 hours, or when cultures reached 90-95% confluence, the standard culture medium was switched to the chondrogenic medium consisting of DMEM/F12, 1% (v/v) FBS, 100 U/ml Pen/Strep, 1% (v/v) sodium pyruvate, 6.5 $\mu\text{g/ml}$ human recombinant insulin, 50 ng/ml ascorbic acid, 10 ng/ml TGF β 1 and 0.1 μM dexamethasone. Control non-induced cells were cultured in DMEM/F12, 1% FBS and 100 u/ml Pen/Strep. Medium was changed every day for the first three days, and every 2-3 days afterwards. Cell morphology was monitored daily by microscopic observation and phase contrast images were taken with a Nikon Eclipse Ti80 microscope (Nikon, China). Differentiation was assessed by Alcian Blue staining at one and two weeks after initiation of induction.

2.5.4 Recombinant human C-C chemokine Receptor 2B (hCCR2B) lentiviral vector design and production

2.5.4.1 hCCR2B cDNA shuttle vector information

The complete Open Reading Frame (ORF) of the human CCR2B gene was purchased from R&D Systems (hCCR2B VersaClone cDNA, RDC0004). The shuttle vector contains the hCCR2B cDNA (1096bp) flanked by multiple cloning sites and preceded by a Kozak consensus sequence for optimal translation initiation. The vector, carrying the gene for ampicillin resistance, has a size of 3830bp. The vector map is shown in figure 2.13. The plasmid DNA sequence and the translated hCCR2B insert sequence are shown in the appendice (appendix 1 and appendix 2 respectively).

RDC0004 Plasmid Map

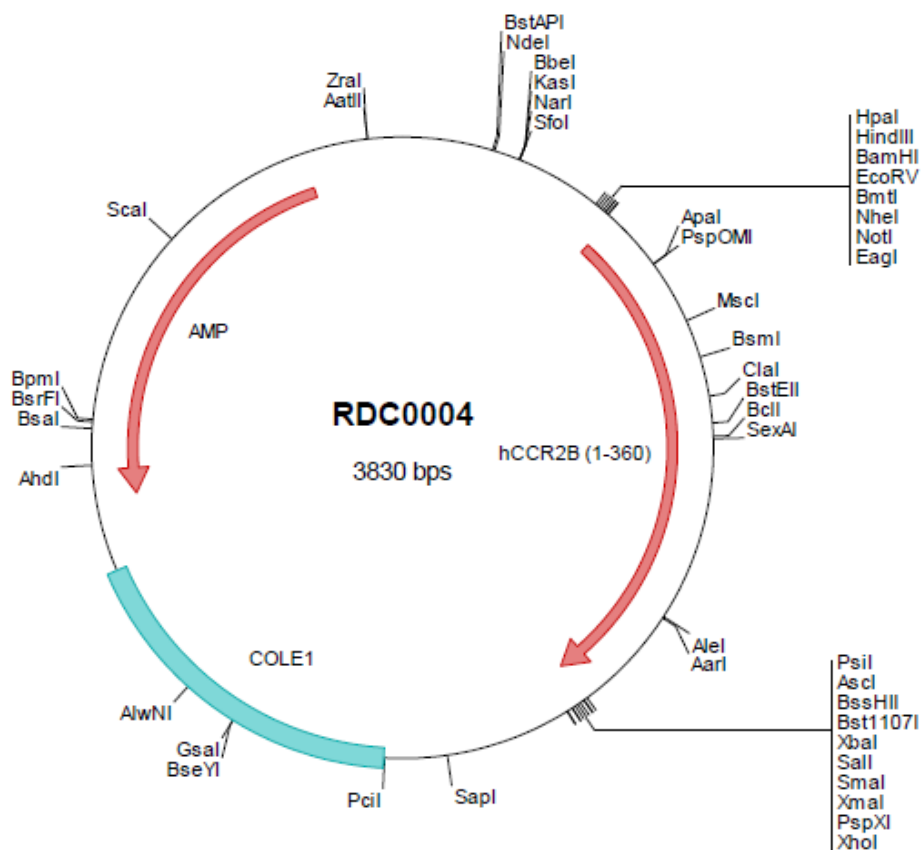


Figure 2.13. hCCR2B cDNA shuttle vector map.

2.5.4.2 pLVX-CMV-IRES-ZsGreen1 plasmid information

The pLVX-IRESZsGreen1 lentivirus vector (pLV-IRES) was purchased from Clontech (632187, Takara Bio Company). pLV-IRES is a HIV-1 based, lentivirus expression vector designed to allow the simultaneous expression of the selected protein of interest and the green fluorescent protein ZsGreen1 from a bicistronic mRNA transcript. The transcript is driven by the cytomegalovirus (CMV) immediate early promoter which is located upstream the multiple cloning site (MCS). The insertion of an internal ribosome entry site (IRES) between the two coding frames allows the translation of the second coding frame from the same mRNA transcript. The vector contains all the viral processing elements for the production of 3rd generation lentivirus particles together with a pUC origin of amplification and an E. Coli ampicillin resistance. In figure 2.14 the lentivirus vector map and the MCS is shown.

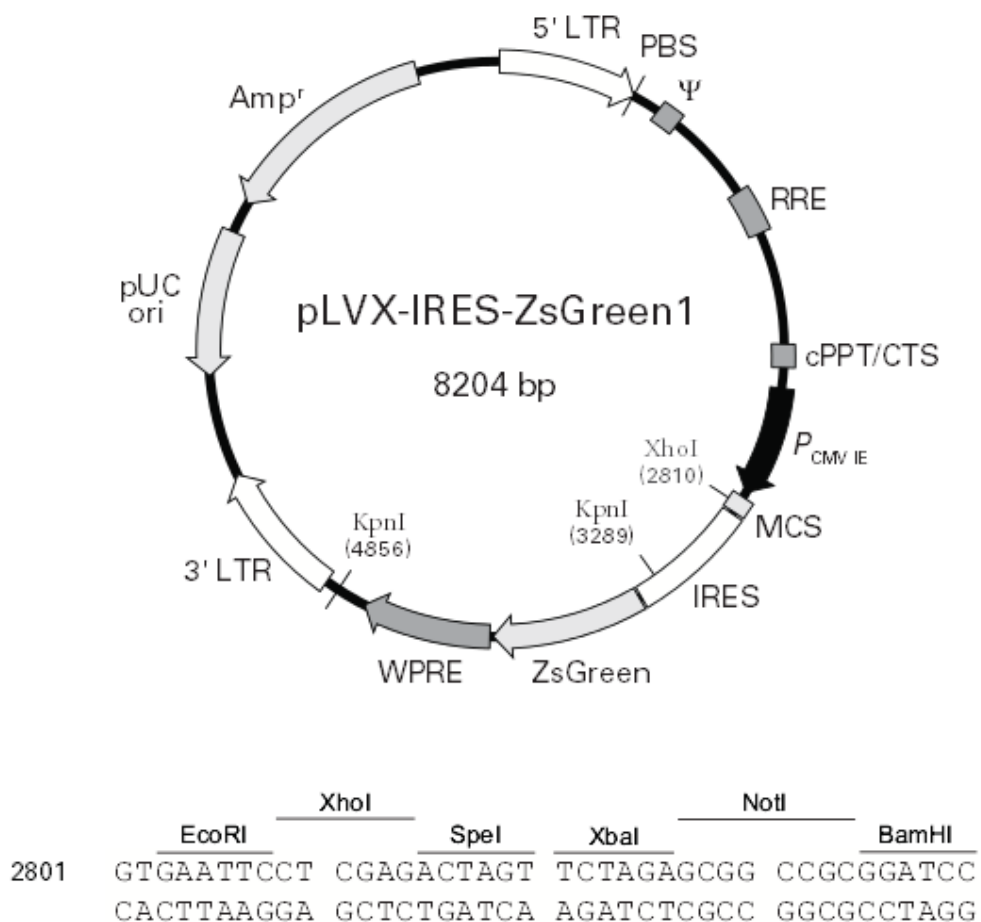


Figure 2.14. pLVX-IRESZsGreen1 lentivirus vector. On the top the vector map. On the bottom the multiple cloning site (MCS).

2.5.4.3 hCCR2B plasmid transformation, purification, digestion and production of bacteria glycerol stocks

In order to make glycerol bacteria stocks and replicate the plasmid, the hCCR2B cDNA shuttle vector was transformed into DH5 α E.Coli chemically competent cells (CB101, Tiangen). Transformation was performed by following the manufacturer recommendations. Briefly, 100 μ l of DH5 α cells stored at -80 $^{\circ}$ were thawed on ice for 20-30 minutes, gently re-suspended to obtain a homogeneous cells solution, and 50 ng of hCCR2B shuttle vector DNA was added. Cells were then incubated on ice for 30 minutes. During the incubation period, pre-made 10 cm agar plates (1% (w/v) tryptone, 1% (w/v) sodium chloride, 0.5% (w/v) yeast extract and 1.5% (w/v) agar) containing 100 μ g/ml of ampicillin were removed from 4 $^{\circ}$ C and allowed to cool at RT. At the end of incubation, cells were heat shocked in a water bath at 42 $^{\circ}$ C for 90 seconds and quickly transferred on ice for at least three minutes. Successively, 900 μ l of sterile Luria-Bertani (LB) broth (1% (w/v) tryptone, 0.5% (w/v) yeast extract and 1% (w/v) sodium chloride) without antibiotic was added to the cell suspension and tubes incubated in a shaker incubator at 37 $^{\circ}$ C, 188 rpm/min for 45 minutes. After incubation, 1/10 (100 μ l) of the outgrowth culture was plated on the agar plate and incubated at 37 $^{\circ}$ C O/N. Compcell control plasmid pUC19 (0.1 ng/ μ l) was transformed as a positive control, while for the negative control ddH $_2$ O was added to the DH5 α cells. The next day, five different single bacterial colonies were picked up from the LB agar plate and individually transferred into 50ml tubes containing 5ml of LB with 100 μ g/ml ampicillin. Bacteria cultures were incubated O/N (16-18 hours) at 37 $^{\circ}$ C in a shaking incubator at 188 rpm/min. After incubation, 500 μ l of the cloudy LB broth (indicating larger bacterial presence) were mixed with 500 μ l of sterile 50% (v/v) glycerol in ddH $_2$ O and stored in cryovials at -20 $^{\circ}$ C. The remaining 4.5 ml were used for plasmid purification using the TIANprep Rapid Mini Plasmid kit (DP105, Tiangen), according to the manufacturer's instructions. At the end of the purification protocol, plasmid DNA was eluted with 20 μ l of free-DNase ddH $_2$ O. DNA concentration was then determined with the NanoDrop 2000C (Thermo Scientific) and stored at -20 $^{\circ}$ C.

The identity of the purified plasmid was revealed by diagnostic restriction digestion. hCCR2B plasmid DNA was digested with fast digest BamHI (FD0054, Thermo Scientific,) and fast digest SmaI (FD0664, Thermo Scientific) restriction enzymes which recognize and cut DNA in two different sites. Specifically, Bam HI upstream and SmaI downstream the hCCR2B insert respectively. Restriction digestion was performed by following the manufacture's protocol. To check for the correct plasmid size, insert and backbone, both single (only one enzyme) and double (both enzymes)

digestions were performed. A single (or double) digestion reaction mixture was prepared as follows:

10X Fast Digest Buffer	2 μ l
Plasmid DNA	1-2 μ l (1 μ g)
Fast digest enzyme	1 μ l (+ 1 μ l)
ddH ₂ O to a final volume of	20 μ l

A master mix containing all the reagents except the DNA plasmid was prepared at RT, gently mixed and aliquoted into each thin PCR tube containing 1 μ g of DNA plasmid from each isolated clone. The tubes were briefly spun down and incubated at 37°C in a water bath for 15 minutes. All the digested products were finally loaded on a 1.5% (w/v) agarose/1xTAE gel matrix containing SYBR Safe DNA Gel Stain (S3310, Invitrogen,) diluted 1:50000 and run for ~40 min at 120mV. Products were visualized with the use of a blue light transilluminator.

2.5.4.4 hCCR2B cloning into the pLV-IRES plasmid by PCR method

Primer Design

Since the MCSs of the hCCR2B and pLV-IRES vectors were not compatible, the polymerase chain reaction (PCR) cloning method was performed. The PCR cloning method allows integration of the desired DNA fragment into a specific vector backbone by amplifying the gene of interest and contemporaneously anchoring the restriction sites that are compatible with the vector MSCs.

Primers to amplify the full-length coding sequences were designed as follow:

5'-end forward primer:

- 5' extension to the restriction site: an extra 5 bases were added at the 5' end of the forward primer to facilitate the restriction enzyme digestion. The extension was designed in order to avoid hairpin structures within the primer.
- Restriction site: the first restriction site was added downstream of the coding sequence. This was chosen with the help of the DNA analysis tool "Addgene's Sequence Analyser" in order to add a restriction site which would not cut within the hCCR2B but was present within the recipient plasmid MSC in the correct orientation.
- Hybridization sequence: in the region that binds to the 5'-end of the hCCR2B DNA sequence (18bp of homology), the kozak consensus sequence (GCCGCCACC) which precedes the ATG start codon was included. For the design, the OligoAnalyzer 3.1 free software (Integrated DNA Technologies,

<http://www.idtdna.com/calc/analyzer>) was used in order to generate an overlapping sequence with a melting temperature (T_m) of at least 60 °C.

- 3'-end: to avoid nonspecific annealing, no more than two G or C bases in sequence were added, nor a T base.

3'-end reverse primer:

- 5' extension to the restriction site: an extra 5 bases were added at the 5' end of the reverse primer to facilitate the restriction enzyme digestion. The extension was designed in order to avoid hairpin structures within the primer.
- Restriction site: the second restriction site was added downstream of the coding sequence. This was chosen with the help of the DNA analysis tool "Addgene's Sequence Analyser" in order to add a restriction site which did not cut within the hCCR2B cDNA and is located within the recipient plasmid MSC in a position next to the restriction site chosen for the forward primer.
- Hybridization sequence: in the region that binds to the stand complement of the 3'-end of the hCCR2B DNA sequence (18bp of homology) the TAA stop codon was included.
- 3'-end: to avoid nonspecific annealing, no more than two G or C bases were added, nor a T base.

Importantly, primers were also designed by following the guidelines below:

- Primer length between 18-30bp
- Repetitive and palindromic sequences were avoided
- Similar annealing temperature for forward and reverse primers (within 2-4 °C) and above 60°C.
- C/G content of approximately 40-60%
- Secondary structures (i.e hairpins, homo- and hetero-dimers) were avoided

Primers were ordered from Sango Biotech (China) and are listed in table 2.8.

Table 2.8. hCCR2B cloning primers detail

Primer Name	Sequence (5'- to 3'-)	Length (bases)	%GC	T_m (°C)
hCCR2B-XbaI-F	CATGATCTAGAGCGGCCGCCACCATGCTG	29	62.1	67.4
hCCR2B-BamHI-R	GCTCACCTAGGGGCGCGCCTTTATAAACC	29	58.6	67.6

Highlight in yellow the 5'- extension sequence; in green the specific restriction site sequence; in red the insert cDNA hybridization sequence.

hCCR2B cDNA amplification by PCR and purification

In order to clone the hCCR2B cDNA into the pLV-IRES expression vector, the complete gene ORF together with the kozak consensus sequence was amplified by PCR. As already described, primers were designed to anchor the insert with XbaI and Bam HI restriction sites which are compatible with the pLV-IRES MCS. In order to minimize mutation events during the cDNA amplification, a high fidelity polymerase with 3'-5' proofreading activity was used. The Fast HiFidelity PCR kit was purchased from Tiangen (KP202, China). DNA amplification was performed on a Veriti Thermal Cycler (4375786, Thermo Fisher Scientific). A single PCR reaction mixture was prepared on ice as follows:

Plasmid DNA template	1 μ l (5ng)
Forward primer	1.5 μ l (0.3 μ M)
Reverse primer	1.5 μ l (0.3 μ M)
5x Fast HI Fidelity buffer	10 μ l
Fast HI Fidelity polymerase	1 μ l
ddH ₂ O	35 μ l
Total Volume	50 μ l

A three-step PCR reaction was chosen and the automated cycling was set as follows:

Step	Temperature	Time	
Initial Denaturation	94 °C	2 min	
Denaturation	94 °C	15 sec	} X 34 cycles
Annealing	65 °C	10 sec	
Elongation	68 °C	30 sec	
Final elongation	68 °C	5 min	
Storage	4 °C	Infinite	

To check whether the PCR product was of the anticipated size, 5 μ l of the PCR reaction was run on a 1.5 % agarose gel together with a positive control (enzymatically digested shuttle vector) and a negative control (PCR reaction without DNA template). After the amplicon size was confirmed, the remaining 45 μ l of the PCR reaction was purified from primers, dNTPs, enzyme, short failed PCR products and salts by using the Universal DNA purification kit (DP214, Tiangen) following the

manufacturer's recommendations. From a single PCR reaction, DNA was eluted with 20 μ l of nuclease-free ddH₂O, and concentration determined with Nanodrop.

pLVX-IRES and hCCR2B DNA restriction digestion and purification from agarose gel

The pLV-IRES backbone was cut with XbaI and Bam HI restriction enzymes by a double enzymatic digestion as described in paragraph 2.5.5.3. The PCR products were also digested with the same enzymes, in order to generate sticky ends compatible with the digested backbone vector. To cut the PCR products the reaction mixture was as follows:

10X Fast Digest Buffer	2 μ l
hCCR2B PCR product	1-2 μ l 0.2 μ g)
Fast digest enzyme	1 μ l (+ 1 μ l)
ddH ₂ O to a final volume of	30 μ l

Both digestions were performed at 37 °C for 20 minutes. Since the two pairs of enzymes do not have compatible overhangs, the use of a phosphatase to prevent re-circularization of the vector was omitted. Successively, 3 μ g of digested pLV-IRES and 0.5 μ g of digested PCR products were run on a 0.8% (w/v) Low-melting agarose gel >480 g/cm² (9012-36-6, BBI), together with a DNA ladder of known fragments size. Electrophoresis was run at 90 Volt for 20-30 minutes on ice. The DNA fragments were then excised from the gel with the help of a blue light transilluminator (Tiangen) and DNA was extracted from the gel using the TIANgel midi DNA purification kit (DP209, Tiangen). DNA was finally recovered in ddH₂O and nucleic acid concentration and purity measured with Nanodrop.

Ligation, transformation, diagnostic digestion and sequencing analysis

The hCCR2B cDNA construct was ligated to the pLV-IRES lentivirus vector by overnight incubation at 16°C with the T4 DNA ligase (M0202, NEB). For ligation, the molar ratios 1:3 and 1:5 vector to insert were tested. NEBcalculator (<http://nebiocalculator.neb.com/#!/ligation>) was used to calculate the DNA molar ratios.

The reaction mixture was set as follows:

Molar ratio vector to insert	1:3	1:5
T4 DNA Ligase Buffer (10X)	2 μ l	2 μ l
pLVX-IRES (8204bp)	70ng (13.81 fmol)	60ng (11.84 fmol)
hCCR2B (1096bp)	28 ng (36.91 fmol)	40ng (59.06f mol)
Fast digest enzyme	1 μ l	1 μ l
ddH ₂ O to a final volume of	20 μ l	20 μ l

The mixture reaction was prepared into a micro centrifuge tube on ice, gently mixed and centrifuged briefly. Samples were then incubated in a thermocycler at 16°C overnight. After incubation, the ligase was heat inactivated at 65°C for 10 minutes. Finally, 7 μ l of the ligation reaction was used to transform DH5 α competent E Coli cells as described in paragraph 2.5.5.3. In parallel, negative controls were included in the experiment. To estimate the background of self-ligating recipient plasmid and uncut plasmid, the ligase reaction of the pLV-IRES plasmid without any DNA insert or the reaction without enzyme was transformed.

After 16 hours, depending on the number of background colonies in the control plates, 5 to 10 single bacterial colonies were picked up, grown overnight and checked for successful ligation by diagnostic digestion with the same pair of enzymes used for the cloning. Finally, the positive colonies were verified by Sanger sequencing method by the Jie Li Biology company (www.genebioseq.com, Shanghai). For sequencing, the universal EGFP-F and EGFP-R primer pairs (flanking the vector MCS) were used. The sequences were received as electropherograms and visualised with Chromas software (Version 2.5, Technelysium Pty).

2.5.5 Production of infectious viral particles with 3rd or 2nd generation packaging plasmids

For lentivirus particle production, HEK 293T cells were transiently co-transfected (calcium-phosphate method) with the lentivirus vector of interest (pLVX-IRES-ZsGreen1 backbone or pLVX-hCCR2B-IRES-ZsGreen1) and with either 3rd generation packaging plasmids (pMDL g/p RRE, pRSV-Rev and pVSV-G), or 2nd generation packaging plasmids (pVSV-G and pCMV. Δ 89).

One day before transfection, HEK 293T cells were plated on 10 cm petri dishes at a concentration of $2.5\text{-}3 \times 10^6$ cells/plate in DMEM containing 10% FBS and incubated at 37°C, 5% CO₂. Transfection was performed when cells reached 70-80 % confluence. When using the 3rd generation packaging plasmids, for each plate, 20 µg of the insert vector, 10 µg of pRRE, 10 µg of pRev and 6 µg of pVSV-G were mixed in a final volume of 250 µl of sterile ddH₂O. For the 2nd generation packaging method, 10 µg of the insert vector, 5.5 µg of pVSV-G and 7.5 µg of pCMV.Δ89 were pooled together and mixed in ddH₂O. The DNA solution was then added dropwise to 250µl of calcium chloride (CaCl₂) 0.5M. Immediately after, 500 µl of RT 2x HBS (280mM NaCl, 100mM HEPES free-acids, 1.5mM Na₂HPO₄, 0.2% (w/v) dextrose in ddH₂O, pH 7.05), were added dropwise to the DNA-CaCl₂ solution while bubbling air with an automated pipette. The solution was left at RT for 10-15 minutes for DNA precipitation. Finally, 1 ml/plate of the precipitated DNA solution was added dropwise to the HEK293T cells, plates were swirled gently and incubated at 37°C, 5% CO₂ for 6 hour to overnight. After incubation, the medium containing the DNA was removed, replaced with 10 ml of fresh new medium and cells incubated for an additional 48 hours. At the end of the incubation period, the virus-containing medium was collected, centrifuged at 1500 RPM for 3 minutes and filtered through a 0.45 µm filter to remove cells and debris. Virus was then used directly for transduction experiments.

2.5.6 hADSCs transduction optimization

Because of unavailability of equipment (ultracentrifuge), it was not possible to obtain high-titre viral preparations. Thus, freshly produced virus was used to directly transduce hADSCs. For transduction optimization hADSCs were plated at a cell density of 8,000 cells/cm² in 6-well culture plates, placed in incubator O/N and the following day transduced with the pLV-IRES backbone or pLV-IRES-CCR2B expressing lentivirus produced with either the 3rd or 2nd generation packaging plasmids. Different conditions were tested. These are summarized in table 2.9.

Table 2.9. hADSCs transduction optimization

Virus	Packaging method	Amount of Virus (ml)	n° of transductions	Polybrene concentration (µg/ml)
pLV-IRES	3 rd generation	1	1 st :16h 2 nd : 6h	10
pLV-IRES	3 rd generation	2	1 st :16h 2 nd : 6h	10

pLV-IRES	3 rd generation	1	1 st :8h 2 nd : 8h 3 rd : 8h	4
pLV-IRES-hCCR2B	3 rd generation	1	1 st :8h 2 nd : 8h 3 rd : 8h	4
pLV-IRES	2 nd generation	1	1 st :8h 2 nd : 8h	4
pLV-IRES-hCCR2B	2 nd generation	1	1 st :8h 2 nd : 8h	4

In one set of experiments, growth medium was replaced with either 1 or 2 ml of the medium containing virus (3rd generation) in the presence of 10 µg/ml polybrene and cells placed in incubator. After 16 hours a second round of transfection with fresh virus was performed for further 6 hours.

In a separate experiment, hADSCs were infected for three rounds of 8 hours each with 1 ml of virus (3rd generation) and 4 µg/ml polybrene.

In the last transduction optimization experiment, hADSCs were infected for two rounds of 8 hours each with 1 ml of virus containing medium (2nd generation) and 4 µg/ml polybrene.

For each of the conditions tested, transduction efficiency was evaluated 5 days post infection by fluorescence microscopy using the Nikon Eclipse Ti inverted microscope and by flow cytometry analysis.

2.5.7 Analysis of hCCR2B expression by Flow Cytometry

hADSCs were transduced with either the pLV-IRES backbone or the pLV-hCCR2B-IRES expressing lentivirus and 5 days post-infection the transduction efficiency and the cell surface expression of hCCR2B were investigated by flow cytometry analysis. Transduction efficiency was measured by quantifying the number of hADSCs expressing the ZsGreen1 protein. The expression of hCCR2B was detected by staining the cells with the mouse anti-human APC-conjugated CCR2 antibody (FAB151A, R&D Systems) following the manufacturer's recommendations. Samples preparation and analysis was carried out as described in paragraph 2.5.2.

2.5.8 Analysis of hCCR2B expression by Western blot

2.5.8.1 Preparation of hADSC lysates for western blot

hADSCs were transduced with lentivirus on 6-well culture plates and 5 days post-transduction cells were collected and cell lysis performed for immunoblotting. Culture medium was discarded and cells washed on ice with ice cold PBS. PBS was removed and 200 μ l of ice cold RIPA buffer (89900, Thermo Fishes Scientific) containing 1mM phenylmethane sulfonyl fluoride (PMSF) (10837091001, Sigma-Aldrich) was added to the well. Cells were then scraped and collected in cold 1.5 ml collection tubes. Cells were homogenised by vigorously pipetting the solution followed by 3 passages through a syringe with needle. Homogenates were incubated on ice for 30 minutes. Following incubation, lysates were clarified by centrifugation at 12,500g for 10 minutes at 4°C and supernatants containing soluble proteins collected. Protein concentration was quantified by optical density using the Quick Start Bradford 1x Dye Reagent (500-0205, Bio-Rad). Cell lysates were then diluted with RIPA buffer containing PMSF to equalize the amount of protein in each sample. Samples were finally mixed with 2X Laemmli buffer (S3401-10VL, Sigma-Aldrich) and heated for 10 minutes at 70°C for protein denaturation and addition of positive charges.

2.5.8.2 SDS-Polyacrilamide Gel Electrophoresis and transfer

Mini-PROTEAN® TGX™ Precast Protein Gels (4–20%, 4561093, Bio-Rad) were inserted into a Mini-PROTEAN® Tetra Vertical Electrophoresis Cell (Bio-Rad), and the apparatus filled with running buffer (25mM Tris, 3.5mM SDS, 20mM glycine). A 3 μ l volume of pre-stained protein ladder (molecular weight marker) was load in the first well of each gel, while 15 μ l of each sample (~25 μ g of soluble proteins) was loaded in the remaining wells. Electrophoresis was run at 50 V for 20 minutes and then at 130 V until the dye reached the bottom of the gel. Following electrophoresis, proteins were transferred into Polyvinylidene difluoride (PVDF) membranes with a wet transfer apparatus. The gel was carefully removed from the electrophoresis apparatus, soaked in transfer buffer (47.9 mM Tris, 38.6mM glycine, 1.38mM, 20% (v/v) methanol) and placed over a PVDF membrane pre-soaked on methanol. Pads, filter papers and transfer foam pre-soaked in transfer buffer were used to assemble the transfer sandwich, which was then placed in the transfer apparatus. Finally, the apparatus was placed in bag of ice and proteins transferred at 0.15A/gel for 1 hour.

2.5.8.3 Immunoblotting

Membranes were blocked in 5% (w/v) milk/Tris Buffered Saline containing Tween® 20 (TBST) (20mM Tris, 137mM NaCl, 0.2% (v/v) Tween 20, pH 7.6) for 1 hour at RT with agitation. After blocking, membranes were stained with the rabbit anti-human CCR2-N-terminal primary antibody (ab155321, Abcam) at a dilution of 1/500 in 5% (w/v) milk/TBST at 4° O/N with agitation. The membranes were washed 3 times in TBST for 5 minutes at RT and incubated for 1 hour at RT with the horseradish peroxidase conjugated (HRP) anti-rabbit secondary antibody (7074S, Cell Signaling Technology) diluted 1/3000 in 5% (w/v) milk/TBST. After 3 x 5 minute washes in TBST, membranes were incubated with enhanced chemiluminescence (ECL) for 1 minute and imaged.

After imaging, the membranes were incubated with Restore Western Blot Stripping buffer (21059, ThermoFisher) for 15 minutes at RT with agitation, following by 3 x 5 minute washes in TBST. The membranes were then blocked in 5% (w/v) milk/TBST for 1 hour at RT and successively stained with the mouse anti-β-Actin primary antibody (ab6276, Abcam) at 1/1000 dilution in 5% (w/v) milk/TBST for 1 hour at RT. Following incubation, membranes were washed in TBST and incubated with the HRP-conjugated anti-mouse secondary antibody (7076S, Cell Signalling Technology) diluted 1/3000 in 5% (w/v) milk/TBST for 1 hour at RT. Finally, membranes were washed in TBST, incubated for 1 minute with ECL and imaged with the G:BOX Chemi XRQ gel doc detection system (Syngene, USA).

2.5.9 Analysis of hCCR2B expression by IF

Cells were seeded onto glass coverslips in 24-well culture plates and cultured for 48 hours under basal conditions. Cells were washed with PBS and fixed with 4% (w/v) PFA / 0.2% (v/v) Triton™-X-100 in PBS for 15-20 minutes at RT. Following 3 quick washes with PBS, cells were blocked with 300 µl of 5% (v/v) donkey serum/PBS for 40 minutes at RT. After blocking, cells were stained with the rabbit anti-human CCR2-N-terminal primary antibody (ab155321, Abcam) in 2% (v/v) donkey serum/PBS at a dilution of 1/250 at 4°C O/N. The following day cells were washed with PBS (3 X 5 min) with constant agitation and incubated with the secondary donkey anti-rabbit (H+L) CF™ 633 conjugated antibody (SAB4600132, Sigma) diluted 1/1000 for 1 hour at RT. As a negative control cells were incubated with the secondary antibody only. At the end of the incubation, coverslips were washed (3 x 5min) with PBS and stained with Hoechst (33258, Sigma) diluted 1/10000 for 10 minutes. Finally, coverslips were washed in PBS and mounted on a glass slide with Organo/Limonene mounting

medium (O8015, Sigma). Slides were left to air dry at RT for at least 24 hours before capturing images with an Upright Nikon Spinning Disk confocal microscope.

2.6 Statistical analysis

All statistical analyses were performed with the use of GraphPad Prism 7 (Graph Pad, San Diego, CA, USA). For data with multiple time points, 2-way ANOVA with Sidak post-hoc test was used. For pair-wise data with normal distribution, the Student's t-test was applied. For pair-wise data with non-normal distribution, the Mann-Whitney U test was used.

The 1-way ANOVA with Sidak's multiple comparison test and the 2-way ANOVA with Tukey's multiple comparison test were used depending on the number of variables in each experiment. All data are presented as mean \pm standard deviation. Statistical significance was considered with a p-value < 0.05 .

3 Characterisation of Mouse Adipose Derived Stem Cells (mADSCs)

3.1 Introduction

Mesenchymal stem cells represent a reliable non-haematopoietic adult source of stem cells, with great capacity for self-renewal, high plasticity, and immunomodulatory and trophic properties. Therefore, MSCs are considered a promising tool to repair and regenerate damaged tissues. Moreover, since MSCs have shown high long-term viability after *ex-vivo* expansion, and do not raise particular ethical issues, they represent attractive candidates for clinical applications. For several years, bone marrow has been considered the reference source of MSCs, however, the cell isolation method from BM aspirate is expensive, invasive and gives rise to a limited cell yield. In recent years, white adipose tissue (WAT) has become a research topic in regenerative medicine, as a promising alternative and more accessible source for MSCs. Indeed, WAT is widely present in the human body and can be relatively easily harvested with a minimally invasive procedure such as liposuction. Also, the stem cell frequency in WAT is estimated to be 40-fold more than in bone marrow aspirate, with ADSCs showing a higher proliferation capacity and a slower senescence ratio than BM-MSCs (Strem et al., 2005, Han et al., 2014).

The isolation of a multipotent stem cell population from human adipose tissue by mechanical and enzymatic techniques was first reported by Zuk et. al in 2001. By adopting the same digestion protocol, several groups have documented the isolation of ADSCs from both human and murine fat tissue, and demonstrated the reproducibility and consistency of this method. The only difference in the isolation procedure of ADSCs from rodents, is the starting biological material, consisting of fragmented fat tissue collected by open surgery, instead of a lipoaspirate. In 2013, the International Federation for Adipose Therapeutics and Science (IFATS) and the International Society for Cellular Therapy (SISCT), released a manuscript stating the minimal criteria to define the culture of expanded ADSCs, with the aim of providing general guidelines to promote and facilitate the development of reproducible and standardized methods amongst the medical and scientific community (Dominici et al., 2006). According to the aforementioned paper, cultured ADSCs are plastic adherent and should exhibit a homogeneous fibroblast-like morphology. Moreover, the cell immunophenotype should be characterized by flow cytometry to validate the relative homogeneity of the cell population. However, the lack of definitive and restricted

markers for ADSCs, imposes a requirement for their functional characterization. Indeed, *ex vivo* expanded ADSCs should preserve and demonstrate their multipotency and capacity for differentiation into cells of mesodermal origin (e.g. osteoblasts, adipocytes and chondrocytes). Therefore, it is important to fully characterise and confirm the mesenchymal stem cell identity of the isolated and expanded ADSCs before proceeding to any further *in vitro* or *in vivo* investigation.

As discussed in chapter 1, a critical parameter in stem cell transplantation is the study of both short- and long-term engraftment of the injected cells. While hADSCs can be easily identified by immunohistochemistry in rodent models, taking advantage of their cross-species nature, mADSCs need to be labelled before transplantation into rodents. Recently, the identification of the cell graft has been performed by labelling stem cells with fluorescent dyes such as Hoechst 33342, bisbenzimidazole, bromodeoxyuridine and Dil, which mark the cell nucleus or the cytoplasm. However, their use may not be appropriate for the study of long-term engraftment, since the dye gradually loses fluorescence intensity naturally and following cell proliferation (Wang et al., 2009b). More importantly, these molecules may easily transfer to host cells, making their use inadequate to study the fate of transplanted cells (Iwashita et al., 2000). One of the options to permanently label stem cells and identify the graft after *in vivo* transplantation, consists of the integration of the green fluorescent protein (GFP) into the cell genome. This can be efficiently achieved by the transduction of stem cells with GFP-encoding lentiviral vectors, which allows permanent GFP expression (Wang et al., 2009b). The efficient transduction of ADSCs with GFP-lentivirus, has already been demonstrated and the viral infection did not affect the immunophenotype, nor the differentiation potential *in vitro* (Wang et al., 2009b, van Vollenstee et al., 2016, Zhang et al., 2014). However, to exclude the eventual toxicity of the viral infection and/or GFP expression, it is important to re-evaluate cell morphology, immunophenotype and multipotency after lentivirus transduction.

In the body of work described in this chapter, ADSCs were isolated from the subcutaneous fat of WT adult mice and fully characterized by studying the morphology, proliferation, immunophenotype and differentiation potential. For *in vivo* tracking purpose, mADSCs were transduced with lentivirus carrying EGFP and a cell bank established.

3.2 Aims

1. To isolate, expand and characterise mADSCs derived from non-transgenic (NTg) healthy C57BL/6J mice.
2. To genetically modify mADSCs to express green fluorescent protein (GFP) for *in vivo* tracking purposes.
3. To establish a cell bank for long-term storage of mADSCs.

3.3 Isolation and expansion of mADSCs

Subcutaneous (inguinal) fat pads were collected from NTg C57BL/6J mice and processed to isolate the stromal vascular fraction (SVF) as described in Chapter 2 (Materials and Methods). With this protocol, $2.1 \pm 0.4 \times 10^6$ vital cells/g fat (mean \pm SD, $n = 3$) were obtained after isolation. The SVF was then cultured to allow mADSCs to attach to the tissue culture dish. After 24 hours, around 30% of the plated cells adhered to the plastic, while non-adherent cells and debris were removed (figure 3.1 A). 48-72 hours after the initiation of the primary culture, mADSCs started to proliferate rapidly in culture with a heterogeneous composition in monolayer (figure 3.1 B and C). The presence of several mADSCs proliferating as single cell-derived colonies was a characteristic feature (figure 3.1D).

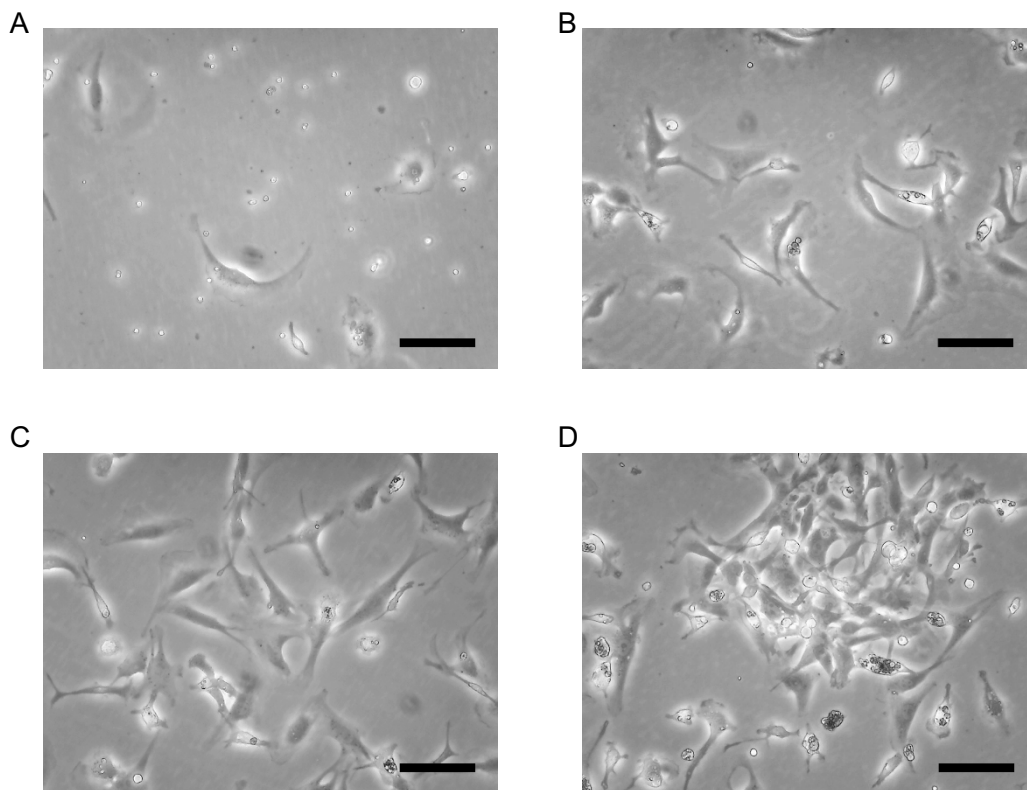


Figure 3.1. Appearance of p0 mADSCs. (A) Phase-contrast images of attached cells 24h after isolation. (B) mADSCs 48h and (C) 72h post-isolation, growing as monolayer with a heterogeneous morphology. (D) Representative image of a proliferating colony of mADSCs. Microphotographs were acquired with the Minigrab camera adapted on an inverted microscope. Scale bars: 50µm.

As mentioned in material and methods, mADSCs were initially cultured in medium containing 10% of the non-USA origin FBS purchased from Sigma. Cells were passaged every 5 to 6 days when cultures reached 80-90% confluence. mADSCs between passage 1-2 (p1-p2) grew as a relatively homogeneous population with a classic fibroblast-like spindle-shape morphology (figure 3.2 A and B). However, cells at passage 3 (p3) started exhibiting classical signs of senescence such as changes in morphology, with cells showing a larger size, flattened shape and increased ratio of cytoplasm/nucleus, and quiescence (figure 3.2 C). After 2 weeks of repeated (every three days) feeding, cells were not able to grow above 60% confluency *in vitro*, and all cells died within 3-4 weeks.

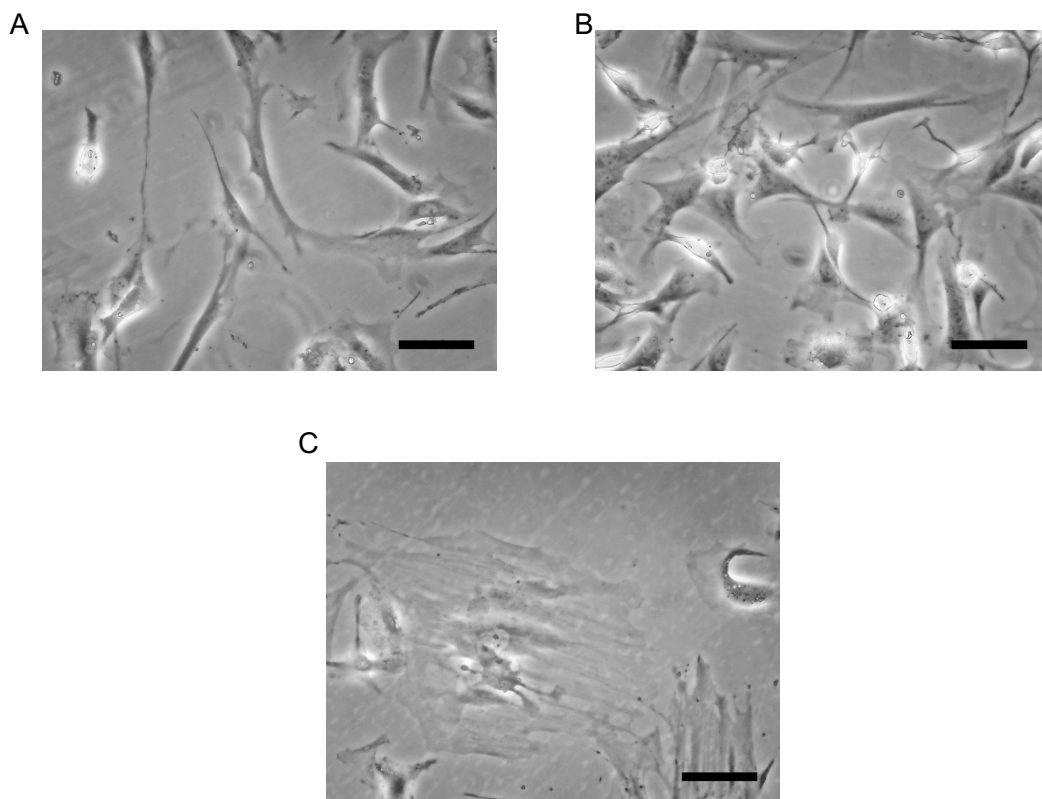


Figure 3.2. Appearance of early passage mADSCs. (A) Representative images of proliferating mADSCs at passage 1 and (B) passage 2 under light microscopy, showing a homogeneous fibroblast-like morphology. (C) mADSCs at passage 3 showed a spread out morphology with elevated cytoplasmic/nucleus ratio and lack of proliferation. Scale bars: 50 μ m.

3.3.1 Foetal Bovine Serum (FBS) test results

In the work published by Zuk and colleagues (Zuk et al., 2001), where the isolation and characterization of human ADSCs were described for the first time in the literature, the importance of testing various lots of FBS was highlighted, in order to achieve the efficient expansion of ADSCs *in vitro*. Given that our ADSC cultures were not able to expand *in vitro* with the FBS purchased from Sigma, three different sources of FBS were screened: 1) FBS of South American origin from Labtech (FBS-SA); 2) Qualified-FBS of USA origin from Gibco (FBS-Q); and 3) Mesenchymal Stem Cell Qualified-FBS of Mexican origin from Gibco (FBS-MS-C). mADSCs obtained from the same batch of isolation, were cultured in parallel with the expansion medium by using the different types of serum, and the cell growth rate was evaluated by estimating the cumulative population doubling level (PDL) at each passage in culture from p1 to p13 as described in materials and methods.

As expected, the growth of mADSCs was affected by the different source and quality of FBS used for cell expansion. The graph in figure 3.3 shows the growth kinetics of mADSCs, represented as cumulative PDLs as a function of the time in culture for the three different sources of FBS.

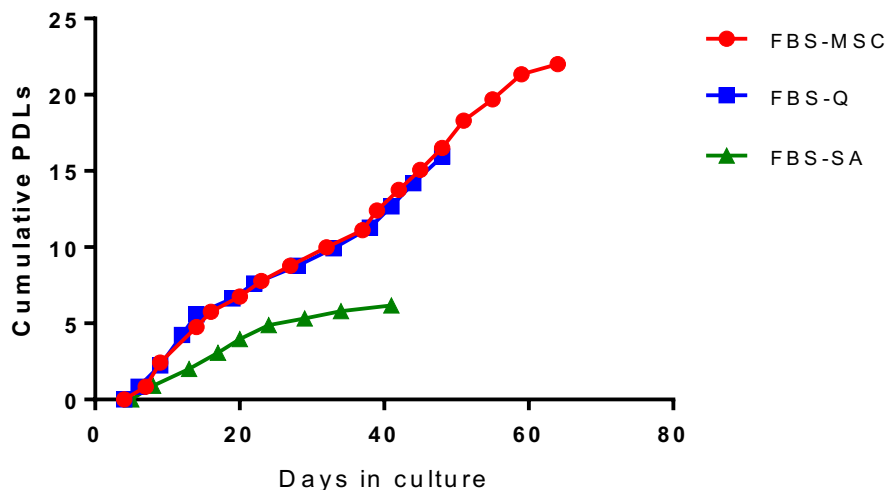


Figure 3.3. Growth kinetics of mADSCs. The graph represents the population doubling potential of mADSCs in three different sources of FBS. Cells were plated at a density of 5.000 cells/cm², harvested at 80-90% confluence, counted and re-plated at the same concentration for 13 passages. Cell growth is illustrated starting from passage 1. The mADSC growth curves are defined by the relationship between the PDL and the days in culture. (FBS-MS-C = Mesenchymal Stem Cell Qualified-FBS of

Mexico origin: FBS-Q = Qualified FBS of USA origin; FBS-SA = FBS of South America origin).

Analysis of the proliferation potential revealed that mADSCs growing in either FBS-MSC or FBS-Q had the highest cumulative PDL after 48 days in culture (p13). Indeed, after 13 passages in culture, mADSCs in the presence of FBS-MSC had expanded for approximately 16.5 generations, characterized by a population doubling rate (PDR) of 0.34. mADSCs cultured in FBS-Q, showed an almost identical growth rate when compared to the FBS-MSC, reaching a PDL of 15.9 with a PDR of 0.33 (figure 3.3). mADSCs cultured either with the FBS-MSC or the FBS-Q were passaged every 3-4 days, without showing morphological signs of senescence until passage 17, when the proliferation activity started to decrease. At the end of the FBS screening, mADSCs growing with the FBS-MSC, could be expanded for at least 22 PDLs. In contrast, mADSCs supplemented with the FBS-SA, showed the lowest proliferation capacity and cells were not able to expand beyond the passage eight (p8) in culture. In the presence of FBS-SA, mADSCs reached a maximum PDL of 6 with a PDR of 0.15. It should be noted that the calculation of PDR is only an estimation of the exponential growth of primary cell cultures, since it does not account for the latent phase of growth, or for the very early proliferation phase between the initiation of the culture (p0) and the first passage (p1).

To investigate whether the different FBS tested to support mADSC growth could alter the cell morphology, mADSCs were monitored and documented at each passage in culture. The FBS lots did not appear to affect the cell morphology, with no appreciable differences observed (figure 3.4). After 1 passage in culture, mADSCs exhibited a relatively homogeneous flat and fusiform appearance, reminiscent of fibroblast morphology. The cell morphology appeared to be stable during culture, however, mADSCs appeared to progressively grow in size as passages progressed.

Since the Mesenchymal Stem Cell Qualified-FBS of Mexican origin (FBS-MSC) better supported the growth of mADSCs among the three FBS tested, it was chosen for further experiments.

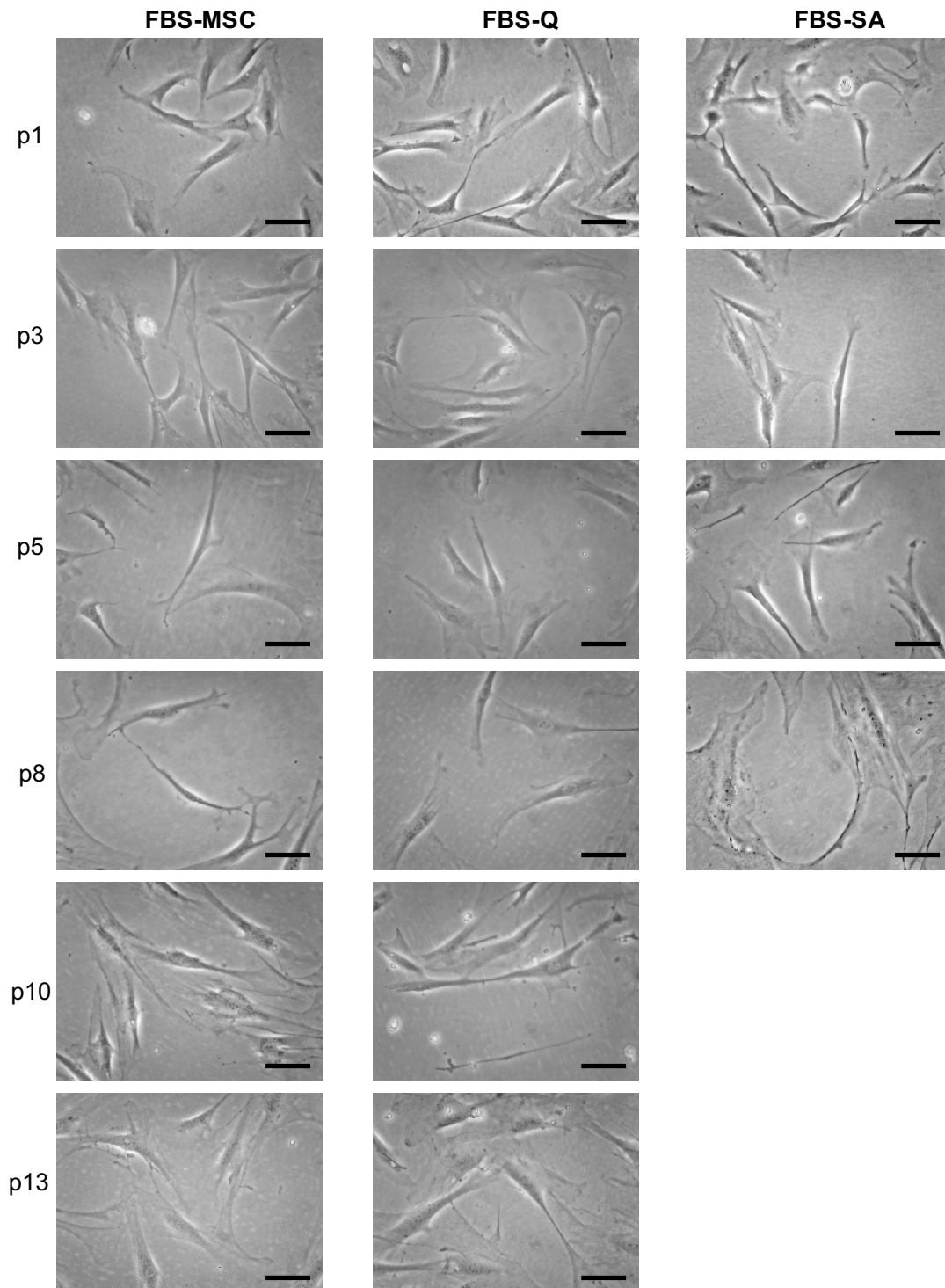


Figure 3.4. Morphology of mADSCs at early and late passages. Light microscopy representative microphotographs of mADSCs cultured in the presence of either FBS-MSC, FBS-Q or FBS-SA serum. Cells cultured with the FBS-SA showed morphological signs of senescence after 8 passages in culture (p8) and stopped proliferating. Cells supplemented with either the FBS-MSC or FBS-Q showed a relatively homogeneous elongated spindle-shape morphology during expansion, with increased cell size during late passages (p10-p13). Scale bars: 50 μ m.

3.4 The immunophenotype of mADSCs: flow cytometry results

The immunophenotype of expanded mADSCs (p5) was analyzed by flow cytometry for specific surface marker expression. A panel of standard MSC (CD90, CD44, CD29, CD106, CD105), haematopoietic (CD34, CD45, CD11b) and endothelial (CD31) markers were individually tested on three separate cell isolation batches. Data were collected with the SLRII FACS instrument (Biosciences Company) and analysed with FlowJow software 7.6.1. For analysis, unstained samples were used to set the gates, exclude cell debris and identify the single cell population (figure 3.5 A-B), while specific matched isotype controls were used to define the antibody specificity as described in the materials and methods chapter (paragraph 2.2.3).

As shown in figure 3.5, mADSCs were strongly positive for the mesenchymal stem cell markers CD90 ($98.9 \pm 0.7\%$ (mean \pm SD)), CD29 ($99.5 \pm 0.5\%$) and CD44 ($99.6 \pm 0.2\%$) (figure 3.5 C-E), while the expression of the MSC marker CD106 (figure 3.5 F) displayed some variability in between separate experiments ($91.4 \pm 3.3\%$). Interestingly, the analysis of the MSC marker CD105 showed the presence of two distinct populations of mADSCs, CD105⁻ ($46 \pm 0.9\%$) and CD105⁺ ($54 \pm 0.9\%$) (figure 3.5 G). Notably, haematopoietic (CD45, CD11b, CD34) and endothelial (CD31) markers were not expressed ($<0.6\%$) by mADSCs (figure 3.5 H-K). The percentage of positive cells for each antibody tested was calculated as average \pm SD from three separate experiments. It is to be noted that each experiment represents a separate batch of stem cell isolation.

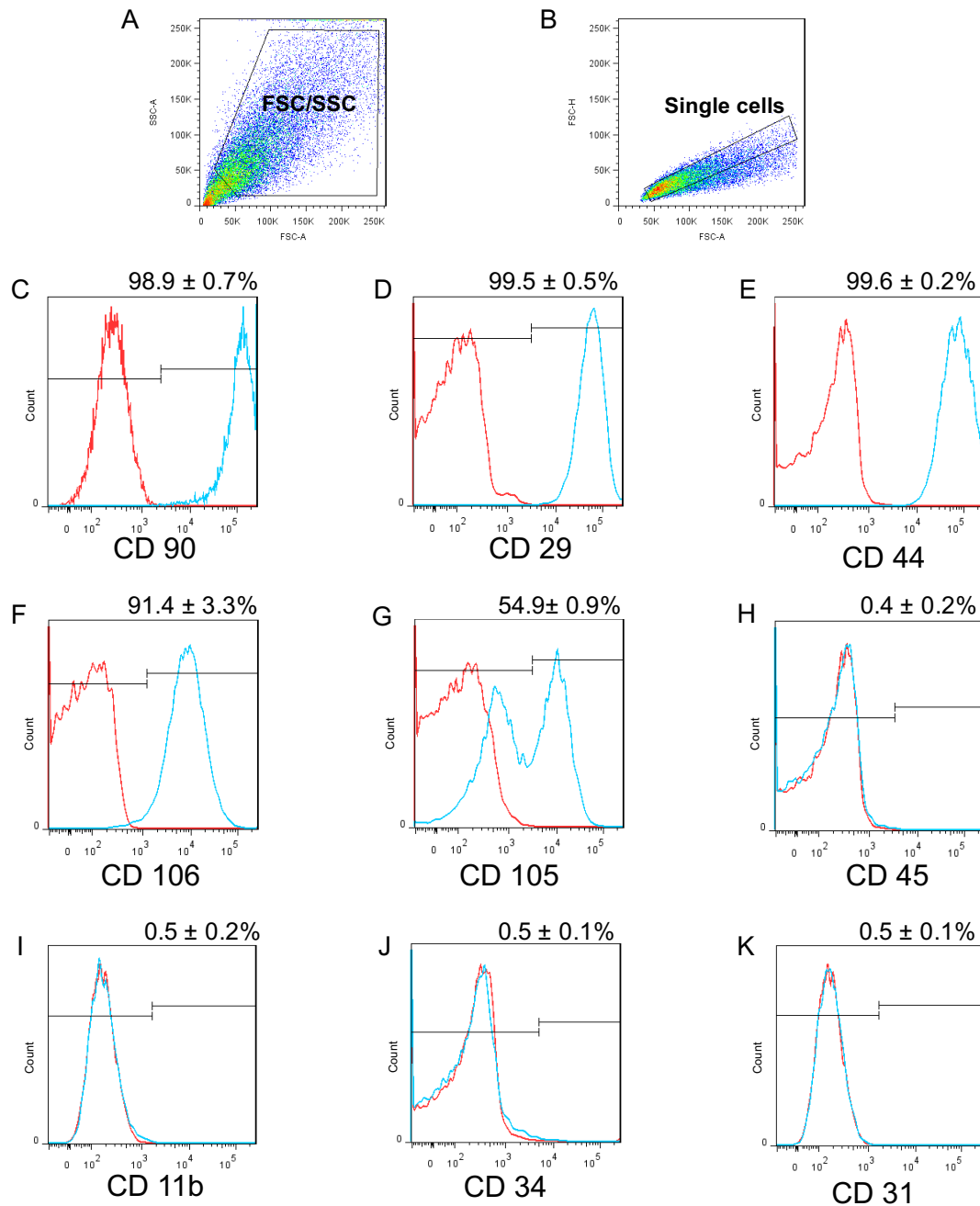


Figure 3.5. Surface marker expression of mADSCs. The immunophenotype profile of mADSCs expanded for 5 passages was analyzed by screening for a panel of fluorescent-labelled antibodies specific for characteristic surface antigens. Unstained cells were used to set the gates and identify the single cell population (A and B). The percentage of positive cells was calculated by setting the red region based on the intensity of isotype controls. mADSCs were positive (>90%) for CD90 (C), CD29 (D), CD44 (E) and CD106 (F) MSC markers. The expression of CD105 was found in ~ 55% of mADSCs (G). mADSCs were negative (<0.5%) for the haematopoietic markers CD45 (H), CD11b (I), CD34 (J) and for the endothelial marker CD31 (K). The histogram in red represents the cells stained with the specific antibody, while in blue

is represented the staining with the isotype-matched control antibody. On the abscissa is indicated the fluorescent intensity, while on the ordinate the cell counts. Percentages represent average from three separate experiments \pm SD.

3.5 Tri-lineage differentiation of mADSCs: results

3.5.1 Adipogenic differentiation

mADSCs after early (p3) and late (p14) passages in culture, were tested for adipogenic differentiation potential. Cells were cultured in the presence of a chemical cocktail of factors, specific for adipogenic induction and maturation of mesenchymal stem cells into adipocytes (see Material and Methods for medium composition). The differentiation process was monitored daily by microscopic observation and documented with the Apex Mingrab camera.

As early as 4 days after incubation in the differentiation media, p3 mADSCs became smaller in size and started changing in structure from an elongated fibroblast-like morphology to a more rounded shape. Cells, also appeared highly refractive under light microscopy, and tiny, circular, light refractive lipid droplets could be observed in the cytoplasm (figure 3.6 A-B).

At day 7 of differentiation, lipid-filled cells were easily detectable under light microscopy (figure 3.6 D-E), while 14 days after induction, mADSCs extensively differentiated into adipocytes, presenting with enlarged lipid droplets (figure 3.6 G-H). mADSCs cultured in control basal medium, did not show morphological changes, nor the presence of intracytoplasmic lipid droplets (figure 3.6 C, F and I).

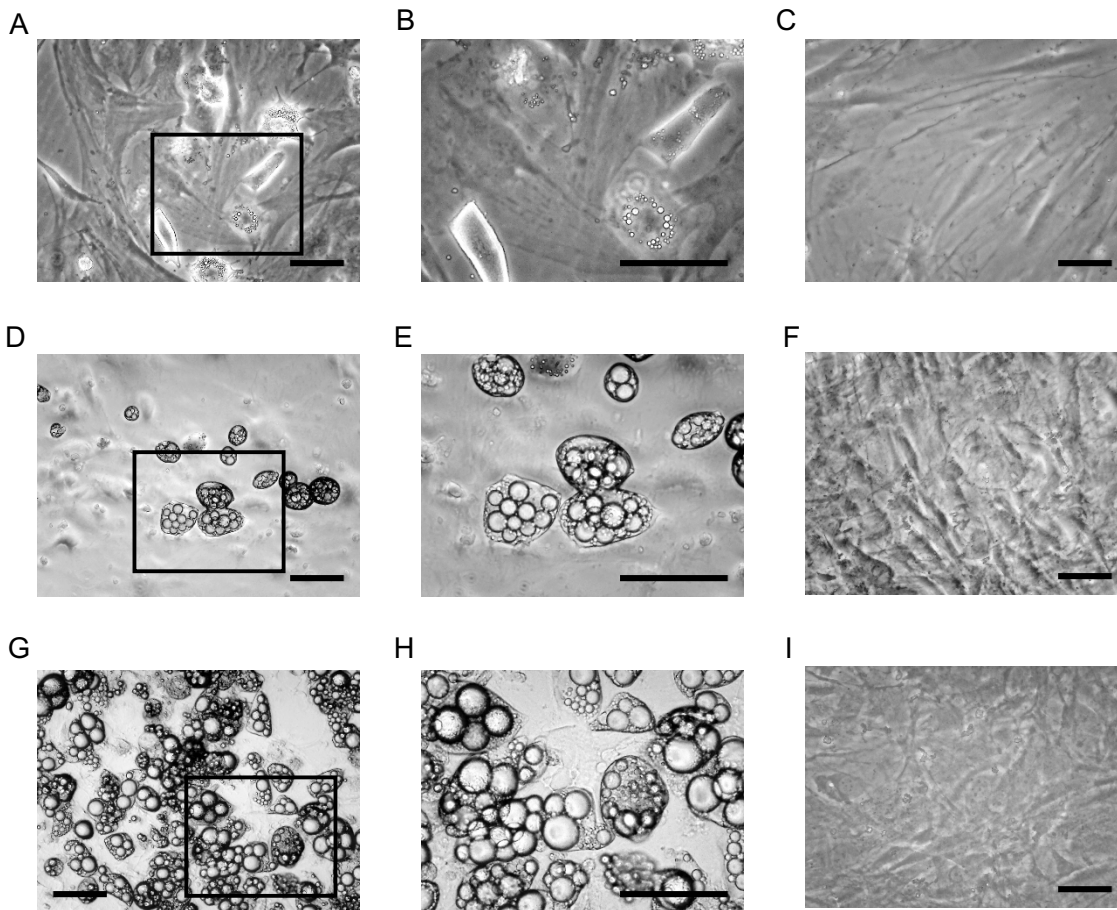


Figure 3.6. Adipogenic induction of p3 mADSCs. Light microscopy pictures of p3 mADSCs showing morphological changes after 4 days (A and B), 7 days (D and E) and 14 days (G and H) in adipogenic induction medium. mADSCs did not show any morphological changes when cultured in standard (control) medium and continued to proliferate at 4 days (C), 7 days (F) and 14 days (I). The boxed areas in A, D and G are magnified in B, E and H respectively. Scale bars: 50 μ m.

Adipogenic differentiation of p3 mADSCs was confirmed by Oil Red O staining after 1 week and 2 weeks of induction (figure 3.7 and 3.8). The lipophilic Oil Red O dye is specific for neutral triglycerides and lipids, and it penetrates the vacuole membranes of intracellular lipid deposits. The Oil Red O staining is widely used to assess differentiation of MSCs into adipocytes. As early as 1 week post-induction, mADSCs showed differentiation into adipocytes. The images in figure 3.7 and 3.8 clearly show intracellular lipid filled droplets, positively stained with the specific red dye. Notably, after 2 weeks in the adipogenic medium, mADSCs massively differentiated into adipocytes characterized by lipid deposits that have grown in size. Although rarely, unilocular lipid cells were observed within the cultures.

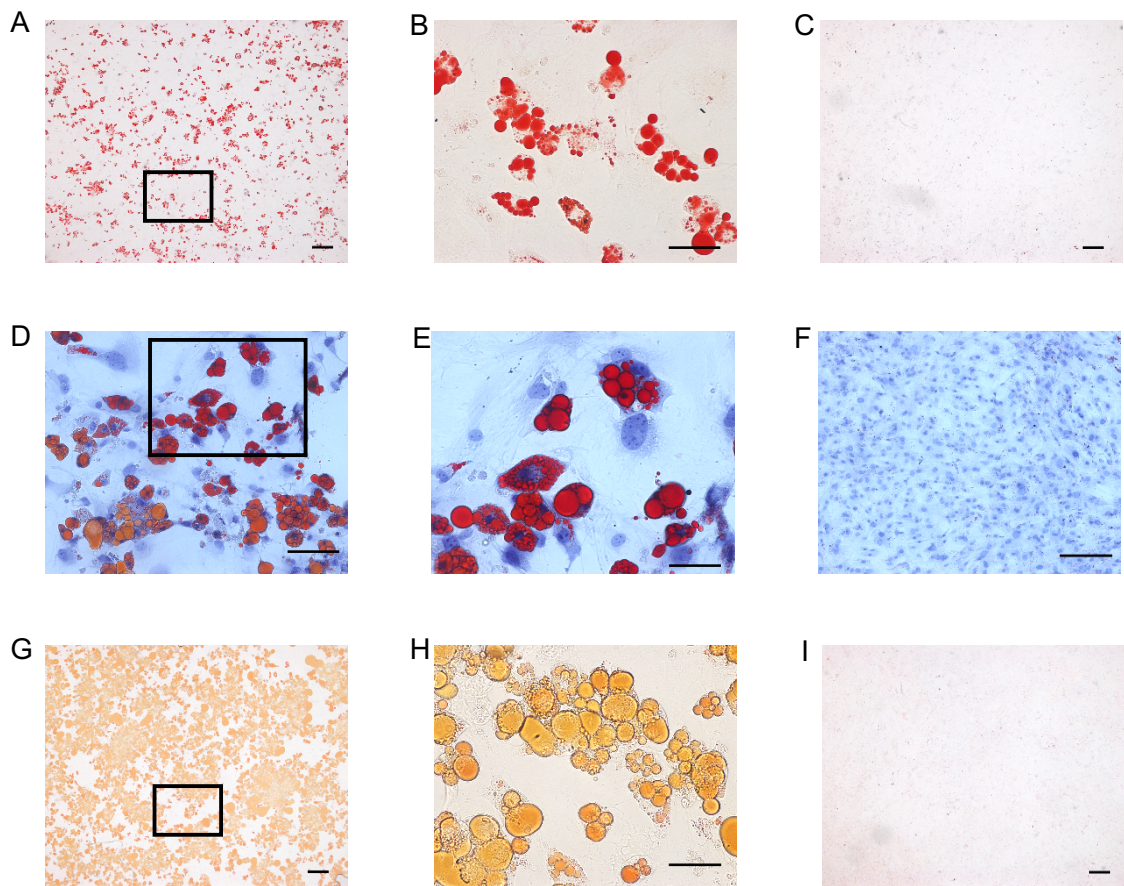


Figure 3.7. Adipogenic differentiation of p3 mADSCs: Oil Red O staining 1. mADSCs were induced to differentiate onto glass coverslips in 24-well plates. Adipogenic differentiation was assessed by Oil Red O staining after 1 and 2 weeks of induction in the conditioned medium. After 1 week of induction, mADSCs stained positively for the lipid dye (A and B). To show the cytoplasmic localization of the lipid vesicles, nuclei were counterstained with Mayer's hematoxylin (D and E). After 2 weeks, the stained lipid droplets increased in size, as well as the number of differentiated cells (G and H). Surprisingly, while after 1 week of differentiation the lipid vesicles stained in red, after 2 weeks, an orange staining was observed. This could be explained by a change in pH during the preparation of the working staining solution. Notably, mADSCs placed in the control media were not stained (C, F and I). The boxed areas in A, D and G are magnified in B, E and H respectively. Images were captured with the Nikon microscope and are representative of at least three separate experiments. Scale bars: 200 μm (A, C, G, I); 100 μm (F); 100 μm (D); 50 μm (B, E,H).

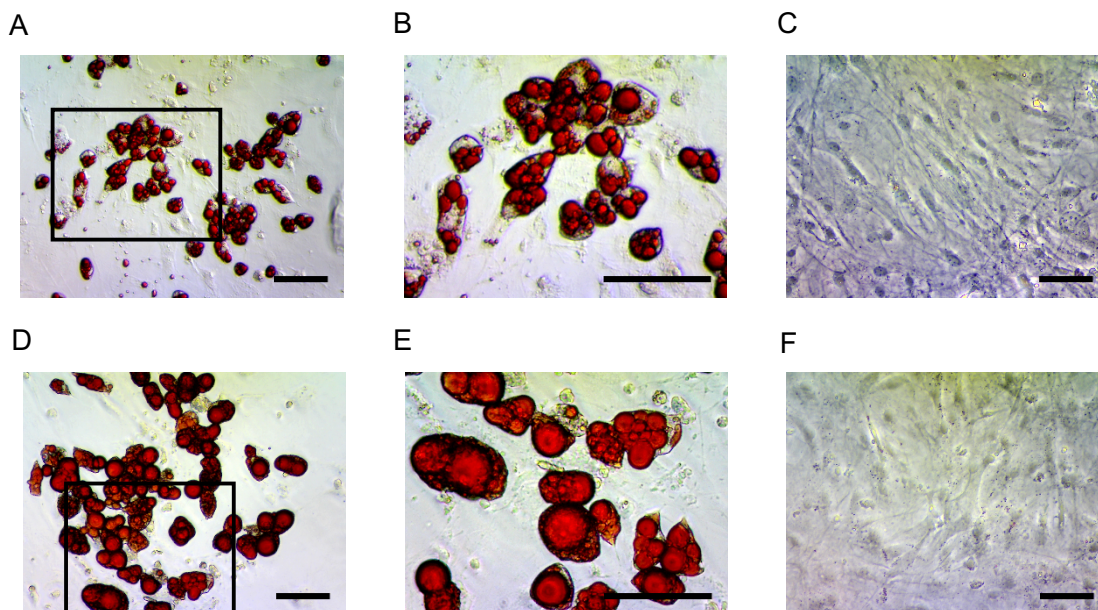


Figure 3.8. Adipogenic differentiation of p3 mADSCs: Oil Red O staining 2. mADSCs were induced to differentiate in 12-well plates. Phase contrast images showing positive staining to Oil Red O after 1 (A, B) and 2 (D, E) weeks of culture in the adipogenic differentiation medium. Intracellular lipid content is visualized as circular bright-red droplets. The boxed areas in A and D are magnified in B and E respectively. mADSCs cultured in non-induction control media were negative for the lipid dye (C, F). Images are representative of at least three separate experiments. Scale bars: 50 μm .

To investigate whether mADSCs retained the adipogenic differentiation capacity after long-term culture, cells were induced to differentiate into adipocytes after *in vitro* expansion for 14 passages (PDL = 18). Although to a lesser extent, p14 mADSCs still readily differentiated into adipocytes, as confirmed by Oil red O staining after 2 weeks of culture with the adipogenic conditioned medium (figure 3.9).

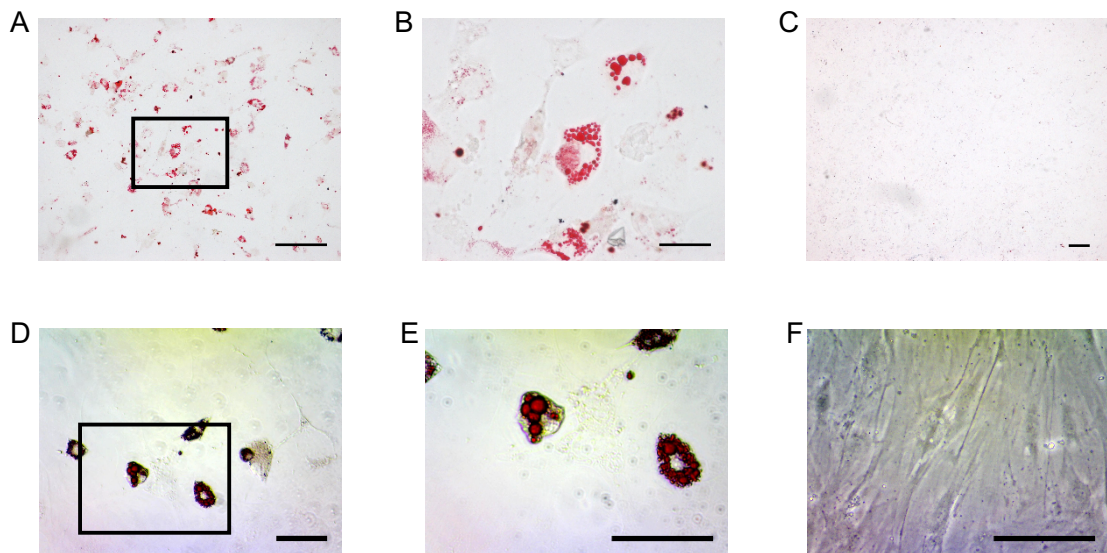


Figure 3.9. Adipogenic differentiation of p14 mADSCs: Oil Red O staining. mADSCs were expanded for 14 passages and induced to differentiate into adipocytes for 2 weeks. Oil red O staining confirmed differentiation of mADSCs cultured onto glass coverslips (A and B) and onto plastic in 12-well plates (D and E). The boxed area in A and D are magnified in B and C respectively. mADSCs cultured in control basal medium did not stain for oil red O (C and F). Representative images of at least three separate experiments. Scale bars: 200µm (A and C); 50µm (B, D, E and F).

3.5.2 Osteogenic differentiation

For osteogenic differentiation, mADSCs were expanded for 3 passages and cultured in the presence of a specific induction medium known to promote the differentiation of MSCs into osteoblasts. After 3 days, morphological changes were observed in mADSCs cultured with the differentiation medium. Cell morphology changed from an elongated spindle shape into an irregular squared shape, with nuclei appearing larger and surrounded by small white spots (figure 3.10 A). After 10 days of induction, cells tended to aggregate in islands and started secreting extracellular matrix as suggested by the presence of white calcium deposits surrounding the cell bodies (figure 3.10 C). At 17 days of induction, granular rounded nodules of calcium deposits were sparsely distributed in the culture and easily detectable by the naked eye (figure 3.10 E). mADSCs kept in basal control medium did not show major morphological changes and did not produce deposits of extracellular matrix (figure 2.10 B, D and F).

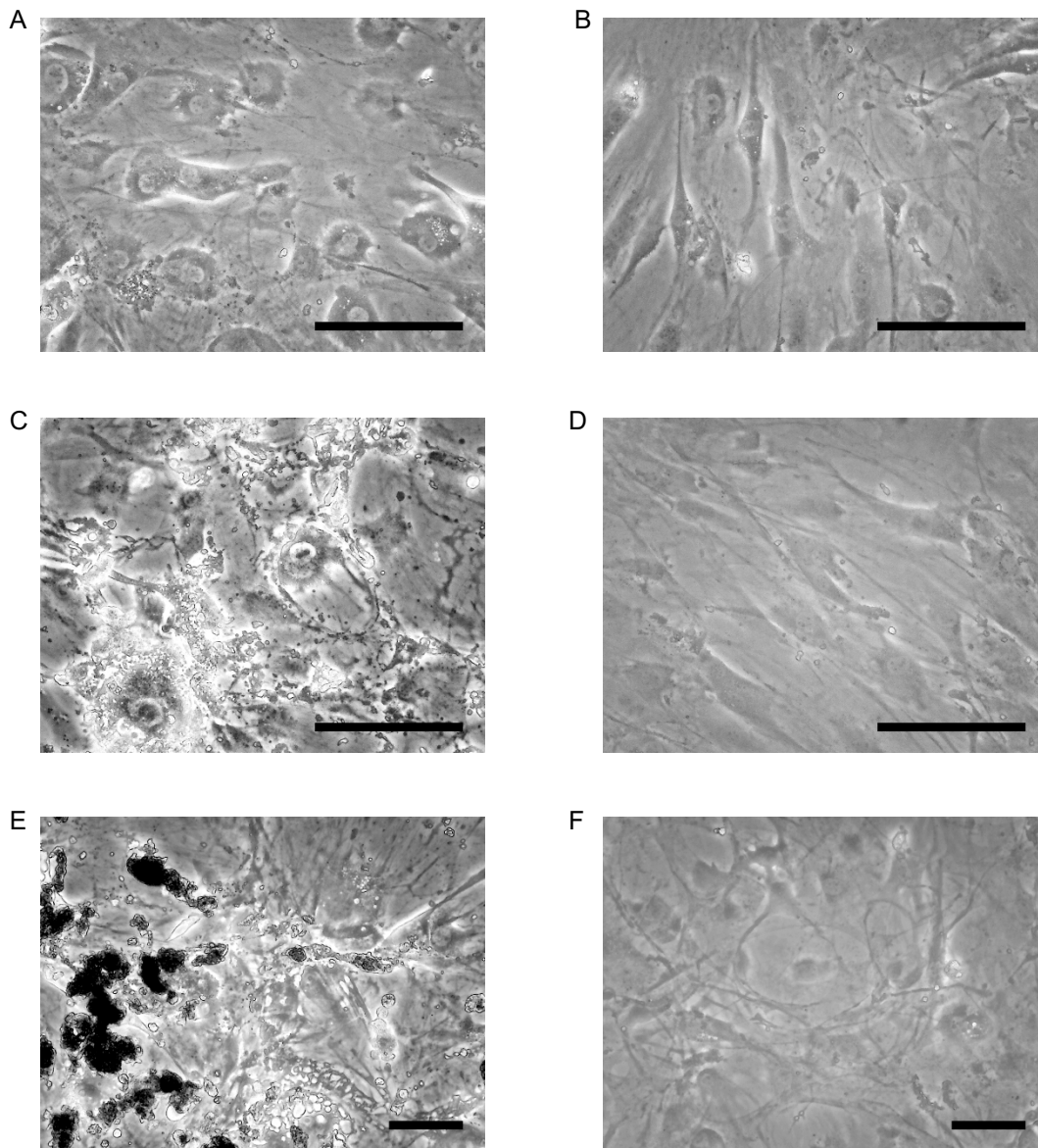


Figure 3.10. Osteogenic induction of p3 mADSCs. Phase contrast images showing morphological changes of p3 mADSCs after 3 days (A), 10 days (C) and 17 days (E) of culture with the osteogenic differentiation medium. Cells maintained with basal culture medium did not show considerable changes in morphology nor the secretion of extracellular matrix detectable by phase contrast microscopy (B, D and F). Scale bars: 50 μ m.

The calcified nature of the extracellular matrix was confirmed by Alizarin Red S staining after 2 and 4 weeks of culture of mADSCs with the osteogenic differentiation medium (figure 3.11). Alizarin Red S is a dye that specifically complexes with calcium deposits, and it is considered a valid method to document the differentiation of MSCs into the osteogenic lineage. At 2 weeks post-differentiation, deposits of calcium containing extracellular matrix were detected as bright-red nodules after Alizarin Red S staining (figure 3.11 A and B). At the end of the differentiation protocol (4 weeks), the cultures were almost completely covered by mineralized calcium deposits (figure 3.11 D), a sign of extensive differentiation of mADSCs into osteoblasts, that actively secrete extracellular matrix.

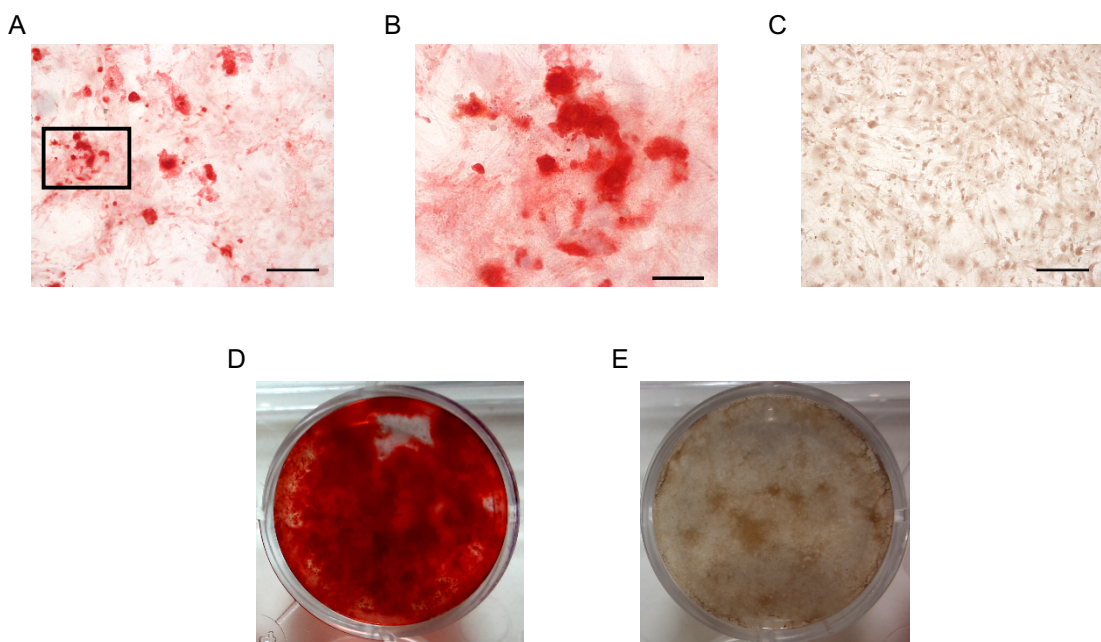


Figure 3.11. Osteogenic differentiation of p3 mADSCs: Alizarin Red S staining. mADSCs were seeded on glass coverslips and cultured in the presence of osteogenic differentiation medium or control medium for 2 weeks. Images, representative of at least three separate experiments, were captured with the Nikon microscope. Extracellular calcium nodules stained intensely in red with Alizarin Red S solution (A and B), while control cultures were negative for this stain (C). The boxed area in A is magnified in B. After 4 weeks of induction, mADSCs extensively differentiated in osteoblasts secreting large amounts of calcium matrix, as shown in the digital picture of the culture well after Alizarin staining (D). Spontaneous differentiation was absent in control cultures (E). Scale bars: 200 μm (A and C); 50 μm (B).

mADSCs preserved the osteogenic differentiation capacity also after expansion for 14 passages in culture, as demonstrated by positive Alizarin Red S Staining at day 21 and 28 of osteogenic differentiation induction (figure 3.12). However, the degree of differentiation was reduced compared to early passage mADSCs.

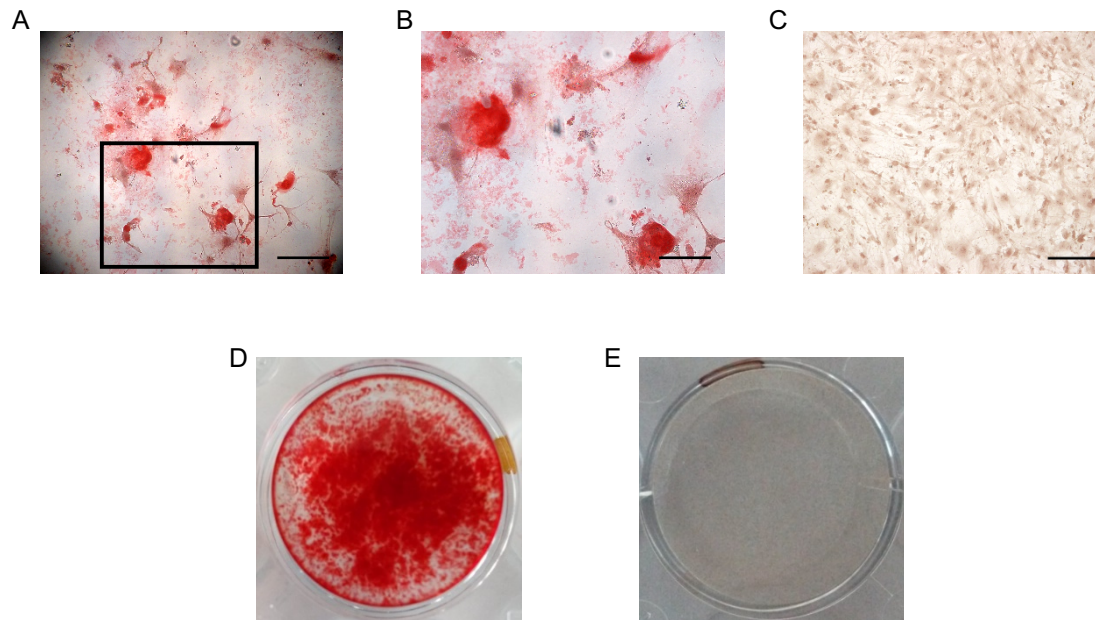


Figure 3.12. Osteogenic differentiation of p12 mADSCs: Alizarin Red S staining. (A and B) mADSCs expanded for 14 passages maintained the osteogenic differentiation potential as confirmed by the presence of extracellular calcium deposits in the culture, positive for Alizarin Red S staining at day 21 of induction. (C) Control cultures were negative for this stain. The boxed area in A is magnified in B. Digital photographs of representative culture wells at day 28 of induction with osteogenic factors (D) or control media (E) after Alizarin Red S staining. Images are representative of at least 3 separate experiments. Scale bar: 200 μm (A and C); 50 μm (B).

3.5.3 Chondrogenic differentiation

Chondrogenic differentiation of mADSCs was performed on three dimensional cell pellets as described in the materials and methods. Chondrocyte differentiation was evaluated after three weeks of induction with the specific cocktail medium. As shown in figure 3.13, in the presence of the differentiation medium, pellet cultures were much bigger than pellets maintained in control basal medium. This might be explained by the secretion of a large amount of extracellular matrix composed of collagenous proteoglycans and elastin.

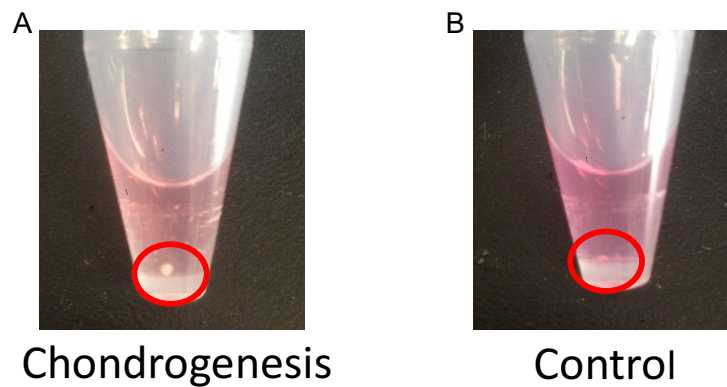


Figure 3.13. Chondrogenic differentiation of p3 mADSCs in 3D pellet cultures. mADSCs were expanded for 3 passages and induced to differentiate into chondrocyte pellets. Cells were cultured as 3D pellets in 15 ml Falcon tubes, in the presence or absence of specific differentiation stimuli. Representative digital photos at the end of the differentiation protocol are shown. Pellets maintained in chondrocyte medium (A) grew bigger than pellets cultured with basal medium (B).

After three weeks of induction, pellets were collected and processed for Alcian Blue staining in order to confirm the chondrocyte nature of the differentiated mADSCs. Alcian blue complexes with acid proteoglycans, which are characteristic components of cartilage tissue. Induced mADSC-pellet cultures stained positively with the basic blue dye (figure 3.14 A and B). In contrast control mADSC pellets did not stain with Alcian blue (figure 3.14 C).

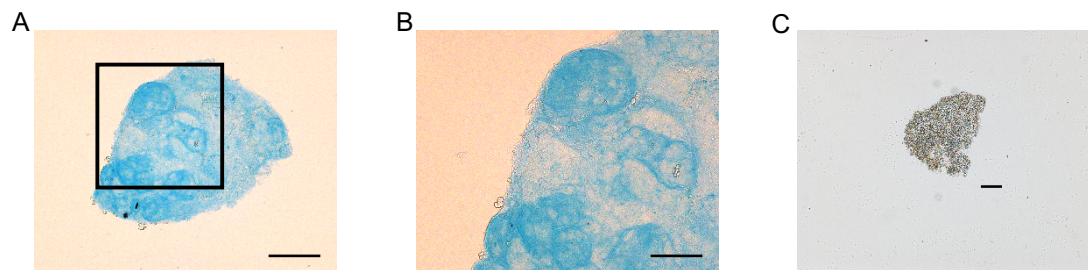


Figure 3.14. Chondrogenic differentiation in 3D pellets cultures: Alcian Blue staining. mADSC pellets were maintained in chondrogenic differentiation medium for 3 weeks. At the end of the differentiation protocol, pellets were fixed, frozen and sectioned using a cryostat. Sections were then stained for Alcian Blue. Differentiated pellets stained intensely with Alcian blue solution (A and B). Control pellets were negative for this stain (C). The boxed area in A is magnified in B. Scale bars: 200 μ m (A); 100 μ m (B); 200 μ m (C).

3.6 EGFP-expressing lentivirus production: titration results

EGFP-lentivirus was packaged by transient co-transfection of HEK 293T cells with four DNA plasmids (pLV-SIN-EGFP, pCMV Δ 8.92, pRSV-Rev, pMDG) as described in the material and methods. Following virus production, viral particles were concentrated by ultracentrifugation and aliquots were stored at -80°C. In order to control for the multiplicity of infection (MOI) in downstream applications, the concentrated virus was then functionally titred by infecting HeLa cells and quantifying the number of transduced cells following infection with serial dilution of the virus stock. GFP-positive cells were quantified by flow cytometry 5 days post transduction. Control untransduced cells were used to identify the single cell population (figure 3.15 A and B) and set the gate in order to discriminate between the GFP-negative and the GFP-positive signal (figure 3.15 C). As shown in figure 3.15, more than 90% of cells were transduced with the 10^{-2} and 10^{-3} dilutions from the concentrated virus stock (figure 3.15 D and E), while around 40% of cells were GFP positive following transduction with a dilution factor of 10^{-4} (figure 3.15 F). Since the functional titring method assumes one virus particle integration event per cell, to avoid underestimation of the viral titre, calculations were made by using the viral dilution of 10^{-4} , which resulted in transduction of the lowest number of HeLa cells. The vector titre calculations are shown in figure 3.15 G. The estimated virus titre was in the range of 4×10^8 transduction unit per millilitre (Tu/ml) (figure 3.15 G).

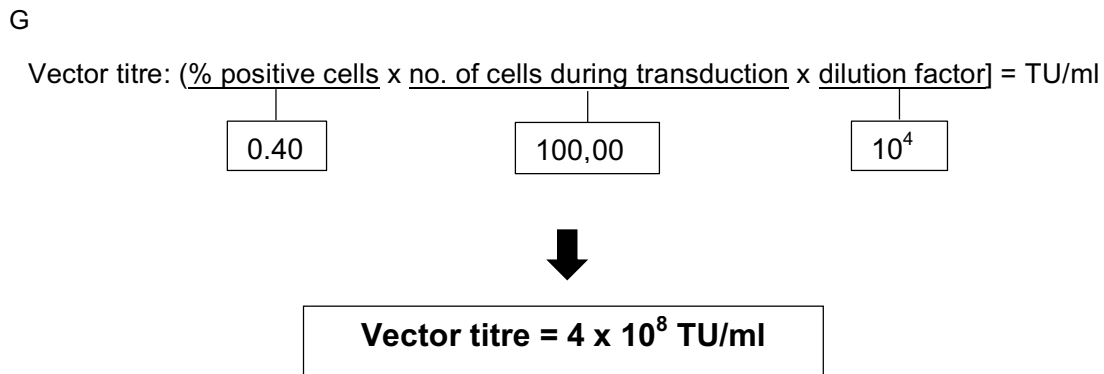
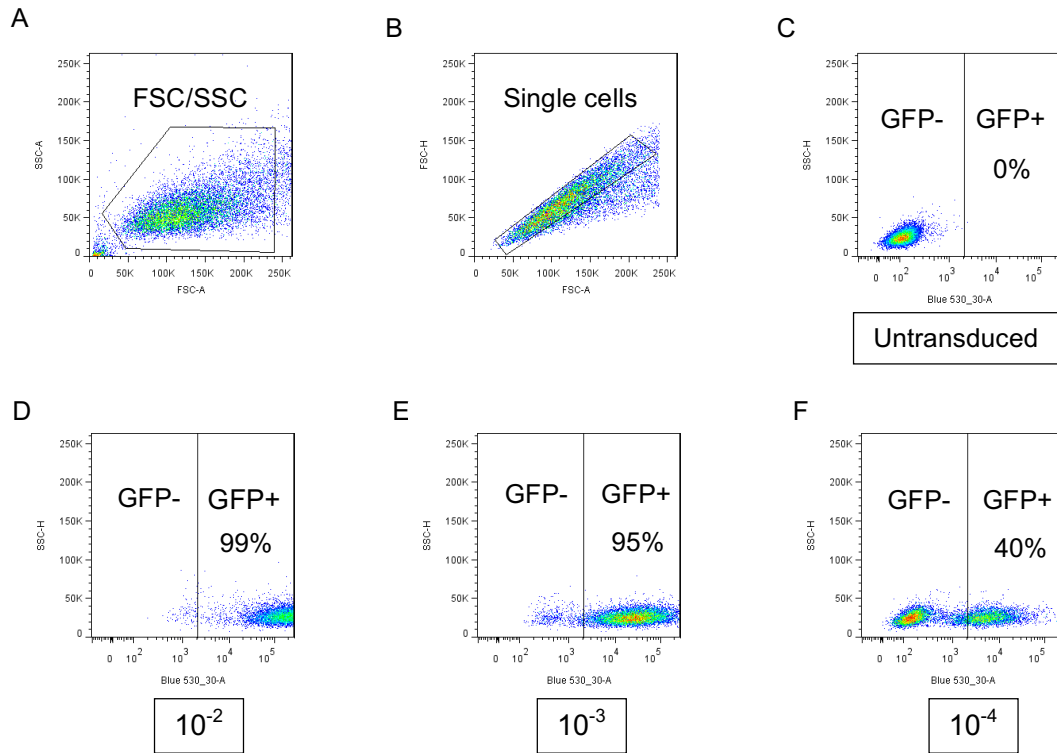


Figure 3.15. EGFP-lentivirus titration by flow cytometry. EGFP-expressing lentivirus particles were produced by transfecting HEK 293T cells, and the virus concentrated by ultracentrifugation. Functional virus titre (TU) was estimated by cytometry analysis by counting the number of GFP-positive HeLa cells 5 days after transduction with serial dilutions (10^{-2} , 10^{-3} and 10^{-4}) of the concentrated viral stock. Untransduced cells were used to identify the single cell population and set the gates (A, B and C). Representative images showing the percentage of GFP⁺/HeLa cells after infection with serial virus dilutions (D, E and F). The percentages of GFP⁺ cells represent average between technical duplicates. The virus titre was calculated by using the dilution factor which resulted in transduction of the lowest number of HeLa cells (10^{-4}) (G).

3.7 Transduction of mADSCs: MOI test results

In order to estimate the optimal titre that would lead to high transduction efficiency and low toxicity, a dose response experiment was performed. Passage 3 ADSCs were infected with viral particles at a multiplicity of infection (MOI) of 30, 50, 80 and 100 in the presence or absence of 4 µg/ml polybrene. Polybrene is a positively-charged polycation which increases lentivirus transduction efficiency by reducing the electrostatic repulsion forces between the cell membrane and the virus envelope (Denning et al., 2013). Following 24 hours incubation with the virus, mADSCs were cultured for a further 4 days and transduction efficiency quantified by flow cytometry analysis on PFA fixed cells.

As shown in figure 3.16, the transduction efficiency of mADSCs improved with increasing MOI. With a MOI of 30, ~ 60% of mADSCs were successfully transduced (figure 3.16 B), while approximately 85% and 94% of cells were transduced with a MOI of 50 and 80 respectively (figure 3.16 C and D). However, cells infected with a MOI of 100 did not show a substantial increase in the number of transduced cells in comparison to the MOI of 80 (figure 3.16 E). Notably, the addition of polybrene during infection improved the transduction efficiency considerably. With a MOI of 30 about 94% of ADSCs were positive for the GFP, in the presence of polybrene (figure 3.16 G). However, infection with higher MOIs mostly resulted in higher fluorescence intensity (figure 3.16 H, I and J), probably due to multiple virus integration events. Importantly, regardless of the presence of polybrene, mADSCs continued to proliferate following transduction with any of the different MOIs tested, and morphological changes were not detectable by microscopic observation. The scope of the MOI assay is exclusively related to transduction optimization, thus the test was carried out as a single experiment.

Given the high transduction efficiency and absence of toxicity, the MOI of 30 in the presence of polybrene was chosen to transduce mADSCs in the following experiments.

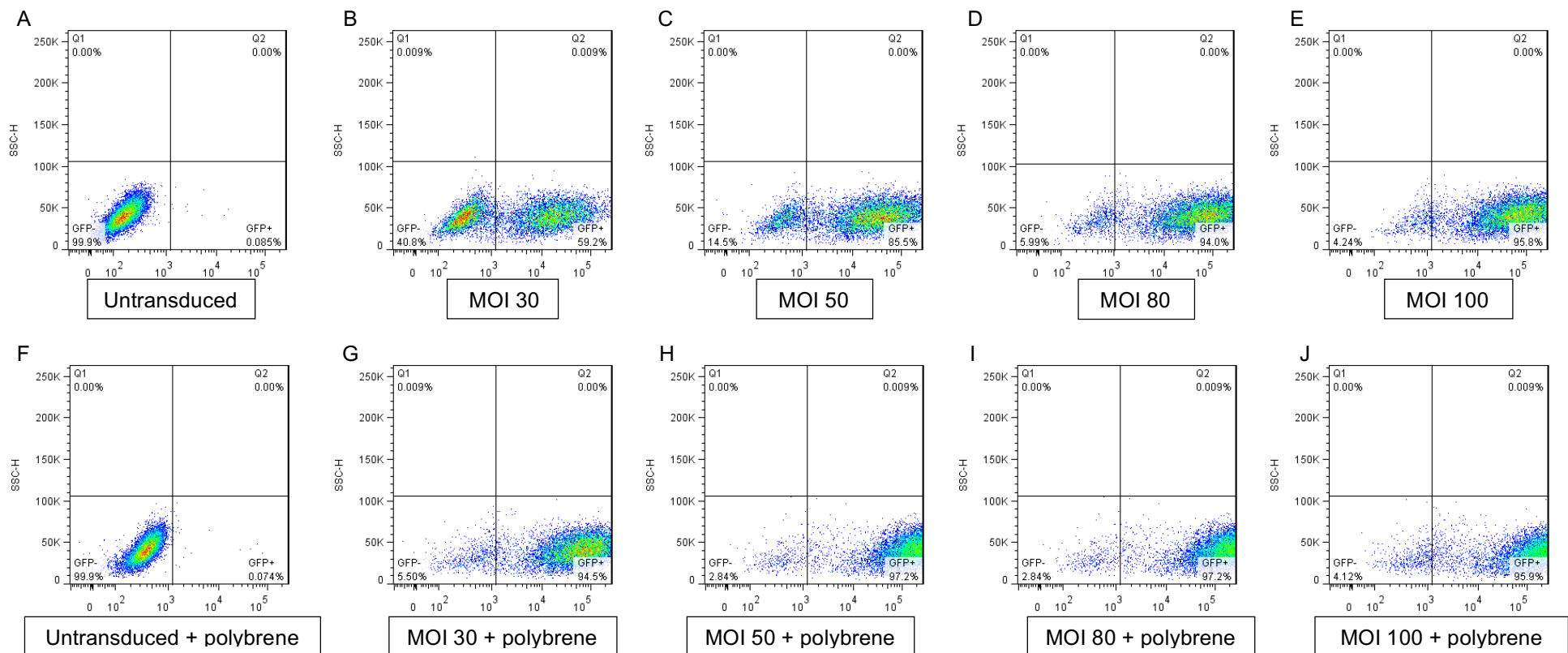


Figure 3.16. Optimization of EGFP-lentivirus transduction of mADSCs. Passage 3 mADSCs were transduced with the EGFP-expressing lentivirus at different MOIs in the presence or absence of polybrene at a concentration of 4 $\mu\text{g/ml}$. Transduction efficiency was compared 5 days post-infection by flow cytometry analysis. Untransduced cells were used to set the gates (A and F). In the absence of polybrene the transduction efficiency improved as increasing levels of MOI were applied, from ~60% transduction (MOI 30) to 96% (MOI 100) (B, C, D and E). The transduction efficiency improved greatly with the addition of polybrene, with about 95% transduced cells at a MOI of 30 (G), while the application of higher MOIs (50, 80 and 100) resulted in greater fluorescence intensity (H, I and J).

3.8 Lentivirus transduction of mADSCs and long-term storage

Freshly isolated mADSCs were expanded for one passage and transduced with the EGFP-expressing lentivirus at a MOI of 30 in the presence of polybrene. Lentivirus transduction was then confirmed by fluorescent microscopy and quantified by flow cytometry 5 days post-infection (figure 3.17). As early as 3 days post-transduction, mADSCs showed high expression of GFP by fluorescence microscopy, a sign of high rate of transduction (figure 3.17 A). Efficiency of transduction was then quantified 5 days post-infection by flow cytometry analysis on PFA fixed cells (figure 2.17). As shown in figure 3.17, $98.8 \pm 0.3\%$ (mean \pm SD, n=3 biological replicates) mADSCs were positive for the GFP, confirming the high rate of transduction seen by microscopy.

In order to create a cell bank of GFP-mADSCs, following transduction, cells were expanded in culture for 2 passages, frozen and stored in liquid nitrogen as described in material and methods (paragraph 2.2.7).

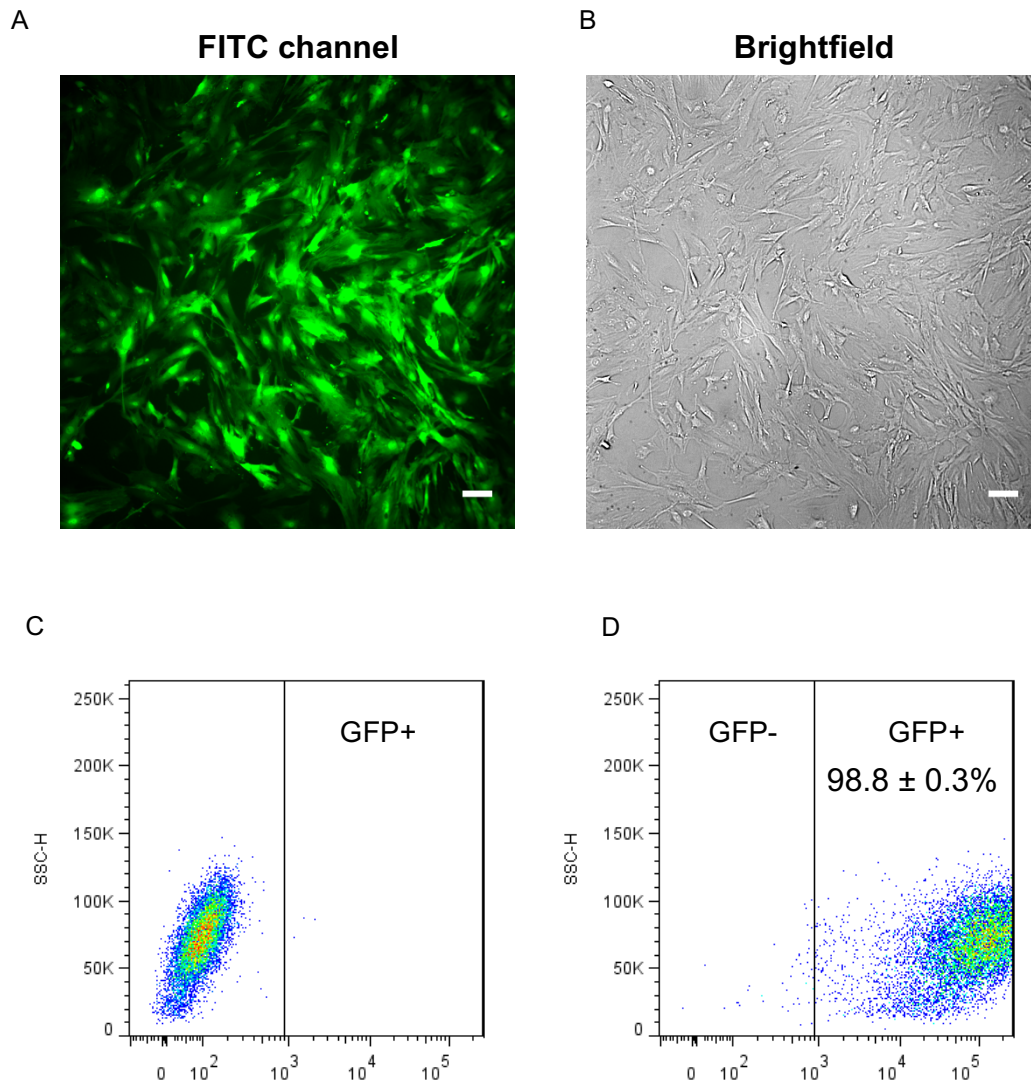


Figure 3.17: Lentivirus transduction of passage 1 mADSCs. mADSCs were infected with the EGFP-expressing lentivirus at a MOI of 30 in the presence of 4 μ g/ml polybrene for 24 hours. Untransduced cells cultured in medium containing polybrene were used as controls. At day 3 post-infection transduction was confirmed by expression of GFP by fluorescent microscopy (A). Transduction was then quantified by flow cytometry 5 days post-infection. Control untransduced cells were used to set the gate (C). The transduction efficiency achieved was extremely high with $98.8 \pm 0.3\%$ mADSCs positive for GFP (mean \pm SD, $n=3$) (D). Fluorescence and brightfield microscopic images were taken with the INCell 2000 GE. Scale bars: 100 μ m.

3.9 Characterization of GFP-mADSC

After 3 months of preservation in liquid nitrogen, 3 separate vials of GFP-mADSCs were recovered and expanded in culture. GFP-mADSCs did not show evident morphological changes in microscopy and maintained their proliferation capacity.

3.9.1 Immunophenotype of GFP-mADSCs: flow cytometry results

Following 2 passages in culture (equivalent to a total of 5 passages), the immunophenotype of GFP-mADSCs was analysed by flow cytometry (figure 3.18). GFP-mADSCs retained expression of classical mesenchymal stem cell markers such as CD90, CD29, CD44, CD106 and CD105 (figure 3.18 B-F). Moreover, cells were negative for the endothelial (CD31) and haematopoietic (CD34) surface cell markers (figure 3.18 G and H).

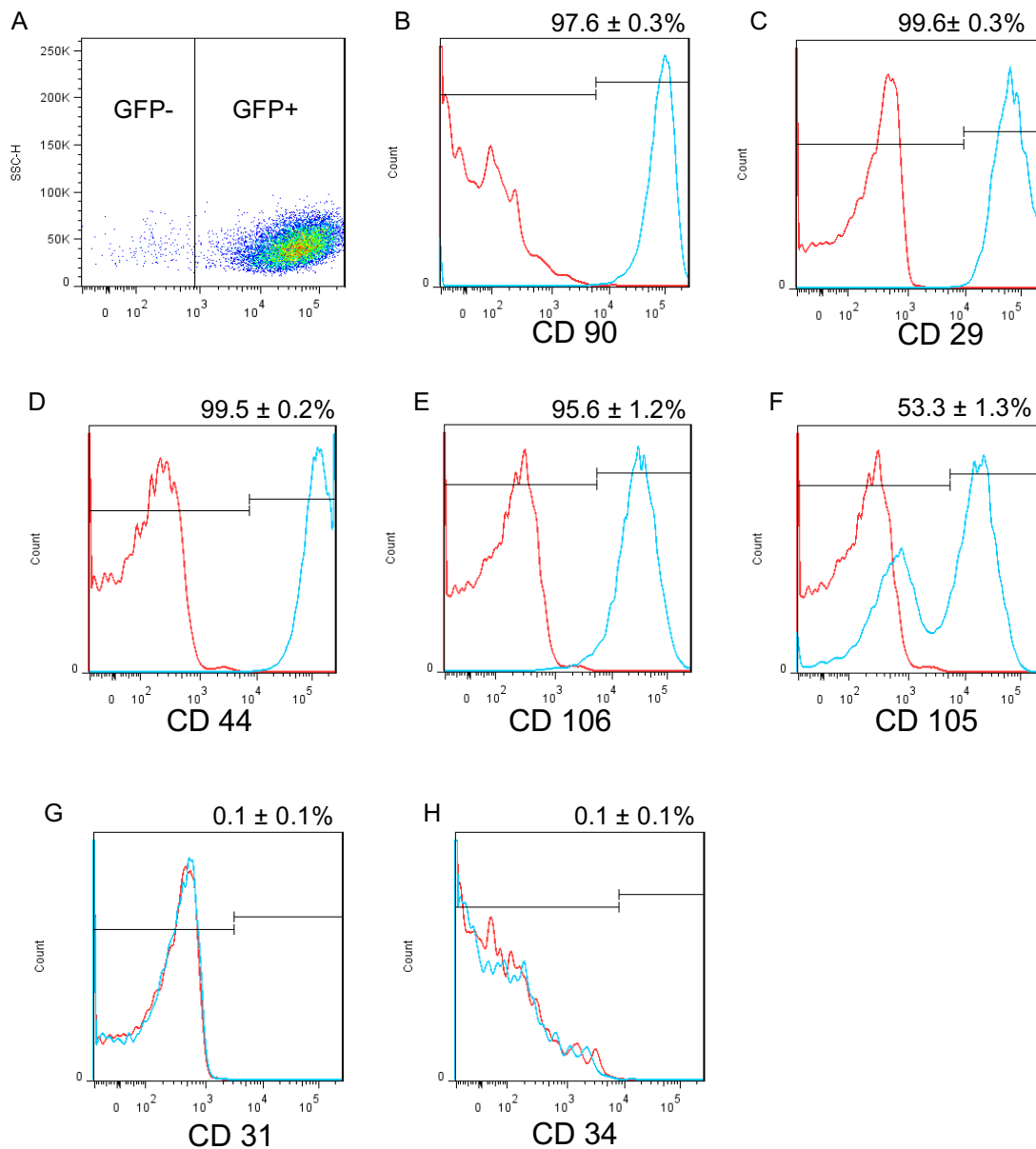


Figure 3.18. Immunophenotype of GFP-mADSCs. Passage 5 GFP-mADSCs were screened for a panel of fluorescent-labelled antibodies specific for mesenchymal, endothelial and haematopoietic surface antigens. Unstained cells were used to identify the single cell population and adjust for fluorescence compensation (A). The histogram in blue represents the cells stained with the specific antibody, while in red is represented the staining with the isotype-matched control antibody. On the abscissa is indicated the fluorescent intensity, while on the ordinate the cell counts. GFP-mADSCs were positive (>90%) for CD90 (B), CD29 (C), CD44 (D) and CD106 (E) MSC markers. The expression of CD105 was found in ~ 53% of cells (F). GFP-mADSCs were negative (<0.2%) for the endothelial marker CD31 (G) and for the hematopoietic marker CD34 (H). Percentages represent average from three separate experiments ± SD.

3.9.2 Tri-lineage differentiation of GFP-mADSCs

GFP-mADSCs were successively tested for their capacity to differentiate into the three different lineages of mesodermal origin: adipocytes, osteocytes and chondrocytes. GFP-mADSCs were induced to differentiate into adipocytes in 12-well culture plates. After 2 weeks of differentiation, cells were imaged with the INCell 2000 (GE) and then stained for the lipid dye Oil-Red-O. GFP-mADSCs successfully differentiated into adipocytes as shown by the morphological shift from the classical fibroblast-like morphology to a more rounded shape containing light refractive cytoplasmic lipid deposits which positively stained with Oil-Red-O staining solution (figure 3.19 A-C). Importantly, cells cultured in basal medium did not show spontaneous differentiation (figure D-F).

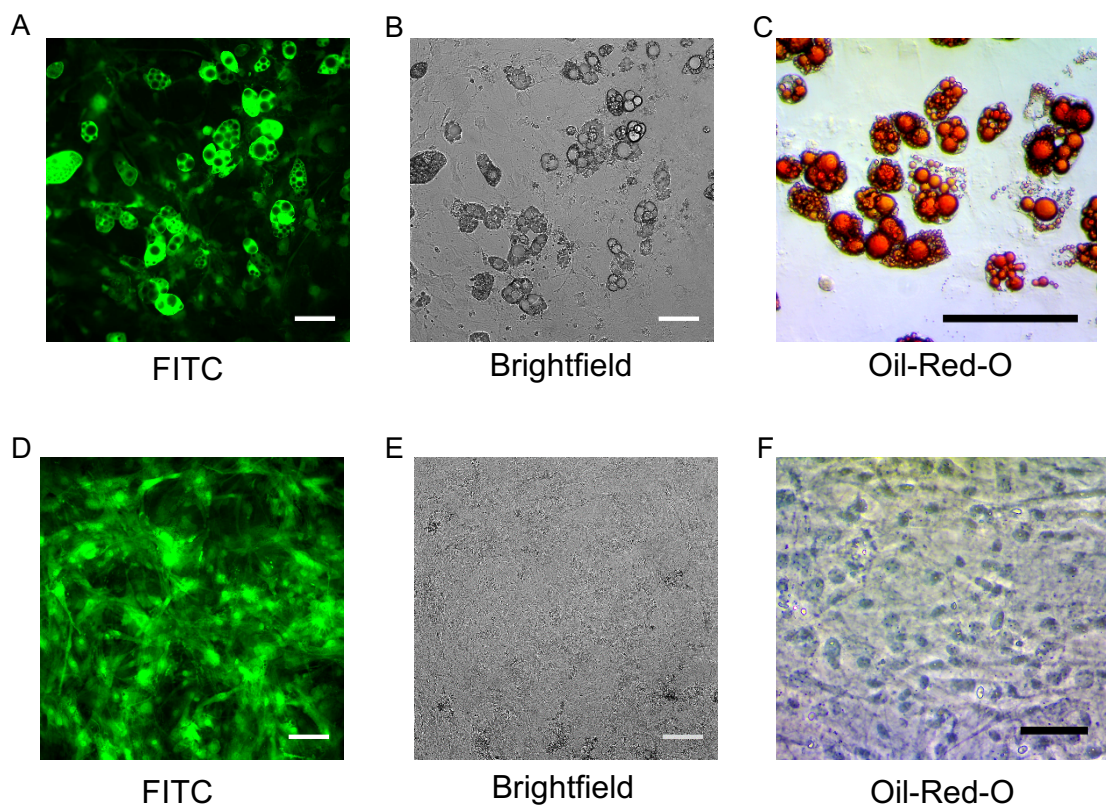


Figure 3.19. Adipogenesis of GFP-mADSCs. Passage 5 GFP-mADSCs were induced to differentiate into adipocytes in 12-well culture plates. (A and B) Representative fluorescent and phase contrast images showing differentiation of GFP-mADSCs 2 weeks after initiation of the induction protocol. (C) Adipocyte differentiation was confirmed by Oil-Red O staining. (D, E and F) GFP-mADSCs cultured in basal medium did not show spontaneous differentiation. Images are representative of 3 separate experiments. Scale bars: 100 μ m.

Osteogenic differentiation was induced in GFP-mADSCs in 6-well culture plates for a period of 3 weeks. Fluorescent images of cultures were acquired 2 weeks after the initiation of the differentiation protocol. Differentiated GFP-mADSCs appeared with a more flattened morphology compared to the spindle shape morphology characteristic of mADSCs cultured in control medium (figure 3.20 A and B). Differentiation of GFP-mADSCs into osteocytes was confirmed by alizarin red staining after 3 weeks from the initiation of the differentiation protocol (figure 3.20 C and D).

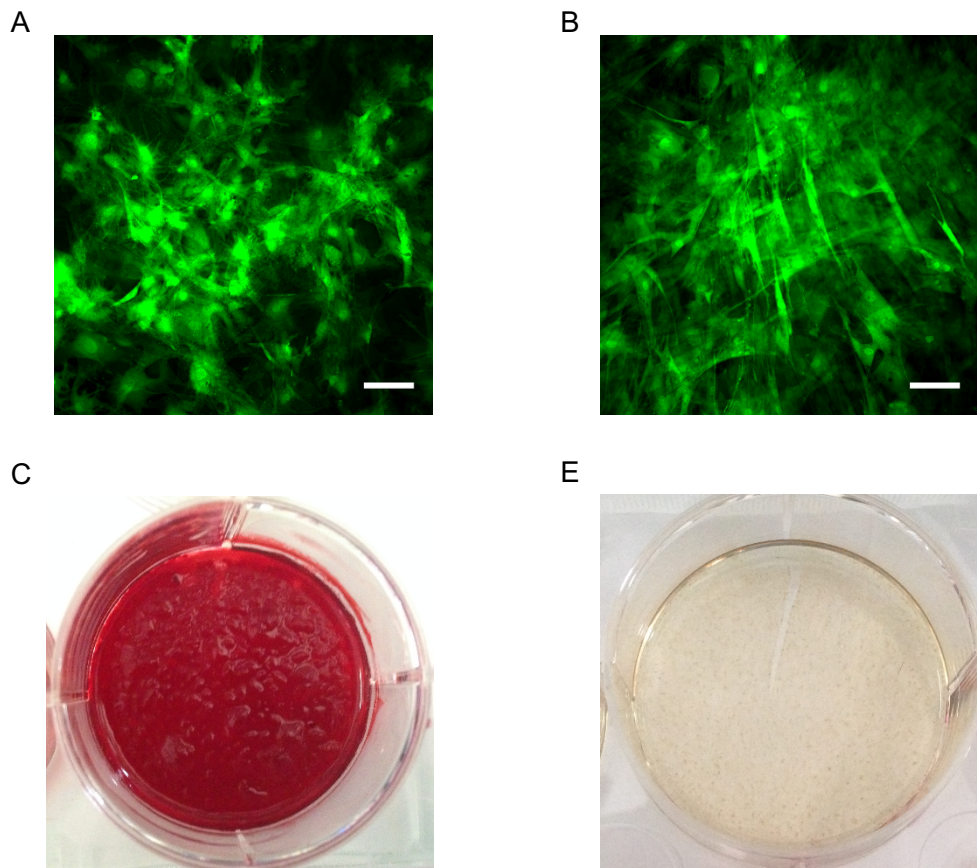


Figure 3.20: Osteogenesis of GFP-mADSCs. Passage 5 GFP-mADSCs were successfully induced to differentiate into osteocytes when cultured in a specific differentiation medium, while they maintained an undifferentiated state in control basal medium. (A) Representative fluorescent image showing morphological changes of GFP-mADSCs 2 weeks after initiation of the induction protocol. (B) GFP-mADSCs cultured in basal medium appeared with a classic fibroblast-like spindle-shape morphology. (C) Osteogenic differentiation was confirmed by alizarin red staining as shown in the digital photograph of a representative culture well. (E) Control cultures did not stain with alizarin red. Images are representative of 3 separate experiments. Scale bars: 100 μ m.

Chondrogenesis was induced in 3D GFP-mADSC pellets as described in Chapter 2 (Materials and Methods). Following 3 weeks culture in differentiation medium, pellets were processed and sectioned for imaging and histology. At the end of the protocol, pellets cultured with the differentiation medium were much more solid and stiff compared to pellets maintained in control basal medium, probably due to the high amount of cartilage produced. This was also visible after fluorescence imaging of the sections, where chondrocyte pellets appeared more circular with well delineated boundaries (figure 3.21 A and B). The cartilaginous nature of the extracellular matrix was confirmed by Alcian Blue staining (figure 3.21 C). Control non induced pellets did not stain with Alcian Blue (figure 3.21 D).

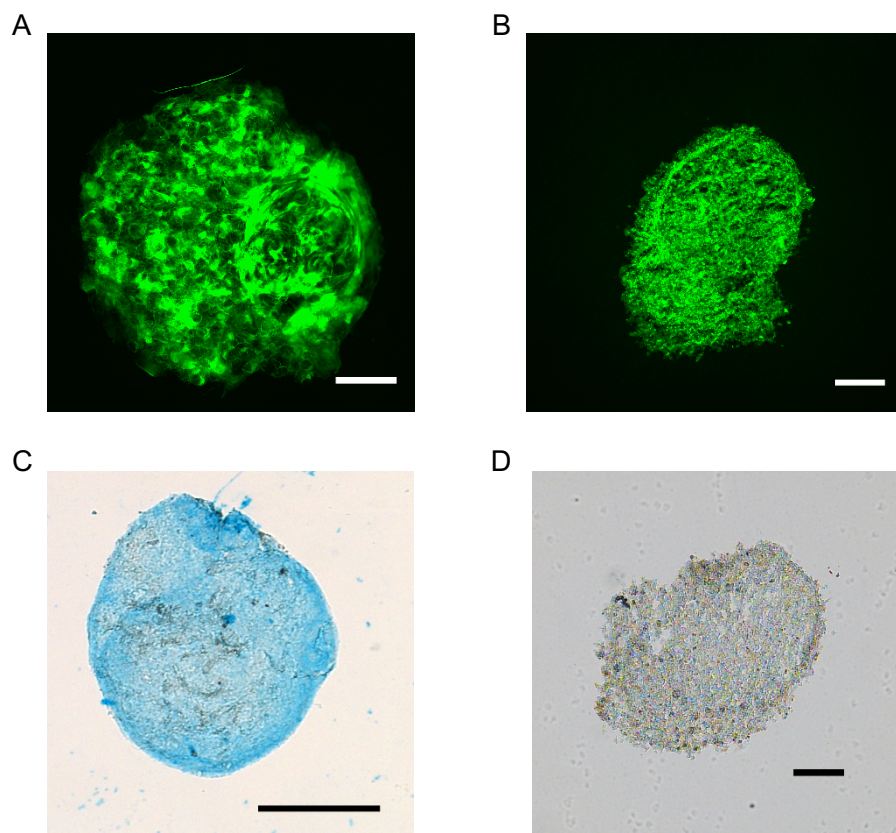


Figure 3.21. Chondrogenesis of GFP-mADSCs. Differentiation of GFP-mADSCs into chondrocytes was achieved on 3D cell pellets. At the end of the differentiation protocol, pellets were collected, processed and sectioned at 25 μm thickness. Representative fluorescence images of GFP-mADSC pellets after 3 weeks in chondrocyte differentiation medium (A) or control basal medium (B). Chondrocyte pellets positively stained with Alcian blue solution (C), while pellets cultured in control medium did not stain (D). Fluorescent images were acquired with the INCell 2000 GE while histology images with the Nikon Eclipse Ni. Scale bars: 100 μm (A, B), 500 μm (C), 200 μm (D).

3.10 Discussion

The first aim of the work described in this chapter was to isolate, expand and fully characterize murine ADSCs in a reproducible manner, with the goal of then investigating the therapeutic potential of mADSCs both *in vitro* and *in vivo* models of ALS as proof-of-concept for the potential of a future ADSC-based therapy in the clinic. Thus, the general IFATS guidelines for the identification of human ADSCs were adapted and applied to identify and fully characterize mADSCs from mice. mADSCs were successively transduced with EGFP-expressing lentivirus and a cell bank was generated to support subsequent *in vivo* transplantation experiments. To exclude toxicity or alteration of cell characteristics following integration of GFP into the genome, GFP-mADSCs were subjected to phenotypic and functional analysis.

3.10.1 Isolation and expansion of mADSCs

The isolation of ADSCs from healthy C57BL/6 mice was successfully achieved by adapting established protocols (Marconi et al., 2013; Cao et al., 2015). After the mechanical and enzymatic digestion of the adipose tissue, the SVF was isolated and a yield of $2.1 \pm 0.4 \times 10^6$ vital cells/g fat (mean \pm SD, n = 3) was obtained, which is consistent with previous reports (Anderson, 2015, Luna et al., 2014).

During the first day of culture of the SVF, a small proportion of cells, consisting of the ADSC population, attached to the plastic culture surface and within a few days started to proliferate rapidly as single cell-derived colonies. The presence of ADSC colonies demonstrated the existence in the culture of progenitors and stem cells with high proliferation capacity. ADSC cultures reached 80% confluency after 4 to 6 days *in vitro*, and were then sub-cultured. After 1-2 passages in culture, ADSCs were grown as a homogeneous monolayer of cells exhibiting a characteristic fibroblast-like morphology. Initially, technical difficulties were encountered in order to expand the ADSCs for more than 3-4 passages in culture.

The maintenance of MSCs *in vitro* relies on the presence of FBS in the culture media, and it is noteworthy that certain serum components such as nutrients, small molecules, toxins and other unidentified factors, may play a critical role in the proliferation and differentiation of MSCs (Lund et al., 2009). Since these components vary considerably between different sources of FBS, and even between different lots of the same serum, screening of sera is critical in achieving the optimal expansion and subsequent differentiation of ADSCs (Zuk et al., 2001) .

Therefore, the three following sources of FBS were tested: FBS of South American origin from Labtech (FBS-SA); Qualified-FBS of USA origin from Gibco (FBS-Q); and Mesenchymal Stem Cell Qualified-FBS of Mexican origin from Gibco (FBS-MSQ). To select the best serum capable of supporting the ADSC expansion, after isolation of the SVF, cells were separately cultured in the presence of the different FBS. The growth kinetics were evaluated and compared by calculating the cumulative PDL from passage 1 to passage 13, and plotting these as a function of the time in culture as described in materials and methods. This is a simple and widely adopted *in vitro* assay to estimate and compare cell growth under different culture conditions or stimuli (Greenwood et al., 2004).

As expected, the proliferation rate of ADSCs was affected by the source of FBS, and the FBS-MSQ was marginally the best choice amongst the sera screened for ADSC expansion. To note, the FBS-MSQ from Gibco is specially designed and pre-tested for the ability to support the *in vitro* expansion of mesenchymal stem cells. Indeed, with the FBS-MSQ serum, ADSCs showed a high proliferation rate and could be expanded for more than 22 PDLs up to 48 days in culture. Despite the differences observed in the growth kinetics, the different sources of FBS did not affect the cell morphology.

3.10.2 Immunophenotype of mADSCs

As described in the IFATS guidelines, human ADSCs must be positive (>90%) for at least three different surface antigens used to identify hMSCs, such as for example CD90, CD73, CD44 and CD29. In addition, to exclude cell contamination, the ADSC population should be negative (<2%) for haematopoietic markers such as CD11b, CD45 and CD34, and negative for the endothelial surface marker CD31. Whereas these guidelines are now widely accepted, and put into practice from most of the laboratories working with human ADSCs, the full characterization of mADSCs is often omitted in papers that investigate the therapeutic potential of these cells. In particular, there is inconsistency and high variability in the choice of the surface markers analyzed to define the ADSC population.

Here, a panel of six different MSC markers (CD90, CD44, CD29, CD73, CD105 and CD106), three haematopoietic markers (CD45, CD11b and CD34) and the endothelial marker (CD31) were tested. mADSCs were nearly 100% positive for the MSC markers CD90, CD44 and CD29, and negative (<0.6%) for the haematopoietic and endothelial surface markers CD45, CD11b, CD34 and CD31. Thus, these results satisfy the minimum criteria established for the identification of cultured ADSCs based

on their characteristic immunophenotype. However, ADSCs isolated in this study differed from their human counterparts for the expression of the surface markers CD73 and CD106. Indeed, mADSCs did not express the MSC marker CD73, but did express CD106, which has been shown to be exclusive to MSCs derived from other sources such as bone marrow and umbilical cord (Yang et al., 2013). These results correlate with other findings in the literature, suggesting the heterogeneous expression of the marker CD73 (depending on species donor and source of MSCs) and the inclusion of CD106 for identification of murine ADSCs (Luna et al., 2014, Anderson, 2015, Peroni et al., 2008, Mohammadpour et al., 2016). Interestingly, CD106 (VCAM-1) is an important cell adhesion molecule involved in haematopoietic stem cells homing from and to the bone marrow, and its expression positively correlates with immunosuppression potential and homing capacity of activated MSCs (Simmons et al., 1992, Ren et al., 2010). The discrepancy in the expression of CD106 amongst mADSCs, hADSCs, and hBM-MSCs could reflect differences in the regulation of homing, mobility and immunomodulation ability of MSCs, and further investigations are needed to address this.

The analysis of the MSC marker CD105 (endoglin) identified two separate populations in our ADSCs cultures: CD105⁺ (52.6 %) and CD105⁻ (47.4 %). The loss of CD105 during *in vitro* expansion has been associated with differentiation processes and loss of stemness of human MSCs (Jin et al., 2009). However, Anderson et al. highlighted the multipotential differentiation and immunomodulation capacity of the CD105⁻ subpopulation of murine ADSCs, showing that CD105⁻ mADSCs are still to be considered in an undifferentiated state (Anderson et al., 2013). Moreover, the CD105⁻ population showed increased capacity to differentiate into osteocytes and adipocytes and were more efficient in modulating CD4⁺ T cells proliferation *in vitro*. These discrepancies might be due to species differences between human and murine ADSCs. However, as suggested by Anderson et al., further investigation would be useful to study differences between the two populations especially when investigating potential therapeutic applications.

3.10.3 Tri-lineage differentiation of mADSCs

A functional hallmark for mesenchymal stem cells is the ability to differentiate *in vitro* toward cells of mesodermal lineage after exposure to specific differentiation chemical cocktails. mADSCs were induced to differentiate towards adipocytes, osteocytes and chondrocytes by culturing cells with defined differentiation media that are widely used to differentiate MSCs.

Following expansion for three generations, mADSCs were cultured in adipogenic medium containing dexamethasone, insulin, IBMX and indomethacin. Under these conditions, mADSCs readily differentiated toward mature adipocytes characterized by the presence of typical intracytoplasmic multilocular fat deposits, whose lipid nature was confirmed by positive Oil Red O staining 1 week and 2 weeks after the initiation of the induction protocol. In particular, after 2 weeks of induction, mADSCs massively differentiated into adipocytes characterized by the presence of large lipid droplets, probably derived from the fusion of the smallest vesicles which appeared during the first week of induction. Rarely, the presence of unilocular fat cells was also observed.

The osteogenic differentiation of the cultured mADSCs was achieved by incubating the cells with a specific differentiation media consisting of DMEM, FBS, dexamethasone, ascorbic acid and β -glycerol phosphate. Although alterations in cell morphology were observable early after the initiation of the induction, the production of calcium extracellular matrix and differentiation of mADSCs into osteoblasts, was detectable only after three weeks of incubation. At this point, white calcium deposits were easily detectable by eye. To confirm osteogenic differentiation, cells cultured for three and four weeks in the osteogenic medium, were stained with Alizarin Red S, the most common assay used to document MSC differentiation into osteocytes. The staining revealed that differentiated mADSCs were able to form characteristic mineralized-bone-nodules *in vitro*.

Chondrogenesis was induced on 3D mADSCs pellets cultured in DMEM in the presence of FBS, insulin-transferrin-selenium, sodium pyruvate, ascorbic acid, dexamethasone and transforming growth factor β 1. At the end of the differentiation, the production and accumulation of extracellular matrix was noticeable, with differentiated pellets appearing bigger and stiffer compared to the pellets cultured in control basal medium. The cartilaginous nature of the extracellular matrix was confirmed by staining the pellets sections with Alcian Blue, which complexes with acid proteoglycans. In contrast, control cultures were negative for this stain.

In the literature, the differentiation of ADSCs is commonly performed after 2-3 passages in culture, since the differentiation potential seems to decrease during repeated passages. However, some authors speculated that the differentiation usually seen in ADSCs, could be the result of a low fraction of contaminant haematopoietic stem cells which is still present after early passages in cultures (Locke et al., 2009).

Here, after 5 passages in culture, the mADSCs were immunophenotypically homogeneous and almost completely free from haematopoietic stem cell contaminants as determined by very low expression (<0.6%) of CD45 and CD34 surface markers. Also, mADSCs retained the capacity to differentiate into mature adipocytes and osteocytes even after 14 passages in culture, equivalent to approximately 18 generations. Thus, it is unlikely that the differentiation here documented can be attributed to contaminant stem cells of haematopoietic origin.

3.10.4 Generation of GFP-mADSCs, long-term storage and characterisation

In order to permanently label mADSCs for *in vivo* tracking purposes, cells were genetically modified to express EGFP by lentivirus transduction. Given their large gene capacity, relatively low cytotoxicity and stable long-term gene expression, lentiviruses are considered potent and efficient vectors for gene delivery in a variety of cell types, including MSCs (Hong et al., 2007).

The lentivirus vector with the EGFP expression under control of the mPGK promoter was chosen because of previous reports in the literature showing that the use of this promoter allowed efficient and stable gene delivery/expression into murine MSCs (Sweeney et al., 2016, Krause et al., 2011, McGinley et al., 2011). Lentivirus particles were generated by transient co-transfection of HEK 293T cells using the phosphate calcium method. The lentivirus was then concentrated by ultracentrifugation, allowing the use of small volumes of virus for downstream applications. Finally, the concentrated lentivirus was functionally titred by infecting HeLa cells. In this study a titre of 4×10^8 TU/ml was obtained. Although the lentivirus titre is only an estimated and arbitrary number relative to several parameters such as type of target cells, cellular density and proliferation rate during infection, it is of extreme utility to check the lentivirus quality and to control for MOI dilution experiments, especially when high transduction efficiency is needed.

In this study, it was important to efficiently transduce mADSCs since non-labeled mADSCs would not be detectable after *in vivo* transplantation, and important information regarding engraftment, distribution and survival of transplanted cells would be missed. To optimize the lentivirus transduction of mADSCs, a MOI titration experiment was carried out. Since previous reports have indicated a relatively low transduction efficiency of MSCs with lentivirus (Lin et al., 2012), the MOI test was also performed in the presence of polybrene which has been shown to improve the transduction efficiency (Denning et al., 2013). As expected, high levels of transduction were obtained only by infecting mADSCs with a relatively high MOI such

as 80. However, infection of primary cells with a high MOI may result in toxicity. Moreover, several lentivirus preparations would be necessary to achieve the transduction of a considerable amount of cells needed for transplantation studies. Remarkably, in the presence of polybrene, more than 94% of ADSCs were successfully transduced with an MOI of 30. The use of polybrene to transduce MSCs has been adopted previously, however, it has also been shown to dramatically affect human BM-MSC proliferation (Lin et al., 2012). Although a proliferation assay was not performed, a decrease in proliferation was not detected. Indeed, polybrene treated cells continued to proliferate as fast as untreated mADSCs for at least 5 passages in culture, allowing for the establishment of a relatively large cell bank. The inconsistency with the Lin work may be related to several aspects such as species differences, MSC source and seeding density.

Given the high transduction efficiency and the retained capacity of transduced ADSCs to proliferate in culture, the MOI of 30 with 4 µg/ml polybrene was chosen to transduce a large amount of freshly isolated p1 mADSCs for future transplantation experiments. Before expanding and cryopreserving GFP-mADSCs, the GFP expression was analyzed. Unexpectedly, the transduction efficiency was slightly higher compared to that observed in the MOI test (98.8% vs 94%). This could be explained by differences in cell density during transduction and proliferation rate. Indeed, since the proliferation rate of passage 1 mADSCs is very high, to avoid over-confluency of cultures before the flow cytometry analysis, cells were plated at a reduced density compared to the seeding density of the MOI test when passage 3 mADSCs were used.

Since GFP-mADSCs were generated for future *in vivo* transplantation experiments, it was important to certify the capacity of GFP-mADSCs to recover from a freezing/thawing cycle and preserve the phenotypic and functional mesenchymal stem cell characteristics following integration of GFP. Thus, three samples of GFP-mADSCs were recovered from the cryopreserved stock and the viability, phenotype profile and pluripotency evaluated. Notably, the GFP-mADSCs fully recovered after being stored for three months in liquid nitrogen. Cells did not show evidence of morphological changes and were successfully expanded for 2 passages in culture before being subjected to immunophenotype analysis by flow cytometry and multipotential capacity by tri-lineage differentiation assay. The immunophenotype of GFP-mADSCs was unaffected by neither the cryopreservation nor the genome integration of GFP. Indeed, cells were strongly positive for the MSC markers (CD90, CD29, CD44, CD106 and CD105) and negative for the endothelial (CD31) and the haematopoietic (CD34) markers.

Finally, GFP-mADSCs were shown to preserve the multilineage differentiation potential towards the mesodermal commitment (adipocytes, osteocytes and chondrocytes), with no effects on GFP expression levels. The retention of GFP expression following differentiation is of considerable importance since this would allow the detection of the transplanted cells in *in vivo* experiments.

3.10.5 Conclusions

In this study mADSCs were successfully isolated and expanded similar to previous reports. Furthermore, these cells were fully characterized by adopting standardized and reproducible phenotypical and functional assays, thus meeting the minimum criteria used to identify human ADSCs, released by the IFATS and the SISCT societies. mADSCs were successfully labelled for transplantation experiments by genomic integration of EGFP following lentivirus infection, with an efficiency of almost 100%. In agreement with previous studies, the integration of GFP did not affect the immunophenotype, nor the differentiation potential of mADSCs *in vitro* (Wang et al., 2009b, van Vollenstee et al., 2016, Zhang et al., 2014). Importantly, GFP-mADSCs maintained their characteristics following a freezing/thawing cycle, which allowed their long-term storage.

4 Intrathecal transplantation of mADSCs in SOD1^{G93A} mice

4.1 Introduction

Several pre-clinical studies have demonstrated beneficial effects of mesenchymal stem cell transplantation in animal models of ALS (Zhao et al., 2007, Uccelli et al., 2012, Boucherie et al., 2009). In most of the previous studies, human MSCs derived from the bone marrow (hBM-MSC) were used, with some authors transplanting murine BM-MSC. As discussed in the introduction, a less invasive procedure such as liposuction may represent a valuable alternative to bone marrow aspiration in order to obtain higher yields of MSCs for clinical application.

At present, only two groups investigated the therapeutic potential of ADSCs in ALS animal models. In 2013, Marconi et al. injected mouse ADSCs intravenously in SOD1^{G93A} mice at disease onset (Marconi et al., 2013). The authors, showed improvement in neurophysiology parameters and motor strength up to 50 days after ADSC treatment compared to controls. However, lifespan and inflammation was not affected by this stem cell treatment. The graft evaluation was performed 4 weeks and 8 weeks following stem cell injection, showing migration and survival of some ADSCs (less than 3 cells/mm²) into the spinal cord parenchyma (Marconi et al., 2013). In the study reported by Kim et al., ADSCs from human lipoaspirates were transplanted either intravenously (IV) or intrathecally by intra-cerebroventricular injections (ICV) into pre-symptomatic SOD1^{G93A} mice (Kim et al., 2014b). Interestingly, both routes of delivery resulted in motor performance improvements and extended survival, but more consistent beneficial effects were observed in the ICV group. The authors showed migration of hADSCs into the spinal cord parenchyma of ICV transplanted mice 4 weeks after injection. However, very few cells in the IV group were detected (Kim et al., 2014b).

In both studies the therapeutic effect of ADSCs was investigated in the commonly used SOD1^{G93A} transgenic mouse strain on a mixed C57BL/6SJL background. The use of the mixed genetic background in the SOD1^{G93A} mouse model can lead to a number of confounding factors which, if not adequately controlled for, can result in spurious results (Alexander et al., 2004, Mead et al., 2011, Scott et al., 2008). In the present study, the therapeutic potential of ADSCs transplantation directly into the CSF of mice was evaluated by using SOD1^{G93A} transgenic mice of the defined C57Bl/6J genetic background. This model shows minimal genetic variation, reduced

background noise in biological readouts and robust reproducibility of disease readouts (Mead et al., 2011). Moreover, in this model significant changes in motor function are detectable as early as 40 days of age before other visible signs of the disease are observable (Mead et al., 2011). This allows the design of a relatively short protocol for preclinical therapeutic investigation before conducting additional studies in which the mice are allowed to reach the end-stage of the disease (Mead et al., 2011).

Amongst different delivery options, intrathecal injection may represent the most clinically translatable delivery method, since the cells would be able to migrate close to sites of neurodegeneration, without the need of a highly invasive surgical procedure. In this study, as a proof of concept we tested whether intrathecal injection of mouse ADSCs before clinical signs of disease, could improve motor performance and delay disease onset in SOD1^{G93A} mice on this defined C57Bl/6J genetic background. There are different methods to assess motor function (Schonfeld et al., 2017). In the SOD1^{G93A} mouse model the most commonly used assessments consist of the rotarod test, grip strength, open field, neurological scoring and gait analysis. In this study, we monitored weight, rotarod performance, gait analysis and neurological score based on extensive previous experience and historical data with these techniques (Mead et al 2011). Moreover, given the central role of inflammation during disease progression in ALS, and the immunomodulatory properties of ADSCs, levels of astrocyte and microglial activation were evaluated, as well as spinal motor neuron survival. Finally, for the first time we evaluated the distribution and survival of intrathecally injected mouse ADSCs in SOD1^{G93A} mice over time at 1 week intervals up to 4 weeks after transplantation.

4.2 Aims

1. To investigate whether GFP-mADSCs could survive and engraft in transgenic SOD1^{G93A} ALS mice following injection directly into the cerebrospinal fluid via the cisterna magna.
2. To investigate whether intrathecal transplantation of GFP-mADSCs could improve motor performance, delay disease onset, reduce neuroinflammation and protect motor neurons in SOD1^{G93A} mice.

4.3 Estimation of cell viability before in vivo transplantation

As described in the material and methods chapter (paragraph 2.3.3), on the day of transplantation ADSCs were collected and suspended in the HypoThermosol® FRS solution in order to maintain their biological stability during the transfer from the tissue culture facility to the animal facility, during the preparation of the mice for the surgical procedure, and eventually during the period occurring in between different injections of several mice on the same day. To confirm the preservation of the ADSCs in the FRS solution, cell samples were suspended in the hypothermal solution and stored for 4 hours at 4°C before checking for viability by the trypan blue exclusion method. Remarkably, the recovery of the stored mADSCs was extremely high, with a viability of $98.8 \pm 0.4\%$ (mean \pm SD, n=3). To check whether cell viability could be affected during transplantation by their passage through the syringe needle, following preservation in FSR, ADSCs (1 million/10 μ l) were loaded into the Hamilton syringe used for transplantation, pushed through the needle by using the programmable syringe pump (1 μ l/min) and viability estimated. Live ADSC recovery after hypothermic preservation and following injection was $97.5 \pm 0.3\%$. Thus, cell preservation in FSR solution and following passage through the syringe needle did not significantly reduce ADSC viability.

4.4 Optimization of cell dosage for transplantation

In order to evaluate the feasibility and safety of the surgical procedure, 2 x 30 days-old SOD1^{G93A} transgenic mice were injected with a total of 1×10^6 GFP-mADSCs via the cisterna magna and the mice were sacrificed 48h post injection. No complications were encountered during the injections nor after the mice recovered from the anaesthesia. Tissue was then collected and processed to evaluate the survival and distribution of the transplanted GFP-mADSCs as described in the materials and methods chapter (paragraph 2.3.4). As shown in figure 4.1, histology examination of the mouse brain revealed GFP⁺ cell clumps of considerable dimensions in the ventricular system accompanied by evidence of abnormal structural changes in the size and shape of the third and fourth ventricles (figure 4.1 A, C and E). The presence of obstructive cell aggregates could cause CSF blockage and subsequent hydrocephalus. Moreover, the aggregation of the injected stem cells could affect CNS cell distribution and potentially result in reduced therapeutic effects. No signal was detected in control PBS-injected mice (figure 4.1 B, D and F).

Thus, to determine the maximum/optimal amount of cells to be injected, a pilot study was conducted. SOD1^{G93A} transgenic mice (n=2 per group) were transplanted with

either 0.3 million, 0.5 million or 1 million GFP-mADSCs and animals were monitored daily to exclude any complications resulting from the transplantation. Mice were then culled 1 week post-transplantation and the whole CNS processed for GFP-mADSC detection. All animals recovered from the surgical procedure and did not show any sign of hydrocephalus during the first week following transplantation. Since most of the detected GFP signal was from clusters of transplanted cells rather than isolated single GFP-mADSCs, it was not possible to quantify the number of engrafted cells. Thus, a qualitative evaluation of cell distribution and survival was performed. As shown in figure 4.2, in all the groups, most of the GFP signal was detected in the IV ventricle, lateral recesses and cisterna pontine (figure 4.2 A-C, G-I, M-O).

In mice injected with 1 million GFP-mADSCs, big cell clumps in the IV ventricle were still present one week after the injection (figure 4.2 A). However, the GFP signal was confined to the edges of the cellular aggregates while no signal was detected in the middle, suggesting that most of the cells died during the first week. Moreover, abnormal structural changes in the IV ventricle were visible, with the cell clump mechanically indenting the brainstem region, which looked deformed. Clumps of GFP-mADSCs were also found in the ventricular system of mice injected with 0.5 or 0.3 million cells, however, these were of a much smaller size and did not cause abnormal changes in the IV ventricle structure (figure 4.2 G and M). As expected, fewer GFP-mADSCs were detected in the lateral recesses (figure 4.2 B, H and N) and around the brainstem (cisterna pontine) (figure 4.2 C, I and O) of mice injected with 0.3 and 0.5 million cells compared to the mice transplanted with 1 million ADSCs. Cells were also detected within the subarachnoid space of the spinal cord at cervical, thoracic and lumbar levels. In mice injected with 1 million cells, most of the GFP-mADSCs were detected around the cervical and thoracic spinal cord, while cells at the lumbar enlargement were rarely detected (figure 4.2 D-F). Surprisingly, in mice injected with 0.5 and 0.3 million cells, a greater amount of GFP-mADSCs were detected in the lumbar segment compared to the mice dosed with 1 million cells (figure 4.2 F, L and R). No major differences were observed in the distribution of cells in the cervical and thoracic spinal cord between the 0.5 and 0.3 million groups (figure 4.2 J-K, P-Q).

Since hydrocephalus or abnormal structural changes in the ventricular system were not observed in mice injected with 0.5 million cells and given that previous reports suggested a greater therapeutic effect when injecting higher numbers of MSCs (Kim et al., 2010), the 0.5 million cells/animal dose was chosen for the subsequent experiments.

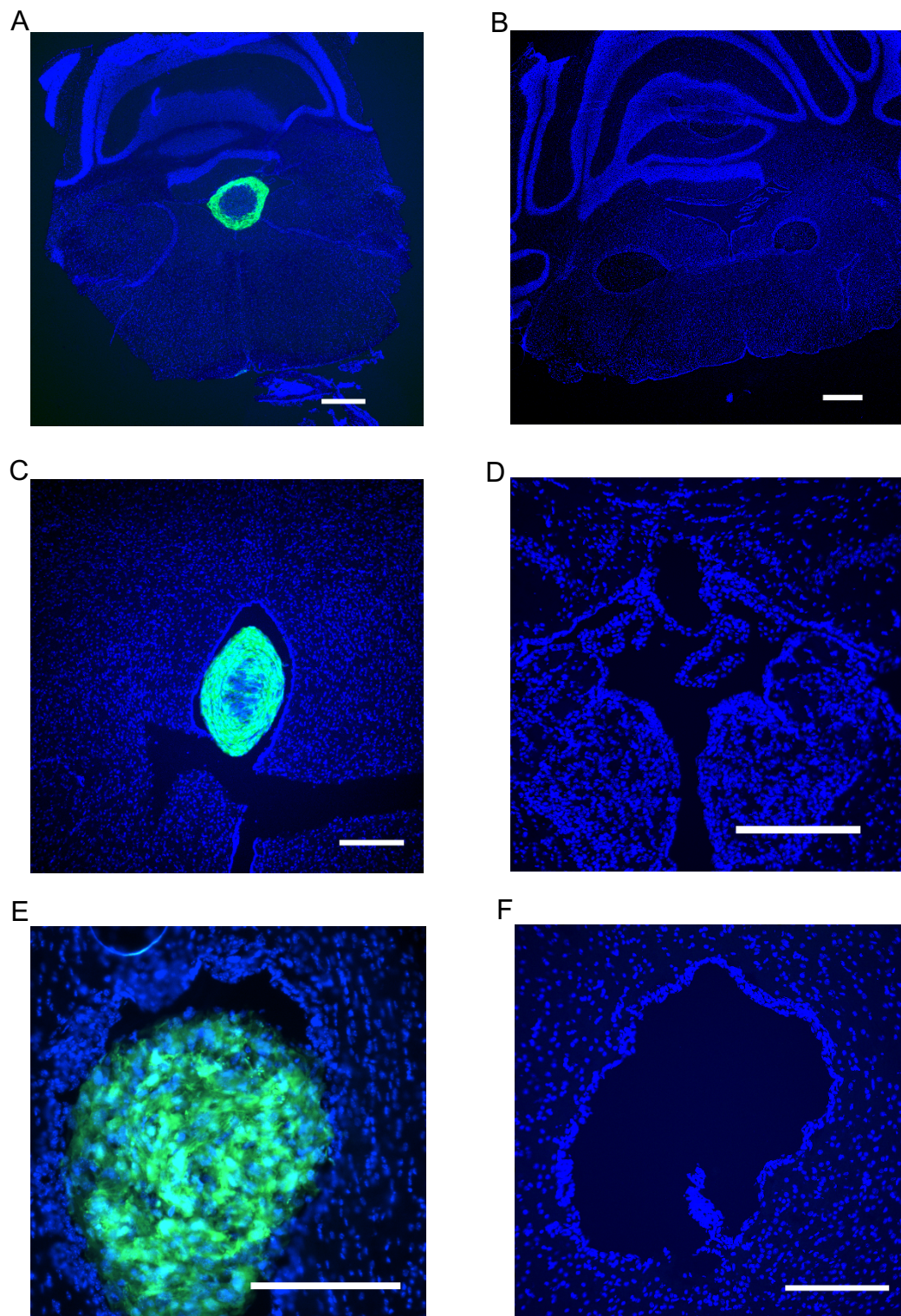


Figure 4.1. GFP-ADSCs engraftment in SOD1^{G93A} mice 48 hours after intrathecal injection of 1×10^6 cells. Representative images showing cell clumps of GFP⁺ cells within the IV ventricle (A), III ventricle (C) and aqueduct (E). In control PBS-injected mice no signal was detected (B, D and F). Nuclei are stained with DAPI. Images were captured with the IN Cell 2000 (GE) and are representative of two separate experiments. Scale Bars: 500 μm (A and B); 250 μm (C and D) and 200 μm (E, F).

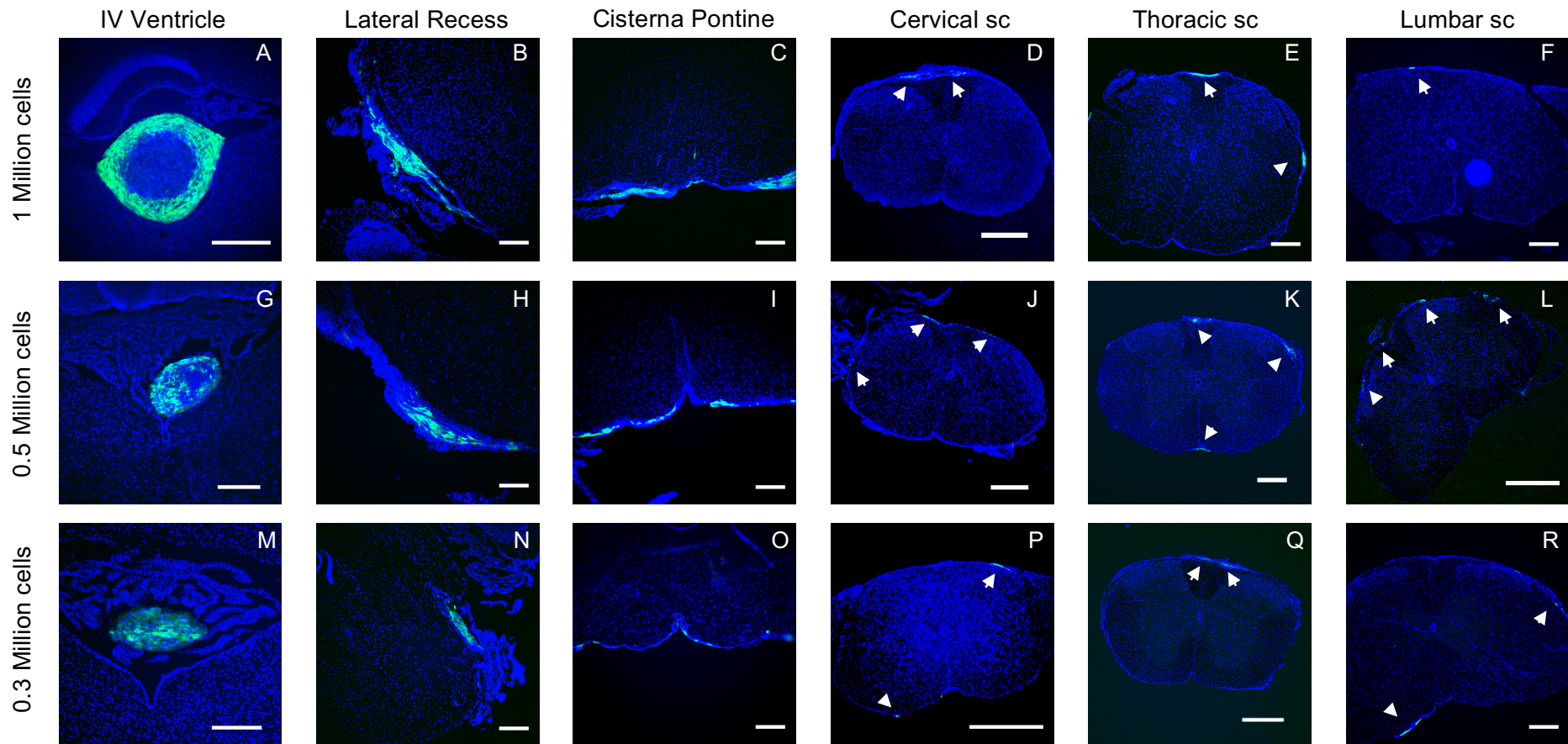


Figure 4.2. Optimization of cell dose for transplantation in $SOD1^{G93A}$ mice. Representative images illustrating the engraftment and distribution of GFP-mADSCs in the CNS of in $SOD1^{G93A}$ mice 1 week after transplantation of different cell doses. Mice were transplanted with 1 million (A-F), 0.5 million (G-L) or 0.3 million (M-R) GFP-mADSCs. Nuclei are stained with DAPI. Images were captured with the IN Cell 2000 (GE) and are representative of two mice per group. Scale Bars: 500 μ m (D, J, L, P and Q); 250 μ m (K); and 200 μ m (A, C, E, F, G, H, I, M, N, O and R). (sc = spinal cord).

4.5 Engraftment, distribution and survival of GFP-mADSCs in SOD1G93A mice

During the preclinical study, groups of mice (n=3/group) were sacrificed at several time points after GFP-mADSC-transplantation to evaluate stem cell engraftment, distribution and survival over time. The whole CNS with intact dura mater was dissected and processed for detection of GFP-positive cells after 1, 2, 3 and 4 weeks from transplantation.

After 1 week, GFP-mADSCs were mostly detected as cell clusters close to the injection site (cisterna magna), in the IV ventricle, underneath the brainstem, and within the meninges of the dorsal cervical spinal cord (figure 4.3 A). GFP-mADSCs were also found close to the choroid plexus in the lateral recess (figure 4.3 B) and in the cisterna pontine (figure 4.3 C). Histology on whole spinal cord showed that the transplanted GFP-mADSCs survived within the subarachnoid space in the cervical (figure 4.4 A), thoracic (figure 4.4 B) and lumbar (figure 4.4 C) regions of the spinal cord.

At week 2 post-injection, GFP-mADSCs were still present in the IV ventricle (figure 4.5 A) and within the cisterna pontine (figure 4.5 B), with some cells migrating into the brainstem parenchyma. Interestingly, a considerable number of cells were found in the lateral recesses close to the choroid plexus (figure 4.5 C). Cells were also detected along the spinal cord, albeit they did not appear to cross the meninges and penetrate into the parenchyma (figure 4.5 D). However, homing of ADSCs close to both dorsal and ventral roots was observed (figure 4.5 D).

After 3 weeks, the survival of GFP-ADSCs within the IV ventricle (figure 4.6 A) and cisterna pontine (figure 4.6B) decreased considerably, while the majority of the surviving cells were detected in the lateral recesses strongly associated with the brainstem border (figure 4.6 C). Cells were still detected in the subarachnoid space of the spinal cord, although not as often as observed during the first two weeks post-injection (figure 4.6 D).

At week 4, few GFP-ADSCs survived within the ventricular system (figure 4.7 A, B and C) and occasionally cells were detected in the lumbar spinal cord confined to the meninges (figure 4.7 D). Figure 4.8 shows that no fluorescent signal was detected in control PBS-injected mice.

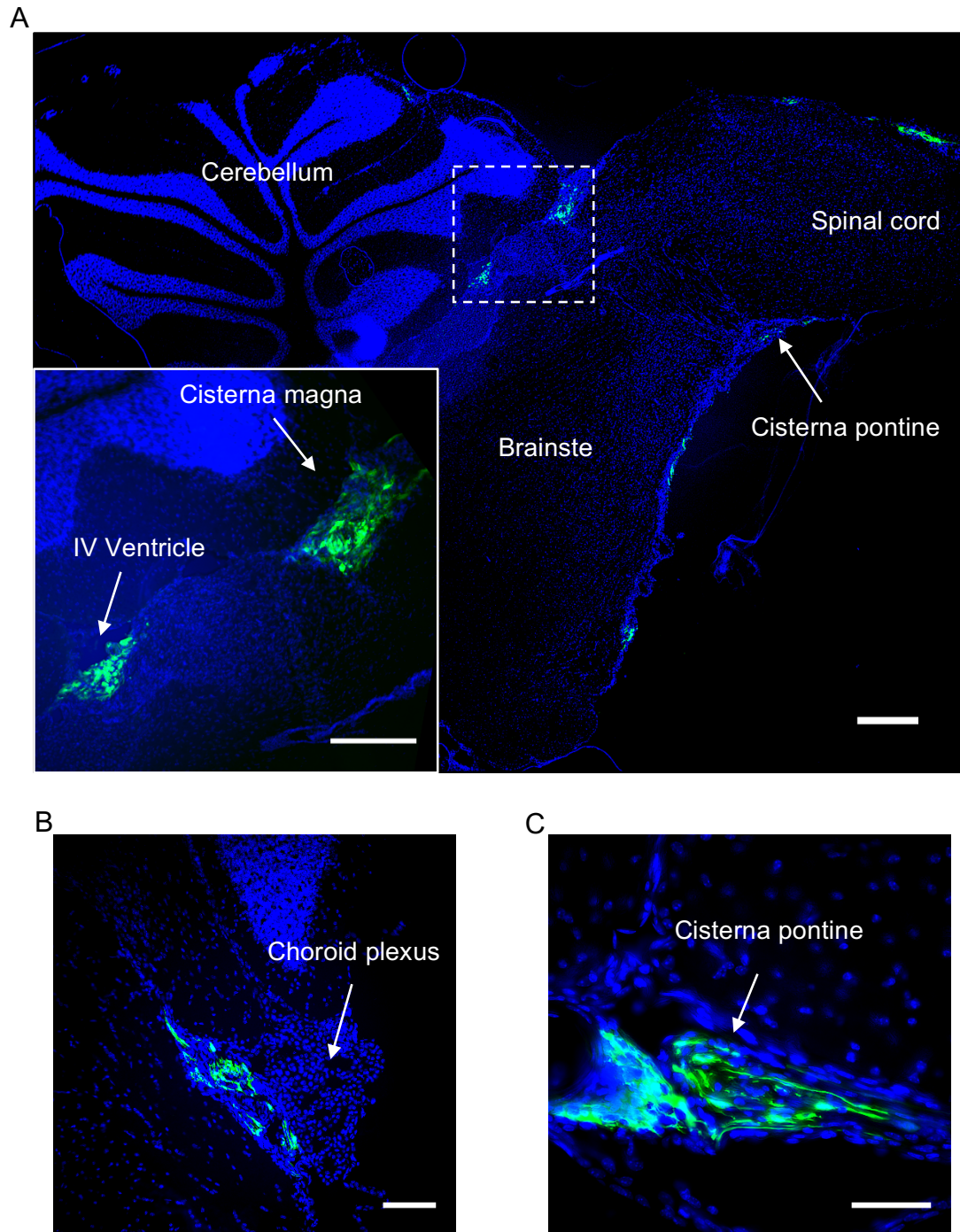


Figure 4.3. Distribution of GFP-mADSCs 1 week post-injection 1. (A) Representative image of a brain sagittal section showing engraftment and distribution of transplanted GFP-mADSCs one week-post injection. Clusters of GFP-positive cells were found in the cisterna magna, IV ventricle, cisterna pontine and dorsal meninges of cervical spinal cord. The dashed area is magnified in the box area. (B) GFP-mADSCs were found in the lateral recesses close to the choroid plexus. (C) Images showing GFP⁺

cell cluster in the cisterna pontine. Nuclei are stained with DAPI. Images were captured with the In Cell 2000 GE. Scale bars: (A) 500 μm ; (B) 100 μm ; (C) 50 μm .

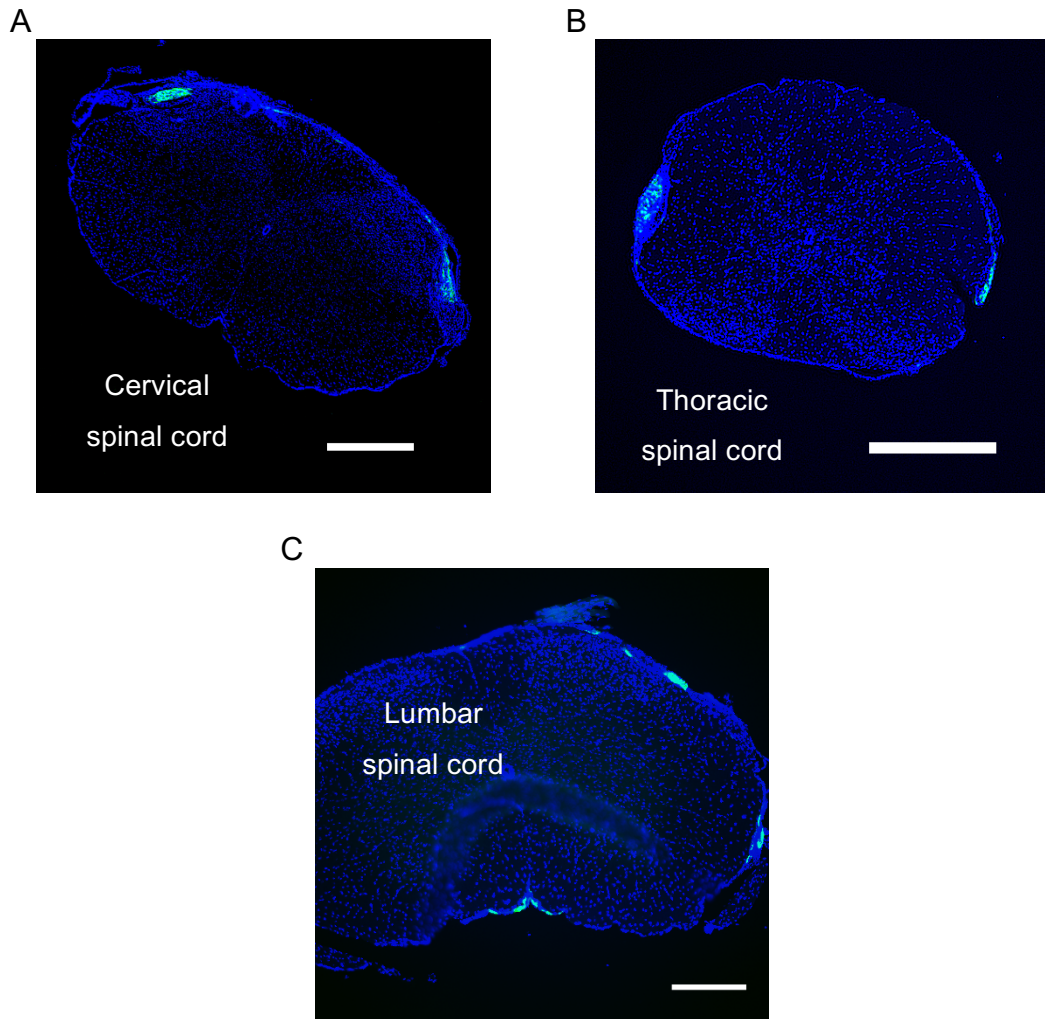


Figure 4.4. Distribution of GFP-mADSCs 1 week post-injection 2. Representative images of spinal cord coronal sections showing engraftment and distribution of transplanted GFP-mADSCs one week-post injection. Cells were detected along the spinal cord confined to the subarachnoid space. Cell clusters were observed at cervical (A), thoracic (B) and lumbar (C) levels. Nuclei are stained with DAPI. Images were captured with the In Cell 2000 GE. Scale bars: 500 μm (A and B); 250 μm (C).

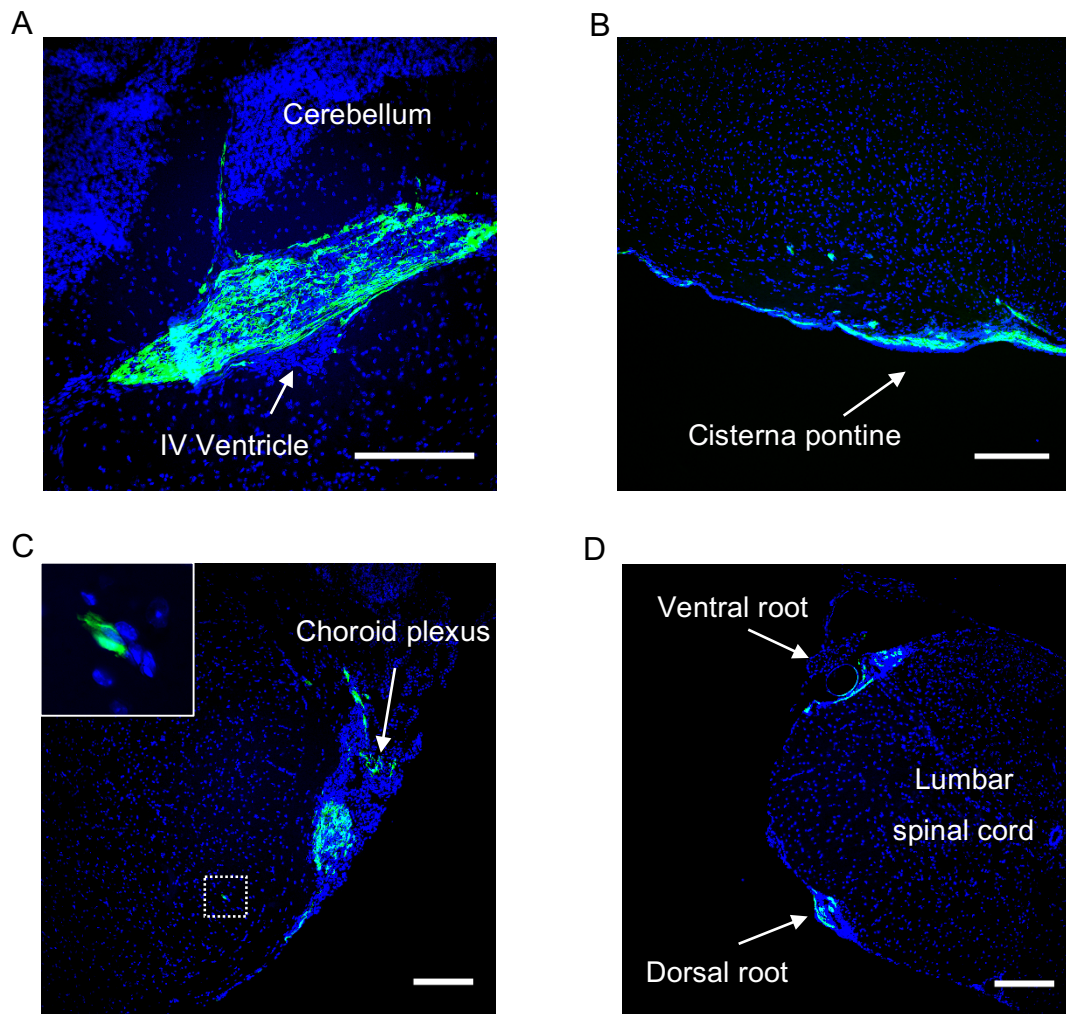


Figure 4.5. Distribution of GFP-mADSCs 2 weeks post-injection. Representative images of coronal brain and spinal cord sections showing survival of GFP-mADSCs 2 weeks after injection. GFP-mADSC were detected in the IV ventricle (A), around the brainstem (B) and in the lateral recesses (C). Occasionally, cells migrated into the brainstem parenchyma (B and C). GFP-mADSCs were also found in the meninges of spinal cord, although they did not migrate into the parenchyma (D) The dashed area is magnified in the box area. Nuclei are stained with DAPI. Images captured with the In Cell 2000 (GE). Scale bars: 200 μm (A, C and D); 250 μm (B).

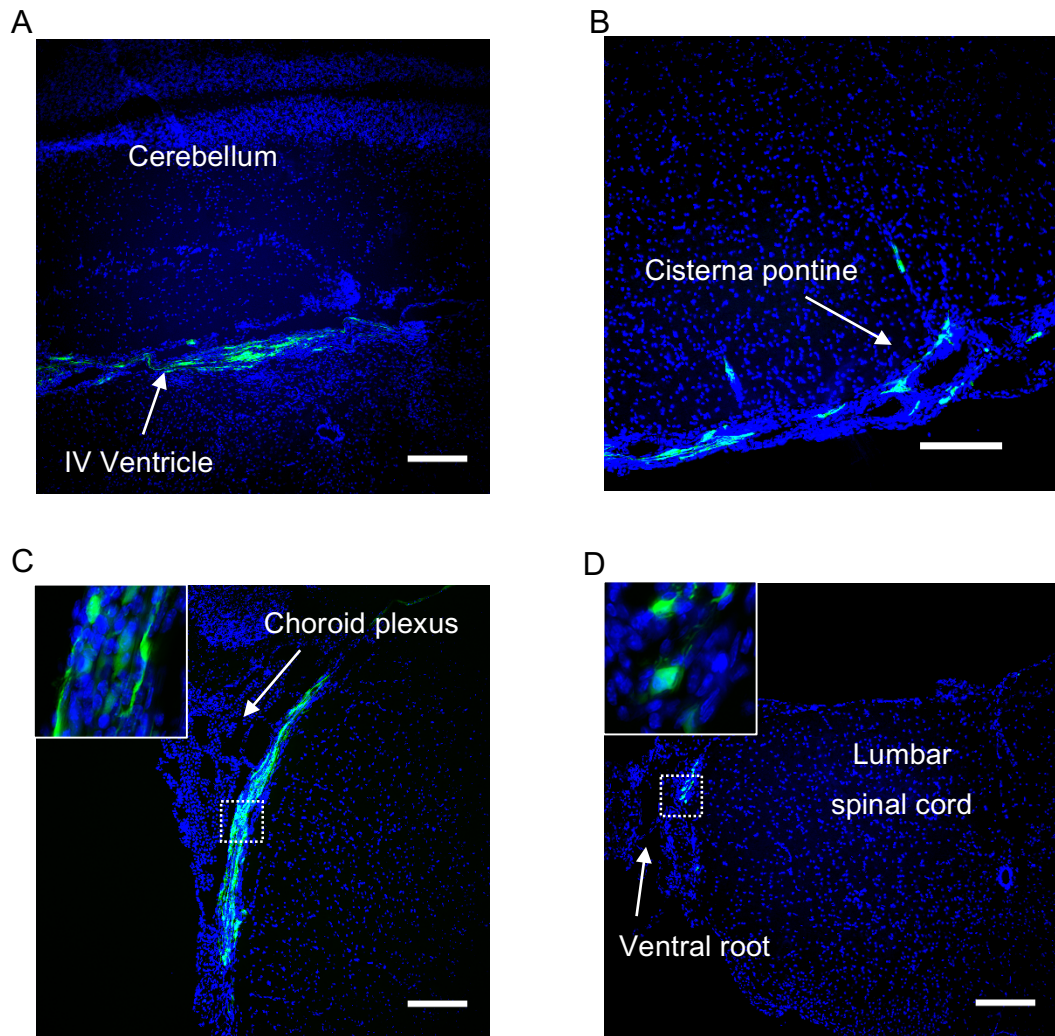


Figure 4.6. Distribution of GFP-mADSCs 3 weeks post-injection. Representative images of coronal brain and spinal cord sections showing distribution of GFP-mADSCs 3 weeks after transplantation. GFP-mADSC were detected in the IV ventricle (A) and in the cisterna pontine (B). Most of the surviving cells were detected in the lateral recesses adjacent to the brainstem (C). Occasionally cells were found in the meninges of spinal cord, at the dorsal root level (D). The dashed areas are magnified in the box areas. Nuclei are stained with DAPI. Images captured with the In Cell 2000 (GE). Scale bars: 200 μ m all.

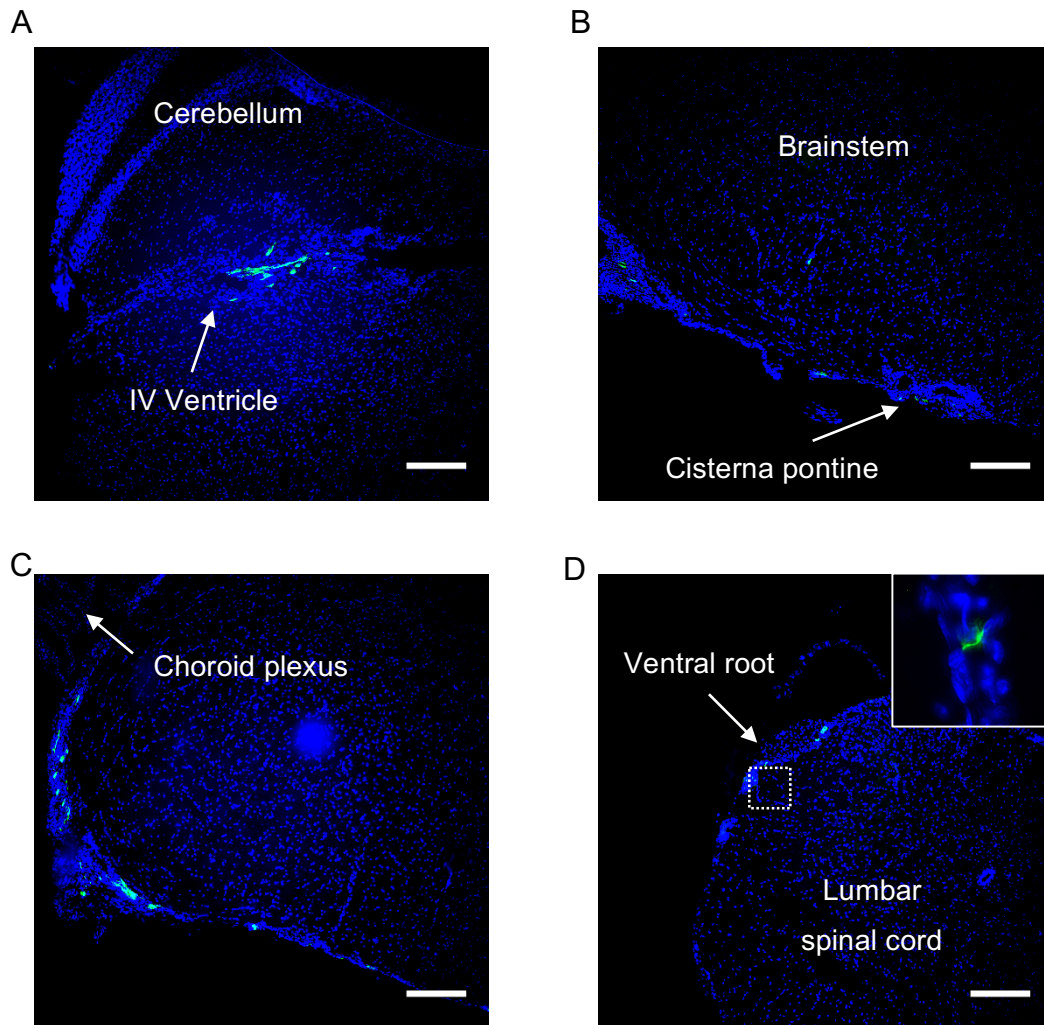


Figure 4.7. Distribution of GFP-mADSCs 4 weeks post-injection. Representative images of coronal brain and spinal cord sections showing distribution of GFP-mADSCs 4 weeks after transplantation. Few GFP-mADSC were detected in the IV ventricle (A) and in the cisterna pontine (B). Cells were also found in the lateral recesses (C). Rarely, cells were detected in the meninges of spinal cord (D). The dashed area is magnified in the box area. Nuclei are stained with DAPI. Images captured with the In Cell 2000 (GE). Scale bars: 200 μ m all.

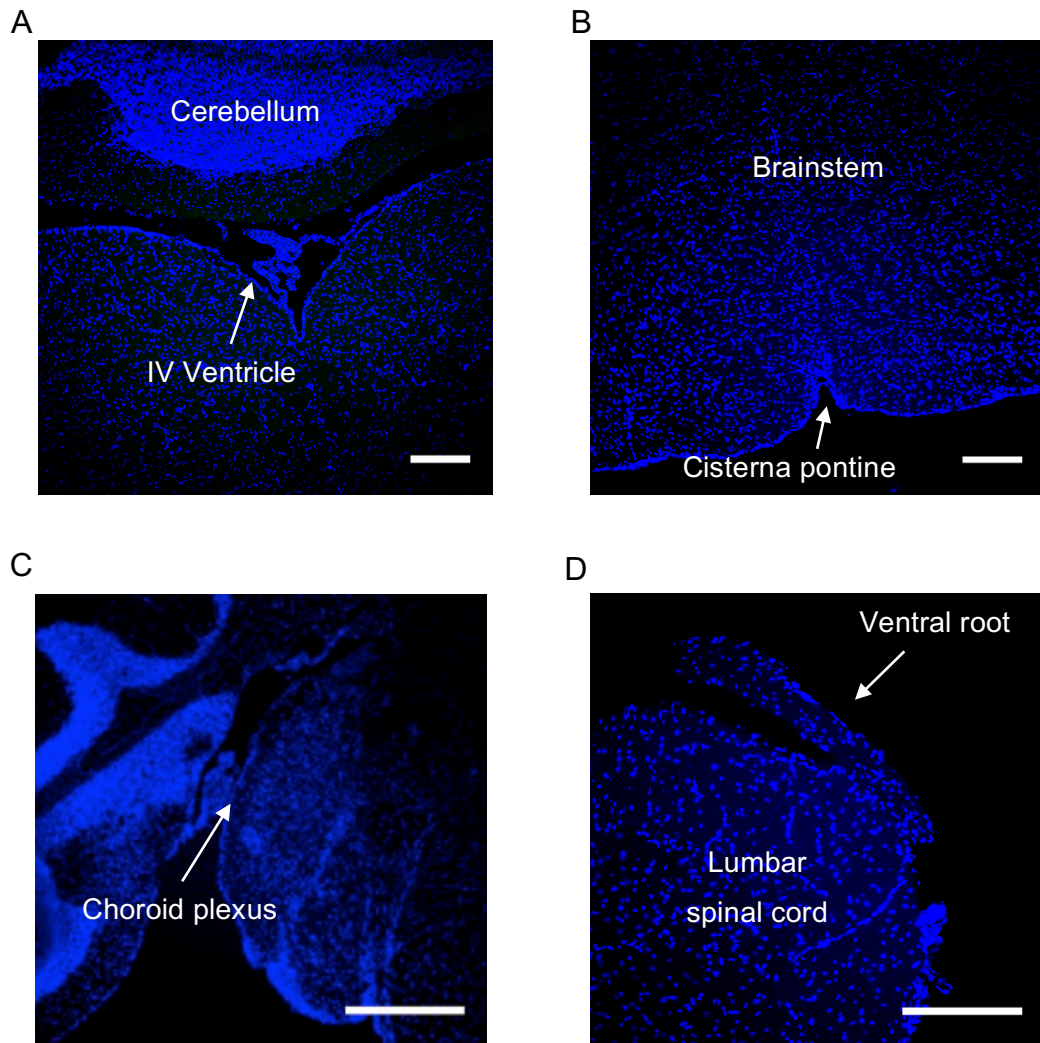


Figure 4.8. Histology on control PBS-Injected mice. Representative images of coronal brain and spinal cord sections showing that no GFP signal was detected in PBS-injected mice (A-D). Nuclei are stained with DAPI. Images captured with the In Cell 2000 (GE). Scale bars: 200 μm.

4.6 mADSCs increase body weight in SOD1G93A mice

Mice were weighed twice per week immediately before behavioural assessments from day 33 until the end of the study. ADSC-injected mice were significantly heavier than PBS-injected controls (vehicle) from 8.5 weeks of age (15.7 ± 1 g for PBS vs 16.9 ± 0.8 for ADSC, $p < 0.05$) (figure 4.9). The difference became more evident from week 10 (15.8 ± 1.1 for PBS vs 17.3 ± 1 for ADSC, $p < 0.001$) and persisted until the end of the study at 12.5 weeks of age (16 ± 0.8 for PBS vs 17.5 ± 0.9 for ADSC, $p < 0.01$). Overall, on a 2-way ANOVA with Bonferroni's multiple comparison test ADSC treated mice were significantly heavier than PBS injected mice throughout the study ($p < 0.0001$).

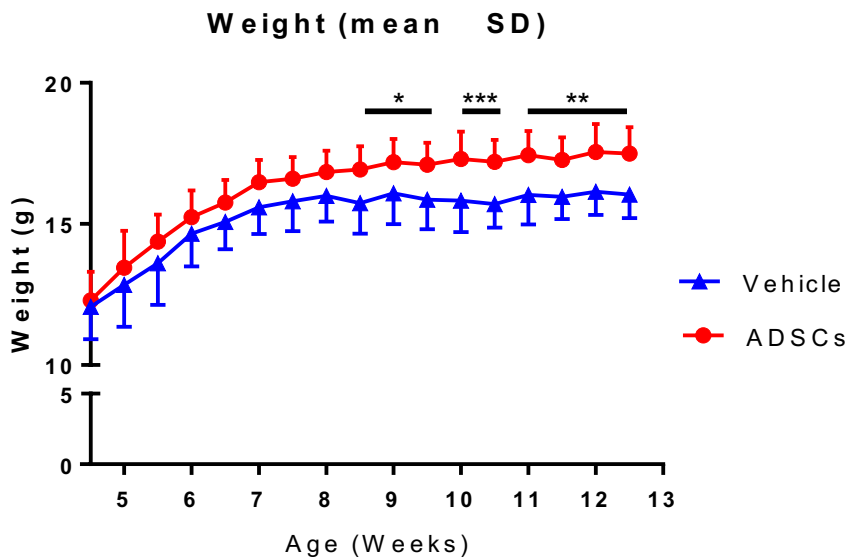
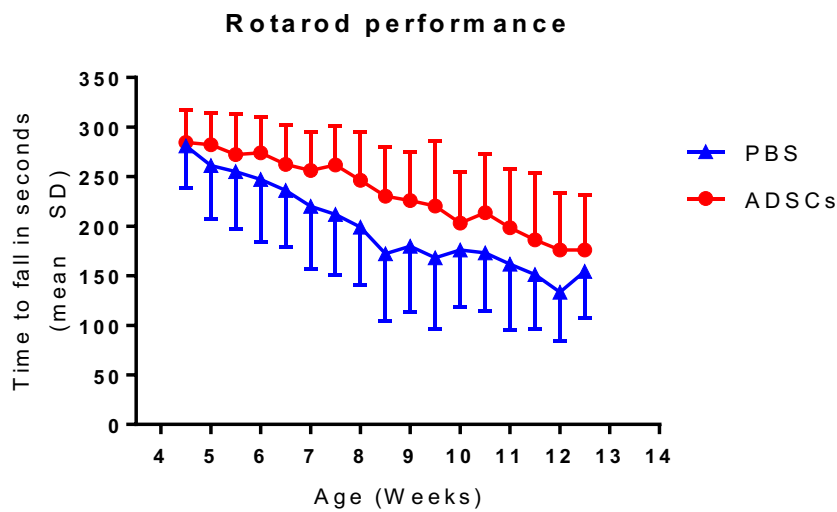


Figure 4.9. Effect of ADSC-transplantation on body weight. ADSC-treated mice ($n=15$) gained more weight compared to the vehicle ($n=15$) from week 8.5. * $p < 0.05$, ** $p < 0.01$, *** $p < 0.001$, 2-way ANOVA with Bonferroni's multiple comparison test. Data is plotted as mean \pm SD.

4.7 mADSCs delay motor performance decline in SOD1^{G93A} mice

Rotarod performance was assessed twice per week from the age of 33 days until the end of the study. SOD1^{G93A} mice showed motor function decline from the age of 35-40 days (figure 4.10 A). The motor performance decline was observed in both ADSC-treated and PBS-treated mice, however, ADSC-treated mice performed significantly better than PBS-injected mice throughout the study (overall treatment effect $p < 0.0397$, 2-way ANOVA with repeated measures) (figure 4.10 A). The improvement in motor performance observed in mice receiving ADSCs was confirmed by analysis of the area under curve (AUC) of the rotarod graph which showed that ADSC-injected mice had a significantly increased latency to fall compared to PBS-treated mice (1582 ± 84 for PBS vs 1870 ± 70 for ADSC, $p < 0.0001$, student's T-test with Welch's correction) (figure 4.10 B). The onset of pronounced motor performance decline, defined by a 20% drop in rotarod task from peak of performance, was delayed by 2.5 weeks (median 7 weeks for PBS vs 9.5 weeks for ADSC, $p = 0.0264$, Mann-Whitney U test) (figure 4.11). Statistical power analysis demonstrated that a group size of 14 mice per group were necessary to detect a 10-day difference in time taken to reach the 20% decline in rotarod performance. A retrospective power analysis of our data showed an achieved statistical power of 79%.

A



B

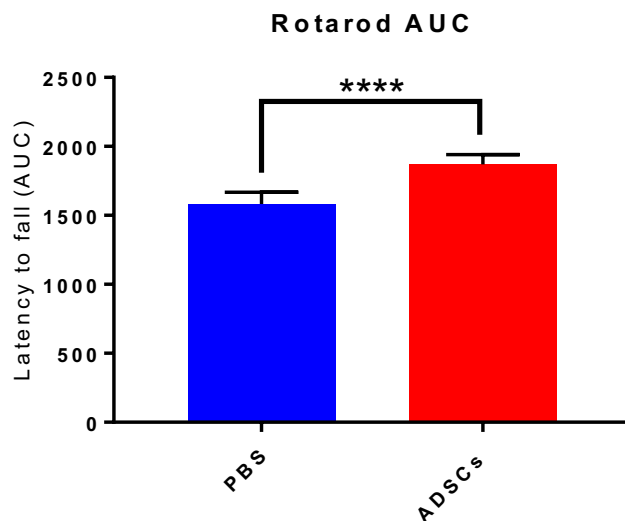


Figure 4.10. Effect of ADSC-transplantation on Rotarod performance. (A) Time to fall in seconds for ADSC-injected and PBS-injected mice. ADSC-treated mice (n=15) performed significantly better than PBS-treated mice (n=15) (overall treatment effect $p=0.0397$, 2-way ANOVA with repeated measures). (B) Area under the curve (AUC) of rotarod performance. ADSC-injected mice had a significant increase in latency to fall compared to the vehicle (1582 ± 84 for PBS vs 1870 ± 70 for ADSC, student's t-test with Welch's correction). **** $p<0.0001$. Values represent mean \pm SD.

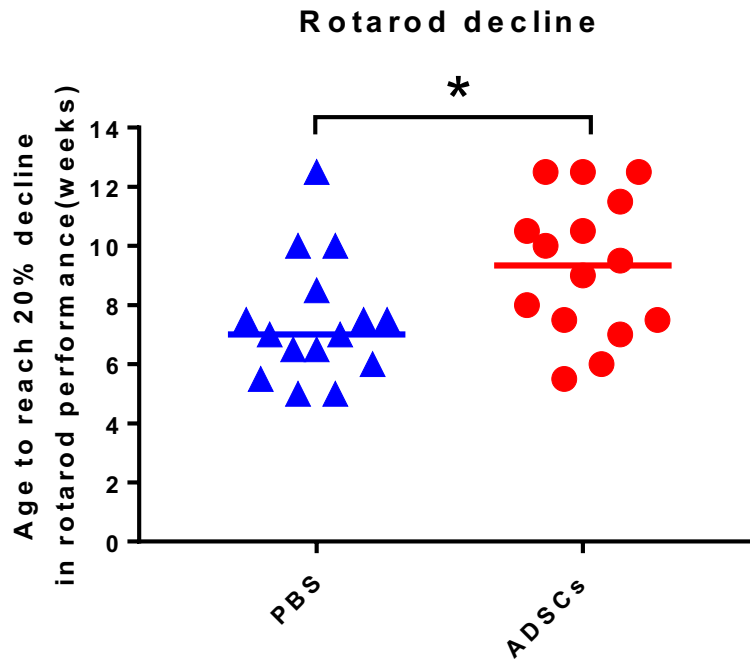


Figure 4.11. Effect of ADSC-transplantation on onset of motor function decline. The marked decline in rotarod performance in $SOD1^{G93A}$ mice (defined as a 20% drop from peak of performance) is visible from 35 days of age. The decline was significantly delayed in mice receiving ADSCs compared to control PBS-injected mice (median 7 weeks for PBS vs 9.5 weeks for ADSC). The horizontal lines indicate the group median. * $p < 0.05$, Mann-Whitney U test.

4.8 mADSCs improve gait parameters in $SOD1^{G93A}$ mice

Gait parameters were analysed at the age of 70 and 84 days in ADSC and PBS injected mice with the use of the catwalk system. The stride length, which is the distance between two consecutive steps of the same paw, did not significantly change from day 70 to day 84 in the two groups (figure 4.12 A and B). However, at day 70 ADSC-injected mice had a significantly longer stride length compared to the vehicle treated mice for both forelimbs ($p=0.0268$, 2-way ANOVA, figure 4.12 A) and hindlimbs ($p=0.0216$, figure 4.12 B). At day 84, the difference between the two groups did not reach statistical significance. The stand time, consisting in the duration of paw contact with the ground in a step cycle, was no different between the two groups at the two individual time points. However, on a 2-way ANOVA with repeated measures, ADSC-transplanted mice showed a significant decrease in forelimb ($p=0.0268$, figure 4.12 C) and hindlimb ($p=0.0374$, figure 4.12 D) stand time compared to the vehicle

group. The duty cycle is the percentage of time that the paw stands on the floor relative to the duration of the complete stride (figure 4.12 E and F). No differences over time were found in duty cycle in both groups. However, on a 2-way ANOVA with repeated measures, the forelimb duty cycle was significantly reduced in ADSC treated mice compared to the controls ($p=0.0253$, figure 4.12 E). No differences were found in the hindlimb duty cycle over time within the same group nor between the two groups (figure 4.12 F). The walking duration, representing the time that the mouse takes to cross the catwalk glass distance (43.8 cm) was similar between 70 and 84 days of age in both groups (figure 4.13 A). In ADSC-transplanted mice the walking duration at day 70, however, was significantly shorter compared to the mice injected with PBS ($p=0.0229$, figure 4.13 A). The percentage of time spent by the mice on diagonal support or three limbs support at day 70 and day 84 of age is reported in figure 4.13 B and C respectively. Surprisingly, the walking pattern of the PBS-treated mice showed a slight increase in the percentage of time spent on diagonal support and decreased percentage of time on three limbs support from day 70 to day 84 of age, however the difference did not reach statistical significance (figure 4.13 B and C). A non-statistically significant decrease in percentage of time with a three limb support walking pattern was also observed in ADSCs-treated mice (figure 4.13 C). On a 2-way ANOVA with repeated measures and Sidak's post-hoc test, ADSC-injected mice showed a significant increase in the percentage of time spent on diagonal paws compared to PBS-injected mice ($p=0.0327$, figure 4.13 B). Conversely, overall the ADSC treated group showed a decrease in percentage of time spent by walking with three limbs support compared to the vehicle group ($p=0.0178$, figure 4.13 C).

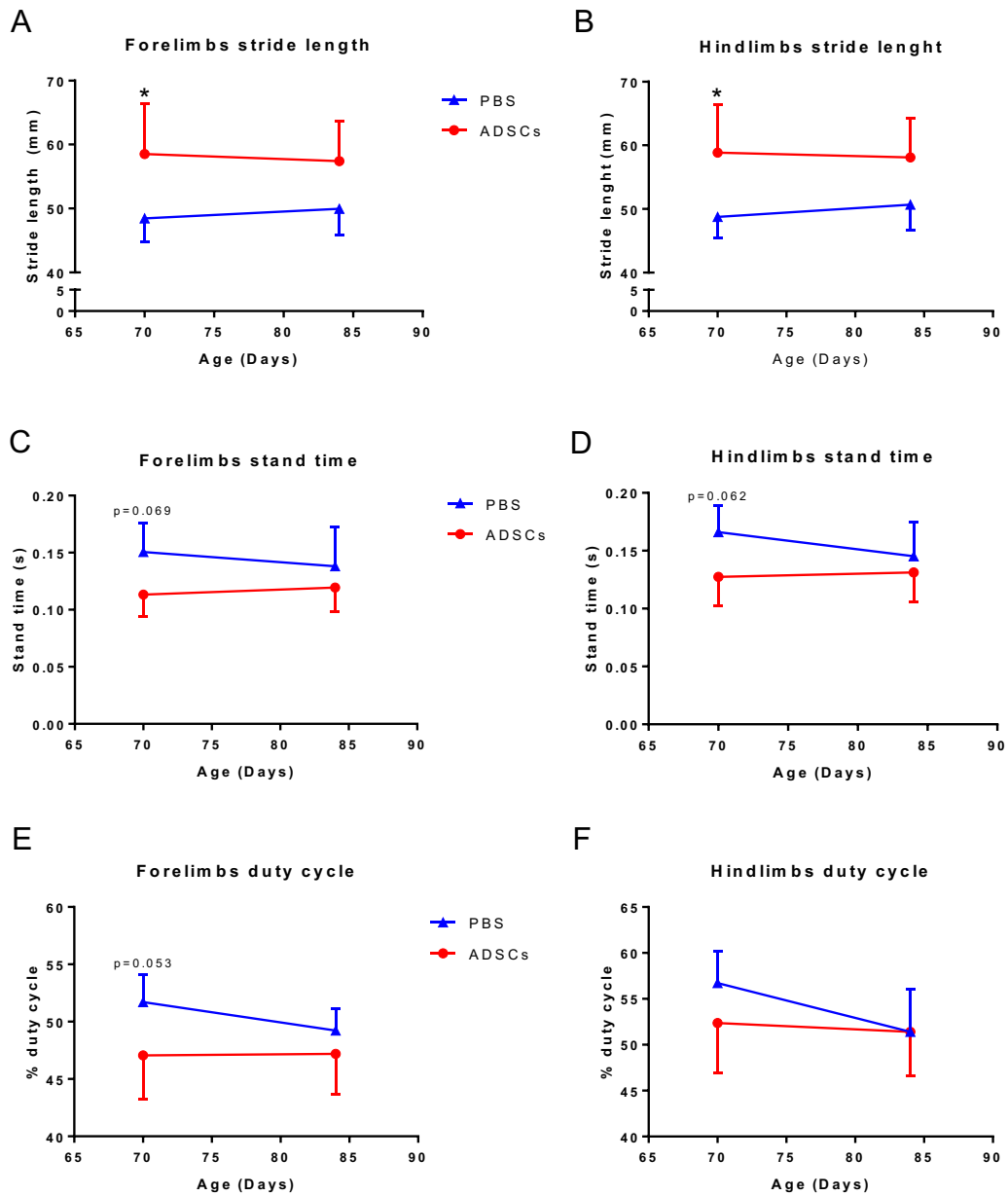


Figure 4.12. Effect of ADSC-transplantation on gait parameters: stride length, stand time and duty cycle. (A and B) Stride length is the distance between successive placements of the same paw. (C and D) Stand time is the duration of contact of a paw with the ground in a step cycle. (E and F) Duty cycle is the stand time expressed as percentage of the duration of the step cycle. Values represent mean \pm SD of the left and right paws for each mouse ($n=5$ /group). * $p < 0.05$, 2-way ANOVA with Sidak's multiple comparison test.

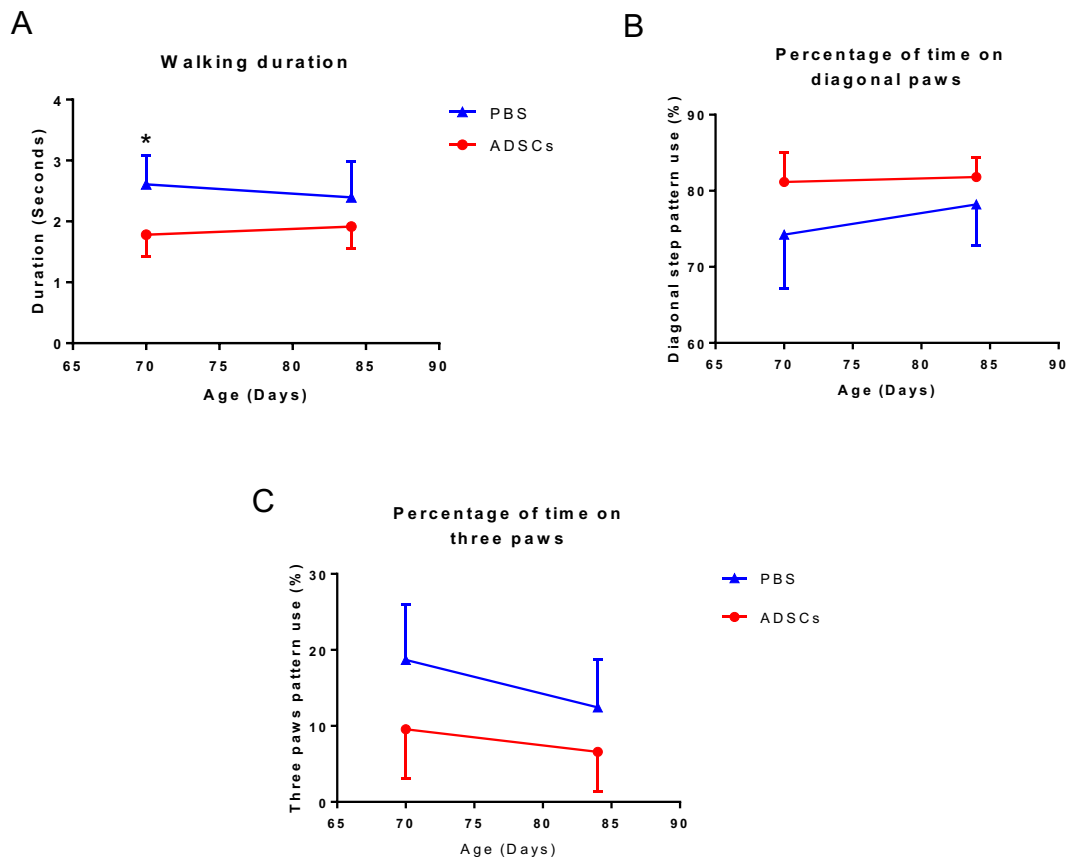


Figure 4.13. Effect of ADSC-transplantation on gait parameters: walking duration, percent of time spent on diagonal paws and percentage of time spent on three paws. (A) Walking duration is the time taken by the mouse to cross the catwalk glass distance. (B) Diagonal step pattern. (C) Three paws step pattern. Values represent mean \pm SD (n=5/group). *p<0.05, 2-way ANOVA with Sidak's multiple comparison test.

4.10 ADSCs increase MN survival in SOD1^{G93A} mice: Nissl staining results

At the end of the therapeutic study (90 days-old mice), spinal cord sections from the lumbar enlargement were stained with cresyl violet (Nissl staining) for motor neuron quantification. α -motor neurons were identified and counted in the spinal cord ventral horns based on the presence of Nissl bodies, a size of at least 25 μ m and the presence of a large nucleus with a detectable nucleolus. Motor neuron counts were performed blinded to the treatment group by the same investigator. In particular, about 96 spinal cord sections were screened for each mouse (n=6 per group).

In figure 4.15 A are representative histology images showing Nissl staining in lumbar spinal cord ventral horns where vacuolated MNs can be observed, a feature which is typical in SOD1^{G93A} mice after disease onset. A significant increase of ~20% in the number of motor neurons was found in lumbar spinal cord of mice that received ADSCs compared to mice receiving PBS injections (2.5 ± 0.2 MNs/ventral horn for PBS vs 3.1 ± 0.4 MNs/ventral horn for ADSC, $p=0.0086$, $n=6$ /group, figure 4.15 B). Thus, ADSC-injection resulted in reduced MN loss in SOD1^{G93A} mice.

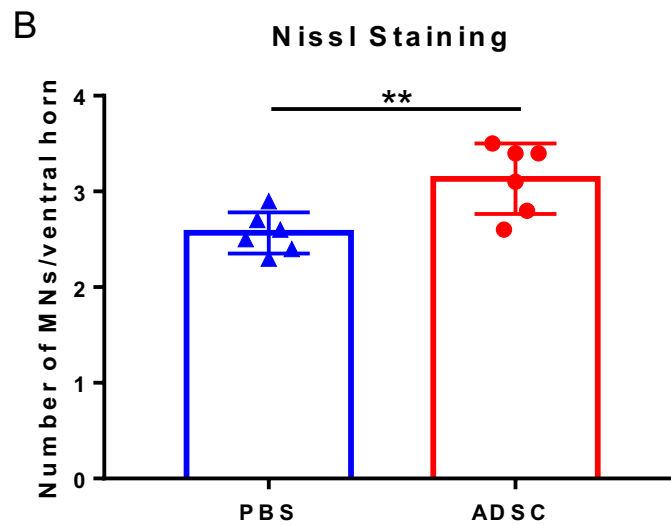
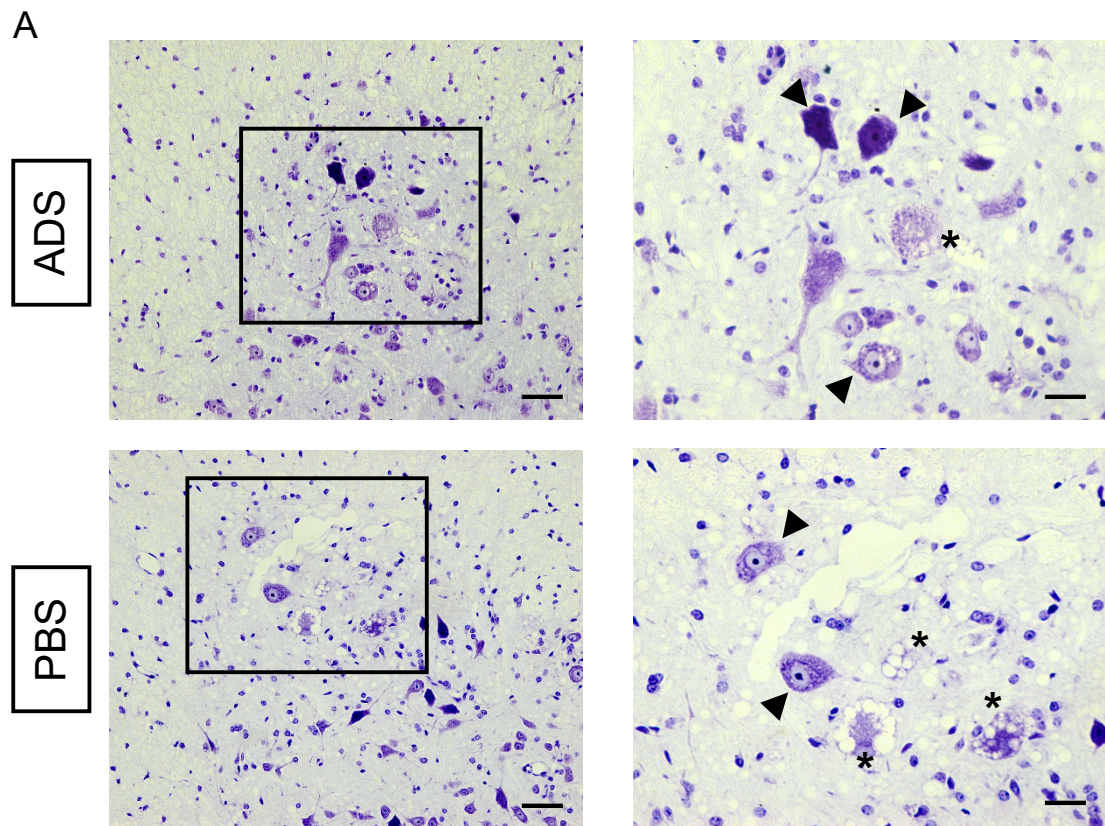
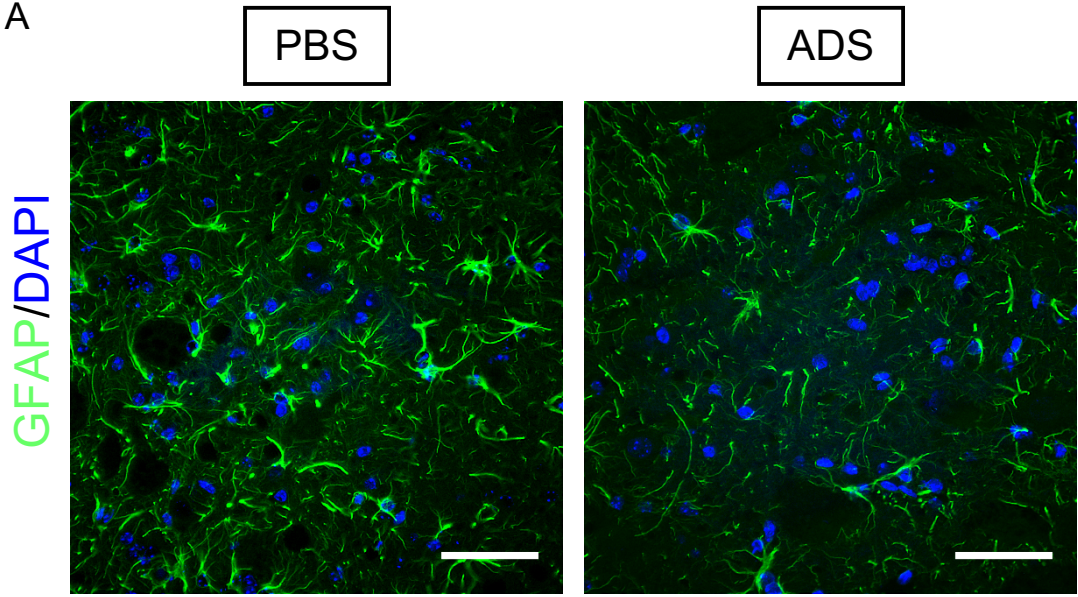


Figure 4.15. Effect of ADSC-transplantation on MN survival in $SOD1^{G93A}$ mice. (A) Representative images showing Nissl staining of the lumbar spinal cord of ADSC and PBS injected mice ($n=6/\text{group}$). The boxed areas are magnified on the right panel. MNs counted for quantification are indicated with an arrow head, while vacuolated dying or death MNs are marked with an asterisk. Scale bars: 50 μm left panel; 25 μm right panel. (B) Quantification of α -MN expressed as number of motor neurons per ventral horn section. Each value represents the average from ~ 192 ventral horn sections. Column values represent mean \pm SD. $**p<0.01$, unpaired Student's t-test.

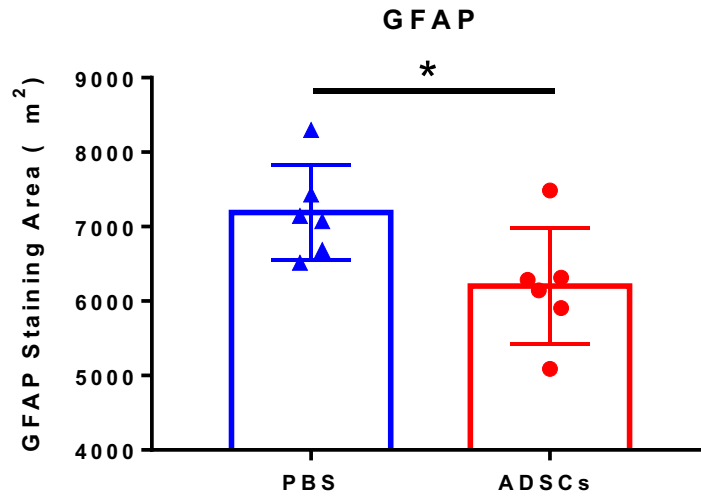
4.11 ADSCs reduce astrogliosis in SOD1^{G93A} mice: glial fibrillary acid protein (GFAP) staining results

At the age of 90 days, tissue was collected and lumbar spinal cord sections stained for GFAP. Immunoreactivity to GFAP is a commonly used staining method to evaluate astrogliosis. In particular, astrogliosis is documented by increased staining levels for GFAP in both area and intensity. Images of spinal cord ventral horns were taken at a magnification of 60x (figure 4.16 A). Astrocyte activation was reduced in ADSC-treated mice (n=6) compared to the vehicle treated mice (n=6) as shown by a significant reduction in the GFAP total staining area ($7,191 \pm 634 \mu\text{m}^2$ in PBS vs $6,203 \pm 774 \mu\text{m}^2$ in ADSC, $p=0.0363$, figure 4.16 B). Staining index (area X intensity) was also reduced in the ADSC group ($2.75 \times 10^6 \pm 0.73 \times 10^6$ in PBS vs $1.95 \times 10^6 \pm 0.5 \times 10^6$ in ADSC, $p=0.0515$, figure 4.16 C) although the difference did not reach statistical significance. Thus, ADSC treatment significantly reduced astrogliosis in SOD1^{G93A} mice.

A



B



C

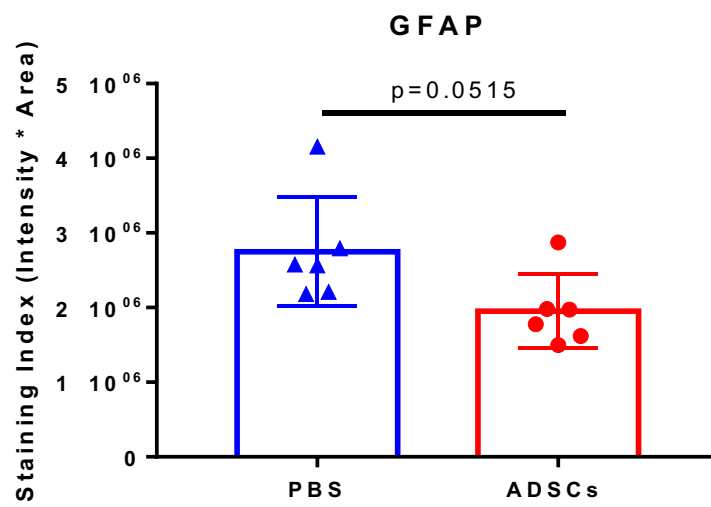


Figure 4.16. Effect of ADSC-transplantation on astrocyte activation in SOD1^{G93A} mice. (A) Representative images of GFAP staining on lumbar spinal cord sections of ADSC and PBS treated mice (n=6/group). Fluorescent images were captured with the IN Cell 2000 (GE) at a 60x magnification. Nuclei are stained with DAPI. Scale bar: 50 μ m. (B) Quantification of GFAP staining area showing reduced astrogliosis in ADSC-injected mice compared to the vehicle (p=0.0363). (C) Staining index (Area x Intensity) was reduced in ADSC-transplanted mice compared to the PBS group (p=0.0515). Each value represents the average from 16 ventral horns. Column values represent mean \pm SD. *p<0.05, unpaired Student's t-test.

4.12 ADSCs reduce microgliosis in SOD1^{G93A} mice: IBA-1 staining results

Lumbar spinal cord microgliosis was evaluated by immunostaining with the microglial marker IBA-1. In figure 4.17 A are representative images of IBA-1 staining in ADSC and PBS injected mice (n=6/group). IBA-1 total staining area was significantly reduced by about 30% in ADSC-transplanted mice compared to mice that received PBS (2921 ± 154 μm² in PBS vs 2075 ± 67 μm² in ADSC, p<0.0001, figure 4.17 B). In addition, clusters of hyperactivated microglia, often observed in PBS injected animals, were more rare in ADSC-transplanted mice.

The ramified (resting) to amoeboid (activated) morphology spectrum of microglia was evaluated by using a morphology metric (M-score) as described in the materials and methods chapter (paragraph 2.3.11). An M-score was given to each individual cell based on roundness and size, with a higher M value corresponding to a more “activated” phagocytic phenotype. The M score was then used to classify microglia into “ramified” and “amoeboid” by setting a threshold. In particular, cells with an M score < of 0.65 were classified as ramified, while cells with an M score > 0.65 were considered amoeboid (figure 4.18 A). Interestingly, the relative percentage of “phagocytic” amoeboid microglia was slightly decreased in ADSC injected mice compared to the vehicle (27.5% ± 5.1% in PBS vs 22.1% ± 1.9% in ADSCs, p=0.0359, figure 4.18 B).

Taken together, these data demonstrated that intrathecal injection of ADSCs significantly attenuated microgliosis in SOD1^{G93A} mice.

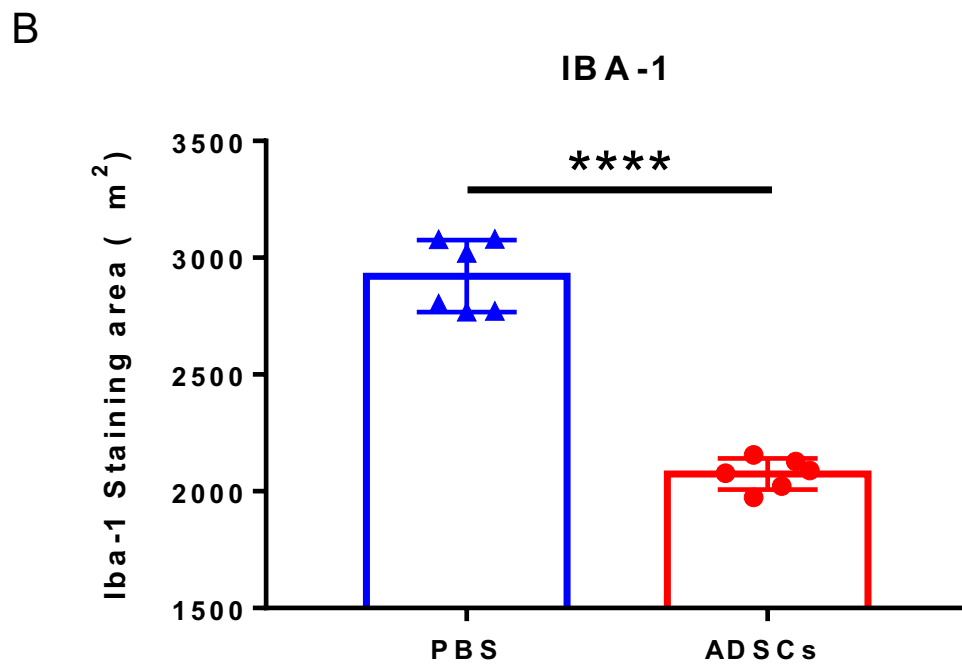
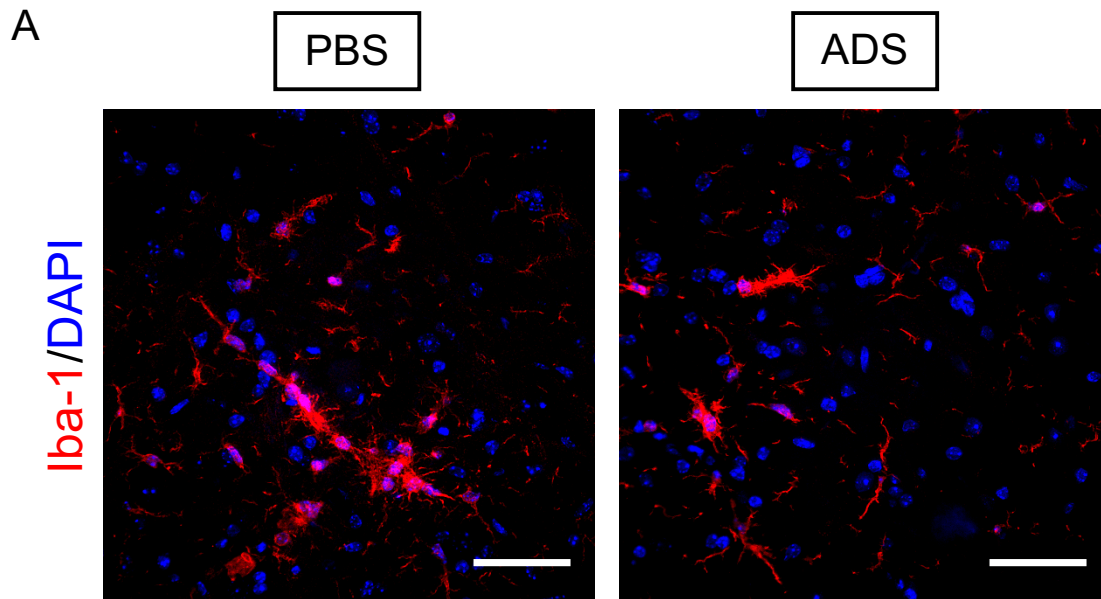


Figure 4.17. Effect of ADSC-transplantation on microgliosis in SOD1^{G93A} mice. (A) Representative images of IBA-1 staining of lumbar spinal cord of ADSC and PBS treated mice (n=6/group). Fluorescent images were captured with the IN Cell 2000 (GE) at 60x magnification. Nuclei are counterstained with DAPI. Scale bar: 50 µm. (B) Quantification of IBA-1 total staining area showing significantly reduced microgliosis in ADSC-injected mice compared to the vehicle (p<0.0001). Each value represents the average from 16 ventral horns. Column values represent mean ± SD. ****p<0.0001, unpaired Student's t-test.

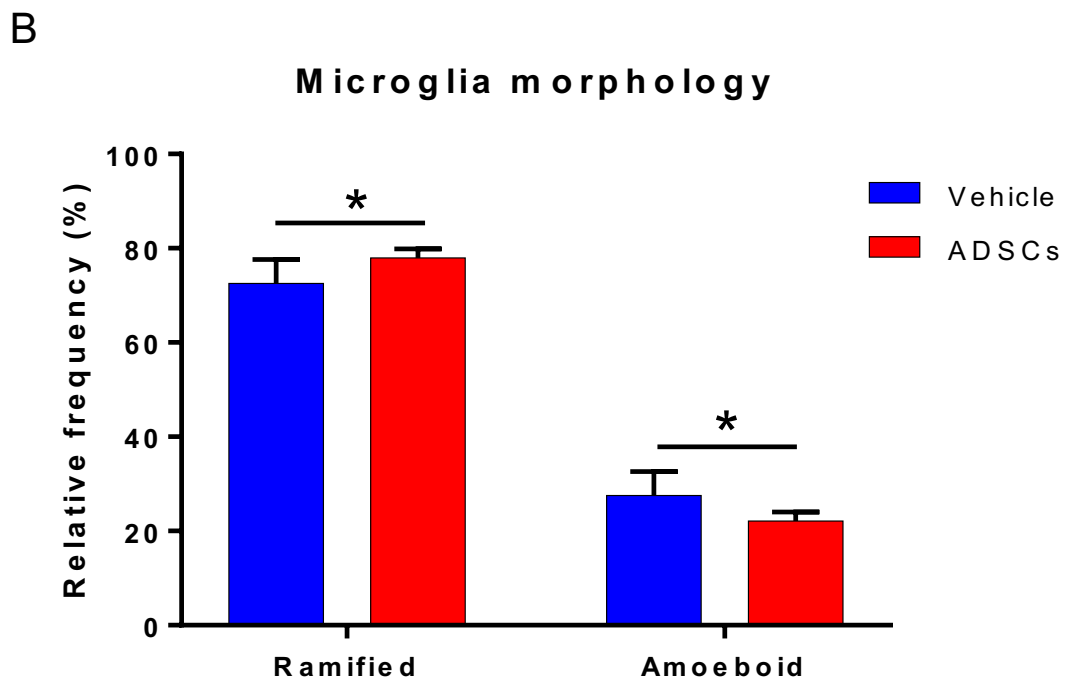
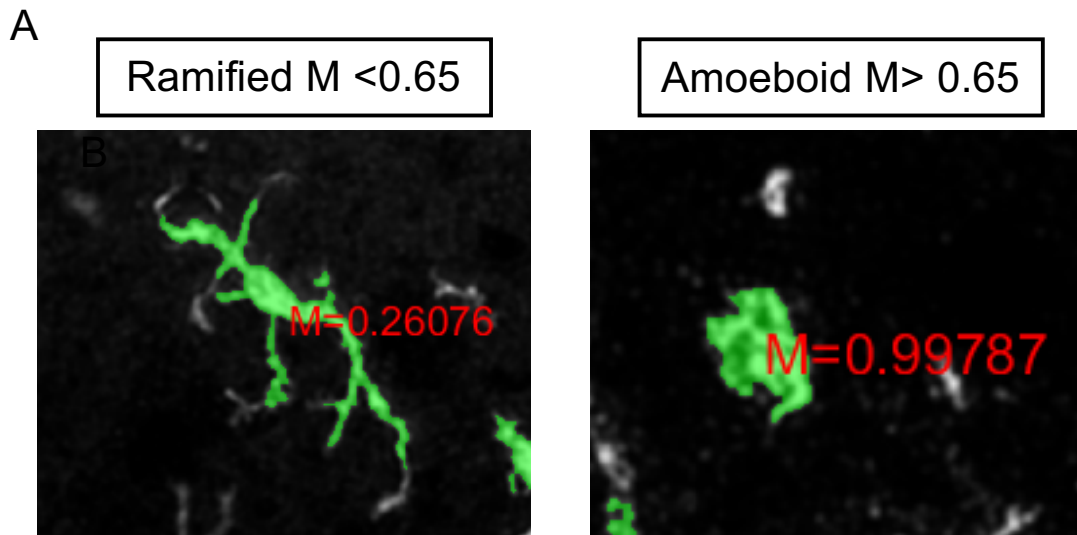


Figure 4.18. Effect of ADSC-transplantation on microglial morphology in SOD1^{G93A} mice. (A) Representative images of IBA-1 positive microglia selected for morphology analysis with the corresponding M score. Cells with an M score < of 0.65 were considered ramified, while cells with an M score > of 0.65 were considered amoeboid. (B) Relative frequency of ramified vs amoeboid microglia in PBS (vehicle) and ADSC injected mice, showing a shift from amoeboid to ramified cell morphology in ADSC transplanted mice. Column values represent mean \pm SD (n=6/group). *p<0.05, unpaired Student's t-test.

4.13 Gene expression analysis in spinal cord tissue: qPCR results

Total RNA was extracted from the lower half of spinal cord from SOD1^{G93A} mice receiving ADSCs (n=7) or PBS (n=7) injections and cDNA synthesised for gene expression analysis by qPCR. For each gene analysed, primer pairs were validated and optimized and primer efficiency assessed. To evaluate whether ADSCs could affect gene expression in the spinal cord of SOD1^{G93A} mice, the levels of expression of inflammatory cytokines/chemokines and growth factors were compared between the two groups (figure 4.19 and 4.20).

Expression of TNF- α was significantly reduced in ADSC-treated mice compared to the vehicle ($p=0.0212$, figure 4.19). Expression levels of IL-6 and TGF- β were also slightly reduced although the difference was not statistically significant (2-way ANOVA, figure 4.19). IL-1 β and MCP-1 expression levels were not affected by ADSC treatment (figure 4.19).

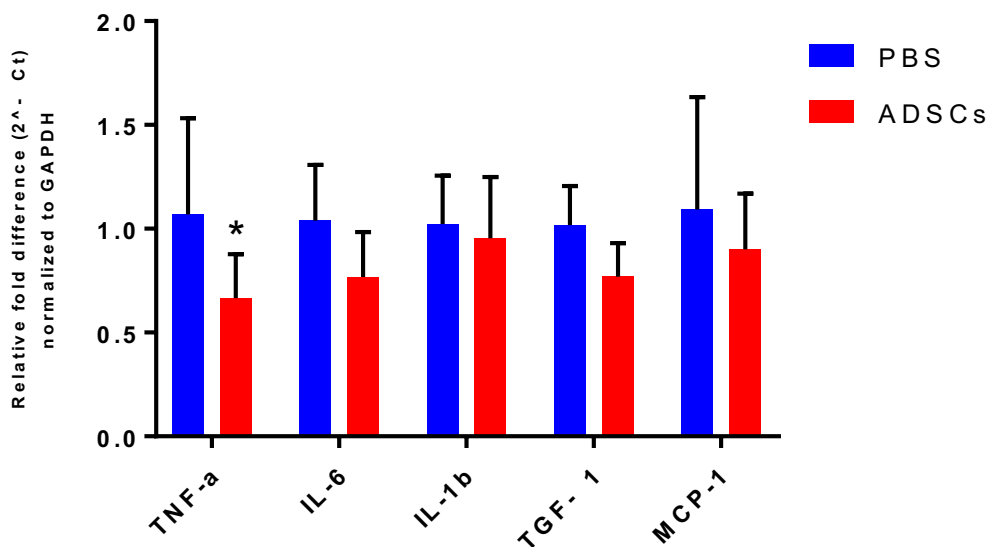


Figure 4.19. Gene expression of inflammatory cytokines/chemokines in spinal cord of SOD1^{G93A} mice. cDNA was obtained from total RNA extracted from the lower half of spinal cords of ADSCs-injected (n=7) and PBS-injected (n=7) mice at 90 days of age. Gene expression was evaluated by qPCR with the double delta Ct method ($\Delta\Delta Ct$) relative to GAPDH. Column values represent mean \pm SD. * $p<0.05$, 2-way ANOVA with Sidak's multiple comparisons.

Analysis of growth factors did not show any significant difference between the two groups on a 2-way ANOVA (figure 4.20).

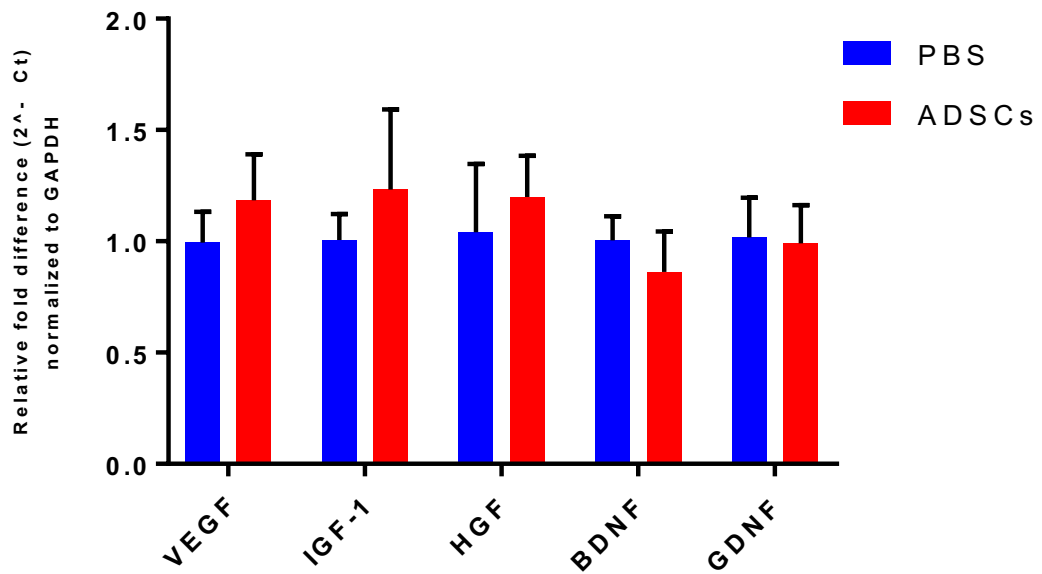


Figure 4.20. Gene expression of growth factors in spinal cord of SOD1^{G93A} mice. cDNA was obtained from total RNA extracted from the lower half of spinal cords of ADSCs-injected (n=7) and PBS-injected (n=7) mice at 90 days of age. Gene expression was evaluated by qPCR with the double delta Ct method ($\Delta\Delta Ct$) relative to GAPDH. Column values represent mean \pm SD. 2-way ANOVA with Sidak's multiple comparisons.

4.14 Discussion

The first aim of the work described in this chapter was to assess whether intrathecal transplantation of GFP-mADSCs into pre-symptomatic SOD1^{G93A} mice via cisterna magna injection was safe and would allow engraftment and wide distribution of cells throughout the CNS. First, the optimal cell dosage was defined and histology studies performed to evaluate stem cell survival over time. The second aim of the study focused on the effect of mADSC transplantation into pre-symptomatic SOD1^{G93A} mice as a proof of concept for their therapeutic potential. Following stem cell transplantation, behavioural and pathological studies were carried out.

4.14.1 Optimization of the cell number to inject in SOD1^{G93A} mice

A critical aspect and major challenge in stem cell therapy is the identification of the optimal cell dose to be transplanted. If on one hand the administration of a large amount of cells could result in enhanced benefits, on the other hand it is fundamental to determine a safe cell dosage. For instance, different cell doses have been previously tested in pre-clinical studies investigating the therapeutic potential of MSCs in animal models of ALS. The cell dosage was mainly determined based on the delivery route and the size of the animal. In ALS mouse models, the injection doses ranged from a minimum of 1×10^4 to a maximum of 1×10^6 MSCs when cells were injected intrathecally (Habisch et al., 2007, Kim et al., 2010, Boido et al., 2014). However, application of low cell dosages (1×10^4 , 1×10^5 and 2×10^5 cells/mouse) resulted in limited or no therapeutic effects (Habisch et al., 2007). On the contrary with a high cell dosage (1×10^6 cells) enhanced therapeutic effects were described (Kim et al., 2010). Based on these previous data, the dosage of 1×10^6 ADSCs was initially chosen. However, most of the cells aggregated in the IV ventricle, thus limiting cell distribution and consequently very few cells reached the lumbar enlargement of the spinal cord. Moreover, morphological changes in the structures of the brain ventricles were observed, probably due to CSF flow blockage. For these reasons, a pilot study aimed to determine the maximum transplantable number of ADSCs was performed by injecting increasing numbers of ADSCs (3×10^5 , 5×10^5 and 1×10^6) and evaluating tolerability of the transplant and cell distribution 1 week after injection. Even though hydrocephalus was not observed in mice transplanted with 1×10^6 cells after 1 week from injection, histology on whole CNS showed that most of the transplanted cells formed a clump in the IV ventricle, resulting in brainstem malformation and limited distribution of cells along the spinal cord. On the contrary, the injection of 5×10^5 GFP-mADSCs appeared to be a reasonable cell dosage.

Indeed, good cell distribution from the brain ventricular system to the lumbar region of the spinal cord was observed, and structural changes in the IV ventricle were not observed. Based on these data, the 5×10^5 cell dosage was finally chosen to test for the therapeutic potential of mADSCs.

4.14.2 Engraftment and distribution of GFP-ADSCs in SOD1^{G93A} mice

During the therapeutic study, groups of mice were sacrificed to investigate the engraftment, distribution and survival of the transplanted GFP-mADSCs. This is the first study in which the distribution and fate of transplanted mADSCs following a single intrathecal injection was evaluated over time at one week intervals in an animal model of ALS. However, a limitation of the study is that only a qualitative evaluation was performed. This was due to the difficulty in quantifying the cells given their aggregation into tight clusters. Notably, a large number of GFP-mADSCs were found to engraft and survive within the ventricular system of SOD1^{G93A} mice for up to 4 weeks after being transplanted into the cisterna magna. Moreover, injection via the cisterna magna allowed the cells to widely distribute within the brain ventricular system and to travel down to the spinal cord at the lumbar level, where lower motor neurons are degenerating.

Achieving a widespread distribution of transplanted cells is particularly important in ALS since the disease is characterized by a widespread neuronal degeneration in various areas of the CNS. Interestingly, the presence of GFP-mADSCs in the IV ventricle after transplantation suggests that cell distribution might initially depend on the fluid pressure during the injection rather than gravitational effects or homing capacity, as already indicated in the literature (Janowski et al., 2008). Also, cells were not found in the III ventricle or lateral ventricles at any time point, meaning that after injection the distribution of transplanted cells was dependent on CSF flow. Two weeks after transplantation, homing of GFP-mADSCs to both ventral and dorsal spinal roots in the lumbar enlargement was observed. However, it is difficult to determine whether this was due to a specific homing response to chemical stimuli or because of limited physical room in the subarachnoid space around the spinal cord at both the dorsal and the ventral surfaces.

As described in the literature, one limitation of intrathecal transplantation is that MSCs are not able to penetrate the spinal cord meninges or migrate into the brain parenchyma (Habisch et al., 2007, Forostyak et al., 2014). Some authors reported the ability of human MSCs to penetrate the spinal cord meninges from the subarachnoid space. However, a very low number of cells was detected in the grey

and white matter of the spinal cord, showing their inability to differentiate into neuronal or glial cells (Kim et al., 2010, Kim et al., 2014b, Boido et al., 2014). The inefficiency of injected human MSCs to migrate, survive and differentiate in ALS mice in those studies might be attributed to species-specific incompatibility. For example, the injection of rat BM-MSCs into the CSF of symptomatic (day 90) SOD1^{G93A} rats resulted in a considerable migration of the transplanted cells into the spinal cord parenchyma (Boucherie et al., 2009). Moreover, the cells found in the grey matter showed substantial differentiation into astrocytes (Boucherie et al., 2009). In our study, GFP-mADSCs were not detected within the spinal cord parenchyma at any time point after transplantation. A possible reason which could explain the discrepancy with the Boucherie findings is that in our study GFP-mADSCs were injected at a pre-symptomatic stage (day 30). At this age, inflammatory chemical signals such as chemokines and cytokines necessary to activate or induce the homing properties of ADSCs might not yet have been secreted at biologically relevant concentrations (Noh et al., 2014). At a later stage of disease, a sustained inflammatory milieu may allow MSCs to enter the parenchyma directly through the pia mater (composed of pial cells and subpial connective tissue) which in non-inflammatory conditions could reach a thickness of 250 µm in the lumbar spinal cord (Kayalioglu, 2009). This impermeable wall would be very difficult to penetrate without active CNS inflammation characterized by production of metalloproteases by immune cells (Wilson et al., 2010). Moreover, once the transplanted cells would have crossed the meninges, a potential way for the cells to migrate into the spinal cord parenchyma may be represented by the perivascular space (Virchow-Robin space), which is in continuity with the subarachnoid space (Wilson et al., 2010, Lam et al., 2017). In the perivascular space, the high concentration of the chemokine CXCL10 secreted by limiting astrocytes in non-inflammatory conditions might further limit the migration of the cells into the parenchyma (Wilson et al., 2010). In addition, the expression of adhesion molecules such as ICAM1, VCAM1 and PECAM1 on the surface of endothelial cells of meningeal vessels, necessary for cell diapedesis, are increased only during CNS inflammation (Wilson et al., 2010). At the same time, the possibility cannot be excluded that intrinsic biological characteristics and different homing capacities of ADSCs compared to BM-MSCs, could limit their ability to penetrate the spinal cord meninges from the CSF in the context of ALS (Elahi et al., 2016). This hypothesis may be supported by the fact that following intrathecal stem cell transplantation into ALS murine models, the degree of engraftment, survival and distribution of MSCs was reported to vary depending on the source and characteristics of the cells (Habisch et al., 2007, Sironi et al., 2017). In particular, a

greater survival capacity of BM-MSCs over UC-MSCs in SOD1^{G93A} mice following intrathecal injection is described in the literature (Habisch et al., 2007, Sironi et al., 2017).

4.14.3 Effect of ADSC injection on body weight

Body weight is a simple and objective parameter to be monitored in the transgenic SOD1^{G93A} mouse model. Weight loss in ALS is observed in both humans and mice and it is a sign of motor neuron loss with resultant muscle atrophy during disease progression (Oliván et al., 2015). ADSC injected mice gained significantly more weight compared to saline injected mice, and the difference persisted for the entire duration of the study. Although the study terminated before weight loss is typically observed in SOD1^{G93A} mice, transgenic mice are generally lighter than control non-transgenic mice even before the evidence of clinical signs of disease in our congenic C57Bl6 SOD1^{G93A} mice and in other SOD1^{G93A} mouse models (Miana-Mena et al., 2005). Since food intake was not monitored, it is difficult to address whether the difference in body weight was due to increase in food intake or changes in metabolic activity. Interestingly, to the best of our best knowledge this is the first time that intrathecal injection of MSCs resulted in an increase in body weight in a murine model of ALS.

4.14.4 Effect of ADSC injection on the rotarod task

The accelerating rotarod test is a method widely used to objectively assess motor performance in mice. It provides a relatively rapid estimation of neuromuscular coordination, balance, grip strength, stamina and endurance. In transgenic SOD1^{G93A} ALS mice on the defined C57Bl6/J genetic background, deficit in motor performance can be detected as early as 40 days of age, before other clinical signs of disease become evident (Mead et al., 2013). This initial deficit can be measured as a 20% drop in rotarod task from peak of performance, which correlates with early denervation of fast-fatigable muscle fibres (Mead et al., 2011). In this study, the age when the motor performance decline was observed in PBS-injected mice (vehicle) was similar compared to previous studies, in which the decline was observed at around 7 weeks of age (Mead et al., 2011, Mead et al., 2013).

ADSC transplantation significantly delayed the motor performance decline by about 2.5 weeks. Moreover, ADSC treated mice performed better in the rotarod task throughout the study when compared to the vehicle group. It has been previously shown that intrathecal injection of human BM-MSCs into pre-symptomatic ALS mice slowed down the decline in rotarod performance (Kim et al., 2010, Zhou et al., 2013).

Improvements in motor performance were also observed in ALS mice that received human ADSCs through intra-cerebroventricular injection (Kim et al., 2014b). Thus, the data generated in this study agree with previous findings, confirming that MSCs (either from BM or adipose tissue) are able to delay motor performance decline in SOD1^{G93A} mice when delivered intrathecally before the evidence of clinical signs of disease.

4.14.5 Effect of ADSC injection on gait parameters

Analysis of gait parameters by using the catwalk system has been previously performed in the congenic SOD1^{G93A} mouse model of ALS for the detection of early signs of disease (Mead et al., 2011) and to test for pharmaceutical intervention (Mead et al., 2013). Decreased stride length, increased stand time, increased duty cycle, decreased percentage of time walking with diagonal support and increased percentage of time on three limbs support are some of the changes which are characteristic of SOD1^{G93A} mice compared to NTg control mice (Mead et al., 2011). Historical data show that significant differences in some gait parameters between SOD1^{G93A} mice and NTg mice can be detected from the age of 70 days, while the majority of changes are detected after the appearance of clinical signs of disease. For this reason, analysis of gait parameters using the Catwalk system was assessed at the age of 70 days and 85 days. To note, this is the first time that the catwalk system was used to investigate changes in gait analysis in an ALS mouse model following transplantation of MSCs.

Differences in stride length

In SOD1^{G93A} mice, reduced stride length in both forelimbs and hindlimbs is usually observed from 77 days of age onward (Mead et al., 2011). Indeed, while in NTg mice stride length slightly increases with age, in SOD1^{G93A} mice it starts declining from the age of 70 days. Surprisingly, the increase in stride length from day 70 to day 84 of age was not observed in the vehicle group. However, ADSC-transplanted mice had a significant longer stride length in both forelimbs and hindlimbs compared to the vehicle treated mice at day 70. The difference was still present at the age of 84 days although not statistically significant. The reason for a decreased stride length in SOD1^{G93A} is motor system degeneration. Therefore, the increased stride length observed in ADSC-injected mice may be due to enhanced muscle strength in both forelimbs and hindlimbs compared to the saline-injected group.

Differences in stand time and duty cycle

Stand time and duty cycle are two strictly correlated parameters which were found to be affected in SOD1^{G93A} mice compared to NTg controls (Mead et al., 2011). Stand time is the duration of the stance phase for a particular paw during a step cycle and it is found to be slightly increased in SOD1^{G93A} mice from the age of 63 days (Mead et al., 2011). Compared to the vehicle group, a marginal (non-statistically significant) decrease in both hindlimb and forelimb stand time was observed in ADSC treated mice at 70 days. However, this trend was lost at the age of 84 days. Duty cycle represents the stance as a percentage of the duration of the complete step cycle. In the ADSC group, for both forelimbs and hindlimbs, the duty cycle was slightly (non-statistically significant) decreased at day 70 compared to the vehicle, but no difference was found at day 80. For instance, a decrease in stand time and duty cycle could reflect the enhanced ability of the mouse to start the movement of the limb off the ground to initiate the successive step.

Differences in walking speed and gait pattern

Walking duration is the time the mouse takes to cross the entire catwalk system and it is an indirect measure of the walking speed. The walking duration did not change between 70 and 84 days of age in either ADSC or PBS injected mice. However, at day 70, ADSC-transplanted mice were significantly faster than the PBS-injected controls. This may be related to enhanced muscle strength and motivation to move. The diagonal limb support is the most used walking step pattern in healthy mice (Bernardes and Oliveira, 2017). However, given the development of impairment in gait stability, ALS mice progressively spend less time on diagonal limbs. This reduction in diagonal step pattern observed in SOD1^{G93A} mice is compensated by an increase in the use of three limbs to support themselves. Although a decrease in time spent on diagonal support with a concomitant increase of time spent on three limbs was not observed over time in the two groups, overall, ADSC-injected mice showed an increase in diagonal stepping compared to vehicle mice. As a consequence, ADSC mice spent less time supporting themselves on three limbs during the stepping pattern. These results suggest that ADSC transplantation increased motor strength and stability in SOD1^{G93A} mice.

4.14.6 Effect of ADSCs on disease onset

Evaluation of neurologic deficits in SOD1^{G93A} mice was performed by following criteria used in previous studies (Mead et al., 2011, Bennett et al., 2014). To detect clinical signs of disease mice were scored every three days from 60 days of age. As

expected for this model, clinical symptoms of disease appeared after the documented deficit in motor performance (Mead et al., 2011). This was also seen in the SOD1^{G93A} mice on the mixed B6SJL genetic background in which running wheel performance started to decline 3 weeks before the evidence of clinical signs of disease (Bruestle et al., 2009). However, in other studies motor performance decline did not precede the appearance of clinical signs of disease (Kim et al., 2010, Kim et al., 2014b). To note, in human patients decline in motor performance is often found before the diagnosis of ALS is established (Bruestle et al., 2009). In this study, intrathecal injection of ADSCs significantly delayed disease onset by 5 days in SOD1^{G93A} mice. Interestingly, Kim et al., reported that transplantation of human ADSCs but not human BM-MSCs into the CSF of pre-symptomatic mice, delayed the appearance of clinical signs of disease (Kim et al., 2010, Kim et al., 2014b). However, later onset (6 days) in ALS mice that received intrathecal injection of human BM-MSCs was also reported from a different group (Zhou et al., 2013). It is difficult to ascertain whether in the report by Kim et al (2010) disease onset was not affected by the treatment because of the intrinsic characteristics of the isolated MSCs or because of biological noise.

4.14.7 Effect of mADSCs on MN loss

ALS is characterized by the selective death of spinal cord motor neurons, a feature which is replicated in rodent models of the disease. SOD1^{G93A} mice are characterized by an initial loss of motor neurons in the pre-symptomatic stage, followed by a further gradual loss during disease progression (Feeney et al., 2001). Various approaches have been adopted in order to perform MN counting through histological techniques (Ferrucci et al., 2018). In this study, MNs were identified by cresyl violet staining. Cresyl violet is a basic organic compound that labels neuronal cells through staining of condensed granules of rough endoplasmic reticulum called Nissl bodies. Moreover, the sensitivity of the stain solution to basophilic substances allows the differentiation of cytoplasm, nucleus and nucleolus within a neuron (Alvarez-Buylla et al., 1990). α -motor neurons were identified following gold-standard features, which include topography (ventral horns), size ($\geq 25\mu\text{m}$) and appearance under histochemical observation (basophilic cytosol, large nucleus and identifiable nucleolus) (Ferrucci et al., 2018).

In this study, transplantation of mADSCs culminated in motor neuron protection as documented by a significant 20% increase in the number of MNs in treated mice compared to the vehicle. Preservation of motor neurons following MSC transplantation in ALS animal models has been previously documented in the

literature (Kim et al., 2010, Boucherie et al., 2009). Although the reduced MN loss may correlate with the improvements in motor performance here documented, care should be taken when interpreting motor neuron survival data by histological counts. For example, reduced motor neuron loss achieved through intrathecal transplantation of human umbilical cord MSCs into symptomatic SOD1^{G93A} mice was not sufficient to prevent muscle denervation and delay disease progression (Sironi et al., 2017).

4.14.8 Effect of ADSCs on astrogliosis

Astrocyte activation is a hallmark of disease progression in ALS (Ferraiuolo et al., 2011). GFAP is one of the most used markers to evaluate astrogliosis in the injured CNS (Keller et al., 2009). In particular, higher levels of GFAP expression are observed as astrogliosis increases in both humans and animal models of the disease (Fujita et al., 1998, Yamanaka et al., 2008b). In ALS, astroglial reactivity appears to be enhanced in the ventral horn of the lumbar spinal cord in proximity to degenerating α -motor neurons (Schiffer et al., 1996). Thus, immunohistochemical analysis of GFAP was performed on spinal cord ventral horn areas with limitation to the grey matter. In line with previous studies where MSCs were injected into ALS or spinal cord injury animal models, transplantation of ADSCs resulted in significant attenuation of astrocyte activation in spinal cord ventral horns (Boido et al., 2014, Wang et al., 2018a). This was documented by a decrease in both GFAP total staining area and staining index in ADSC recipient mice, suggesting a reduction in the number of activated astrocytes and in the degree of activation respectively. Since astrogliosis is thought to be mostly driven by activation of pre-existing resident astrocytes, which start displaying morphological changes and alterations in the expression of specific markers (i.e. downregulation of GLT-1), it is likely that ADSCs directly affected astrocyte activation rather than inhibiting proliferation (Philips and Rothstein, 2014, Wang et al., 2018a). This hypothesis is supported by the ability of MSCs to down-regulate the expression of inflammatory cytokines while up-regulating the expression of growth factors and the expression of the glutamate transporter 1 (GLT-1) both *in vitro* and *in vivo* models of ALS (Gu et al., 2010, Uccelli et al., 2012, Sun et al., 2013). Moreover, even though *in vivo* proliferation of astrocytes has been documented in neurodegenerative and neuroinflammation models, this was reported to be very modest in ALS (Liddel and Barres, 2017).

4.14.9 Effects of ADSCs on microgliosis

Microgliosis is a well documented feature in ALS and it intensifies during disease progression (Geloso et al., 2017). In the spinal cord of ALS animal models, it has

been shown that resident microglia increase in number and switch from a neuroprotective state (M2) to an alternative toxic state (M1) during disease progression (Boillée et al., 2006). The M1 microglia activation state exerting neurotoxic effects can be documented by increased secretion levels of pro-inflammatory cytokines (Saijo and Glass, 2011), changes in morphology (from classical “ramified” to “amoeboid”) (Sampson et al., 2016) and cell proliferation (Geloso et al., 2017). In this study, microgliosis was evaluated and semi-quantified through immunohistochemistry on the lumbar spinal cord using the microglia marker IBA-1 (Korzhevskii and Kirik, 2016). Since IBA-1 intensity immunoreactivity does not change with microgliosis, the total staining area was quantified. Interestingly, in mice that received ADSCs the IBA-1 total staining area was significantly reduced compared to mice that received a saline injection, indicating reduced microgliosis. Moreover, mice injected with ADSCs showed a reduction in the percentage of amoeboid (activated) microglia compared to the vehicle group, accompanied by an increase in the percentage of cells presenting with a more ramified (resting) morphology. Inhibition of microgliosis in the spinal cord of SOD1^{G93A} mice following transplantation of MSCs, with consequent increased levels of anti-inflammatory cytokines (IL-10, IL-4 and TGF-β) and reduced levels of inflammatory mediators (TNF-α, IL-6 and IL-1β) has been previously shown by other groups (Zhou et al., 2013, Vercelli et al., 2008, Boido et al., 2014). Moreover, the capacity of MSCs to inhibit microgliosis has been described in *in vitro* models of ALS (Ooi et al., 2015, Noh et al., 2016, Sun et al., 2013). In particular, the capacity of MSCs to switch the detrimental M1 activated microglia state into the beneficial M2 activated state, appears to be mediated by paracrine mechanisms following exposure of MSCs to inflammatory molecules (Zhou et al., 2013). For instance, it has been shown that the release of CX3CL1, prostaglandin E₂ and TGF-β from MSCs, induced LPS-activated microglia to secrete increased levels of neuroprotective mediators such as IL-10, CD200, IGF-1 and MKP-1, while reducing the release of pro-inflammatory cytokines such as example TNF-α, IL-1β, IL-6 and iNOS (Giunti et al., 2012, Boido et al., 2014, Noh et al., 2016). In addition, the capacity of MSCs to inhibit microglial proliferation by modulation of the cell cycle dependent on TNF-α reduction has been reported (Jose et al., 2014).

4.14.10 Effect of ADSCs on cytokines and growth factor gene expression

As already mentioned, the paracrine influence of MSCs on microglia and astrocytes has been documented both *in vivo* and *in vitro* models of ALS (Boido et al., 2014, Sun et al., 2013). In particular, transplanted MSCs showed the ability to reduce expression of inflammatory mediators and increase expression of neurotrophic factors in the

spinal cord of ALS murine models (Boido et al., 2014, Kim et al., 2014b). In this study, gene expression analysis on spinal cords of SOD1^{G93A} mice did not reveal major changes in growth factor expression between the ADSC-injected and the saline-injected mice. However, a slight, non-statistically significant increase in the expression levels of VEGF and IGF-1 was observed in the ADSCs group. Interestingly, MSCs have been reported to show the ability to enhance the level of expression of VEGF and IGF-1 in astrocytes and microglia, resulting in anti-apoptotic effects and neuroprotection both *in vivo* and *in vitro* models of ALS (Marconi et al., 2013, Knippenberg et al., 2012a, Sun et al., 2013). Regarding expression of inflammatory mediators, a significant reduction in the expression of TNF- α and a trend towards the reduction of IL-6 and TGF- β 1 was observed in mice transplanted with ADSCs. Interestingly, enhanced expression levels of TNF- α , IL-6 and TGF- β 1 have been shown to positively correlate with disease progression in SOD1^{G93A} mice and to induce motor neuron death *in vitro* (Endo et al., 2015, Garbuzova-Davis et al., 2018, Tripathi et al., 2017, Kia et al., 2018).

Taken together, our gene expression data does not fully correlate with the literature, where substantial changes in gene expression following MSC transplantation were documented. One explanation might be related to the time of intervention and the age of the mice when the tissue was collected. For example, in Boido *et al.* gene expression analysis was performed at disease end-stage, which is characterized by high levels of inflammation and thus substantial expression of pro-inflammatory cytokines (Boido et al., 2014). In this study, tissue was collected at an early symptomatic stage in which expression of inflammatory mediators might not be at their highest expression levels yet (Noh et al., 2014). However, control wild-type NTg mice have not been included in the study to identify genes differentially expressed in SOD1^{G93A} mice at the symptomatic age of 90 days. Another reason may be that in previous studies changes in gene expression were documented only two or three weeks following stem cell transplantation, when MSCs were still present either in spinal cord tissue or subarachnoid space of mice (Boido et al., 2014, Kim et al., 2014b, Zhou et al., 2013). In this study, gene expression analysis was performed 2 months after transplantation of ADSCs. Since ADSCs did not migrate into the spinal cord parenchyma and did not survive for more than 4 weeks in the subarachnoid space, one could speculate that the modulation effects of MSCs reported in literature are the result of paracrine effects with short-term efficacy. On the one hand, the reduction in astrocyte activation documented by immunohistology could not have been sufficiently large to allow the detection of changes in gene expression for growth

factors by means of RT-qPCR. On the other hand, the reduction observed in TNF- α , IL-6 and TGF- β 1 expression may reflect the substantial reduction in microgliosis. It is noteworthy that microglia represent the main source of production for TNF- α during inflammation (Welser-Alves and Milner, 2013).

4.15 Conclusions

In conclusion, a single intrathecal dose of mouse ADSCs into SOD1^{G93A} mice at the pre-symptomatic stage was able to improve motor performance and gait parameters, and delay the appearance of the first clinical signs of disease. Pathological studies revealed an increase in MN numbers in the lumbar spinal cord, accompanied by reduced glial activation in ADSC-treated mice compared to those which received the vehicle. ADSCs were able to survive in the ventricular system and spinal cord subarachnoid space of mice up to 4 weeks post-transplantation, however, cells were not able to migrate into the brain or spinal cord parenchyma. Thus, it is highly likely that the beneficial effects observed are due to a transient paracrine activity of ADSCs, which culminate in motor neuron protection and reduced gliosis.

This study further validated the therapeutic potential of ADSCs in the SOD1^{G93A} mouse model of ALS. In particular, for the first time treatment with ADSCs showed the capacity to delay the early motor performance decline in SOD1^{G93A} mice on the defined C57Bl/6J genetic background. Since in this model the early detection of motor performance dysfunction is a direct consequence of the initial denervation of motor-end plates (Mead et al., 2011), we could speculate that through paracrine mechanisms ADSCs were able to directly support motor neurons during the very first stages of neuronal degeneration characterized by the loss of NMJ. However, further investigation using methods such as electrophysiology and immunohistochemistry to directly evaluate the histology and function of NMJ are needed to address this hypothesis.

Remarkably, a single intrathecal dose of ADSCs was able to reduce glial activation up to the early symptomatic stage at a distance of two months from injection. Since glial activation increases as disease progresses, further pre-clinical studies focused on the potential effect of ADSC transplantation on disease progression and survival would be of significant interest.

For the first time the engraftment of mouse ADSCs following intrathecal transplantation was evaluated over time, providing new insights on how these cells

distribute and survive within the cerebrospinal fluid of SOD1^{G93A} mice. Importantly, unlike most of the previous studies transplanting human MSCs in ALS rodents, here stem cell transplantation was performed without the use of immunosuppressive agents that could potentially affect both behavioral and pathology readouts.

5 The therapeutic potential of ADSCs on in vitro models of ALS

5.1 Introduction

As discussed in chapter 1, a growing body of evidence points to the involvement of astrocytes in ALS pathology. Astrocytes contribute to disease progression through both loss of homeostatic functions and secretion of neurotoxic factors (Yamanaka and Komine, 2018). For instance, astrocytes derived from SOD1^{G93A} mice are less supportive and/or toxic to healthy motor neurons *in vitro* (Di Giorgio et al., 2008, Ferraiuolo et al., 2011). In chapter 4, we showed that the beneficial effects observed in SOD1^{G93A} mice following ADSC transplantation are in part mediated by motor neuron protection and attenuation of astrocyte activation. Moreover, since the ADSCs were not able to migrate within the brain or spinal cord parenchyma, we hypothesize that those effects were mediated by paracrine mechanisms.

In this chapter we first wanted to test whether through release of soluble factors, ADSCs were able to protect MNs from SOD1^{G93A} astrocyte mediated toxicity. In order to evaluate the paracrine effects of ADSCs on astrocytes/MNs co-cultures we adopted a triple separated co-culture system in which ADSCs were physically separated from astrocytes/MNs but able to communicate through the exchange of soluble factors, thus in part mimicking the *in vivo* conditions.

It has been demonstrated that the toxic effects of ALS astrocytes is selective to MNs and may be in part mediated by the release of toxic mediators considering that conditioned medium from ALS astrocytes is sufficient to kill MNs (Ferraiuolo et al., 2011, Di Giorgio et al., 2008). Amongst several mediators identified as responsible for motor neuron damage both *in vivo* and *in vitro* models of ALS, there is evidence that reactive astrocytes actively contribute to inflammation-mediated neurotoxicity by releasing pro-inflammatory cytokines and chemokines (Philips and Robberecht, 2011, Farina et al., 2007, Schafer et al., 2012). It is also widely accepted that MSCs, and in particular ADSCs, possess anti-inflammatory and immunomodulatory

properties which culminate in neuroprotection (Shalaby et al., 2016, Marconi et al., 2013, Sironi et al., 2017). Most of the literature investigating the immunomodulatory properties of MSCs in ALS, focused on the modulation of microglia and peripheral immune cell functions rather than astrocytes (Ooi et al., 2015, Noh et al., 2016, Luz-Crawford et al., 2013, Kwon et al., 2014). Here, through separated co-culture experiments we investigated the immunomodulatory potential of ADSCs on mouse astrocytes derived from symptomatic SOD1^{G93A} mice and control non-transgenic (NTg) mice. The expression and secretion of cytokines and chemokines known to be secreted by astrocytes and relevant in ALS pathology were evaluated. Specifically we analyzed levels of IL-6, TNF- α , IL-1 β and MCP-1, for which high expression and/or concentrations were documented in both ALS murine models and in biological samples obtained from human ALS patient (Ono et al., 2001, Sekizawa et al., 1998, Ehrhart et al., 2015, Hu et al., 2017, van der Meer and Simon, 2010, Jeyachandran et al., 2015, Tortarolo et al., 2017).

Another mechanism by which ALS astrocytes contribute to either damage or reduced support to MNs in ALS is due to impairment in the synthesis and release of growth factors (Staats and Van Den Bosch, 2009). The production of growth factors from astrocytes is of extreme importance in supporting and regulating several activities in the nervous system. Growth factors directly affect neurons by increasing survival, promoting neurogenesis and regulating neuroplasticity (Henriques et al., 2010). Moreover, growth factors are important in potentiating the anti-oxidative response, preserving the BBB and participating in the repair and maintenance of the CNS following injury or disease (Cabezas et al., 2016). Altered levels of growth factors in SOD1^{G93A} mice and CSF, blood, muscle and brain of ALS patients have been reported (Ekester, 2004, Peters et al., 2017). In addition, strategies to enhance the levels of growth factors in SOD1^{G93A} rodents resulted in motor neuron protection, NMJ preservation and increased survival (Henriques et al., 2010). On the basis of a previous finding showing the ability of MSCs to modify the astrocytic secretome, we then asked whether ADSCs could modulate expression of growth factors in our SOD1^{G93A} and NTg astrocytic cultures following a separated co-culture assay (Sun et al., 2013).

In addition to modulation of astrocytic functions, one of the mechanisms by which ADSCs are thought to mediate neuroprotection in ALS models is through the direct release of a high concentration of several growth factors (Marconi et al., 2013, Kim et al., 2014b). Since MSCs previously showed the capacity to respond to inflammatory stimuli by modulating the expression of growth factors, we wanted to investigate

whether ADSCs could in turn be influenced by SOD1^{G93A} astrocytes in our *in vitro* model, by measuring levels of expression and secretion of growth factors known to be produced at high levels by ADSCs (Nicaise et al., 2011, Zachar et al., 2016, Chen et al., 2015a).

Although SOD1^{G93A} mice represent a robust and well characterized model of ALS, and primary cultures derived from these mice are widely used to study pathogenic mechanisms of disease, SOD1 mutations are responsible for only ~2% of human ALS cases, and unfortunately several promising therapeutic approaches tested in this model failed during translation into the clinic. Indeed, because of high heterogeneity in ALS disease pathophysiology, therapies that might show positive effects in SOD1 models may not be effective in sALS or in non-SOD1 fALS cases, for example caused by mutations in C9orf72. Similar to astrocytes derived from murine SOD1^{G93A} models of ALS, human astrocytes differentiated from neuronal progenitor cells (NPCs) obtained from post-mortem tissue of ALS patients, display MN toxicity *in vitro* (Haidet-Phillips et al., 2011).

In 2014, Meyer et al. established a method to rapidly and efficiently obtain human astrocytes from ALS patients with either sporadic or familial disease through direct conversion of fibroblasts into induced neural progenitor cells (iNPCs). These cells, called induced astrocytes (iAstrocytes), reproduce MN toxicity similar to ALS astrocytes obtained from post-mortem tissue (Meyer et al., 2014). In addition to the opportunity to study sALS *in vitro*, this model allows testing for therapeutic strategies on cells obtained when the patient was still alive, thus more closely reproducing the human “*in vivo* conditions” compared to the use of post-mortem tissue. Also, the generation of iAstrocytes allows avoidance of issues related to the use of biopsies, such as for example sample limitation, tissue degradation and incomplete maturation of NPC-derived astrocytes (Myszczyńska and Ferraiuolo, 2016). As a proof of concept for potential therapeutic translation into human disease, we thus wanted to investigate whether ADSCs could protect MNs from human ALS iAstrocyte toxicity by using the Meyer et al. *in vitro* model of disease adapted to our triple co-culture system. In particular, we used iAstrocytes derived from healthy controls, sALS patients and fALS patients carrying the SOD1^{A4V} mutation or the C9orf72 repeat expansion mutation. Finally, through the separated co-culture method, the modulatory effects of ADSCs on expression of cytokines and growth factors in iAstrocytes was evaluated.

5.2 Aims

1. To investigate whether, through paracrine mechanisms, ADSCs could protect MNs from SOD1^{G93A} astrocytes derived from symptomatic mice *in vitro*.
2. To investigate the capacity of ADSCs to modulate astrocytic functions by reducing the pro-inflammatory signature of SOD1^{G93A} astrocytes.
3. To investigate whether through paracrine mechanisms ADSCs could protect MNs from human iAstrocytes derived from ALS patients with both sporadic and familial disease.

5.3 Purity of mouse astrocyte cultures

Mouse astrocytes were isolated from the brain cortex of Tg SOD1^{G93A} and NTg 90 day-old female mice. For each genotype, astrocytes were obtained from three separate preparations. Astrocytes were purified from microglia by mild-trypsinisation and expanded for 3/4 generations before being analyzed by flow cytometry to test for the purity of the cultures (figure 5.1 A). As shown in figure 5.1 B, the astrocyte populations were positive (>98%) for the astrocyte marker CD44 and negative (<0.4%) for the microglia marker CD11b, regardless of the genotype.

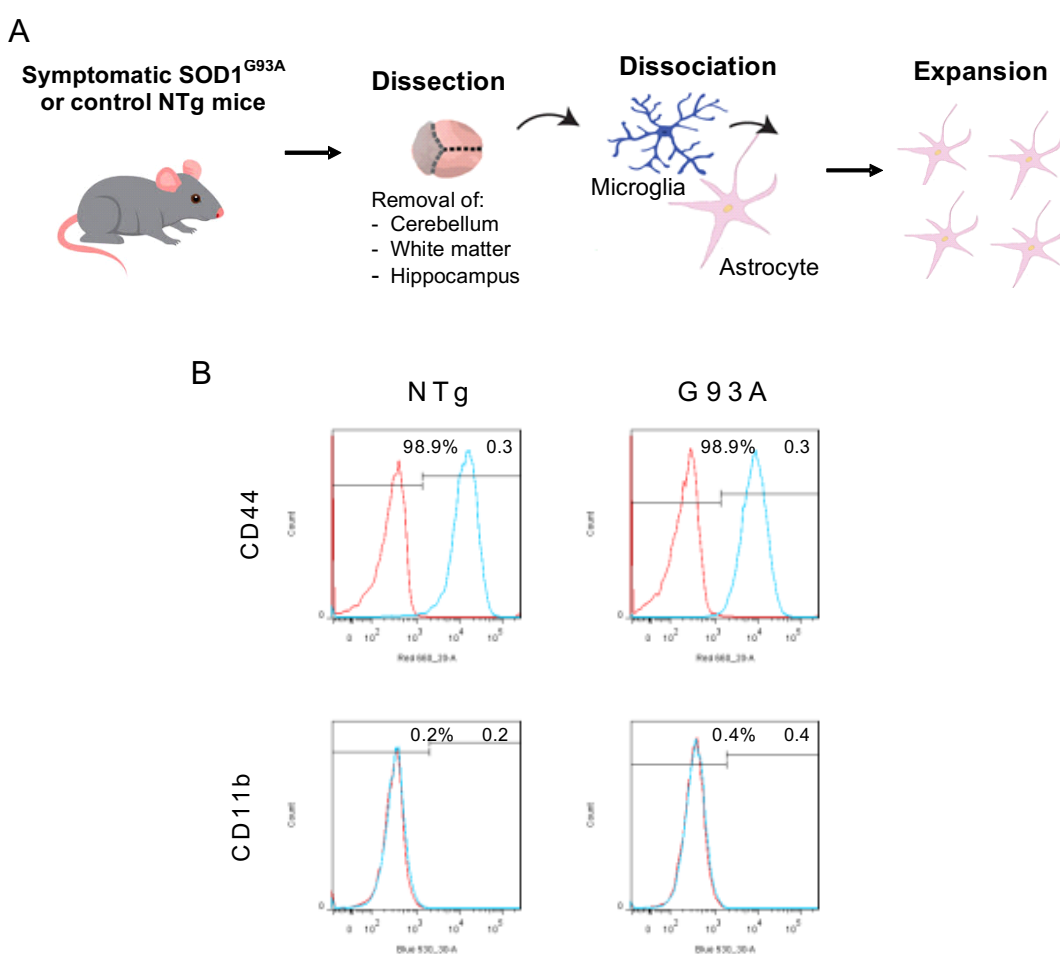


Figure 5.1. Characteristics of mouse astrocytes. (A) Schematic diagram showing the procedure to obtain mAstrocytes. (B) Passage 3-4 mAstrocytes were stained for the astrocyte surface marker CD44 and for the microglia marker CD11b, before being analysed by flow cytometry. Purity of NTg astrocytes was estimated to be $98.9 \pm 0.3\%$ with minimal presence of microglia cells ($0.2 \pm 0.2\%$). G93A astrocytes were $98.9 \pm 0.3\%$ positive for CD44 and negative ($0.4 \pm 0.4\%$) for CD11b. The histograms in blue represent the cells stained with the specific antibody, while in red is the control isotype

antibody staining. Percentages represent mean \pm SD from three separate culture preparations.

5.4 ADSCs protect MNs from SOD1^{G93A}-linked mouse astrocyte toxicity

It has been previously demonstrated that astrocytes derived from SOD1^{G93A} mice are toxic to wild-type mouse motor neurons in co-culture systems (Ferraiuolo et al., 2011, Tripathi et al., 2017). To test whether ADSCs could protect MNs from astrocyte toxicity through paracrine mechanisms, a triple separated co-culture system was designed and used. Briefly, healthy wild-type HB9-GFP-MNs were co-cultured with mAstrocytes derived from either NTg or SOD1^{G93A} symptomatic mice. mADSCs were seeded onto modified glass coverslips containing paraffin wax dots, so that coverslips with adherent mADSCs could be inverted and added on top of the astrocyte/MN mixed co-culture without being physically connected. The separated co-culture method is described in detail in the materials and methods chapter (paragraph 2.4.5, figure 2.8). Before starting the triple co-culture experiments, the separated co-culture method was validated in order to confirm that the ADSCs growing on coverslips would not migrate down to the plastic culture well where astrocytes are attached. Mouse SOD1^{G93A} astrocytes and GFP-ADSCs were co-cultured with the separated method for 7 days. At the end of the co-culture, coverslips containing the GFP-ADSCs were removed and plates imaged with the In Cell 2000 (GE). As shown in figure 5.2, GFP-ADSCs were not found within the astrocyte cultures, where the only GFP signal that was detected came from the presence of ADSC cell debris. This experiment confirmed that the GFP-ADSCs remained attached to the coverslips for the entire co-culture period.

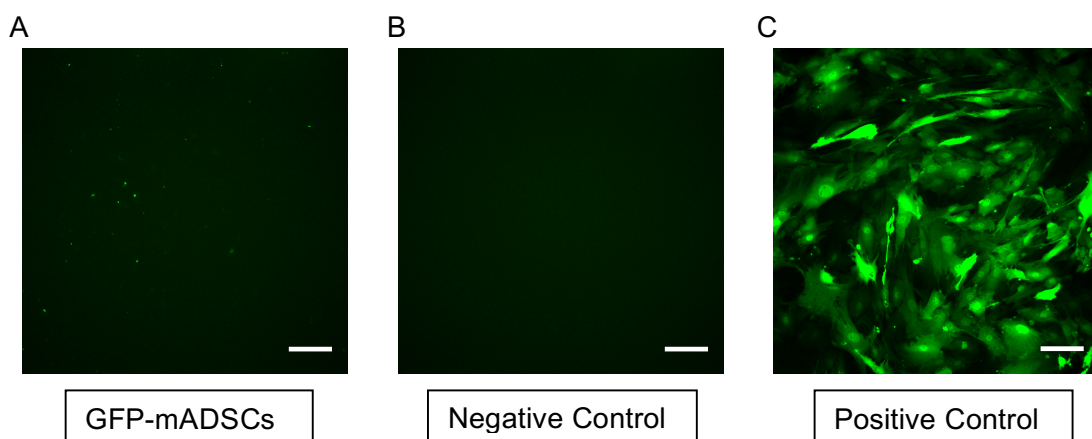


Figure 5.2. Validation of the separated co-culture method. Representative fluorescent images of mouse astrocytes after 1 week of separated co-culture with GFP-mADSCs (A) or cultured alone (B). GFP-mADSCs were used as a positive control (C). GFP-mADSCs did not migrate from the coverslip to the bottom plastic culture well where astrocytes were growing. Images were taken with the In Cell 2000 (GE). Scale bars: 50 μ m.

After validating the method, the triple co-culture experiments were performed with naïve GFP-negative ADSCs. The HB9-GFP-MNs used in this study were differentiated from mouse embryonic stem cells previously obtained from healthy mice genetically modified to express GFP under control of the motor neuron specific promoter HB9. The differentiation protocol, which gives rise to a 70 – 90% MN-enriched fraction was performed within the lab of Dr Laura Ferraiuolo.

At day 1 and day 7 of co-culture, HB9-GFP-MNs were imaged with the In Cell 2000 Analyser (GE) and counted with the use of the Columbus software. The percentage of MN survival was calculated as the number of viable MN at day 7 as a percentage of the number of viable MN at day 1. Only GFP positive cell bodies with at least one axon were considered to be viable MNs.

At basal level, after 7 days of co-culture there was a modest but significant reduction of ~15% ($p=0.0079$, figure 5.3 A and B) in motor neuron survival in the SOD1^{G93A} astrocytes cultures compared to control NTg cultures. In particular, without ADSC treatment the percentage of MN survival from day 1 to day 7 with NTg astrocytes was $72.1\% \pm 3.9$ (mean \pm SD), while with SOD1^{G93A} astrocytes it was $61.6\% \pm 3.4$ (mean \pm SD). Thus, SOD1^{G93A} astrocytes were shown to be toxic and/or less supportive to healthy MNs compared to NTg wild-type astrocytes. Notably, when compared to the untreated astrocytes, the presence of ADSCs in the SOD1^{G93A} co-culture significantly increased MN viability by ~23% ($61.1\% \pm 6.3$ MN survival in untreated SOD1^{G93A} vs $79.7\% \pm 2.2$ MN survival in ADSCs treated SOD1^{G93A}, $p=0.0002$, figure 5.3 A and B). Thus, the presence of ADSCs protected MNs from SOD1^{G93A} astrocytes, completely abolishing the toxicity observed under basal conditions. Furthermore, MN survival in SOD1^{G93A} cultures containing ADSCs was 7% higher than untreated NTg cultures ($p=0.0426$, figure 5.3 A and B). Remarkably, ADSCs also affected NTg astrocyte cultures increasing MN survival by ~ 15% ($72.1\% \pm 9.9$ MN survival in untreated NTg vs $85\% \pm 0.4$ MN survival in ADSC treated NTg, $p=0.0021$, figure 5.3 A and B) compared to untreated NTg astrocytes.

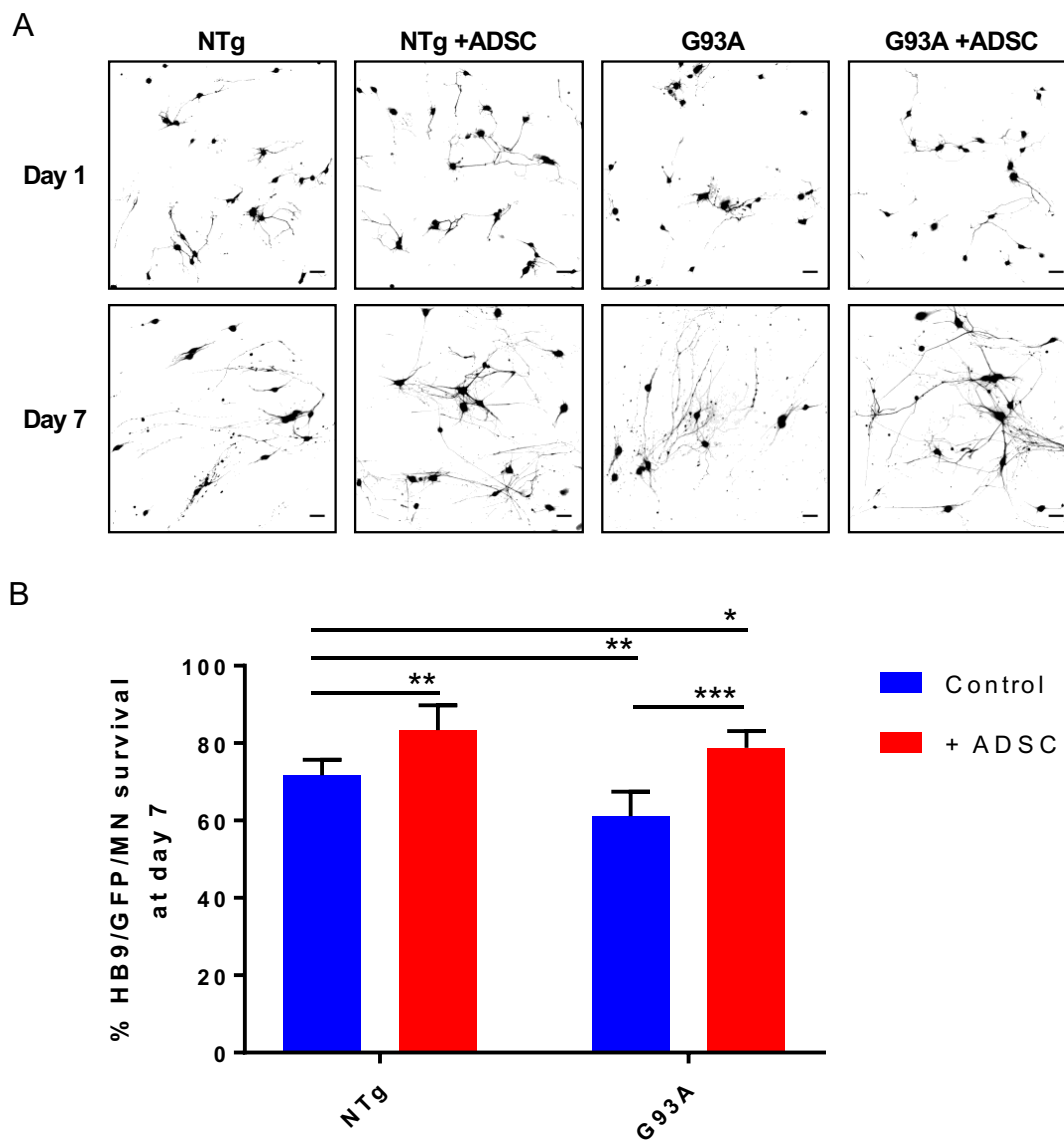


Figure 5.3. Effect of ADSC exposure on MN survival after co-culture with NTg and SOD1G93A astrocytes. (A) Representative images of HB9-GFP-MNs at day 1 and day 7 of co-culture with G93A or NTg astrocytes under basal conditions or in the presence of ADSCs (scale bars: 50 μ m). (B) Percentage of motor neurons that survived from day 1 to day 7 of co-culture. G93A astrocytes were toxic to MNs compared to NTg astrocyte co-cultures (71% \pm 4 MN survival in NTG vs 61% \pm 6 in G93A). ADSCs protected MNs from G93A astrocyte toxicity (61% \pm 6 in untreated vs

79% \pm 4 in ADSC treated) and increased MN survival when compared to untreated NTg astrocytes (7%). ADSCs increased MN survival on NTg astrocyte co-cultures compared to untreated NTg astrocytes (71% \pm 4 MN survival in untreated vs 83% \pm 6 in ADSC treated). MN quantification is representative of 3 independent experiments, where each experiment is in triplicate (2-way ANOVA, followed by Tukey's multiple comparisons test). * p <0.05, ** p <0.01, *** p <0.001 Error bars represent SD. MN = Motor neurons; NTg = Non transgenic astrocytes; G93A = SOD1^{G93A} astrocytes.

5.5 Expression of growth factors in ADSCs is modulated by SOD1^{G93A} mouse astrocytes

ADSCs are known to secrete several growth factors including VEGF, HGF, IGF-1 and FGF-2. Moreover, the capacity of MSCs to modulate their own growth factor expression and secretion in response to specific changes in the microenvironment has been reported (Gu et al., 2010). Gene expression analysis for growth factors in ADSCs following 48 hours co-culture with either NTg or SOD1^{G93A} astrocytes and in control mono-cultures was evaluated by RT-qPCR.

Before gene expression analysis, RT-qPCR amplicons were run on an agarose gel to confirm that the growth factor transcripts were present in ADSCs (figure 5.4 A). VEGF expression was significantly increased in ADSCs co-cultured with NTg astrocytes compared to control ADSC mono-cultures (p =0.0289, figure 5.4 B). Moreover, co-culture with SOD1^{G93A} further enhanced VEGF expression as shown by comparison with ADSC cultured with NTg astrocytes (p =0.0443, figure 5.4 B).

Expression levels for IGF-1 in ADSCs cultured with SOD1^{G93A} astrocytes were increased by \sim 5-fold when compared to ADSCs alone (p <0.0001), and by \sim 3-fold compared to ADSCs cultured with NTg astrocytes (p =0.0002, figure 5.4 B). Although the difference was not statistically significant, co-culture with NTg astrocytes increased IGF-1 expression in ADSCs by \sim 2-fold compared to unstimulated ADSCs (p =0.0785, figure 5.4 C).

Similar to the changes observed in IGF-1 expression, co-culture with SOD1^{G93A}, stimulated ADSCs to express higher levels of FGF-2 when compared to either unstimulated ADSCs (p =0.0016) or ADSCs co-cultured with NTg astrocytes (p =0.0081, figure 5.4 D).

HGF expression was increased by \sim 3 fold in ADSCs cultured with NTg astrocytes compared to ADSCs alone (p =0.0156, figure 5.4 E). This effect was not observed when ADSCs were co-cultured with SOD1^{G93A} astrocytes.

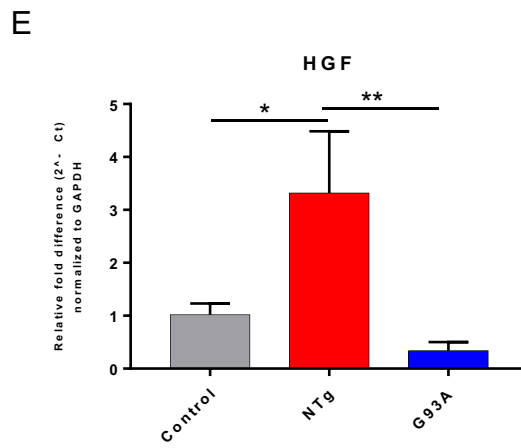
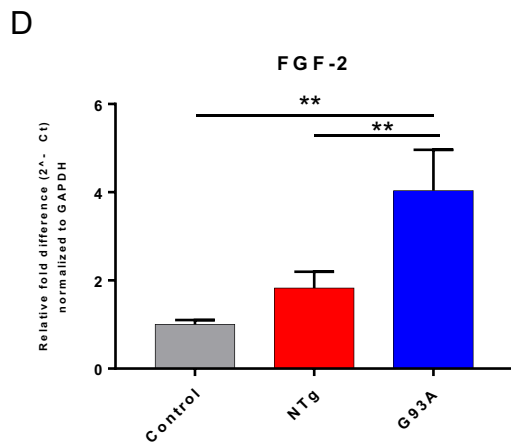
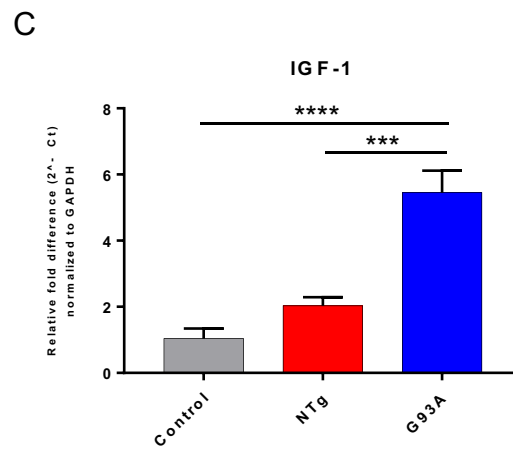
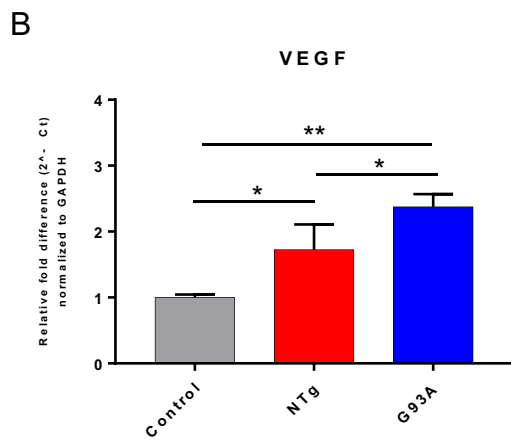
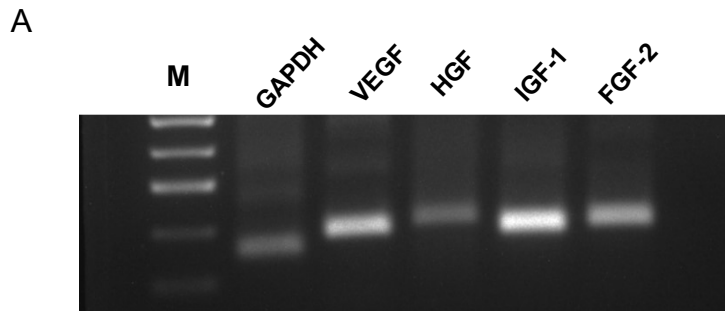


Figure 5.4. Growth factor gene expression in ADSCs. Gene expression was evaluated by RT-qPCR. (A) Representative agarose gel picture showing amplification of growth factor transcripts in ADSCs. (B) Expression levels of VEGF were increased in ADSCs co-cultured with either NTg or SOD1G93A astrocytes compared to control ADSC mono-cultures. In comparison to NTg astrocytes, co-cultured with SOD1G93A astrocytes further stimulated VEGF expression in ADSCs. (C) IGF-1 expression was increased by 5-fold in ADSCs cultured with SOD1G93A astrocytes compared to ADSCs alone, while co-culture with NTg astrocytes was not sufficient to induce a statistically significant increase in IGF-1 expression. (D) In comparison to unstimulated ADSCs, co-culture with SOD1G93A astrocytes induced a 4-fold increase in FGF-2 expression in ADSCs. FGF-2 expression was not statistically different between ADSCs alone and ADSCs cultured with NTg astrocytes. (E) HGF expression was significantly increased in ADSCs co-cultured with NTG astrocytes. A massive reduction in the expression of HGF was found in ADSCs co-cultured with SOD1G93A astrocytes, compared to ADSCs co-cultured with NTg astrocytes. Gene expression was calculated relative to GAPDH expression and results normalized to the expression in control unstimulated ADSCs. Data are presented as mean \pm SD, n=3, where each n consists of a different astrocyte culture preparation. Data were analysed with 1-way ANOVA followed by Tukey's multiple comparison test. **p<0.01, ***p<0.001, ****p<0.0001. NTg = Non transgenic astrocytes; G93A = SOD1G93A astrocytes.

To validate the qPCR data, following 48 hours of separated co-culture, ADSCs and astrocytes were separated and cultured individually for a further 24 hours before measuring secretion levels of VEGF and IGF-1 in the culture supernatant using an ELISA assay.

In 24 hours, ADSCs secreted 2.94 ± 0.1 ng/ml (mean \pm SD) of VEGF (figure 5.5 A). In line with the gene expression data, VEGF secretion following co-culture with either NTg or SOD1^{G93A} astrocytes was significantly higher compared to ADSC mono-cultures. VEGF secretion in ADSCs was increased by ~27% ($p=0.0135$) and by ~46% ($p=0.0002$) after co-culture with NTg or SOD1^{G93A} astrocytes respectively. In particular, ADSCs secreted 3.99 ± 0.3 ng/ml of VEGF when cultured with NTg astrocytes and 5.4 ± 0.4 ng/ml of VEGF when cultured with SOD1^{G93A} astrocytes (figure 5.5 A).

IGF-1 concentration in supernatant of control ADSC mono-cultures was of 62.39 ± 15.11 pg/ml (mean \pm SD) (figure 5.5 B). Notably, following co-culture with SOD1^{G93A} astrocytes, ADSCs secreted IGF-1 at a concentration of 350.2 ± 61.79 pg/ml (mean \pm SD), resulting in a significant increase in protein secretion of ~5-fold compared to unstimulated ADSCs ($p=0.0003$, figure 5.5 B). ADSCs co-cultured with NTg astrocytes secreted 114.5 ± 24.8 (mean \pm SD) of IGF-1, equivalent to an increase of ~27% compared to mono-culture ADSCs. However, the difference was not statistically significant ($p=0.1563$, figure 5.5 B).

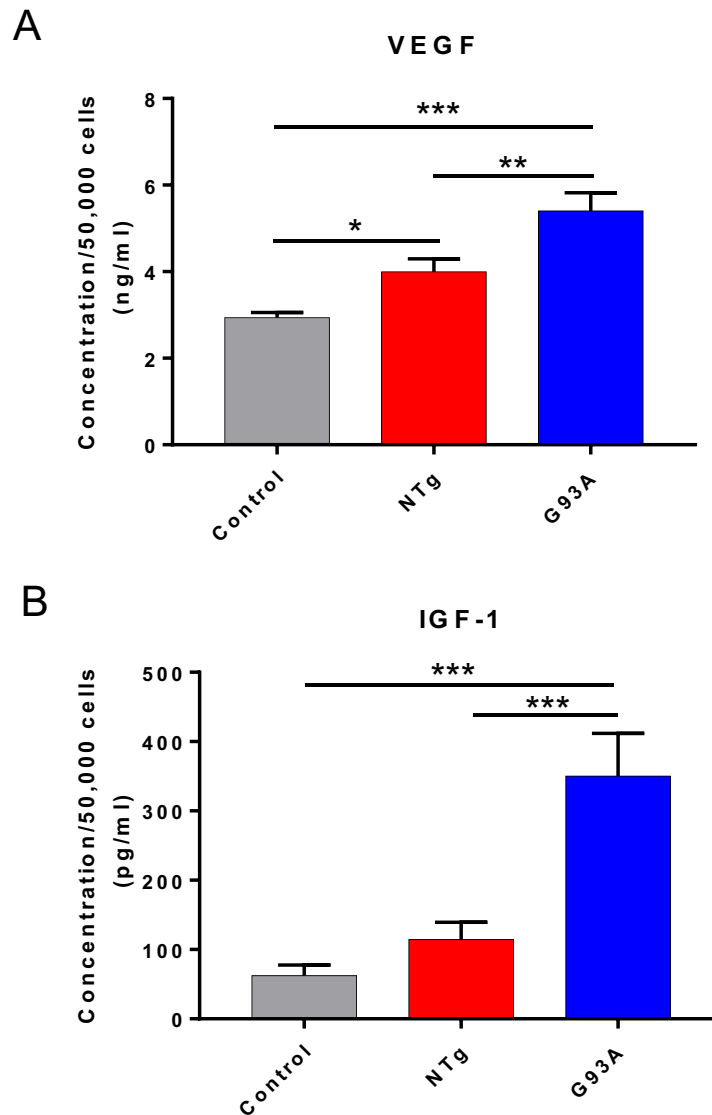


Figure 5.5. Secretion levels of VEGF and IGF-1 in ADSCs. ADSCs were cultured for 48 hours either alone, with NTg astrocytes or SOD1^{G93A} astrocytes. At the end of the separated co-culture period, fresh medium was added and growth factor secretion evaluated after a further 24 hours of culture by ELISA. (A) Co-culture with SOD1^{G93A} astrocytes induced ADSCs to secrete significantly higher levels of VEGF (5.4 ± 0.4 ng/ml) compared to ADSCs co-cultured with NTg astrocytes (3.99 ± 0.3 ng/ml) or ADSCs alone (2.94 ± 0.1 ng/ml). (B) Secretion levels of IGF-1 were significantly increased in ADSCs co-cultured with SOD1^{G93A} astrocytes (350.2 ± 61.79 pg/ml), compared to control ADSCs mono-cultures (62.39 ± 15.11 pg/ml) or compared to NTg astrocytes co-cultures (114.5 pg/ml ± 24.8). Data are presented as mean ± SD, n=3, where each n consists of a different astrocyte culture preparation. Data were analysed with 1-way ANOVA followed by Tukey's multiple comparison test *p<0.05, **p<0.01, ***p<0.001, NTg = Non transgenic astrocytes; G93A = SOD1^{G93A} astrocytes.

5.6 ADSCs modulate the expression of growth factors in SOD1^{G93A} astrocytes

Since astrocytes are known to secrete growth factors important in supporting the survival and function of MNs, we investigated whether ADSCs could affect SOD1^{G93A} astrocytic functions by potentiating the expression and secretion of growth factors. First, the expression levels of BDNF, GDNF, VEGF and IGF-1 in SOD1^{G93A} or NTg astrocytes in the presence or absence of ADSCs were evaluated by qPCR analysis (figure 5.6).

At basal levels, no differences were detected in the expression of BDNF between NTg and SOD1^{G93A} astrocytes. However, in SOD1^{G93A} cultures, the presence of ADSCs significantly increased the expression of BDNF by ~ 7-fold compared to untreated astrocytes ($p=0.0045$, figure 5.6 A).

The expression of GDNF was massively decreased in SOD1^{G93A} astrocytes when compared to NTg cultures ($p=0.0001$, figure 5.6 B). Interestingly, co-culture with ADSCs induced a significant increase of ~ 7-fold in GDNF expression in SOD1^{G93A} astrocytes ($p=0.0058$, figure 5.6 B), in contrast to the induction of a significant decrease of ~ 2-fold in NTg cultures ($p=0.0098$, figure 5.6 B).

Without ADSC treatment, expression of VEGF was slightly increased in SOD1^{G93A} astrocytes compared to NTg astrocytes, although the difference was not statistically significant (figure 5.6 C). ADSC treatment induced an increase of VEGF expression of ~ 10-fold in SOD1^{G93A} astrocytes ($p<0.0001$, figure 5.6 C), while in NTg astrocytes the increase was not statistically significant ($p=0.2849$, figure 5.6 C).

IGF-1 expression was found to be strongly decreased in SOD1^{G93A} astrocytes compared to NTg astrocytes ($p=0.0016$, figure 5.6 D). In SOD1^{G93A} astrocytes, ADSCs induced a significant increase by ~ 9-fold in IGF-1 expression ($p=0.0004$), while there was no significant effect in NTg cultures (figure 5.6 D).

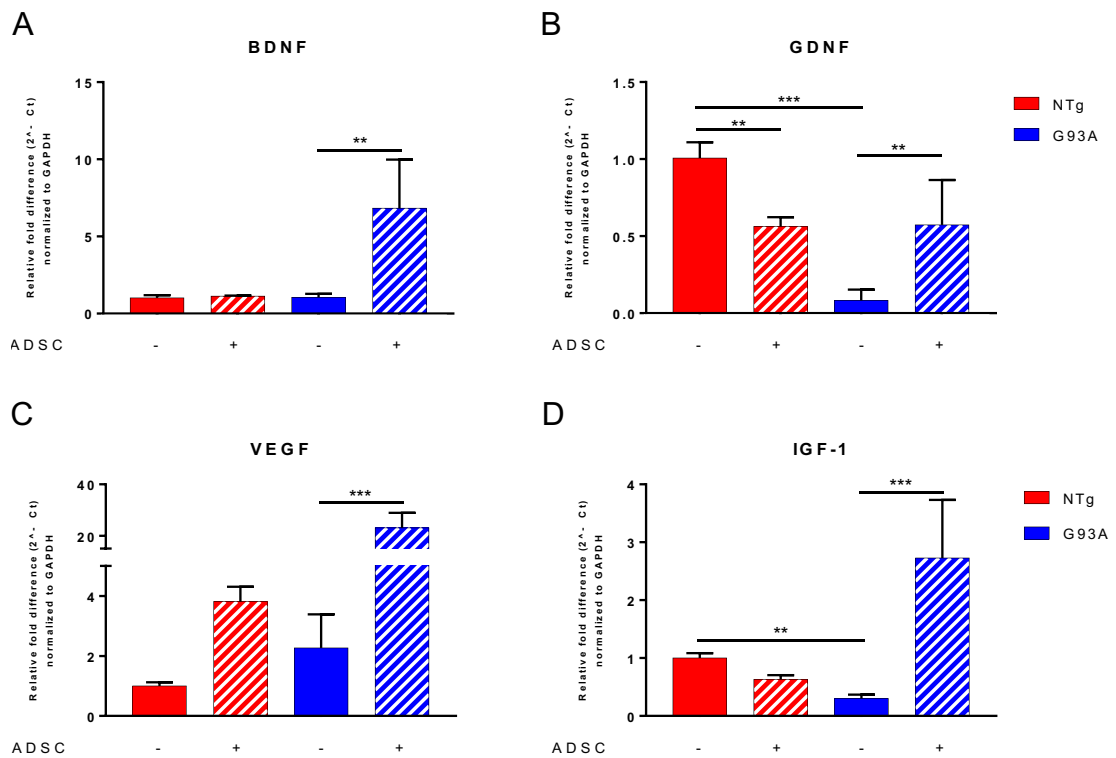


Figure 5.6. Growth factor expression in SOD1^{G93A} and NTg astrocytes. Gene expression was evaluated by RT-qPCR. (A) Expression levels of BDNF were unchanged between SOD1^{G93A} and NTg astrocytes. ADSC treatment significantly increased BDNF expression by 7-fold in SOD1^{G93A} astrocytes. (B) GDNF expression was substantially decreased in SOD1^{G93A} astrocytes and ADSC treatment induced its up-regulation by 7-fold. On the contrary, ADSCs inhibited the expression of GDNF in NTg astrocytes. (C) No statistically significant changes were found between NTg and SOD1^{G93A} astrocytes in basal levels of VEGF expression. A 10-fold increase in VEGF expression was found in SOD1^{G93A} astrocytes co-cultured with ADSCs. (D) IGF-1 expression was significantly reduced in SOD1^{G93A} astrocytes compared to NTg cultures. ADSC treatment induced IGF-1 expression by 9-fold in SOD1^{G93A} astrocytes. Gene expression for growth factors was calculated relative to GAPDH expression and results normalized to untreated NTg control astrocytes. Data are presented as mean \pm SD, n=3, where each n consists of a different astrocyte culture preparation. Data were analysed with 1-way ANOVA followed by Sidak's multiple comparisons test *p<0.05, **p<0.01, ***p<0.001, ****p<0.0001. NTg = Non transgenic astrocytes; G93A = SOD1^{G93A} astrocytes.

In a separate set of experiments, the secretion levels of VEGF and IGF-1 from NTg and SOD1^{G93A} astrocytes following co-culture with ADSCs or without any treatment were quantified by ELISA.

In 24 hours, SOD1^{G93A} astrocytes secreted a significantly higher amount of VEGF compared to NTg astrocytes (612 pg/ml ± 62.5 for NTg vs 1,531 pg/ml ± 129.1 for SOD1^{G93A}, p=0.0001, figure 5.7 A). Unexpectedly, in contrast with the gene expression data, while ADSC treatment significantly enhanced secretion of VEGF in NTg astrocytes (612 pg/ml ± 62.5 in untreated vs 1001 pg/ml ± 255.6 in ADSC-treated, p=0.0178, figure 5.7 B), secretion levels in SOD1^{G93A} astrocytes were unchanged (1,531 pg/ml ± 129.1 in untreated vs 1678 pg/ml ± 129.3 in ADSC-treated, p=0.2953, figure 5.7 A).

In agreement with the qPCR data, secretion of IGF-1 from untreated SOD1^{G93A} astrocytes was significantly reduced by ~ 19-fold compared to untreated control NTg astrocytes (131.6 pg/ml ± 13.92 for NTg vs 6.6 pg/ml ± 3 for SOD1^{G93A}, p<0.0001, figure 5.7 B). Notably, the presence of ADSCs in the culture enhanced the secretion of IGF-1 in both NTg and SOD1^{G93A} astrocytes. In particular, IGF-1 secretion in SOD1^{G93A} astrocytes was increased by ~ 5-fold (6.6 pg/ml ± 3 in untreated vs 38.6 pg/ml ± 9 in ADSC-treated, p=0.0386, figure 5.7 B).

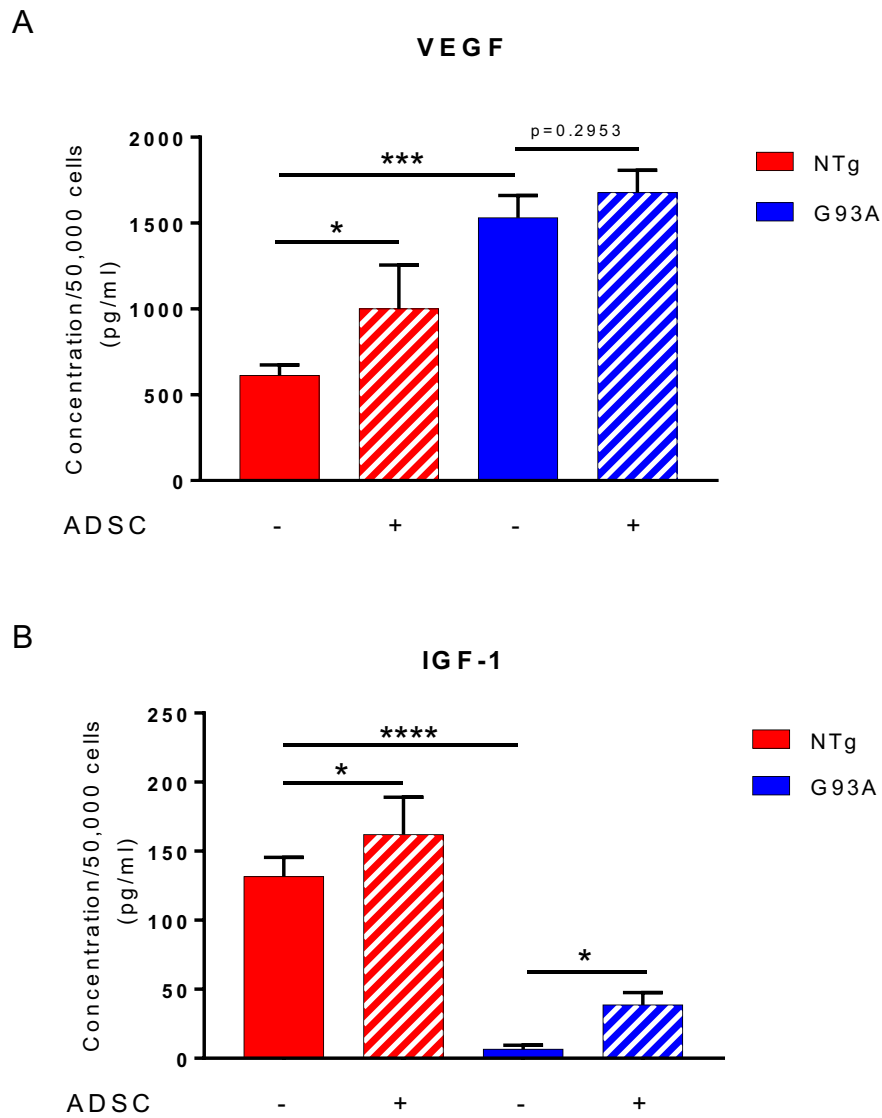


Figure 5.7. Growth factor secretion from SOD1^{G93A} and NTg astrocytes. (A) At basal levels SOD1^{G93A} astrocytes secreted significantly more VEGF (1,531 pg/ml ± 129.1) compared to control NTg astrocytes (612 pg/ml ± 62.5). Co-culture with ADSCs induced a significant increase in VEGF secretion in NTg astrocytes (1001 pg/ml ± 255.6). In SOD1^{G93A} astrocytes, the presence of ADSCs did not significantly alter VEGF secretion (1678 pg/ml ± 129.3 in ADSC-treated). (B) Secretion levels of IGF-1 were significantly reduced in SOD1^{G93A} astrocytes (6.6 pg/ml) compared to control NTg astrocytes (131.6 pg/ml ± 13.92). The presence of ADSCs in the culture induced the secretion of IGF-1 in both NTg (162 pg/ml ± 27) and SOD1^{G93A} astrocytes (6.6 pg/ml ± 3 in untreated vs 38.6 pg/ml ± 9 in ADSC-treated). Data are presented as mean ± SD, n=3, where each n consists of a different astrocyte culture preparation. Data were analysed with 1-way ANOVA followed by Sidak's multiple comparisons test *p<0.05, **p<0.01, ***p<0.001, ****p<0.0001. NTg = Non transgenic astrocytes; G93A = SOD1^{G93A} astrocytes.

5.7 ADSCs modulate the expression of cytokines/chemokines in SOD1^{G93A} astrocytes

Amongst several mechanisms by which ALS astrocytes exert neuronal toxicity, the increased secretion of pro-inflammatory mediators such as cytokines and chemokines have been reported (Endo et al., 2015, Kia et al., 2018, Yamanaka and Komine, 2018). Given the immunomodulatory properties of ADSCs, their effects on the expression and secretion of pro-inflammatory molecules in astrocyte cultures have been investigated. As already described, separated co-cultures between mAstrocytes (NTg or SOD1^{G93A}) and ADSCs were maintained for 48 hours. At the end of the separated co-culture, ADSCs were removed, total RNA was extracted from astrocytes and gene expression for IL-6, MCP-1, IL1 β and TNF- α was evaluated by RT-qPCR. To evaluate gene expression at basal levels, astrocytes were cultured in the presence of empty coverslips.

Without ADSCs, transcription levels of IL-6 were slightly but significantly higher in SOD1^{G93A} compared to NTg astrocytes ($p=0.0211$, figure 5.8 A). The presence of ADSCs in the co-culture reduced the expression of IL-6 in both SOD1^{G93A} and NTg astrocytes. In particular, expression of IL-6 was reduced by about 3-fold in ADSC-treated SOD1^{G93A} astrocytes compared to untreated cultures ($p<0.0001$, figure 5.8 A).

At basal level, SOD1^{G93A} astrocytes displayed increased expression of MCP-1 compared to control NTg astrocytes ($p=0.0341$, figure 5.8 B), however, this was significantly reduced by 9-fold in cells co-cultured with ADSCs ($p=0.0002$, figure 5.8 B).

The transcription levels of IL1- β were significantly increased in SOD1^{G93A} astrocytes compared to controls ($p=0.0287$, figure 5.8 C). However, a 5-fold reduction in SOD1^{G93A} astrocytes following co-culture with ADSCs was observed ($p=0.0081$, figure 5.8 C).

Finally, although no difference was found between SOD1^{G93A} and NTg astrocytes, TNF- α expression in SOD1^{G93A} astrocytes was significantly reduced by 5-fold after co-culture with ADSCs ($p=0.0003$, figure 5.8 D).

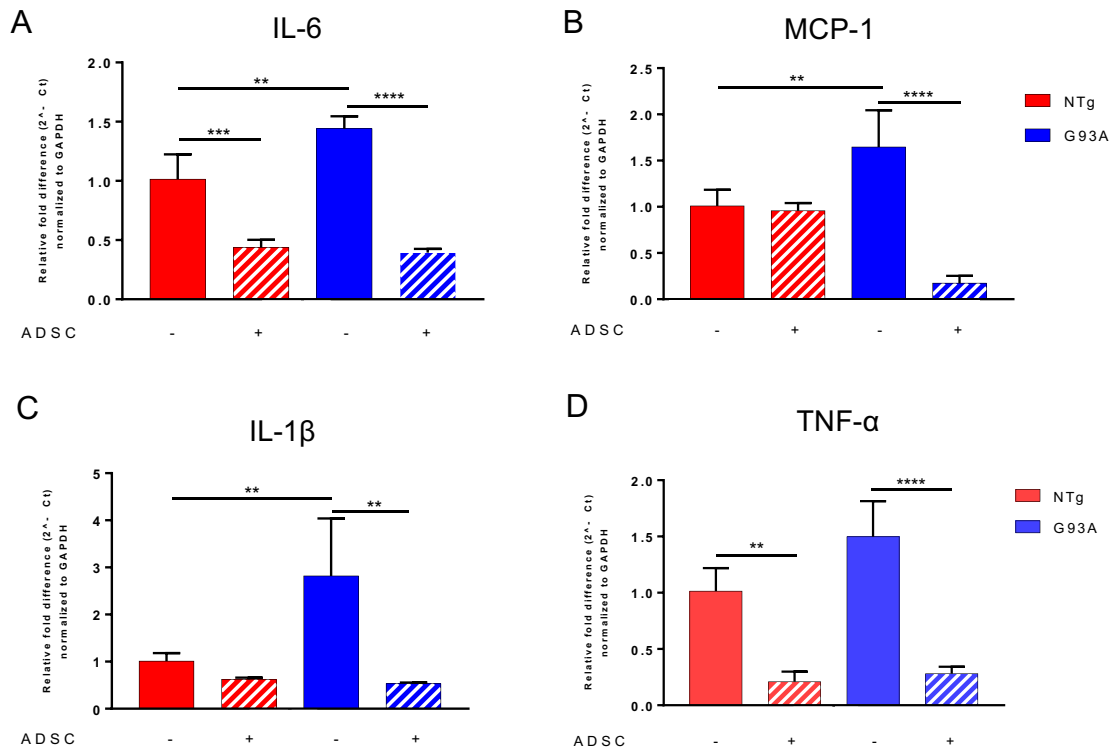


Figure 5.8. Cytokine/chemokine expression in SOD1^{G93A} and NTg astrocytes. (A) Expression levels of IL-6 were increased in SOD1^{G93A} astrocytes compared to NTg astrocytes. ADSC treatment reduced IL-6 expression by 3-fold in SOD1^{G93A} astrocytes and by 2-fold in NTg astrocyte cultures. (B) MCP-1 expression was slightly increased in SOD1^{G93A} astrocytes compared to NTg cultures and reduced by 9-fold in SOD1^{G93A} cultured with ADSCs. (C) IL-1 β expression was increased by 3-fold in SOD1^{G93A} astrocytes compared to controls. ADSCs inhibited IL-1 β expression by 5-fold in SOD1^{G93A} astrocytes. (D) TNF- α expression was decreased by 5-fold in SOD1^{G93A} astrocytes and by 4-fold in NTg astrocytes after co-culture with ADSCs. Gene expression for cytokines was calculated relative to GAPDH expression and results normalized to untreated NTg control astrocytes. Data are presented as mean \pm SD, n=3, where each n consists of a different astrocyte culture preparation. Data were analysed with 1-way ANOVA followed by Sidak's multiple comparisons *p<0.05, **p<0.01, ***p<0.001, ****p<0.0001. NTg = Non transgenic astrocytes; G93A = SOD1^{G93A} astrocytes.

To validate the qPCR data, the secretion levels of IL-6, MCP-1, IL1 β and TNF- α were measured. Briefly, following 48 hours of separated co-culture between astrocytes and ADSCs, the stem cells were removed from the culture and astrocytes cultured for a further 24 hours in control serum free medium before protein detection in the supernatants. Protein concentration of soluble cytokines was evaluated with the use of the BDTM Cytometric Bead Array (CBA) Flex Set Multiplexed Bead-Based Immunoassay, the principles of which are described in the material and methods chapter (paragraph 2.4.9).

Under basal conditions, SOD1^{G93A} astrocytes secreted significantly higher levels of IL-6 (96.8 pg/ml \pm 31.4 for NTg vs 3,374 pg/ml \pm 339.2 for SOD1^{G93A}, $p < 0.0001$, figure 5.9 A) and MCP-1 (811 pg/ml \pm 83 for NTg vs 8,133 pg/ml \pm 543 for SOD1^{G93A}, $p < 0.0001$, figure 5.9 B) when compared to NTg control astrocytes, while no difference was found in IL-1 β secretion (440 fg/ml \pm 340 for NTg vs 301 fg/ml \pm 206 for SOD1^{G93A}, figure 5.9 C). Levels of TNF- α were also increased in SOD1^{G93A} astrocyte supernatant although the difference did not reach statistical significance (59.4 pg/ml \pm 19.6 for NTg vs 81.7 pg/ml \pm 6.7 for SOD1^{G93A}, $p = 0.0596$, figure 5.9 D).

Co-culture with ADSCs inhibited the secretion of all the four cytokines tested in SOD1^{G93A} astrocytes (figure 5.9 A-D). In particular, secretion of IL-6 was reduced by 68% ($p < 0.0001$, figure 5.9 A), MCP-1 by 22% ($p < 0.0002$, figure 5.9 B) and TNF- α by 69% ($p = 0.0006$, figure 5.9 D), while IL-1 β levels were not detectable in supernatant from ADSCs treated astrocytes (figure 5.9 C). Moreover, ADSCs inhibited the secretion of IL-1 β in NTg astrocytes, which levels were below the detection limit of the kit (figure 5.9 C). IL

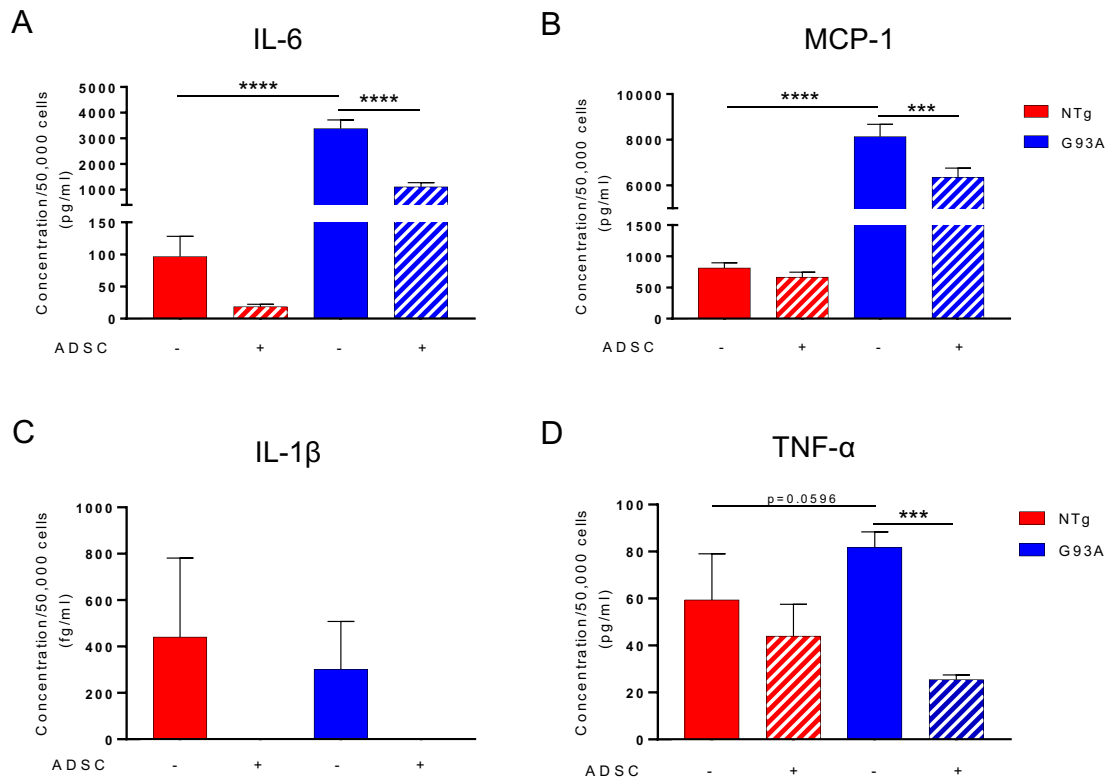


Figure 5.9. Cytokine/chemokine secretion from SOD1^{G93A} and NTg astrocytes. (A) SOD1^{G93A} astrocytes secreted more IL-6 than control astrocytes (96.8 pg/ml \pm 31.4 for NTg vs 3,374 pg/ml \pm 339.2 for SOD1^{G93A}), the concentration of which was reduced after co-culture with ADSCs (1104 pg/ml \pm 167). (B) Secretion levels of the chemokine MCP-1 were increased in SOD1^{G93A} astrocytes (811 pg/ml \pm 83 for NTg vs 8,133 pg/ml \pm 543 for SOD1^{G93A}) and ADSCs treatment reduced its secretion (6,346 pg/ml \pm 414). (C) No difference was found between SOD1^{G93A} and control astrocytes in IL-1 β secretion (440 fg/ml \pm 340 for Ntg vs 301 fg/ml \pm 206 for SOD1^{G93A}). However, no detectable levels of IL-1 β were found in the supernatant of astrocytes cultured with ADSCs. (D) SOD1^{G93A} astrocytes secreted more TNF- α compared to controls (59.4 pg/ml \pm 19.6 for NTg vs 81.7 pg/ml \pm 6.7 for SOD1^{G93A}) the levels of which decreased after ADSC treatment (25.45 pg/ml \pm 2). Data are presented as mean \pm SD, n=3, where each n consists of a different astrocyte culture preparation. Data were analysed with 1-way ANOVA followed by Sidak's multiple comparisons. **p<0.01, ***p<0.001, ****p<0.0001. NTg = Non transgenic astrocytes; G93A = SOD1^{G93A} astrocytes.

5.8 mADSCs protect MNs from human ALS iAstrocyte toxicity

After showing that ADSCs could protect MNs from SOD1^{G93A} astrocyte toxicity, we wanted to validate our results in a human model of disease by using human astrocytes derived from ALS patients with both sporadic and familial disease. In this study, human control healthy iAstrocytes and ALS iAstrocytes were differentiated from iNPCs previously obtained by direct conversion of adult skin fibroblasts using the method of Meyer et al. 2014. Similar to mouse astrocytes and human spinal cord astrocytes isolated from post-mortem tissue, iAstrocytes derived from ALS patients recapitulate non-cell autonomous toxicity towards MNs *in vitro* (Haidet-Phillips et al., 2011, Meyer et al., 2014). The human iAstrocytes were generated by Dr Laura Ferraiuolo's lab group (Sheffield Institute for Translational Neuroscience, University of Sheffield, United Kingdom) and kindly provided for use in our co-culture experiments. Following differentiation, the iAstrocytes are routinely characterized for expression of specific astrocyte markers by the Ferraiuolo lab. In figure 5.10, are some representative immunocytochemistry images of Ctr3050 iAstrocytes that positively express the astrocytic markers CD44, GFAP, vimentin and the glutamate transporter EAAT2.

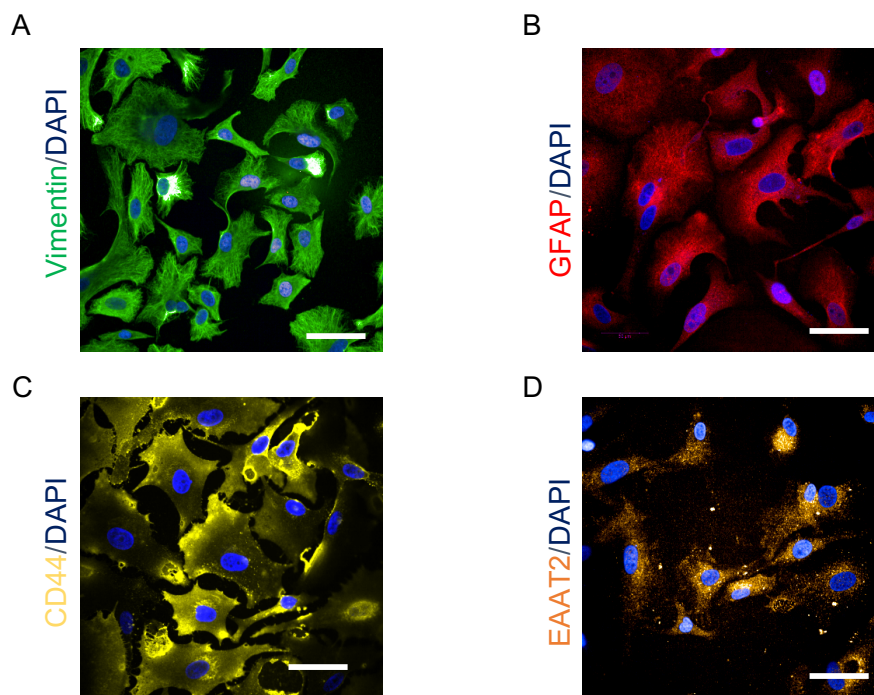


Figure 5.10. iAstrocyte characterization by ICC. iNPC obtained through genetic reprogramming from skin fibroblast are differentiated into iAstrocytes which positively express the astrocytic markers vimentin (A), GFAP (B), CD44 (C) and EAAT2 (D). Images are representative of the Ctr155 cell line and were provided by PhD candidate Noemi Gatto (SITraN, Sheffield). Scale bars: 50 μ m.

The iAstrocytes used in this study were obtained from two healthy control donors (Ctr3050 and Ctr155), two ALS patients with sporadic disease (Pat12 and Pat17), two ALS patients with the C9orf72 repeat expansion mutation (Pat78 and Pat183) and two ALS patients with the SOD1^{A4V} mutation (Pat100 and Pat102). Clinical details are summarized in table 2.5 in the material and methods chapter (paragraph 2.4.3). To test the potential of ADSCs to protect healthy HB9-GFP-MNs from iAstrocyte toxicity, the same triple co-culture method described for the mouse model was adopted. The only difference consisted of a reduction in the co-culture duration to 3 days.

In the absence of ADSCs, MN survival at 3 days was not different in the two control cell lines (67% ± 4.9 MN survival in Ctr3050 and 68.2% ± 6.8 in Ctr155, figure 5.11). As expected, MN survival in ALS iAstrocyte co-cultures was significantly reduced compared to control iAstrocytes (figure 5.12). Specifically, compared to controls, MN survival was reduced by ~34% in the C9orf72 Pat78 line ($p < 0.0001$) and by ~59% in the C9orf72 Pat183 line ($p < 0.0001$). MN death in the sALS Pat17 line and sALS Pat12 line was increased by ~32% ($p < 0.0001$) and by ~33% ($p < 0.0001$) respectively when compared to controls. Finally, survival of MNs in the SOD1^{A4V} iAstrocyte cultures was reduced by ~41% in the Pat102 cell line ($p < 0.0001$) and by ~24% in the Pat100 cell line ($p < 0.005$).

The presence of ADSCs protected MNs from both sporadic and familial ALS iAstrocytes regardless of the genetic mutation. In particular, the presence of ADSCs in the C9orf72 Pat78 iAstrocyte culture increased MN survival by ~25% compared to untreated iAstrocytes ($p < 0.005$), restoring the level of MN survival to those documented when culturing the MNs with the untreated control iAstrocytes. In the C9orf72 Pat183 culture, ADSCs protected MNs as documented by an increase in MN survival of ~47% compared to the untreated culture ($p < 0.0001$). As for the sporadic ALS cell lines, ADSCs completely abolished MN toxicity in the sALS Pat12 cell line, increasing MN survival by ~34% ($p < 0.0001$), however, no significant protective effect was observed in the sALS Pat17 line. In the SOD1^{A4V} Pat102 iAstrocyte line, ADSCs increased MN survival by ~31% compared to untreated cultures ($p < 0.005$) thus, restoring MN survival to levels not statistically different from those observed in the control healthy untreated cultures. In contrast, although a small increase in MN survival (~15%) was observed, treatment with ADSCs did not significantly reduced MN death in the SOD1^{A4V} Pat100 iAstrocyte line. However, in the presence of ADSCs, the SOD1^{A4V} Pat100 line did not show significant differences in MN survival compared to the control iAstrocyte lines. Interestingly, the presence of ADSCs also supported MNs in the Ctr3050 iAstrocyte line by significantly increasing MN survival by ~23%

compared to the survival at basal level ($p < 0.0001$). In the Ctr155 iAstrocyte line, ADSCs did not significantly improve MN survival compared to untreated iAstrocytes.

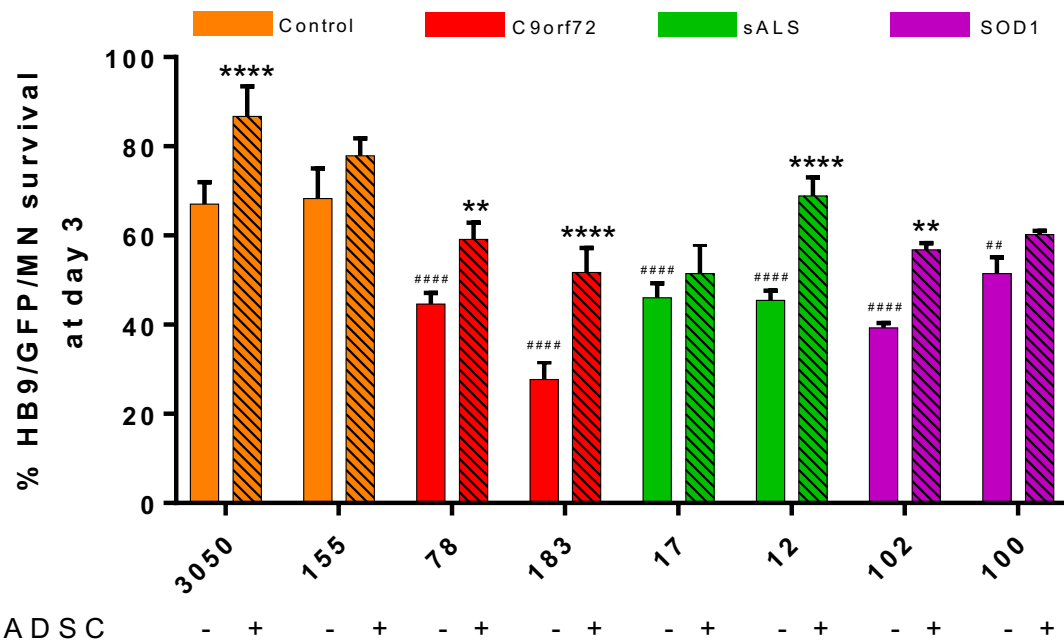


Figure 5.11. Effect of ADSCs on MN survival after co-culture with control or ALS derived human iAstrocytes. The graph shows the percentage of MNs that survived from day 1 to day 3 of co-culture with human iAstrocytes in the presence or absence of mADSCs. The orange bars represent the healthy control cell lines; in red the cell lines with the C9orf72 repeat expansion mutation; in green the cell lines derived from sporadic patients; in purple the cell lines with the SOD1^{A4V} mutation. MN survival was significantly reduced in co-culture with iAstrocytes derived from ALS patients compared to control iAstrocytes obtained from healthy donors. The presence of ADSCs protected MNs from iAstrocyte ALS toxicity, restoring MN survival at levels in some cases comparable to those observed in control non-ALS cultures. The ability of ADSCs to reduce MN death appeared to be patient specific, since in the sALS Pat17 and SOD1 Pat100 iAstrocyte cultures ADSCs did not significantly improve MN survival. Quantification is representative of 3 to 4 independent experiments, where each experiment is in quintuplicate. Data were analysed with 2-way ANOVA, followed by Tukey's multiple comparison test, * $p < 0.05$, ** $p < 0.01$, *** $p < 0.001$, **** $p < 0.0001$; ## $p < 0.005$, #### $p < 0.0001$. Error bars represent SD. (*) symbols denote significant differences between ADSC-treated and non-treated iAstrocytes for the same line; (#) symbols denote significant differences between ALS-iAstrocytes and control iAstrocytes.

Taken together, these data showed that, as seen for the SOD1^{G93A} mouse astrocyte *in vitro* model, through the release of soluble factors mADSCs were able to protect MNs against toxicity exerted by human iAstrocytes derived from ALS patients with either sporadic or familial disease. However, the magnitude of the effect observed was patient specific.

Given that in the presence of ADSCs an increase in MN survival was also observed in the control iAstrocytes cultures, further co-culture experiments were carried out in order to determine whether the mechanism of protection was due to direct MN support rather than the ability of ADSCs to reduce the ALS astrocyte toxicity.

First, the effect of ASDCs on MN mono-cultures was assessed. HB9-GFP-MNs were seeded on laminin coated plates and cultured for 3 days alone or in the presence of ADSCs (separated co-culture). The relative percentage of MN survival from day 1 to day 3 was then calculated and compared. Although non-statistically significant ($p=0.0707$), an increase of ~17% in MN survival was observed when the cells were co-cultured with ADSCs (figure 5.12).

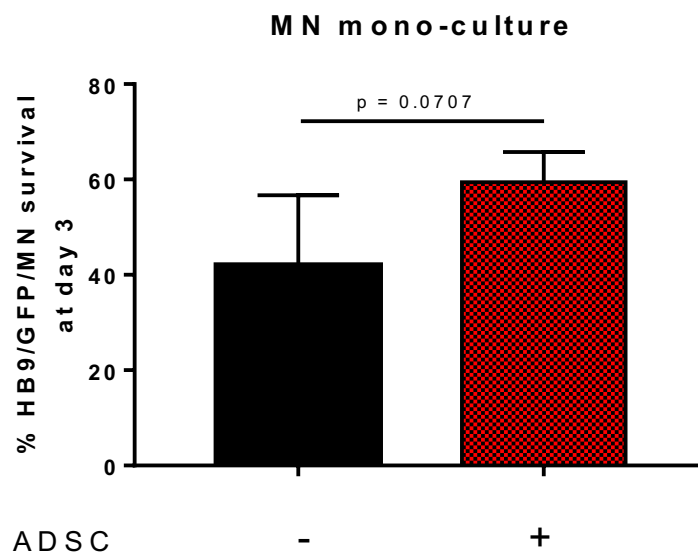


Figure 5.12. Effect of ADSCs on MN mono-cultures. HB9-GFP-MNs were cultured alone or with ADSCs and the relative percentage of MN survival at day 3 was estimated. A non-statistically significant increase in MN survival was observed in the presence of ADSCs. Data are representative of 3 independent experiments, where each experiment is in triplicate. Data were analysed with paired t-test. Error bars represent SD.

To evaluate whether the ADSCs could directly reduce the toxicity of ALS-derived astrocytes, an experiment with the SOD1^{A4V} Pat102 iAstrocyte line was carried out as a proof of principle. Briefly, SOD1 Pat102 iAstrocytes at day 4 of differentiation were plated, and 24 hours later, coverslips containing ADSCs were added to the culture. Following 48 hours of separated co-culture (day 7 of the differentiation), ADSCs were withdrawn and HB9-GFP-MNs seeded on top of the iAstrocytes. Plates were then imaged 24 hours (day 1) and 72 hours (day 3) later to calculate the relative percentage of MN survival, and this was compared to the survival in untreated iAstrocyte cultures. The triple separated co-culture system, in which ADSCs are added at day 7 of iAstrocyte differentiation and maintained in the co-culture for the whole experimental period, was used as a positive control. As expected, the presence of ADSCs for the whole duration of the co-culture protected MN by increasing the survival by ~ 50% compared to control untreated iAstrocytes ($p=0.0067$, figure 5.13). Interestingly, pretreatment of iAstrocytes with ADSCs had a similar effect on MN survival, as documented by an increase of ~ 36% in survival when compared to controls ($p=0.0347$). Although the presence of ADSCs during the MN/iAstrocyte co-culture had a greater effect on MN survival compared to the pretreatment with ADSCs, the difference was not statistically different ($p=0.3547$, figure 5.13).

Taken together these data suggest that the paracrine mechanisms of protection of ADSCs are mainly due to the ability of these cells to modulate astrocytic functions, and in part due to direct MN trophic support.

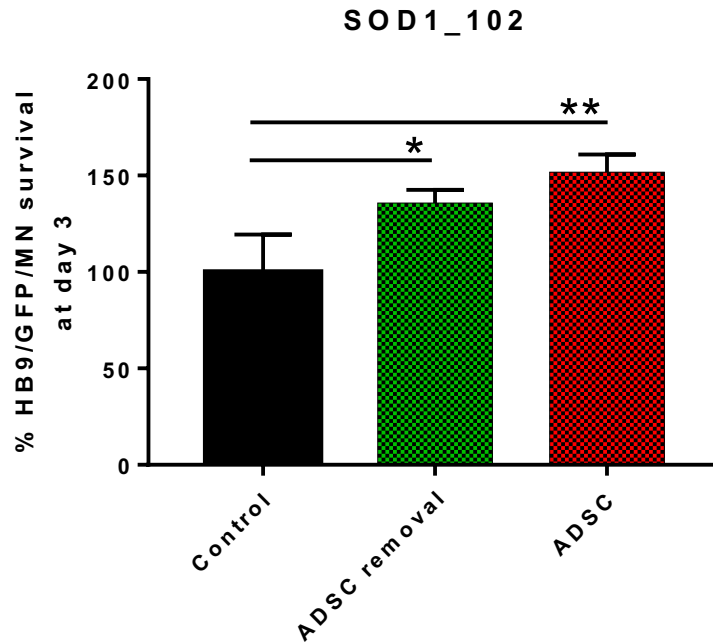


Figure 5.13. Effect on MN survival of SOD1_102 iAstrocytes exposed and then withdrawn from ADSCs. SOD1_102 iAstrocytes were cultured in the presence or not (control) of ADSCs for 48 hours. At the end of the co-culture, ADSC were removed and HB9-GFP-MNs seeded on top of the iAstrocytes (ADSC withdraw). Plates were then imaged 24 and 72 hours later and the relative percentage of MN survival calculated. The triple separated co-culture, in which ADSCs were added 5 hours after seeding the MN and left until the end of the experiment, was used as positive control. Pre-treatment of iAstrocyte with ADSCs resulted in a significant increase in MN survival when compared to untreated iAstrocytes. However, no differences were found between ADSCs removal and the positive control. The relative percentage of MN survival was normalized to the survival in control untreated iAstrocytes. Data are representative of 3 independent experiments, where each experiment is in triplicate. Data were analysed with 1-way ANOVA followed by Tukey's post hoc test; * $p < 0.05$, ** $p < 0.01$, *. Error bars represent SD.

5.9 iAstrocytes/ADSCs separated co-culture: gene expression analysis for inflammatory cytokines and growth factors

After confirming that ADSCs were able to protect MNs from ALS-linked iAstrocyte toxicity we asked whether the cells could also modulate the expression of pro-inflammatory cytokines and growth factors in the human ALS iAstrocytes as seen in the mouse SOD1^{G93A} astrocytes/ADSCs separated co-culture system. At day 5 of differentiation, iAstrocytes were cultured with or without ADSCs for 48 hours, total RNA extracted, cDNA synthesised and gene expression evaluated by qPCR.

First, the relative expression levels of the pro-inflammatory cytokines IL-1 β , TNF- α and IL-6 in ALS iAstrocytes compared to control iAstrocytes were evaluated. Gene expression was calculated relative to GAPDH by normalizing the data to the pooled expression in the control cell lines (Ctr3050 and Ctr155). IL-6 expression was increased by ~3-fold in both sALS iAstrocyte cell lines (Pat12 and Pat17) compared to control iAstrocytes, while the expression in C9orf72 (Pat183 and Pat78) and SOD1 (Pat100 and Pat102) iAstrocyte lines was not significantly different to the controls (figure 5.14 A). Analysis of TNF- α expression revealed a significant reduction in all the iAstrocyte lines (C9orf72, sALS and SOD1) when compared to control iAstrocytes (figure 5.14 B). For IL-1 β , the C9orf72 Pat183 line showed a marked reduction in its expression compared to controls (figure 5.14 C). Conversely, expression of IL-1 β was strongly increased in SOD1 Pat100 iAstrocytes. Interestingly, IL-1 β expression in both sALS cell lines, in the C9orf72 Pat78 line and in the SOD1 Pat102 iAstrocytes was not altered (figure 5.14 C).

We then evaluated whether co-culture with ADSCs could modulate gene expression in iAstrocytes (figure 5.15). ADSCs did not modulate cytokine expression in control (figure 5.15 A), C9orf72 Pat78 (figure 5.15 B) or sALS (figure 5.15 C) iAstrocyte cell lines. In C9orf72 Pat183 iAstrocytes, ADSCs consistently induced the expression of IL-1 β , while no differences in IL-6 and TNF- α were detected when compared to untreated cultures (figure 5.15 B). In both SOD1 iAstrocyte lines, ADSCs induced the expression of IL-6 (figure 5.15 D).

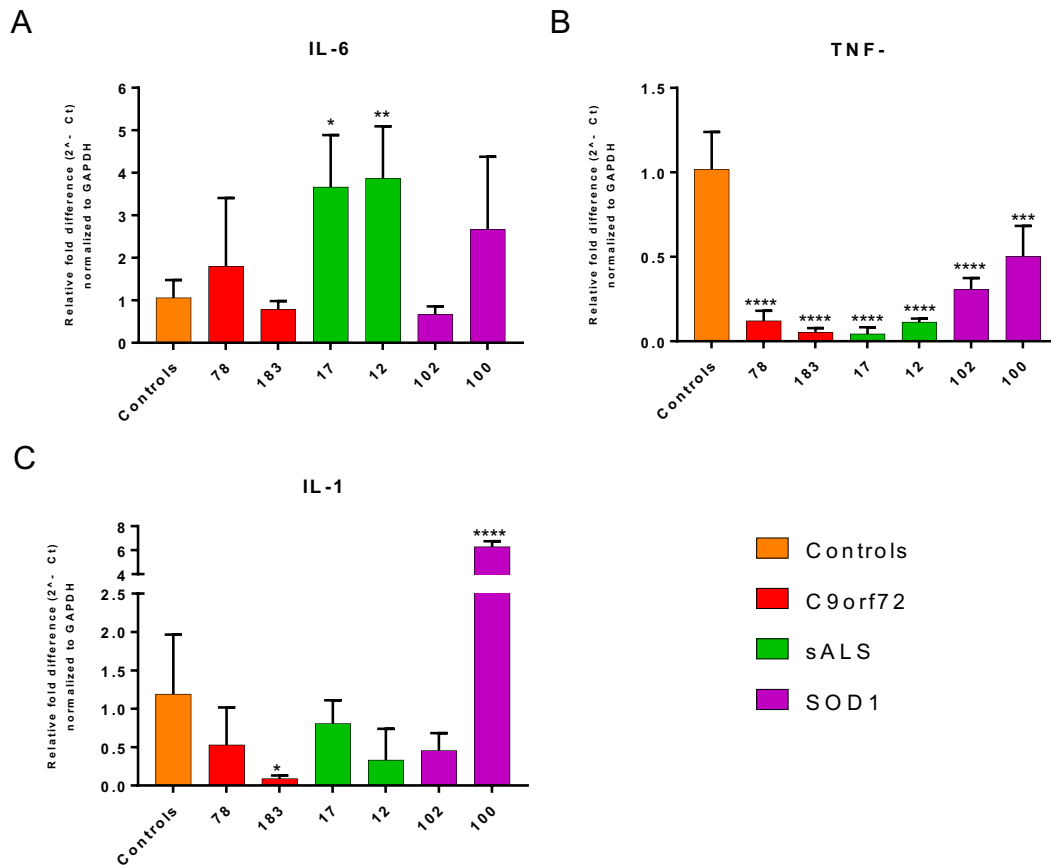


Figure 5.14. Gene expression of pro-inflammatory cytokines in iAstrocytes at basal levels. Gene expression was calculated relative to GAPDH expression and results normalized to control iAstrocytes. (A) Expression levels of IL-6 were significantly increased in both sALS iAstrocyte lines (Pat17 and Pat12) compared to control iAstrocytes, while no differences were found between fALS iAstrocytes and controls. (B) TNF- α expression was decreased in all the ALS iAstrocyte lines compared to control iAstrocytes. (C) Compared to controls, IL-1 β expression was strongly increased in one SOD1 iAstrocyte line (Pat100) and decreased in one C9Orf72 line (Pat183). Data are presented as mean \pm SD, n=3, where each n consists of a different iAstrocyte culture preparation. Data were analysed with 1-way ANOVA followed by Sidak's multiple comparisons *p<0.05, **p<0.01, ***p<0.001, ****p<0.0001.

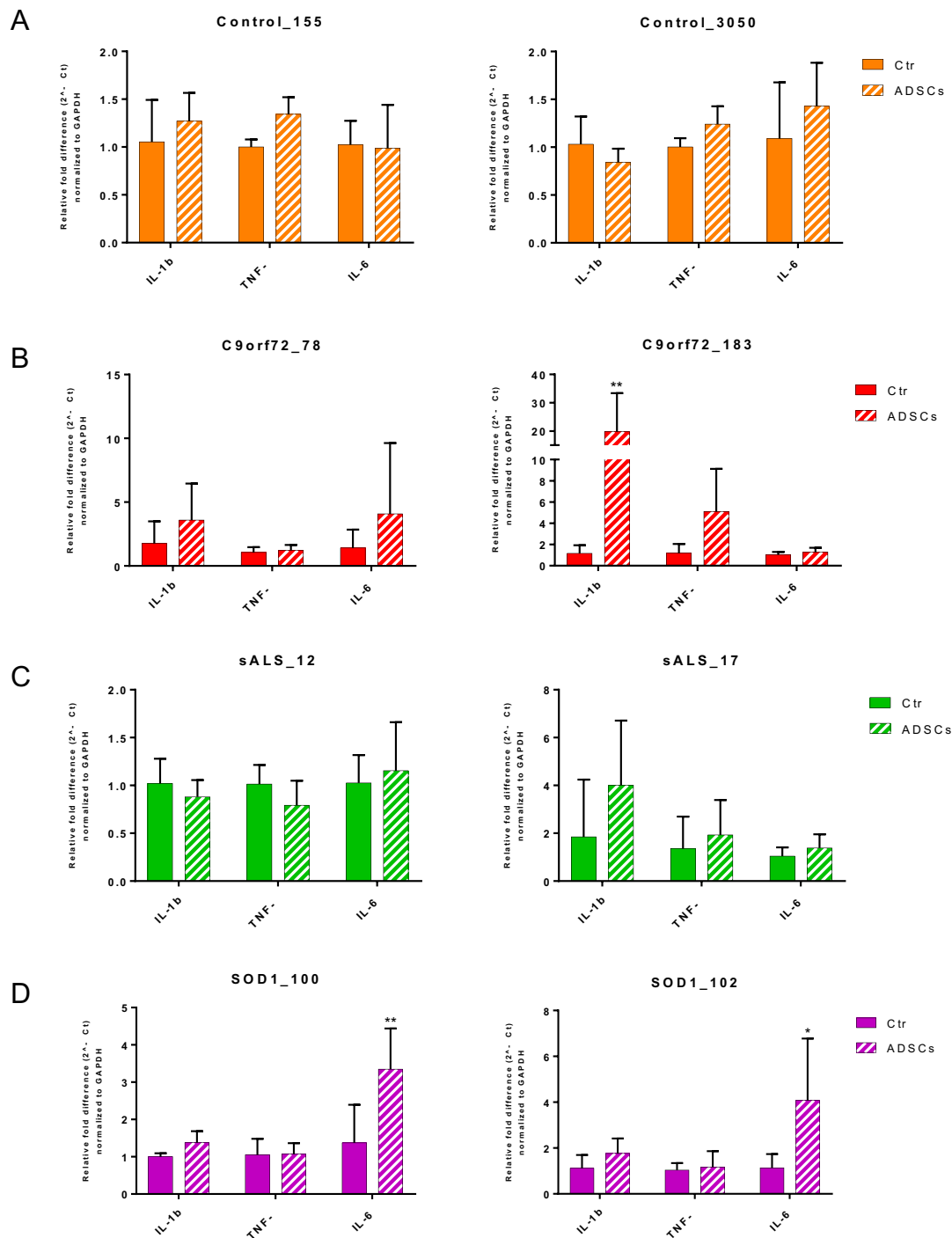


Figure 5.15. Gene expression of pro-inflammatory cytokines in iAstrocytes after co-culture with ADSCs. Gene expression for individual cytokines was calculated relative to GAPDH expression and results normalized to untreated iAstrocytes. The presence of ADSCs did not alter the expression of cytokines in control iAstrocytes, nor in sALS iAstrocytes (A and C). ADSCs induced the expression of IL-1 β in C9orf72 Pat183 iAstrocytes. (D) ADSCs induced expression of IL-6 in both SOD1 iAstrocyte patient cell lines. Data are presented as mean \pm SD, n=3, where each n consists of a different iAstrocyte culture preparation. Data were analysed with 1-way ANOVA followed by Sidak's multiple comparison test *p<0.05, **p<0.01.

As described for the analysis of cytokines, differences in gene expression for BDNF, GDNF and VEGF between control and ALS iAstrocytes were first investigated (figure 5.16). Compared to control iAstrocytes, the levels of BDNF expression were strongly increased in the C9orf72 patient cell lines and in the sALS Pat12 iAstrocytes (figure 5.16 A). BDNF expression was also slightly increased in sALS Pat17 iAstrocytes and in the SOD1 patient cell lines, although the difference was not statistically significant compared to controls (figure 5.16 A). GDNF expression was increased in the sALS Pat17 cell line and in the SOD1 Pat100 cell line in comparison to controls (figure 5.16 B). In the two C9orf72 iAstrocyte lines, BDNF expression was slightly decreased compared to controls, although the difference was not significant (figure 5.16 B). Interestingly, VEGF expression was reduced in all the iAstrocyte cell lines in comparison to the controls (figure 5.16 C).

Co-culture with ADSCs did not significantly modulate the expression of either BDNF, GDNF or VEGF in any of the iAstrocyte cell lines (figure 5.17).

In conclusion, the gene expression analysis for cytokines and growth factors in human iAstrocytes did not match with the gene expression data observed in mouse astrocytes. Moreover, ADSCs derived from mice did not have a detectable impact on modulating iAstrocyte gene expression as observed for the SOD1^{G93A} mouse astrocytes.

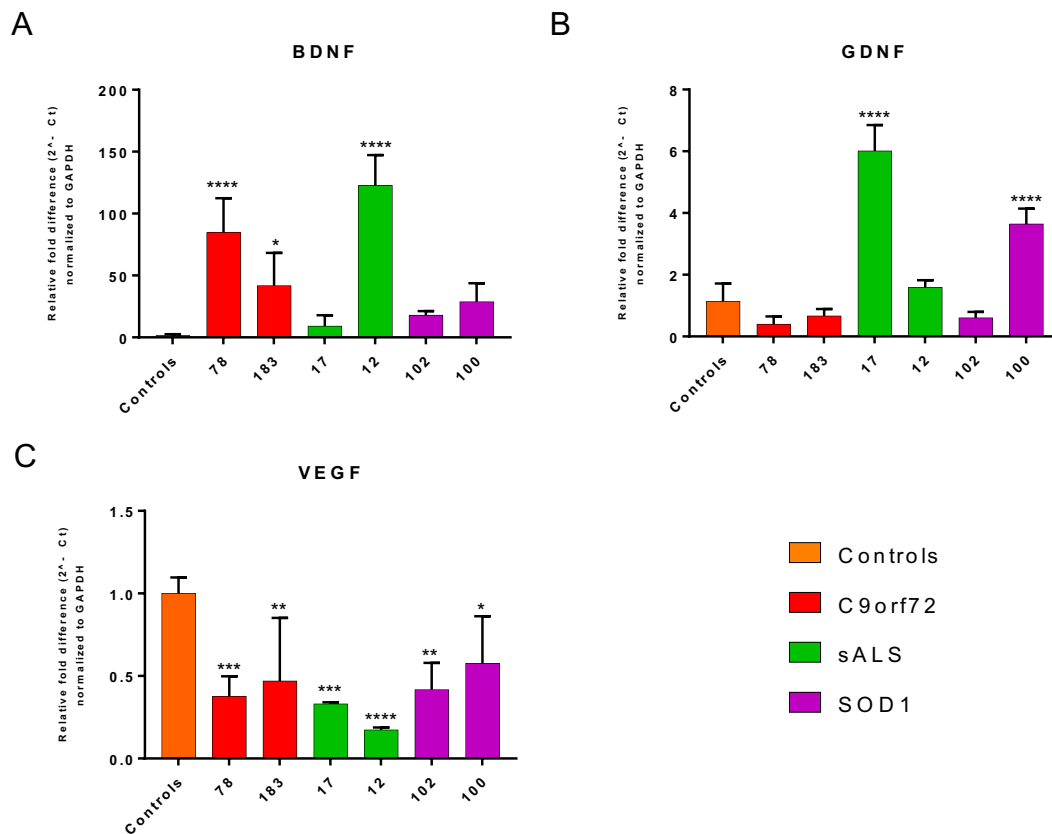


Figure 5.16. Gene expression of growth factors in iAstrocytes at basal levels. Gene expression was calculated relative to GAPDH expression and results normalized to control iAstrocytes. (A) BDNF expression was significantly increased in both C9orf72 iAstrocyte lines and in sALS Pat12 iAstrocytes. BDNF up-regulation in the SOD1 iAstrocyte cell lines did not reach statistical significance. (B) Compared to controls, GDNF expression was increased in sALS Pat17 and SOD1 Pat100 iAstrocytes. (C) Expression of VEGF was decreased in all ALS iAstrocyte lines compared to controls. Data are presented as mean \pm SD, n=3, where each n consists of a different iAstrocyte culture preparation. Data were analysed with 1-way ANOVA followed by Sidak's multiple comparisons *p<0.05, **p<0.01, ***p<0.001, ****p<0.0001.

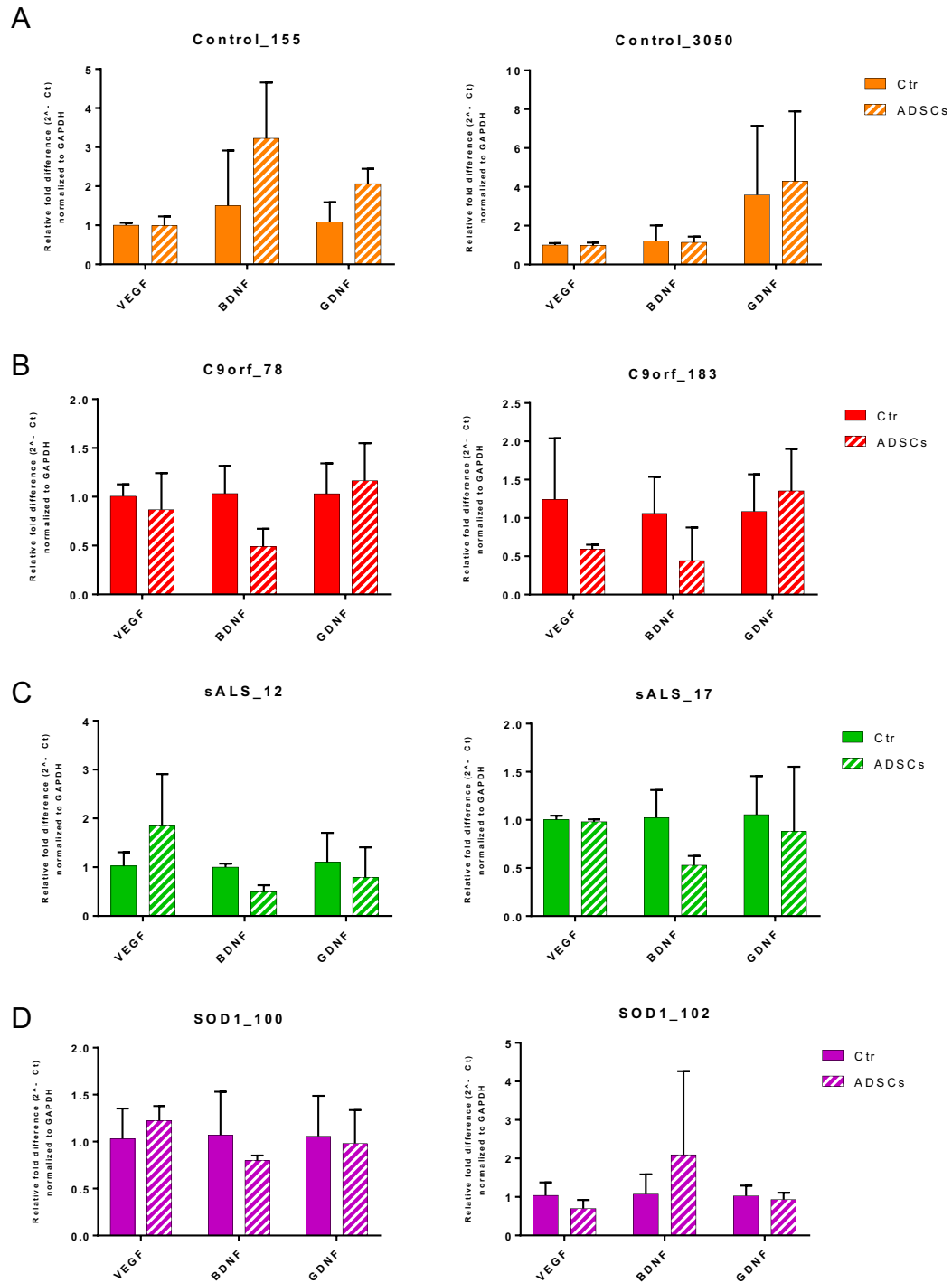


Figure 5.17. Gene expression of growth factors in iAstrocyte after co-culture with ADSCs. Gene expression was calculated relative to GAPDH expression and results normalized to untreated iAstrocytes. The presence of ADSCs did not significantly modulate growth factor expression in control iAstrocytes (A), C9orf72 iAstrocytes (B), sALS iAstrocytes (C) or SOD1 iAstrocytes (D). Data are presented as mean \pm SD, $n=3$, where each n consists of a different iAstrocyte culture preparation. Data were analysed with 1-way ANOVA followed by Sidak's multiple comparison test.

5.10 Discussion

The first aim of the work described in this chapter was to assess whether ADSCs, through paracrine mechanisms, could protect healthy MNs from SOD1^{G93A} mouse astrocyte toxicity *in vitro*. A separated triple co-culture assay to assess MN survival was designed and used. Viable MNs were identified by live imaging thanks to the expression of the GFP under control of the MN-specific promoter HB9. The separated co-culture system allowed ADSCs to be physically separated from a mixed astrocyte/MN co-culture, but able to exchange soluble factors. The second aim of the study focused on unraveling potential *in vitro* molecular mechanisms underpinning the neuroprotection. By using the separated co-culture method, the mutual modulation in growth factor expression and secretion between ADSCs and mouse astrocytes was investigated. Moreover, the paracrine effects of ADSCs on expression and secretion of pro-inflammatory mediators from SOD1^{G93A} astrocytes were investigated. Finally, the neuroprotective potential of ADSCs on a human cell model of disease by using iAstrocytes derived from ALS patients was evaluated. In particular, by using iAstrocytes derived from patients the therapeutic potential of ADSCs could be tested in both sporadic and familial ALS cases.

5.10.1 ADSCs protect MNs from SOD1^{G93A} mAstrocyte toxicity

Before performing the co-culture experiments, the purity of mAstrocytes was analyzed by flow cytometry staining for the astrocyte marker CD44 and the microglial marker CD11b. Since mAstrocytes were obtained by mild-trypsinization, it was fundamental to check for microglia contamination. Indeed, even the presence of a few microglia in the culture might be responsible for effects that would be erroneously attributed to astrocytes (Saura, 2007). Notably, microglial contamination was found to be minimal representing less than 0.5% in all the preparations.

Without the presence of ADSCs, mAstrocytes isolated from the cortex of symptomatic SOD1^{G93A} mice displayed MN toxicity as evidenced by a significant reduction in MN viability after 7 days in culture when compared to MN survival in NTg mAstrocyte co-cultures. These data are in agreement with previous studies in which astrocytes derived from either the cortex or the spinal cord of murine models of ALS were less-supportive and/or selectively detrimental to healthy MNs in culture (Ferraiuolo et al., 2011, Di Giorgio et al., 2008, Kia et al., 2018). Notably, ADSCs had a substantial positive impact on MN survival in the SOD1^{G93A} astrocyte co-cultures, with the number of viable MNs at the end of the culture exceeding the number of MNs that survived in untreated NTg cultures. Moreover, since ADSCs slightly promoted MN survival in NTg

astrocytic cultures, the protective effect on MNs seen in the astrocyte/MN mixed culture may be attributed to the capacity of ADSCs to both directly support MN through the release of neurotrophic factors, and indirectly by affecting astrocytic functions. Previous studies showed that conditioned medium from MSCs protected MNs against mechanical, oxidative and apoptotic stress *in vitro* (Sun et al., 2013, Rajan et al., 2017, Kim et al., 2014b). However, in these studies application of external stimuli such as treatment with H₂O₂, staurosporine or manual scratch were necessary in order to induce MN damage. In the present study, through the secretion of soluble factors, ADSCs were able to protect motor neurons from intrinsic SOD1^{G93A} astrocyte toxicity. Thus, for the first time the neuroprotective potential of ADSCs has been demonstrated by adopting an *in vitro* system that more closely recapitulates the ALS environment.

5.10.2 Expression and secretion of growth factors in ADSCs is modulated by SOD1^{G93A} astrocytes

One of the proposed mechanisms by which ADSCs exert neuroprotection is related to the capacity of these cells to secrete several growth factors which can potentially protect MNs both directly and indirectly (Baloh et al., 2018). Moreover, there is evidence that MSCs have the ability to “activate” and respond differently according to the external stimuli they are exposed to (Chen et al., 2015a, Nicaise et al., 2011). For example, growth factor expression in rat BM-MSCs was shown to be differentially regulated following exposure to brain and spinal cord extracts obtained from NTg or SOD1^{G93A} rats (Nicaise et al., 2011).

The transcript expression levels of growth factors with neuroprotective potential such as VEGF, IGF-1, FGF-2 and HGF in ADSCs were first confirmed by qPCR. Then we evaluated whether co-culture with SOD1^{G93A} or NTg astrocytes could affect the expression levels of these growth factors. Interestingly, compared to unstimulated ADSC mono-cultures, the expression of VEGF, IGF-1, FGF-2 and HGF was altered following co-culture with either NTg or SOD1^{G93A} astrocytes, confirming that ADSCs can modulate their own growth factor expression in response to changes in the microenvironment. Notably, compared to stimulation with NTg astrocytes, ADSC expression of VEGF, IGF-1 and FGF-2 was significantly increased following co-culture with SOD1^{G93A} astrocytes. On the contrary, expression of HGF was increased only when ADSCs were stimulated with NTg astrocytes. These data are in part in line with a previous study that investigated the capacity of human ADSCs to modulate SOD1^{G93A} astrocyte functions *in vitro*. In this study, human ADSCs induced an

increase in the expression levels of VEGF, HGF and IGF-1 following co-culture with postnatal spinal cord SOD1^{G93A} astrocytes, compared to control NTg astrocytes (Gu et al., 2010). These data were further confirmed at the protein level by measuring growth factor concentration in culture supernatants (Gu et al., 2010). However, protein concentrations were measured in the supernatant from mixed astrocyte/ADSC co-cultures, thus without taking into account the contribution of astrocytes, which as shown in our study, secrete both VEGF and IGF-1 with considerable differences depending on the genotype. Here, the gene expression data was confirmed by measuring the protein levels of VEGF and IGF-1 in culture supernatants of ADSCs cultured alone for 24 hours following pretreatment with NTg and SOD1^{G93A} astrocytes.

At basal levels, secretion of VEGF by ADSCs was relatively high. In addition, the release of VEGF consistently increased after ADSCs were exposed to SOD1^{G93A} astrocytes. VEGF is a potent neurotrophic factor which has been shown to protect MNs from hypoxia, oxidative insult and glutamate-excitotoxicity both *in vivo* and *in vitro* experimental models (Lladó et al., 2013). It has also been proposed that VEGF can indirectly protect MNs by enhancing neurotrophic factor secretion from astrocytes (Bogaert et al., 2006). Moreover, strategies to enhance VEGF concentration in brain, spinal cord or muscle of SOD1^{G93A} mice improved motor performance, slowed down disease progression and extended life span through motor neuron protection, preservation of NMJ and reduction of microgliosis (Azzouz et al., 2004, Storkebaum et al., 2005, Dodge et al., 2010, Wang et al., 2016). Thus, the secretion of VEGF from ADSCs could have had a great impact on MN survival in our experiments.

Similar to VEGF, analysis of IGF-1 content by ELISA confirmed the qPCR data, in which SOD1^{G93A} astrocytes induced ADSCs to secrete enhanced levels of IGF-1 compared to control NTg astrocytes or unstimulated ADSCs. IGF-1 is another potent growth factor that has been shown to directly support MN survival by protecting against glutamate excitotoxicity and oxidative stress in both *in vivo* and *in vitro* models of neurodegeneration (Henriques et al., 2010). IGF-1 also reduces neuroinflammation by inhibiting astrocyte activation and by promoting a neuroprotective phenotype in microglia *in vitro* (Bellini et al., 2011). Recently, it has been shown that IGF-1 has anti-inflammatory properties in primary LPS-stimulated astrocytes probably mediated by activation of Notch signaling following the inhibition of the classical NF-κB pathway (Acáz-Fonseca et al., 2019). In addition, gene therapy strategies aimed to deliver IGF-1 in SOD1^{G93A} mice protected MNs and reduced astroglial activation, resulting in improved motor performance and prolonged survival compared to placebo (Kaspar

et al., 2003, Dodge et al., 2008, Hu et al., 2018, Wang et al., 2018b, Wang et al., 2018a). Very recently, IGF-1 was shown to protect mitochondria in both *in vivo* and *in vitro* models of ALS (Wen et al., 2019). Also, IGF-1 reduced inflammation in the sciatic nerve of SOD1^{G93A} mice by inhibiting macrophage invasion and reducing local levels of TNF- α (Ji et al., 2018).

It is noteworthy that, amongst several growth factors secreted by ADSCs, VEGF and IGF-1 showed the greatest capacity to ameliorate neuronal cell death *in vitro* (Kim et al., 2014b). The secretion of large amounts of VEGF and IGF-1 from our ADSCs, especially following stimulation with SOD1^{G93A} astrocytes, could have contributed significantly to the therapeutic effects observed in the SOD1^{G93A} mice and to the motor neuron protection documented in our *in vitro* ALS model. However, we do not have direct evidence showing that IGF-1 and VEGF released by ADSCs are responsible for the reduced MN death observed in our triple co-culture system. The use of neutralizing antibodies against VEGF and IGF-1 during the co-culture assay may allow this question to be addressed. Alternatively, expression of VEGF and IGF-1 by ADSCs could be silenced by short hairpin RNAs (shRNA) to test whether the neuroprotective properties of ADSCs are affected by the absence of these growth factors.

5.10.3 ADSCs modulate the expression and secretion of neurotrophic factors in mAstrocytes

In addition to the uninterrupted secretion of growth factors, previous evidence suggested that MSCs have the capacity to modulate the astrocytic expression of growth factors (Sun et al., 2013). Astrocyte secretion of growth factors is of considerable importance in both neurophysiology and in response to neuronal damage (Cabezas et al., 2016). Also, there is evidence suggesting that the synthesis and secretion of neurotrophic factors may be impaired in ALS (Harandi et al., 2014). Thus, the modulatory potential of ADSCs on the expression and secretion of growth factors in NTg and SOD1^{G93A} mAstrocytes following separated co-culture was evaluated by means of qPCR and ELISA respectively.

We first focused on the expression of BDNF and GDNF, which are considered “classic” neurotrophic factors known to be secreted from astrocytes. In our cultures, SOD1^{G93A} adult astrocytes expressed significantly lower levels of GDNF compared to NTg astrocytes, and GDNF expression was significantly increased following co-culture with ADSCs. GDNF is a potent protective factor for spinal motor neurons and strategies to enhance CNS concentrations showed encouraging results in both *in vivo*

and *in vitro* neurodegenerative models (Henriques et al., 2010). To the best of our knowledge, this is the first time that cortical SOD1^{G93A} astrocytes displayed impairment of GDNF expression. However, astrocytes derived from SOD1^{G93A} rats showed a senescent phenotype characterized by reduced motor neuron support *in vitro*, which could be improved by addition of exogenous GDNF (Das and Svendsen, 2015). Although the expression and secretion of GDNF from rat SOD1^{G93A} astrocytes was not directly measured, it is noteworthy that GDNF levels in astrocytes decrease with aging (Das and Svendsen, 2015). In addition, stimulation of healthy wild-type rat astrocytes with CSF from ALS patients reduced the expression of GDNF when compared to astrocytes exposed to CSF from healthy donors, indicating that GDNF expression in ALS astrocytes may be impaired (Ouali Alami et al., 2018). Intriguingly, increased levels of GDNF were found in the CSF and spinal cord post-mortem tissue from ALS cases in comparison to healthy controls (Ekester, 2004). Increased levels of GDNF were also found in SOD1^{G93A} mice over the course of the disease, indicating that GDNF production may be a protective response in ALS as seen for example following spinal cord ischemia (Tovar-Y-Romo et al., 2014). Indeed, disruption of the astrocytic TNFR1-GDNF axis in SOD1^{G93A} mice, caused acceleration of disease progression (Brambilla et al., 2016). The increased expression of GDNF in SOD1^{G93A} astrocytes following co-culture with ADSCs is in line with previous studies (Sun et al., 2013, Marconi et al., 2013). In Sun et al, treatment of neonatal SOD1^{G93A} astrocytes with human BM-MSCs conditioned medium, resulted in a significant increase in GDNF expression at mRNA level (Sun et al., 2013). Moreover, intravenous injection of mADSCs in SOD1^{G93A} mice resulted in a higher concentration of GDNF in spinal cord tissue. Since mADSCs did not secrete GDNF *in vitro*, the authors proposed that transplantation of ADSCs might have influenced the astrocytic secretome (Marconi et al., 2013). Interestingly, NTg astrocytes treated with ADSCs showed a significant reduction in the expression of GDNF, the reasons for which are unknown.

Although analysis of BDNF gene expression did not show differences between NTg and SOD1^{G93A} astrocytes, ADSC treatment resulted in increased expression of this growth factor in mutant astrocytes. Unlike GDNF, strategies aimed to increase BDNF concentration in SOD1^{G93A} mice did not result in behavioural improvements (Tovar-Y-Romo et al., 2014). Moreover, levels of BDNF were found unaltered in muscle biopsies and CSF of ALS patients compared to healthy controls, indicating that BDNF may not be relevant in motor neuron degeneration (Ekester, 2004). In addition, although BDNF has been shown to protect against excitotoxicity *in vivo*, other studies have suggested that, through the p75 receptor, BDNF could activate the pro-apoptotic

pathway (Henriques et al., 2010). Thus, it is unclear whether the up-regulation of BDNF seen in SOD1^{G93A} astrocytes following stimulation with ADSCs may have provided neuroprotection.

Besides “classic” neurotrophic factors, astrocytes can also secrete other potent neuroprotective growth factors such as VEGF and IGF-1. We evaluated their expression and secretion in mouse astrocytes both at basal levels and following co-culture with ADSCs.

At mRNA level, SOD1^{G93A} astrocytes showed a slight increase in the expression of VEGF which was significantly enhanced following co-culture with ADSCs. Secretion of VEGF was then measured in the culture supernatant by ELISA assay. Interestingly, in the absence of ADSCs, SOD1^{G93A} astrocytes secreted significantly more VEGF than NTg astrocytes. Although dysregulation in VEGF signaling may be relevant in ALS, conflicting data about the concentration in CSF, plasma and serum of ALS patients have been reported (Pronto-Laborinho et al., 2014, Just et al., 2007). Some studies described reduced or unaltered VEGF levels in the plasma and serum of ALS patients compared to healthy controls (Lambrechts et al., 2009, Just et al., 2007, Nygren et al., 2002), while others reported increased concentration of this growth factor (Nygren et al., 2002, Ilzecka, 2004, Gupta et al., 2011, Gao et al., 2014a). Moreover, Brockington et al. showed that expression of VEGF and VEGFR-2 in the spinal cord of ALS patients was reduced compared to controls (Brockington et al., 2006). In line with the hypothesis that VEGF may be protective in ALS, high levels of VEGF in the CSF of ALS patients inversely correlated with disease progression rate and disease duration (Gupta et al., 2011, Ilzecka, 2004, Gao et al., 2014a). Similarly, studies investigating the role of VEGF in SOD1^{G93A} mice also reported conflicting results. Murakami et al. showed elevated levels of VEGF in the spinal cord of both pre-symptomatic and symptomatic SOD1^{G93A} mice compared to NTg mice (Murakami et al., 2003). In contrast, Van Den Bosch *et al.* did not find differences between SOD1^{G93A} and control NTg mice in VEGF concentration in the spinal cord (Van Den Bosch et al., 2004). Finally, Lu *et al.*, reported down-regulation of VEGF expression in the spinal cord of SOD1^{G93A} mice, the levels of which further reduced during disease progression (Lu et al., 2007). Of interest, VEGF expression in the brain of ALS mice was found unaltered compared to control NTg mice (Lu et al., 2007). To the best of our knowledge, this is the first study to report increased secretion of VEGF from SOD1^{G93A} cortical astrocytes compared to control NTg cortical astrocytes. It is well known that in other neurological conditions or in the presence of pro-inflammatory cytokines, activated astrocytes increase the expression of VEGF as a protective

response (Lladó et al., 2013). However, whether the increase in VEGF secretion seen in our SOD1^{G93A} astrocytes is a response to brain inflammation in symptomatic SOD1^{G93A} mice or it is merely due to an *in vitro* artifact is unclear.

In contrast to the qPCR data, treatment with ADSCs did not show a significant increase in VEGF protein secretion from SOD1^{G93A} astrocytes. However, an increase in mRNA expression does not always necessarily translate into increased production and secretion of proteins. VEGF secretion is finely regulated by post-transcriptional events at several levels such as mRNA stabilization, translation and cellular localization (Yoo et al., 2006). In addition, VEGF concentration was quantified only after 24 hours of culture, which may not have been enough time to allow protein build-up in culture supernatants, and so to detect an increase in VEGF secretion. On the other hand, in line with the qPCR data, secretion of VEGF from NTg astrocytes was significantly increased following co-culture with ADSCs. However, since at basal levels NTg astrocytes secreted much less VEGF than SOD1^{G93A} astrocytes, 24 hours might have been long enough for the detection of an increase in protein release.

qPCR analysis showed that SOD1^{G93A} astrocytes express reduced levels of IGF-1 compared to NTg astrocytes. This reduction was confirmed at the protein level, indicating that IGF-1 regulation and secretion is impaired in our SOD1^{G93A} astrocyte cultures. Notably, the presence of ADSCs induced up-regulation of IGF-1 expression both at the transcriptional and the protein level in SOD1^{G93A} astrocytes. However, the amount of IGF-1 released did not equate to the levels of secretion documented in NTg astrocytes. IGF-1 is considered a potent agent with both neuroprotective and anti-inflammatory properties, and impairment in IGF-1 signaling have been associated with neurodegenerative conditions (Labandeira-Garcia et al., 2017). It has been previously reported that microglia obtained from SOD1^{G93A} mice have reduced ability to secrete IGF-1 when stimulated with LPS, indicating that increased levels of pro-inflammatory cytokines during chronic inflammation may inhibit the expression and release of IGF-1 (Zhao et al., 2006). Impairment of IGF-1 secretion from ALS astrocytes has not been previously reported and this is the first study showing that reduced secretion levels of IGF-1 from SOD1^{G93A} astrocytes was partially restored by ADSC treatment. Whether IGF-1 concentrations in spinal cord and blood of ALS patients are impaired remains controversial. Some studies showed unaltered levels of IGF-1 in the spinal cord and serum of ALS patients when compared to healthy controls (Ekestern, 2004). On the contrary, others reported elevated IGF-1 serum levels and increased spinal cord IGF-1 immunoreactivity in ALS cases compared to controls (Henriques et al., 2010). In SOD1^{G93A} mice, IGF-1 expression was found

elevated in the spinal cord compared to NTg mice, indicating that increasing IGF-1 levels might be a protective response as observed in other brain injury models (Marconi et al., 2013, Sironi et al., 2017, Sakowski et al., 2009). However, increased expression of the IGF-1 receptor in reactive astrocytes, and elevated immunoreactivity to IGF binding proteins in SOD1^{G93A} mice, may suggest the development of mechanisms of resistance and thus decreased responsiveness to IGF-1, which in turn would aggravate disease progression during chronic neuroinflammation (Sakowski et al., 2009, Labandeira-Garcia et al., 2017).

Taken together, our data showed that ADSCs are able to modify the expression of growth factors in SOD1^{G93A} astrocytes both at transcriptional and protein level, where direct cell contact is not necessary. Although the underlying molecular mechanisms responsible for this modulation remain unknown, our data suggest that regulation of trophic factor production in SOD1^{G93A} astrocytes may contribute to the neuroprotective effects observed both *in vivo* and *in vitro*.

5.10.4 ADSCs reduce the inflammatory signature of SOD1^{G93A} astrocytes

ALS astrocytes are known to contribute to inflammation-mediated neurotoxicity through the secretion of pro-inflammatory mediators, and MSCs demonstrated the ability to attenuate the inflammatory response in activated microglia, dendritic cells and pro-inflammatory Th1 and Th17 cells *in vitro*. We therefore explored whether ADSCs could modify the inflammatory signature of SOD1^{G93A} astrocytes. We analyzed the expression and secretion of pro-inflammatory mediators from SOD1^{G93A} astrocytes and NTg astrocytes under basal conditions and following separated co-culture with ADSCs. We chose to analyze levels of the cytokines IL-6, TNF- α and IL-1 β and the chemokine MCP-1 since they are known to be secreted from astrocytes and they have been linked to the pathological microenvironment in ALS.

Compared to NTg cultures, SOD1^{G93A} astrocytes showed up-regulation of IL-6, TNF- α and MCP-1 both at transcriptional and protein levels. As described in the general introduction chapter, elevated concentrations of these pro-inflammatory mediators have been found in biological samples obtained from ALS patients and also in animal models of the disease. In a previous study it has been shown that following LPS stimulation, astrocytes derived from pre-symptomatic (1-2 days old) SOD1^{G93A} mice, had enhanced mRNA levels of inflammatory cytokines such as TNF- α , IL-6 and COX-2 compared to stimulated Ntg astrocytes (Sun et al., 2013). However, gene expression analysis under basal conditions without an inflammatory stimulus, did not reveal differences in the levels of pro-inflammatory cytokines between SOD1^{G93A} and

Ntg astrocytes (Sun et al., 2013). The difference with this study might be due to the fact that the neonatal SOD1^{G93A} astrocytes used in Sun et al. had not yet been exposed to an inflammatory environment *in vivo*, thus being unable to reproduce the pro-inflammatory phenotype of adult SOD1^{G93A} astrocytes used in our study. This hypothesis is supported by the evidence that astrocytes derived from neonatal SOD1^{G93A} mice do not express genes known to be characteristic of reactive astrocytes in contrast to findings documented in astrocytes derived from adult symptomatic SOD1^{G93A} mice (Tripathi et al., 2017). Moreover, the transition from a neuroprotective phenotype during the pre-symptomatic phase to a reactive neurotoxic phenotype during disease progression is accompanied by changes in astrocyte gene expression in SOD1^{G93A} mice (Ouali Alami et al., 2018).

IL-1 β expression was increased in SOD1^{G93A} astrocytes at transcriptional level, but no difference in protein secretion was observed. This could be the result of post-transcriptional modification events. IL-1 β is synthesized as a precursor protein, pro-IL-1 β , which is then cleaved by the inflammasome through activation of caspase-1 (Zhu and Kanneganti, 2017). How the inflammasome regulates the maturation of pro-IL-1 β and thus the secretion of bioactive IL-1 β , is not fully understood. However, expression of pro-IL-1 β and activation of the inflammasome may be regulated by separate mechanisms (Gallagher-Beckley et al., 2013). Also, IL-1 β secretion was measured after 24 hours of culture which may not have been long enough to allow the build-up of the mature cytokine in the supernatant.

Remarkably, through paracrine mechanisms ADSCs were able to significantly reduce the expression of IL-6, TNF- α , IL-1 β and MCP-1 in SOD1^{G93A} astrocytes. Previous findings showed that treatment of adult healthy LPS-stimulated astrocytes and neonatal SOD1^{G93A} LPS-stimulated astrocytes with BM-MSCs conditioned media reduced the expression of pro-inflammatory genes. However, these data were not confirmed at the protein level (Sun et al., 2013, Schafer et al., 2012). Here, for the first time, we showed that ADSCs were able to significantly reduce both the expression and secretion of pro-inflammatory mediators in adult SOD1^{G93A} astrocytes, where LPS treatment was not necessary to induce a pro-inflammatory phenotype. Importantly, this is the first report showing the capacity of ADSCs to reduce secretion levels of MCP-1 in transgenic SOD1^{G93A} astrocytes. Interestingly, in the Oh et al. 2018 phase 2 clinical trial investigating the safety and effect of two intrathecal BM-MSCs injections in patients with ALS, cytokine measurements in CSF showed that MSC injection significantly reduced the levels of TNF- α and MCP-1 (Oh et al., 2018). Moreover, post-hoc analysis revealed a positive correlation between

decreased MCP-1 levels in CSF and good responsiveness to the therapy, defined by a reduction in the absolute ALSFRS-R decline after 4- and 6-month follow-up, in comparison to the control group (Oh et al., 2018). Interestingly, this study found elevated levels of IL-6 in CSF of patient treated with MSCs. However, post-hoc analysis showed that increased expression of IL-6 was characteristic of the poor-responder subgroup (Oh et al., 2018).

Taken together, our data reinforce the concept that one of the mechanisms contributing to the therapeutic effects of ADSCs in ALS models is mediated through immunosuppression not only of peripheral immune cells and resident microglia but also of astrocytes, which contribute to inflammation-mediated neurotoxicity through the production and secretion of high concentrations of potent pro-inflammatory neurotoxic factors. Moreover, given the constant interaction of astrocytes with microglia and the important interplay between these two cell populations in mediating the neuroinflammatory response in ALS, the manipulation of the astrocytic pro-inflammatory signature by ADSCs *in vivo*, may potentially amplify the anti-inflammatory effects by indirectly promoting a neuroprotective phenotype in reactive microglia.

Interestingly, NTg astrocytes responded differently to the presence of ADSCs. Indeed, ADSC treatment in NTg astrocytes resulted in a slight reduction in IL-6 and IL-1 β secretion, while the secretion levels of MCP-1 and TNF- α were not altered. These data highlight the capacity of astrocytes to respond differently to the MSC secretome. This response is dependent on both the activation state and on the genetic background of the astrocytes (Sun et al., 2013, Schafer et al., 2012).

5.10.5 ADSCs protect MNs from human ALS iAstrocyte toxicity

As described in the introduction section of this chapter, there is an urgent need to test whether therapeutic strategies that show positive effects in SOD1-linked ALS murine models could be translated into the human disease which is mostly sporadic in origin. Moreover, since abnormalities in the C9orf72 hexanucleotide repeat expansion account for approximately 40% of fALS and 7% of sALS it is important to investigate therapeutic approaches in C9orf72 models (Renton et al., 2014).

We tested the capacity of ADSCs to protect healthy murine HB9-GFP-MNs from cell death induced by iAstrocytes derived from ALS patients with either sporadic or familial disease caused by mutations in the C9orf72 repeat expansion or in the SOD1 gene. As already mentioned, the use of iAstrocytes represents a reproducible and unique *in vitro* model to study the human disease and to screen for therapeutic approaches

in both sALS and fALS (Meyer et al., 2014). More importantly, given the high genetic and clinical heterogeneity of ALS, the MN survival screening method adopted in our study enables the investigation of efficacy and responses to therapeutic agents in patient subpopulations, establishing a so called “in vitro clinical trial” and opening the doors for a personalized medicine approach in ALS (Li et al., 2015, Grskovic et al., 2011, Kim and Lee, 2013).

After 3 days of co-culture, compared to control iAstrocytes derived from healthy donors, iAstrocytes derived from ALS patients with either sporadic or familial disease induced an increase of about 30-50% in MN death which is similar to what was reported previously (Meyer et al., 2014, Varcianna et al., 2019, Allen et al., 2019). Remarkably, through paracrine activity, ADSCs reduced MN death in both sporadic, C9Orf72 and SOD1 iAstrocytes. However, the level of MN protection was patient specific. In particular, ADSC treatment restored MN survival in sALS Pat12 iAstrocytes, while it had no significant effect in the sALS Pat17 cell line. Similarly, in the SOD1 Pat102 iAstrocyte line MN survival was completely rescued in the presence of ADSCs, while in the SOD1 Pat100 cell line MN survival was not significantly improved compared to untreated iAstrocytes. However, MN survival in ADSCs-treated SOD1 Pat100 iAstrocytes was not different from survival in untreated control astrocytes, indicating that ADSCs had actually had a beneficial effect on MNs. Interestingly, the SOD1 iAstrocyte cell line Pat102, which positively responded to the ADSCs treatment, was derived from a pre-symptomatic donor (daughter of patient 100) which at the time of fibroblast collection did not present with clinical signs of ALS. Finally, ADSCs completely rescued MN survival in the C9orf72 Pat78 line, while only partially in the C9orf72 Pat183 cell line, although the latter iAstrocyte line displayed a really high level of MN toxicity.

Unfortunately, given the small sample size it is difficult to find a clinical correlation between good-responders and poor- or non-responders in our “*in vitro* clinical trial”. In addition, there were not essential differences in disease duration and thus disease aggressivity between sALS Pat17 and sALS Pat12 or between C9orf72 Pat78 and C9orf72 Pat183, thus hypothetically excluding correlations between disease severity and degree of MN protection by ADSCs in our co-culture system.

The lack of specific disease biomarkers makes the identification of the mechanisms of protection in patient cell lines that positively responded to the presence of ADSCs even more complicated. However, this diverges from the main aim of this study, in which we wanted to demonstrate the potential therapeutic translational of ADSCs in

human disease as a proof of concept. The main finding of our experiments is that, for the first time, the therapeutic potential of ADSCs was extended to a human ALS *in vitro* model, showing that potentially, and considering all the limitations of artificial models, the use of ADSCs as a cell therapy approach could have a positive effect in both sporadic and familial ALS characterized by genetic mutation in either the SOD1 or C9orf72 genes. Moreover, by pretreating SOD1 Pat102 iAstrocytes with ADSCs before starting the co-culture with MNs, we showed that ADSCs are able to reduce MN death by directly reducing the iAstrocyte toxicity.

Finally, our findings highlight the importance of controlling for clinical and genetic heterogeneity in clinical trial enrolment, the need for patient stratification methods when evaluating therapies, and the inclusion of post-hoc analysis in ALS clinical trials. Indeed, therapies that may have a positive effect in specific patient subgroups may be masked during analysis of overall clinical trials outcomes. Additional co-culture experiments using more iAstrocytes cell lines, and further investigation of the specific molecular mechanisms of protection of ADSCs, might be useful in the identification of such stratification markers.

5.10.6 Gene expression of cytokines and growth factors in iAstrocytes: differences with murine SOD1^{G93A} astrocytes

Based on the evidence that ADSCs were able to protect MNs from human ALS iAstrocyte toxicity similarly to what was found with the mouse astrocyte *in vitro* model, we investigated whether the gene expression pattern for cytokines and growth factors with or without the presence of ADSCs found in the SOD1^{G93A} mAstrocytes could be validated in the human iAstrocyte model. This would have also been an opportunity to potentially identify markers in responders and non-responders iAstrocyte patient cell lines.

Intriguingly, gene expression analysis of pro-inflammatory cytokines and growth factors revealed conflicting data between mouse and human astrocytes. Moreover, the high variability in gene expression observed among biological replicates in the human model hampered the detection of statistically significant differences between untreated and ADSC-treated iAstrocytes. Also, a clear correlation between the gene expression profile of patient cell lines and responsiveness to ADSC treatment was not found. But again, this may be explained by the limited sample size and also the limited amount of genes that were analysed.

In relation to the inflammatory phenotype of ALS iAstrocytes, under basal conditions expression of TNF- α at the transcript level was decreased in all the ALS iAstrocyte

cell line compared to control iAstrocytes; IL-6 was increased only in the sALS iAstrocyte lines; while IL-1 β was increased in the SOD1 Pat100 line and decreased in the C9orf72 Pat183 line. Although these results might seem surprising, there are several reasons that could explain the differences found between mouse and human astrocytes. First of all, the qPCR data will need to be confirmed at the protein level, which could differ significantly from gene expression. Second, although about 90% of genes are in common between mouse and human astrocytes, the cells differ considerably in cell behaviour and gene expression in culture (Zhang et al., 2016). For instance, human and mouse astrocytes responded differently to glutamate stimulation and immune activation *in vitro* (Zhang et al., 2016, Tarassishin et al., 2014). Moreover, there are several subtypes of astrocytes that differ in phenotype and functions depending on, for example, the anatomical region of origin (Molofsky and Deneen, 2015). While with primary cultures obtained from animal models there is the opportunity to isolate subpopulations of astrocytes from a specific anatomical region, the protocol adopted in this study to obtain human iAstrocytes does not allow the derivation of specific astrocytes subpopulations (Chandrasekaran et al., 2016). Thus, the differences in the transcriptomic profile might be linked to a difference in regional heterogeneity between mouse cortical astrocytes and human iAstrocytes.

In addition, iAstrocytes were derived from skin fibroblasts, which had never been exposed to the ALS neuroinflammatory microenvironment *in vivo*, and similar to astrocytes derived from neonatal SOD1^{G93A} mice, iAstrocytes would perhaps need an external stimulus such as for example the presence of MNs to display the transcriptomic profile of reactive astrocytes. It would be interesting to expose the iAstrocytes to LPS or pro-inflammatory cytokines and repeat the gene expression analysis. This would reveal whether the iAstrocytes derived from ALS patients respond differently to an inflammatory stimulus when compared to control healthy iAstrocytes. Finally, the high variability in gene expression found amongst different patient cell lines, and even amongst lines with the same mutated gene is not surprising, given human genetic variation, and probably, variation related to the different stage of disease at the time of fibroblast collection.

ADSCs did not show the ability to extensively modulate the expression of cytokines in iAstrocytes. Nevertheless, the modulatory effect was in the opposite direction to that observed in the mouse astrocytes. Indeed, instead of inhibiting expression of pro-inflammatory cytokines, ADSCs induced the expression of IL-6 in the two sALS iAstrocyte lines and increased the levels of IL-1 β in the C9orf72 Pat183 astrocyte line.

This might be explained by species incompatibility, with mouse-specific soluble factors that may have induced a pro-inflammatory response in human astrocytes.

Similarly, in contrast to the mouse astrocyte data, compared to control iAstrocytes VEGF expression in all the ALS iAstrocyte lines was reduced, BDNF expression increased and GDNF levels were unaltered or increased in patient iAstrocytes. Moreover, mouse ADSCs were not able to significantly modulate the expression of any of the tested growth factors in any of the iAstrocyte cell lines. Again, it is important to bear in mind that analysis of the expression of these factors at the protein level was not performed.

The fact that ADSCs were unable to affect the expression of pro-inflammatory cytokines and growth factors in iAstrocytes, but still able to protect MNs, suggests that the mechanisms of protection in the human model are in part different from the ones observed in the murine model. However, at the same time we do not have direct evidence that the modulation of inflammatory cytokines and growth factors in the SOD1^{G93A} mouse astrocytes by ADSCs is entirely responsible for the MN protection observed in our *in vitro* model. These data, together with the fact that ADSCs were able to increase MN survival in the control iAstrocyte co-cultures and that the presence of ADSCs in MN mono-cultures slightly improved the survival, is suggestive of a direct mechanisms of protection limited to the provision of growth factor to the MNs. However, when iAstrocytes (SOD1 Pat102) were pretreated for 48 hours with ADSCs before being co-cultured with MNs, the level of MN protection was comparable to the level seen when ADSCs were present during the entire co-culture period. This experiment demonstrated that the increase in MN survival observed in the presence of ADSCs in the human co-cultures might not be exclusively associated with direct trophic support to MNs, but that ADSCs are able to affect and modify iAstrocyte functions. Further studies investigating molecular mechanisms of action of ADSCs on iAstrocytes are essential. For example, RNA-sequencing or microarray analysis on iAstrocytes co-cultured in the presence or not of ADSCs, would potentially enable the identification of affected molecular pathways that can be corrected by ADSCs. However, the use of ADSCs derived from humans would be more relevant compared to the use of murine ADSCs in investigating molecular mechanisms of action of these cells in human ALS iAstrocytes, so avoiding misinterpretation of data due to cross-species incompatibility.

5.11 Conclusions

Based on the evidence from the *in vivo* therapeutic study (Chapter 3) and the hypothesis that the potential benefit of ADSC therapy resides in the capacity of these cells to release multiple bioactive soluble molecules, able in turn to modify the toxic microenvironment in ALS, the main aim of the work described in this chapter was to investigate whether through paracrine mechanisms ADSCs could protect MNs from SOD1^{G93A} adult astrocytes which display toxicity *in vitro*. Although the specific factors or mechanisms by which SOD1^{G93A} astrocytes kill MNs are not fully understood, the use of astrocyte-based cell models provided a unique opportunity to study the non-cell autonomous degeneration processes in ALS, and more importantly it provided a tool for the development of drug screening methods. In addition, extensive gene expression studies using the SOD1^{G93A} murine model, showed an extraordinary overlap between astrocytes co-cultured with MNs and *in vivo* spinal cord tissue, thus validating the co-culture model (Phatnani et al., 2013). By designing a separated co-culture system integrated with the astrocyte/MN mixed co-culture model, we first validated our hypothesis that ADSCs can promote MN survival in the SOD1^{G93A} murine model of ALS, without the need of physical cell contact between the stem cells and the neuronal/glial cell populations. This in part explains the beneficial effects observed following intrathecal cell transplantation in SOD1^{G93A} mice where the ADSCs did not migrate into the CNS parenchyma. We also provided evidence that ADSCs can positively modulate astrocytic functions by reducing the pro-inflammatory signature and increasing the neurotrophic properties of SOD1^{G93A} astrocytes. Moreover, we confirmed that SOD1^{G93A} astrocytes can potentiate the production of growth factor in ADSCs which can be considered as a protective response of these cells to the ALS toxic microenvironment. Finally, by using iAstrocytes derived from ALS patients we demonstrated for the first time potential therapeutic translation of ADSCs into the human disease, showing that as a proof-of-concept these cells may be neuroprotective in both sporadic and familial ALS, regardless of the genetic mutation.

Nonetheless, the specific molecular mechanisms by which ADSCs protect MNs from ALS-linked astrocyte toxicity remain elusive and further investigation focused on how these cells modify astrocytic functions, together with the identification of the secreted molecules that are responsible for their modulatory capacity is still needed.

6 CCR2 overexpression in human Adipose Derived Stem Cells (hADSCs)

6.1 Introduction

The work described in this chapter was carried out in Professor Jun Xu's laboratory in the Department of Regenerative Medicine at Tongji University (Shanghai, China).

In the first part of the chapter, the phenotypic and functional characterization of human ADSCs (hADSCs) isolated after processing a liposuction aspirate sample which was previously obtained from a healthy donor volunteer, is presented.

As already described, one limitation of cell therapy in ALS is represented by the limited capacity of MSCs to migrate into the spinal cord parenchyma when the cells are injected either intravenously or intrathecally. MSCs express several chemokine receptors and homing properties similar to those of immune cells such as lymphocytes and monocytes which allow them to migrate into damaged or inflamed tissues. However, donor age and the number of passages in culture were shown to negatively influence expression of homing factors on stem cells (Zhang et al., 2017). For example, it has been shown that at early passage, cultures of BM-MSCs express high levels of chemokine receptors such as CXCR4, CXCR5, CCR1 and CCR7. However, during *ex vivo* expansion, BM-MSCs gradually lose expression of these chemokine receptors, and after 12-16 passages in culture the cells are not able to respond or migrate towards chemokine gradients *in vitro* (Honczarenko et al., 2006). Other studies showed that compared to freshly isolated cells, BM-MSCs expanded in culture lose their migratory capacity when injected into animal models (Rombouts and Ploemacher, 2003, Eggenhofer et al., 2014).

In order to maximize the potential benefits of stem cell transplantation, strategies aimed to improve migratory and homing capacity of MSCs are of great interest. This could be achieved by genet modification of MSCs in order to overexpress chemokine receptors, thus potentiating their innate properties. For instance, genetic engineering of MSCs showed that overexpression of chemokine receptors such as CXCR4 and CXCR7, which recognize the chemokine stromal-derived-factor 1 (SDF-1), significantly improved the migratory capacity of the cells towards SDF-1 gradients *in vitro*, and also the homing of MSCs towards areas of damaged tissues in animal models of kidney injury, partial liver regeneration, myocardial infarction and stroke (Chen et al., 2013, Cao et al., 2013, Yu et al., 2012, Liu et al., 2013, Wang et al.,

2014, Cheng et al., 2008). Other groups have genetically modified MSCs to express on their cell surface enhanced levels of chemokine receptors such as CXCR5 or CCR1, which are specific for CXCL13 and CCL7 respectively (Zhang et al., 2017, Huang et al., 2010). Overexpression of CXCR5 increased the homing capacity and therapeutic efficacy of injected MSCs in a mouse model of contact hypersensitivity (Zhang et al., 2017). In another study, CCR1-expressing MSCs, but not CXCR2-expressing MSCs, showed improved migration and engraftment capacity in a model of injured myocardium compared to native MSCs (Huang et al., 2010).

Undoubtedly, for engineered MSCs to be able to target a specific injured tissue, it is fundamental to select a receptor that interacts with chemokines that are secreted from that specific damaged area. One of the most studied and characterized chemokines in ALS is represented by MCP-1, for which the principal receptor is CCR2. Increased levels of MCP-1 have been documented in both CSF samples of ALS patients and in the CSF and spinal cord of SOD1^{G93A} mice (Henkel et al., 2004, Tateishi et al., 2010, Martinez et al., 2017). In particular, extensive research demonstrated that local gradients of MCP-1, the concentration of which increases during disease progression in SOD1^{G93A} mice, plays a major role in the development of neuroinflammation by attracting and recruiting microglia and immune cells into the damaged area in the CNS (Kawaguchi-Niida et al., 2013, Henkel et al., 2006, Beers et al., 2011). Immunohistochemistry on the spinal cord of ALS mice, also showed that MCP-1 is mainly expressed in motor neurons (Kawaguchi-Niida et al., 2013). Thus, overexpression of CCR2 could potentially improve the homing, migratory and engraftment efficiency of MSCs towards areas of neurodegeneration, when transplanted into symptomatic ALS mice.

Interestingly, CCR2 overexpression on BM-MSCs improved cell migration towards MCP-1 *in vitro*, and towards ischaemic lesions in a rat model of stroke (Huang et al., 2018). In addition, Belema-Bedada et al. elegantly showed that efficient homing of mouse BM-MSCs to sites of injury in a myocardial ischemia reperfusion animal model, is dependent on activation and clustering of CCR2 which, by inducing cytoskeletal reorganization, promotes polarization events and thus chemotaxis (Belema-Bedada et al., 2008). Finally, it has been shown that exosomes released by MSCs express high levels of CCR2, which by binding soluble MCP-1 can diminish the local levels of the free chemokine, resulting in suppression of macrophage recruitment and activation (Shen et al., 2016).

Although a limited number of studies characterized the expression of chemokine receptors on MSCs derived from the adipose tissue, ADSCs do not seem to express CCR2 either on the cell surface or at the transcriptional level (Albersen et al., 2013, Baek et al., 2011). Thus, we hypothesized that expression of CCR2 on the cell surface of ADSCs could potentially improve both the homing capacity and the therapeutic potential of these cells when delivered intrathecally in mouse models of ALS. In this chapter, hADSCs were genetically manipulated to express high levels of the chemokine receptor CCR2 by infecting the cells with a lentiviral vector. The resultant CCR2-hADSCs were then fully characterized to assess whether induced expression of CCR2 could affect intrinsic phenotypic and functional cell characteristics.

6.2 Aims

1. To isolate, expand and characterise hADSCs derived from a lipoaspirate sample obtained from a healthy human donor.
2. To genetically modify hADSCs to stably overexpress the human C-C chemokine receptor 2B (hCCR2B) on the cell surface.

6.3 hADSCs isolation and expansion

Subcutaneous abdominal lipoaspirate was obtained from a healthy donor and processed within 24 hours upon receipt. The stromal vascular fraction (SVF) was isolated as described in the material and methods chapter. At the end of the isolation procedure, the SVF was cultured under specific conditions which allow the selective attachment and growth of adipose derived stem cells. With the protocol described, we were able to seed one 10 cm culture dish for every 8 ml of starting biological material.

After plating the SVF, cultures were left undisturbed in the incubator for 48 hours and then washed with PBS to eliminate debris and contaminating red blood cells. At this stage, cultures were around 20-30% confluent. After a stationary phase of 24 hours, cells started to proliferate rapidly as single cell-derived colonies and cultures reached 80-90% confluence within 5 to 6 days after isolation. Cells exhibited a homogeneous fibroblast-like morphology composition in a monolayer after 1-2 passages. hADSCs were passaged every 4-5 days at a seeding density of 10,000 cells/cm² for at least 10 generations without showing signs of senescence, such as for example changes in morphology or a reduction in proliferation activity. Figure 6.1 shows representative microscopic images of cultured hADSCs during the first 7 passages in culture.

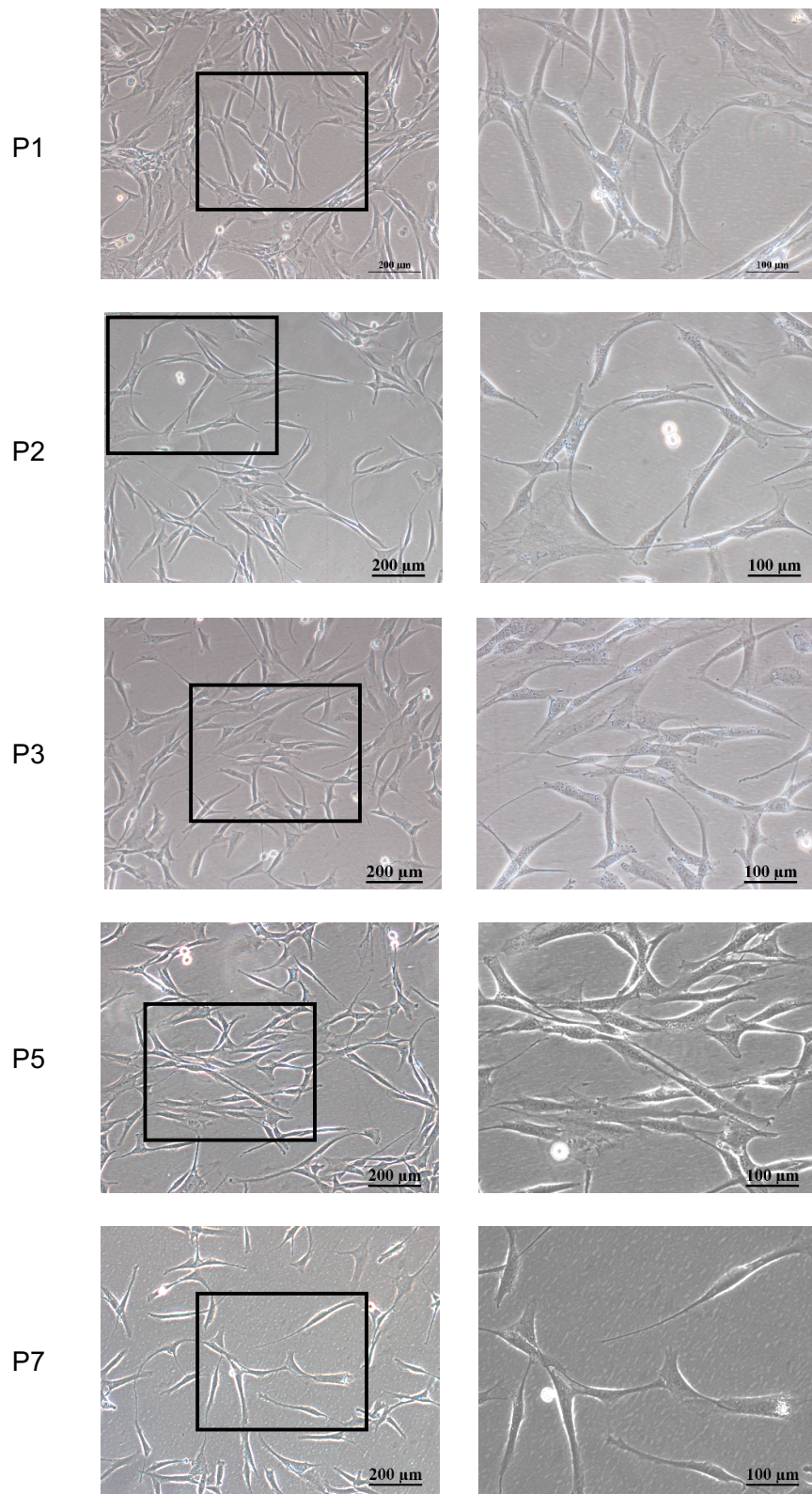


Figure 6.1. Morphology of cultured hADSCs. Phase-contrast images of cultured hADSCs during culture passages. Cells grow as a homogeneous composition in monolayer with classic spindle-shape morphology. The boxed areas on the left panels are magnified on the right panels. Scale bars: 200 μm (left panel), 100 μm (right panel). Images were captured with a Nikon Eclipse Ti inverted microscope.

6.4 hADSC characterisation by flow cytometry

hADSCs expanded for 5 passages *in vitro* were immunophenotypically characterised by flow cytometry. A panel of standard mesenchymal stem cell (CD90, CD73, CD105, CD44), endothelial (CD31), haematopoietic (CD45 CD34, CD11b, CD19) and HLA-DR surface markers were tested either individually or together by performing a complex multicolor analysis. Data were analysed with FlowJow 7.6.1 software. Unstained samples were used to set the FSC and SSC frequencies parameters and to discriminate between single cells and doublets (figure 6.2 A), while the cells stained with the specific matched isotype fluorescent conjugated antibodies were used to set the plot gates and to define the antibody specificity (figure 6.2 B and C).

ADSCs were nearly 100% positive for the MSC markers CD73, CD44 and CD90 (figure 6.2 D, E and F), and ~ 94% of cells were positive for CD105 (figure 6.2 G). Importantly, no sign of contamination from haematopoietic or endothelial cells was detected (Figure 6.2 H).

Notably, in the complex multicolor analysis, in which cells are stained with different antibodies contemporaneously, $91.2 \pm 0.4\%$ (mean \pm SD) of hADSCs were shown to be positive for the mesenchymal stem cell markers CD90, CD73 and CD105, while they were negative for the endothelial, haematopoietic and HLA-DR markers (figure 6.3).

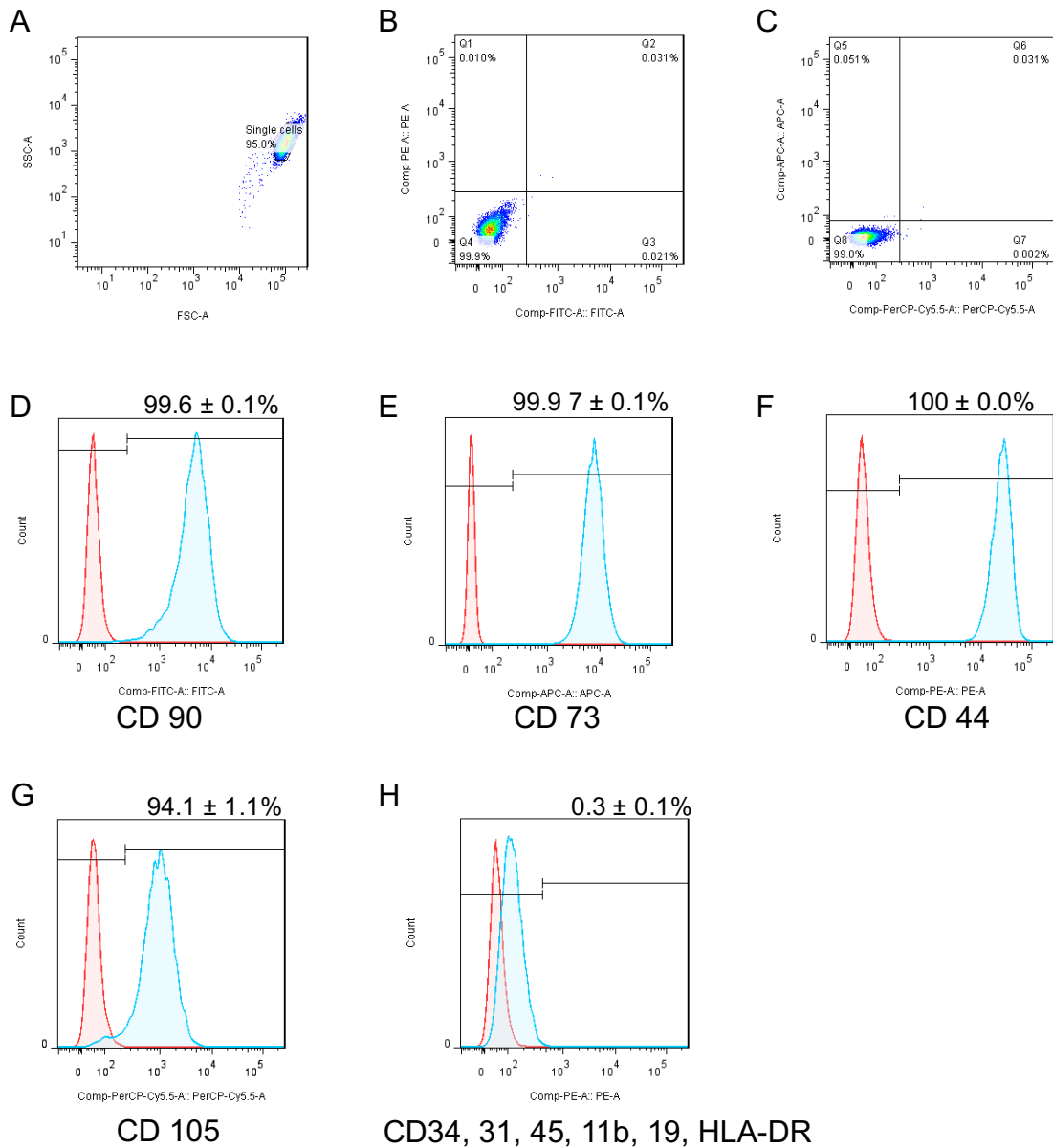


Figure 6.2. Immunophenotype of hADSCs. For hADSC characterisation, a panel of antibodies for markers recognized by the IFATS and SISCT societies were screened by flow cytometry. Unstained samples were used to set the gates and to identify the single cell populations using a logarithmic scale (A). Matched fluorescent conjugated isotype control antibodies were used to determine the positive gates (B and C). hADSCs were positive for CD90 (D), CD73 (E), CD 44 (F) and CD105 (G), but negative for CD34, CD31, CD45, CD11b, CD 19 and HLA-DR (H). The histogram in red represents the signal relative to the isotype negative control, while the histogram in blue represents the cells stained with the specified antibody. On the abscissae is indicated the fluorescence intensity, on the ordinate the cell counts. Values are representative of three separate experiments and indicate mean \pm SD percentage of positive cells.

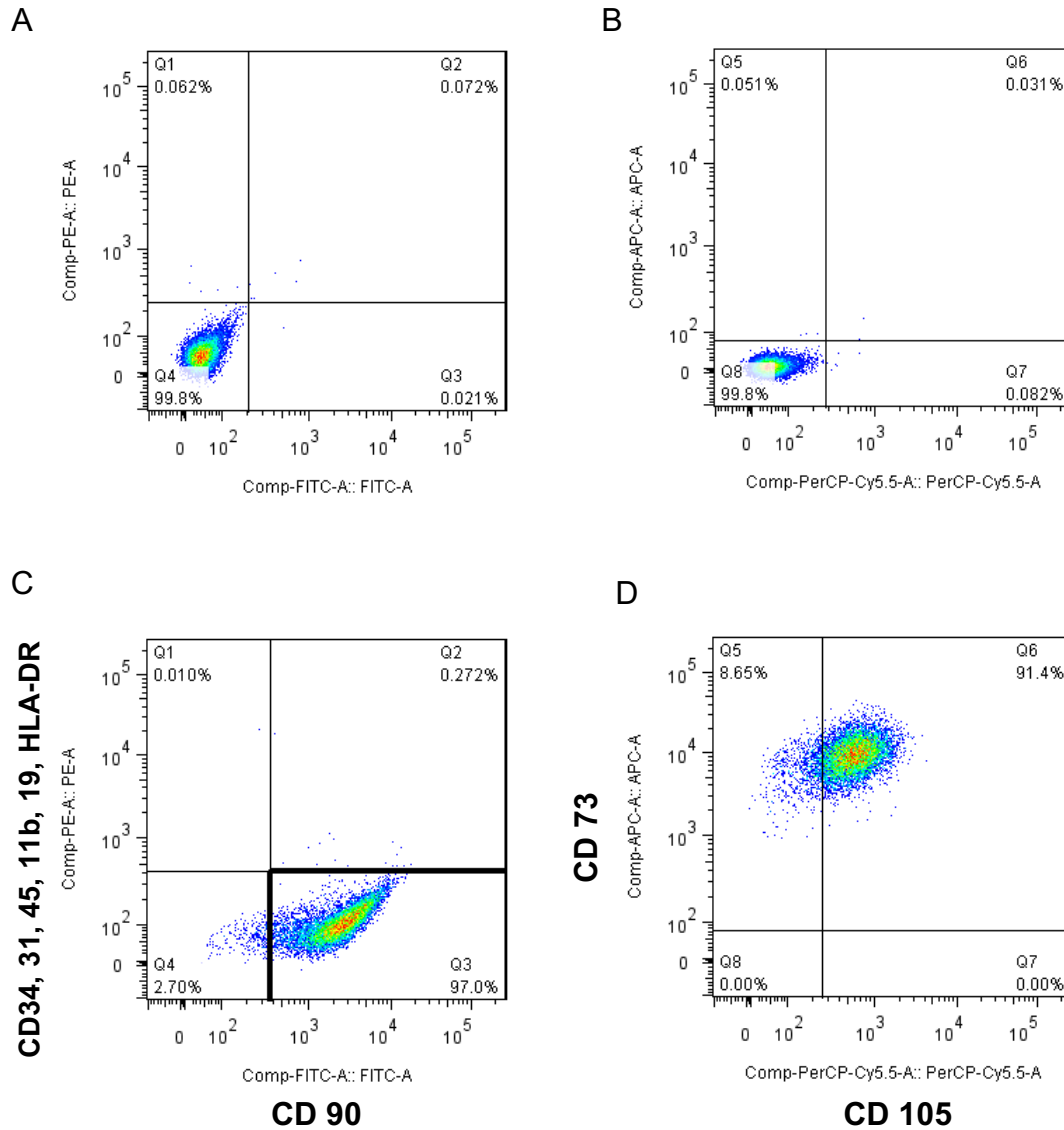


Figure 6.3. Flow Cytometry multicolour analysis of hADSCs. The surface marker expression of hADSCs was characterized by a multicolour analysis. Cells were contemporaneously stained for CD73, CD90, and CD105, together with the cocktail of negative antibodies (CD45, CD31, CD34, CD11b, CD19 and HLA-DR). Unstained cells were used to select the single cell population, while isotype control staining was used to define the positive regions (A, B). hADSCs did not stain ($< 0.3\%$) with the negative antibodies cocktail (C). The CD90 positive region (Q3 in C) was selected and analysed for the concomitant expression of CD73 and CD105 (D). From the multicolour analysis $91.2 \pm 0.4\%$ of uncontaminated hADSCs stained positively for CD90, CD73, and CD105. Values are representative of three separate experiments and indicate mean \pm SD percentage of positive cells.

6.5 Tri-lineage differentiation of hADSCs

6.5.1 Adipogenic differentiation

hADSCs were expanded for three passages and induced to differentiate into adipocytes using a chemical cocktail of factors as described in the materials and methods chapter (paragraph 2.5.3.1).

At day 4 of differentiation, cells switched from the characteristic fibroblast morphology to a more rounded shape with cytoplasmic extensions characteristic of pre-adipocytes. Moreover, tiny light-reflective fat droplets started to appear in the cytoplasm (figure 6.4 A and B). After one week, clusters of differentiated adipocytes filled with lipid droplets were observed (figure 6.4 D and E), and two weeks later a greater number of hADSCs differentiated with lipid droplets which also increased in size and number (figure 6.4 G and H). hADSCs cultured in basal medium did not change in morphology, nor did they exhibit the presence of lipid deposits (figure 6.4 C, F and I).

To confirm adipogenic differentiation, Oil red O staining was performed one week and two weeks post induction as described in the materials and methods. As shown in figure 6.5, after one week from the initiation of the differentiation protocol, the cytoplasmic lipid droplets positively stained with the red dye (figure 6.5 A and B). However, a significant increase in differentiation efficiency was obtained after incubation with the induction medium for an additional week, as documented by an increase in differentiated adipocytes and greater production of Oil red O positive lipids (figure 6.5 D and E). Importantly, hADSCs cultured in the absence of the differentiation chemical cocktail did not stain with oil red solution (figure 6.5 C and F).

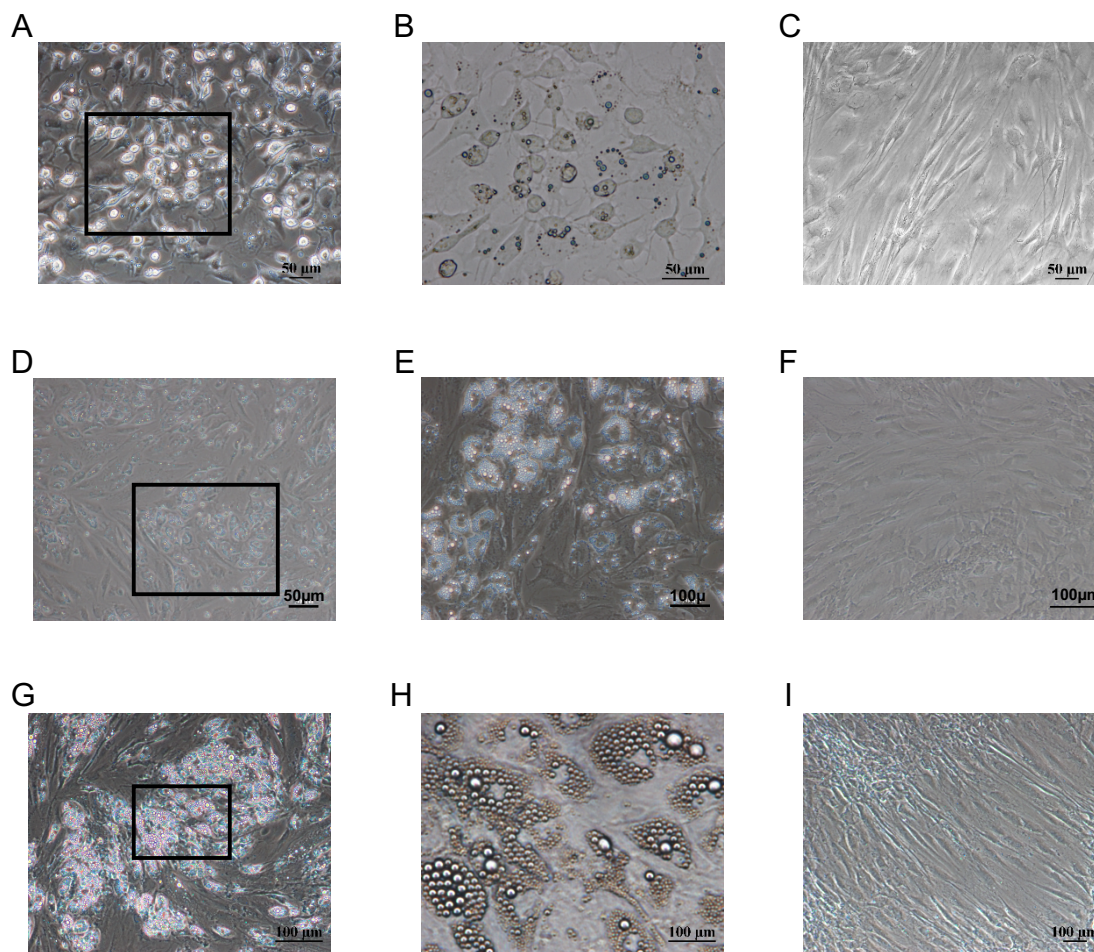


Figure 6.4. Adipogenesis of hADSCs: phase-contrast microscopic images. After 4 days in induction media, hADSCs changed morphology and started exhibiting tiny and translucent lipid deposits (A and B). One week post-induction, differentiated cells showed lipid vesicles in the cytoplasm (D and E). At the end of the differentiation protocol, hADSCs massively differentiated into adipocytes characterized by the presence of large lipid droplets which filled all the cell cytoplasm (G and H). As expected, hADSCs cultured in control medium did not show any sign of adipogenesis (C, F and I). The boxed areas in A, D and G are magnified in B, E and H respectively. Images are representative of at least 3 separate experiments. Scale bars: 50µm (A, B, C, D); 100µm (E, F, G, H, I).

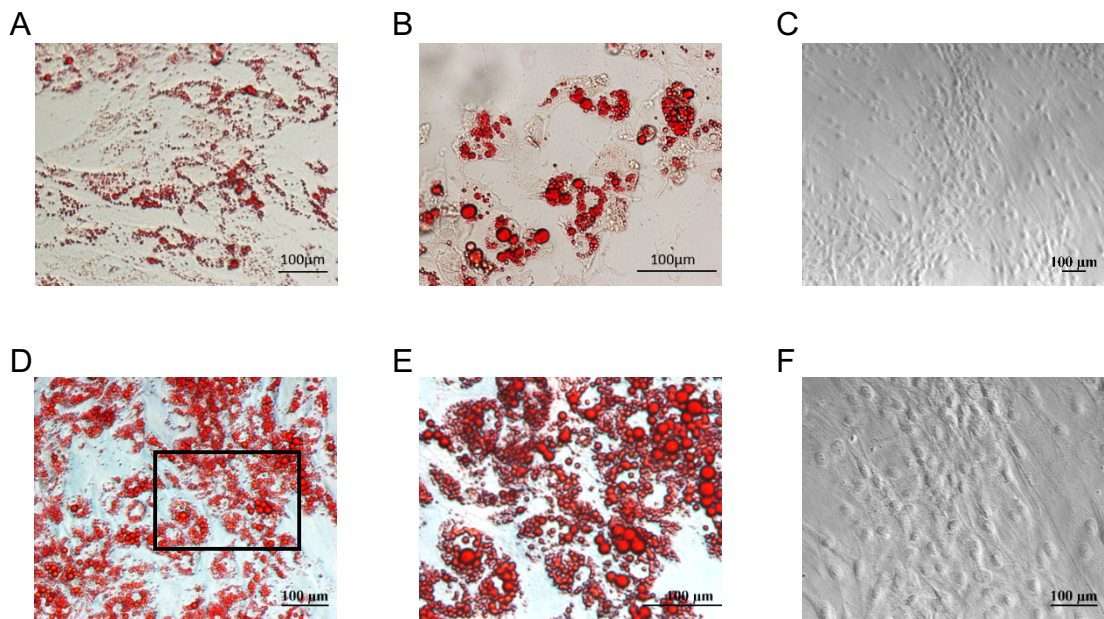


Figure 6.5. Adipogenesis of hADSCs: Oil Red O staining. Representative phase-contrast images of hADSCs differentiated into mature adipocytes which stained positively after exposure to Oil Red O solution. Differentiation was evaluated 1 week (A and B) and 2 weeks (D and E) post-induction. hADSCs cultured with control basal medium showed no signs of differentiation (C and F). The boxed area in D is magnified in E. Images are representative of at least 3 separate experiments. Images were captured with the Nikon 80i microscope. Scale bars: 100μm.

6.5.2 Osteogenic differentiation

hADSCs were expanded for three passages *in vitro* and cultured under specific conditions to stimulate osteogenic differentiation as described in the materials and methods (paragraph 2.5.3.2). Changes in cell morphology were not evident during the differentiation protocol. However, after 10 days of induction white deposits of extracellular matrix were visible by microscopic evaluation (figure 6.6 A and B). These deposits increased in size and number during the following days of osteogenic induction, ultimately covering the whole plate at the end of the differentiation protocol (day 24). In contrast, hADSCs cultured in basal proliferating medium, did not show synthesis of white extracellular matrix (figure 6.6 C).

Osteogenic differentiation was confirmed by Alizarin Red O staining at 12, 18 and 24 days post-induction as described in materials and method. Alizarin Red specifically complexed with mineralized calcium deposits, resulting in a bright orange/red staining. As described, synthesis of calcium matrix was evident after 10-12 days of induction. Alizarin Red staining confirmed the calcium content of these deposits, which appeared as vivid-red nodules (figure 6.7 A and B). After one week (day 18 of differentiation), differentiated hADSCs continued to produce calcium extracellular matrix (figure 6.7 D and E), which covered the whole well after one additional week of differentiation (figure 6.7 G and H). Notably, control cultures did not stain with the red dye (figure 6.7 C, F and I).

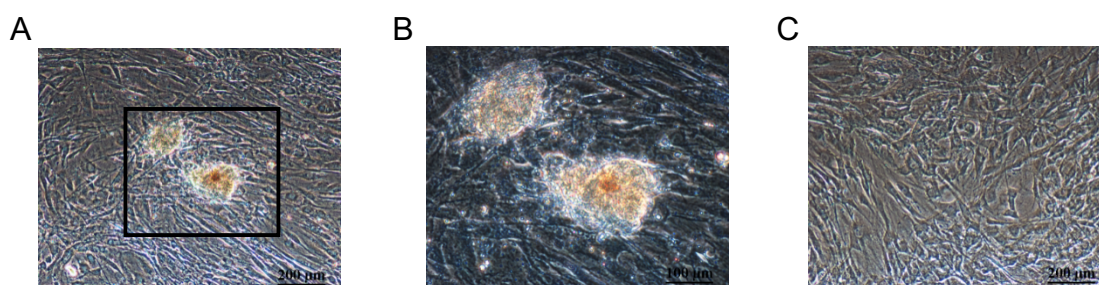


Figure 6.6. Osteogenesis of hADSCs: phase-contrast microscopic images. After 10-12 days of differentiation, the presence of white nodules of extracellular matrix suggested the differentiation of hADSCs into mature osteocytes actively producing calcium matrix (A and B). Calcium deposits were absent in hADSCs cultures which were maintained in control basal medium (C). The boxed area in A is magnified in B. Scale bars: 200 μm (A, C); 100 μm (B).

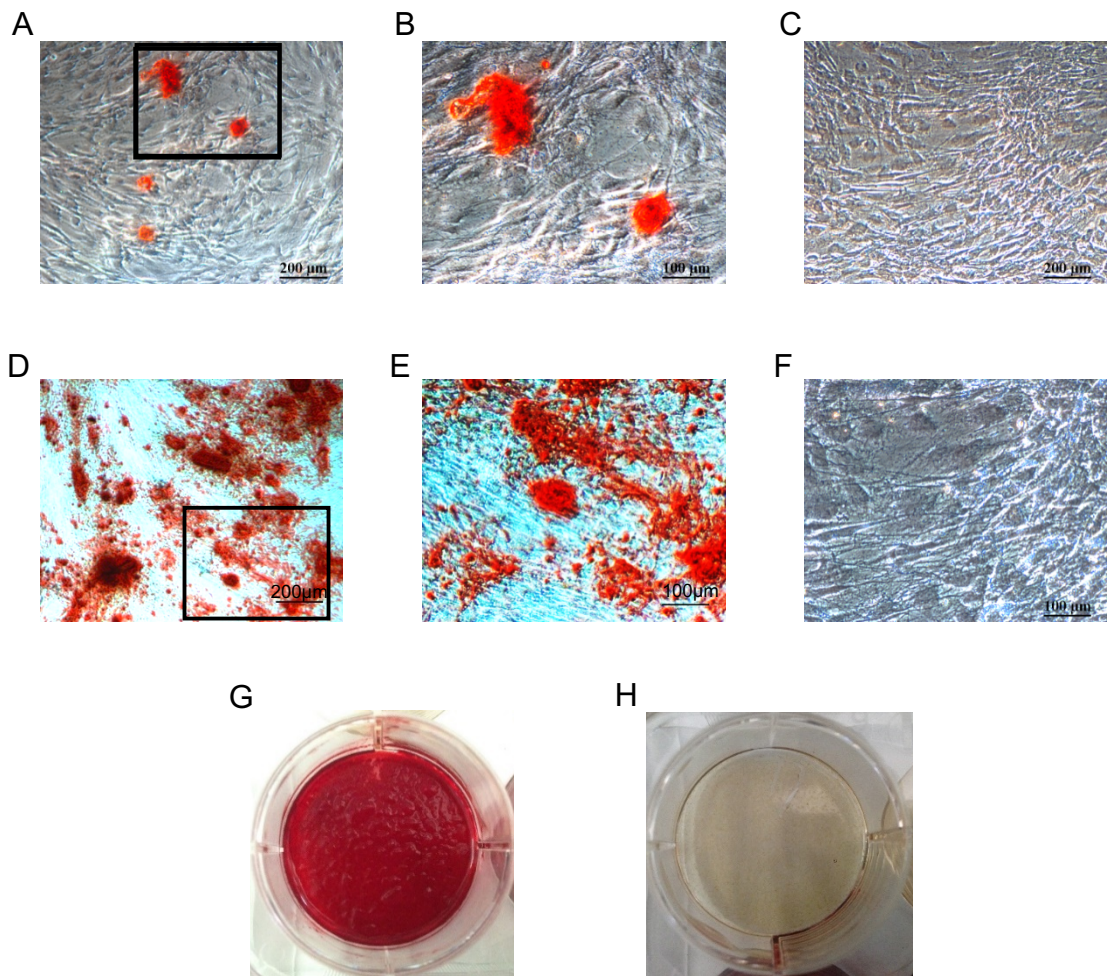


Figure 6.7. Osteogenesis of hADSCs: Alizarin Red O staining. hADSCs were cultured in the presence of osteogenic differentiation medium up to 24 days. 12 days post induction, mineralized calcium nodules stained positively with the red alizarin dye (A and B). The bone nodules grew in size and number after a further week of stimulation (D and E). At the end of the differentiation protocol, cultures were completely covered by alizarin positive extracellular calcium deposits, as evident in the digital photo of the culture well (G). Control cultures did not secrete calcium matrix and did not stain with alizarin red (C, F and H). The boxed areas in A and D are magnified in B and E respectively. Images are representative of at least three separate experiments. Scale bars: 200 μm (A, C, D); 100 μm (B, E, F).

6.5.3 Chondrogenic differentiation

hADSCs were differentiated into chondrocytes by adopting two different methods as described in the materials and methods (paragraph 2.5.3.3). hADSCs were differentiated by adopting a 3D culture method or by culturing confluent hADSCs as a monolayer in culture dishes.

With the 3D pellet culture method, hADSCs took 3 weeks to differentiate into chondrocytes as confirmed by Alcian Blue staining performed on sectioned cell pellets (figure 6.8 A and B).

During the 2-dimensional differentiation of hADSCs, it was possible to observe and document chondrogenesis over time. Interestingly, as early as 4 days post-induction, cells started to migrate and aggregate into islands (figure 6.9 A and B). During differentiation, cells continued to aggregate and formed characteristic dense cartilage nodules, which were clearly visible to the naked-eye as isolated and condensed cell aggregates two weeks post-induction (figure 6.9 D and E). On the contrary, hADSCs cultured in basal medium did not migrate, aggregate or produce extracellular matrix (figure 6.9 C and F).

Chondrogenic differentiation on monolayer cultures was finally confirmed by Alcian blue staining (1 and 2 weeks post-induction) by following the same method used for the detection of acid proteoglycans in the 3D differentiation system (figure 6.10).

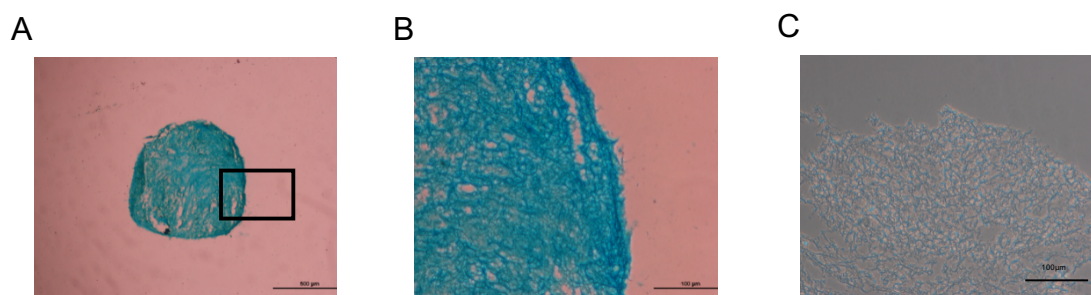


Figure 6.8. 3-dimensional chondrogenesis of hADSCs: Alcian Blue staining. Representative images of hADSC-pellets differentiated into chondrocytes. At the end of the differentiation protocol, pellets were collected and processed for Alcian Blue staining. Images were taken with a Nikon 80Ti microscope and are representative of at least three separate experiments. Differentiated pellets stained intensely in blue with Alcian blue solution (A and B). Control pellets were negative for this stain (C). The boxed area in A is magnified in B. Scale bars: 500µm (A); 100 µm (B, C).

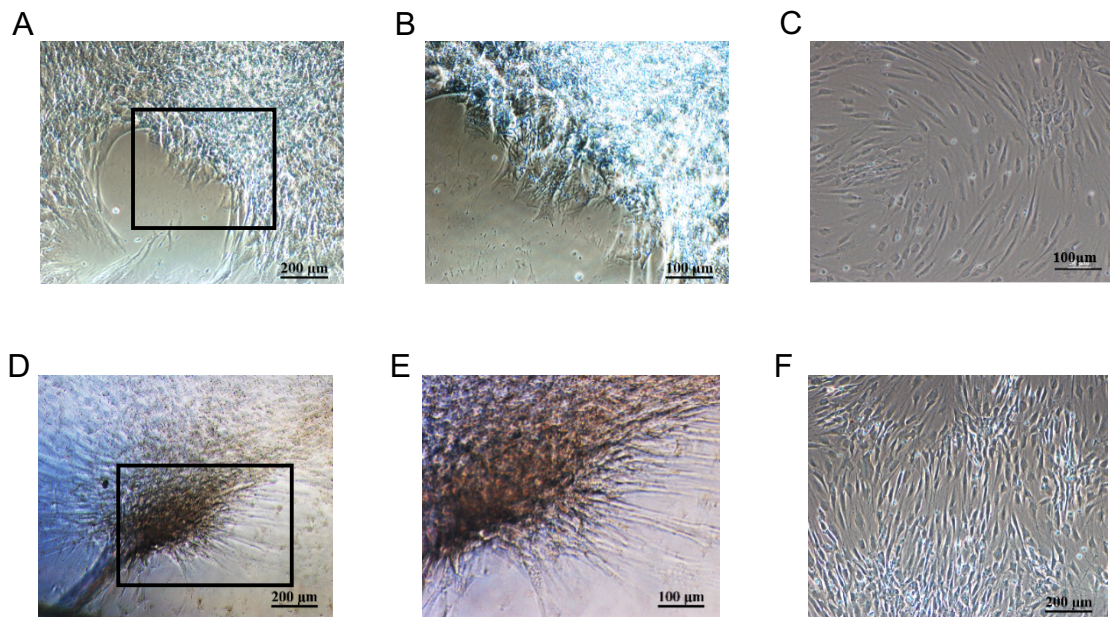


Figure 6.9. 2-dimensional chondrogenesis of hADSC. Representative phase-contrast images of hADSCs differentiation into chondrocytes. After 4 days in induction medium, hADSCs started to migrate (A and B). One week post-induction, differentiated cells aggregated in clusters and started secreting extracellular matrix. At the end of the differentiation protocol (2 weeks), culture plates were characterised by the presence of sparse cartilage nodules (D and E). hADSCs cultured in control medium did not migrate, or produce extracellular matrix (C and F). The boxed areas in A and D are magnified in B and E respectively. Images are representative of at least 3 separate experiments. Scale bars: 200μm (A,C, D, F); 100μm (B, E).

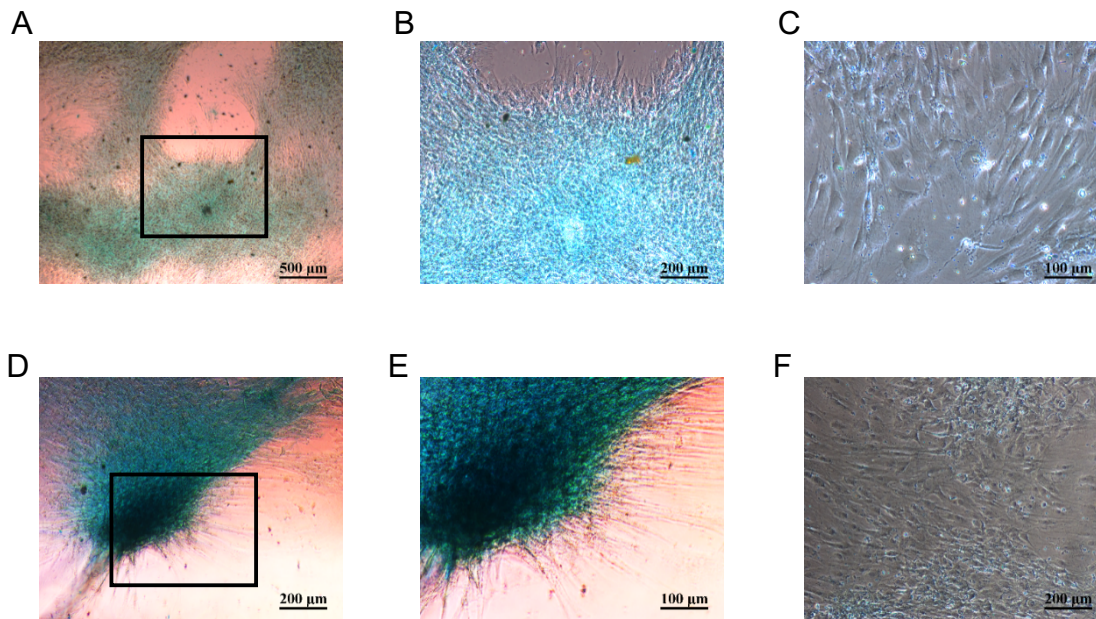


Figure 6.10. 2-dimensional chondrogenesis of hADSC: Alcian Blue staining. Representative images of monolayer cultures of hADSC differentiated into chondrocytes. One week after initiation of the differentiation, the cartilaginous nature of the secreted extracellular matrix was confirmed by Alcian blue staining (A and B). At the end of the differentiation, the cartilaginous nodules strongly stained for the basic dye (D and E). On the contrary, control cultures were negative for the blue dye (C and F). The boxed areas in A and D are magnified in B and E respectively. Images are representative of at least three separate experiments. Scale Bars: 500 μm (A); 100 μm (C, E); 200 μm (B, D, F).

6.6 Construction of hCCR2B-IRES-ZsGreen1 lentivirus vector

The hCCR2B cDNA shuttle vector was purchased from R&D systems technology. The plasmid was firstly transformed into E. Coli competent cells for plasmid replication and to generate bacteria glycerol stocks. After transformation, five single colonies were picked up, grown in LB broth and DNA plasmids purified as described in the materials and methods. To check the identity and integrity of the recovered plasmids, both single and double enzymatic diagnostic digestion were performed. Plasmids were digested with XbaI and BamHI restriction enzymes that specifically cut at the two extremities of the hCCR2B cDNA fragment. Digested DNA fragments and undigested plasmids were then loaded on agarose gel and run by electrophoresis. Figure 6.11 shows the gel electrophoresis results, in which the originally purchased hCCR2B shuttle plasmid was used as a positive control.

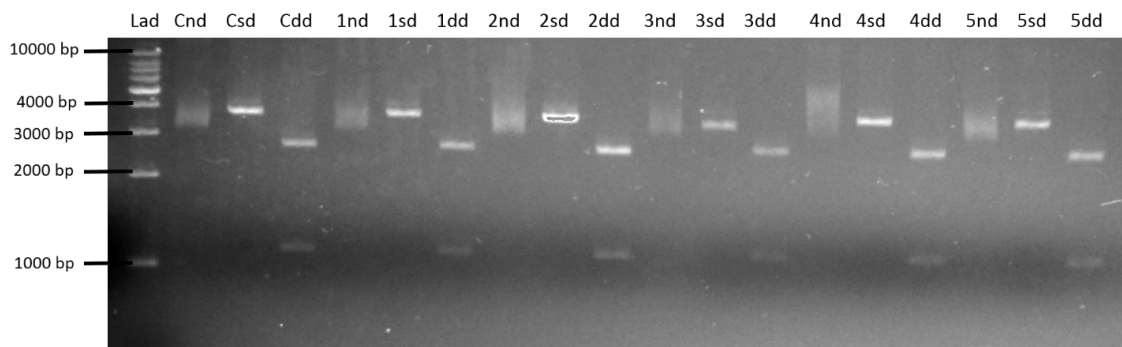


Figure 6.11. Enzymatic diagnostic digestion of hCCR2B shuttle vector clones. After transformation of E. Coli with the hCCR2B shuttle vector, five different colonies were picked up from the agar plate, grown overnight and plasmid DNA isolated. Plasmids were then digested with XbaI and BamHI restriction enzymes either alone (sd) or in combination (dd). Linear DNA fragments, or undigested plasmids, were run on agarose gel by electrophoresis and analyzed by checking the correct size with the help of a DNA ladder of known fragment size. As positive control, the hCCR2B vector from the originally purchased stock was used. The presence of the hCCR2B insert and its correct size (1096bp) was confirmed in all of the plasmids isolated from the five different colonies. Lad = DNA Ladder; C = hCCR2B positive control; nd = undigested; sd = single digestion (i.e. BamHI); dd = double digestion (i.e. BamHI + XbaI); 1 = clone 1; 2 = clone 2; 3 = clone 3; 4 = clone 4; 5 = clone 5. hCCR2B insert length = 1096bp; hCCR2B shuttle vector length = 3830bp.

As described in the materials and methods, the hCCR2B cDNA complete coding frame was amplified by PCR and cloned into the pLVx-IRES-ZsGreen1 backbone vector (pLVx-IRES). For DNA amplification, primers were designed in order to anchor the insert with restriction sites compatible with the pLVx-IRES multiple cloning site (MCS). Moreover, to limit mutagenesis events during the DNA amplification process, a high-fidelity polymerase with a proofreading domain was used. Following the amplification, the hCCR2B PCR product size was then confirmed by gel electrophoresis by running the digested control shuttle plasmid vector as a reference control (figure 6.12). Once the size of the amplified fragment was confirmed, the PCR product was purified with a DNA purification kit. The purification allowed elimination of primer-dimers, large quantities of unused primers, the enzyme, and salts which could have reduced the efficiency of the successive cloning steps.

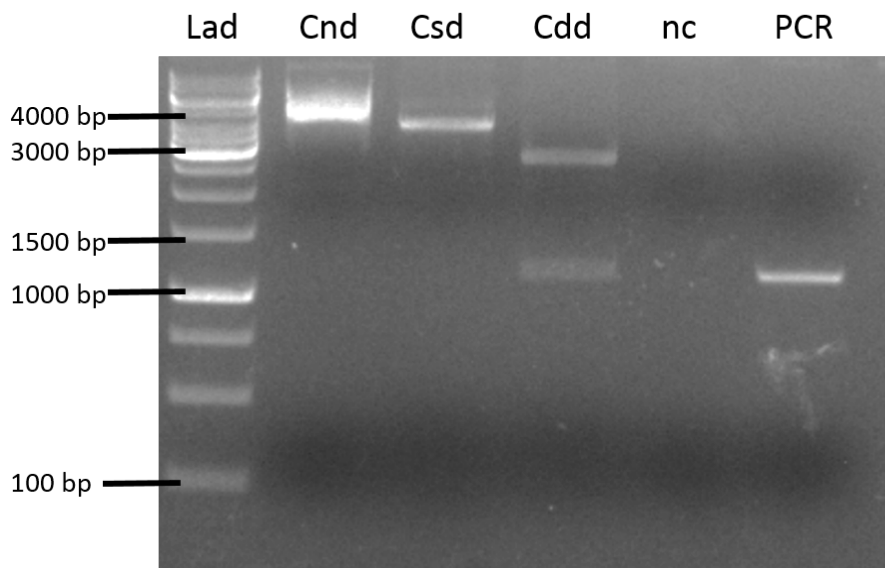


Figure 6.12. Gel electrophoresis of hCCR2B cDNA PCR amplification product. The complete coding region of hCCR2B together with the Kozak consensus sequence was amplified by PCR. XbaI and BamHI restriction sites, which are compatible with the MCS of the lentivirus backbone vector, were anchored to the cDNA. In the figure is the agarose gel image showing the hCCR2B PCR product band, the size of which corresponded to the size of the hCCR2B DNA band obtained after enzymatic digestion of the control plasmid shuttle vector. A negative control containing no DNA template during the PCR reaction was also included.

Lad = DNA Ladder; C = control shuttle plasmid vector; nd = undigested; sd = single digestion; dd = double digestion; nc = negative control; PCR = hCCR2B PCR amplification product.

The pLVx-IRES vector and the hCCR2B PCR product were then cut with XbaI and BamHI restriction enzymes in order to generate compatible sticky ends and the digested products were run on a 0.8% low melting point agar gel by electrophoresis. Successively, with the help of a blue trans-illuminator, the bands corresponding to the linearized vector and the cDNA insert were cut from the agarose gel and purified using a commercially available kit. After purification, the DNA concentration and purity were evaluated by spectrophotometry using the NanoDrop™ 2000/2000c.

The hCCR2B was then cloned into the pLVx-IRES backbone vector by using the T4 DNA ligase enzyme at molar ratios of 1:3 or 1:5 vector to insert. From 20 µl of ligation reaction, 7 µl were used to transform E. Coli chemically competent cells. For the negative controls, a ligation reaction with the linearized pLVx-IRES vector without any insert or a reaction with the linearized pLVx-IRES in absence of the enzyme were also transformed. After 16 hours of incubation of the agar plates, the number of colonies were evaluated. In the plates containing the cells transformed with the molar ratios 1:3 the number of colonies exceeded the ones in the molar ratio 1:5 plate. Thus, single colonies were picked up from the 1:3 molar ratio plate. Importantly, very few colonies (5 to 7) were found in the negative control plates.

Five separate colonies were picked up and grown for plasmid propagation. Plasmid DNA was then purified and subjected to diagnostic enzymatic digestion in order to isolate the “positive” clones harboring the pLVx-hCCR2B-IRES vector plasmid. Plasmids were cut with the two restriction enzymes used for the cloning. As shown in figure 6.13, all of the selected clones were positive for the presence of the lentivirus vector plasmid containing the hCCR2B cDNA.

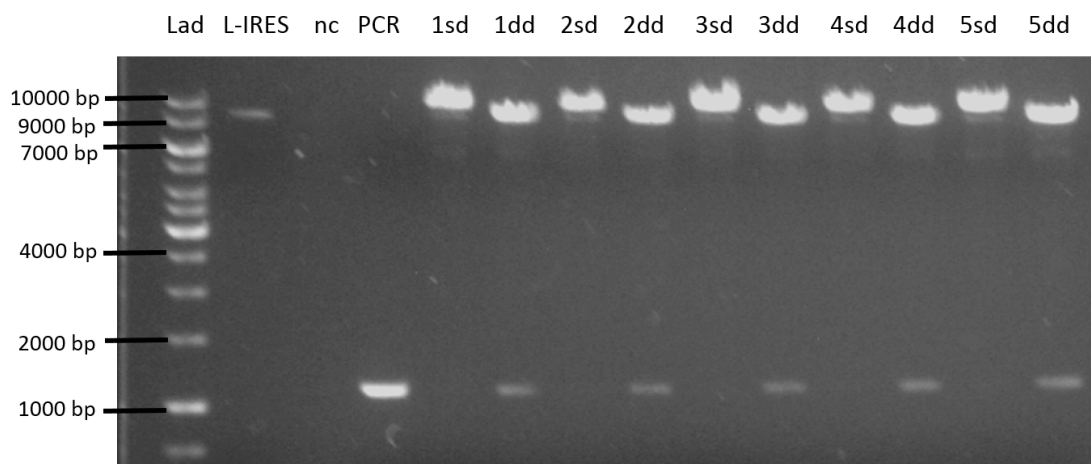


Figure 6.13. Enzymatic diagnostic digestion of pLVx-hCCR2B-IRES vector clones. After DNA ligation and transformation into *E. Coli* cells, five separate single colonies were picked up and subjected to diagnostic digestion by using the same enzymes used for the cloning (XbaI and BamHI). All of the five colonies carried the pLVx-hCCR2B-IRES ligation product. Digested clones were run together with the hCCR2B PCR product (1034bp) and linearized pLVx-IRES plasmid (8204bp) to check the correct size of the DNA fragments. Lad = DNA Ladder; L-IRES = linearized pLVx-IRES control; sd = single digestion; dd = double digestion; nc= negative control; PCR = hCCR2B amplification product; 1= clone 1; 2 = clone 2; 3 = clone 3; 4 = clone 4; 5 = clone 5.

Finally, the plasmid cloning products were subjected to DNA sequencing in order to confirm the presence and correct orientation of the hCCR2B insert, but also to exclude mutagenesis events.

DNA samples were sent for sequencing at the Jie Li Biology company (www.genebioseq.com, Shanghai). The universal EGFP-F and EGFP-R primer pairs (flanking the pLVx-IRES's multiple site cloning) were used for bi-directional sequencing. Sequences were received as electropherograms and analysed with Chromas software (Technelysium, 2.6.6). In figure 6.14 are representative images of the chromatogram DNA sequencing results relative to the pLVx-hCCR2B-IRES clone number 1. The presence of the hCCR2B insert and its correct orientation within the pLVx-IRES were confirmed. Importantly, nucleotide mutations were not found within the construct on analysis of the entire sequence.

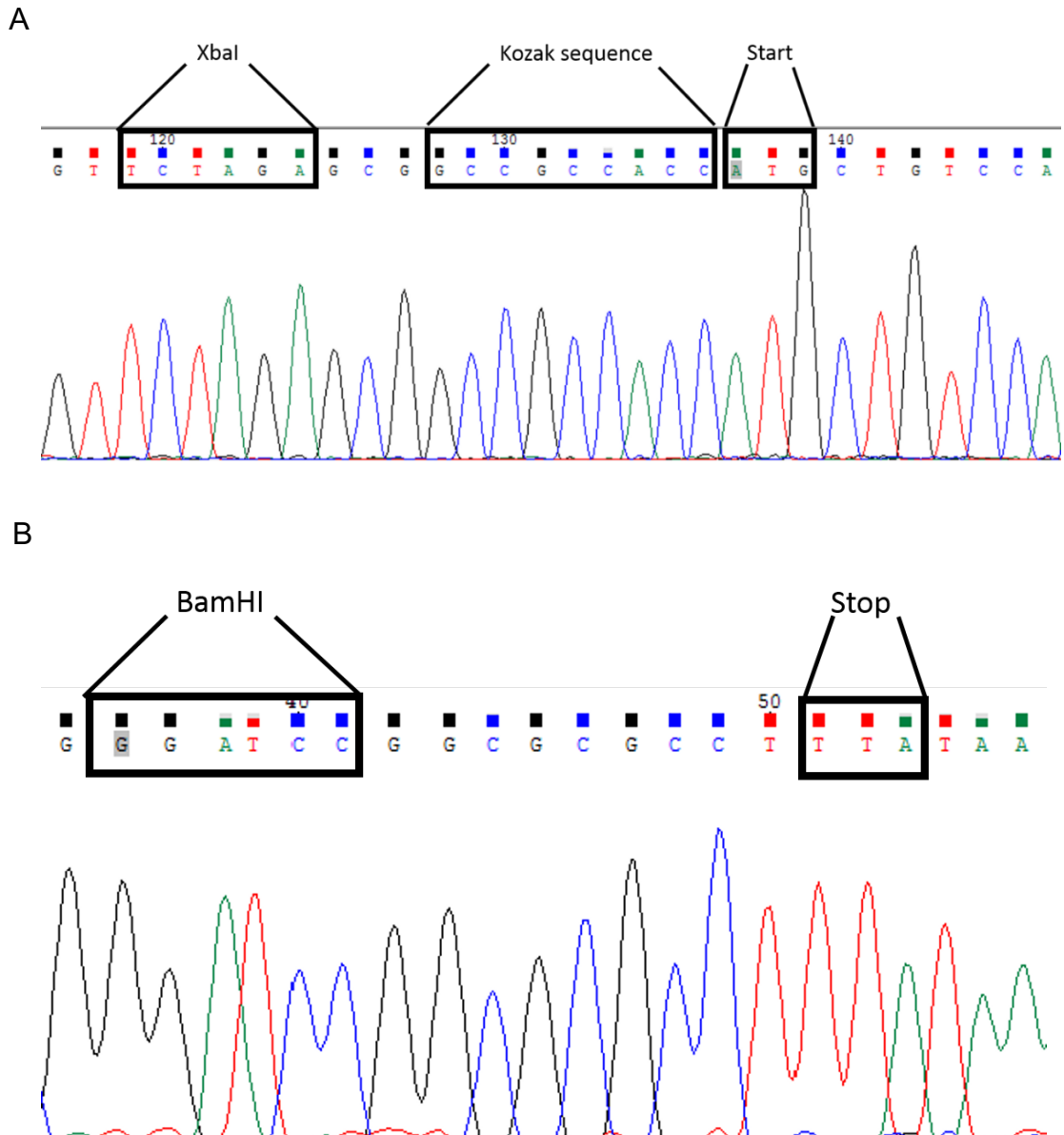


Figure 6.14. pLVx-hCCR2B-IRES vector sequencing. Partial sequence chromatograms of the pLVx-hCCR2B-IRES vector isolated from the clone number 1. Bi-directional automated sequencing was carried out by using the universal EGFP-Forward and EGFP-Reverse primers pair. In the top eletropherogram (A), the XbaI restriction site, the Kozak consensus sequence and the start codon of the hCCR2B cDNA are indicated. In the bottom eletropherogram (B), the reverse sequence shows the stop codon and the BamHI restriction site.

6.7 CCR2 overexpression in hADSCs

6.7.1 Lentivirus transduction optimization

Optimization of hADSCs lentivirus transduction was performed by infecting the cells with the control scramble pLVx-IRES lentivirus (pLV-SCR), which express the ZsGreen1 fluorescent protein but not hCCR2B. Cells at passage 3 were infected with different volumes of fresh prepared medium containing the pLV-SCR lentivirus. hADSCs growing in 48-well culture plates were transduced with 1 or 2 ml of virus which was generated with 3rd generation packaging plasmids. Two rounds of infection in the presence of 10 µg/ml polybrene were carried out: the first round was carried out for 16 hours and the second round for 8 hours. As shown in figure 6.15, regardless of the volume of virus used for infection, 5 days after transduction most of the cells showed high expression of ZsGreen1 by fluorescent microscopy.

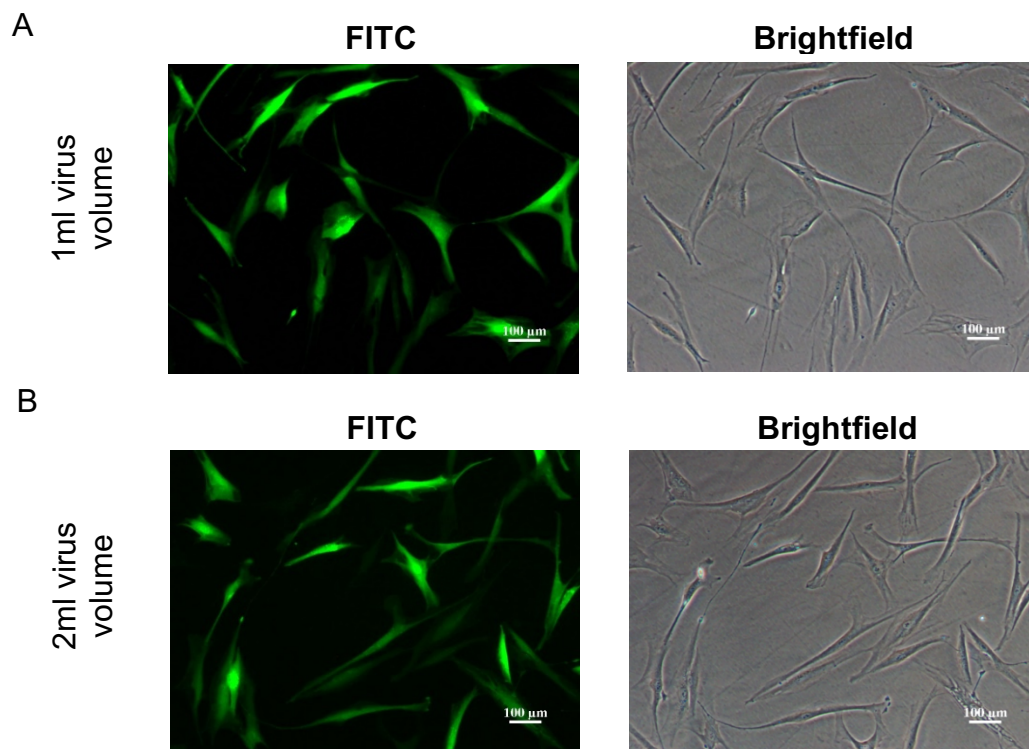


Figure 6.15. hADSCs lentivirus transduction optimization: volume test. Representative fluorescence and phase contrast microscopic images of hADSCs transduced with 1ml (A) or 2ml (B) of media containing pLV-SCR lentivirus particles in the presence of 10 µg/ml polybrene. Images were captured with a Nikon Eclipse Ti inverted microscope 5 days post-infection. Scale bars: 100µm.

Although most of the hADSCs were successfully transduced, during further culture, cells grew in size, stopped proliferating and died within two weeks of repeated medium changes. To assess whether the toxicity was due to the relatively high concentration levels of polybrene used during transduction, in a separate set of experiments cells were transduced with three separate rounds (8 hours each) of infection where the concentration of polybrene was reduced to 4 $\mu\text{g}/\text{ml}$. By using reduced levels of polybrene, transduced hADSCs did not stop proliferating and the majority of the cells expressed high levels of the fluorescent ZsGreen by fluorescent microscopic observation (figure 6.16).

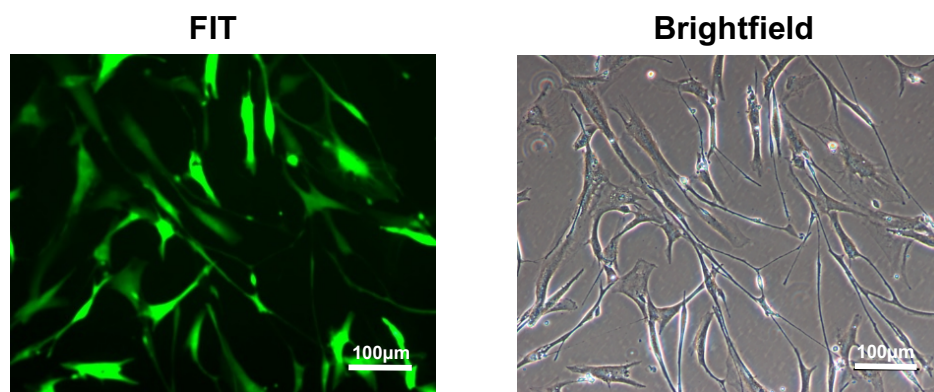


Figure 6.16. hADSCs lentivirus transduction optimization: polybrene test. Representative fluorescence and phase contrast microscopic images of hADSCs transduced with 1ml of media containing pLV-SCR lentivirus particles in the presence of 4 $\mu\text{g}/\text{ml}$ polybrene. Scale bars: 100 μm .

Given the high transduction efficiency and low toxicity, cells were then transduced with the pLV-hCCR2B-IRES-ZsGreen1 lentivirus (pLV-CCR2) following the same transduction conditions used with the pLV-SCR virus. Transduction efficiency was evaluated 5 days post-infection by fluorescence microscopy and by flow cytometry analysis. Moreover, expression of CCR2 was measured by flow cytometric cell surface staining with an anti-hCCR2 APC-conjugated antibody. Unexpectedly, the resulting transduction efficiency appeared to be relatively low (< 50%) and only ~ 34% of hADSCs expressed hCCR2 on the cell surface (figure 6.17).

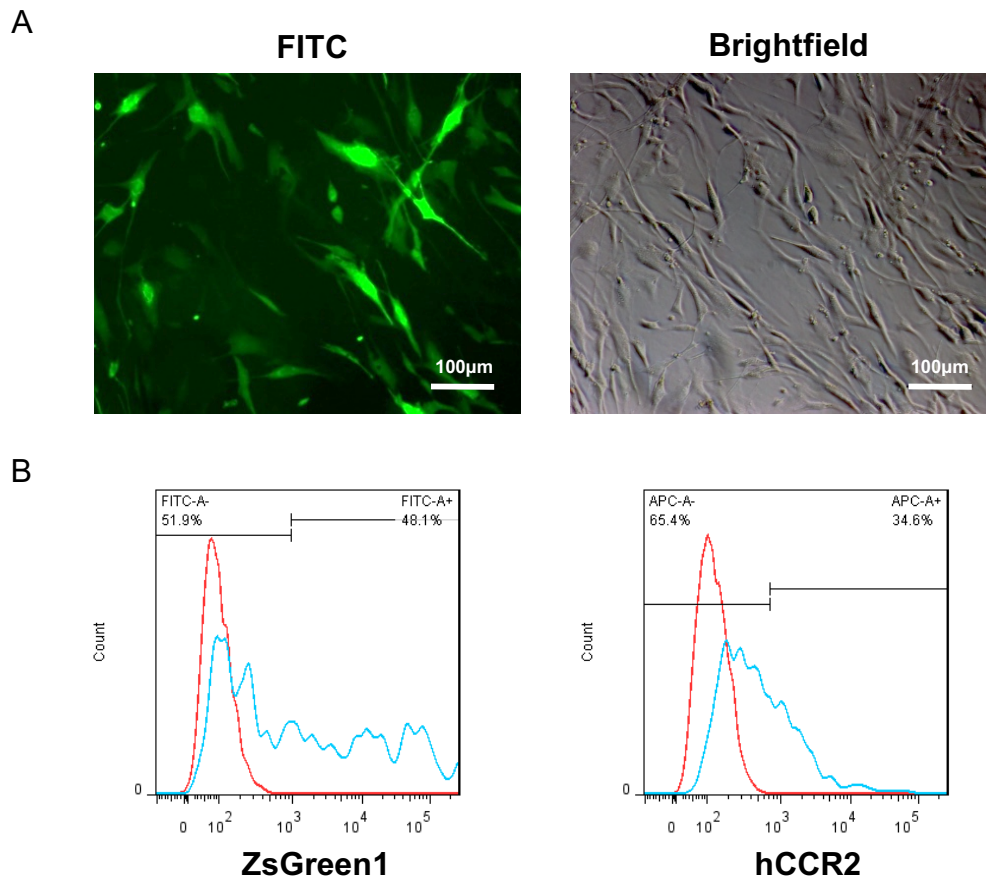


Figure 6.17. Transduction of hADSCs with pLV-CCR2B 3rd generation lentivirus. (A) Representative fluorescence and phase contrast microscopic images of hADSCs transduced with 1ml of media containing pLV-CCR2B lentivirus particles in the presence of 4 µg/ml polybrene. (B) Flow cytometry analysis of infected cells showed that ~ 48% of hADSCs were successfully transduced (left panel), with ~ 34% of cells expressing the hCCR2B receptor on the cell surface (right panel).

To improve the transduction efficiency, hADSCs were successively infected with lentiviruses generated with 2nd generation packaging plasmids. To generate lentivirus with 3rd generation packaging systems, three different packaging plasmids need to be co-transfected, while with the 2nd generation systems only two packaging plasmids are required. Thus, the 2nd generation packaging method is usually expected to give rise to a greater lentivirus titre. Notably, hADSCs transduced with two rounds (8 hours each) of pLV-CCR2B lentivirus (2nd generation) in the presence of 4 µg/ml polybrene resulted in a transduction efficiency of ~ 86% (figure 6.18). Moreover, ~ 78% of cells expressed the CCR2 receptor on the cell surface. The transduction efficiency of hADSCs with the pLV-SCR lentivirus (2nd generation) was similar, with ~ 86% of

transduced cells (figure 6.19). Importantly, hADSCs transduced with the pLV-SCR virus did not express CCR2 on the cell surface (figure 6.19 B).

Based on these data, for the following experiments hADSCs were transduced with lentivirus generated with 2nd generation packaging system, by infecting the cells for two rounds of 8 hours each in the presence of 4 µg/ml polybrene.

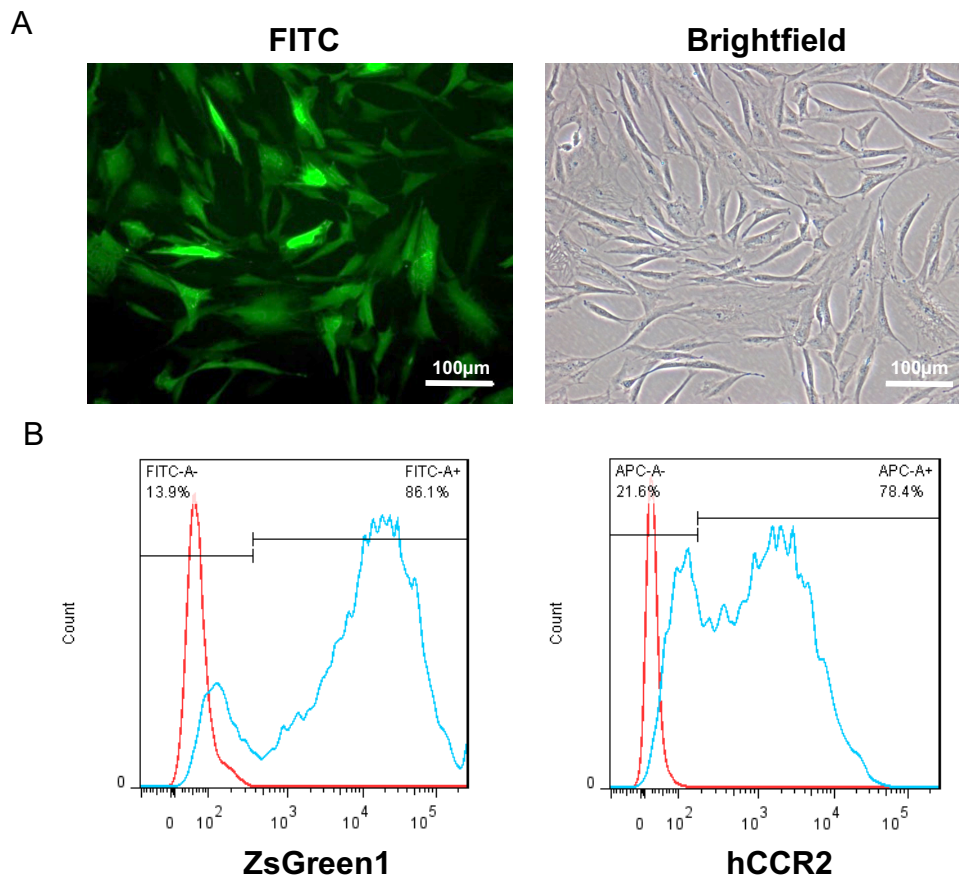


Figure 6.18. Transduction of hADSCs with pLV-CCR2B 2nd generation lentivirus. (A) Representative fluorescence and phase contrast microscopic images of hADSCs transduced with pLV-CCR2B lentivirus in the presence of 4 µg/ml polybrene. (B) Flow cytometry analysis of infected cells showed that ~ 86% of hADSCs were successfully transduced (left panel) with ~ 78% of cells expressing the hCCR2 receptor on the cell surface (right panel).

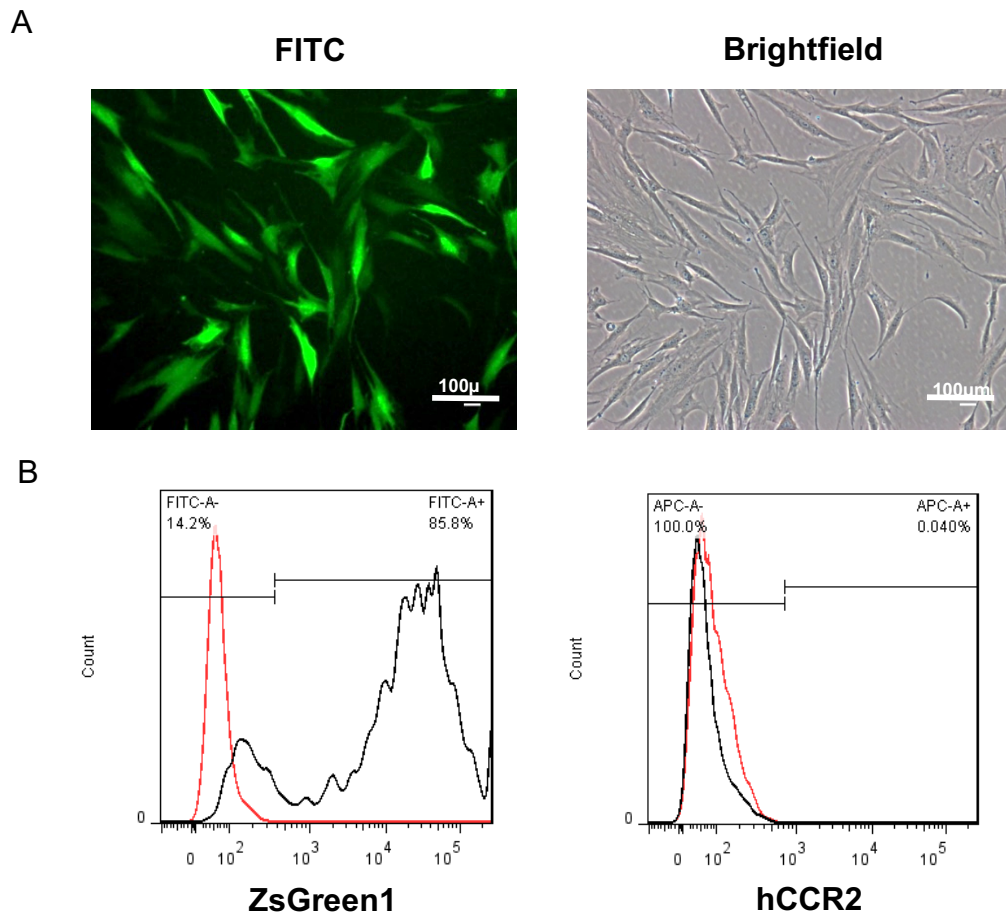


Figure 6.19. Transduction of hADSCs with pLV-SCR 2nd generation lentivirus. (A) Representative fluorescence and phase contrast microscopic images of hADSCs transduced with pLV-SCR lentivirus in the presence of 4 $\mu\text{g/ml}$ polybrene. (B) Flow cytometry analysis of infected cells showed that $\sim 85\%$ of hADSCs were successfully transduced (left panel) and no expression of CCR2 was detected on the cell surface (right panel).

6.7.2 Quantification of CCR2 overexpression in hADSC by Western blotting

Passage 2 ADSCs were transduced with either pLV-SCR or pLV-CCR2B lentivirus and expanded for one passage in culture before processing the cells for western blot analysis. Expression of hCCR2 in hADSCs was evaluated by western blot on total cell lysates with an anti-hCCR2 antibody. As can be seen from the immunoblot image, untransduced control cells or hADSCs transduced with the pLV-SCR lentivirus (SCR-hADSCs) did not express hCCR2, while the cells transduced with the pLV-CCR2B lentivirus (hCCR2B-hADSCs) showed the presence of a single band of the expected CCR2 size, between 40 and 50 kD (figure 6.20).

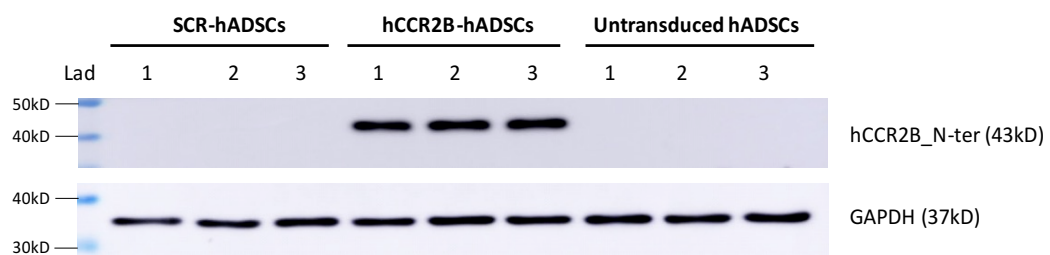


Figure 6.20. CCR2 overexpression in hADSCs: western blot analysis. The immunoblot showed a single band corresponding to the human CCR2 (43kD) in the hCCR2B-transduced cell samples, while no bands were detected in the SCR-transduced or control untransduced lysates. The CCR2 band was of the expected size, at a level between the 40kD and 50kD bands of the protein ladder. GAPDH (37kD) was used as internal loading control. The blot shows a representative image of SCR-transduced, hCCR2B-transduced and untransduced lysate samples obtained from 3 separate experiments.

6.7.3 CCR2 overexpression in hADSCs: immunocytochemistry

hADSCs transduced with either the pLV-CCR2 or pLV-SCR and control untransduced cells were seeded onto glass coverslips and stained with the anti-hCCR2 antibody as described in the materials and methods. At confocal microscopy, pLV-CCR2 transduced cells showed high expression of nuclear and cytoplasmic ZsGreen1 and expression of cytoplasmic CCR2 which seemed to localize around the cell membrane (figure 6.21). On the contrary, no signal for CCR2 was detected in pLV-SCR transduced cells nor in control untransduced cells.

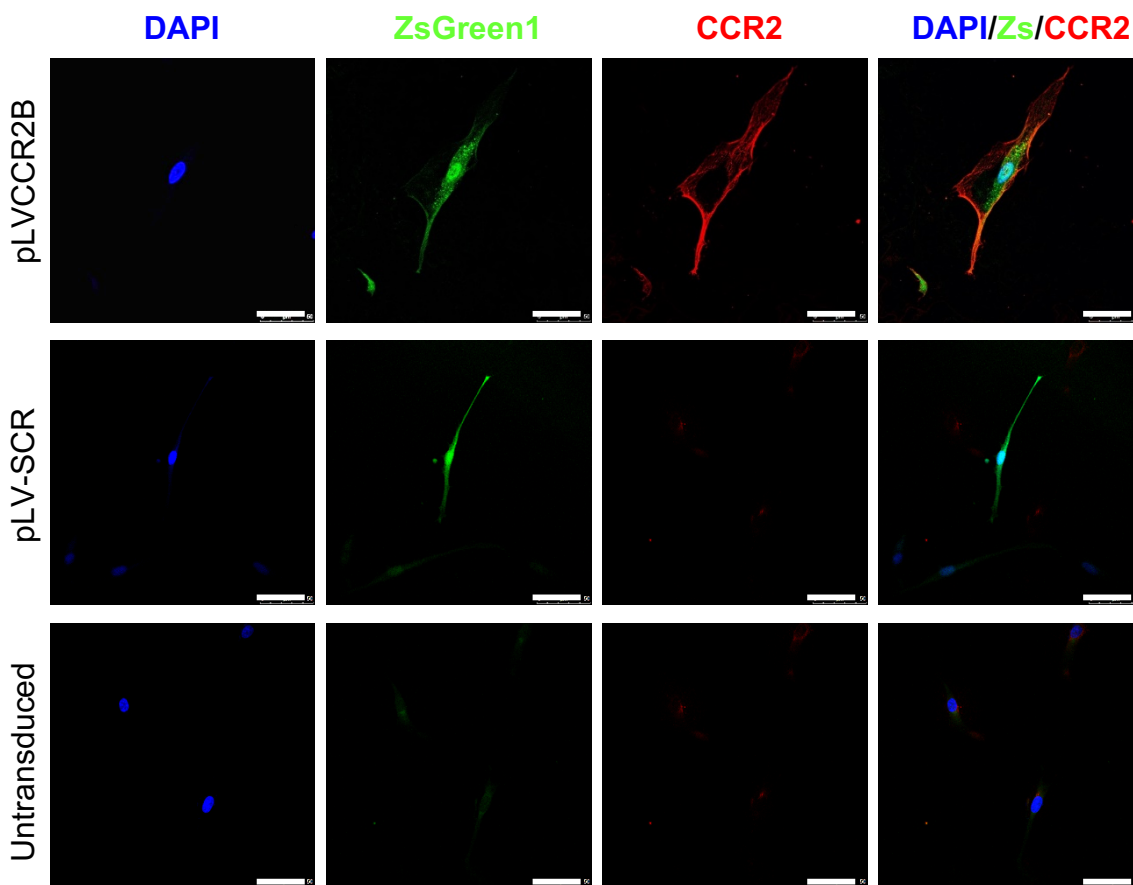


Figure 6.21. CCR2 overexpression in hADSCs: immunocytochemistry. Staining of hADSCs with an anti-CCR2 antibody. pLV-CCR2 transduced cells showed high expression of ZsGreen1 and cytoplasmic expression of CCR2. hADSCs transduced with the pLV-SCR virus and control untransduced cells did not stain for CCR2. Nuclei are stained with DAPI. Images were captured with an Upright Nikon Spinning Disk confocal microscope. Scale bars: 50 μ m.

6.7.4 Phenotypic and functional characterization of CCR2-hADSCs

Following genetic manipulation, hADSCs expressing CCR2 were expanded for 8 passages and tested for specific surface marker expression by flow cytometry. Importantly, 28 days post-transduction, ~ 83% of hADSCs were positive for the reporter gene ZsGreen1, with ~ 75% of transduced cells expressing the hCCR2. Notably, CCR2-hADSCs were positive for the mesenchymal stem cell markers CD44, CD73 and CD105 (figure 6.22 C-E). By contrast, cells were negative for the endothelial (CD31) and hematopoietic (CD34, CD34, CD45, CD11b, CD19) markers and for HLA-DR (figure 6.22 F).

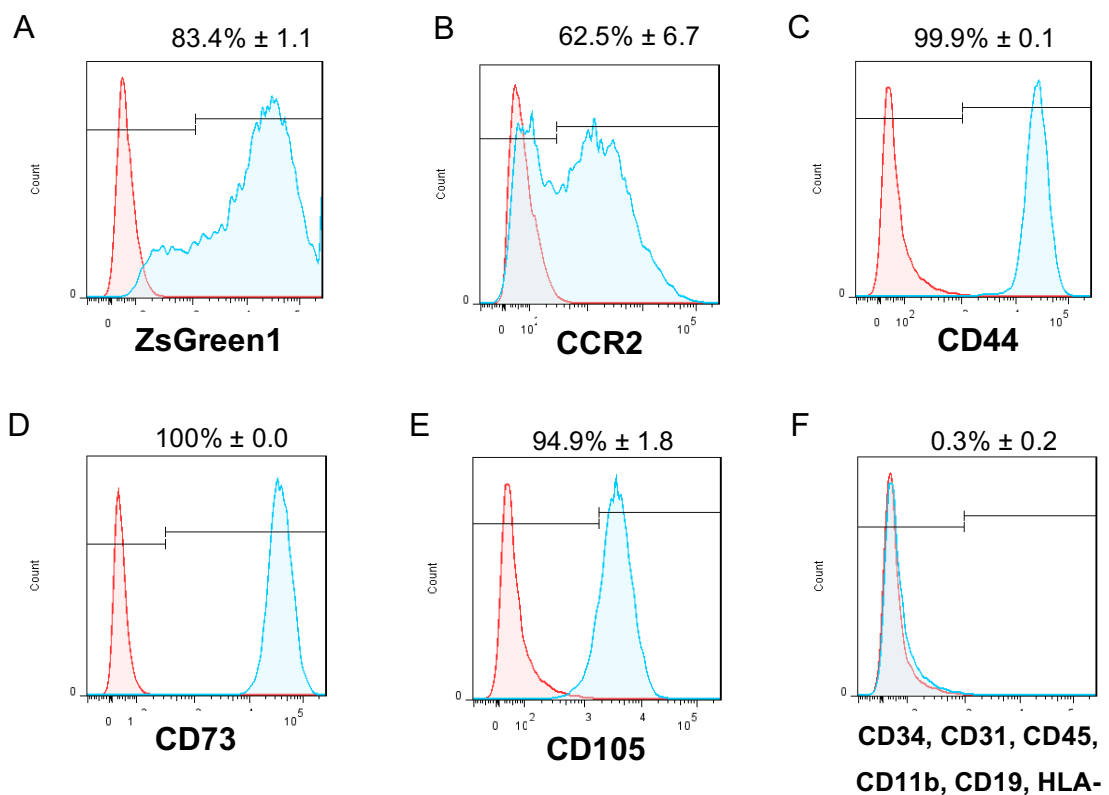


Figure 6.22. Immunophenotype of CCR2-hADSCs. After 28 days of lentivirus infection, hADSCs were positive for the reporter gene ZsGreen1 (A), with ~ 62% of cells expressing the hCCR2 receptor on the cell surface (B). CCR2-hADSCs were positive for CD44 (C), CD73 (D), and CD105 (E) and negative for CD34, CD31, CD45, CD11b, CD19 and HLA-DR (F). The histogram in red represents the signal relative to the isotype negative control, while the histogram in blue represents the cells stained with the specified antibody. On the abscissa is indicated the fluorescence intensity, on the ordinate the cell counts. Values are representative of three separate experiments and indicate mean \pm SD percentage of positive cells.

Finally, CCR2-hADSCs at passage 5 (14 days post-transduction) retained their potential to differentiate into mature cells of the mesodermal lineage (figure 6.23).

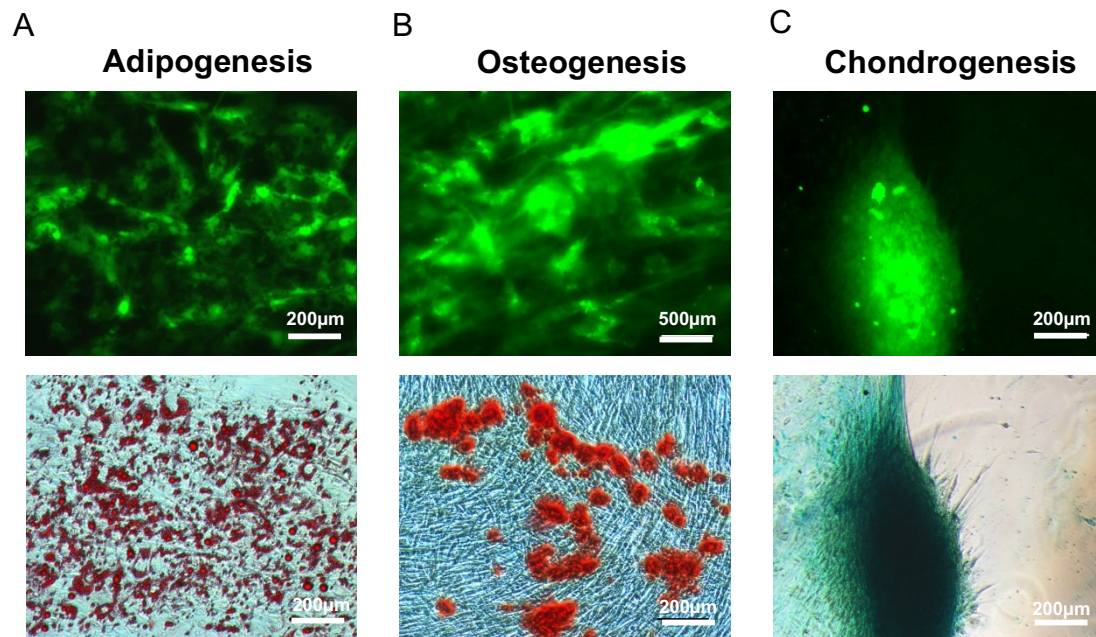


Figure 6.23. Tri-lineage differentiation of CCR2-hADSCs. Representative fluorescence and phase-contrast images showing differentiation of CCR2-hADSCs into adipocytes (Oil-Red staining) (A), osteocytes (Alizarin Red staining) (B) and chondrocytes (Alcian Blue staining) (C). Pictures are representative of at least three separate experiments. Scale bars: 200µm.

6.8 Discussion

6.8.1 Isolation, expansion and characterisation of human ADSCs

In the first part of this chapter, the morphology, immunophenotype and functional characterization of *ex vivo* expanded hADSCs was shown. hADSCs were successfully isolated by enzymatic digestion of a sample of subcutaneous lipoaspirate obtained from a healthy donor volunteer. The protocol to isolate the cells was adapted from the literature and gave rise to a considerable amount of cells after the first four passages in culture. Specifically, with only 10 ml of starting biological material, corresponding to about 3 ml of fat after washing out contaminating serum and plasma, it was possible to obtain about 8 million cells (passage 1) within less than one week of expansion in culture. Considering the high proliferation rate of these cells and that for experiments or clinical application the hADSCs are expanded for 4-5 passages before being used, with 10 ml of lipoaspirate it would be possible to generate a frozen cell bank of about 2.5×10^9 passage 5 hADSCs in less than a month. This confirms that by using standardized and simple isolation methods for processing a lipoaspirate sample, it is possible to obtain a greater (~ 100-fold higher) number of MSCs compared to the isolation from an equal volume of bone marrow aspirate (Meyer et al., 2015).

As expected, the expanded hADSCs appeared as fibroblast-like cells and could be expanded for at least 10 generations without evident changes in cell morphology. Upon flow cytometric analysis, the expanded cell population was strongly positive for mesenchymal stem cells markers (CD90, CD105, CD73 and CD44) and almost completely devoid of contaminants such as endothelial (CD31) and haematopoietic (CD45, CD34, CD11b and CD19) cells. Importantly, the MHC class II cell surface receptor (HLA-DR) was not detected, confirming the hypo-immunogenicity of the isolated ADSCs (Ryan et al., 2005). Remarkably, the complex multicolor flow cytometry analysis, which is required for the characterization of clinical grade MSCs, confirmed the high purity of our culture (Dominici et al., 2006). Finally, hADSCs were able to differentiate into mature cells of the three different mesodermal lineages represented by adipocytes, osteocytes and chondrocytes. Taken together, these data confirmed the mesenchymal stem cell nature of the isolated and expanded hADSCs, where the general guidelines released by the IFATS society to identify ADSCs were followed (Bourin et al., 2013).

6.8.2 Rationale behind CCR2B overexpression on hADSCs

The second part of this chapter aimed to achieve the genetic manipulation of hADSCs to potentially improve the intrinsic homing, migratory and therapeutic properties of the cells. As described in the introduction, during *ex vivo* expansion MSCs gradually lose the expression of chemokine receptors which are important for the cells to migrate towards specific damaged or inflamed areas when transplanted. Based on the specific tissue microenvironment and the nature of the lesion or damage, several groups have engineered MSC to overexpress chemokine receptors and successfully potentiated the homing and therapeutic effects of the cells following transplantation into, for example, animal models of stroke and cardiac injury (Yu et al., 2012, Huang et al., 2010).

Increased levels of MCP-1 have been consistently documented in both ALS patients and in the brain and spinal cord of SOD1^{G93A} mice (Henkel et al., 2006, Beers et al., 2011, Martinez et al., 2017). MCP-1 is considered as the most potent chemoattractant molecule for microglia, monocytes and dendritic cells in the CNS during inflammation and neurodegeneration (Jiang et al., 2012). Moreover, since during disease progression in SOD1^{G93A} mice, high levels of the chemoattractant molecule specifically co-localize with degenerating lower MNs, expression of the chemokine receptor specific for MCP-1 (CCR2) in ADSCs could represent a valid strategy to enhance the homing of injected cells toward the site of neuronal injury and inflammation.

6.8.3 CCR2B overexpression on hADSCs by lentivirus gene delivery

In order to induce human ADSCs to constitutively express the hCCR2B gene, lentivirus infection was chosen as the gene delivery method to efficiently and stably integrate the cDNA ORFs into the host genome. Although different viral vectors have been previously tested to transform MSCs, transgene delivery with lentivirus vectors has been shown to be one of the most efficient delivery methods, which did not alter cell properties (Rostami et al., 2018).

The pLVX-CMV-IRES-ZsGreen1 lentivirus vector (pLVX-IRES) was chosen because of its capacity to induce co-expression of the selected protein of interest, together with the ZsGreen1 fluorescent protein as separated translation products from the same mRNA transcript. This ensures that transduced cells expressing the reporter gene (ZsGreen1) also express the selected transgene, but at the same time, the generation of a fusion protein is avoided. Since from the literature there is a lack of evidence on whether the fluorescent ZsGreen1 protein, when fused to CCR2, may affect the

receptor properties and functions, the pLVX-IRES lentiviral system may represent a good strategy, allowing simultaneous expression of CCR2 and ZsGreen1 in hADSCs.

In humans, two different isoforms of CCR2 exist that are found to be differentially expressed in cell subtypes: CCR2A and CCR2B (Bartoli et al., 2001). The two isoforms result from alternative splicing of the same gene and differ by the carboxyl-terminus (Charo et al., 1994). Although the functional differences between the two isoforms remain unknown, CCR2B represents the most expressed isoform in human monocytes and it is detected on the cell surface of either native cells or after induced overexpression (Wong et al., 1997, Sanders et al., 2000). The CCR2A isoform is mostly located within the cytoplasmic compartment and it is unable to translocate to the cell membrane in transfected cells (Wong et al., 1997). Since our main goal was to improve hADSC migration towards a MCP-1 chemokine gradient, the CCR2B isoform was chosen for transduction.

6.8.4 Lentivirus transduction optimization

Efficient lentivirus transduction of hMSCs is usually obtained by infecting the cells with relatively high concentrations of precipitated virus. Moreover, the use of precipitation methods allows optimization of the transduction efficiency by testing for multiplicity of infection (MOI). Unfortunately, due to limited availability of ultracentrifugation equipment in the Xu laboratory, it was not possible to concentrate the lentivirus preparations by ultracentrifugation, which is considered to be the most efficient precipitation method to obtain high-titre virus stocks (Ichim and Wells, 2011). Thus, transduction optimization was performed by using freshly prepared virus and by varying the volume of medium containing virus, the time and number of transfection cycles, and the concentration of the polycation polybrene during viral infection. The scrambled lentivirus was used to optimize the transduction conditions.

First, different volumes of medium containing virus in the presence of 10 ng/ml polybrene were tested. Although the ADSCs were transduced with high efficiency regardless of the volume of virus applied, a critical decline in cell proliferation, accompanied by changes in morphology was observed during the first week post-infection. Ultimately, all the cells died within two weeks. It is well known that to obtain high transduction efficiency in MSCs the use of additive such as polybrene is needed (Pisano et al., 2018, Kallifatidis et al., 2008). Polybrene is a cationic polymer that, by neutralizing the electrostatic repulsion between the virus and sialic acid groups on the cell membrane, together with inhibition of virus aggregation, massively increases transduction efficiency (Davis et al., 2004, Denning et al., 2013). However, at

relatively high concentrations (>10ng/ml) polybrene can be toxic to some cell types, and it has been reported to have a negative effect on proliferation and differentiation potential of BM-MSCs (Lin et al., 2012). Thus, we tested whether reducing the concentration of polybrene to 4ng/ml, which is the lowest concentration proven to have an effect on transduction efficiency, would reduce the toxic and anti-proliferative effects on ADSCs. Indeed, by using lower concentrations of the polybrene, transduced ADSCs did not stop proliferating and could be expanded for at least 3 passages in culture.

After optimising the lentivirus transduction conditions, ADSCs were infected with the lentivirus expressing CCR2. Unexpectedly, compared to the pLV-SCR virus, the transduction efficiency with the pLV-CCR2 lentivirus was very low. In addition to inter-batch variability, the low level of transduction obtained with the pLV-CCR2 virus could be the consequence of a lower virus titre compared to the pLV-SCR lentivirus. However, since it was not possible to concentrate the virus and perform viral titration or an MOI response on ADSCs, the reason behind the lower transduction efficiency with the pLV-CCR2 lentivirus when compared to the pLV-SCR virus remain elusive. Initially, virus was produced with a four-plasmid system (3rd generation system).

To overcome the low transduction efficiency, transduction of ADSCs with lentivirus produced with a three-plasmid system (2nd generation system) was performed. The two systems differ only in the packaging system, with the 3rd generation system being safer. In the 2nd generation system, all the genes for the packaging (Gag, Pol and Rev) are in one plasmid, while in the 3rd generation system, these are split into two separate plasmids (Gag and Pol + Rev) (Merten et al., 2016). Since the 3rd generation system requires the transient transfection of an additional plasmid for packaging, the lentivirus titre is generally lower compared to virus obtained with the 2nd generation system (Lu et al., 2004b). Notably, infection with the pLV-CCR2 packaged with the 2nd generation system resulted in high ADSC transduction efficiency (~ 85%), with transduction levels similar to that observed when transfecting the cells with the pLV-SCR (2nd generation) lentivirus (~ 86%).

6.8.5 CCR2B overexpression in hADSCs is feasible and does not alter the MSC characteristics

Once the transduction protocol was optimised, early passage (p2) hADSCs were transduced with either pLV-SCR or pLV-CCR2 lentivirus, expanded for one passage, and expression of hCCR2B evaluated by western blot and flow cytometry. As expected, untransduced cells and ADSCs transduced with the scrambled lentivirus

did not show expression of CCR2 at the protein level, confirming transcriptomic data from the literature (Albersen et al., 2013, Baek et al., 2011). Following ADSC infection with the pLV-CCR2 lentivirus, expression of CCR2 was confirmed by western blot on total cell lysate. More importantly, the receptor was able to translocate to the cell membrane as confirmed by flow cytometry analysis. In particular, more than 90% of the transduced cells showed CCR2 expression on the cell surface.

hADSCs expressing CCR2 (CCR2-hADSCs) retained the ability to proliferate and they could be expanded for at least 8 passages in culture. Moreover, stable long-term expression of CCR2 on the cell surface was confirmed by flow cytometry at about 30 days following virus infection. Importantly, the expression of CCR2 did not alter the phenotypic or functional characteristics of ADSCs. To the best of our knowledge, this is the first time that hADSCs have been genetically modified to express CCR2, and similarly to a previous study using hBM-MSCs, overexpression of hCCR2 did not alter the stem cell biological characteristics (Huang et al., 2018).

6.9 Conclusions

In this chapter, the isolation of ADSCs from a human lipoaspirate sample was achieved. The cells were successfully expanded and characterized following standardized guidelines released by the IFATS society.

In addition, hADSCs were successfully transduced with lentivirus expressing the gene for the human CCR2B receptor. In agreement with previous studies, the integration into the ADSC genome of CCR2, together with a fluorescent reporter gene (ZsGreen1) was feasible and did not alter the mesenchymal stem cell morphological, phenotypic or functional characteristics. In order to verify whether the expressed CCR2 is functional and improves the homing capacity of ADSCs, further investigation is needed. For example, the use of transwell chambers would be useful to test whether CCR2B-hADSCs have increased migratory capacity towards an exogenous MCP-1 gradient *in vitro*. Finally, transplantation experiments in symptomatic SOD1^{G93A} mice, will reveal whether expression of CCR2 could improve the chemotaxis of ADSCs towards the area of neurodegeneration, and perhaps, allow the cells to penetrate the brain and spinal cord parenchyma to a greater extent.

7 Discussion

7.1 ADSCs for cell therapy of amyotrophic lateral sclerosis

ALS is a devastating adult-onset neurodegenerative condition where several affected molecular pathways contribute to the aetiology and progression of the disease. Although the disease is characterized by the selective loss of the motor neuron population, ALS is considered a non-cell autonomous condition in which non-neuronal neighboring cells such as astrocytes, microglia and oligodendrocytes play a major role during disease progression, also contributing to the development of a sustained inflammatory microenvironment. Unfortunately, single drugs or targeted treatment have failed as effective therapeutic options and ALS remains a disease with very high unmet medical needs (Hardiman et al., 2017b). During the last decade, the use of stem cells as a cell therapy approach brought new hope for patients. For instance, because of their homing properties, the release of neuroprotective factors and differentiation capacity, the use of stem cells could pave the way for a new therapeutic era in treating neurodegenerative conditions (Lunn et al., 2011). Indeed, the transplanted stem cells may support MN survival, promote neurogenesis, remyelination and axonal sprouting, and improve glial functions (Ciervo et al., 2017).

Various types of stem cells, including embryonic stem cells, foetal stem cells, induced pluripotent stem cells, glial restricted precursors and neuronal progenitors have been shown to ameliorate the phenotype and pathology of transgenic SOD1^{G93A} mice when transplanted either systemically or into the spinal cord (Wyatt et al., 2011, Xu et al., 2009, Nizzardo et al., 2014, Lepore et al., 2008). However, tumorigenicity, restricted availability, ethical issues, safety concerns, immune rejection and low reprogramming/differentiation efficiency are examples of limiting factors that are preventing clinical translation. The use of stem cells obtained from adult individuals may circumvent the aforementioned obstacles. Amongst different types of adult stem cells, mesenchymal stem cells may represent a good candidate for clinical translation for several reasons. First, MSCs are adult stem cells with theoretically unlimited availability in an easy to access location. In contrast to embryonic or foetal derived stem cells there are significantly reduced ethical issues related to their use (Sugarman, 2008). Furthermore, MSCs are a multipotent stem cell population with limited proliferation capacity, and thus, reduced risk of *in vivo* tumour formation compared to the use of neural progenitors derived from ESCs or iPSCs (Toma et al., 2015). Finally, although potential engraftment rejection could be circumvented by using autologous stem cells, MSCs have low immunogenicity, thus potentially

allowing allogenic transplantation without the need for immunosuppressive regimes (Pittenger et al., 1999).

MSCs are multipotent adult stem cells which, in response to the specific surrounding microenvironment, can secrete a large number of trophic factors, cytokines, immunomodulatory molecules and exosomes that, once transplanted, could modulate a plethora of cellular functions in the neighboring cells of the host (Ferreira et al., 2018). Several studies investigating the effect of human or murine bone marrow derived MSCs in animal models of ALS have shown that intrathecal, intravenous or intramuscular injection of these cells can be beneficial, improving motor function, slowing down disease progression and extending survival (Chan-II et al., 2013, Uccelli et al., 2012, Kim et al., 2010, Forostyak et al., 2014, Boucherie et al., 2009, Boido et al., 2014, Suzuki et al., 2008).

For more than a decade, the bone marrow has been considered the reference source for mesenchymal stem cells. However, bone marrow aspiration is an expensive and often painful procedure which gives rise to a very limited yield of MSCs after sample processing. In addition, the proliferation rate, differentiation capacity and therapeutic potential of BM-MSCs rapidly decline during *ex vivo* expansion and manipulation (Zuk et al., 2001). Adipose tissue may represent a valid alternative source of MSCs for clinical translation, with several advantages over the use of MB-MSCs. Indeed, ADSCs can be obtained through a minimally invasive procedure such as liposuction, they are relatively abundant, and display greater proliferation capacity with reduced senescence ratio when compared to MSCs derived from the bone marrow (Frese et al., 2016). In addition, in contrast to BM-MSCs, the proliferation activity, clonogenic capacity, senescence and differentiation potential of ADSCs did not appear to decline with the age of the donor (Beane et al., 2014). Although there are some differences in the immunophenotype, transcriptome profile and differentiation capacity, BM-MSCs and ADSCs possess similar biological characteristics and it is still unclear which cell population would be more effective for clinical application (Strioga et al., 2012, Mohamed-Ahmed et al., 2018, Niemeyer et al., 2007).

7.2 Choosing mouse derived ADSCs for *in vivo* therapeutic investigation

In the current study, we evaluated the therapeutic potential of mouse ADSCs in ALS by using both *in vivo* and *in vitro* models of disease. In most of the previous studies investigating the therapeutic potential of BM-MSCs in the SOD1^{G93A} murine model of ALS, cells derived from human samples were transplanted. However, immunosuppression in recipient rodents was often required in order to avoid rejection

of the transplanted human stem cells. The use of immunocompromised ALS animals for the study of MSC transplantation is disadvantageous for several reasons. Given that one of the protective mechanisms of action of MSCs in ALS is based upon their immunomodulatory activity, the use of immunosuppressive agents could significantly alter and/or mask important features of the transplanted cells and how they respond to the ALS microenvironment. Moreover, an important characteristic of MSCs is their low immunogenic profile, which would enable both autologous and allogenic transplantation in humans. So the introduction of an immunosuppressive regime when investigating the therapeutic potential of MSC *in vivo* could be controversial. For these reasons, most of the work here presented focused on the use of mouse ADSCs which avoided the need for immunosuppressive agents. In the current study, mADSCs were successfully isolated from the inguinal subcutaneous fat pads of healthy wild type mice. The *ex vivo* expanded mADSCs displayed phenotypic and functional properties characteristic of MSCs, which complied with the general guidelines released by the ISCT and IFATS societies (Dominici et al., 2006). In order to track the cells following injection into SOD1^{G93A} mice, mADSCs were successfully transduced with lentivirus expressing the GFP protein. Importantly, similar to previous studies neither the genome integration of the GFP, nor the freezing/thawing cycle of GFP-mADSCs altered the stem cell qualities (van Vollenstee et al., 2016, Zhang et al., 2014, Ginis et al., 2012).

7.3 Intrathecal injection of ADSCs into SOD1^{G93A} ALS mice

One of the major technical issues in the development of cell therapy for ALS is to effectively deliver stem cells into the CNS. Figure 7.1 is a representation of different proposed strategies to deliver MSCs into ALS patients with the relative advantages and disadvantages.

Several studies demonstrated that injecting human stem cells directly into the spinal cord of ALS rodents is feasible, safe and efficient (Vercelli et al., 2008, Knippenberg et al., 2012b, Knippenberg et al., 2015, Xu et al., 2011). The surgical procedure for intraspinal infusion of hMSCs into the spinal cord of ALS patients by specifically designed microinjection manipulators has also been shown to be safe in open-label clinical trials (Mazzini et al., 2010, Mazzini et al., 2012, Blanquer et al., 2010, Blanquer et al., 2012, Riley et al., 2014). However, direct CNS injection remains an invasive procedure which could cause serious clinical complications and permanent damage to CNS areas already affected by the disease. Thus, it might be a considerable ethical issue in clinical trials when investigating the efficacy of the therapy, especially where

placebo controls are required. Nevertheless, given the disseminated nature of neuronal degeneration in ALS in both cortex and spinal cord, injection of stem cells into multiple sites would be needed, making the intraspinal delivery route impractical.

Since early pathologic mechanisms of disease involve destruction of neuromuscular junctions before motor neuron death, intramuscular injection of MSCs at an early stage of disease has also been proposed. Intramuscular injections of hMSCs engineered to overexpress GDNF into SOD1^{G93A} rats resulted in delayed disease onset and prolonged survival, but MSCs were not able to regenerate motor endplates, nor to ameliorate motor neuron loss (Suzuki et al., 2008). Nevertheless, the very poor muscle engraftment efficiency with few transplanted cells surviving for no more than 1 week is an important limitation (Rehorova et al., 2019).

Given their immunomodulatory properties, together with the homing capacity in response to inflammatory signals, hMSCs showed beneficial effects when infused intravenously in ALS animal models (Zhao et al., 2007, Chan-Il et al., 2013). However, even though intravenous infusion could be the easiest and safest way for stem cell delivery, cells are instantly trapped in the lungs, distributed to the liver and spleen within 24 hours and rapidly cleared from the body (Galipeau and Sensebe, 2018, Eggenhofer et al., 2012). Thus, a really small proportion of the initial infused cell dose could actually migrate and engraft into sites of injury, and a large number of cells may need to be transplanted in order to be effective in human subjects.

The delivery of stem cells into the CSF surrounding the spinal cord by intrathecal injection may be an attractive option, since the stem cells would be placed in proximity to damaged areas without direct delivery into the spinal cord parenchyma. Furthermore, it would be possible to perform multiple injections both at the cervical and lumbar levels, allowing the stem cells to migrate towards more affected areas of neurodegeneration/inflammation (Zhou et al., 2013). In some preclinical studies, stem cells were able to migrate from the CSF into the parenchyma, however, the mechanism of migration remains unknown (Boido et al., 2014, Kim et al., 2010). In the current study, we showed that cisterna magna injection allowed the ADSCs to widely distribute within the brain ventricular system and also to travel down to the lumbar region of the spinal cord. However, the cells did not survive for more than 4 weeks post-injection and did not appear to migrate within the brain or spinal cord parenchyma. Our observations are similar to those reported in previous studies, in which intrathecally transplanted MSCs did not show the ability to penetrate the spinal cord meninges (Habisch et al., 2007, Forostyak et al., 2014, Violatto et al., 2015).

Nevertheless, despite the short-term survival and limited engraftment efficiency, injected ADSCs resulted in beneficial effects in SOD1^{G93A} mice, which had a later disease onset and improved motor function (rotarod performance and gait parameters) compared to vehicle treated animals. The improvements in behaviour were further confirmed at the pathological level, where ADSC-injected mice showed partial preservation of motor neurons, reduced astrocyte activation, and decreased microgliosis in the lumbar region of the spinal cord. Our data are in agreement with previous studies in which intrathecal transplantation of human or mouse MSC derived from the bone marrow, alleviated the clinical phenotype of transgenic ALS rodents by protecting MNs and by reducing neuroinflammation (Kim et al., 2010, Boucherie et al., 2009, Boido et al., 2014, Kim et al., 2014b). In the aforementioned studies, the transplanted MSCs displayed a very limited capacity to migrate into the spinal cord. Moreover, the engrafted MSCs were not able to differentiate into neurons and thus functionally integrate with the hosts complex neural circuits. Although partial *in vivo* differentiation of MSCs into cells expressing markers characteristic of mature glial cells was documented, the main mechanism of protection was attributed to the capacity of MSCs to secrete growth factors, cytokines and exosomes, which could in turn support MN survival, reduce inflammation and modulate host glial functions (Marconi et al., 2013, Kim et al., 2014b, Zhou et al., 2013).

In our study and all the previous pre-clinical studies investigating the therapeutic potential of MSCs in the SOD1^{G93A} model of ALS, the control placebo group consisted of animals injected with either PBS, DMEM or CSF alone, depending on what solution was used to re-suspend the cells to be injected in the treatment group. Although it is scientifically and ethically accepted to use PBS or CSF as a control in clinical trials that include a placebo sham-operated arm, this could be a limitation in pre-clinical testing. It might be relevant, in future studies, to include a control group represented by mice injected with either dead MSCs, MSCs isolated from ALS mice or even different cell types such as for example fibroblasts. This would definitively confirm whether the beneficial effects observed in SOD1^{G93A} mice are given to the activity of live MSCs, and would also assess whether MSCs carrying SOD1 mutations could be therapeutically effective.

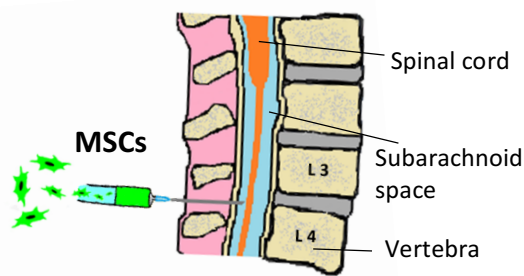
An important factor to be considered in our study is the possibility of dropped copies of the transgene. Indeed, in SOD1^{G93A} mice a reduction in transgene copy number would significantly alter the disease course, resulting in a delayed disease onset (Alexander et al., 2014). However, in our SOD1^{G93A} colonies, variation in transgene copy number is rarely observed. Moreover, in case of a reduction in copy number,

the mouse would be easily detected at the age of 85-90 days because of the lack of a motor impairment phenotype (Mead et al., 2011). In our studies we did not suspect any case of reduced copy number, however, this could have been formally assessed by quantitative PCR (Q-PCR).

Another limitation of our *in vivo* study is the exclusive use of SOD1^{G93A} transgenic females for pre-clinical testing, and it will be important to confirm our data in transgenic males. If on the one hand, significant differences between females and males in the phenotypic parameters measured are not observed in our SOD1^{G93A} model, on the other hand, the differences in male and female physiology and pathophysiology must be considered in translational research. Indeed, sex is considered as a basic biological variable in both animals and humans, and researchers are expected to include the variable sex in both pre-clinical and clinical experimental design (Clayton et al., 2016).

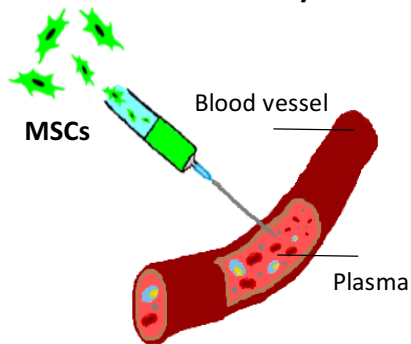
Overall, our data support the hypothesis that the beneficial effects observed in the transgenic ALS mice injected with ADSCs, are due to the release of soluble factors from the transplanted cells that have the potential to target multiple disease pathways, which ultimately culminate in the modulation of the toxic microenvironment that leads to motor neuron loss. This, was also confirmed in our *in vitro* experiments, where through paracrine mechanisms, the ADSCs were able to protect MNs from ALS-derived toxic astrocytes, by directly secreting neuroprotective factors and also by modulating astrocytic functions. Since the *in vivo* study terminated before the animals reached the terminal end-stage of disease, it remains to be seen whether the protective paracrine effects of ADSCs are only transient, and thus strictly depend on the presence of the cells in the host. For instance, it has been shown that the neuroprotective effects of MSCs is dose-dependent, suggesting that in order to obtain long-lasting effects repeated injections may be needed (Zhang et al., 2009, Kim et al., 2010).

A) Intrathecal delivery of MSCs

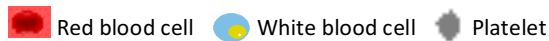


Advantages	Disadvantages
<ul style="list-style-type: none"> • Relatively easy and safe • In proximity to damaged areas (CSF) • Bypass BBB obstacle • Possibility of multiple injections both at cervical and lumbar levels 	<ul style="list-style-type: none"> • Limited migration into parenchyma • Low chance of differentiation

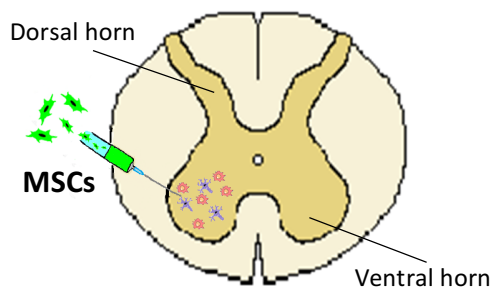
B) Intravenous delivery of MSCs



Advantages	Disadvantages
<ul style="list-style-type: none"> • Easy and safe procedure • Possibility of multiple injections 	<ul style="list-style-type: none"> • Very poor engraftment efficiency • Cells rapidly sequestered by lungs and spleen • No migration into the spinal cord parenchyma (BBB) • Limited beneficial effects



C) Intraspinal delivery of MSCs



Advantages	Disadvantages
<ul style="list-style-type: none"> • Injection site close to areas of degeneration • High engraftment efficiency • Higher chance of differentiation 	<ul style="list-style-type: none"> • Very invasive procedure • Multilevel injections would be needed



Figure 7.1. Delivery strategies for the transplantation of MSCs in ALS. (A) Intrathecal delivery of MSCs into the spinal cord CSF. (B) Systemic delivery of MSCs. (C) Local delivery of MSCs directly into the spinal cord parenchyma. For each delivery route, advantages and disadvantages are summarized. Adapted with permission from Ciervo et al., Advantages, challenges and future directions for stem cell therapy in amyotrophic lateral sclerosis, *Molecular Neurodegeneration*, 2017.

7.4 Triple separated co-culture: a method to screen for ADSC therapeutic potential and to investigate the molecular mechanisms of protection

The capacity of the MSC's secretome to protect MNs from oxidative insult and apoptotic stress has been recently demonstrated (Sun et al., 2013, Kim et al., 2014b). Moreover, previous *in vitro* studies showed that MSC conditioned medium was able to modify the phenotype of LPS-activated astrocytes by inducing the expression of the glutamate transporter 1 (Gu et al., 2010), by reducing the expression of pro-inflammatory genes (Schafer et al., 2012) and by modulating the expression of growth factors (Sun et al., 2013). Although these studies elucidated important mechanisms of protection of MSCs, the data were generated by using *in vitro* systems in which either MNs or astrocytes are exposed to H₂O₂ or LPS in order to induce MN damage or astrocyte activation respectively.

In the current study, we developed and validated a triple separated co-culture method that enable us to demonstrate for the first time, without using external factors, that ADSCs have the potential to protect MNs from ALS-linked astrocyte toxicity through paracrine mechanisms. More importantly, our system enabled testing of the therapeutic potential of ADSCs on human disease by using iAstrocytes derived from ALS patients. As a proof of principle we showed that ADSCs derived from mice were able to protect healthy MNs from toxic human iAstrocytes obtained from patients with either sporadic or familial ALS. Although we observed that the protective effect was patient specific, further studies using human ADSCs are needed to confirm our data, and to potentially categorise patients into responders and non-responders.

This complex *in vitro* co-culture system also enables the investigation of potential therapeutic mechanisms, since the different cell components can be separated and collected for analysis at any time point during the experiment. For instance, we showed mutual paracrine effects between ADSCs and astrocytes, and how the two cell components can influence each other depending on the astrocyte's genotype (NTg vs SOD1^{G93A}). Interestingly, ADSCs induced the expression and secretion of the anti-inflammatory factor IGF-1, and reduced the release of pro-inflammatory mediators including MCP-1, TNF- α , Il-6 and IL-1 β in cortical astrocytes derived from symptomatic SOD1^{G93A} transgenic mice. These data indicate that ADSCs have the potential to reduce neuro-inflammation by suppressing not only pro-inflammatory activated microglia, but also toxic reactive astrocytes (Noh et al., 2016). In addition, we showed that after exposure to ALS astrocytes, ADSCs express and secrete enhanced levels of IGF-1. In agreement with previous data, this could be considered

a positive protective response of ADSCs to the toxic ALS microenvironment (Nicaise et al., 2011).

Although mouse ADSCs protected MNs from the toxicity of human iAstrocytes derived from ALS patients, we did not observe significant changes in the gene expression of either growth factors or cytokines in human iAstrocytes following exposure to ADSCs. The discrepancy with the mouse astrocyte co-culture system, may suggest different mechanism of protection in humans. However, cross-species incompatibility and differences in the models (post-mortem tissue vs genetic reprogramming) may also account for the differences in data observed between the two systems data.

7.5 From the bench to the clinic: trial design for cell therapy in ALS

During the past two decades, several clinical trials investigated the use of stem cells in patients with ALS, mostly focusing on the safety and feasibility of the intervention. Nonetheless, as reported by Appel and Armon, stem cells have often been transplanted into ALS patients with limited preclinical data, without providing details on adverse effects and using small numbers of participants (Appel and Armon, 2016). Moreover, the long-term safety of stem cell transplantation (e.g. non acceleration of disease progression associated with the cell implantation) has been evaluated by comparison with historical control groups. This is an important limitation since heterogeneity in the patient population and differences in clinical care between the treated group and historical controls may affect the readouts (Appel and Armon, 2016). Although single-armed, small phase I/II clinical trials found that cell-based therapy for ALS is relatively safe and feasible, it is uncertain whether stem cell transplantation may be clinically beneficial leading to functional improvements or slowing of disease progression. The majority of the clinical trials were principally focused on the safety and feasibility of the surgical procedure related to the stem cell implantation. Secondly, these clinical trials were not powered to demonstrate any clinical benefit (Abdul Wahid et al., 2016).

In 2016, Abdul *et al.* published a systematic review aiming to assess the effectiveness of stem cell therapy in people with ALS, compared with a placebo or no additional treatment (Abdul Wahid et al., 2016). However, the authors could not identify any randomized controlled trial (RCT), quasi-RCT or clustered RCT involving the use of stem cells in ALS/MND patients. Thus, there is an absence of high-quality published evidence to assess the safety and efficacy of stem cell transplantation in ALS (Abdul Wahid et al., 2016). Moreover, when analyzing the single arm phase I/II clinical studies available in the literature, the authors found substantial variability between

clinical trials in terms of selection criteria, intervention methods and objective outcomes, with the involvement of small numbers of participants and a short-term follow-up period (Abdul Wahid et al., 2016). To investigate the long-term safety and efficacy of cellular therapy for ALS, well-designed prospective randomized-controlled trials with a larger sample size, long-term-follow up and standardization of cell products, are urgently needed (Abdul Wahid et al., 2016). Brainstorm Cell Therapeutics is currently recruiting ALS patients for the first worldwide phase 3 clinical trial evaluating the safety and efficacy of repeated intrathecal injections of MSC-NTFs. Importantly, this study will be the first to include a placebo sham/operation control group (NCT03280056).

Recently, the ALS Clinical Trials Workshop (Airlie Conference, Virginia, 2016), driven by the ALS community, clinicians, researchers, industry representatives, government representatives, ALS patients and family members, released and submitted to the FDA the draft version of the “Guidance for Industry on Drug Development for Amyotrophic Lateral Sclerosis” (van den Berg et al., 2019). The manuscript has been drafted with the intention of improving and accelerating the drug development process, including guidelines for a more effective clinical trial design in ALS. In particular, the guideline highlighted the importance of reducing clinical and genetic heterogeneity when establishing the patient selection criteria. With regards to clinical heterogeneity, inclusion and exclusion criteria for patient enrolment must be well justified for each study, which could vary depending on the phase of development. Selection criteria should also depend on the specific trial goals, since some therapies may be more effective in early stages of disease or in specific sub-groups of patients. Thus, investigators should endeavor to incorporate reliable predictive and prognostic biomarkers for clinical trial eligibility or stratification criteria (van den Berg et al., 2019). Because of the multifactorial nature of ALS, post-hoc analysis of reliable biological markers and neurophysiological data is extremely important, since in specific sub-groups of patients a beneficial effect could be missed during the analysis. However, responder analyses must only be used for hypothesis generation, which will need to be confirmed and further investigated in future trials.

Importantly, although early phase trials are not meant to investigate efficacy, for cell-based therapies which embrace potentially invasive delivery methods and lifelong biological effects, evaluation of efficacy should be included in the design of phase I trials. Furthermore, a long-term monitoring plan to evaluate tumorigenesis, stem cell engraftment and long-term efficacy should be included (van den Berg et al., 2019).

Finally, RCTs with placebo controls is considered the gold standard for clinical investigation. However, in rare, rapidly progressive and untreatable diseases such as ALS, the requirement for a placebo could be revisited, especially if the intervention involves invasive methods. While in phase III clinical trials a randomized placebo group is required, in earlier phase studies, the use of historical controls and predictive algorithms could be accepted. However, the development of target-specific biomarkers, standardization of outcome measures and validation of surrogate endpoints is essential, especially in cell-based studies in which the mechanisms mediating the therapeutic effect are not well established (van den Berg et al., 2019).

7.6 Concluding remarks and future directions

During the last decade, the great advances achieved in regenerative medicine have created an unprecedented enthusiasm and new hope for amelioration of the devastating and until now incurable disease such as ALS. The initial exciting idea of replacing loss of motor neurons, with MSCs is unlikely to be achieved, although other strategies may provide some promise for stem cell derived motor neuron replacement (Bryson et al., 2014). Indeed, transplanted cells should differentiate and integrate with the host spinal motor circuits within the toxic and non-permissive environment that characterizes ALS. However, the neuroprotective and immunomodulatory potential of MSCs could match perfectly with the multifactorial nature of ALS.

Among different tissue sources, ADSCs represent a promising candidate for clinical application. In the current study, we showed that when injected directly into the CSF of pre-symptomatic SOD1^{G93A} transgenic mice, ADSCs provide trophic support to MNs and possess the capacity to modulate the toxic ALS microenvironment, resulting in motor function improvements and delayed disease onset. The therapeutic potential of these cells was also confirmed *in vitro*, where ADSCs were able to protect MNs from ALS-linked astrocyte toxicity, without the need of being physically in contact with either MNs or astrocytes. In particular, for the first time we showed that ADSCs could reduce and inhibit the inflammatory phenotype of activated ALS astrocytes, while improving their trophic functions. Importantly, ADSCs also protected MNs from astrocytes derived from human ALS patients with either familial or sporadic disease, indicating that these cells could potentially be therapeutically effective in human disease regardless of the nature and genetic sub-type of the disease. A limitation of the current study is the exclusive use of the SOD1^{G93A} model to test for *in vivo* therapeutic intervention. Although these mice represent a robust and well characterized model of ALS, the model reflects the pathological features of only a

very small proportion of patients (Abel et al., 2012). Thus, transplantation studies in other ALS models such those driven by mutant TDP-43 and C9ORF72 expansions would be of interest (Arnold et al., 2013, Liu et al., 2016). In addition, further studies injecting cells after the onset of clinical signs of disease and evaluating disease progression and survival are needed. In particular, it would be interesting to determine whether multiple repeated injections of ADSCs would be more effective compared to a single stem cell injection. Although we provided insight into the potential mechanisms of protection, it will be crucial to study and identify which specific factors secreted by ADSCs are important in supporting MNs and modulating glial functions. In addition to the discovery of pathways that could be modified or corrected in ALS, the identification of the specific molecular mechanisms of protection could allow the identification of biomarkers that would be useful to perform quality control analysis on ADSCs to be used for clinical application.

Overall, several technical issues still need to be addressed including the identification of the best route for stem cell administration, the optimal cell dose, and the neuroprotective mechanisms of the transplanted cells. In addition, it needs to be considered that rate of proliferation, stemness properties, longevity and differentiation capacity of MSCs declines considerably with time when culturing cells as monolayers (Cheng et al., 2012). The advent of 3D culture systems, along with enormous progress in the fabrication of biomaterials must be considered. When maintained in 3D culture systems such as hanging drops, low-adhesion plates, porous scaffolds or hydrogels, hMSCs showed increased proliferation and migration capacity, enhanced colony-forming efficiency, higher expression of stem cell markers, greater neuronal differentiation ability and greater cellular engraftment after transplantation in animals (Cheng et al., 2012, Gao et al., 2014b, Cheng et al., 2013). Moreover, culture of MSCs as 3D spheroids induces a decrease in cell size which could be advantageous (Ge et al., 2014). Indeed, the relatively large size of MSCs expanded in a 2D system is a limiting factor, both in terms of maximum injectable cell dose, vascular obstruction and limited migratory capacity. Thus, the regenerative potential of stem cells could be considerably improved by adopting 3D culture methods. Transplantation of bio-scaffolds or encapsulating MSCs to sustain favorable conditions for stem cell survival, growth, migration and maturation is showing promising results in experimental models of spinal cord injury, traumatic brain injury and nerve regeneration, and must be considered in ALS models where the presence of a hostile microenvironment is one of the main factors that negatively affects stem cell engraftment and therefore therapeutic potential (Gao et al., 2014b, Shen et al., 2012, Shrestha et al., 2014).

The optimal maturation level for the transplantation of stem cells to obtain the greatest therapeutic benefit is also unclear. If undifferentiated cells may represent the best way to achieve immunomodulation and trophic factor production, induced neural progenitors may overcome the possibility of tumor formation, along with the possibility of *in vivo* maturation and integration into existing neuronal circuits.

In addition, although intrathecal delivery may represent the preferred route of administration of MSCs in ALS patients, methods to improve cell migration and engraftment into the spinal cord parenchyma are needed. If on the one hand, clinical benefits could be achieved without integration into the host spinal cord parenchyma, on the other hand, multiple and repeated injections might be necessary. This may represent an important limitation, because of the large amount of cells needed and consequently the high costs related to manufacturing, cell banking and patient care/hospitalization. Genetic manipulation of ADSCs in order to induce expression of chemokine receptors or other cell membrane components important in adhesion and migration may represent a potential strategy to enhance the homing capacity of these cells (Chen et al., 2013, Zhang et al., 2017). In the current study we showed that induced expression of the CCR2 receptor in human ADSCs by lentivirus transduction is feasible and well tolerated by the cells. Further *in vitro* and pre-clinical studies aiming to investigate whether the migratory capacity of hADSCs towards a MCP-1 gradient is improved by CCR2 expression are needed. Historically, the evaluation of the presence of injected cells in the host has been carried out by the exclusive use of immunohistochemistry. Adopting advanced microscopy techniques such as confocal and two-photon microscopy would be of great interest to confirm stem cell engraftment, which could also allow tracking *in vivo* the fate of transplanted cells (Scott et al., 2014, Malide et al., 2014).

Although autologous transplantation can reduce the probability of immune rejection, it has been reported that patient-derived MSCs may have impaired or reduced therapeutic effects (Koh et al., 2012, Cho et al., 2010). Other evidence indicates no functional alteration or accelerated cellular senescence in BM-MSCs derived from sporadic cases of ALS (Ferrero et al., 2008). Moreover, it has been shown that there was the possibility of functionally restoring defective ALS-derived MSCs by correcting alterations in DNA methylation (Oh et al., 2016, Ferrero et al., 2008). However, the identification of MSC biological markers predictive of a positive/negative therapeutic response in ALS patients would be of great value (Kim et al., 2014a). In relation to the use of autologous MSCs in patients carrying ALS causative genetic mutations, stem cells could be genetically corrected by adopting CRISPR-Cas9-mediated gene

editing technology (Wu et al., 2015). Nevertheless, it would be interesting to test the therapeutic potential of MSCs derived from ALS patients in the SOD1^{G93A} mouse model, and compare the effects with MSCs derived from healthy donors.

Finally, although MSCs are currently considered as advanced therapy medical products (ATMP), and both the Food and Drug Administration (FDA) and the European Medicines Agency (EMA) have released guidelines about isolation, manipulation and manufacturing quality control methods, the majority of published culture protocols appear less than optimal (Lukomska et al., 2019). The main concerns are related to the use of enzymes for tissue dissociation, culture supplements of animal origins for cell expansion, and standardization of culture protocol in compliance with GMP requirement (Lukomska et al., 2019). Thus, development and optimization of methods for the isolation, expansion and manipulation of clinical grade MSCs is essential before moving towards clinical translation.

In conclusion, the use of ADSCs as a cell therapy approach for ALS holds great promise, however, several hurdles still need to be addressed. All the discussed parameters should be reconsidered and optimized before the translation of stem cell therapy from mice to humans in order to avoid undesirable delays or therapy failure as has happened for most of the promising results derived from SOD1^{G93A} transgenic mouse models, with failure of translation into clinical benefits for ALS patients.

8 References

- Guidance for Industry Drug Development for Amyotrophic Lateral Sclerosis. 2016. <http://www.alsa.org/advocacy/fda/assets/als-drug-development-guidance-for-public-comment-5-2-16.pdf> . Accessed 23 Aug 2017.
- ABDANIPOUR, A. & TIRAIHI, T. 2012. Induction of adipose-derived stem cell into motoneuron-like cells using selegiline as preinducer. *Brain Res*, 1440, 23-33.
- ABDUL WAHID, S. F., LAW, Z. K., ISMAIL, N. A., AZMAN ALI, R. & LAI, N. M. 2016. Cell-based therapies for amyotrophic lateral sclerosis/motor neuron disease. *Cochrane Database Syst Rev*, 11, Cd011742.
- ABEL, O., POWELL, J. F., ANDERSEN, P. M. & AL-CHALABI, A. 2012. ALSod: A user-friendly online bioinformatics tool for amyotrophic lateral sclerosis genetics. *Hum Mutat*, 33, 1345-51.
- ACAZ-FONSECA, E., ORTIZ-RODRIGUEZ, A., AZCOITIA, I., GARCIA-SEGURA, L. M. & AREVALO, M. A. 2019. Notch signaling in astrocytes mediates their morphological response to an inflammatory challenge. *Cell Death Discov*, 5, 85.
- AEBISCHER, J., CASSINA, P., OTSMANE, B., MOUMEN, A., SEILHEAN, D., MEININGER, V., BARBEITO, L., PETTMANN, B. & RAOUL, C. 2010. IFN γ triggers a LIGHT-dependent selective death of motoneurons contributing to the non-cell-autonomous effects of mutant SOD1. *Cell Death And Differentiation*, 18, 754.
- AHMADI, N., RAZAVI, S., KAZEMI, M. & ORYAN, S. 2012. Stability of neural differentiation in human adipose derived stem cells by two induction protocols. *Tissue Cell*, 44, 87-94.
- ALBERSEN, M., BERKERS, J., DEKONINCK, P., DEPREST, J., LUE, T. F., HEDLUND, P., LIN, C.-S., BIVALACQUA, T. J., VAN POPPEL, H., DE RIDDER, D. & VAN DER AA, F. 2013. Expression of a Distinct Set of Chemokine Receptors in Adipose Tissue-Derived Stem Cells is Responsible for In Vitro Migration Toward Chemokines Appearing in the Major Pelvic Ganglion Following Cavernous Nerve Injury. *Sexual medicine*, 1, 3-15.
- ALEXANDER, G. M., DEITCH, J. S., SEEBURGER, J. L., DEL VALLE, L. & HEIMAN-PATTERSON, T. D. 2000. Elevated cortical extracellular fluid glutamate in transgenic mice expressing human mutant (G93A) Cu/Zn superoxide dismutase. *J Neurochem*, 74, 1666-73.
- ALEXANDER, G. M., ERWIN, K. L., BYERS, N., DEITCH, J. S., AUGELLI, B. J., BLANKENHORN, E. P. & HEIMAN-PATTERSON, T. D. 2004. Effect of transgene copy number on survival in the G93A SOD1 transgenic mouse model of ALS. *Brain Res Mol Brain Res*, 130, 7-15.
- ALEXIANU, M. E., KOZOVSKA, M. & APPEL, S. H. 2001. Immune reactivity in a mouse model of familial ALS correlates with disease progression. *Neurology*, 57, 1282-9.
- ALLEN, S. P., HALL, B., CASTELLI, L. M., FRANCIS, L., WOOF, R., SISKOS, A. P., KOULOURA, E., GRAY, E., THOMPSON, A. G., TALBOT, K., HIGGINBOTTOM, A., MYSZCZYNSKA, M., ALLEN, C. F., STOPFORD, M. J., HEMINGWAY, J., BAUER, C. S., WEBSTER, C. P., DE VOS, K. J., TURNER, M. R., KEUN, H. C., HAUTBERGUE, G. M., FERRAIUOLO, L. &

- SHAW, P. J. 2019. Astrocyte adenosine deaminase loss increases motor neuron toxicity in amyotrophic lateral sclerosis. *Brain*, 142, 586-605.
- ALSHIKHO, M. J., ZURCHER, N. R., LOGGIA, M. L., CERNASOV, P., REYNOLDS, B., PIJANOWSKI, O., CHONDE, D. B., IZQUIERDO GARCIA, D., MAINERO, C., CATANA, C., CHAN, J., BABU, S., PAGANONI, S., HOOKER, J. M. & ATASSI, N. 2018. Integrated magnetic resonance imaging and [(11) C]-PBR28 positron emission tomographic imaging in amyotrophic lateral sclerosis. *Ann Neurol*, 83, 1186-1197.
- ALVAREZ-BUYLLA, A., LING, C. Y. & KIRN, J. R. 1990. Cresyl violet: a red fluorescent Nissl stain. *J Neurosci Methods*, 33, 129-33.
- ANDERSEN, P. M. & AL-CHALABI, A. 2011. Clinical genetics of amyotrophic lateral sclerosis: what do we really know? *Nat Rev Neurol*, 7, 603-15.
- ANDERSON, P., CARRILLO-GALVEZ, A. B., GARCIA-PEREZ, A., COBO, M. & MARTIN, F. 2013. CD105 (endoglin)-negative murine mesenchymal stromal cells define a new multipotent subpopulation with distinct differentiation and immunomodulatory capacities. *PLoS One*, 8, e76979.
- ANDERSON, P., CARRILLO-GÁLVEZ, A. B. AND MARTÍN, F. 2015. Isolation of Murine Adipose Tissue-derived Mesenchymal Stromal Cells (mASCs) and the Analysis of Their Proliferation in vitro. *BioProtocol*, 5.
- AOKI, Y., MANZANO, R., LEE, Y., DAFINCA, R., AOKI, M., DOUGLAS, A. G. L., VARELA, M. A., SATHYAPRAKASH, C., SCABER, J., BARBAGALLO, P., VADER, P., MAGER, I., EZZAT, K., TURNER, M. R., ITO, N., GASCO, S., OHBAYASHI, N., EL ANDALOUSSI, S., TAKEDA, S., FUKUDA, M., TALBOT, K. & WOOD, M. J. A. 2017. C9orf72 and RAB7L1 regulate vesicle trafficking in amyotrophic lateral sclerosis and frontotemporal dementia. *Brain*, 140, 887-897.
- APPEL, S. H. & ARMON, C. 2016. Stem cells in amyotrophic lateral sclerosis: Ready for prime time? *Neurology*. United States.
- ARNOLD, E. S., LING, S. C., HUELGA, S. C., LAGIER-TOURENNE, C., POLYMENIDOU, M., DITSWORTH, D., KORDASIEWICZ, H. B., MCALONIS-DOWNES, M., PLATOSHYN, O., PARONE, P. A., DA CRUZ, S., CLUTARIO, K. M., SWING, D., TESSAROLLO, L., MARSALA, M., SHAW, C. E., YEO, G. W. & CLEVELAND, D. W. 2013. ALS-linked TDP-43 mutations produce aberrant RNA splicing and adult-onset motor neuron disease without aggregation or loss of nuclear TDP-43. *Proc Natl Acad Sci U S A*, 110, E736-45.
- ASHJIAN, P. H., ELBARBARY, A. S., EDMONDS, B., DEUGARTE, D., ZHU, M., ZUK, P. A., LORENZ, H. P., BENHAIM, P. & HEDRICK, M. H. 2003. In vitro differentiation of human processed lipoaspirate cells into early neural progenitors. *Plast Reconstr Surg*, 111, 1922-31.
- AZZOUZ, M., RALPH, G. S., STORKEBAUM, E., WALMSLEY, L. E., MITROPHANOUS, K. A., KINGSMAN, S. M., CARMELIET, P. & MAZARAKIS, N. D. 2004. VEGF delivery with retrogradely transported lentivector prolongs survival in a mouse ALS model. *Nature*, 429, 413-417.
- BAEK, S. J., KANG, S. K. & RA, J. C. 2011. In vitro migration capacity of human adipose tissue-derived mesenchymal stem cells reflects their expression of receptors for chemokines and growth factors. *Exp Mol Med*, 43, 596-603.
- BAGLIONI, S., FRANCALANCI, M., SQUECCO, R., LOMBARDI, A., CANTINI, G., ANGELI, R., GELMINI, S., GUASTI, D., BENVENUTI, S., ANNUNZIATO, F., BANI, D., LIOTTA, F., FRANCINI, F., PERIGLI, G., SERIO, M. & LUCONI, M. 2009. Characterization of human adult stem-cell populations isolated from visceral and subcutaneous adipose tissue. *Faseb j*, 23, 3494-505.
- BAHAT-STROOMZA, M., BARHUM, Y., LEVY, Y. S., KARPOV, O., BULVIK, S., MELAMED, E. & OFFEN, D. 2009. Induction of adult human bone marrow

- mesenchymal stromal cells into functional astrocyte-like cells: potential for restorative treatment in Parkinson's disease. *J Mol Neurosci*, 39, 199-210.
- BAHMANI, L., TAHA, M. F. & JAVERI, A. 2014. Coculture with embryonic stem cells improves neural differentiation of adipose tissue-derived stem cells. *Neuroscience*, 272, 229-39.
- BALOH, R. H., GLASS, J. D. & SVENDSEN, C. N. 2018. Stem cell transplantation for amyotrophic lateral sclerosis. *Curr Opin Neurol*, 31, 655-661.
- BARBER, S. C. & SHAW, P. J. 2010. Oxidative stress in ALS: key role in motor neuron injury and therapeutic target. *Free Radic Biol Med*, 48, 629-41.
- BARON, P., BUSSINI, S., CARDIN, V., CORBO, M., CONTI, G., GALIMBERTI, D., SCARPINI, E., BRESOLIN, N., WHARTON, S. B., SHAW, P. J. & SILANI, V. 2005. Production of monocyte chemoattractant protein-1 in amyotrophic lateral sclerosis. *Muscle Nerve*, 32, 541-4.
- BARTOLI, C., CIVATTE, M., PELLISSIER, J. F. & FIGARELLA-BRANGER, D. 2001. CCR2A and CCR2B, the two isoforms of the monocyte chemoattractant protein-1 receptor are up-regulated and expressed by different cell subsets in idiopathic inflammatory myopathies. *Acta Neuropathol*, 102, 385-92.
- BASSO, M., POZZI, S., TORTAROLO, M., FIORDALISO, F., BISIGHINI, C., PASETTO, L., SPALTRO, G., LIDONNICI, D., GENSANO, F., BATTAGLIA, E., BENDOTTI, C. & BONETTO, V. 2013. Mutant copper-zinc superoxide dismutase (SOD1) induces protein secretion pathway alterations and exosome release in astrocytes: implications for disease spreading and motor neuron pathology in amyotrophic lateral sclerosis. *The Journal of biological chemistry*, 288, 15699-15711.
- BEANE, O. S., FONSECA, V. C., COOPER, L. L., KOREN, G. & DARLING, E. M. 2014. Impact of aging on the regenerative properties of bone marrow-, muscle-, and adipose-derived mesenchymal stem/stromal cells. *PLoS One*, 9, e115963.
- BEERS, D. R. & APPEL, S. H. 2019. Immune dysregulation in amyotrophic lateral sclerosis: mechanisms and emerging therapies. *Lancet Neurol*, 18, 211-220.
- BEERS, D. R., HENKEL, J. S., XIAO, Q., ZHAO, W., WANG, J., YEN, A. A., SIKLOS, L., MCKERCHER, S. R. & APPEL, S. H. 2006. Wild-type microglia extend survival in PU.1 knockout mice with familial amyotrophic lateral sclerosis. *Proceedings of the National Academy of Sciences of the United States of America*, 103, 16021-16026.
- BEERS, D. R., ZHAO, W., LIAO, B., KANO, O., WANG, J., HUANG, A., APPEL, S. H. & HENKEL, J. S. 2011. Neuroinflammation modulates distinct regional and temporal clinical responses in ALS mice. *Brain Behav Immun*, 25, 1025-35.
- BELEMA-BEDADA, F., UCHIDA, S., MARTIRE, A., KOSTIN, S. & BRAUN, T. 2008. Efficient homing of multipotent adult mesenchymal stem cells depends on FROUNT-mediated clustering of CCR2. *Cell Stem Cell*, 2, 566-75.
- BELLINI, M. J., HERENU, C. B., GOYA, R. G. & GARCIA-SEGURA, L. M. 2011. Insulin-like growth factor-I gene delivery to astrocytes reduces their inflammatory response to lipopolysaccharide. *J Neuroinflammation*, 8, 21.
- BENKLER, C., BARHUM, Y., BEN-ZUR, T. & OFFEN, D. 2016. Multifactorial Gene Therapy Enhancing the Glutamate Uptake System and Reducing Oxidative Stress Delays Symptom Onset and Prolongs Survival in the SOD1-G93A ALS Mouse Model. *J Mol Neurosci*, 58, 46-58.
- BENNETT, E. J., MEAD, R. J., AZZOUZ, M., SHAW, P. J. & GRIERSON, A. J. 2014. Early Detection of Motor Dysfunction in the SOD1G93A Mouse Model of Amyotrophic Lateral Sclerosis (ALS) Using Home Cage Running Wheels. *PLoS One*, 9, e107918.

- BERNARDES, D. & OLIVEIRA, A. L. R. 2017. Comprehensive catwalk gait analysis in a chronic model of multiple sclerosis subjected to treadmill exercise training. *BMC neurology*, 17, 160-160.
- BLANQUER, M., MORALEDA, J. M., INIESTA, F., GOMEZ-ESPUGH, J., MECALALLANA, J., VILLAVERDE, R., PEREZ-ESPEJO, M. A., RUIZ-LOPEZ, F. J., GARCIA SANTOS, J. M., BLEDA, P., IZURA, V., SAEZ, M., DE MINGO, P., VIVANCOS, L., CARLES, R., JIMENEZ, J., HERNANDEZ, J., GUARDIOLA, J., DEL RIO, S. T., ANTUNEZ, C., DE LA ROSA, P., MAJADO, M. J., SANCHEZ-SALINAS, A., LOPEZ, J., MARTINEZ-LAGE, J. F. & MARTINEZ, S. 2012. Neurotrophic bone marrow cellular nests prevent spinal motoneuron degeneration in amyotrophic lateral sclerosis patients: a pilot safety study. *Stem Cells*, 30, 1277-85.
- BLANQUER, M., PEREZ-ESPEJO, M. A., MARTINEZ-LAGE, J. F., INIESTA, F., MARTINEZ, S. & MORALEDA, J. M. 2010. A surgical technique of spinal cord cell transplantation in amyotrophic lateral sclerosis. *J Neurosci Methods*, 191, 255-7.
- BOGAERT, E., VAN DAMME, P., VAN DEN BOSCH, L. & ROBBERECHT, W. 2006. Vascular endothelial growth factor in amyotrophic lateral sclerosis and other neurodegenerative diseases. *Muscle Nerve*, 34, 391-405.
- BOIDO, M., PIRAS, A., VALSECCHI, V., SPIGOLON, G., MARESCHI, K., FERRERO, I., VIZZINI, A., TEMI, S., MAZZINI, L., FAGIOLI, F. & VERCELLI, A. 2014. Human mesenchymal stromal cell transplantation modulates neuroinflammatory milieu in a mouse model of amyotrophic lateral sclerosis. *Cytotherapy*, 16, 1059-72.
- BOILLEE, S., YAMANAKA, K., LOBSIGER, C. S., COPELAND, N. G., JENKINS, N. A., KASSIOTIS, G., KOLLIAS, G. & CLEVELAND, D. W. 2006. Onset and progression in inherited ALS determined by motor neurons and microglia. *Science*, 312, 1389-92.
- BOILLÉE, S., YAMANAKA, K., LOBSIGER, C. S., COPELAND, N. G., JENKINS, N. A., KASSIOTIS, G., KOLLIAS, G. & CLEVELAND, D. W. 2006. Onset and Progression in Inherited ALS Determined by Motor Neurons and Microglia. *Science*, 312, 1389.
- BONAFEDE, R., SCAMBI, I., PERONI, D., POTRICH, V., BOSCHI, F., BENATI, D., BONETTI, B. & MARIOTTI, R. 2015. Exosome derived from murine adipose-derived stromal cells: Neuroprotective effect on in vitro model of amyotrophic lateral sclerosis. *Exp Cell Res*.
- BONAFEDE, R., SCAMBI, I., PERONI, D., POTRICH, V., BOSCHI, F., BENATI, D., BONETTI, B. & MARIOTTI, R. 2016. Exosome derived from murine adipose-derived stromal cells: Neuroprotective effect on in vitro model of amyotrophic lateral sclerosis. *Exp Cell Res*, 340, 150-8.
- BORCHELT, D. R. 2006. Amyotrophic lateral sclerosis--are microglia killing motor neurons? *N Engl J Med*, 355, 1611-3.
- BORCHELT, D. R., LEE, M. K., SLUNT, H. S., GUARNIERI, M., XU, Z. S., WONG, P. C., BROWN, R. H., JR., PRICE, D. L., SISODIA, S. S. & CLEVELAND, D. W. 1994. Superoxide dismutase 1 with mutations linked to familial amyotrophic lateral sclerosis possesses significant activity. *Proc Natl Acad Sci U S A*, 91, 8292-6.
- BOUCHERIE, C., SCHAFER, S., LAVAND'HOMME, P., MALOTEAUX, J. M. & HERMANS, E. 2009. Chimerization of astroglial population in the lumbar spinal cord after mesenchymal stem cell transplantation prolongs survival in a rat model of amyotrophic lateral sclerosis. *J Neurosci Res*, 87, 2034-46.
- BOURIN, P., BUNNELL, B. A., CASTEILLA, L., DOMINICI, M., KATZ, A. J., MARCH, K. L., REDL, H., RUBIN, J. P., YOSHIMURA, K. & GIMBLE, J. M. 2013. Stromal cells from the adipose tissue-derived stromal vascular fraction and culture expanded adipose tissue-derived stromal/stem cells: a joint

- statement of the International Federation for Adipose Therapeutics and Science (IFATS) and the International Society for Cellular Therapy (ISCT). *Cytotherapy*, 15, 641-8.
- BRAMBILLA, L., GUIDOTTI, G., MARTORANA, F., IYER, A. M., ARONICA, E., VALORI, C. F. & ROSSI, D. 2016. Disruption of the astrocytic TNFR1-GDNF axis accelerates motor neuron degeneration and disease progression in amyotrophic lateral sclerosis. *Hum Mol Genet*, 25, 3080-3095.
- BRITES, D. & VAZ, A. R. 2014. Microglia Centered Pathogenesis in ALS: Insights in Cell Interconnectivity. *Frontiers in Cellular Neuroscience*, 8:117.
- BROCKINGTON, A., WHARTON, S. B., FERNANDO, M., GELSTHORPE, C. H., BAXTER, L., INCE, P. G., LEWIS, C. E. & SHAW, P. J. 2006. Expression of vascular endothelial growth factor and its receptors in the central nervous system in amyotrophic lateral sclerosis. *J Neuropathol Exp Neurol*, 65, 26-36.
- BRUESTLE, D. A., CUTLER, R. G., TELLJOHANN, R. S. & MATTSON, M. P. 2009. Decline in daily running distance presages disease onset in a mouse model of ALS. *Neuromolecular medicine*, 11, 58-62.
- BRUIJN, L. I., BECHER, M. W., LEE, M. K., ANDERSON, K. L., JENKINS, N. A., COPELAND, N. G., SISODIA, S. S., ROTHSTEIN, J. D., BORCHELT, D. R., PRICE, D. L. & CLEVELAND, D. W. 1997. ALS-linked SOD1 mutant G85R mediates damage to astrocytes and promotes rapidly progressive disease with SOD1-containing inclusions. *Neuron*, 18, 327-38.
- BRYSON, J. B., MACHADO, C. B., CROSSLEY, M., STEVENSON, D., BROSFACER, V., BURRONE, J., GREENSMITH, L. & LIEBERAM, I. 2014. Optical control of muscle function by transplantation of stem cell-derived motor neurons in mice. *Science*, 344, 94-7.
- CABEZAS, R., AVILA-RODRIGUEZ, M., VEGA-VELA, N. E., ECHEVERRIA, V., GONZALEZ, J., HIDALGO, O. A., SANTOS, A. B., ALIEV, G. & BARRETO, G. E. 2016. Growth Factors and Astrocytes Metabolism: Possible Roles for Platelet Derived Growth Factor. *Med Chem*, 12, 204-10.
- CAO, M., PAN, Q., DONG, H., YUAN, X., LI, Y., SUN, Z., DONG, X. & WANG, H. 2015. Adipose-derived mesenchymal stem cells improve glucose homeostasis in high-fat diet-induced obese mice. *Stem Cell Res Ther*, 6, 208.
- CAO, Z., ZHANG, G., WANG, F., LIU, H., LIU, L., HAN, Y., ZHANG, J. & YUAN, J. 2013. Protective effects of mesenchymal stem cells with CXCR4 up-regulation in a rat renal transplantation model. *PLoS One*, 8, e82949.
- CARRI, M. T., VALLE, C., BOZZO, F. & COZZOLINO, M. 2015. Oxidative stress and mitochondrial damage: importance in non-SOD1 ALS. *Front Cell Neurosci*, 9, 41.
- CASSINA, P., CASSINA, A., PEHAR, M., CASTELLANOS, R., GANDELMAN, M., DE LEÓN, A., ROBINSON, K. M., MASON, R. P., BECKMAN, J. S., BARBEITO, L. & RADI, R. 2008. Mitochondrial Dysfunction in SOD1^{G93A}-Bearing Astrocytes Promotes Motor Neuron Degeneration: Prevention by Mitochondrial-Targeted Antioxidants. *The Journal of Neuroscience*, 28, 4115.
- CEDARBAUM, J. M., STAMBLER, N., MALTA, E., FULLER, C., HILT, D., THURMOND, B. & NAKANISHI, A. 1999. The ALSFRS-R: a revised ALS functional rating scale that incorporates assessments of respiratory function. BDNF ALS Study Group (Phase III). *J Neurol Sci*, 169, 13-21.
- CHAN-IL, C., YOUNG-DON, L., HEEJAUNG, K., KIM, S. H., SUH-KIM, H. & KIM, S. S. 2013. Neural induction with neurogenin 1 enhances the therapeutic potential of mesenchymal stem cells in an amyotrophic lateral sclerosis mouse model. *Cell Transplant*, 22, 855-70.

- CHANDRASEKARAN, A., AVCI, H. X., LEIST, M., KOBOLÁK, J. & DINNYÉS, A. 2016. Astrocyte Differentiation of Human Pluripotent Stem Cells: New Tools for Neurological Disorder Research. *Frontiers in cellular neuroscience*, 10, 215-215.
- CHARO, I. F., MYERS, S. J., HERMAN, A., FRANCI, C., CONNOLLY, A. J. & COUGHLIN, S. R. 1994. Molecular cloning and functional expression of two monocyte chemoattractant protein 1 receptors reveals alternative splicing of the carboxyl-terminal tails. *Proc Natl Acad Sci U S A*, 91, 2752-6.
- CHEN, H., MIN, X. H., WANG, Q. Y., LEUNG, F. W., SHI, L., ZHOU, Y., YU, T., WANG, C. M., AN, G., SHA, W. H. & CHEN, Q. K. 2015a. Pre-activation of mesenchymal stem cells with TNF-alpha, IL-1beta and nitric oxide enhances its paracrine effects on radiation-induced intestinal injury. *Sci Rep*, 5, 8718.
- CHEN, H., QIAN, K., CHEN, W., HU, B., BLACKBOURN, L. W. T., DU, Z., MA, L., LIU, H., KNOBEL, K. M., AYALA, M. & ZHANG, S.-C. 2015b. Human-derived neural progenitors functionally replace astrocytes in adult mice. *The Journal of clinical investigation*, 125, 1033-1042.
- CHEN, W., LI, M., CHENG, H., YAN, Z., CAO, J., PAN, B., SANG, W., WU, Q., ZENG, L., LI, Z. & XU, K. 2013. Overexpression of the mesenchymal stem cell Cxcr4 gene in irradiated mice increases the homing capacity of these cells. *Cell Biochem Biophys*, 67, 1181-91.
- CHENG, N. C., CHEN, S. Y., LI, J. R. & YOUNG, T. H. 2013. Short-term spheroid formation enhances the regenerative capacity of adipose-derived stem cells by promoting stemness, angiogenesis, and chemotaxis. *Stem Cells Transl Med*, 2, 584-94.
- CHENG, N. C., WANG, S. & YOUNG, T. H. 2012. The influence of spheroid formation of human adipose-derived stem cells on chitosan films on stemness and differentiation capabilities. *Biomaterials*, 33, 1748-58.
- CHENG, Z., OU, L., ZHOU, X., LI, F., JIA, X., ZHANG, Y., LIU, X., LI, Y., WARD, C. A., MELO, L. G. & KONG, D. 2008. Targeted migration of mesenchymal stem cells modified with CXCR4 gene to infarcted myocardium improves cardiac performance. *Mol Ther*, 16, 571-9.
- CHERRY, J. D., OLSCHOWKA, J. A. & O'BANION, M. K. 2014. Neuroinflammation and M2 microglia: the good, the bad, and the inflamed. *J Neuroinflammation*, 11, 98.
- CHO, G. W., NOH, M. Y., KIM, H. Y., KOH, S. H., KIM, K. S. & KIM, S. H. 2010. Bone marrow-derived stromal cells from amyotrophic lateral sclerosis patients have diminished stem cell capacity. *Stem Cells Dev*, 19, 1035-42.
- CHOI, Y. K., LEE, D. H., SEO, Y. K., JUNG, H., PARK, J. K. & CHO, H. 2014. Stimulation of neural differentiation in human bone marrow mesenchymal stem cells by extremely low-frequency electromagnetic fields incorporated with MNPs. *Appl Biochem Biotechnol*, 174, 1233-45.
- CIERVO, Y., NING, K., JUN, X., SHAW, P. J. & MEAD, R. J. 2017. Advances, challenges and future directions for stem cell therapy in amyotrophic lateral sclerosis. *Mol Neurodegener*, 12, 85.
- CIRULLI, E. T., LASSEIGNE, B. N., PETROVSKI, S., SAPP, P. C., DION, P. A., LEBLOND, C. S., COUTHOUIS, J., LU, Y. F., WANG, Q., KRUEGER, B. J., REN, Z., KEEBLER, J., HAN, Y., LEVY, S. E., BOONE, B. E., WIMBISH, J. R., WAITE, L. L., JONES, A. L., CARULLI, J. P., DAY-WILLIAMS, A. G., STAROPOLI, J. F., XIN, W. W., CHESI, A., RAPHAEL, A. R., MCKENNA-YASEK, D., CADY, J., VIANNEY DE JONG, J. M., KENNA, K. P., SMITH, B. N., TOPP, S., MILLER, J., GKAZI, A., AL-CHALABI, A., VAN DEN BERG, L. H., VELDINK, J., SILANI, V., TICOZZI, N., SHAW, C. E., BALOH, R. H., APPEL, S., SIMPSON, E., LAGIER-TOURENNE, C., PULST, S. M., GIBSON, S., TROJANOWSKI, J. Q., ELMAN, L., MCCLUSKEY, L., GROSSMAN, M., SHNEIDER, N. A., CHUNG, W. K., RAVITS, J. M.,

- GLASS, J. D., SIMS, K. B., VAN DEERLIN, V. M., MANIATIS, T., HAYES, S. D., ORDUREAU, A., SWARUP, S., LANDERS, J., BAAS, F., ALLEN, A. S., BEDLACK, R. S., HARPER, J. W., GITLER, A. D., ROULEAU, G. A., BROWN, R., HARMS, M. B., COOPER, G. M., HARRIS, T., MYERS, R. M. & GOLDSTEIN, D. B. 2015. Exome sequencing in amyotrophic lateral sclerosis identifies risk genes and pathways. *Science*, 347, 1436-41.
- CLAYTON, J. A. 2016. Studying both sexes: a guiding principle for biomedicine. *Faseb Journal*, 30, 519-524.
- CLEMENT, A. M., NGUYEN, M. D., ROBERTS, E. A., GARCIA, M. L., BOILLEE, S., RULE, M., MCMAHON, A. P., DOUCETTE, W., SIWEK, D., FERRANTE, R. J., BROWN, R. H., JR., JULIEN, J. P., GOLDSTEIN, L. S. & CLEVELAND, D. W. 2003. Wild-type nonneuronal cells extend survival of SOD1 mutant motor neurons in ALS mice. *Science*, 302, 113-7.
- CLEVELAND, D. W., BRUIJN, L. I., WONG, P. C., MARSZALEK, J. R., VECHIO, J. D., LEE, M. K., XU, X. S., BORCHELT, D. R., SISODIA, S. S. & PRICE, D. L. 1996. Mechanisms of selective motor neuron death in transgenic mouse models of motor neuron disease. *Neurology*, 47, S54-61; discussion S61-2.
- CONDUCTIER, G., BLONDEAU, N., GUYON, A., NAHON, J. L. & ROVERE, C. 2010. The role of monocyte chemoattractant protein MCP1/CCL2 in neuroinflammatory diseases. *J Neuroimmunol*, 224, 93-100.
- COOPER-KNOCK, J., KIRBY, J., HIGHLEY, R. & SHAW, P. J. 2015. The Spectrum of C9orf72-mediated Neurodegeneration and Amyotrophic Lateral Sclerosis. *Neurotherapeutics*, 12, 326-39.
- COOPER-KNOCK, J., MOLL, T., RAMESH, T., CASTELLI, L., BEER, A., ROBINS, H., FOX, I., NIEDERMOSER, I., VAN DAMME, P., MOISSE, M., ROBBERECHT, W., HARDIMAN, O., PANADES, M. P., ASSIALIOU, A., MORA, J. S., BASAK, A. N., MORRISON, K. E., SHAW, C. E., AL-CHALABI, A., LANDERS, J. E., WYLES, M., HEATH, P. R., HIGGINBOTTOM, A., WALSH, T., KAZOKA, M., MCDERMOTT, C. J., HAUTBERGUE, G. M., KIRBY, J. & SHAW, P. J. 2019. Mutations in the Glycosyltransferase Domain of GLT8D1 Are Associated with Familial Amyotrophic Lateral Sclerosis. *Cell Rep*, 26, 2298-2306.e5.
- CROSIO, C., VALLE, C., CASCIATI, A., IACCARINO, C. & CARRI, M. T. 2011. Astroglial inhibition of NF-kappaB does not ameliorate disease onset and progression in a mouse model for amyotrophic lateral sclerosis (ALS). *PLoS One*, 6, e17187.
- DARVISHI, M., TIRAIHI, T., MESBAH-NAMIN, S. A., DELSHAD, A. & TAHERI, T. 2016. Motor Neuron Transdifferentiation of Neural Stem Cell from Adipose-Derived Stem Cell Characterized by Differential Gene Expression. *Cell Mol Neurobiol*.
- DAS, M. M. & SVENDSEN, C. N. 2015. Astrocytes show reduced support of motor neurons with aging that is accelerated in a rodent model of ALS. *Neurobiol Aging*, 36, 1130-9.
- DAVID, K. S., OLIVEIRA, E. R. A., HORTA, B. A. C., VALENTE, A. P. & DE PAULA, V. S. 2017. Insights into CC Chemokine Ligand 2/Chemokine Receptor 2 Molecular Recognition: A Step Forward toward Antichemotactic Agents. *Biochemistry*, 56, 3197-3210.
- DAVIS, H. E., ROSINSKI, M., MORGAN, J. R. & YARMUSH, M. L. 2004. Charged polymers modulate retrovirus transduction via membrane charge neutralization and virus aggregation. *Biophysical journal*, 86, 1234-1242.
- DEJESUS-HERNANDEZ, M., MACKENZIE, I. R., BOEVE, B. F., BOXER, A. L., BAKER, M., RUTHERFORD, N. J., NICHOLSON, A. M., FINCH, N. A., FLYNN, H., ADAMSON, J., KOURI, N., WOJTAS, A., SENGDY, P., HSIUNG, G. Y., KARYDAS, A., SEELEY, W. W., JOSEPHS, K. A., COPPOLA, G., GESCHWIND, D. H., WSZOLEK, Z. K., FELDMAN, H.,

- KNOPMAN, D. S., PETERSEN, R. C., MILLER, B. L., DICKSON, D. W., BOYLAN, K. B., GRAFF-RADFORD, N. R. & RADEMAKERS, R. 2011. Expanded GGGGCC hexanucleotide repeat in noncoding region of C9ORF72 causes chromosome 9p-linked FTD and ALS. *Neuron*, 72, 245-56.
- DENG, H. X., CHEN, W., HONG, S. T., BOYCOTT, K. M., GORRIE, G. H., SIDDIQUE, N., YANG, Y., FECTO, F., SHI, Y., ZHAI, H., JIANG, H., HIRANO, M., RAMPERSAUD, E., JANSEN, G. H., DONKERVOORT, S., BIGIO, E. H., BROOKS, B. R., AJROUD, K., SUFIT, R. L., HAINES, J. L., MUGNAINI, E., PERICAK-VANCE, M. A. & SIDDIQUE, T. 2011. Mutations in UBQLN2 cause dominant X-linked juvenile and adult-onset ALS and ALS/dementia. *Nature*, 477, 211-5.
- DENG, H. X., SHI, Y., FURUKAWA, Y., ZHAI, H., FU, R., LIU, E., GORRIE, G. H., KHAN, M. S., HUNG, W. Y., BIGIO, E. H., LUKAS, T., DAL CANTO, M. C., O'HALLORAN, T. V. & SIDDIQUE, T. 2006. Conversion to the amyotrophic lateral sclerosis phenotype is associated with intermolecular linked insoluble aggregates of SOD1 in mitochondria. *Proc Natl Acad Sci U S A*, 103, 7142-7.
- DENNING, W., DAS, S., GUO, S., XU, J., KAPPES, J. C. & HEL, Z. 2013. Optimization of the transductional efficiency of lentiviral vectors: effect of sera and polycations. *Molecular biotechnology*, 53, 308-314.
- DI GIORGIO, F. P., BOULTING, G. L., BOBROWICZ, S. & EGGAN, K. C. 2008. Human Embryonic Stem Cell-Derived Motor Neurons Are Sensitive to the Toxic Effect of Glial Cells Carrying an ALS-Causing Mutation. *Cell Stem Cell*, 3, 637-648.
- DI GIORGIO, F. P., CARRASCO, M. A., SIAO, M. C., MANIATIS, T. & EGGAN, K. 2007. Non-cell autonomous effect of glia on motor neurons in an embryonic stem cell-based ALS model. *Nat Neurosci*, 10, 608-14.
- DIDIER, N., ROMERO, I. A., CREMINON, C., WIJKHUISEN, A., GRASSI, J. & MABONDZO, A. 2003. Secretion of interleukin-1beta by astrocytes mediates endothelin-1 and tumour necrosis factor-alpha effects on human brain microvascular endothelial cell permeability. *J Neurochem*, 86, 246-54.
- DIMOS, J. T., RODOLFA, K. T., NIAKAN, K. K., WEISENTHAL, L. M., MITSUMOTO, H., CHUNG, W., CROFT, G. F., SAPHIER, G., LEIBEL, R., GOLAND, R., WICHTERLE, H., HENDERSON, C. E. & EGGAN, K. 2008. Induced pluripotent stem cells generated from patients with ALS can be differentiated into motor neurons. *Science*, 321, 1218-21.
- DODGE, J. C., HAIDET, A. M., YANG, W., PASSINI, M. A., HESTER, M., CLARKE, J., ROSKELLEY, E. M., TRELEAVEN, C. M., RIZO, L., MARTIN, H., KIM, S. H., KASPAR, R., TAKSIR, T. V., GRIFFITHS, D. A., CHENG, S. H., SHIHABUDDIN, L. S. & KASPAR, B. K. 2008. Delivery of AAV-IGF-1 to the CNS Extends Survival in ALS Mice Through Modification of Aberrant Glial Cell Activity. *Molecular Therapy*, 16, 1056-1064.
- DODGE, J. C., TRELEAVEN, C. M., FIDLER, J. A., HESTER, M., HAIDET, A., HANDY, C., RAO, M., EAGLE, A., MATTHEWS, J. C., TAKSIR, T. V., CHENG, S. H., SHIHABUDDIN, L. S. & KASPAR, B. K. 2010. AAV4-mediated expression of IGF-1 and VEGF within cellular components of the ventricular system improves survival outcome in familial ALS mice. *Mol Ther*, 18, 2075-84.
- DOMINICI, M., LE BLANC, K., MUELLER, I., SLAPER-CORTENBACH, I., MARINI, F., KRAUSE, D., DEANS, R., KEATING, A., PROCKOP, D. & HORWITZ, E. 2006. Minimal criteria for defining multipotent mesenchymal stromal cells. The International Society for Cellular Therapy position statement. *Cytotherapy*, 8, 315-7.

- EGGENHOFER, E., BENSELER, V., KROEMER, A., POPP, F. C., GEISLER, E. K., SCHLITT, H. J., BAAN, C. C., DAHLKE, M. H. & HOOGDUIJN, M. J. 2012. Mesenchymal stem cells are short-lived and do not migrate beyond the lungs after intravenous infusion. *Front Immunol*, 3, 297.
- EGGENHOFER, E., LUK, F., DAHLKE, M. H. & HOOGDUIJN, M. J. 2014. The life and fate of mesenchymal stem cells. *Frontiers in immunology*, 5, 148-148.
- EHRHART, J., SMITH, A. J., KUZMIN-NICHOLS, N., ZESIEWICZ, T. A., JAHAN, I., SHYTLER, R. D., KIM, S.-H., SANBERG, C. D., VU, T. H., GOOCH, C. L., SANBERG, P. R. & GARBUZOVA-DAVIS, S. 2015. Humoral factors in ALS patients during disease progression. *Journal of Neuroinflammation*, 12, 127.
- EKESTERN, E. 2004. Neurotrophic Factors and Amyotrophic Lateral Sclerosis. *Neurodegenerative Diseases*, 1, 88-100.
- ELAHI, K. C., KLEIN, G., AVCI-ADALI, M., SIEVERT, K. D., MACNEIL, S. & AICHER, W. K. 2016. Human Mesenchymal Stromal Cells from Different Sources Diverge in Their Expression of Cell Surface Proteins and Display Distinct Differentiation Patterns. *Stem cells international*, 2016, 5646384-5646384.
- ENDO, F., KOMINE, O., FUJIMORI-TONOU, N., KATSUNO, M., JIN, S., WATANABE, S., SOBUE, G., DEZAWA, M., WYSS-CORAY, T. & YAMANAKA, K. 2015. Astrocyte-derived TGF-beta1 accelerates disease progression in ALS mice by interfering with the neuroprotective functions of microglia and T cells. *Cell Rep*, 11, 592-604.
- FARG, M. A., SUNDARAMOORTHY, V., SULTANA, J. M., YANG, S., ATKINSON, R. A. K., LEVINA, V., HALLORAN, M. A., GLEESON, P. A., BLAIR, I. P., SOO, K. Y., KING, A. E. & ATKIN, J. D. 2014. C9ORF72, implicated in amyotrophic lateral sclerosis and frontotemporal dementia, regulates endosomal trafficking. *Human molecular genetics*, 23, 3579-3595.
- FARINA, C., ALOISI, F. & MEINL, E. 2007. Astrocytes are active players in cerebral innate immunity. *Trends Immunol*, 28, 138-45.
- FEENEY, S. J., MCKELVIE, P. A., AUSTIN, L., JEAN-FRANCOIS, M. J., KAPSA, R., TOMBS, S. M. & BYRNE, E. 2001. Presymptomatic motor neuron loss and reactive astrocytosis in the SOD1 mouse model of amyotrophic lateral sclerosis. *Muscle Nerve*, 24, 1510-9.
- FENG, N., HAN, Q., LI, J., WANG, S., LI, H., YAO, X. & ZHAO, R. C. 2014. Generation of highly purified neural stem cells from human adipose-derived mesenchymal stem cells by Sox1 activation. *Stem Cells Dev*, 23, 515-29.
- FERRAIUOLO, L. 2014. The non-cell-autonomous component of ALS: new in vitro models and future challenges. *Biochem Soc Trans*, 42, 1270-4.
- FERRAIUOLO, L., HEATH, P. R., HOLDEN, H., KASHER, P., KIRBY, J. & SHAW, P. J. 2007. Microarray analysis of the cellular pathways involved in the adaptation to and progression of motor neuron injury in the SOD1 G93A mouse model of familial ALS. *J Neurosci*, 27, 9201-19.
- FERRAIUOLO, L., HIGGINBOTTOM, A., HEATH, P. R., BARBER, S., GREENALD, D., KIRBY, J. & SHAW, P. J. 2011. Dysregulation of astrocyte-motoneuron cross-talk in mutant superoxide dismutase 1-related amyotrophic lateral sclerosis. *Brain*, 134, 2627-41.
- FERRAIUOLO, L., MEYER, K., SHERWOOD, T. W., VICK, J., LIKHTE, S., FRAKES, A., MIRANDA, C. J., BRAUN, L., HEATH, P. R., PINEDA, R., BEATTIE, C. E., SHAW, P. J., ASKWITH, C. C., MCTIGUE, D. & KASPAR, B. K. 2016. Oligodendrocytes contribute to motor neuron death in ALS via SOD1-dependent mechanism. *Proceedings of the National Academy of Sciences of the United States of America*, 113, E6496-E6505.
- FERREIRA, J. R., TEIXEIRA, G. Q., SANTOS, S. G., BARBOSA, M. A., ALMEIDA-PORADA, G. & GONÇALVES, R. M. 2018. Mesenchymal Stromal Cell

- Secretome: Influencing Therapeutic Potential by Cellular Pre-conditioning. *Frontiers in Immunology*, 9, 2837.
- FERRERO, I., MAZZINI, L., RUSTICHELLI, D., GUNETTI, M., MARESCHI, K., TESTA, L., NASUELLI, N., OGGIONI, G. D. & FAGIOLI, F. 2008. Bone marrow mesenchymal stem cells from healthy donors and sporadic amyotrophic lateral sclerosis patients. *Cell Transplant*, 17, 255-66.
- FERRUCCI, M., LAZZERI, G., FLAIBANI, M., BIAGIONI, F., CANTINI, F., MADONNA, M., BUCCI, D., LIMANAQI, F., SOLDANI, P. & FORNAI, F. 2018. In search for a gold-standard procedure to count motor neurons in the spinal cord. *Histol Histopathol*, 33, 1021-1046.
- FOROSTYAK, S., HOMOLA, A., TURNOVCOVA, K., SVITIL, P., JENDELOVA, P. & SYKOVA, E. 2014. Intrathecal delivery of mesenchymal stromal cells protects the structure of altered perineuronal nets in SOD1 rats and amends the course of ALS. *Stem Cells*, 32, 3163-72.
- FORSBERG, K., GRAFFMO, K., PAKKENBERG, B., WEBER, M., NIELSEN, M., MARKLUND, S., BRANNSTROM, T. & ANDERSEN, P. M. 2019. Misfolded SOD1 inclusions in patients with mutations in C9orf72 and other ALS/FTD-associated genes. *J Neurol Neurosurg Psychiatry*.
- FORSBERG, K., JONSSON, P. A., ANDERSEN, P. M., BERGEMALM, D., GRAFFMO, K. S., HULTDIN, M., JACOBSSON, J., ROSQUIST, R., MARKLUND, S. L. & BRANNSTROM, T. 2010. Novel antibodies reveal inclusions containing non-native SOD1 in sporadic ALS patients. *PLoS One*, 5, e11552.
- FRAKES, A. E., FERRAIUOLO, L., HAIDET-PHILLIPS, A. M., SCHMELZER, L., BRAUN, L., MIRANDA, C. J., LADNER, K. J., BEVAN, A. K., FOUST, K. D., GODBOUT, J. P., POPOVICH, P. G., GUTTRIDGE, D. C. & KASPAR, B. K. 2014. Microglia induce motor neuron death via the classical NF- κ B pathway in amyotrophic lateral sclerosis. *Neuron*, 81, 1009-1023.
- FREISCHMIDT, A., WIELAND, T., RICHTER, B., RUF, W., SCHAEFFER, V., MULLER, K., MARROQUIN, N., NORDIN, F., HUBERS, A., WEYDT, P., PINTO, S., PRESS, R., MILLECAMPS, S., MOLKO, N., BERNARD, E., DESNUELLE, C., SORIANI, M. H., DORST, J., GRAF, E., NORDSTROM, U., FEILER, M. S., PUTZ, S., BOECKERS, T. M., MEYER, T., WINKLER, A. S., WINKELMAN, J., DE CARVALHO, M., THAL, D. R., OTTO, M., BRANNSTROM, T., VOLK, A. E., KURSULA, P., DANZER, K. M., LICHTNER, P., DIKIC, I., MEITINGER, T., LUDOLPH, A. C., STROM, T. M., ANDERSEN, P. M. & WEISHAUPT, J. H. 2015. Haploinsufficiency of TBK1 causes familial ALS and fronto-temporal dementia. *Nat Neurosci*, 18, 631-6.
- FRESE, L., DIJKMAN, P. E. & HOERSTRUP, S. P. 2016. Adipose Tissue-Derived Stem Cells in Regenerative Medicine. *Transfusion medicine and hemotherapy : offzielles Organ der Deutschen Gesellschaft fur Transfusionsmedizin und Immunhamatologie*, 43, 268-274.
- FRITZ, E., IZAURIETA, P., WEISS, A., MIR, F. R., ROJAS, P., GONZALEZ, D., ROJAS, F., BROWN, R. H., JR., MADRID, R. & VAN ZUNDERT, B. 2013. Mutant SOD1-expressing astrocytes release toxic factors that trigger motoneuron death by inducing hyperexcitability. *J Neurophysiol*, 109, 2803-14.
- FU, L., ZHU, L., HUANG, Y., LEE, T. D., FORMAN, S. J. & SHIH, C. C. 2008. Derivation of neural stem cells from mesenchymal stem cells: evidence for a bipotential stem cell population. *Stem Cells Dev*, 17, 1109-21.
- FUJITA, K., KATO, T., YAMAUCHI, M., ANDO, M., HONDA, M. & NAGATA, Y. 1998. Increases in Fragmented Glial Fibrillary Acidic Protein Levels in the Spinal Cords of Patients with Amyotrophic Lateral Sclerosis. *Neurochemical Research*, 23, 169-174.

- GALIEVA, L. R., JAMES, V., MUKHAMEDSHINA, Y. O. & RIZVANOV, A. A. 2019. Therapeutic Potential of Extracellular Vesicles for the Treatment of Nerve Disorders. *Frontiers in neuroscience*, 13, 163-163.
- GALIPEAU, J. & SENSEBE, L. 2018. Mesenchymal Stromal Cells: Clinical Challenges and Therapeutic Opportunities. *Cell Stem Cell*, 22, 824-833.
- GALLIHER-BECKLEY, A. J., LAN, L.-Q., AONO, S., WANG, L. & SHI, J. 2013. Caspase-1 activation and mature interleukin-1 β release are uncoupled events in monocytes. *World journal of biological chemistry*, 4, 30-34.
- GAO, L., ZHOU, S., CAI, H., GONG, Z. & ZANG, D. 2014a. VEGF levels in CSF and serum in mild ALS patients. *J Neurol Sci*, 346, 216-20.
- GAO, S., ZHAO, P., LIN, C., SUN, Y., WANG, Y., ZHOU, Z., YANG, D., WANG, X., XU, H., ZHOU, F., CAO, L., ZHOU, W., NING, K., CHEN, X. & XU, J. 2014b. Differentiation of human adipose-derived stem cells into neuron-like cells which are compatible with photocurable three-dimensional scaffolds. *Tissue Eng Part A*, 20, 1271-84.
- GARBUZOVA-DAVIS, S., EHRHART, J., SANBERG, P. R. & BORLONGAN, C. V. 2018. Potential Role of Humoral IL-6 Cytokine in Mediating Pro-Inflammatory Endothelial Cell Response in Amyotrophic Lateral Sclerosis. *Int J Mol Sci*, 19.
- GE, J., GUO, L., WANG, S., ZHANG, Y., CAI, T., ZHAO, R. C. & WU, Y. 2014. The size of mesenchymal stem cells is a significant cause of vascular obstructions and stroke. *Stem Cell Rev Rep*, 10, 295-303.
- GELOSO, M. C., CORVINO, V., MARCHESE, E., SERRANO, A., MICHETTI, F. & D'AMBROSI, N. 2017. The Dual Role of Microglia in ALS: Mechanisms and Therapeutic Approaches. *Front Aging Neurosci*, 9, 242.
- GINIS, I., GRINBLAT, B. & SHIRVAN, M. H. 2012. Evaluation of bone marrow-derived mesenchymal stem cells after cryopreservation and hypothermic storage in clinically safe medium. *Tissue Eng Part C Methods*, 18, 453-63.
- GIUNTI, D., PARODI, B., USAI, C., VERGANI, L., CASAZZA, S., BRUZZONE, S., MANCARDI, G. & UCCELLI, A. 2012. Mesenchymal Stem Cells Shape Microglia Effector Functions Through the Release of CX3CL1. *STEM CELLS*, 30, 2044-2053.
- GONG, Y. H., PARSADANIAN, A. S., ANDREEVA, A., SNIDER, W. D. & ELLIOTT, J. L. 2000. Restricted expression of G86R Cu/Zn superoxide dismutase in astrocytes results in astrocytosis but does not cause motoneuron degeneration. *J Neurosci*, 20, 660-5.
- GOTHELF, Y., ABRAMOV, N., HAREL, A. & OFFEN, D. 2014. Safety of repeated transplantations of neurotrophic factors-secreting human mesenchymal stromal stem cells. *Clinical and translational medicine*, 3, 21-21.
- GOTHELF, Y., KASPI, H., ABRAMOV, N. & ARICHA, R. 2017. miRNA profiling of NurOwn(R): mesenchymal stem cells secreting neurotrophic factors. *Stem Cell Res Ther*, 8, 249.
- GOWING, G., PHILIPS, T., VAN WIJMEERSCH, B., AUDET, J. N., DEWIL, M., VAN DEN BOSCH, L., BILLIAU, A. D., ROBBERECHT, W. & JULIEN, J. P. 2008. Ablation of proliferating microglia does not affect motor neuron degeneration in amyotrophic lateral sclerosis caused by mutant superoxide dismutase. *J Neurosci*, 28, 10234-44.
- GRAVEL, M., BELAND, L. C., SOUCY, G., ABDELHAMID, E., RAHIMIAN, R., GRAVEL, C. & KRIZ, J. 2016. IL-10 Controls Early Microglial Phenotypes and Disease Onset in ALS Caused by Misfolded Superoxide Dismutase 1. *J Neurosci*, 36, 1031-48.
- GREENWOOD, S. K., HILL, R. B., SUN, J. T., ARMSTRONG, M. J., JOHNSON, T. E., GARA, J. P. & GALLOWAY, S. M. 2004. Population doubling: a simple and more accurate estimation of cell growth suppression in the in vitro assay

- for chromosomal aberrations that reduces irrelevant positive results. *Environ Mol Mutagen*, 43, 36-44.
- GRSKOVIC, M., JAVAHERIAN, A., STRULOVICI, B. & DALEY, G. Q. 2011. Induced pluripotent stem cells--opportunities for disease modelling and drug discovery. *Nat Rev Drug Discov*, 10, 915-29.
- GU, R., HOU, X., PANG, R., LI, L., CHEN, F., GENG, J., XU, Y. & ZHANG, C. 2010. Human adipose-derived stem cells enhance the glutamate uptake function of GLT1 in SOD1(G93A)-bearing astrocytes. *Biochem Biophys Res Commun*, 393, 481-6.
- GUASTI, L., PRASONGCHEAN, W., KLEFTOURIS, G., MUKHERJEE, S., THRASHER, A. J., BULSTRODE, N. W. & FERRETTI, P. 2012. High plasticity of pediatric adipose tissue-derived stem cells: too much for selective skeletogenic differentiation? *Stem Cells Transl Med*, 1, 384-95.
- GUO, H., LAI, L., BUTCHBACH, M. E., STOCKINGER, M. P., SHAN, X., BISHOP, G. A. & LIN, C. L. 2003. Increased expression of the glial glutamate transporter EAAT2 modulates excitotoxicity and delays the onset but not the outcome of ALS in mice. *Hum Mol Genet*, 12, 2519-32.
- GUPTA, P. K., PRABHAKAR, S., SHARMA, S. & ANAND, A. 2011. Vascular endothelial growth factor-A (VEGF-A) and chemokine ligand-2 (CCL2) in amyotrophic lateral sclerosis (ALS) patients. *J Neuroinflammation*, 8, 47.
- GURNEY, M. E., PU, H., CHIU, A. Y., DAL CANTO, M. C., POLCHOW, C. Y., ALEXANDER, D. D., CALIENDO, J., HENTATI, A., KWON, Y. W., DENG, H. X. & ET AL. 1994. Motor neuron degeneration in mice that express a human Cu,Zn superoxide dismutase mutation. *Science*, 264, 1772-5.
- HABISCH, H. J., JANOWSKI, M., BINDER, D., KUZMA-KOZAKIEWICZ, M., WIDMANN, A., HABICH, A., SCHWALENSTOCKER, B., HERMANN, A., BRENNER, R., LUKOMSKA, B., DOMANSKA-JANIK, K., LUDOLPH, A. C. & STORCH, A. 2007. Intrathecal application of neuroectodermally converted stem cells into a mouse model of ALS: limited intraparenchymal migration and survival narrows therapeutic effects. *J Neural Transm (Vienna)*, 114, 1395-406.
- HAIDET-PHILLIPS, A. M., GROSS, S. K., WILLIAMS, T., TUTEJA, A., SHERMAN, A., KO, M., JEONG, Y. H., WONG, P. C. & MARAGAKIS, N. J. 2013. Altered astrocytic expression of TDP-43 does not influence motor neuron survival. *Exp Neurol*, 250, 250-9.
- HAIDET-PHILLIPS, A. M., HESTER, M. E., MIRANDA, C. J., MEYER, K., BRAUN, L., FRAKES, A., SONG, S., LIKHITE, S., MURTHA, M. J., FOUST, K. D., RAO, M., EAGLE, A., KAMMESHEIDT, A., CHRISTENSEN, A., MENDELL, J. R., BURGHESE, A. H. & KASPAR, B. K. 2011. Astrocytes from familial and sporadic ALS patients are toxic to motor neurons. *Nat Biotechnol*, 29, 824-8.
- HALL, E. D., OOSTVEEN, J. A. & GURNEY, M. E. 1998. Relationship of microglial and astrocytic activation to disease onset and progression in a transgenic model of familial ALS. *Glia*, 23, 249-56.
- HAN, C., SUN, X., LIU, L., JIANG, H., SHEN, Y., XU, X., LI, J., ZHANG, G., HUANG, J., LIN, Z., XIONG, N. & WANG, T. 2016. Exosomes and Their Therapeutic Potentials of Stem Cells. *Stem Cells Int*, 2016, 7653489.
- HAN, C., ZHANG, L., SONG, L., LIU, Y., ZOU, W., PIAO, H. & LIU, J. 2014. Human adipose-derived mesenchymal stem cells: a better cell source for nervous system regeneration. *Chin Med J (Engl)*, 127, 329-37.
- HARANDI, V. M., LINDQUIST, S., KOLAN, S. S., BRÄNNSTRÖM, T. & LIU, J.-X. 2014. Analysis of neurotrophic factors in limb and extraocular muscles of mouse model of amyotrophic lateral sclerosis. *PLoS one*, 9, e109833-e109833.
- HARDIMAN, O., AL-CHALABI, A., CHIO, A., CORR, E. M., LOGROSCINO, G., ROBBERECHT, W., SHAW, P. J., SIMMONS, Z. & VAN DEN BERG, L. H.

- 2017a. Amyotrophic lateral sclerosis. *Nature Reviews Disease Primers*, 3, 17071.
- HARDIMAN, O., AL-CHALABI, A., CHIO, A., CORR, E. M., LOGROSCINO, G., ROBBERECHT, W., SHAW, P. J., SIMMONS, Z. & VAN DEN BERG, L. H. 2017b. Amyotrophic lateral sclerosis. *Nat Rev Dis Primers*, 3, 17071.
- HARDIMAN, O. & VAN DEN BERG, L. H. 2017. Edaravone: a new treatment for ALS on the horizon? *Lancet Neurol*, 16, 490-491.
- HE, M., DONG, H., HUANG, Y., LU, S., ZHANG, S., QIAN, Y. & JIN, W. 2016. Astrocyte-Derived CCL2 is Associated with M1 Activation and Recruitment of Cultured Microglial Cells. *Cellular Physiology and Biochemistry*, 38, 859-870.
- HENKEL, J. S., BEERS, D. R., SIKLOS, L. & APPEL, S. H. 2006. The chemokine MCP-1 and the dendritic and myeloid cells it attracts are increased in the mSOD1 mouse model of ALS. *Mol Cell Neurosci*, 31, 427-37.
- HENKEL, J. S., BEERS, D. R., WEN, S., RIVERA, A. L., TOENNIS, K. M., APPEL, J. E., ZHAO, W., MOORE, D. H., POWELL, S. Z. & APPEL, S. H. 2013. Regulatory T-lymphocytes mediate amyotrophic lateral sclerosis progression and survival. *EMBO Mol Med*, 5, 64-79.
- HENKEL, J. S., ENGELHARDT, J. I., SIKLOS, L., SIMPSON, E. P., KIM, S. H., PAN, T., GOODMAN, J. C., SIDDIQUE, T., BEERS, D. R. & APPEL, S. H. 2004. Presence of dendritic cells, MCP-1, and activated microglia/macrophages in amyotrophic lateral sclerosis spinal cord tissue. *Ann Neurol*, 55, 221-35.
- HENRIQUES, A., PITZER, C. & SCHNEIDER, A. 2010. Neurotrophic Growth Factors for the Treatment of Amyotrophic Lateral Sclerosis: Where Do We Stand? *Front Neurosci*, 4.
- HENSLEY, K., ABDEL-MOATY, H., HUNTER, J., MHATRE, M., MOU, S., NGUYEN, K., POTAPOVA, T., PYE, Q. N., QI, M., RICE, H., STEWART, C., STROUKOFF, K. & WEST, M. 2006. Primary glia expressing the G93A-SOD1 mutation present a neuroinflammatory phenotype and provide a cellular system for studies of glial inflammation. *Journal of neuroinflammation*, 3, 2-2.
- HERMANN, A., GASTL, R., LIEBAU, S., POPA, M. O., FIEDLER, J., BOEHM, B. O., MAISEL, M., LERCHE, H., SCHWARZ, J., BRENNER, R. & STORCH, A. 2004. Efficient generation of neural stem cell-like cells from adult human bone marrow stromal cells. *J Cell Sci*, 117, 4411-22.
- HIGHLEY, J. R., KIRBY, J., JANSWEIJER, J. A., WEBB, P. S., HEWAMADDUMA, C. A., HEATH, P. R., HIGGINBOTTOM, A., RAMAN, R., FERRAIUOLO, L., COOPER-KNOCK, J., MCDERMOTT, C. J., WHARTON, S. B., SHAW, P. J. & INCE, P. G. 2014. Loss of nuclear TDP-43 in amyotrophic lateral sclerosis (ALS) causes altered expression of splicing machinery and widespread dysregulation of RNA splicing in motor neurones. *Neuropathol Appl Neurobiol*, 40, 670-85.
- HONCZARENKO, M., LE, Y., SWIERKOWSKI, M., GHIRAN, I., GLODEK, A. M. & SILBERSTEIN, L. E. 2006. Human bone marrow stromal cells express a distinct set of biologically functional chemokine receptors. *Stem Cells*, 24, 1030-41.
- HONG, S., HWANG, D.-Y., YOON, S., ISACSON, O., RAMEZANI, A., HAWLEY, R. G. & KIM, K.-S. 2007. Functional analysis of various promoters in lentiviral vectors at different stages of in vitro differentiation of mouse embryonic stem cells. *Molecular therapy : the journal of the American Society of Gene Therapy*, 15, 1630-1639.
- HOWLAND, D. S., LIU, J., SHE, Y., GOAD, B., MARAGAKIS, N. J., KIM, B., ERICKSON, J., KULIK, J., DEVITO, L., PSALTIS, G., DEGENNARO, L. J., CLEVELAND, D. W. & ROTHSTEIN, J. D. 2002. Focal loss of the glutamate

- transporter EAAT2 in a transgenic rat model of SOD1 mutant-mediated amyotrophic lateral sclerosis (ALS). *Proc Natl Acad Sci U S A*, 99, 1604-9.
- HU, H., LIN, H., DUAN, W., CUI, C., LI, Z., LIU, Y., WANG, W., WEN, D., WANG, Y. & LI, C. 2018. Intrathecal Injection of scAAV9-hIGF1 Prolongs the Survival of ALS Model Mice by Inhibiting the NF- κ B Pathway. *Neuroscience*, 381, 1-10.
- HU, Y., CAO, C., QIN, X.-Y., YU, Y., YUAN, J., ZHAO, Y. & CHENG, Y. 2017. Increased peripheral blood inflammatory cytokine levels in amyotrophic lateral sclerosis: a meta-analysis study. *Scientific reports*, 7, 9094-9094.
- HUANG, C., TONG, J., BI, F., ZHOU, H. & XIA, X. G. 2012. Mutant TDP-43 in motor neurons promotes the onset and progression of ALS in rats. *J Clin Invest*, 122, 107-18.
- HUANG, J., ZHANG, Z., GUO, J., NI, A., DEB, A., ZHANG, L., MIROTSOU, M., PRATT, R. E. & DZAU, V. J. 2010. Genetic modification of mesenchymal stem cells overexpressing CCR1 increases cell viability, migration, engraftment, and capillary density in the injured myocardium. *Circ Res*, 106, 1753-62.
- HUANG, Y., WANG, J., CAI, J., QIU, Y., ZHENG, H., LAI, X., SUI, X., WANG, Y., LU, Q., ZHANG, Y., YUAN, M., GONG, J., CAI, W., LIU, X., SHAN, Y., DENG, Z., SHI, Y., SHU, Y., ZHANG, L., QIU, W., PENG, L., REN, J., LU, Z. & XIANG, A. P. 2018. Targeted homing of CCR2-overexpressing mesenchymal stromal cells to ischemic brain enhances post-stroke recovery partially through PRDX4-mediated blood-brain barrier preservation. *Theranostics*, 8, 5929-5944.
- IANNITTI, T., SCARROTT, J. M., LIKHTE, S., COLDICOTT, I. R. P., LEWIS, K. E., HEATH, P. R., HIGGINBOTTOM, A., MYSZCZYNSKA, M. A., MILO, M., HAUTBERGUE, G. M., MEYER, K., KASPAR, B. K., FERRAIUOLO, L., SHAW, P. J. & AZZOUZ, M. 2018. Translating SOD1 Gene Silencing toward the Clinic: A Highly Efficacious, Off-Target-free, and Biomarker-Supported Strategy for fALS. *Molecular therapy. Nucleic acids*, 12, 75-88.
- ICHIM, C. V. & WELLS, R. A. 2011. Generation of high-titer viral preparations by concentration using successive rounds of ultracentrifugation. *J Transl Med*, 9, 137.
- ILIEVA, H., POLYMERIDOU, M. & CLEVELAND, D. W. 2009. Non-cell autonomous toxicity in neurodegenerative disorders: ALS and beyond. *J Cell Biol*, 187, 761-72.
- ILZECKA, J. 2004. Cerebrospinal fluid vascular endothelial growth factor in patients with amyotrophic lateral sclerosis. *Clin Neurol Neurosurg*, 106, 289-93.
- IWASHITA, Y., CRANG, A. J. & BLAKEMORE, W. F. 2000. Redistribution of bisbenzimidazole Hoechst 33342 from transplanted cells to host cells. *Neuroreport*, 11, 1013-6.
- JAARSMA, D., TEULING, E., HAASDIJK, E. D., DE ZEEUW, C. I. & HOOGENRAAD, C. C. 2008. Neuron-specific expression of mutant superoxide dismutase is sufficient to induce amyotrophic lateral sclerosis in transgenic mice. *J Neurosci*, 28, 2075-88.
- JANG, S., CHO, H. H., CHO, Y. B., PARK, J. S. & JEONG, H. S. 2010. Functional neural differentiation of human adipose tissue-derived stem cells using bFGF and forskolin. *BMC Cell Biol*, 11, 25.
- JANOWSKI, M., KUZMA-KOZAKIEWICZ, M., BINDER, D., HABISCH, H. J., HABICH, A., LUKOMSKA, B., DOMANSKA-JANIK, K., LUDOLPH, A. C. & STORCH, A. 2008. Neurotransplantation in mice: the concorde-like position ensures minimal cell leakage and widespread distribution of cells transplanted into the cisterna magna. *Neurosci Lett*, 430, 169-74.
- JEYACHANDRAN, A., MERTENS, B., MCKISSICK, E. A. & MITCHELL, C. S. 2015. Type I Vs. Type II Cytokine Levels as a Function of SOD1 G93A Mouse

- Amyotrophic Lateral Sclerosis Disease Progression. *Frontiers in cellular neuroscience*, 9, 462-462.
- JI, Y., DUAN, W., LIU, Y., LIU, Y., LIU, C., LI, Y., WEN, D., LI, Z. & LI, C. 2018. IGF1 affects macrophage invasion and activation and TNF- α production in the sciatic nerves of female SOD1G93A mice. *Neuroscience Letters*, 668, 1-6.
- JIANG, J., ZHU, Q., GENDRON, T. F., SABERI, S., MCALONIS-DOWNES, M., SEELMAN, A., STAUFFER, J. E., JAFAR-NEJAD, P., DRENNER, K., SCHULTE, D., CHUN, S., SUN, S., LING, S. C., MYERS, B., ENGELHARDT, J., KATZ, M., BAUGHN, M., PLATOSHYN, O., MARSALA, M., WATT, A., HEYSER, C. J., ARD, M. C., DE MUYNCK, L., DAUGHRITY, L. M., SWING, D. A., TESSAROLLO, L., JUNG, C. J., DELPOUX, A., UTZSCHNEIDER, D. T., HEDRICK, S. M., DE JONG, P. J., EDBAUER, D., VAN DAMME, P., PETRUCCELLI, L., SHAW, C. E., BENNETT, C. F., DA CRUZ, S., RAVITS, J., RIGO, F., CLEVELAND, D. W. & LAGIER-TOURENNE, C. 2016. Gain of Toxicity from ALS/FTD-Linked Repeat Expansions in C9ORF72 Is Alleviated by Antisense Oligonucleotides Targeting GGGGCC-Containing RNAs. *Neuron*, 90, 535-50.
- JIANG, X.-S., NI, Y.-Q., LIU, T.-J., ZHANG, M., REN, H., JIANG, R., HUANG, X. & XU, G.-Z. 2012. CCR2 overexpression promotes the efficient recruitment of retinal microglia in vitro. *Molecular vision*, 18, 2982-2992.
- JIN, H. J., PARK, S. K., OH, W., YANG, Y. S., KIM, S. W. & CHOI, S. J. 2009. Down-regulation of CD105 is associated with multi-lineage differentiation in human umbilical cord blood-derived mesenchymal stem cells. *Biochem Biophys Res Commun*, 381, 676-81.
- JOE, I. S., JEONG, S.-G. & CHO, G.-W. 2014. Resveratrol-induced SIRT1 activation promotes neuronal differentiation of human bone marrow mesenchymal stem cells. *Neuroscience Letters*, 584, 97-102.
- JOHNSON, B. S., SNEAD, D., LEE, J. J., MCCAFFERY, J. M., SHORTER, J. & GITLER, A. D. 2009. TDP-43 is intrinsically aggregation-prone, and amyotrophic lateral sclerosis-linked mutations accelerate aggregation and increase toxicity. *J Biol Chem*, 284, 20329-39.
- JOHNSON, J. O., MANDRIOLI, J., BENATAR, M., ABRAMZON, Y., VAN DEERLIN, V. M., TROJANOWSKI, J. Q., GIBBS, J. R., BRUNETTI, M., GRONKA, S., WUU, J., DING, J., MCCLUSKEY, L., MARTINEZ-LAGE, M., FALCONE, D., HERNANDEZ, D. G., AREPALLI, S., CHONG, S., SCHYMICK, J. C., ROTHSTEIN, J., LANDI, F., WANG, Y. D., CALVO, A., MORA, G., SABATELLI, M., MONSURRO, M. R., BATTISTINI, S., SALVI, F., SPATARO, R., SOLA, P., BORGHERO, G., GALASSI, G., SCHOLZ, S. W., TAYLOR, J. P., RESTAGNO, G., CHIO, A. & TRAYNOR, B. J. 2010. Exome sequencing reveals VCP mutations as a cause of familial ALS. *Neuron*, 68, 857-64.
- JONSSON, P. A., GRAFFMO, K. S., BRANNSTROM, T., NILSSON, P., ANDERSEN, P. M. & MARKLUND, S. L. 2006. Motor neuron disease in mice expressing the wild type-like D90A mutant superoxide dismutase-1. *J Neuropathol Exp Neurol*, 65, 1126-36.
- JOSE, S., TAN, S. W., OOI, Y. Y., RAMASAMY, R. & VIDYADARAN, S. 2014. Mesenchymal stem cells exert anti-proliferative effect on lipopolysaccharide-stimulated BV2 microglia by reducing tumour necrosis factor- α levels. *Journal of neuroinflammation*, 11, 149-149.
- JUST, N., MOREAU, C., LASSALLE, P., GOSSET, P., PEREZ, T., BRUNAUD-DANEL, V., WALLAERT, B., DESTEE, A., DEFEBVRE, L., TONNEL, A. B. & DEVOS, D. 2007. High erythropoietin and low vascular endothelial growth factor levels in cerebrospinal fluid from hypoxemic ALS patients suggest an abnormal response to hypoxia. *Neuromuscul Disord*, 17, 169-73.

- KABASHI, E., VALDMANIS, P. N., DION, P., SPIEGELMAN, D., MCCONKEY, B. J., VANDE VELDE, C., BOUCHARD, J. P., LACOMBLEZ, L., POCHIGAEVA, K., SALACHAS, F., PRADAT, P. F., CAMU, W., MEININGER, V., DUPRE, N. & ROULEAU, G. A. 2008. TARDBP mutations in individuals with sporadic and familial amyotrophic lateral sclerosis. *Nat Genet*, 40, 572-4.
- KALININA, N., KHARLAMPIEVA, D., LOGUINOVA, M., BUTENKO, I., POBEGUTS, O., EFIMENKO, A., AGEEVA, L., SHARONOV, G., ISCHENKO, D., ALEKSEEV, D., GRIGORIEVA, O., SYSOEVA, V., RUBINA, K., LAZAREV, V. & GOVORUN, V. 2015. Characterization of secretomes provides evidence for adipose-derived mesenchymal stromal cells subtypes. *Stem Cell Res Ther*, 6, 221.
- KALLIFATIDIS, G., BECKERMANN, B. M., GROTH, A., SCHUBERT, M., APEL, A., KHAMIDJANOV, A., RYSCHICH, E., WENGER, T., WAGNER, W., DIEHLMANN, A., SAFFRICH, R., KRAUSE, U., ECKSTEIN, V., MATTERN, J., CHAI, M., SCHUTZ, G., HO, A. D., GEBHARD, M. M., BUCHLER, M. W., FRIESS, H., BUCHLER, P. & HERR, I. 2008. Improved lentiviral transduction of human mesenchymal stem cells for therapeutic intervention in pancreatic cancer. *Cancer Gene Ther*, 15, 231-40.
- KANG, S. H., LI, Y., FUKAYA, M., LORENZINI, I., CLEVELAND, D. W., OSTROW, L. W., ROTHSTEIN, J. D. & BERGLES, D. E. 2013. Degeneration and impaired regeneration of gray matter oligodendrocytes in amyotrophic lateral sclerosis. *Nat Neurosci*, 16, 571-9.
- KARUMBAYARAM, S., NOVITCH, B. G., PATTERSON, M., UMBACH, J. A., RICHTER, L., LINDGREN, A., CONWAY, A. E., CLARK, A. T., GOLDMAN, S. A., PLATH, K., WIEDAU-PAZOS, M., KORNBLUM, H. I. & LOWRY, W. E. 2009. Directed differentiation of human-induced pluripotent stem cells generates active motor neurons. *Stem Cells*, 27, 806-11.
- KARUSSIS, D., KARAGEORGIU, C., VAKNIN-DEMBINSKY, A., GOWDA-KURKALLI, B., GOMORI, J. M., KASSIS, I., BULTE, J. W., PETROU, P., BEN-HUR, T., ABRAMSKY, O. & SLAVIN, S. 2010. Safety and immunological effects of mesenchymal stem cell transplantation in patients with multiple sclerosis and amyotrophic lateral sclerosis. *Arch Neurol*, 67, 1187-94.
- KASPAR, B. K., LLADO, J., SHERKAT, N., ROTHSTEIN, J. D. & GAGE, F. H. 2003. Retrograde viral delivery of IGF-1 prolongs survival in a mouse ALS model. *Science*, 301, 839-42.
- KAWAGUCHI-NIIDA, M., YAMAMOTO, T., KATO, Y., INOSE, Y. & SHIBATA, N. 2013. MCP-1/CCR2 signaling-mediated astrocytosis is accelerated in a transgenic mouse model of SOD1-mutated familial ALS. *Acta Neuropathol Commun*, 1, 21.
- KAYALIOGLU, G. 2009. Chapter 3 - The Vertebral Column and Spinal Meninges. *In: WATSON, C., PAXINOS, G. & KAYALIOGLU, G. (eds.) The Spinal Cord*. San Diego: Academic Press.
- KELLER, A. F., GRAVEL, M. & KRIZ, J. 2009. Live imaging of amyotrophic lateral sclerosis pathogenesis: disease onset is characterized by marked induction of GFAP in Schwann cells. *Glia*, 57, 1130-42.
- KERN, R., CUDKOWICZ, M., BERRY, J., WINDEBANK, A., NATHAN, STAFF, OWEGI, M., LEBOVITS, C., GOTHELF, Y. & BROWN, R. 2018. NurOwn® Phase 2 ALS study: ALSFRS-R subscale responder analysis. *In: TECHNOLOGY, B. C. (ed.) 70th Annual Meeting of the American Academy of Neurology*. Los Angeles, USA.

- KIA, A., MCAVOY, K., KRISHNAMURTHY, K., TROTTI, D. & PASINELLI, P. 2018. Astrocytes expressing ALS-linked mutant FUS induce motor neuron death through release of tumor necrosis factor-alpha. *Glia*, 66, 1016-1033.
- KIERDORF, K. & PRINZ, M. 2013. Factors regulating microglia activation. *Frontiers in cellular neuroscience*, 7, 44-44.
- KIM, H., KIM, H. Y., CHOI, M. R., HWANG, S., NAM, K. H., KIM, H. C., HAN, J. S., KIM, K. S., YOON, H. S. & KIM, S. H. 2010. Dose-dependent efficacy of ALS-human mesenchymal stem cells transplantation into cisterna magna in SOD1-G93A ALS mice. *Neurosci Lett*, 468, 190-4.
- KIM, H. Y., KIM, H., OH, K. W., OH, S. I., KOH, S. H., BAIK, W., NOH, M. Y., KIM, K. S. & KIM, S. H. 2014a. Biological markers of mesenchymal stromal cells as predictors of response to autologous stem cell transplantation in patients with amyotrophic lateral sclerosis: an investigator-initiated trial and in vivo study. *Stem Cells*, 32, 2724-31.
- KIM, J. M., LEE, S. T., CHU, K., JUNG, K. H., SONG, E. C., KIM, S. J., SINN, D. I., KIM, J. H., PARK, D. K., KANG, K. M., HYUNG HONG, N., PARK, H. K., WON, C. H., KIM, K. H., KIM, M., KUN LEE, S. & ROH, J. K. 2007. Systemic transplantation of human adipose stem cells attenuated cerebral inflammation and degeneration in a hemorrhagic stroke model. *Brain Res*, 1183, 43-50.
- KIM, K. S., LEE, H. J., AN, J., KIM, Y. B., RA, J. C., LIM, I. & KIM, S. U. 2014b. Transplantation of human adipose tissue-derived stem cells delays clinical onset and prolongs life span in ALS mouse model. *Cell Transplant*, 23, 1585-97.
- KIM, Y. J. & LEE, G. 2013. Candidate ALS therapeutics motor toward "in vitro clinical trials". *Cell Stem Cell*, 12, 633-4.
- KINGHAM, P. J., KOLAR, M. K., NOVIKOVA, L. N., NOVIKOV, L. N. & WIBERG, M. 2014. Stimulating the neurotrophic and angiogenic properties of human adipose-derived stem cells enhances nerve repair. *Stem Cells Dev*, 23, 741-54.
- KITAMURA, A., INADA, N., KUBOTA, H., MATSUMOTO, G., KINJO, M., MORIMOTO, R. I. & NAGATA, K. 2014. Dysregulation of the proteasome increases the toxicity of ALS-linked mutant SOD1. *Genes Cells*, 19, 209-24.
- KNIPPENBERG, S., RATH, K. J., BOSELT, S., THAU-HABERMANN, N., SCHWARZ, S. C., DENGLER, R., WEGNER, F. & PETRI, S. 2015. Intraspinal administration of human spinal cord-derived neural progenitor cells in the G93A-SOD1 mouse model of ALS delays symptom progression, prolongs survival and increases expression of endogenous neurotrophic factors. *J Tissue Eng Regen Med*.
- KNIPPENBERG, S., THAU, N., DENGLER, R., BRINKER, T. & PETRI, S. 2012a. Intracerebroventricular injection of encapsulated human mesenchymal cells producing glucagon-like peptide 1 prolongs survival in a mouse model of ALS. *PLoS One*, 7, e36857.
- KNIPPENBERG, S., THAU, N., SCHWABE, K., DENGLER, R., SCHAMBACH, A., HASS, R. & PETRI, S. 2012b. Intraspinal injection of human umbilical cord blood-derived cells is neuroprotective in a transgenic mouse model of amyotrophic lateral sclerosis. *Neurodegener Dis*, 9, 107-20.
- KOBAYASHI, Z., KAWAKAMI, I., ARAI, T., YOKOTA, O., TSUCHIYA, K., KONDO, H., SHIMOMURA, Y., HAGA, C., AOKI, N., HASEGAWA, M., HOSOKAWA, M., OSHIMA, K., NIIZATO, K., ISHIZU, H., TERADA, S., ONAYA, M., IKEDA, M., OYANAGI, K., NAKANO, I., MURAYAMA, S., AKIYAMA, H. & MIZUSAWA, H. 2013. Pathological features of FTL-D-FUS in a Japanese population: analyses of nine cases. *J Neurol Sci*, 335, 89-95.
- KOH, S. H., BAIK, W., NOH, M. Y., CHO, G. W., KIM, H. Y., KIM, K. S. & KIM, S. H. 2012. The functional deficiency of bone marrow mesenchymal stromal cells

- in ALS patients is proportional to disease progression rate. *Exp Neurol*, 233, 472-80.
- KONDO, T., FUNAYAMA, M., TSUKITA, K., HOTTA, A., YASUDA, A., NORI, S., KANEKO, S., NAKAMURA, M., TAKAHASHI, R., OKANO, H., YAMANAKA, S. & INOUE, H. 2014. Focal transplantation of human iPSC-derived glial-rich neural progenitors improves lifespan of ALS mice. *Stem cell reports*, 3, 242-249.
- KORZHEVSKII, D. E. & KIRIK, O. V. 2016. Brain Microglia and Microglial Markers. *Neuroscience and Behavioral Physiology*, 46, 284-290.
- KRAKORA, D., MULCRONE, P., MEYER, M., LEWIS, C., BERNAU, K., GOWING, G., ZIMPRICH, C., AEBISCHER, P., SVENDSEN, C. N. & SUZUKI, M. 2013. Synergistic effects of GDNF and VEGF on lifespan and disease progression in a familial ALS rat model. *Mol Ther*, 21, 1602-10.
- KRAMPERA, M., MARCONI, S., PASINI, A., GALIE, M., RIGOTTI, G., MOSNA, F., TINELLI, M., LOVATO, L., ANGHILERI, E., ANDREINI, A., PIZZOLO, G., SBARBATI, A. & BONETTI, B. 2007. Induction of neural-like differentiation in human mesenchymal stem cells derived from bone marrow, fat, spleen and thymus. *Bone*, 40, 382-90.
- KRAUSE, C. D., IZOTOVA, L. S., REN, G., YUAN, Z.-R., SHI, Y., CHEN, C.-C., RON, Y. & PESTKA, S. 2011. Efficient co-expression of bicistronic proteins in mesenchymal stem cells by development and optimization of a multifunctional plasmid. *Stem Cell Research & Therapy*, 2, 15.
- KWIATKOWSKI, T. J., JR., BOSCO, D. A., LECLERC, A. L., TAMRAZIAN, E., VANDERBURG, C. R., RUSS, C., DAVIS, A., GILCHRIST, J., KASARSKIS, E. J., MUNSAT, T., VALDMANIS, P., ROULEAU, G. A., HOSLER, B. A., CORTELLI, P., DE JONG, P. J., YOSHINAGA, Y., HAINES, J. L., PERICAK-VANCE, M. A., YAN, J., TICOZZI, N., SIDDIQUE, T., MCKENNA-YASEK, D., SAPP, P. C., HORVITZ, H. R., LANDERS, J. E. & BROWN, R. H., JR. 2009. Mutations in the FUS/TLS gene on chromosome 16 cause familial amyotrophic lateral sclerosis. *Science*, 323, 1205-8.
- KWON, M. S., NOH, M. Y., OH, K. W., CHO, K. A., KANG, B. Y., KIM, K. S., KIM, Y. S. & KIM, S. H. 2014. The immunomodulatory effects of human mesenchymal stem cells on peripheral blood mononuclear cells in ALS patients. *J Neurochem*, 131, 206-18.
- LABANDEIRA-GARCIA, J. L., COSTA-BESADA, M. A., LABANDEIRA, C. M., VILLAR-CHEDA, B. & RODRÍGUEZ-PEREZ, A. I. 2017. Insulin-Like Growth Factor-1 and Neuroinflammation. *Frontiers in aging neuroscience*, 9, 365-365.
- LAGIER-TOURENNE, C., POLYMERIDOU, M., HUTT, K. R., VU, A. Q., BAUGHN, M., HUELGA, S. C., CLUTARIO, K. M., LING, S. C., LIANG, T. Y., MAZUR, C., WANCEWICZ, E., KIM, A. S., WATT, A., FREIER, S., HICKS, G. G., DONOHUE, J. P., SHIUE, L., BENNETT, C. F., RAVITS, J., CLEVELAND, D. W. & YEO, G. W. 2012. Divergent roles of ALS-linked proteins FUS/TLS and TDP-43 intersect in processing long pre-mRNAs. *Nat Neurosci*, 15, 1488-97.
- LAM, M. A., HEMLEY, S. J., NAJAFI, E., VELLA, N. G. F., BILSTON, L. E. & STOODLEY, M. A. 2017. The ultrastructure of spinal cord perivascular spaces: Implications for the circulation of cerebrospinal fluid. *Scientific Reports*, 7, 12924.
- LAMBRECHTS, D., POESEN, K., FERNANDEZ-SANTIAGO, R., AL-CHALABI, A., DEL BO, R., VAN VUGHT, P. W., KHAN, S., MARKLUND, S. L., BROCKINGTON, A., VAN MARION, I., ANNESER, J., SHAW, C., LUDOLPH, A. C., LEIGH, N. P., COMI, G. P., GASSER, T., SHAW, P. J., MORRISON, K. E., ANDERSEN, P. M., VAN DEN BERG, L. H., THIJIS, V., SIDDIQUE, T., ROBBERECHT, W. & CARMELIET, P. 2009. Meta-analysis

- of vascular endothelial growth factor variations in amyotrophic lateral sclerosis: increased susceptibility in male carriers of the -2578AA genotype. *J Med Genet*, 46, 840-6.
- LEE, J. S., LEE, S. M., JEONG, S. W., SUNG, Y. G., LEE, J. H. & KIM, K. W. 2016a. Effects of age, replicative lifespan and growth rate of human nucleus pulposus cells on selecting age range for cell-based biological therapies for degenerative disc diseases. *Biotech Histochem*, 1-9.
- LEE, M., BAN, J. J., KIM, K. Y., JEON, G. S., IM, W., SUNG, J. J. & KIM, M. 2016b. Adipose-derived stem cell exosomes alleviate pathology of amyotrophic lateral sclerosis in vitro. *Biochem Biophys Res Commun*, 479, 434-439.
- LEE, Y., MORRISON, B. M., LI, Y., LENGACHER, S., FARAH, M. H., HOFFMAN, P. N., LIU, Y., TSINGALIA, A., JIN, L., ZHANG, P. W., PELLERIN, L., MAGISTRETTI, P. J. & ROTHSTEIN, J. D. 2012. Oligodendroglia metabolically support axons and contribute to neurodegeneration. *Nature*, 487, 443-8.
- LEE, Y. B., CHEN, H. J., PERES, J. N., GOMEZ-DEZA, J., ATTIG, J., STALEKAR, M., TROAKES, C., NISHIMURA, A. L., SCOTTER, E. L., VANCE, C., ADACHI, Y., SARDONE, V., MILLER, J. W., SMITH, B. N., GALLO, J. M., ULE, J., HIRTH, F., ROGELJ, B., HOUART, C. & SHAW, C. E. 2013. Hexanucleotide repeats in ALS/FTD form length-dependent RNA foci, sequester RNA binding proteins, and are neurotoxic. *Cell Rep*, 5, 1178-86.
- LEPORE, A. C., RAUCK, B., DEJEA, C., PARDO, A. C., RAO, M. S., ROTHSTEIN, J. D. & MARAGAKIS, N. J. 2008. Focal transplantation-based astrocyte replacement is neuroprotective in a model of motor neuron disease. *Nature neuroscience*, 11, 1294-1301.
- LEWIS, C. M. & SUZUKI, M. 2014. Therapeutic applications of mesenchymal stem cells for amyotrophic lateral sclerosis. *Stem Cell Res Ther*, 5, 32.
- LI, Y., BALASUBRAMANIAN, U., COHEN, D., ZHANG, P. W., MOSMILLER, E., SATTLER, R., MARAGAKIS, N. J. & ROTHSTEIN, J. D. 2015. A comprehensive library of familial human amyotrophic lateral sclerosis induced pluripotent stem cells. *PLoS One*, 10, e0118266.
- LIAO, B., ZHAO, W., BEERS, D. R., HENKEL, J. S. & APPEL, S. H. 2012. Transformation from a neuroprotective to a neurotoxic microglial phenotype in a mouse model of ALS. *Exp Neurol*, 237, 147-52.
- LIDDELOW, S. A. & BARRES, B. A. 2017. Reactive Astrocytes: Production, Function, and Therapeutic Potential. *Immunity*, 46, 957-967.
- LIN, P., LIN, Y., LENNON, D. P., CORREA, D., SCHLUCHTER, M. & CAPLAN, A. I. 2012. Efficient Lentiviral Transduction of Human Mesenchymal Stem Cells That Preserves Proliferation and Differentiation Capabilities. *Stem Cells Translational Medicine*, 1, 886-897.
- LINO, M. M., SCHNEIDER, C. & CARONI, P. 2002. Accumulation of SOD1 mutants in postnatal motoneurons does not cause motoneuron pathology or motoneuron disease. *J Neurosci*, 22, 4825-32.
- LIU, J. & WANG, F. 2017. Role of Neuroinflammation in Amyotrophic Lateral Sclerosis: Cellular Mechanisms and Therapeutic Implications. *Frontiers in Immunology*, 8, 1005.
- LIU, N., PATZAK, A. & ZHANG, J. 2013. CXCR4-overexpressing bone marrow-derived mesenchymal stem cells improve repair of acute kidney injury. *Am J Physiol Renal Physiol*, 305, F1064-73.
- LIU, Y., PATTAMATTA, A., ZU, T., REID, T., BARDHI, O., BORCHELT, D. R., YACHNIS, A. T. & RANUM, L. P. 2016. C9orf72 BAC Mouse Model with Motor Deficits and Neurodegenerative Features of ALS/FTD. *Neuron*, 90, 521-34.

- LLADÓ, J., TOLOSA, L. & OLMOS, G. 2013. Cellular and molecular mechanisms involved in the neuroprotective effects of VEGF on motoneurons. *Frontiers in Cellular Neuroscience*, 7, 181.
- LOCKE, M., WINDSOR, J. & DUNBAR, P. R. 2009. Human adipose-derived stem cells: isolation, characterization and applications in surgery. *ANZ J Surg*, 79, 235-44.
- LU, L., ZHENG, L., VIERA, L., SUSWAM, E., LI, Y., LI, X., ESTEVEZ, A. G. & KING, P. H. 2007. Mutant Cu/Zn-superoxide dismutase associated with amyotrophic lateral sclerosis destabilizes vascular endothelial growth factor mRNA and downregulates its expression. *J Neurosci*, 27, 7929-38.
- LU, P., BLESCH, A. & TUSZYNSKI, M. H. 2004a. Induction of bone marrow stromal cells to neurons: differentiation, transdifferentiation, or artifact? *J Neurosci Res*, 77, 174-91.
- LU, X., HUMEAU, L., SLEPUSHKIN, V., BINDER, G., YU, Q., SLEPUSHKINA, T., CHEN, Z., MERLING, R., DAVIS, B., CHANG, Y.-N. & DROPULIC, B. 2004b. Safe two-plasmid production for the first clinical lentivirus vector that achieves >99% transduction in primary cells using a one-step protocol. *The Journal of Gene Medicine*, 6, 963-973.
- LUDOLPH, A. C., BENDOTTI, C., BLAUGRUND, E., CHIO, A., GREENSMITH, L., LOEFFLER, J. P., MEAD, R., NIESSEN, H. G., PETRI, S., PRADAT, P. F., ROBBERECHT, W., RUEGG, M., SCHWALENSTOCKER, B., STILLER, D., VAN DEN BERG, L., VIEIRA, F. & VON HORSTEN, S. 2010. Guidelines for preclinical animal research in ALS/MND: A consensus meeting. *Amyotroph Lateral Scler*, 11, 38-45.
- LUKOMSKA, B., STANASZEK, L., ZUBA-SURMA, E., LEGOSZ, P., SARZYNSKA, S. & DRELA, K. 2019. Challenges and Controversies in Human Mesenchymal Stem Cell Therapy. *Stem Cells Int*, 2019, 9628536.
- LUNA, A. C., MADEIRA, M. E., CONCEICAO, T. O., MOREIRA, J. A., LAISO, R. A. & MARIA, D. A. 2014. Characterization of adipose-derived stem cells of anatomical region from mice. *BMC Res Notes*, 7, 552.
- LUND, P., PILGAARD, L., DUROUX, M., FINK, T. & ZACHAR, V. 2009. Effect of growth media and serum replacements on the proliferation and differentiation of adipose-derived stem cells. *Cytotherapy*, 11, 189-97.
- LUNN, J. S., SAKOWSKI, S. A., HUR, J. & FELDMAN, E. L. 2011. Stem cell technology for neurodegenerative diseases. *Annals of neurology*, 70, 353-361.
- LUZ-CRAWFORD, P., KURTE, M., BRAVO-ALEGRÍA, J., CONTRERAS, R., NOVA-LAMPERTI, E., TEJEDOR, G., NOÉL, D., JORGENSEN, C., FIGUEROA, F., DJOUAD, F. & CARRIÓN, F. 2013. Mesenchymal stem cells generate a CD4+CD25+Foxp3+ regulatory T cell population during the differentiation process of Th1 and Th17 cells. *Stem Cell Res Ther*, 4, 65.
- MADJI HOUNOUM, B., MAVEL, S., COQUE, E., PATIN, F., VOURC'H, P., MAROUILLAT, S., NADAL-DESBARATS, L., EMOND, P., CORCIA, P., ANDRES, C. R., RAOUL, C. & BLASCO, H. 2017. Wildtype motoneurons, ALS-Linked SOD1 mutation and glutamate profoundly modify astrocyte metabolism and lactate shuttling. *Glia*, 65, 592-605.
- MAJOUNIE, E., RENTON, A. E., MOK, K., DOPPER, E. G., WAITE, A., ROLLINSON, S., CHIO, A., RESTAGNO, G., NICOLAOU, N., SIMON-SANCHEZ, J., VAN SWIETEN, J. C., ABRAMZON, Y., JOHNSON, J. O., SENDTNER, M., PAMPHLETT, R., ORRELL, R. W., MEAD, S., SIDLE, K. C., HOULDEN, H., ROHRER, J. D., MORRISON, K. E., PALL, H., TALBOT, K., ANSORGE, O., HERNANDEZ, D. G., AREPALLI, S., SABATELLI, M., MORA, G., CORBO, M., GIANNINI, F., CALVO, A., ENGLUND, E., BORGHERO, G., FLORIS, G. L., REMES, A. M., LAAKSOVIRTA, H., MCCLUSKEY, L., TROJANOWSKI, J. Q., VAN DEERLIN, V. M.,

- SCHELLENBERG, G. D., NALLS, M. A., DRORY, V. E., LU, C. S., YEH, T. H., ISHIURA, H., TAKAHASHI, Y., TSUJI, S., LE BER, I., BRICE, A., DREPPER, C., WILLIAMS, N., KIRBY, J., SHAW, P., HARDY, J., TIENARI, P. J., HEUTINK, P., MORRIS, H. R., PICKERING-BROWN, S. & TRAYNOR, B. J. 2012. Frequency of the C9orf72 hexanucleotide repeat expansion in patients with amyotrophic lateral sclerosis and frontotemporal dementia: a cross-sectional study. *Lancet Neurol*, 11, 323-30.
- MALIDE, D., METAIS, J. Y. & DUNBAR, C. E. 2014. In vivo clonal tracking of hematopoietic stem and progenitor cells marked by five fluorescent proteins using confocal and multiphoton microscopy. *J Vis Exp*, e51669.
- MARCHETTO, M. C., MUOTRI, A. R., MU, Y., SMITH, A. M., CEZAR, G. G. & GAGE, F. H. 2008. Non-cell-autonomous effect of human SOD1 G37R astrocytes on motor neurons derived from human embryonic stem cells. *Cell Stem Cell*, 3, 649-57.
- MARCONI, S., BONACONSA, M., SCAMBI, I., SQUINTANI, G. M., RUI, W., TURANO, E., UNGARO, D., D'AGOSTINO, S., BARBIERI, F., ANGIARI, S., FARINAZZO, A., CONSTANTIN, G., DEL CARRO, U., BONETTI, B. & MARIOTTI, R. 2013. Systemic treatment with adipose-derived mesenchymal stem cells ameliorates clinical and pathological features in the amyotrophic lateral sclerosis murine model. *Neuroscience*, 248, 333-43.
- MARTINEZ, H. R., ESCAMILLA-OCANAS, C. E., CAMARA-LEMARROY, C. R., GONZALEZ-GARZA, M. T., MORENO-CUEVAS, J. & GARCIA SARREON, M. A. 2017. Increased cerebrospinal fluid levels of cytokines monocyte chemoattractant protein-1 (MCP-1) and macrophage inflammatory protein-1beta (MIP-1beta) in patients with amyotrophic lateral sclerosis. *Neurologia*.
- MARUYAMA, H., MORINO, H., ITO, H., IZUMI, Y., KATO, H., WATANABE, Y., KINOSHITA, Y., KAMADA, M., NODERA, H., SUZUKI, H., KOMURE, O., MATSUURA, S., KOBATAKE, K., MORIMOTO, N., ABE, K., SUZUKI, N., AOKI, M., KAWATA, A., HIRAI, T., KATO, T., OGASAWARA, K., HIRANO, A., TAKUMI, T., KUSAKA, H., HAGIWARA, K., KAJI, R. & KAWAKAMI, H. 2010. Mutations of optineurin in amyotrophic lateral sclerosis. *Nature*, 465, 223-6.
- MAYO, L., TRAUGER, S. A., BLAIN, M., NADEAU, M., PATEL, B., ALVAREZ, J. I., MASCANFRONI, I. D., YESTE, A., KIVISAKK, P., KALLAS, K., ELLEZAM, B., BAKSHI, R., PRAT, A., ANTEL, J. P., WEINER, H. L. & QUINTANA, F. J. 2014. Regulation of astrocyte activation by glycolipids drives chronic CNS inflammation. *Nat Med*, 20, 1147-56.
- MAZZINI, L., FAGIOLI, F., BOCCALETTI, R., MARESCHI, K., OLIVERI, G., OLIVIERI, C., PASTORE, I., MARASSO, R. & MADON, E. 2003. Stem cell therapy in amyotrophic lateral sclerosis: a methodological approach in humans. *Amyotroph Lateral Scler Other Motor Neuron Disord*, 4, 158-61.
- MAZZINI, L., FERRERO, I., LUPARELLO, V., RUSTICHELLI, D., GUNETTI, M., MARESCHI, K., TESTA, L., STECCO, A., TARLETTI, R., MIGLIORETTI, M., FAVA, E., NASUELLI, N., CISARI, C., MASSARA, M., VERCELLI, R., OGGIONI, G. D., CARRIERO, A., CANTELLO, R., MONACO, F. & FAGIOLI, F. 2010. Mesenchymal stem cell transplantation in amyotrophic lateral sclerosis: A Phase I clinical trial. *Exp Neurol*, 223, 229-37.
- MAZZINI, L., MARESCHI, K., FERRERO, I., MIGLIORETTI, M., STECCO, A., SERVO, S., CARRIERO, A., MONACO, F. & FAGIOLI, F. 2012. Mesenchymal stromal cell transplantation in amyotrophic lateral sclerosis: a long-term safety study. *Cytotherapy*, 14, 56-60.
- MAZZINI, L., MARESCHI, K., FERRERO, I., VASSALLO, E., OLIVERI, G., NASUELLI, N., OGGIONI, G. D., TESTA, L. & FAGIOLI, F. 2008. Stem cell treatment in Amyotrophic Lateral Sclerosis. *J Neurol Sci*, 265, 78-83.

- MCCOMBE, P. A. & HENDERSON, R. D. 2011. The Role of immune and inflammatory mechanisms in ALS. *Current molecular medicine*, 11, 246-254.
- MCGINLEY, L., MCMAHON, J., STRAPPE, P., BARRY, F., MURPHY, M., O'TOOLE, D. & O'BRIEN, T. 2011. Lentiviral vector mediated modification of mesenchymal stem cells & enhanced survival in an in vitro model of ischaemia. *Stem Cell Research & Therapy*, 2, 12.
- MEAD, R. J., BENNETT, E. J., KENNERLEY, A. J., SHARP, P., SUNYACH, C., KASHER, P., BERWICK, J., PETTMANN, B., BATTAGLIA, G., AZZOUZ, M., GRIERSON, A. & SHAW, P. J. 2011. Optimised and rapid pre-clinical screening in the SOD1(G93A) transgenic mouse model of amyotrophic lateral sclerosis (ALS). *PLoS One*, 6, e23244.
- MEAD, R. J., HIGGINBOTTOM, A., ALLEN, S. P., KIRBY, J., BENNETT, E., BARBER, S. C., HEATH, P. R., COLUCCIA, A., PATEL, N., GARDNER, I., BRANCALE, A., GRIERSON, A. J. & SHAW, P. J. 2013. S[+] Apomorphine is a CNS penetrating activator of the Nrf2-ARE pathway with activity in mouse and patient fibroblast models of amyotrophic lateral sclerosis(). *Free Radical Biology & Medicine*, 61, 438-452.
- MEISSNER, F., MOLAWI, K. & ZYCHLINSKY, A. 2010. Mutant superoxide dismutase 1-induced IL-1beta accelerates ALS pathogenesis. *Proceedings of the National Academy of Sciences of the United States of America*, 107, 13046-13050.
- MERTEN, O.-W., HEBBEN, M. & BOVOLENTA, C. 2016. Production of lentiviral vectors. *Molecular therapy. Methods & clinical development*, 3, 16017-16017.
- MEYER, J., SALAMON, A., HERZMANN, N., ADAM, S., KLEINE, H. D., MATTHIESEN, I., UEBERREITER, K. & PETERS, K. 2015. Isolation and Differentiation Potential of Human Mesenchymal Stem Cells From Adipose Tissue Harvested by Water Jet-Assisted Liposuction. *Aesthet Surg J*, 35, 1030-9.
- MEYER, K., FERRAIUOLO, L., MIRANDA, C. J., LIKHTE, S., MCELROY, S., RENUSCH, S., DITSWORTH, D., LAGIER-TOURENNE, C., SMITH, R. A., RAVITS, J., BURGHESE, A. H., SHAW, P. J., CLEVELAND, D. W., KOLB, S. J. & KASPAR, B. K. 2014. Direct conversion of patient fibroblasts demonstrates non-cell autonomous toxicity of astrocytes to motor neurons in familial and sporadic ALS. *Proc Natl Acad Sci U S A*, 111, 829-32.
- MIANA-MENA, F. J., MUNOZ, M. J., YAGUE, G., MENDEZ, M., MORENO, M., CIRIZA, J., ZARAGOZA, P. & OSTA, R. 2005. Optimal methods to characterize the G93A mouse model of ALS. *Amyotroph Lateral Scler Other Motor Neuron Disord*, 6, 55-62.
- MISHRA, P.-S., DHULL, D. K., NALINI, A., VIJAYALAKSHMI, K., SATHYAPRABHA, T. N., ALLADI, P. A. & RAJU, T. R. 2016. Astroglia acquires a toxic neuroinflammatory role in response to the cerebrospinal fluid from amyotrophic lateral sclerosis patients. *Journal of neuroinflammation*, 13, 212-212.
- MITCHELL, J. D., CALLAGHER, P., GARDHAM, J., MITCHELL, C., DIXON, M., ADDISON-JONES, R., BENNETT, W. & O'BRIEN, M. R. 2010. Timelines in the diagnostic evaluation of people with suspected amyotrophic lateral sclerosis (ALS)/motor neuron disease (MND)--a 20-year review: can we do better? *Amyotroph Lateral Scler*, 11, 537-41.
- MOHAMED-AHMED, S., FRISTAD, I., LIE, S. A., SULIMAN, S., MUSTAFA, K., VINDENES, H. & IDRIS, S. B. 2018. Adipose-derived and bone marrow mesenchymal stem cells: a donor-matched comparison. *Stem Cell Res Ther*, 9, 168.
- MOHAMMADPOUR, H., POURFATHOLLAH, A. A., NIKOUGOFTAR ZARIF, M. & HASHEMI, S. M. 2016. Increasing proliferation of murine adipose tissue-

- derived mesenchymal stem cells by TNF-alpha plus IFN-gamma. *Immunopharmacol Immunotoxicol*, 38, 68-76.
- MOLOFSKY, A. V. & DENEEN, B. 2015. Astrocyte development: A Guide for the Perplexed. *Glia*, 63, 1320-9.
- MORI, K., WENG, S. M., ARZBERGER, T., MAY, S., RENTZSCH, K., KREMMER, E., SCHMID, B., KRETZSCHMAR, H. A., CRUTS, M., VAN BROECKHOVEN, C., HAASS, C. & EDBAUER, D. 2013. The C9orf72 GGGGCC repeat is translated into aggregating dipeptide-repeat proteins in FTL/ALS. *Science*, 339, 1335-8.
- MOTHE, A. & TATOR, C. H. 2015. Isolation of Neural Stem/Progenitor Cells from the Periventricular Region of the Adult Rat and Human Spinal Cord. *J Vis Exp*, e52732.
- MURAKAMI, T., ILIEVA, H., SHIOTE, M., NAGATA, T., NAGANO, I., SHOJI, M. & ABE, K. 2003. Hypoxic induction of vascular endothelial growth factor is selectively impaired in mice carrying the mutant SOD1 gene. *Brain Research*, 989, 231-237.
- MYSZCZYNSKA, M. & FERRAIUOLO, L. 2016. New In Vitro Models to Study Amyotrophic Lateral Sclerosis. *Brain Pathol*, 26, 258-65.
- NAGAI, M., RE, D. B., NAGATA, T., CHALAZONITIS, A., JESSELL, T. M., WICHTERLE, H. & PRZEDBORSKI, S. 2007. Astrocytes expressing ALS-linked mutated SOD1 release factors selectively toxic to motor neurons. *Nat Neurosci*, 10, 615-22.
- NAKAMURA, M., ITO, H., WATE, R., NAKANO, S., HIRANO, A. & KUSAKA, H. 2008. Phosphorylated Smad2/3 immunoreactivity in sporadic and familial amyotrophic lateral sclerosis and its mouse model. *Acta Neuropathologica*, 115, 327-334.
- NEUHUBER, B., GALLO, G., HOWARD, L., KOSTURA, L., MACKAY, A. & FISCHER, I. 2004. Reevaluation of in vitro differentiation protocols for bone marrow stromal cells: disruption of actin cytoskeleton induces rapid morphological changes and mimics neuronal phenotype. *J Neurosci Res*, 77, 192-204.
- NICAISE, C., MITRECIC, D. & POCHET, R. 2011. Brain and spinal cord affected by amyotrophic lateral sclerosis induce differential growth factors expression in rat mesenchymal and neural stem cells. *Neuropathol Appl Neurobiol*, 37, 179-88.
- NIEMEYER, P., KORNACKER, M., MEHLHORN, A., SECKINGER, A., VOHRER, J., SCHMAL, H., KASTEN, P., ECKSTEIN, V., SUDKAMP, N. P. & KRAUSE, U. 2007. Comparison of immunological properties of bone marrow stromal cells and adipose tissue-derived stem cells before and after osteogenic differentiation in vitro. *Tissue Eng*, 13, 111-21.
- NIZZARDO, M., SIMONE, C., RIZZO, F., RUGGIERI, M., SALANI, S., RIBOLDI, G., FARAVELLI, I., ZANETTA, C., BRESOLIN, N., COMI, G. P. & CORTI, S. 2014. Minimally invasive transplantation of iPSC-derived ALDHhiSSCloVLA4+ neural stem cells effectively improves the phenotype of an amyotrophic lateral sclerosis model. *Hum Mol Genet*, 23, 342-54.
- NOH, M. Y., CHO, K. A., KIM, H., KIM, S.-M. & KIM, S. H. 2014. Erythropoietin modulates the immune-inflammatory response of a SOD1G93A transgenic mouse model of amyotrophic lateral sclerosis (ALS). *Neuroscience Letters*, 574, 53-58.
- NOH, M. Y., LIM, S. M., OH, K. W., CHO, K. A., PARK, J., KIM, K. S., LEE, S. J., KWON, M. S. & KIM, S. H. 2016. Mesenchymal Stem Cells Modulate the Functional Properties of Microglia via TGF-beta Secretion. *Stem Cells Transl Med*, 5, 1538-1549.

- NYGREN, I., LARSSON, A., JOHANSSON, A. & ASKMARK, H. 2002. VEGF is increased in serum but not in spinal cord from patients with amyotrophic lateral sclerosis. *Neuroreport*, 13, 2199-201.
- O'ROURKE, J. G., BOGDANIK, L., MUHAMMAD, A., GENDRON, T. F., KIM, K. J., AUSTIN, A., CADY, J., LIU, E. Y., ZARROW, J., GRANT, S., HO, R., BELL, S., CARMONA, S., SIMPKINSON, M., LALL, D., WU, K., DAUGHRITY, L., DICKSON, D. W., HARMS, M. B., PETRUCCELLI, L., LEE, E. B., LUTZ, C. M. & BALOH, R. H. 2015. C9orf72 BAC Transgenic Mice Display Typical Pathologic Features of ALS/FTD. *Neuron*, 88, 892-901.
- OH, K. W., MOON, C., KIM, H. Y., OH, S. I., PARK, J., LEE, J. H., CHANG, I. Y., KIM, K. S. & KIM, S. H. 2015. Phase I trial of repeated intrathecal autologous bone marrow-derived mesenchymal stromal cells in amyotrophic lateral sclerosis. *Stem Cells Transl Med*, 4, 590-7.
- OH, K. W., NOH, M. Y., KWON, M. S., KIM, H. Y., OH, S. I., PARK, J., KIM, H. J., KI, C. S. & KIM, S. H. 2018. Repeated Intrathecal Mesenchymal Stem Cells for Amyotrophic Lateral Sclerosis. *Ann Neurol*, 84, 361-373.
- OH, Y. S., KIM, S. H. & CHO, G. W. 2016. Functional Restoration of Amyotrophic Lateral Sclerosis Patient-Derived Mesenchymal Stromal Cells Through Inhibition of DNA Methyltransferase. *Cell Mol Neurobiol*, 36, 613-20.
- OLIVÁN, S., CALVO, A. C., RANDO, A., MUÑOZ, M. J., ZARAGOZA, P. & OSTA, R. 2015. Comparative study of behavioural tests in the SOD1G93A mouse model of amyotrophic lateral sclerosis. *Experimental animals*, 64, 147-153.
- ONO, S., HU, J., SHIMIZU, N., IMAI, T. & NAKAGAWA, H. 2001. Increased interleukin-6 of skin and serum in amyotrophic lateral sclerosis. *J Neurol Sci*, 187, 27-34.
- OOI, Y. Y., DHEEN, S. T. & TAY, S. S. 2015. Paracrine effects of mesenchymal stem cells-conditioned medium on microglial cytokines expression and nitric oxide production. *Neuroimmunomodulation*, 22, 233-42.
- OUALI ALAMI, N., SCHURR, C., OLDE HEUVEL, F., TANG, L., LI, Q., TASDOGAN, A., KIMBARA, A., NETTEKOVEN, M., OTTAVIANI, G., RAPOSO, C., ROVER, S., ROGERS-EVANS, M., ROTHENHAUSLER, B., ULLMER, C., FINGERLE, J., GREYER, U., KNUESSEL, I., BOECKERS, T. M., LUDOLPH, A., WIRTH, T., ROSELLI, F. & BAUMANN, B. 2018. NF-kappaB activation in astrocytes drives a stage-specific beneficial neuroimmunological response in ALS. *Embo j*, 37.
- PAEZ-COLASANTE, X., FIGUEROA-ROMERO, C., SAKOWSKI, S. A., GOUTMAN, S. A. & FELDMAN, E. L. 2015. Amyotrophic lateral sclerosis: mechanisms and therapeutics in the epigenomic era. *Nat Rev Neurol*, 11, 266-79.
- PAPADEAS, S. T., KRAIG, S. E., O'BANION, C., LEPORE, A. C. & MARAGAKIS, N. J. 2011. Astrocytes carrying the superoxide dismutase 1 (SOD1G93A) mutation induce wild-type motor neuron degeneration in vivo. *Proc Natl Acad Sci U S A*, 108, 17803-8.
- PARDO, A. C., WONG, V., BENSON, L. M., DYKES, M., TANAKA, K., ROTHSTEIN, J. D. & MARAGAKIS, N. J. 2006. Loss of the astrocyte glutamate transporter GLT1 modifies disease in SOD1(G93A) mice. *Exp Neurol*, 201, 120-30.
- PARK, D., YANG, G., BAE, D. K., LEE, S. H., YANG, Y. H., KYUNG, J., KIM, D., CHOI, E. K., CHOI, K. C., KIM, S. U., KANG, S. K., RA, J. C. & KIM, Y. B. 2013. Human adipose tissue-derived mesenchymal stem cells improve cognitive function and physical activity in ageing mice. *J Neurosci Res*, 91, 660-70.
- PEHAR, M., HARLAN, B. A., KILLOY, K. M. & VARGAS, M. R. 2017. Role and Therapeutic Potential of Astrocytes in Amyotrophic Lateral Sclerosis. *Current pharmaceutical design*, 23, 5010-5021.

- PEISTER, A., MELLAD, J. A., LARSON, B. L., HALL, B. M., GIBSON, L. F. & PROCKOP, D. J. 2004. Adult stem cells from bone marrow (MSCs) isolated from different strains of inbred mice vary in surface epitopes, rates of proliferation, and differentiation potential. *Blood*, 103, 1662-8.
- PERETS, N., SEGAL-GAVISH, H., GOTHELF, Y., BARZILAY, R., BARHUM, Y., ABRAMOV, N., HERTZ, S., MOROZOV, D., LONDON, M. & OFFEN, D. 2017. Long term beneficial effect of neurotrophic factors-secreting mesenchymal stem cells transplantation in the BTBR mouse model of autism. *Behav Brain Res*, 331, 254-260.
- PERONI, D., SCAMBI, I., PASINI, A., LISI, V., BIFARI, F., KRAMPERA, M., RIGOTTI, G., SBARBATI, A. & GALIE, M. 2008. Stem molecular signature of adipose-derived stromal cells. *Exp Cell Res*, 314, 603-15.
- PERRY, V. H. & TEELING, J. 2013. Microglia and macrophages of the central nervous system: the contribution of microglia priming and systemic inflammation to chronic neurodegeneration. *Seminars in immunopathology*, 35, 601-612.
- PETERS, O. M., CABRERA, G. T., TRAN, H., GENDRON, T. F., MCKEON, J. E., METTERVILLE, J., WEISS, A., WIGHTMAN, N., SALAMEH, J., KIM, J., SUN, H., BOYLAN, K. B., DICKSON, D., KENNEDY, Z., LIN, Z., ZHANG, Y. J., DAUGHRITY, L., JUNG, C., GAO, F. B., SAPP, P. C., HORVITZ, H. R., BOSCO, D. A., BROWN, S. P., DE JONG, P., PETRUCCELLI, L., MUELLER, C. & BROWN, R. H., JR. 2015. Human C9ORF72 Hexanucleotide Expansion Reproduces RNA Foci and Dipeptide Repeat Proteins but Not Neurodegeneration in BAC Transgenic Mice. *Neuron*, 88, 902-909.
- PETERS, S., ZITZELSPERGER, E., KUESPERT, S., IBERL, S., HEYDN, R., JOHANNESSEN, S., PETRI, S., AIGNER, L., THAL, D. R., HERMANN, A., WEISHAUPT, J. H., BRUUN, T.-H. & BOGDAHN, U. 2017. The TGF- β System As a Potential Pathogenic Player in Disease Modulation of Amyotrophic Lateral Sclerosis. *Frontiers in neurology*, 8, 669-669.
- PETROU, P., GOTHELF, Y., ARGOV, Z., GOTKINE, M., LEVY, Y. S., KASSIS, I., VAKNIN-DEMBINSKY, A., BEN-HUR, T., OFFEN, D., ABRAMSKY, O., MELAMED, E. & KARUSSIS, D. 2016. Safety and Clinical Effects of Mesenchymal Stem Cells Secreting Neurotrophic Factor Transplantation in Patients With Amyotrophic Lateral Sclerosis: Results of Phase 1/2 and 2a Clinical Trials. *JAMA Neurol*, 73, 337-44.
- PETROV, D., MANSFIELD, C., MOUSSY, A. & HERMINE, O. 2017. ALS Clinical Trials Review: 20 Years of Failure. Are We Any Closer to Registering a New Treatment? *Frontiers in aging neuroscience*, 9, 68-68.
- PHATNANI, H. P., GUARNIERI, P., FRIEDMAN, B. A., CARRASCO, M. A., MURATET, M., O'KEEFFE, S., NWAKEZE, C., PAULI-BEHN, F., NEWBERRY, K. M., MEADOWS, S. K., TAPIA, J. C., MYERS, R. M. & MANIATIS, T. 2013. Intricate interplay between astrocytes and motor neurons in ALS. *Proceedings of the National Academy of Sciences of the United States of America*, 110, E756-E765.
- PHILIPS, T., BENTO-ABREU, A., NONNEMAN, A., HAECK, W., STAATS, K., GEELLEN, V., HERSMUS, N., KUSTERS, B., VAN DEN BOSCH, L., VAN DAMME, P., RICHARDSON, W. D. & ROBBERECHT, W. 2013. Oligodendrocyte dysfunction in the pathogenesis of amyotrophic lateral sclerosis. *Brain*, 136, 471-82.
- PHILIPS, T. & ROBBERECHT, W. 2011. Neuroinflammation in amyotrophic lateral sclerosis: role of glial activation in motor neuron disease. *Lancet Neurol*, 10, 253-63.
- PHILIPS, T. & ROTHSTEIN, J. D. 2014. Glial cells in amyotrophic lateral sclerosis. *Experimental neurology*, 262 Pt B, 111-120.

- PISANO, F., MURA, M., CIUFFREDA, M. C., CALABRÒ, F., LANZO, N. & GNECCHI, M. 2018. Optimized lentiviral transduction of human amniotic mesenchymal stromal cells. *Pharmacological Research*, 127, 49-57.
- PITTENGER, M. F., MACKAY, A. M., BECK, S. C., JAISWAL, R. K., DOUGLAS, R., MOSCA, J. D., MOORMAN, M. A., SIMONETTI, D. W., CRAIG, S. & MARSHAK, D. R. 1999. Multilineage potential of adult human mesenchymal stem cells. *Science*, 284, 143-7.
- POKRISHEVSKY, E., GRAD, L. I., YOUSEFI, M., WANG, J., MACKENZIE, I. R. & CASHMAN, N. R. 2012. Aberrant localization of FUS and TDP43 is associated with misfolding of SOD1 in amyotrophic lateral sclerosis. *PLoS One*, 7, e35050.
- POLYMENIDOU, M., LAGIER-TOURENNE, C., HUTT, K. R., HUELGA, S. C., MORAN, J., LIANG, T. Y., LING, S. C., SUN, E., WANCEWICZ, E., MAZUR, C., KORDASIEWICZ, H., SEDAGHAT, Y., DONOHUE, J. P., SHIUE, L., BENNETT, C. F., YEO, G. W. & CLEVELAND, D. W. 2011. Long pre-mRNA depletion and RNA missplicing contribute to neuronal vulnerability from loss of TDP-43. *Nat Neurosci*, 14, 459-68.
- POPESCU, I. R., NICAISE, C., LIU, S., BISCH, G., KNIPPENBERG, S., DAUBIE, V., BOHL, D. & POCHET, R. 2013. Neural progenitors derived from human induced pluripotent stem cells survive and differentiate upon transplantation into a rat model of amyotrophic lateral sclerosis. *Stem Cells Transl Med*, 2, 167-74.
- POPPE, L., RUE, L., ROBBERECHT, W. & VAN DEN BOSCH, L. 2014. Translating biological findings into new treatment strategies for amyotrophic lateral sclerosis (ALS). *Exp Neurol*, 262 Pt B, 138-51.
- PRADA, I., GABRIELLI, M., TUROLA, E., IORIO, A., D'ARRIGO, G., PAROLISI, R., DE LUCA, M., PACIFICI, M., BASTONI, M., LOMBARDI, M., LEGNAME, G., COJOC, D., BUFFO, A., FURLAN, R., PERUZZI, F. & VERDERIO, C. 2018. Glia-to-neuron transfer of miRNAs via extracellular vesicles: a new mechanism underlying inflammation-induced synaptic alterations. *Acta Neuropathol*, 135, 529-550.
- PRADAT, P. F., KABASHI, E. & DESNUELLE, C. 2015. Deciphering spreading mechanisms in amyotrophic lateral sclerosis: clinical evidence and potential molecular processes. *Curr Opin Neurol*, 28, 455-61.
- PRAMATAROVA, A., LAGANIERE, J., ROUSSEL, J., BRISEBOIS, K. & ROULEAU, G. A. 2001. Neuron-specific expression of mutant superoxide dismutase 1 in transgenic mice does not lead to motor impairment. *J Neurosci*, 21, 3369-74.
- PRONTO-LABORINHO, A. C., PINTO, S. & DE CARVALHO, M. 2014. Roles of vascular endothelial growth factor in amyotrophic lateral sclerosis. *Biomed Res Int*, 2014, 947513.
- QIAN, D. X., ZHANG, H. T., MA, X., JIANG, X. D. & XU, R. X. 2010. Comparison of the efficiencies of three neural induction protocols in human adipose stromal cells. *Neurochem Res*, 35, 572-9.
- QIAN, K., HUANG, H., PETERSON, A., HU, B., MARAGAKIS, N. J., MING, G.-L., CHEN, H. & ZHANG, S.-C. 2017. Sporadic ALS Astrocytes Induce Neuronal Degeneration In Vivo. *Stem cell reports*, 8, 843-855.
- RAJAN, T. S., DIOMEDE, F., BRAMANTI, P., TRUBIANI, O. & MAZZON, E. 2017. Conditioned medium from human gingival mesenchymal stem cells protects motor-neuron-like NSC-34 cells against scratch-injury-induced cell death. *Int J Immunopathol Pharmacol*, 30, 383-394.
- RAMASAMY, R., FAZEKASOVA, H., LAM, E. W., SOEIRO, I., LOMBARDI, G. & DAZZI, F. 2007. Mesenchymal stem cells inhibit dendritic cell differentiation and function by preventing entry into the cell cycle. *Transplantation*, 83, 71-6.

- RAMIREZ-JARQUIN, U. N., ROJAS, F., VAN ZUNDERT, B. & TAPIA, R. 2017. Chronic infusion of SOD1(G93A) astrocyte-secreted factors induces spinal motoneuron degeneration and neuromuscular dysfunction in healthy rats. *J Cell Physiol*, 232, 2610-2615.
- RANSOHOFF, R. M. 2016. A polarizing question: do M1 and M2 microglia exist? *Nature Neuroscience*, 19, 987.
- RE, DIANE B., LE VERCHE, V., YU, C., AMOROSO, MACKENZIE W., POLITI, KRISTIN A., PHANI, S., IKIZ, B., HOFFMANN, L., KOOLEN, M., NAGATA, T., PAPADIMITRIOU, D., NAGY, P., MITSUMOTO, H., KARIYA, S., WICHTERLE, H., HENDERSON, CHRISTOPHER E. & PRZEDBORSKI, S. 2014. Necroptosis Drives Motor Neuron Death in Models of Both Sporadic and Familial ALS. *Neuron*, 81, 1001-1008.
- REHOROVA, M., VARGOVA, I., FOROSTYAK, S., VACKOVA, I., TURNOVCOVA, K., KUPCOVA SKALNIKOVA, H., VODICKA, P., KUBINOVA, S., SYKOVA, E. & JENDELOVA, P. 2019. A Combination of Intrathecal and Intramuscular Application of Human Mesenchymal Stem Cells Partly Reduces the Activation of Necroptosis in the Spinal Cord of SOD1(G93A) Rats. *Stem Cells Transl Med*, 8, 535-547.
- REN, G., ZHAO, X., ZHANG, L., ZHANG, J., L'HUILLIER, A., LING, W., ROBERTS, A. I., LE, A. D., SHI, S., SHAO, C. & SHI, Y. 2010. Inflammatory Cytokine-Induced Intercellular Adhesion Molecule-1 and Vascular Cell Adhesion Molecule-1 in Mesenchymal Stem Cells Are Critical for Immunosuppression. *J Immunol*, 184, 2321-8.
- RENTON, A. E., CHIO, A. & TRAYNOR, B. J. 2014. State of play in amyotrophic lateral sclerosis genetics. *Nat Neurosci*, 17, 17-23.
- RENTON, A. E., MAJOUNIE, E., WAITE, A., SIMON-SANCHEZ, J., ROLLINSON, S., GIBBS, J. R., SCHYMICK, J. C., LAAKSOVIRTA, H., VAN SWIETEN, J. C., MYLLYKANGAS, L., KALIMO, H., PAETAU, A., ABRAMZON, Y., REMES, A. M., KAGANOVICH, A., SCHOLZ, S. W., DUCKWORTH, J., DING, J., HARMER, D. W., HERNANDEZ, D. G., JOHNSON, J. O., MOK, K., RYTEN, M., TRABZUNI, D., GUERREIRO, R. J., ORRELL, R. W., NEAL, J., MURRAY, A., PEARSON, J., JANSEN, I. E., SONDERVAN, D., SEELAAR, H., BLAKE, D., YOUNG, K., HALLIWELL, N., CALLISTER, J. B., TOULSON, G., RICHARDSON, A., GERHARD, A., SNOWDEN, J., MANN, D., NEARY, D., NALLS, M. A., PEURALINNA, T., JANSSON, L., ISOVIITA, V. M., KAIVORINNE, A. L., HOLTTA-VUORI, M., IKONEN, E., SULKAVA, R., BENATAR, M., WUU, J., CHIO, A., RESTAGNO, G., BORGHERO, G., SABATELLI, M., HECKERMAN, D., ROGAEVA, E., ZINMAN, L., ROTHSTEIN, J. D., SENDTNER, M., DREPPER, C., EICHLER, E. E., ALKAN, C., ABDULLAEV, Z., PACK, S. D., DUTRA, A., PAK, E., HARDY, J., SINGLETON, A., WILLIAMS, N. M., HEUTINK, P., PICKERING-BROWN, S., MORRIS, H. R., TIENARI, P. J. & TRAYNOR, B. J. 2011. A hexanucleotide repeat expansion in C9ORF72 is the cause of chromosome 9p21-linked ALS-FTD. *Neuron*, 72, 257-68.
- RILEY, J., GLASS, J., FELDMAN, E. L., POLAK, M., BORDEAU, J., FEDERICI, T., JOHE, K. & BOULIS, N. M. 2014. Intraspinal stem cell transplantation in amyotrophic lateral sclerosis: a phase I trial, cervical microinjection, and final surgical safety outcomes. *Neurosurgery*, 74, 77-87.
- RIVERA, F. J., COUILLARD-DESPRES, S., PEDRE, X., PLOETZ, S., CAIONI, M., LOIS, C., BOGDAHN, U. & AIGNER, L. 2006. Mesenchymal stem cells instruct oligodendrogenic fate decision on adult neural stem cells. *Stem Cells*, 24, 2209-19.
- ROBBERECHT, W. & PHILIPS, T. 2013. The changing scene of amyotrophic lateral sclerosis. *Nat Rev Neurosci*, 14, 248-64.

- ROJAS, F., CORTES, N., ABARZUA, S., DYRDA, A. & VAN ZUNDERT, B. 2014. Astrocytes expressing mutant SOD1 and TDP43 trigger motoneuron death that is mediated via sodium channels and nitroxidative stress. *Front Cell Neurosci*, 8, 24.
- ROMBOUITS, W. J. & PLOEMACHER, R. E. 2003. Primary murine MSC show highly efficient homing to the bone marrow but lose homing ability following culture. *Leukemia*, 17, 160-70.
- ROSEN, D. R., SIDDIQUE, T., PATTERSON, D., FIGLEWICZ, D. A., SAPP, P., HENTATI, A., DONALDSON, D., GOTO, J., O'REGAN, J. P., DENG, H. X. & ET AL. 1993. Mutations in Cu/Zn superoxide dismutase gene are associated with familial amyotrophic lateral sclerosis. *Nature*, 362, 59-62.
- ROSSI, S. L., NISTOR, G., WYATT, T., YIN, H. Z., POOLE, A. J., WEISS, J. H., GARDENER, M. J., DIJKSTRA, S., FISCHER, D. F. & KEIRSTEAD, H. S. 2010. Histological and functional benefit following transplantation of motor neuron progenitors to the injured rat spinal cord. *PLoS One*, 5, e11852.
- ROSTAMI, M., HAIDARI, K. & SHAHBAZI, M. 2018. Genetically Engineered Adipose Mesenchymal Stem Cells Using HIV-Based Lentiviral Vectors as Gene Therapy for Autoimmune Diseases. *Cell Reprogram*.
- ROTHSTEIN, J. D., MARTIN, L. J. & KUNCL, R. W. 1992. Decreased Glutamate Transport by the Brain and Spinal Cord in Amyotrophic Lateral Sclerosis. *New England Journal of Medicine*, 326, 1464-1468.
- ROTHSTEIN, J. D., PATEL, S., REGAN, M. R., HAENGGELI, C., HUANG, Y. H., BERGLES, D. E., JIN, L., DYKES HOBERG, M., VIDENSKY, S., CHUNG, D. S., TOAN, S. V., BRUIJN, L. I., SU, Z.-Z., GUPTA, P. & FISHER, P. B. 2005. β -Lactam antibiotics offer neuroprotection by increasing glutamate transporter expression. *Nature*, 433, 73-77.
- ROTHSTEIN, J. D., VAN KAMMEN, M., LEVEY, A. I., MARTIN, L. J. & KUNCL, R. W. 1995. Selective loss of glial glutamate transporter GLT-1 in amyotrophic lateral sclerosis. *Annals of Neurology*, 38, 73-84.
- RUTHERFORD, N. J., ZHANG, Y. J., BAKER, M., GASS, J. M., FINCH, N. A., XU, Y. F., STEWART, H., KELLEY, B. J., KUNTZ, K., CROOK, R. J., SREEDHARAN, J., VANCE, C., SORENSON, E., LIPPA, C., BIGIO, E. H., GESCHWIND, D. H., KNOPMAN, D. S., MITSUMOTO, H., PETERSEN, R. C., CASHMAN, N. R., HUTTON, M., SHAW, C. E., BOYLAN, K. B., BOEVE, B., GRAFF-RADFORD, N. R., WSZOLEK, Z. K., CASELLI, R. J., DICKSON, D. W., MACKENZIE, I. R., PETRUCCELLI, L. & RADEMAKERS, R. 2008. Novel mutations in TARDBP (TDP-43) in patients with familial amyotrophic lateral sclerosis. *PLoS Genet*, 4, e1000193.
- RUTKOVE, S. B. 2015. Clinical Measures of Disease Progression in Amyotrophic Lateral Sclerosis. *Neurotherapeutics*, 12, 384-93.
- RYAN, J. M., BARRY, F. P., MURPHY, J. M. & MAHON, B. P. 2005. Mesenchymal stem cells avoid allogeneic rejection. *Journal of inflammation (London, England)*, 2, 8-8.
- SADAN, O., BAHAT-STROMZA, M., BARHUM, Y., LEVY, Y. S., PISNEVSKY, A., PERETZ, H., ILAN, A. B., BULVIK, S., SHEMESH, N., KREPEL, D., COHEN, Y., MELAMED, E. & OFFEN, D. 2009. Protective effects of neurotrophic factor-secreting cells in a 6-OHDA rat model of Parkinson disease. *Stem Cells Dev*, 18, 1179-90.
- SADAN, O., MELAMED, E. & OFFEN, D. 2012. Intrastratial transplantation of neurotrophic factor-secreting human mesenchymal stem cells improves motor function and extends survival in R6/2 transgenic mouse model for Huntington's disease. *PLoS currents*, 4, e4f7f6dc013d4e-e4f7f6dc013d4e.
- SADAN, O., SHEMESH, N., BARZILAY, R., BAHAT-STROMZA, M., MELAMED, E., COHEN, Y. & OFFEN, D. 2008. Migration of neurotrophic factors-secreting

- mesenchymal stem cells toward a quinolinic acid lesion as viewed by magnetic resonance imaging. *Stem Cells*, 26, 2542-51.
- SAFFORD, K. M., HICOK, K. C., SAFFORD, S. D., HALVORSEN, Y. D., WILKISON, W. O., GIMBLE, J. M. & RICE, H. E. 2002. Neurogenic differentiation of murine and human adipose-derived stromal cells. *Biochem Biophys Res Commun*, 294, 371-9.
- SAIJO, K. & GLASS, C. K. 2011. Microglial cell origin and phenotypes in health and disease. *Nat Rev Immunol*, 11, 775-87.
- SAKOWSKI, S. A., SCHUYLER, A. D. & FELDMAN, E. L. 2009. Insulin-like growth factor-I for the treatment of amyotrophic lateral sclerosis. *Amyotrophic lateral sclerosis : official publication of the World Federation of Neurology Research Group on Motor Neuron Diseases*, 10, 63-73.
- SAMPSON, T. R., DEBELIUS, J. W., THRON, T., JANSSEN, S., SHASTRI, G. G., ILHAN, Z. E., CHALLIS, C., SCHRETTER, C. E., ROCHA, S., GRADINARU, V., CHESSELET, M. F., KESHAVARZIAN, A., SHANNON, K. M., KRAJMALNIK-BROWN, R., WITTUNG-STAFSHED, P., KNIGHT, R. & MAZMANIAN, S. K. 2016. Gut Microbiota Regulate Motor Deficits and Neuroinflammation in a Model of Parkinson's Disease. *Cell*, 167, 1469-1480 e12.
- SANCHEZ-RAMOS, J., SONG, S., CARDOZO-PELAEZ, F., HAZZI, C., STEDEFORD, T., WILLING, A., FREEMAN, T. B., SAPORTA, S., JANSSEN, W., PATEL, N., COOPER, D. R. & SANBERG, P. R. 2000. Adult bone marrow stromal cells differentiate into neural cells in vitro. *Exp Neurol*, 164, 247-56.
- SANDERS, S. K., CREAN, S. M., BOXER, P. A., KELLNER, D., LAROSA, G. J. & HUNT, S. W., 3RD 2000. Functional differences between monocyte chemotactic protein-1 receptor A and monocyte chemotactic protein-1 receptor B expressed in a Jurkat T cell. *J Immunol*, 165, 4877-83.
- SARGSYAN, S. A., BLACKBURN, D. J., BARBER, S. C., MONK, P. N. & SHAW, P. J. 2009. Mutant SOD1 G93A microglia have an inflammatory phenotype and elevated production of MCP-1. *Neuroreport*, 20, 1450-5.
- SAURA, J. 2007. Microglial cells in astroglial cultures: a cautionary note. *Journal of Neuroinflammation*, 4, 26.
- SAURA, J., TUSELL, J. M. & SERRATOSA, J. 2003. High-yield isolation of murine microglia by mild trypsinization. *Glia*, 44, 183-9.
- SAXENA, S., CABUY, E. & CARONI, P. 2009. A role for motoneuron subtype-selective ER stress in disease manifestations of FALS mice. *Nat Neurosci*, 12, 627-36.
- SCHAFFER, S., CALAS, A. G., VERGOUTS, M. & HERMANS, E. 2012. Immunomodulatory influence of bone marrow-derived mesenchymal stem cells on neuroinflammation in astrocyte cultures. *J Neuroimmunol*, 249, 40-8.
- SCHIFFER, D., CORDERA, S., CAVALLA, P. & MIGHELI, A. 1996. Reactive astrogliosis of the spinal cord in amyotrophic lateral sclerosis. *J Neurol Sci*, 139 Suppl, 27-33.
- SCHONFELD, L. M., DOOLEY, D., JAHANSHAH, A., TEMEL, Y. & HENDRIX, S. 2017. Evaluating rodent motor functions: Which tests to choose? *Neurosci Biobehav Rev*, 83, 298-312.
- SCHWARTZ, J. C., CECH, T. R. & PARKER, R. R. 2015. Biochemical Properties and Biological Functions of FET Proteins. *Annu Rev Biochem*, 84, 355-79.
- SCHWERK, A., ALTSCHULER, J., ROCH, M., GOSEN, M., WINTER, C., BERG, J., KURTZ, A., AKYUZ, L. & STEINER, B. 2015. Adipose-derived human mesenchymal stem cells induce long-term neurogenic and anti-inflammatory effects and improve cognitive but not motor performance in a rat model of Parkinson's disease. *Regen Med*, 10, 431-46.

- SCOTT, M. K., AKINDURO, O. & LO CELSO, C. 2014. In vivo 4-dimensional tracking of hematopoietic stem and progenitor cells in adult mouse calvarial bone marrow. *J Vis Exp*, e51683.
- SCOTT, S., KRANZ, J. E., COLE, J., LINCECUM, J. M., THOMPSON, K., KELLY, N., BOSTROM, A., THEODOSS, J., AL-NAKHALA, B. M., VIEIRA, F. G., RAMASUBBU, J. & HEYWOOD, J. A. 2008. Design, power, and interpretation of studies in the standard murine model of ALS. *Amyotroph Lateral Scler*, 9, 4-15.
- SCOTTER, E. L., CHEN, H. J. & SHAW, C. E. 2015. TDP-43 Proteinopathy and ALS: Insights into Disease Mechanisms and Therapeutic Targets. *Neurotherapeutics*, 12, 352-63.
- SEKIZAWA, T., OPENSHAW, H., OHBO, K., SUGAMURA, K., ITOYAMA, Y. & NILAND, J. C. 1998. Cerebrospinal fluid interleukin 6 in amyotrophic lateral sclerosis: immunological parameter and comparison with inflammatory and non-inflammatory central nervous system diseases. *J Neurol Sci*, 154, 194-9.
- SERIO, A., BILICAN, B., BARMADA, S. J., ANDO, D. M., ZHAO, C., SILLER, R., BURR, K., HAGHI, G., STORY, D., NISHIMURA, A. L., CARRASCO, M. A., PHATNANI, H. P., SHUM, C., WILMUT, I., MANIATIS, T., SHAW, C. E., FINKBEINER, S. & CHANDRAN, S. 2013. Astrocyte pathology and the absence of non-cell autonomy in an induced pluripotent stem cell model of TDP-43 proteinopathy. *Proc Natl Acad Sci U S A*, 110, 4697-702.
- SHALABY, S. M., SABBAH, N. A., SABER, T. & ABDEL HAMID, R. A. 2016. Adipose-derived mesenchymal stem cells modulate the immune response in chronic experimental autoimmune encephalomyelitis model. *IUBMB Life*, 68, 106-15.
- SHAW, C. E. 2010. Capturing VCP: another molecular piece in the ALS jigsaw puzzle. *Neuron*, 68, 812-4.
- SHEN, B., LIU, J., ZHANG, F., WANG, Y., QIN, Y., ZHOU, Z., QIU, J. & FAN, Y. 2016. CCR2 Positive Exosome Released by Mesenchymal Stem Cells Suppresses Macrophage Functions and Alleviates Ischemia/Reperfusion-Induced Renal Injury. *Stem Cells Int*, 2016, 1240301.
- SHEN, C. C., YANG, Y. C. & LIU, B. S. 2012. Peripheral nerve repair of transplanted undifferentiated adipose tissue-derived stem cells in a biodegradable reinforced nerve conduit. *J Biomed Mater Res A*, 100, 48-63.
- SHI, P., GAL, J., KWINTER, D. M., LIU, X. & ZHU, H. 2010. Mitochondrial dysfunction in amyotrophic lateral sclerosis. *Biochim Biophys Acta*, 1802, 45-51.
- SHIN, S., DALTON, S. & STICE, S. L. 2005. Human motor neuron differentiation from human embryonic stem cells. *Stem Cells Dev*, 14, 266-9.
- SREEDHARAN, J., BLAIR, IP., TRIPATHI, VB., HU, X., VANCE, C., ROGELJ, B., ACKERLEY, S., DURRALL, JC., WILLIAMS, KL., BURATTI, E., BARALLE, F., de BELLEORCHE, J., MITCHELL, JD., LEIGH, PN., AL-CHALABI, A., MILLER, CC., NICHOLSON, G., SHAW, CE. 2008. TDP-43 mutations in familial and sporadic amyotrophic lateral sclerosis. *Science*, 319, 1668-72.
- SHRESTHA, B., COYKENDALL, K., LI, Y., MOON, A., PRIYADARSHANI, P. & YAO, L. 2014. Repair of injured spinal cord using biomaterial scaffolds and stem cells. *Stem Cell Res Ther*, 5, 91.
- SIMMONS, P. J., MASINOVSKY, B., LONGENECKER, B. M., BERENSON, R., TOROK-STORB, B. & GALLATIN, W. M. 1992. Vascular cell adhesion molecule-1 expressed by bone marrow stromal cells mediates the binding of hematopoietic progenitor cells. *Blood*, 80, 388-95.
- SIRONI, F., VALLAROLA, A., VIOLATTO, M. B., TALAMINI, L., FRESCHI, M., DE GIOIA, R., CAPELLI, C., AGOSTINI, A., MOSCATELLI, D., TORTAROLO, M., BIGINI, P., INTRONA, M. & BENDOTTI, C. 2017. Multiple

- intracerebroventricular injections of human umbilical cord mesenchymal stem cells delay motor neurons loss but not disease progression of SOD1G93A mice. *Stem Cell Res*, 25, 166-178.
- SONG, S., MIRANDA, C. J., BRAUN, L., MEYER, K., FRAKES, A. E., FERRAIUOLO, L., LIKHITE, S., BEVAN, A. K., FOUST, K. D., MCCONNELL, M. J., WALKER, C. M. & KASPAR, B. K. 2016. Major histocompatibility complex class I molecules protect motor neurons from astrocyte-induced toxicity in amyotrophic lateral sclerosis. *Nature medicine*, 22, 397-403.
- STAATS, K. A. & VAN DEN BOSCH, L. 2009. Astrocytes in amyotrophic lateral sclerosis: direct effects on motor neuron survival. *Journal of biological physics*, 35, 337-346.
- STAFF, N. P., MADIGAN, N. N., MORRIS, J., JENTOFT, M., SORENSON, E. J., BUTLER, G., GASTINEAU, D., DIETZ, A. & WINDEBANK, A. J. 2016. Safety of intrathecal autologous adipose-derived mesenchymal stromal cells in patients with ALS. *Neurology*, 87, 2230.
- STORKEBAUM, E., LAMBRECHTS, D., DEWERCHIN, M., MORENO-MURCIANO, M.-P., APPELMANS, S., OH, H., VAN DAMME, P., RUTTEN, B., MAN, W. Y., DE MOL, M., WYNS, S., MANKA, D., VERMEULEN, K., VAN DEN BOSCH, L., MERTENS, N., SCHMITZ, C., ROBBERECHT, W., CONWAY, E. M., COLLEN, D., MOONS, L. & CARMELIET, P. 2005. Treatment of motoneuron degeneration by intracerebroventricular delivery of VEGF in a rat model of ALS. *Nature Neuroscience*, 8, 85-92.
- STREM, B. M., HICOK, K. C., ZHU, M., WULUR, I., ALFONSO, Z., SCHREIBER, R. E., FRASER, J. K. & HEDRICK, M. H. 2005. Multipotential differentiation of adipose tissue-derived stem cells. *Keio J Med*, 54, 132-41.
- STRIOGA, M., VISWANATHAN, S., DARINSKAS, A., SLABY, O. & MICHALEK, J. 2012. Same or not the same? Comparison of adipose tissue-derived versus bone marrow-derived mesenchymal stem and stromal cells. *Stem Cells Dev*, 21, 2724-52.
- SUGARMAN, J. 2008. Ethical issues in stem cell research and treatment. *Cell Research*, 18, S176.
- SUN, H., BENARDAIS, K., STANSLOWSKY, N., THAU-HABERMANN, N., HENSEL, N., HUANG, D., CLAUS, P., DENGLER, R., STANGEL, M. & PETRI, S. 2013. Therapeutic potential of mesenchymal stromal cells and MSC conditioned medium in Amyotrophic Lateral Sclerosis (ALS)--in vitro evidence from primary motor neuron cultures, NSC-34 cells, astrocytes and microglia. *PLoS One*, 8, e72926.
- SUZUKI, M., MCHUGH, J., TORK, C., SHELLY, B., HAYES, A., BELLANTUONO, I., AEBISCHER, P. & SVENDSEN, C. N. 2008. Direct muscle delivery of GDNF with human mesenchymal stem cells improves motor neuron survival and function in a rat model of familial ALS. *Mol Ther*, 16, 2002-10.
- SWARUP, V., PHANEUF, D., DUPRE, N., PETRI, S., STRONG, M., KRIZ, J. & JULIEN, J. P. 2011. Deregulation of TDP-43 in amyotrophic lateral sclerosis triggers nuclear factor kappaB-mediated pathogenic pathways. *J Exp Med*, 208, 2429-47.
- SWEENEY, N. P., REGAN, C., LIU, J., GALLEU, A., DAZZI, F., LINDEMANN, D., RUPAR, C. A. & MCCLURE, M. O. 2016. Rapid and Efficient Stable Gene Transfer to Mesenchymal Stromal Cells Using a Modified Foamy Virus Vector. *Molecular Therapy*, 24, 1227-1236.
- TAKAHASHI, K., TANABE, K., OHNUKI, M., NARITA, M., ICHISAKA, T., TOMODA, K. & YAMANAKA, S. 2007. Induction of pluripotent stem cells from adult human fibroblasts by defined factors. *Cell*, 131, 861-72.

- TAKAHASHI, K. & YAMANAKA, S. 2006. Induction of pluripotent stem cells from mouse embryonic and adult fibroblast cultures by defined factors. *Cell*, 126, 663-76.
- TARASSISHIN, L., SUH, H. S. & LEE, S. C. 2014. LPS and IL-1 differentially activate mouse and human astrocytes: role of CD14. *Glia*, 62, 999-1013.
- TATEISHI, T., YAMASAKI, R., TANAKA, M., MATSUSHITA, T., KIKUCHI, H., ISOBE, N., OHYAGI, Y. & KIRA, J. 2010. CSF chemokine alterations related to the clinical course of amyotrophic lateral sclerosis. *J Neuroimmunol*, 222, 76-81.
- THERY, C., ZITVOGEL, L. & AMIGORENA, S. 2002. Exosomes: composition, biogenesis and function. *Nat Rev Immunol*. England.
- THOMSON, J. A., ITSKOVITZ-ELDOR, J., SHAPIRO, S. S., WAKNITZ, M. A., SWIERGIEL, J. J., MARSHALL, V. S. & JONES, J. M. 1998. Embryonic stem cell lines derived from human blastocysts. *Science*, 282, 1145-7.
- TOMA, J. S., SHETTAR, B. C., CHIPMAN, P. H., PINTO, D. M., BOROWSKA, J. P., ICHIDA, J. K., FAWCETT, J. P., ZHANG, Y., EGGAN, K. & RAFUSE, V. F. 2015. Motoneurons Derived from Induced Pluripotent Stem Cells Develop Mature Phenotypes Typical of Endogenous Spinal Motoneurons. *J Neurosci*, 35, 1291-306.
- TONG, J., HUANG, C., BI, F., WU, Q., HUANG, B., LIU, X., LI, F., ZHOU, H. & XIA, X. G. 2013. Expression of ALS-linked TDP-43 mutant in astrocytes causes non-cell-autonomous motor neuron death in rats. *Embo j*, 32, 1917-26.
- TORTAROLO, M., LO COCO, D., VEGLIANESE, P., VALLAROLA, A., GIORDANA, M. T., MARCON, G., BEGHI, E., POLONI, M., STRONG, M. J., IYER, A. M., ARONICA, E. & BENDOTTI, C. 2017. Amyotrophic Lateral Sclerosis, a Multisystem Pathology: Insights into the Role of TNFalpha. *Mediators Inflamm*, 2017, 2985051.
- TOVAR-Y-ROMO, L. B., RAMÍREZ-JARQUÍN, U. N., LAZO-GÓMEZ, R. & TAPIA, R. 2014. Trophic factors as modulators of motor neuron physiology and survival: implications for ALS therapy. *Frontiers in cellular neuroscience*, 8, 61-61.
- TRIPATHI, P., RODRIGUEZ-MUELA, N., KLIM, J. R., DE BOER, A. S., AGRAWAL, S., SANDOE, J., LOPES, C. S., OGLIARI, K. S., WILLIAMS, L. A., SHEAR, M., RUBIN, L. L., EGGAN, K. & ZHOU, Q. 2017. Reactive Astrocytes Promote ALS-like Degeneration and Intracellular Protein Aggregation in Human Motor Neurons by Disrupting Autophagy through TGF-β1. *Stem cell reports*, 9, 667-680.
- TURNER, M. R., BOWSER, R., BRUIJN, L., DUPUIS, L., LUDOLPH, A., MCGRATH, M., MANFREDI, G., MARAGAKIS, N., MILLER, R. G., PULLMAN, S. L., RUTKOVE, S. B., SHAW, P. J., SHEFNER, J. & FISCHBECK, K. H. 2013. Mechanisms, models and biomarkers in amyotrophic lateral sclerosis. *Amyotroph Lateral Scler Frontotemporal Degener*, 14 Suppl 1, 19-32.
- UCCELLI, A., MILANESE, M., PRINCIPATO, M. C., MORANDO, S., BONIFACINO, T., VERGANI, L., GIUNTI, D., VOCI, A., CARMINATI, E., GIRIBALDI, F., CAPONNETTO, C. & BONANNO, G. 2012. Intravenous mesenchymal stem cells improve survival and motor function in experimental amyotrophic lateral sclerosis. *Mol Med*, 18, 794-804.
- VAN DEN BERG, L. H., SORENSON, E., GRONSETH, G., MACKLIN, E. A., ANDREWS, J., BALOH, R. H., BENATAR, M., BERRY, J. D., CHIO, A., CORCIA, P., GENGE, A., GUBITZ, A. K., LOMEN-HOERTH, C., MCDERMOTT, C. J., PIORO, E. P., ROSENFELD, J., SILANI, V., TURNER, M. R., WEBER, M., BROOKS, B. R., MILLER, R. G. & MITSUMOTO, H. 2019. Revised Airlie House consensus guidelines for design and implementation of ALS clinical trials. *Neurology*, 92, e1610.

- VAN DEN BOSCH, L., STORKEBAUM, E., VLEMINCKX, V., MOONS, L., VANOPDENBOSCH, L., SCHEVENEELS, W., CARMELIET, P. & ROBBERECHT, W. 2004. Effects of vascular endothelial growth factor (VEGF) on motor neuron degeneration. *Neurobiology of Disease*, 17, 21-28.
- VAN DER MEER, J. W. M. & SIMON, A. 2010. Blocking IL-1beta to slow down progression of ALS? *Proceedings of the National Academy of Sciences of the United States of America*, 107, 12741-12742.
- VAN VOLLENSTEE, F. A., JACKSON, C., HOFFMANN, D., POTGIETER, M., DURANDT, C. & PEPPER, M. S. 2016. Human adipose derived mesenchymal stromal cells transduced with GFP lentiviral vectors: assessment of immunophenotype and differentiation capacity in vitro. *Cytotechnology*.
- VANCE, C., ROGELJ, B., HORTOBAGYI, T., DE VOS, K. J., NISHIMURA, A. L., SREEDHARAN, J., HU, X., SMITH, B., RUDDY, D., WRIGHT, P., GANESALINGAM, J., WILLIAMS, K. L., TRIPATHI, V., AL-SARAJ, S., AL-CHALABI, A., LEIGH, P. N., BLAIR, I. P., NICHOLSON, G., DE BELLEROCHE, J., GALLO, J. M., MILLER, C. C. & SHAW, C. E. 2009. Mutations in FUS, an RNA processing protein, cause familial amyotrophic lateral sclerosis type 6. *Science*, 323, 1208-11.
- VARCIANNA, A., MYSZCZYNSKA, M. A., CASTELLI, L. M., O'NEILL, B., KIM, Y., TALBOT, J., NYBERG, S., NYAMALI, I., HEATH, P. R., STOPFORD, M. J., HAUTBERGUE, G. M. & FERRAIUOLO, L. 2019. Micro-RNAs secreted through astrocyte-derived extracellular vesicles cause neuronal network degeneration in C9orf72 ALS. *EBioMedicine*.
- VARGAS, M. R., JOHNSON, D. A., SIRKIS, D. W., MESSING, A. & JOHNSON, J. A. 2008. Nrf2 Activation in Astrocytes Protects against Neurodegeneration in Mouse Models of Familial Amyotrophic Lateral Sclerosis. *The Journal of Neuroscience*, 28, 13574.
- VERBER, N. S., SHEPHEARD, S. R., SASSANI, M., MCDONOUGH, H. E., MOORE, S. A., ALIX, J. J. P., WILKINSON, I. D., JENKINS, T. M. & SHAW, P. J. 2019. Biomarkers in Motor Neuron Disease: A State of the Art Review. *Front Neurol*, 10, 291.
- VERCELLI, A., MEREUTA, O. M., GARBOSSA, D., MURACA, G., MARESCHI, K., RUSTICHELLI, D., FERRERO, I., MAZZINI, L., MADON, E. & FAGIOLI, F. 2008. Human mesenchymal stem cell transplantation extends survival, improves motor performance and decreases neuroinflammation in mouse model of amyotrophic lateral sclerosis. *Neurobiol Dis*, 31, 395-405.
- VIOLATTO, M. B., SANTANGELO, C., CAPELLI, C., FRAPOLLI, R., FERRARI, R., SITIA, L., TORTAROLO, M., TALAMINI, L., PREVIDI, S., MOSCATELLI, D., SALMONA, M., INTRONA, M., BENDOTTI, C. & BIGINI, P. 2015. Longitudinal tracking of triple labeled umbilical cord derived mesenchymal stromal cells in a mouse model of Amyotrophic Lateral Sclerosis. *Stem Cell Research*, 15, 243-253.
- WALLING, A. D. 1999. Amyotrophic lateral sclerosis: Lou Gehrig's disease. *Am Fam Physician*, 59, 1489-96.
- WANG, L., GUTMANN, D. H. & ROOS, R. P. 2011a. Astrocyte loss of mutant SOD1 delays ALS disease onset and progression in G85R transgenic mice. *Hum Mol Genet*, 20, 286-93.
- WANG, L., PEI, S., HAN, L., GUO, B., LI, Y., DUAN, R., YAO, Y., XUE, B., CHEN, X. & JIA, Y. 2018a. Mesenchymal Stem Cell-Derived Exosomes Reduce A1 Astrocytes via Downregulation of Phosphorylated NFκB P65 Subunit in Spinal Cord Injury. *Cellular Physiology and Biochemistry*, 50, 1535-1559.
- WANG, L., SHARMA, K., GRISOTTI, G. & ROOS, R. P. 2009a. The effect of mutant SOD1 dismutase activity on non-cell autonomous degeneration in familial amyotrophic lateral sclerosis. *Neurobiol Dis*, 35, 234-40.

- WANG, Q., STEIGELMAN, M. B., WALKER, J. A., CHEN, S., HORNSBY, P. J., BOHNENBLUST, M. E. & WANG, H. T. 2009b. In vitro osteogenic differentiation of adipose stem cells after lentiviral transduction with green fluorescent protein. *J Craniofac Surg*, 20, 2193-9.
- WANG, R., YANG, B. & ZHANG, D. 2011b. Activation of interferon signaling pathways in spinal cord astrocytes from an ALS mouse model. *Glia*, 59, 946-958.
- WANG, W., WEN, D., DUAN, W., YIN, J., CUI, C., WANG, Y., LI, Z., LIU, Y. & LI, C. 2018b. Systemic administration of scAAV9-IGF1 extends survival in SOD1(G93A) ALS mice via inhibiting p38 MAPK and the JNK-mediated apoptosis pathway. *Brain Res Bull*, 139, 203-210.
- WANG, Y., DUAN, W., WANG, W., DI, W., LIU, Y., LI, Z., HU, H., LIN, H., CUI, C., LI, D., DONG, H. & LI, C. 2016. scAAV9-VEGF prolongs the survival of transgenic ALS mice by promoting activation of M2 microglia and the PI3K/Akt pathway. *Brain Res*, 1648, 1-10.
- WANG, Y., FU, W., ZHANG, S., HE, X., LIU, Z., GAO, D. & XU, T. 2014. CXCR-7 receptor promotes SDF-1 α -induced migration of bone marrow mesenchymal stem cells in the transient cerebral ischemia/reperfusion rat hippocampus. *Brain Res*, 1575, 78-86.
- WEBSTER, C. P., SMITH, E. F., GRIERSON, A. J. & DE VOS, K. J. 2018. C9orf72 plays a central role in Rab GTPase-dependent regulation of autophagy. *Small GTPases*, 9, 399-408.
- WELSER-ALVES, J. V. & MILNER, R. 2013. Microglia are the major source of TNF- α and TGF- β 1 in postnatal glial cultures; regulation by cytokines, lipopolysaccharide, and vitronectin. *Neurochemistry international*, 63, 47-53.
- WEN, D., CUI, C., DUAN, W., WANG, W., WANG, Y., LIU, Y., LI, Z. & LI, C. 2019. The role of insulin-like growth factor 1 in ALS cell and mouse models: A mitochondrial protector. *Brain Research Bulletin*, 144, 1-13.
- WEYDT, P., YUEN, E. C., RANSOM, B. R. & MOLLER, T. 2004. Increased cytotoxic potential of microglia from ALS-transgenic mice. *Glia*, 48, 179-82.
- WILMS, H., SIEVERS, J., DENGLER, R., BUFLER, J., DEUSCHL, G. & LUCIUS, R. 2003. Intrathecal synthesis of monocyte chemoattractant protein-1 (MCP-1) in amyotrophic lateral sclerosis: further evidence for microglial activation in neurodegeneration. *J Neuroimmunol*, 144, 139-42.
- WILSON, E. H., WENINGER, W. & HUNTER, C. A. 2010. Trafficking of immune cells in the central nervous system. *J Clin Invest*, 120, 1368-79.
- WINKLER, E. A., SENGILLO, J. D., SAGARE, A. P., ZHAO, Z., MA, Q., ZUNIGA, E., WANG, Y., ZHONG, Z., SULLIVAN, J. S., GRIFFIN, J. H., CLEVELAND, D. W. & ZLOKOVIC, B. V. 2014. Blood-spinal cord barrier disruption contributes to early motor-neuron degeneration in ALS-model mice. *Proceedings of the National Academy of Sciences of the United States of America*, 111, E1035-E1042.
- WISLET-GENDEBIEN, S., HANS, G., LEPRINCE, P., RIGO, J. M., MOONEN, G. & ROGISTER, B. 2005. Plasticity of cultured mesenchymal stem cells: switch from nestin-positive to excitable neuron-like phenotype. *Stem Cells*, 23, 392-402.
- WONG, L. M., MYERS, S. J., TSOU, C. L., GOSLING, J., ARAI, H. & CHARO, I. F. 1997. Organization and differential expression of the human monocyte chemoattractant protein 1 receptor gene. Evidence for the role of the carboxyl-terminal tail in receptor trafficking. *J Biol Chem*, 272, 1038-45.
- WONG, P. C., PARDO, C. A., BORCHELT, D. R., LEE, M. K., COPELAND, N. G., JENKINS, N. A., SISODIA, S. S., CLEVELAND, D. W. & PRICE, D. L. 1995. An adverse property of a familial ALS-linked SOD1 mutation causes motor neuron disease characterized by vacuolar degeneration of mitochondria. *Neuron*, 14, 1105-16.

- WOODBURY, D., REYNOLDS, K. & BLACK, I. B. 2002. Adult bone marrow stromal stem cells express germline, ectodermal, endodermal, and mesodermal genes prior to neurogenesis. *J Neurosci Res*, 69, 908-17.
- WOODBURY, D., SCHWARZ, E. J., PROCKOP, D. J. & BLACK, I. B. 2000. Adult rat and human bone marrow stromal cells differentiate into neurons. *J Neurosci Res*, 61, 364-70.
- WU, Y., ZHOU, H., FAN, X., ZHANG, Y., ZHANG, M., WANG, Y., XIE, Z., BAI, M., YIN, Q., LIANG, D., TANG, W., LIAO, J., ZHOU, C., LIU, W., ZHU, P., GUO, H., PAN, H., WU, C., SHI, H., WU, L., TANG, F. & LI, J. 2015. Correction of a genetic disease by CRISPR-Cas9-mediated gene editing in mouse spermatogonial stem cells. *Cell Res*, 25, 67-79.
- WYATT, T. J., ROSSI, S. L., SIEGENTHALER, M. M., FRAME, J., ROBLES, R., NISTOR, G. & KEIRSTEAD, H. S. 2011. Human motor neuron progenitor transplantation leads to endogenous neuronal sparing in 3 models of motor neuron loss. *Stem Cells Int*, 2011, 207230.
- XIAO, Q., ZHAO, W., BEERS, D. R., YEN, A. A., XIE, W., HENKEL, J. S. & APPEL, S. H. 2007. Mutant SOD1(G93A) microglia are more neurotoxic relative to wild-type microglia. *J Neurochem*, 102, 2008-2019.
- XU, L., RYUGO, D. K., PONGSTAPORN, T., JOHE, K. & KOLIATSOS, V. E. 2009. Human neural stem cell grafts in the spinal cord of SOD1 transgenic rats: differentiation and structural integration into the segmental motor circuitry. *J Comp Neurol*, 514, 297-309.
- XU, L., SHEN, P., HAZEL, T., JOHE, K. & KOLIATSOS, V. E. 2011. Dual transplantation of human neural stem cells into cervical and lumbar cord ameliorates motor neuron disease in SOD1 transgenic rats. *Neurosci Lett*, 494, 222-6.
- XU, L., YAN, J., CHEN, D., WELSH, A. M., HAZEL, T., JOHE, K., HATFIELD, G. & KOLIATSOS, V. E. 2006. Human neural stem cell grafts ameliorate motor neuron disease in SOD-1 transgenic rats. *Transplantation*, 82, 865-75.
- YAMANAKA, K., BOILLEE, S., ROBERTS, E. A., GARCIA, M. L., MCALONIS-DOWNES, M., MIKSE, O. R., CLEVELAND, D. W. & GOLDSTEIN, L. S. 2008a. Mutant SOD1 in cell types other than motor neurons and oligodendrocytes accelerates onset of disease in ALS mice. *Proc Natl Acad Sci U S A*, 105, 7594-9.
- YAMANAKA, K., CHUN, S. J., BOILLEE, S., FUJIMORI-TONOU, N., YAMASHITA, H., GUTMANN, D. H., TAKAHASHI, R., MISAWA, H. & CLEVELAND, D. W. 2008b. Astrocytes as determinants of disease progression in inherited amyotrophic lateral sclerosis. *Nature neuroscience*, 11, 251-253.
- YAMANAKA, K. & KOMINE, O. 2018. The multi-dimensional roles of astrocytes in ALS. *Neurosci Res*, 126, 31-38.
- YAN, J., XU, L., WELSH, A. M., CHEN, D., HAZEL, T., JOHE, K. & KOLIATSOS, V. E. 2006. Combined immunosuppressive agents or CD4 antibodies prolong survival of human neural stem cell grafts and improve disease outcomes in amyotrophic lateral sclerosis transgenic mice. *Stem Cells*, 24, 1976-85.
- YAN, J., XU, L., WELSH, A. M., HATFIELD, G., HAZEL, T., JOHE, K. & KOLIATSOS, V. E. 2007. Extensive neuronal differentiation of human neural stem cell grafts in adult rat spinal cord. *PLoS Med*, 4, e39.
- YAN, Y., MA, T., GONG, K., AO, Q., ZHANG, X. & GONG, Y. 2014. Adipose-derived mesenchymal stem cell transplantation promotes adult neurogenesis in the brains of Alzheimer's disease mice. *Neural Regen Res*, 9, 798-805.
- YANG, Z. X., HAN, Z. B., JI, Y. R., WANG, Y. W., LIANG, L., CHI, Y., YANG, S. G., LI, L. N., LUO, W. F., LI, J. P., CHEN, D. D., DU, W. J., CAO, X. C., ZHUO, G. S., WANG, T. & HAN, Z. C. 2013. CD106 identifies a subpopulation of mesenchymal stem cells with unique immunomodulatory properties. *PLoS One*, 8, e59354.

- YOO, P. S., MULKEEN, A. L. & CHA, C. H. 2006. Post-transcriptional regulation of vascular endothelial growth factor: implications for tumor angiogenesis. *World journal of gastroenterology*, 12, 4937-4942.
- YU, X., CHEN, D., ZHANG, Y., WU, X., HUANG, Z., ZHOU, H. & ZHANG, Z. 2012. Overexpression of CXCR4 in mesenchymal stem cells promotes migration, neuroprotection and angiogenesis in a rat model of stroke. *J Neurol Sci*, 316, 141-9.
- ZACHAR, L., BAČENKOVÁ, D. & ROSOCHA, J. 2016. Activation, homing, and role of the mesenchymal stem cells in the inflammatory environment. *Journal of inflammation research*, 9, 231-240.
- ZAPPIA, E., CASAZZA, S., PEDEMONTE, E., BENVENUTO, F., BONANNI, I., GERDONI, E., GIUNTI, D., CERAVOLO, A., CAZZANTI, F., FRASSONI, F., MANCARDI, G. & UCCELLI, A. 2005. Mesenchymal stem cells ameliorate experimental autoimmune encephalomyelitis inducing T-cell anergy. *Blood*, 106, 1755-61.
- ZHANG, B., TU, P., ABTAHIAN, F., TROJANOWSKI, J. Q. & LEE, V. M. 1997. Neurofilaments and orthograde transport are reduced in ventral root axons of transgenic mice that express human SOD1 with a G93A mutation. *J Cell Biol*, 139, 1307-15.
- ZHANG, C., ZHOU, C., TENG, J. J., ZHAO, R. L. & SONG, Y. Q. 2009. Multiple administrations of human marrow stromal cells through cerebrospinal fluid prolong survival in a transgenic mouse model of amyotrophic lateral sclerosis. *Cytotherapy*, 11, 299-306.
- ZHANG, X., HUANG, W., CHEN, X., LIAN, Y., WANG, J., CAI, C., HUANG, L., WANG, T., REN, J. & XIANG, A. P. 2017. CXCR5-Overexpressing Mesenchymal Stromal Cells Exhibit Enhanced Homing and Can Decrease Contact Hypersensitivity. *Mol Ther*, 25, 1434-1447.
- ZHANG, Y., LIU, N., TANG, Y., YANG, E., DONG, S., HUANG, M., PAN, C., ZHANG, P., CHEN, H. & TANG, Z. 2014. Efficient generation of neural stem cell-like cells from rat adipose derived stem cells after lentiviral transduction with green fluorescent protein. *Mol Neurobiol*, 50, 647-54.
- ZHANG, Y., SLOAN, S. A., CLARKE, L. E., CANEDA, C., PLAZA, C. A., BLUMENTHAL, P. D., VOGEL, H., STEINBERG, G. K., EDWARDS, M. S., LI, G., DUNCAN, J. A., 3RD, CHESHER, S. H., SHUER, L. M., CHANG, E. F., GRANT, G. A., GEPHART, M. G. & BARRES, B. A. 2016. Purification and Characterization of Progenitor and Mature Human Astrocytes Reveals Transcriptional and Functional Differences with Mouse. *Neuron*, 89, 37-53.
- ZHAO, C. P., ZHANG, C., ZHOU, S. N., XIE, Y. M., WANG, Y. H., HUANG, H., SHANG, Y. C., LI, W. Y., ZHOU, C., YU, M. J. & FENG, S. W. 2007. Human mesenchymal stromal cells ameliorate the phenotype of SOD1-G93A ALS mice. *Cytotherapy*, 9, 414-26.
- ZHAO, W., BEERS, D. R., BELL, S., WANG, J., WEN, S., BALOH, R. H. & APPEL, S. H. 2015. TDP-43 activates microglia through NF-kappaB and NLRP3 inflammasome. *Exp Neurol*, 273, 24-35.
- ZHAO, W., BEERS, D. R., HENKEL, J. S., ZHANG, W., URUSHITANI, M., JULIEN, J. P. & APPEL, S. H. 2010. Extracellular mutant SOD1 induces microglial-mediated motoneuron injury. *Glia*, 58, 231-43.
- ZHAO, W., XIE, W., XIAO, Q., BEERS, D. R. & APPEL, S. H. 2006. Protective effects of an anti-inflammatory cytokine, interleukin-4, on motoneuron toxicity induced by activated microglia. *J Neurochem*, 99, 1176-87.
- ZHENG, B., CAO, B., LI, G. & HUARD, J. 2006. Mouse adipose-derived stem cells undergo multilineage differentiation in vitro but primarily osteogenic and chondrogenic differentiation in vivo. *Tissue Eng*, 12, 1891-901.

- ZHOU, C., ZHANG, C., ZHAO, R., CHI, S. & GE, P. 2013. Human marrow stromal cells reduce microglial activation to protect motor neurons in a transgenic mouse model of amyotrophic lateral sclerosis. *J Neuroinflammation*, 10, 52.
- ZHU, Q. & KANNEGANTI, T. D. 2017. Cutting Edge: Distinct Regulatory Mechanisms Control Proinflammatory Cytokines IL-18 and IL-1beta. *J Immunol*, 198, 4210-4215.
- ZUK, P. A., ZHU, M., ASHJIAN, P., DE UGARTE, D. A., HUANG, J. I., MIZUNO, H., ALFONSO, Z. C., FRASER, J. K., BENHAIM, P. & HEDRICK, M. H. 2002. Human adipose tissue is a source of multipotent stem cells. *Mol Biol Cell*, 13, 4279-95.
- ZUK, P. A., ZHU, M., MIZUNO, H., HUANG, J., FUTRELL, J. W., KATZ, A. J., BENHAIM, P., LORENZ, H. P. & HEDRICK, M. H. 2001. Multilineage cells from human adipose tissue: implications for cell-based therapies. *Tissue Eng*, 7, 211-28.
- ZURCHER, N. R., LOGGIA, M. L., LAWSON, R., CHONDE, D. B., IZQUIERDO-GARCIA, D., YASEK, J. E., AKEJU, O., CATANA, C., ROSEN, B. R., CUDKOWICZ, M. E., HOOKER, J. M. & ATASSI, N. 2015. Increased in vivo glial activation in patients with amyotrophic lateral sclerosis: assessed with [(11)C]-PBR28. *Neuroimage Clin*, 7, 409-14.

Appendices

Appendix 1: Plasmid DNA sequence of the hCCR2B shuttle vector

In bold the cDNA hCCR2B sequence together with the Kozak consensus sequences.

tcgcgcttt cggatgatgac ggtgaaaacc tctgacacat gcagctccc gagacggtca cagctgtct gtaagcggat
gccgggagca gacaagccc tcagggcgcg tcagcgggtg ttggcgggtg tcggggctgg ctaactatg
cggcatcaga gcagattgta ctgagagtgc accatagcgc gtgtgaaata ccgcacagat gcgtaaggag
aaaataccgc atcaggcgcc atcgccatt caggctgcgc aactgtggg aagggcgatc ggtgcgggcc tctcgctat
tacgccagct ggcgaaaggg gatgtgctg caagcgcatt aagtgggta acgccagggt ttcccagtc acgacgtgt
aaaacgacgg ccagtgaatt ggagacgtgt taacaagctt ggatccgata tcgtagcgc **ggccgccacc**
atgctgtcca catctcgttc tcggttatc agaaatacca acgagagcgg tgaagaagtc accaccttt
ttgattatga ttacggtgct ccctgcata aattgacgt gaagcaaatt ggggccaac tctgctcc
gctctactcg ctggtgtca tctttggtt tgtgggcaac atgctgctg tctcatctt aataaactgc aaaaactga
agtgtgtgac tgacatttac ctgctcaacc tggccatctc tgatctgctt tttctatta ctctccatt gtgggctcac
tctgtgcaa atgagtgggt ctttggaat gcaatgtgca aattattcac agggctgtat cacatcgggt
atttggcgg aatctcttc atcatcctc tgacaatcga tagatactg gctattgtcc atgctgtgtt tgcttaaaa
gccaggacgg tcaccttgg ggtggtgaca agtgtgatca cctggttggt ggctgtgttt gcttctgctc
caggaatcat cttactaaa tgccagaaag aagattctgt ttatgtctgt ggccctatt ttccagagg
atggaataat ttccacaaa taatgaggaa cttttgggg ctggtcctgc cgctgctcat catggtcatc
tgctactcgg gaatcctgaa aaccctgctt cgggtgcaaa acgagaagaa gagcatagg gcagtgagag
tcacttcac catcatgatt gttacttct tctctggac tcctataat attgcattc tctgaacac ctccaggaa
ttctcggcc tgagtaactg tgaagcacc agtcaactgg accaagccac gcaggtgaca gagactctg
ggatgactca ctgctgcatc aatccatca tctatgcctt cgttggggag aagttcagaa ggtatctctc
ggtgttctc cgaaagcaca tcaccaagcg cttctgcaaa caatgtccag tttctacag ggagacagtg
gatggagtga ctcaacaaa cacgccttc actggggagc aggaagtctc ggctggtta taaaggcgcg
ccagtatact ctagagtga caccgggga atcctcagc cgctcgtctc tagctggcg taatcatggt catagctgtt
tctgtgtga aattgtatc cgctcacaat tccacacaac atacgagccg gaagcataaa gtgtaaagcc tggggtcct

aatgagtgag ctaactaca ttaattgctg tgcgctcact gcccgcttc cagtcgggaa acctgctg cagctgcat
taatgaatcg gccaacgcgc ggggagaggc ggtttgcgta ttggcgctc ttccgcttc tcgctcactg actcgctg
ctcggtcgtt cggctgcggc gagcggatc agctcactca aaggcggtaa tacggtatc cacagaatca ggggataacg
caggaaagaa catgtgagca aaaggccagc aaaaggccag gaaccgtaaa aaggccgcgt tgctggcgtt
ttccatagg ctccgcccc ctgacgagca tcacaaaaat cgacgctcaa gtcagagggtg gcgaaacccg acaggactat
aaagatacca ggcggttccc cctggaagct cctcgtgctg ctctcctgtt ccgaccctgc cgcttaccg atacctgtcc
gcctttctcc ctccgggaag cgtggcgctt tctcaatgct cagcctgtag gtatctcagt tcgggttagg tcgttcgctc
caagctgggc tgtgtgcag aacccccgt tcagcccgcg cgctgcgctt tatccggtaa ctatcgtctt gagtccaacc
cggaagaca cgacttatcg cactggcag cagccactgg taacaggatt agcagagcga ggtatgtagg cgtgtctaca
gagttctga agtggtggc taactacgc tactagaa ggacagtatt tggtatctg gctctgctga agccagtac
ctcggaaaa agagttgga gctctgac cggcaaaaa accaccgctg gtagcgggtg tttttgtt tgcaagcagc
agattacgcg cagaaaaaaaa ggatctcaag aagatcctt gatctttct acggggtctg acgctcagt gaacgaaac
tcacgtaag ggatttgg catgagatta tcaaaaagga tctcaccta gatccttta aataaaaaat gaagtttaa
atcaatctaa agtatatg agtaaactg gctgacagt taccaatgct taatcagga ggcacctatc tcagcagct
gtctattcg tcatccata gttgcctgac tcccgtcgt gtagataact acgatacggg agggcttacc atctggccc
agtgtgcaa tgataccgc agaccacgc tcaccggctc cagattatc agcaataaac cagccagccg
gaagggccga gcgagaagt ggtcctgcaa ctatccgc ctccatccag tctattaatt gttccggga agctagagta
agtagtgc cagtaatag tttgcgaac gttgtgcca ttgctacag catcgtggtg tcacgctcgt cgttggat
ggcttctc agtcccgtt cccaacgac aaggcaggt acatgatccc ccatgttg caaaaagc gtagctct
tcggtctcc gatcgtgtc agaagtaagt tggccgaggt gttatcactc atggttatg cagcactgca taattctt
actgtatgc catcgtatg atgctttct gtgactggtg agtactcaac caagctcctc tgagaatagt gtagcggc
accgagttgc tctgcccgc ctcaatag ggataatacc gcgccacata gcagaacttt aaaagtgtc atcattgaa
aacgttctc gggcgaaaa ctctcaagga tctaccgct gttgagatcc agttcagatg aaccactcgc tgcaccaac
tgatctcag catctttac ttcaccagc gttctgggt gagcaaaaac aggaaggcaa aatgccgcaa aaaaggaat
aagggcgaca cggaaatgtt gaatactcat actcttctt ttcaatatt attgaagcat ttatcaggtt tattgtctca
tgagcggata catattgaa tttattaga aaaataaaca aataggggtt ccgcgcat ttcccgaaa agtccacct
gagctcaag aaaccattat tatcatgaca ttaacctata aaaataggcg taccagag cctttcgtc

Appendix 2: Translated amino acid sequence of hCCR2B (360aa)

mlstsrfrl rntnesgeev tffdydyga pchkfdvkqi gaqllpplys lvfifgvgn mlvvlilinc kklkcltdiy
llnlaisdll flitlplwah saanewvfgn amcklftgly higyfggiff iilltidryl aivhavfalk artvtfgvvt
svitwlvavf asvpgiifk cqkedsyvc gpyfprgwnn fhtimrnilg lvpplimvi cysgilktil crnekkrrh
avrvtfimi vyflfwtpyn ivillntfqc fflsncest sqldqatqvt etlgmthcci npiiyafvge kfrrylsvff
rkhitkrfck qcpvyfretv dgtvtstnps tgeqevsagl

Project Outputs and Achievements

Publications

- *Manuscript in preparation.* Ciervo et al. (2019) Adipose derived stem cells protect motor neurons and reduce glial activation in both *in vitro* and *in vivo* models of ALS.
- Ciervo et al. (2017) Advances, challenges and future directions for stem cell therapy in amyotrophic lateral sclerosis, *Molecular Neurodegeneration*, 12,85 (DOI: 10.1186/s13024-017-0227-3). *Review article*

Oral Presentations

- Selected Special Fairbairn oral presentation at the British Society for Gene and Cell Therapy (BSGCT) national meeting (Sheffield, 2019).
- 15th Annual University of Sheffield Medical School research Meeting (Sheffield, 2019).
- NIHR Sheffield BRC Training Academy (Sheffield, 2019).

Poster Presentations

- Poster at The European Network for the Cure of ALS (ENCALS) meeting (Tours, France 2019).

- Best Biomedical poster at The 29th international MNDA symposium on ALS (Glasgow, 2018)
- Moderated poster at the 13th Annual University of Sheffield Medical School research Meeting (Sheffield, 2018).